気相を介する新規合成法による
ゼオライト膜の調製とその機能の評価

09555247

平成9年度～平成11年度

科学研究費補助金

基盤研究(B)(2)研究成果報告書

平成13年4月

研究代表者　松方　正彦

（早稲田大学・理工学部・助教授）

はじめに

本報告書は、題記の研究費によって援助を受けて実施した、DGC 法によるゼオライト合成そのものに関する研究成果、および DGC 法を用いたゼオライト膜の合成と膜分離特性に関する研究成果についてまとめました。無機膜、なかでもゼオライト膜研究が本格的に行われるようになってから約 10 年が経ちます。筆者にとっても、本報告書の多くの部分で用いられている DGC 法によるゼオライト合成の開発に着手してからちょうど 10 年が経ちました。

もともと、ゼオライト膜を合成するためには、アルミノシリケートゲルをあらかじめ薄膜化し、これをゼオライト化することによって均質な膜が得られるのではないかと考えてはじめた研究でした。しかし、幸運なことに、DGC 法自身が、既往の水熱合成とは異なる組成、構造、物性をもつゼオライトが合成でき、ゼオライト合成法そのものとして特長ある手法であることが徐々に明らかとなってきました。このようにして、DGC 法によるゼオライト合成自身の研究を本研究の大きな柱として育てることができました。なかでも、ゼオライトベータの結晶化機構を明らかにできたことは、筆者らにとって重要なステップであったと考えています。

いっぽう、DGC 法を用いたゼオライト膜の合成と、膜分離特性の研究は国際的に多くの競争相手が次々と良い成果を報告するなか、質とスピードの両方が必要とされました。本研究を開始した当初は、ゼオライト膜を用いた炭化水素分離に対して懐疑的な意見も多く、まず炭化水素をゼオライト膜によって分離することが可能であることを実験的に示すことが研究の目標となりました。幸いになことに、C4 異性体混合物、キシレン異性体混合物など炭化水素混合物が、ゼオライト膜によって分離可能であることが示すことができ、この分野における先駆的な成果を継続的に発表することができたのではないかと考えています。

ゼオライト膜は最近、アルコール水溶液の分離では工業化されるに至りました。しかし、本研究で目標としたような、蒸気、ガス分離の分野では、透過流束、選択性について、まだまだ実用的なものを得るに至っていませんし、合成レシピも必ずしも再現性があるものではありません。本研究費のご援助に深謝するとともに、さらに本研究分野の発展に力を尽すべく、努力を傾注したいと思います。

Zeolitic Membranes: Synthesis, Properties and Prospects,
M. Matsukata, and E. Kikuchi,
Bull. Chem. Soc. Jpn., **70(10)**, 2341-2356(1997)

Synthesis of a Zeolitic Thin Layer by a Vapor-phase Transport Method: Appearance of a Preferential Orientation of MFI Zeolite
E. Kikuchi, K. Yamashita, S Hiromoto , K. Ueyama, M. Matsukata,
Micropor. Mater., **11**, 107-116 (1997)

Gas Permeation through Zeolite-Alumina Composite Membranes
N. Nishiyama, K. Ueyama, M. Matsukata,
AIChE J., **43(11A)**, 2724-2730 (1997)

FER Membrane Synthesized by a Vapor-phase Transport Method: Its Structure and Separation Properties
N. Nishiyama, T. Matsufuji, K. Ueyama, M. Matsukata,
Micropor. Mater., **12**, 293-303 (1997)

Effect of Pinholes on Permselectivities of MFI Membranes
M.Matsukata, J.D. Wang, N. Nishiyama, M. Nomura, K. Ueyama,
Proc. the 12th Intern. Zeolite Conf., Baltimore, 1998, Ed. by M.M.J. Treacy, B. Marcus, J.B. Higgins, M.E. Bisher, Mater. Res. Soc., 613-620(1999)

Crystallization of FER on a Porous Alumina Support by a Vapor-phase Transport Method
T. Matsufuji, N. Nishiyama, K. Ueyama, M. Matsukata
Micropor. and Mesopor. Mater., **32(1-2)**, 159-168(1999)

Permeation Characteristics of butane Isomers through MFI-type Zeolitic Membranes
T. Matsufuji, N. Nishiyama, K. Ueyama, M. Matsukata,
Catal. Today, **56(1-3)**, 265-273(2000)

Synthesis and Permeation Studies of FER/Alumina Composite Membranes
T. Matsufuji, S. Nakagawa, N. Nishiyama, M. Matsukata, K. Ueyama,
Micropor. and Mesopor. Mater., **38**, 43-50(2000)

Separation of Butane and Xylene Isomers with MFI-type Zeolitic Membranes Synthesized by a Vapor-phase Transport Method
T. Matsufuji, N. Nishiyama, M. Matsukata, K. Ueyama,
J. Membr. Sci., **178,** 25-34(2000)

Permeation of Hexane Isomers through an MFI Membrane
T. Matsufuji, K. Watanabe, N. Nishiyama, Y. Egashira, M. Matsukata, K. Ueyama,
Ind. Eng. Chem. Res., **39,** 2434-2438 (2000)

Preparation of Mordenite membranes on a-Alumina Tubular Supports for Pervaporation of

Water-Isopropyl Alcohol Mixtures
X. Lin, E. Kikuchi, M. Matsukata,
Chem. Comm., 957-958(2000)

ゼオライトの合成および膜作成技術の最近の進歩
松方正彦
セラミックス, **32(5)**, 351-355(1997)

無機ガス分離膜の開発動向
松方正彦
最近の化学工学の進歩４９「膜技術の動向と将来展望」化学工学会編, 化学工業社, pp101-109(1997)

無機膜による炭化水素分離
松方正彦
膜, **23(2)**, 55-61 (1998)

新しいゼオライト合成法とその展開
松方正彦
化学工学, **63(8)**, 40-41 (1999)

無機膜の最近の開発動向
松方正彦, 野村幹弘
工業材料, **47(7)**, 22-25(1999)

Microscopic Structure of a Ferrierite Membrane Synthesized by a Vapor-phase Transport Technique
M. Matsukata, N. Nishiyama, T. Matsufuji, K. Ueyama,
Proc. 15th North American Catalysis Society Meeting, Chicago, USA(1997)

Selective Permeation of Hydrocarbons through A Zeolitic Membrane
A. Takahashi, T. Takahashi, K. Ueyama, N. Nishiyama, M. Matsukata,
Proc. Fifth International Conference on Inorganic Membranes, Nagoya, 184-187 (1998)

Permeation Studies of Butane Isomers through MFI-type Zeolitic Membranes
T. Matsufuji, N. Nishiyama, K. Ueyama, M. Matsukata,
Proc. Fifth International Conference on Inorganic Membranes, Nagoya, 568-571(1998)

Crystallization of High Silica BEA by Dry Gel Conversion
P.R.H. Prasad Rao, K. Ueyama, M. Matsukata,
Appl. Catal. A, **166**, 97-103 (1998)

Phase Transformation of BEA Zeolite by Dry Gel Conversion
P.R.H. Prasad Rao, K. Ueyama, E. Kikuchi, M. Matsukata,
Chem. Lett., 311-312 (1998)

Synthesis of BEA by Dry Gel Conversion and Its Characterization
P.R.H. Prasad Rao, C.A. Leon y Leon, K. Ueyama, M. Matsukata,
Micropor. and Mesopor. Mater., **21**, 305-313(1998)

Synthesis of Pure Silica BEA and Al-free Ti-BEA Using TEAOH and Their Characterization
P.R.H. Prasad Rao, K. Ueyama, E. Kikuchi, M. Ogura, M. Matsukata,
Proc. the 12th Intern. Zeolite Conf., Baltimore, 1998, Ed. by M.M.J. Treacy, B. Marcus, J.B. Higgins, M.E. Bisher, Mater. Res. Soc., 1515-1522 (1999)

Synthesis of OU-1, a Large-Pore, High Silica Zeolite, by Dry Gel Conversion
M. Matsukata, M. Kato, T. Suzuki, Y. Sasaki, E. Kikuchi, K. Ueyama, P.R.H. Prasad Rao,
Proc. the 12th Intern. Zeolite Conf., Baltimore, 1998, Ed. by M.M.J. Treacy, B. Marcus, J.B. Higgins, M.E. Bisher, Mater. Res. Soc., 2009-2014 (1999)

Conversion of Dry Gel to Microporous Crystals in Gas Phase
M. Matsukata, M. Ogura, T. Osaki, P.R.H. Prasad Rao, M. Nomura, E. Kikuchi
Topics in Catalysis, **9**, 77-92 (1999)

Conversion of Dry Gels to Zeolites
M. Matsukata, P.R.H. Prasad Rao, T. Osakai, M. Ogura, E. Kikuchi
Proc. of Intern. Conf. on Solid-Solid Phase Trans., '99, Ed. by M. Koiwa, K. Otsuka, T. Miyazaki
The Japan Institute of Metals, pp1421-1424 (1999)

ドライゲルコンバージョン法を中心とする新しいゼオライトの合成とその特性
松方正彦
触媒技術の動向と展望 1998，触媒学会編，pp.27-35(1998)

ゼオライト OU-1 合成の経緯と構造
松方正彦
ゼオライト，**15(4)**, 8-12 (1998)

Dry Gel Conversion Synthesis of beta and EMT Zeolites
M. Matsukata, P.R.H. Prasad Rao
Proc. 15th North American Catalysis Society Meeting, Chicago, USA(1997)

ドライゲルコンバージョン法によるゼオライト合成
松方正彦、小倉賢
機能材料，**20(10)**, 64-73 (2000)

Bull. Chem. Soc. Jpn., 70, 2341—2356 (1997)

Accounts

Zeolitic Membranes: Synthesis, Properties, and Prospects

Masahiko Matsukata* and Eiichi Kikuchi†

Department of Chemical Engineering, Osaka University, 1-3 Machikaneyama, Toyonaka, Osaka 560

†School of Science and Engineering, Waseda University, 3-4-1 Okubo, Shinjyuku-ku, Tokyo 169

(Received January 7, 1997)

This article is intended to describe recent progress in the synthesis of zeolitic membranes and their permeation properties. While hydrothermal synthesis has been widely employed for zeolitic-membrane synthesis, the development of a new technique for zeolite synthesis, vapor-phase transport (VPT), has enabled us to prepare pinhole-free, zeolite-porous support composite membranes. This article consists of three sections that describe: a survey of the hydrothermal synthesis of zeolitic membranes, our synthesis results and the formation mechanism of zeolitic membranes by the VPT method as well as some permeation results to show the prospects of zeolitic membranes.

Inorganic membranes were the first membranes which found practical application in large-scale gas-separation processes in the 1940's. An alumina membrane was used to separate isotopes of uranium based on the difference in the molecular weights of their hexafluorides. New sophisticated techniques of thin polymeric membrane preparation, gas-separation processes using polymeric membranes, were commercialized. Polymeric membranes had both high permselectivity and rapid permeation. For several decades, the research and development efforts in membrane processes were directed to polymeric membranes, while inorganic membranes were largely forgotten. Due to their instability in organic solvents and at high temperatures, however, practical applications of polymeric membranes have been limited to these processes operating at slightly above room temperature.

There is strong interest in membranes made of inorganic materials, such as ceramics and metals for applications in separation processes, owing to their superior characteristics of thermal, mechanical and structural stabilities, and of chemical resistance. In order to develop a new generation of high-temperature resistant membranes, researchers have turned back to the development of inorganic membranes.

Inorganic membranes can be classified into two types, nonporous (dense) and porous membranes. The first well-studied inorganic membranes were dense palladium[1] and its alloys,[2] which are permeable only to hydrogen. Following palladium-based membranes, other types of dense inorganic membranes permselective to oxygen, for instance, silver and stabilized zirconia, have been developed.[3] The types of permselective dense membranes, however, are limited to motivate the development of porous inorganic membranes.

Based on the definition by the International Union of Pure and Applied Chemistry (IUPAC), porous materials, such as adsorbents and porous membranes, are classified in relation to their pore size, as follows:

1. Pores with widths exceeding about 50 nm are called *macropores*;
2. Pores with widths between 2 and 50 nm are called *mesopores*; and
3. Pores with widths not exceeding about 2 nm are called *micropores*.

The membranes used in the practical applications today are mostly macroporous with pore diameters of 0.1—100 μm. They include alumina, zirconia, and porous glass membranes. Porous metal membranes are available, though they are relatively limited in the extent of industrial use because of their costs.

The transport of gases in macropores is governed by the viscosity of the gas (Poiseuille flow), Knudsen diffusion, or flow in the transition between them. Membranes with macropores are, thus, not expected to show sufficient selectivities for gas separation, although they show high permeability. In smaller pores, mesopores, surface diffusion and capillary condensation phenomena can play an important role in the transport of molecules in addition to Knudsen diffusion. Mesoporous membranes, including γ-alumina, titania and zirconia, with an average pore diameters of 2—10 nm have been prepared by sol–gel techniques. When the pore size is comparable to the molecular dimensions, a molecular sieving property appears, thereby leading to large selectivity.

Therefore, the current research is mainly focusing on the development of microporous membranes.

The first study that attracted attention to microporous membranes was on a silica membrane, reported by Gavalas et al., who prepared a SiO_2 layer within the pores of a Vycor glass tube by SiH_4 oxidation.[4—6] This SiO_2 membrane was highly selective to H_2 permeation with a permselectivity of H_2/N_2 = ca. 3000 at 723 K. Following this study, they succeeded to prepare of H_2-permselective SiO_2, TiO_2, Al_2O_3, B_2O_3 membranes by chemical-vapor deposition using their chloride precursors within the pores of a Vycor glass tube. These membranes show permselectivities of H_2/N_2 = 1000—5000 at 723 K. Another noteworthy H_2-permselective membrane was a SiO_2 membrane, which was prepared on an alumina support with an average pore diameter of 1 μm by a sol–gel method.[7] Its permselectivity of H_2/N_2 was about 400. Microporous glass membranes with the pore width of $0.5 < d < 2.0$ nm were prepared by attenuation from glass melts.[8,9] The permselectivities of H_2/N_2 and He/CH_4 at 303 K were 235 and 11700, respectively. Another method for preparing microporous membranes has been to use carbon of which membranes are obtained by carbonization of polymeric precursors.[10,11]

Besides the amorphous materials mentioned above, microporous crystals have been of interest as membrane materials in recent years because they have extremely narrow pore-size distributions, which is not the case for amorphous materials.

Zeolites, a class of microporous crystalline aluminosilicate materials, have been extensively studied and utilized in chemical and physical processes, such as in gas separation and heterogeneous catalysis. Adsorptive separation processes with granular molecular sieves are operated in a batchwise manner. If membranes could be composed of a sort of zeolites, it would be possible to carry out separation continuously without any changes in the phase, and to substitute these processes with the membrane separation ones.

Apart from their high thermal resistance, high mechanical strength and chemical inertness, zeolites have the following advantageous features when used as a membrane.

1. Micropore systems of zeolites are inherent for the structure. Pore diameters in zeolites are determined by the aperture with 4, 6, 8, 10 or 12-membered rings of oxygen anions. The maximum values of the pore opening were calculated to be 0.26, 0.34, 0.42, 0.63, and 0.74 nm, respectively.

2. Inner surface of zeolites can be readily modified. Both the actual pore size and the affinity between adsorbed molecules and the pore-wall depend on the type of cation, and are precisely controllable by ion-exchange. The outer surface can also be selectively modified by chemical-vapor deposition.[12]

3. The hydrophilic/hydrophobic nature of zeolites can be tuned by changing the SiO_2/Al_2O_3 ratio in the framework of zeolites. The cation that balances the negative charge associated with the framework aluminum ions causes an electrostatic field in zeolites. Thus, the pores of aluminum-rich zeolites are occupied by water molecules, while a decrease in the aluminum content leads to the hydrophobic nature.

4. Since zeolites exhibit catalytic properties, they can be applied to catalytic membrane reactors. A few concepts of membrane reactors using zeolitic membranes have been proposed.[13,14]

Due to the reasons described above, increasing attention has been paid to the preparation of zeolitic membranes. Whereas zeolitic membranes were first proposed in the 1980's,[15—18] studies of them started to be reported in scientific journals in the early 1990's. In this account, previous reports on the preparation of zeolitic membranes will be reviewed first. We have proposed a new synthetic method, a dry-gel conversion technique to prepare zeolitic membranes via vapor-phase transport. Recent progress of our studies concerning the preparation of zeolitic membranes and their properties will be summarized.

Hydrothermal Synthesis of Zeolitic Membranes

Zeolitic membranes have typically been prepared from hydrogels or sols composed of SiO_2, Al_2O_3, Na_2O, H_2O, and organic templating agents. More or less, most of the studies have employed a conventional hydrothermal synthe

Table 1. Self-Supporting MFI Membranes

	Silica source	Alumina source	Gel composition (Na_2O : SiO_2 : Al_2O_3 : TPA : H_2O)	Substrate	Crystallization	Thickness μm
Sano et al.[19]	CS	$Al(NO_3)_3$	0.05 : 1 : 0.01 : 0.1 : 40—100	Teflon®	373—473 K 2—17 d	30—100
Sano et al.[20,21]	CS	$Al(NO_3)_3$	0.05 : 1 : 0.01 : 0.1 : 80	Teflon®	443 K 2 d	30—100
Tsikoyiannis and Haag[22]	CS	—	2.2 : 100 : 0 : 5.22 : 2832	Teflon® Silver Stainless steel Vycor® disk	453 K 0.3—9 d	20—250
Sano et al.[23]	CS	$Al(NO_3)_3$	0.05 : 1 : 0—0.01 : 0.1 : 80	Cellulose	443 K 2 d	500
Kiyozumi et al.[24]	CS	$Al(NO_3)_3$	0.01 : 0.05—0.1 : 1 : 0—0.02 : 20—400	Mercury	393—453 K 2 d	

CS: colloidal silica.

Table 2. Supported-MFI Membranes

	Si source	Al source	Gel composition ($Na_2O : SiO_2 : Al_2O_3 : TPA : H_2O$)	Support (pore diameter)	Crystallization	Thickness μm
Geus et al.[25]	Aerosil 200	—	1.6 : 1 : 0 : 1.5 : 166.66	Clay, zirconia	453 K, 1—5 d	100
Geus et al.[26]	Aerosil 200, CS	—	— : 100 : 0 : 6 : 6330	Sintered metal (10 μm), Stainless steel	453 K, 1—7 d	60—400
Jia et al.[27]	Aerosil 130	—	0.75 : 9 : 0 : 1.0 : 70	Ceramic disk	453 K, 3—72 h	5
Sano et al.[28]	CS	—	0.05 : 1 : 0 : 0.1 : 80	Stainless steel (0.5—2 μm)	443 K, 2 d	400—500
Masuda et al.[29]	SS	$Al_2(SO_4)_3$	34 : 71 : 1 : —	α-Alumina (2 μm)	473 K, 2 d	10—25
Jia et al.[30]	Aerosil 130	—		γ-Alumina (5 nm)	453 K, 3—72 h	10
Meriaudeau et al.[31]	TEOS	—	— : 1 : 0 : 0.051 : 22.5	Porous glass (10—20 μm)	448 K, 72 h	150
Bai et al.[32]	Aerosol	—	0.071 : 1 : 0 : 0.071 : 42	γ-Alumina (5 nm)	453 K, 12 h	10
Yan et al.[33]	CS	—	2 : 6 : 0.005 : 1 : 571 : 1	α-Alumina (0.5 μm)	448 K, 16 h	10
Yan et al.[34]	TEOS	Al foil	0—4 : 6 : 0—0.06 : 1 : 96—700	α-Alumina (0.5 μm)	448 K, 4—24 h	10
Vroon et al.[35]	Silica	—	5.3 : 100 : 0 : 30 : 1420	α-Alumina	393 K, 3 d	5
Chiou et al.[36]	TEOS	—	5 : 100 : 0 : 10 : 10000	Anodic alumina (0.2 μm)	473 K, 1—4 d	130
Kusakabe et al.[37]	Aerosil 200	—	— : 1 : 0 : 1.0 : 100	γ-Alumina (5—10 nm) α-Alumina (0.95, 0.15 μm)	448 K, 12—24 h	20 —30

TPA: tetrapropylammonium ion, IPA: isopropylalcohol, TEOS: tetraethylorthosilicate, CS: colloidal silica, SS: sodium silicate solution.

Table 3. Supported-Zeolitic Membranes Other than MFI

	Products	Si	Al	Composition ($Na_2O : SiO_2 : Al_2O_3 : TPA : H_2O$)	Crystallization	Support	Thickness μm
Suzuki et al.[38]	MOR	CS	$Al_2(SO_4)_3$	0.38 : 1 : 0.025 : 0 : 40	433 K 40 h	Silica–alumina, Quartz glass	23
Geus et al.[25]	ANA	Aerosil 200	—	1.6 : 1 : 0 : 1.5 : 166.66	453 K 1—5 d	α-Alumina	
Masuda et al.[39]	LTA	Na_2SiO_3	$Al(OH)_3$	—	343—373 K 6—18 h	α-Alumina	5—25
Mimura et al.[40]	ANA	CS	PNC	67.5 : 67.3 : 1.0 : 1.0 : 3375	423—453 K 0.1—3 d	α-Alumina	60
Kita et al.[41]	LTA	SS	$Al(OH)_3$	2 : 2 : 1 : 0 : 120	373 K 3.5 h	α-Alumina	30
Yamazaki and Tsutsumi[42]	LTA	SS	$Al_2(SO_4)_3$	4.25 : 2.5 : 1.0 : 0 : 111	433 K 40 h	Silica	
Yamazaki and Tsutsumi[43]	MOR	CS	$NaAlO_2$	3 : 20 : 1 : 0 : 200	453 K 1—5 d	Stainless-steel filter	

PNC: Powdered natural clinoptilolite.

sis to produce a zeolitic thin layer. Typical silica sources for synthesizing MFI (particularly known as ZSM-5 zeolite) membranes are colloidal silica and silica powder (Aerosil). The tetrapropylammonium (TPA) cation has mainly been used as a templating agent.

Self-supporting zeolitic membranes can be synthesized on various substrates. Table 1 summarizes studies concerning the preparation of self-supporting zeolitic membranes. Sano and coworkers[19—21] first synthesized self-supporting MFI membranes on a Teflon® sleeve using a clear aqueous solution with a composition of 0.1 TPABr : 0.05 Na_2O : 0.01 Al_2O_3 : SiO_2 : 40—100 H_2O. Synthesis mixtures with H_2O/SiO_2 ratios > 70 were crystallized to form MFI membranes without stirring. Tsikoyiannis and Haag hydrothermally synthesized MFI layers with 20—250 μm thickness on various non-porous supports, such as a Teflon® slab.[22]

The mechanical strength of self-supporting zeolitic membranes is insufficient for their application in separation processes. Most of the studies on the synthesis of zeolitic membranes have been directed for use on porous supports.

High-silica MFI membranes have mainly been studied as summarized in Table 2. Supported MFI membranes have typically been prepared from hydrogels or sols composed of SiO_2, Al_2O_3, Na_2O, and TPA cation, similarly to the preparation of self-supporting membranes. A reactant mixture, in which a porous support is immersed, is placed in an autoclave. Typical MFI membranes have been synthesized on macroporous supports with a pore size of 0.1—10 μm, such as α-alumina and sintered stainless steel. A support with γ-alumina top layer with an average pore size of 5 nm was also used by Jia et al.[30] Table 3 summarizes the studies concerning other kinds of zeolitic membranes. The preparation of zeolite A (LTA)[29,41,42] and mordenite (MOR)[38,43] membranes have been extensively investigated.

Myatt et al.[44] claimed four possibilities for the formation of zeolitic membranes, as depicted in Fig. 1a: 1) The production of nuclei and the growth of crystals in the bulk solution, followed by their attraction to, or collision and association with, a substrate; 2) the production of nuclei in bulk solution, but diffusion to, and accumulation at, the support before significant growth has occurred; 3) the diffusion of colloidal amorphous aluminosilicate to, and concentration at, the substrate, providing more favorable conditions of nucleation and growth in the vicinity of the substrate; and 4) production of nuclei on the substrate surface, followed by growth. Figure 1b shows the mechanism proposed by Sano et al.,[21] who claimed that an MFI membrane forms through a successive accumulation of large MFI crystals of 5 to 10 μm and filling of voids among the large crystals with microcrystals. This corresponds to the first case of Myatt's mechanism. Valtchev et al.[46] studied the growth of MFI and FAU (Y type) zeolites on a copper substrate, and reported that there were three stages of film growth: 1) initial nucleation on the substrate, 2) a linear increase in crystal size, and 3) saturation of film growth, which is similar to the fourth mechanism proposed by Myatt et al. On the other hand, Kita et al.[41] suggested that a gel layer was first formed on the surface of a support, and then the gel layer was crystallized to LTA, being similar to the third mechanism. The MFI crystals prepared by Jansen et al.[45] were preferentially oriented parallel to the *b*-direction, and, thus, the straight channels of the pore system were perpendicular to the support surface. According to an in situ observation of crystallization, they proposed a formation mechanisms of such a preferentially oriented zeolite layer, as shown in Fig. 1c. First, large gel spheres containing no TPA were formed in the liquid phase, and the crystallization started at the interface of the gel spheres and the liquid

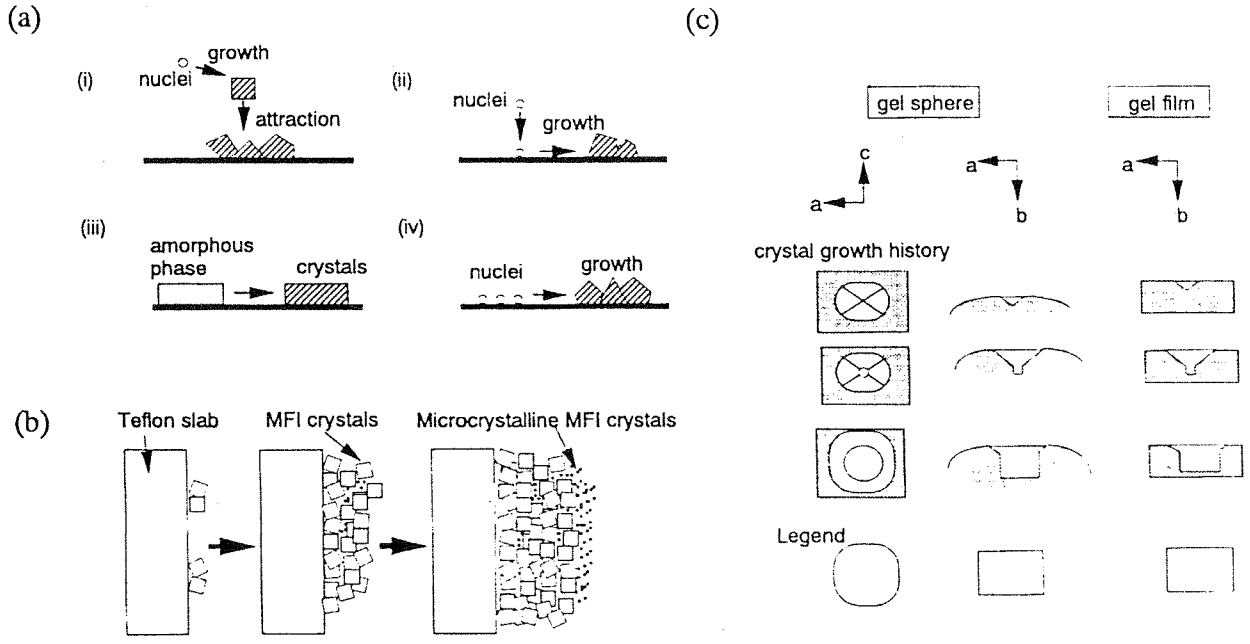

Fig. 1. Proposed growth mechanisms of zeolitic membranes. a) Sano et al.,[21] b) Myatt et al.,[44] and c) Jansen et al.[45]

phase. As soon as the gel spheres on which MFI crystals was formed attached the support surface, the support surface was attracted to the *ac*-plane, the largest plane of the crystal. As a result, the crystals were laterally oriented to the support surface. This is also similar to the third mechanism proposed by Myatt et al.

The intergrowth of zeolite crystals has often been observed,[22,27,33] and Yan et al.[33] have claimed that the intergrowth of zeolite crystals to fill the voids among crystals is cruicial for the synthesis of a compact zeolitic membrane under hydrothermal conditions.

The controlling factors for synthesizing a compact zeolitic layer have not yet been elucidated. However, a partial dissolution of the support during crystallization was often reported. Alumina[25,28,36] and glass[42] are easily leached during synthesis, and the dissolved Si^{4+} and Al^{3+} ions are expected to encourage nucleation and crystallization of zeolites on the support surface, leading to the formation of a continuos layer of zeolites. Additionally, the incorporation of dissolved Si or Al atoms into the framework of the resultant zeolite should greatly affect the types of zeolites formed.

Under these hydrothermal syntheses, the way to place the supports seems to affect the formation process of the zeolitic membranes, because nuclei or crystals homogeneously formed in the solution could deposit on the support by convection or diffusion.

Typically, porous supports were horizontally placed on the bottom of a Teflon® vessel.[28,40] On the other hand, Jansen et al.[45] adopted a vertical placement of the support. The support was positioned in the upper part of the synthesis mixture with the help of a Teflon® holder.

To form zeolite crystals only on the inner wall of a tube with γ-alumina top layer, Jia et al.[30] transferred a gel into the alumina tube, and plugged both ends with Teflon® caps. The tube was then placed in a Teflon®-lined autoclave. Yan et al.[33,34] placed a porous plate in an autoclave horizontally using a Teflon® holder. The upper level of the synthesis solution was, however, kept to dip only the bottom side of the support in the solution in order to grow zeolite crystals on the bottom side of the support.

A more sophisticated synthesis method has very recently been developed by Tsapatsis et al.,[47] who demonstrated that stable, colloidal suspensions of nano-sized zeolite L (LTL) particles can be formed from a clear solution, and then used for thin-film preparation. The average size of zeolite particles in the suspension was as small as 20 nm. A thin layer consisting of nano-LTL particles can be grown in an aluminosilicate sol. This was the first successful case to separate the nucleation process from the growth of zeolites during membrane synthesis in the hydrothermal method.

Synthesis of Zeolitic Membranes by Solid Dry-Gel Conversion via Vapor-Phase Transport

Bibby and Dale[48] first synthesized a zeolite from a non-aqueous system, suggesting that water is not essential as a solvent for the crystallization of zeolites. Pure silica zeolites with a sodalite (SOD) structure were obtained using ethylene glycol as a solvent. Since their study, several types of zeolites like MFI, FER, and MTN have been synthesized using organic solvents.[49,50]

Xu et al.[51] first found that an aluminosilicate dry gel was transformed to MFI in contact with vapors of water, ethylenediame (EDA) and triethylamine (Et_3N) at 453 K. Kim et al.[52] and we[53,54] followed this report, and confirmed that this solid dry-gel conversion technique is useful for synthesizing various types of zeolites. Kim et al. called this method vapor-phase transport (VPT).[52]

In addition, several advantages have been shown to be drawn from the VPT method.[53,54] If the aluminum content would be appropriate, aluminum could be fully incorporated in the zeolitic framework during the early stage of crystallization; crystallization of a Si-rich phase followed. A dry gel can be completely converted to a zeolite by selecting the proper synthetic conditions. This synthetic method offers promising prospects for the synthesis of zeolites possessing the same SiO_2/Al_2O_3 ratio as with that of the parent gel, and the production of zeolites shaped in advance. We therefore expected that the VPT method is prospective for the production of zeolite thin layers on a porous support with a variety of shapes.

Membrane Synthesis. The typical preparation procedure that we have employed for synthesizing zeolitic membranes is as follows. A parent aluminosilicate gel is prepared. Either of two kinds of silica sources, colloidal silica or sodium silicate solution, is used. Anhydrous aluminum sulfate, $Al_2(SO_4)_3$, is used as an alumina source. An aqueous solution of NaOH or H_2SO_4 is added to colloidal silica or sodium silicate solution, respectively, and the resultant silicate gel is mixed with an $Al_2(SO_4)_3$ aqueous solution.

A porous α-alumina support with an average pore diameter of 0.1 μm was used throughout our study. The parent aluminosilicate gel is applied on the support surface by means of conventional dip coating.

After Et_3N, EDA, and water as the vapor source are poured into the bottom of an autoclave, the alumina support coated with the aluminosilicate dry gel is set horizontally in the autoclave, as shown in Fig. 2. The gel is crystallized in the mixed vapors of Et_3N, EDA, and water under autogeneous pressure at 453 K for 4 d.

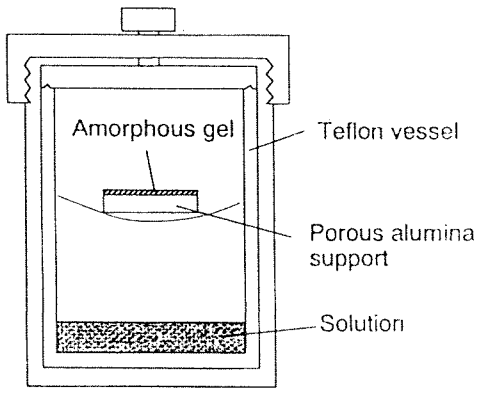

Fig. 2. Schematic diagram of the special autoclave for vapor-phase transport synthesis.

An as-synthesized membrane is calcined in air at 773 K for 4 h. In order to prevent crack formation in the zeolite layer, we employed a heating rate of 0.1 K min^{-1} in the temperature range of 473—773 K.

The formation of a compact dry amorphous gel on the support prior to crystallization is required to form for the preparation of zeolitic membranes in a compact form.[55,56] Numerous cracks were visually observed during the course of drying, even at room temperature when the gel prepared at pH of 11 had been applied to the alumina support. Moreover, the gel which had been prepared at pH of 10 easily scaled off the support during the drying process.

The compactness of the gel can be evaluated by its specific surface area. Figure 3[56] shows the specific surface area of aluminosilicate gel dried at 363 K overnight as a function of the pH at which the gel was prepared. The specific surface areas of both dry gels with SiO_2/Al_2O_3 ratios = 25 and 50 exhibited the same pH dependence, and steeply decreased with increasing pH in the range of 9.5—11.5. This trend indicates that the dry gel becomes compact when the gel is prepared at pH > 11.5.

Further details of the pH dependence were studied using gels prepared at pH of 11.0—12.0. A glass plate was dipped in a gel prepared at a given pH and room temperature. The resultant gel film on the glass plate was dried at 363 K for 1 h. The compactness of the film was visually evaluated, as listed in Table 4.[54] When a sodium silicate solution was used, a compact continuous film with SiO_2/Al_2O_3 ratio = 50 was obtained on a glass plate at pH = 11.66, while numerous cracks were visually observed on a gel film prepared at pH = 11.45. A gel with SiO_2/Al_2O_3 ratio = 25 gave similar results when a sodium silicate solution was used. A value of pH = 12.13 was required for the formation of a continuous compact film when colloidal silica was used. Table 4 also lists the specific surface areas of dry gels. As described above, the specific surface area of either dry gel decreased with increasing pH, indicating that the dry gel became denser at higher pH. In conclusion, it is essential to precisely control the value of the pH for obtaining a compact continuous layer of a dry amorphous gel on the support.

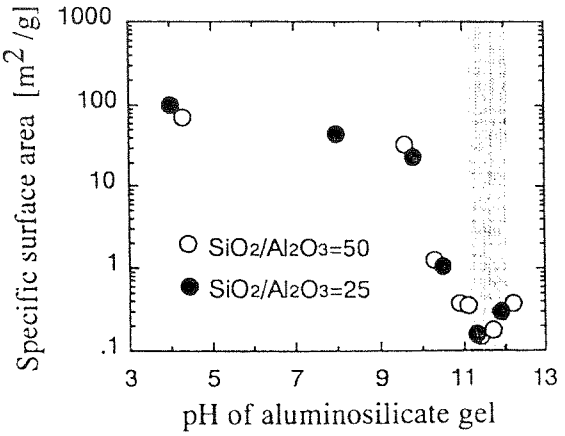

Fig. 3. Effect of pH of at which gel was prepared on its specific area.

Table 4. Effect of pH at Which Gel Was Prepared on the Surface Area and the Compactness of the Dry Gel Film on a Glass Plate

Silica source	SiO_2/Al_2O_3	pH	Specific surface area [M^2 g^{-1}]	Compactness
Sodium silicate Solution	50	11.66	0.21	Good
		11.45	0.27	Poor
	25	11.82	0.20	Good
		11.58	0.43	Poor
		11.28	5.22	Poor
Colloidal silica	25	12.13	0.11	Good
		11.81	0.16	Poor
		11.54	0.20	Poor

$SiO_2/Na_2 = 2.1$.

Elucidating the chemistry of aluminosilicate gel is clearly essential to prepare a nicely compact dry gel layer on a support surface. In general, silicic species exist both in the form of a dissolved state and in solid particles in the synthesis solution. The content of dissolved siliceous species dramatically decreases, and, instead, particles are formed as the pH decreases from 12 to 10.[57] Namely, a larger amount of dissolved silica was transformed into particles during the gelation of a silicic solution at a lower pH. The gel prepared at a higher pH becomes compact, because dissolved siliceous species act as a binder of the particles during drying. A compact gel can thus be prepared using a silica solution containing a sufficient amount of dissolved silica. This discussion suggests that a higher pH value is favorable for preparing a compact gel layer on a support, being in good agreement with our results shown in Fig. 3 and Table 4.

Table 5 summarizes the typical results of crystallization of aluminosilicate gels applied on an alumina support. Aluminosilicate gels were formed at pH = 11.7 and 12.0 from a sodium silicate solution and colloidal silica, respectively, applied to the alumina support, and crystallized at 453 K for 4 d by the VPT method. The results on a Teflon® plate are tabulated together. It should be noted that different products were obtained on the alumina support and the Teflon® plate when the gel with the same composition was applied to both supports. Sodium silicate resulted in analcime (ANA) on the alumina support, while ferrierite (FER) was formed on the Teflon® plate. Colloidal silica gave MOR on the alumina support, while MFI was formed on the Teflon® plate. The

Table 5. Synthesis of Zeolitic Membranes on Porous Alumina Support with and without Surface Treatment

	Silica source	pH	Products
No treatment	Sodium silicate solution	11.7	ANA
	Colloidal silica	12.0	MOR
Surface treatment	Sodium silicate solution	11.7	FER
	Colloidal silica	12.0	MFI
On Teflon® plate	Sodium silicate solution	11.7	FER
	Colloidal silica	12.0	MFI

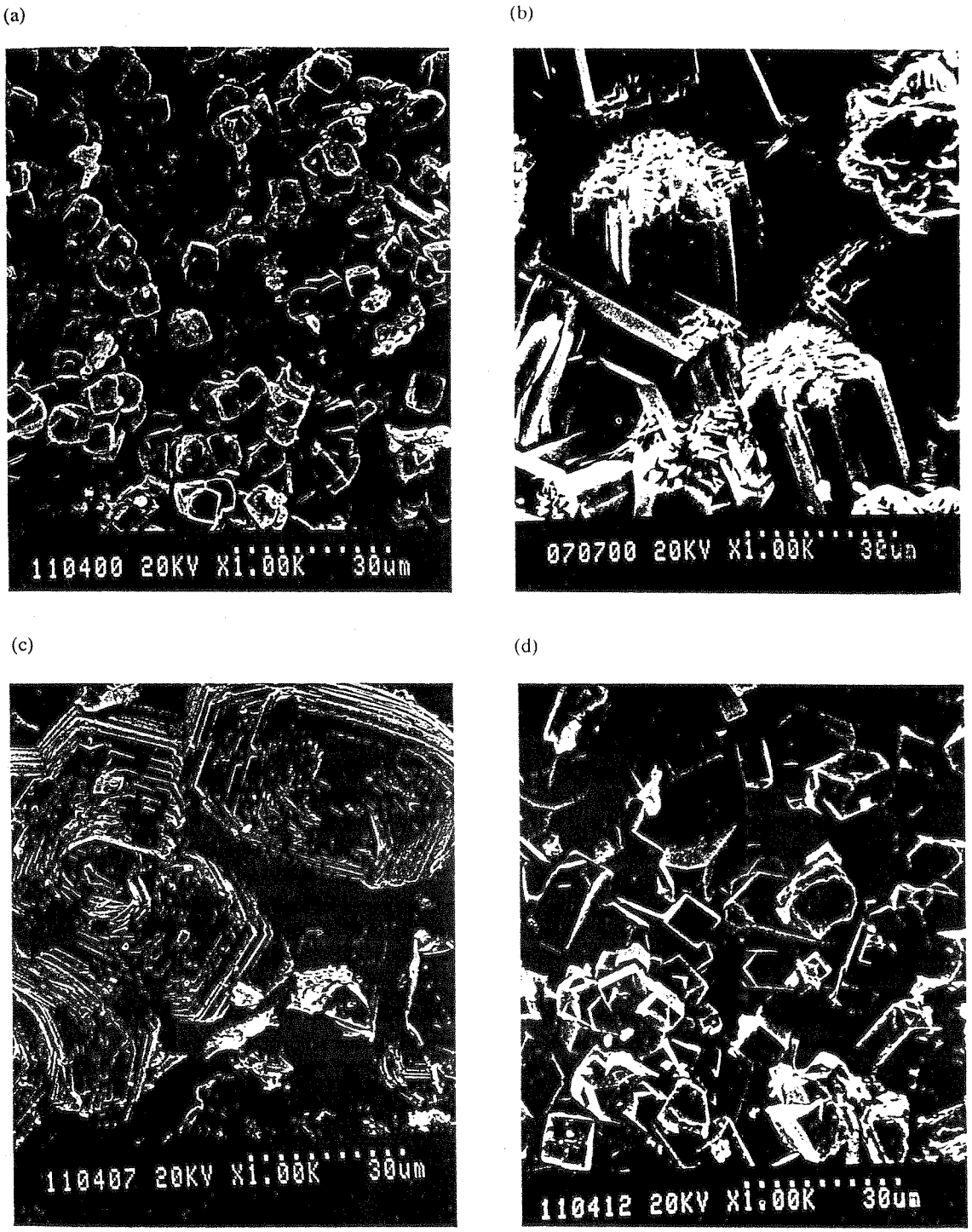

Fig. 4. SEM images for the top views of zeolitic membranes. (a) ANA, (b) MOR, (c) FER, and (d) MFI membranes.

Table 6. Effect of Pore Blocking by Benzene Molecules on Hydrogen Permeation through MOR Membrane

	Permeability of H_2 [mol m^{-2} s^{-1} Pa^{-1}]
Before permeation of benzene	1.12×10^{-7} (310 K)
After permeation of benzene	
Accompanied by evacuation (383 K, 1 h)	2.47×10^{-10} (310 K)
Accompanied by evacuation (400 K, 10 h)	3.48×10^{-8} (310 K)

Permeability of $C_6H_6 = 1.14\times10^{-9}$ (323 K), $\Delta p(C_6H_6) = 0.036$ MPa.

Fig. 5. SEM images for the top views of MOR membranes after (a) 1, (b) 2, and (c) 4 days of crystallization.

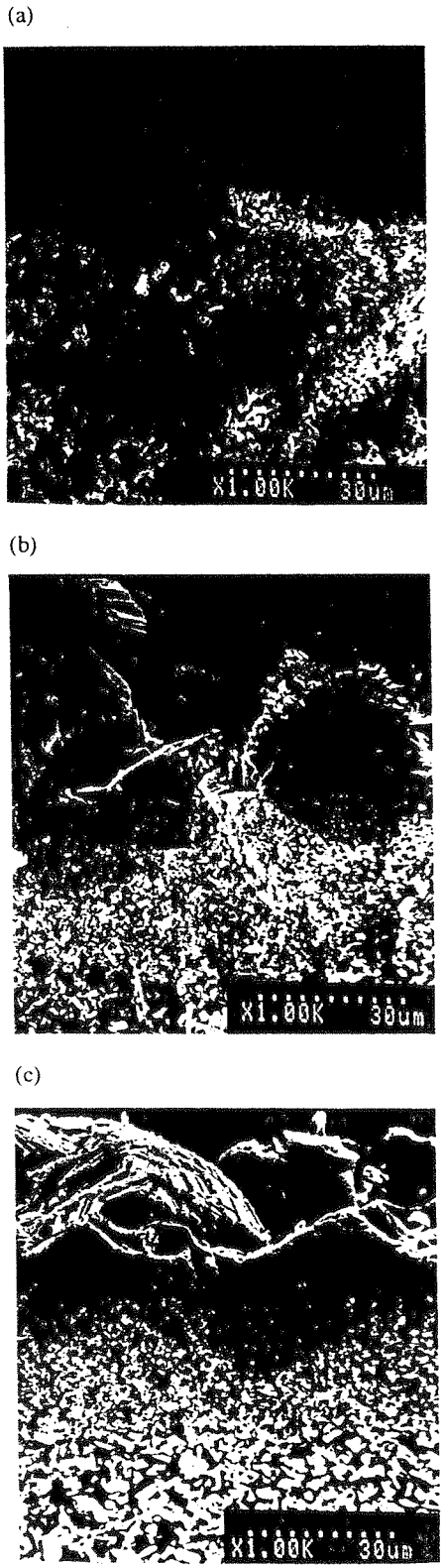

Fig. 6. SEM images for the cross-section of MOR membranes after (a) 1, (b) 2, and (c) 4 days of crystallization.

Fig. 7. FE-SEM images for the cross-section of MOR membrane.

SiO_2/Al_2O_3 ratios of ANA and MOR are generally lower than those of FER and MFI: The SiO_2/Al_2O_3 ratios of ANA and FER are typically 4 and 15—20, respectively. Those of MOR and MFI are 8—20 and greater than 20, respectively. These results should be attributed to the dissolution of the alumina support and its incorporation into the framework of zeolite, as found in the studies on hydrothermal synthesis.[25,36]

The surface treatment of the support with colloidal silica, which has a pH of about 10, successfully depressed the dissolution of alumina in our study.[55,56] As can be seen in Table 5, the same crystallization results as those on the Teflon® plate were obtained on the silica-coated alumina support.

Figure 4[56] shows typical SEM images of the top view of the ANA, MOR, FER, and MFI membranes. Each image shows a typical morphology of the corresponding zeolite crystals, the results of which are very different from those observed for those membranes prepared hydrothermally. The top layers of the zeolitic membranes consist of randomly-oriented, isolated crystals. The top views of the zeolitic layers which formed on the surface of the alumina support were clearly incompact.

Fig. 9. SEM image for a preferentially oriented MFI membrane prepared on porous alumina support.

The pervaporation of 1,3,5-triisopropylbenzene (TIPB), which has a kinetic diameter (0.85 nm) greater than the pore dimensions of FER (0.42×0.54 nm) and MOR (0.65×0.70 nm), was carried out for 10 h at room temperature using the MOR and FER membranes.

No permeation of TIPB through both MOR and FER membranes was detected by gas chromatogram, indicating that the flux of TIPB was less than 1.0×10^{-9} mol m^{-2} s^{-1}, the minimum flux of which can be determined in the experimental procedure used (Table 6). It should be noted that these re-

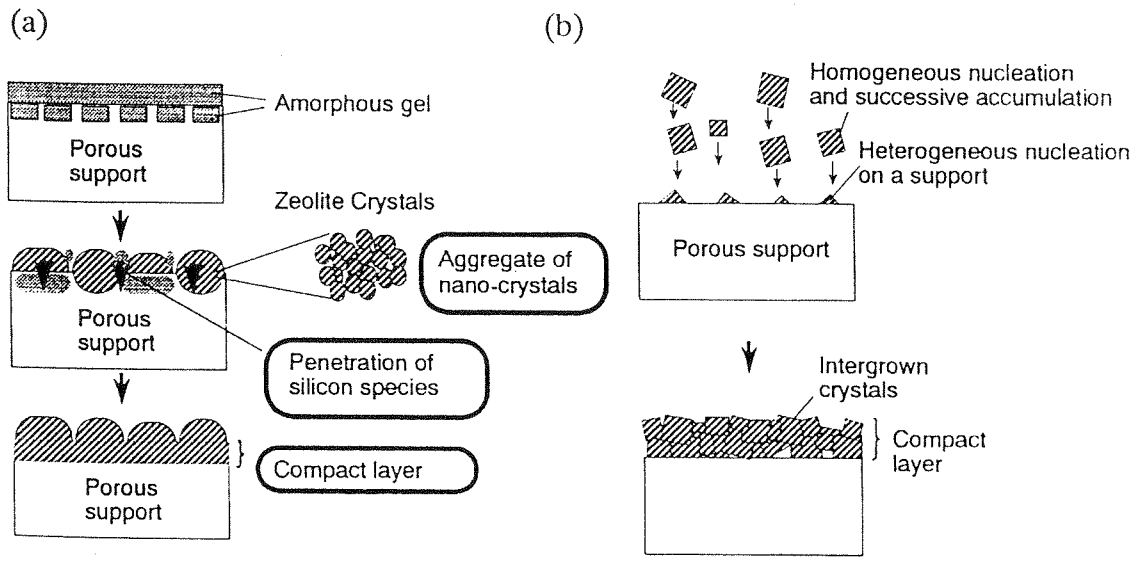

Fig. 8. Formation mechanism of zeolitic membrane (a) by vapor-phase transport method and (b) by hydrothermal synthesis.

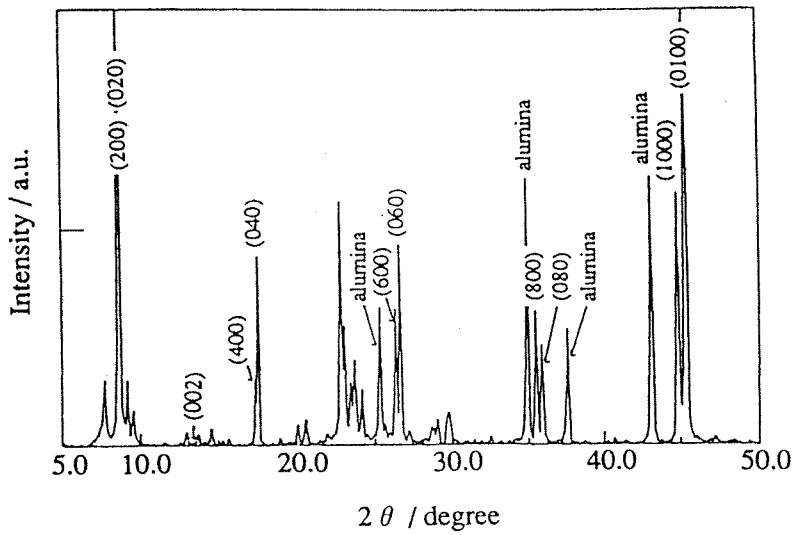

Fig. 10. XRD pattern for a preferentially oriented MFI membrane prepared on porous alumina support.

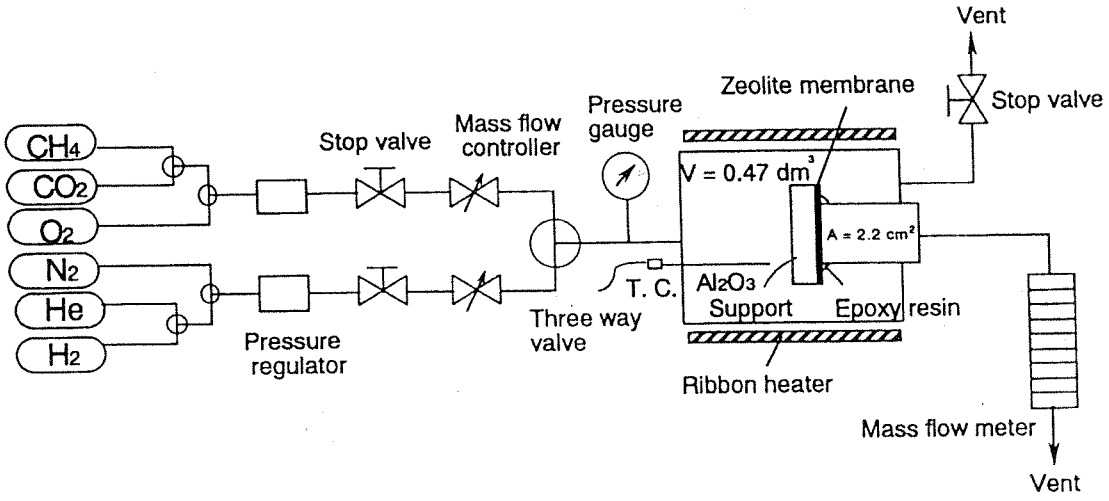

Fig. 11. Schematic diagram of the experimental apparatus for gas permeation measurements.

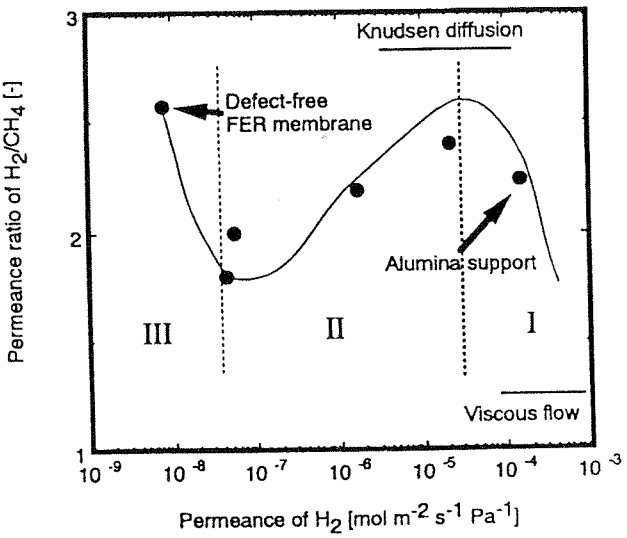

Fig. 12. Permeance ratios of H_2/CH_4 as a function of H_2 permeation through FER membranes. Temperature: 303 K.

sults of permeation tests with TIPB do not necessarily mean that there is no pinhole between the zeolite crystals. We can at least conclude that there practically existed no pinhole greater than the molecular dimension of TIPB in the MOR and FER membranes.

Formation Mechanism of Zeolitic Membranes. It is interesting to note that although numerous voids have been observed among zeolite crystals on an alumina support, as shown in Fig. 4, the MOR and FER membranes are confirmed to be pinhole-free. We have studied the formation mechanism of pinhole-free zeolitic membranes.[55,56,58—60]

We now describe the results of studies on the MOR membrane. Figure 5[56] shows a series of SEM images for the top view of MOR membranes. Figure 5a shows that MOR crystals began to form on the alumina support within 1 d of crystallization. While MOR crystals continued to grow in 2 d (Fig. 5b), the morphology of the MOR crystals was further changed after 4 d (Fig. 5c). Though the MOR membrane was pinhole-free, as previously described, numerous voids were observed among the MOR crystals on the surface of the

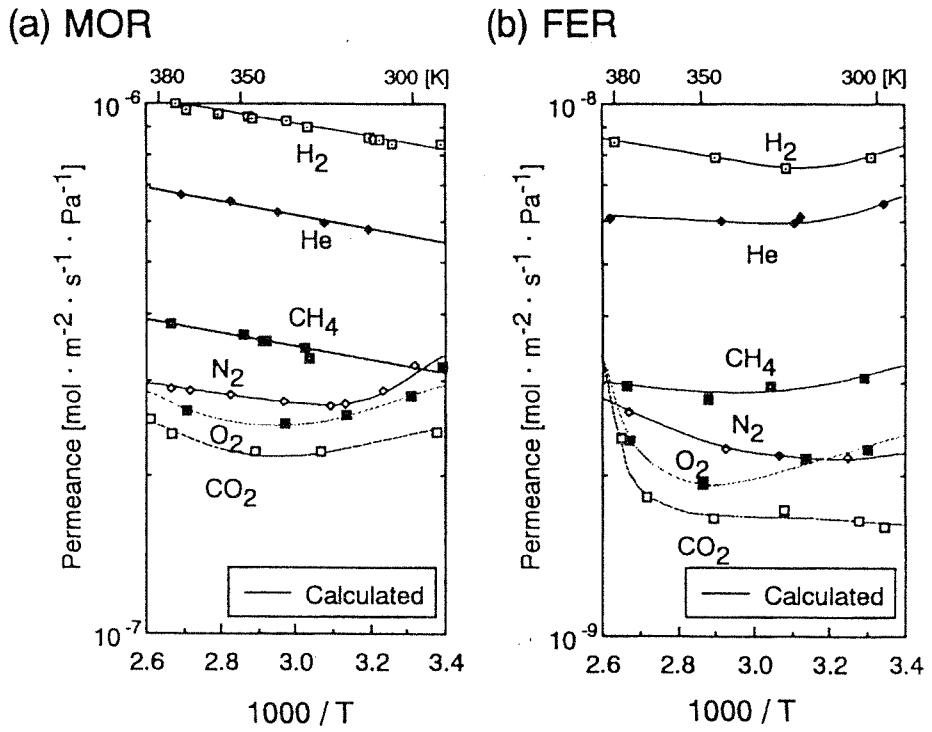

Fig. 13. Permeances of single gases through (a) MOR and (b) FER membranes.

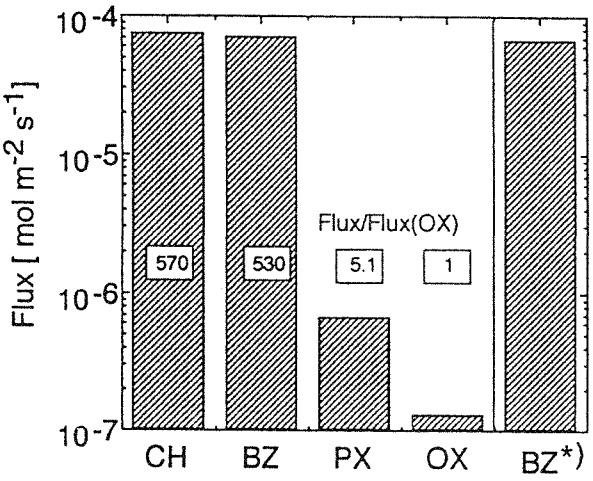

Fig. 14. Pervaporation results for single liquid components using FER membrane. (T = 303 K) CH: cyclohexane, BZ: benzene, PX: *p*-xylene, OX: *o*-xylene. *) After permeation test for 1,3,5-triisopropylebenzene.

alumina support. As can be seen from the top views of the MOR layers which formed on the surface of alumina support, the surface of these membranes was clearly not compact.

Figure 6 shows SEM images for the cross-sectional view of the MOR membranes crystallized in different times. It is noteworthy that the part which is bound with MOR crystals formed on the surface of alumina support gave a dark contrast, as shown in Figs. 6a and b. These dark contrast parts spread with the crystallization time, and finally link together after 4 d. Accordingly, these parts seem to be MOR-alumina composite layers.

Judging from Figs. 6b and c, crystallization started at the outer surface, and proceeded to the pores of alumina support to give a continuous MOR-alumina composite layer of 10—20 μm thickness after 4 d. The crystallization mechanism can explain that the MOR-alumina composite layer is pinhole-free, in spite of the fact that there are numerous voids among the MOR crystals on the support.

Figure 7 shows a typical FE-SEM image for the cross section of the MOR membrane. We found that nano-particles fill up the alumina pores. It is believed that these nano-particles are nano-crystals of MOR. Namely, a composite layer consisting of nano-crystals of zeolite and porous alumina can be formed in a compact form. We obtained the same conclusion for the case of an FER membrane.[60,61] During the course of crystallization, Si and Al species can migrate from the outer surface to the interior of alumina pores to fill up the pores.[61] The driving force of such migration might be a concentration gradient, or a capillary force.

Figure 8 schematically illustrates the plausible formation process of zeolitic membranes by the VPT method. Aluminosilicate gel partly penetrates into the pores of the alumina support during the course of dip coating. The crystallization starts on the surface of the alumina support. Then, the crystallization proceeds on both the alumina support and in the pores of alumina. The gel is successively supplied into the pores of the alumina support from the gel layer on the support. The zeolite crystals formed in the pores of alumina support comprize nano-particles. Finally, a zeolite–alumina composite layer is formed in a compact form, while voids remain among the crystals on the alumina support.

The formation mechanisms of zeolitic membranes by hydrothermal synthesis are compared in Fig. 8. Briefly, there are two possibilities for membrane formation, heterogeneous

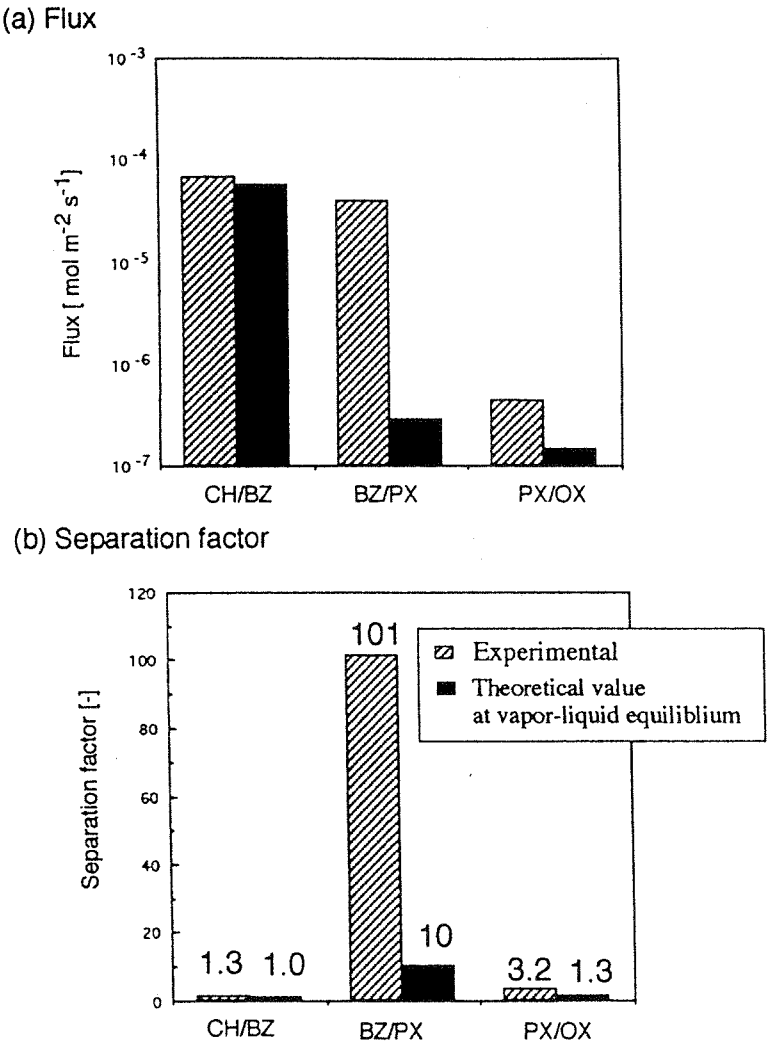

Fig. 15. Pervaporation results for mixtures using FER membrane at 303 K. CH: cyclohexane, BZ: benzene, PX: *p*-xylene, OX: *o*-xylene. Feed mole ratios of CH/BZ, BZ/PX, and PX/OX were 0.95, 1.34, and 0.96, respectively.

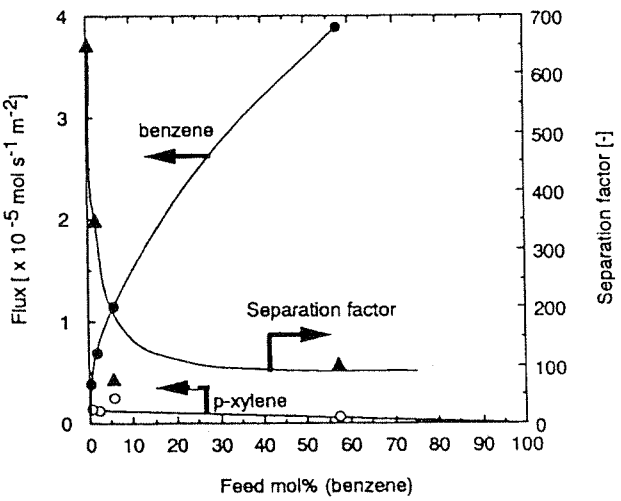

Fig. 16. Effect of benzene feed concentration on the fluxes of benzene and *p*-xylene and separation factor in pervaporation of benzene/*p*-xylene mixtures using FER membranes. Temperature: 303 K, ●: flux of benzene, ○: flux of *p*-xylene, △: separation factor.

and homogeneous nucleation, as discussed above. Irrespective of these mechanisms, once a zeolite layer is formed on the surface of a support, an aluminosilicate solution should find it difficult to penetrate into the support to fill up the pores. Consequently, the intergrowth of crystals formed on the surface of support is probably essential to obtain a pinhole-free zeolitic membrane under hydrothermal conditions, as previously suggested.[22,25,26,33,34,45] The zeolitic membranes prepared by the VPT method, thus, show different morphological features from those prepared by the conventional hydrothermal synthetic method.

Preferentially-Oriented Membrane.[62] Apart from the studies described above, we recently found that preferentially oriented-MFI membrans can be synthesized by the VPT method. The synthesis of pinhole-less, oriented crystals on a porous ceramic support is of great interests for understanding the ultimate permeation properties of zeolitic membranes, and also for sensor and devise applications. Figures 9 and 10 show a typical SEM image and their XRD pattern. These membranes are obtained by using sodium aluminate as an aluminum sourse. Other synthetic procedures are the same as those described above. When aluminum sulfate was used, the MFI layer consisted of an accumulation of randomly ori-

ented polygonal crystals, as shown in Fig. 4. The relative reflection intensities of the (a 0 0) and (0 b 0) crystal faces of MFI are peculiarly high (Fig. 10), indicating that the (a 0 0) and (0 b 0) faces of MFI crystals are oriented pallarel along the surface of the alumina plate. The MFI layer comprizes hexagonal large crystals with a diameter of 50—100 μm; the surfaces of these large crystals are smooth (Fig. 9). It is noteworthy that such an oriented-MFI can be syntheized from a dry gel layer on the support, while the role of the aluminum source involved in the parent gel on the orientation of resultant zeolite crystals is open question.

Permeation Properties of Zeolitic Membranes

Gas Permeation. Although numerous single gas and mixed gas permeation measurements have been reported, the types of zeolitic membranes that have been used for gas-permeation tests are still limited. MFI membranes, especially silicalite (Al-free MFI) membranes, were used frequently. The permeance ratio of n-butane to isobutane has been widely used as an indication of the compactness of MFI membranes. However, the relations between the compactness of zeolitic membranes with their permeation and separation properties have not been clearly understood. Compact MFI membranes generally show a high selectivity to n-butane, while the selectivity ranges from 1 to 64.[26,27,32—34,63,64]

We carried out permeation tests of H_2 and CH_4 at room temperature with five FER membranes, including a pinhole-free FER membrane and four incompact FER membranes. Figure 11 shows a schematic diagram of the experimental apparatus for determining the permeance of the gas. The pressure difference between the feed and permeate sides was kept at 0.2 MPa. The permeation side was set at atmospheric pressure.

Figure 12 shows the variation in the permeance ratios of H_2/CH_4 plotted as a function of the H_2 permeance through the FER membranes. The H_2 permeance should be an indication of the compactness of FER membranes.

The H_2/CH_4 permeance ratio through the alumina support, itself, was 2.24. The theoretical value for viscous flow and Knudsen diffusion are 1.25 and 2.82, respectively. The H_2/CH_4 permeance ratio through the alumina support is between these two theoretical values. Taking it into account that the average pore diameter of alumina pore is 0.1 μm, this result suggests that the transport of H_2 and CH_4 was governed by the flow in the transition region between viscous flow and Knudsen diffusion. The zeolitic membranes were stuck on a glass or stainless-steel tube with a resin. The effective membrane area was 2.2 cm^2.

The behavior of the H_2/CH_4 permeation ratio can be classified into three regions, as shown in Fig. 12. The H_2/CH_4 permeance ratio approached the theoretical value for the Knudsen diffusion with decreasing H_2 permeance in region I. In region II, the H_2/CH_4 permeance ratio decreased with decreasing H_2 permeance. In this region, the surface diffusion of CH_4, which is more absorbable than H_2, appeared in addition to the Knudsen diffusion. Thus, the H_2/CH_4 permeance ratio is less than the theoretical value for the Knudsen diffusion. In region III, the H_2/CH_4 permeance ratio, again, increases with decreasing H_2 permeance. The extreme left plot in Fig. 12 was obtained with a pinhole-free FER membrane. This behavior seems to be due to configurational diffusion, which influences the permeation of CH_4 more than that of H_2. As a result of this discussion, we suppose that pinhole-free membranes may be essential for separation on the basis of configurational diffusion or shape selectivity. In other words, the smaller number of piholes could greatly influence the permeation and separation properties.

There exists little information on the relation between the separation properties of zeolitic membranes and their structures. We preliminary compared the permeances of inorganic gases through two different types of zeolitic membranes, FER and MOR, synthesized on a porous alumina support.

The permeances of H_2, He, CH_4, N_2, O_2 and CO_2 through these two membranes are shown in Fig. 13.[65] The permeance of each gas through the MOR membrane was about 100-times greater than those through the FER membrane. This was presumably due to the pore diameter of MOR being larger than that of FER, since the thickness of the compact layer in the MOR membrane, about 20 μm, was almost comparable to that of the FER.

The permeances of H_2, He, and CH_4 through the MOR membrane monotonously increased with increasing temperature, indicating that the controlling mechanism of permeation did not change in this temperature region. This temperature dependence of the permeances is evidently caused by activated diffusion. Other permeances of gases through the MOR and FER membranes have minimums with increasing temperature, suggesting that the controlling mechanism changes. The appreance of these minimums can be explained by a combination of activated diffusion and the contribution of sorption. Namely, inorganic gas permeation is governed by an activated diffusion mechanism at higher temperatures, and an increasing amount of gas adsorbed on micropore wall causes an increase in permeance with decreasing temperature. A theoretical analysis of gas permeation through zeolitic membranes was described elsewhere.[65]

Most gas-permeation measurements have so far been carried out below 450 K, except for those described in several reports.[14,32,63,66] This is because it is difficult to seal between a membrane and an apparatus at a high temperature where polymeric sealing materials cannot be used. One of the attractive targets for zeolitic membranes is to develop a highly selective membrane reactor operating at high temperatures. The sealing problems should be overcome in the near future.

Pervaporation Performance. Pervaporation is useful to separate liquid mixtures. Recent studies on separation tests by pervaporation have indicated that zeolitic membranes posses a high separation potential for a variety of organic/water mixtures including water/ethanol[21,24,25] and water/methylethylketone.[68] This separation performance is governed by the hydrophilic/hydrophobic nature of zeolites.

The separation of aromatic hydrocarbons can be achieved by the shape selectivity and/or the adsorption property of zeolites. However, only a few attempts have so far been made

to separate aromatic hydrocarbons. We examined the pervaporation of cyclohexane and three aromatic hydrocarbons, i.e., benzene, *p*-xylene and *o*-xylene, through FER and MOR membranes prepared by the VPT method.[59—61]

Figure 14[61] shows the pervaporation results using the FER membrane for unary systems of cyclohexane, benzene, *p*-xylene and *o*-xylene at 303 K. The zeolitic membrane was set in the solution and the permeate side was kept under a vacuum.

The separation factor ($\alpha(a/b)$) was calculated as follows:

$$\alpha(a/b) = \frac{(x_a/x_b)_{\text{permeate}}}{(x_a/x_b)_{\text{feed}}}.$$

where x represents the mole fraction [–].

The ratios of each flux to that of *o*-xylene are shown together in Fig. 14. The fluxes of cyclohexane and benzene are about one-hundred times greater than those of *p*- and *o*-xylene. The flux of *p*-xylene is about five-times greater than that of *o*-xylene.

Pervaporation tests were carried out consecutively in the order from the left to the right-hand side in Fig. 14. The permeation test for TIPB was carried out after that for *o*-xylene, and no permeation of TIPB was detected. After a permeation test for TIPB, pervaporation using benzene was performed again. The flux of benzene observed was comparable to that before the TIPB permeation test, as shown in Fig. 14. These results prove that no TIPB existed in the micropore of FER, and TIPB adsorbed around the entrance of micropores was easily substituted by benzene. This is in good agreement with the conclusion that there existed no pinhole which would allow the entrance of TIPB into the FER membrane.

Figure 15[61] shows the pervaporation results using the FER membrane for binary mixtures, cyclohexane/benzene, benzene/*p*-xylene and *p*-xylene/*o*-xylene at 303 K. The theoretical separation factors from vapor–liquid equilibrium were calculated, and are shown in Fig. 15 together. The separation factors for these three mixtures were greater than those at vapor-liquid equilibrium. It is noteworthy that a separation factor α(*p*-xylene/*o*-xylene) was about 3, taking into account that a MFI membrane which possesses pinholes with a diameter of about 1 nm showed no selectivity for the *p*-xylene/*m*-xylene mixture.[28]

The fluxes of both benzene and *p*-xylene through the FER membrane were about a quarter of those through the MOR membrane. The difference in the fluxes between two types of zeolitic membrane can be attributed to the difference in the pore dimensions of MOR (0.70×0.65 nm) and FER (0.54×0.42 nm). The separation factors for the benzene/*p*-xylene mixture exceeded 100, which was much greater than 10.3 predicted based on the vapor–liquid equilibrium.

The vapor permeation of *p*-xylene, *m*-xylene, ethylbenzene, and toluene through an MFI membrane was carried out by Baertsch et al.,[69] who reported that no separation was achieved for binary mixtures of *p*-xylene/*o*-xylene, *p*-xylene/ethylbenzene, *p*-xylene/toluene, and *m*-xylene/ethylbenzene at 380—480 K. They claimed that the molecule with the slowest permeation rate limits the diffusion, and slows the other species down to its own rate in single-file transport.

When single-file transport occurs in the membrane, the overall selectivity is always governed by the selectivity on the feed side of the membrane. Thus, taking into account that the FER–alumina composite layer is compact, high selectivities for the benzene/*p*-xylene mixtures suggest that the shape selectivity for the benzene/*p*-xylene mixture appears at the pore mouths of FER on the feed side of the FER–alumina composite layer. The intracrystalline diffusivities of benzene in MFI crystals were reported to be comparable to those of *p*-xylene.[70] Therefore, it seems that the difference in the sorption rates of benzene and *p*-xylene molecules into the zeolite pores on the feed side governed the selectivity in the present pervaporation.

Figure 16[60] shows the variation in the fluxes of benzene and *p*-xylene and the separation factor as a function of the feed concentration of benzene. When the molar fraction of benzene in the feed solution was 57 mol%, the separation factors for the benzene/*p*-xylene mixture exceeded 100, which was much greater than 10.3 predicted based on the vapor–liquid equilibrium. The separation factor for benzene/*p*-xylene mixtures greatly increased with decreasing benzene concentration in the feed. The separation factor α (benzene/*p*-xylene) was surprisingly as high as 600 when the feed concentration of benzene was 0.5 mol%. Although the flux of *p*-xylene was varied in proportion to the *p*-xylene concentration in the feed, that of benzene did not monotonously decrease with decreasing feed concentration, suggesting that even when the concentration of benzene in feed solution is extremely small, the sorption rate of benzene into the FER pores still exceeds that of *p*-xylene. Therefore, a high separation factor was obtained at the low feed concentration of benzene.

Concluding Remarks

Only about ten reports on zeolitic membranes were published in 1992. Since then, attention has rapidly been paid to the research on zeolitic membranes and in 1995 more than 150 papers were reported. With this steeply increasing attention, application fields of zeolitic membranes have been expanding, for instance, catalytic membranes, sensors, devices, and modification of electrodes. One can believe that excellent separation properties reported so far prove promising prospects of zeolitic membranes. We have demonstrated that the novel synthetic method, vapor-phase transport, is useful for preparing zeolitic membranes which can be pinhole-free.

On the other hand, the reproducibility is now the most critical problem to be overcome. Most researchers have reported their best results. This is due probably to a lack of knowledge concerning the mechanisms of nucleation and the growth of zeolites. Also, intracrystalline diffusion and sorption properties are still open for discussion. Further fundamental studies in a wide variety of fields of zeolite science are required.

References

1) B. J. Grashoff, C. E. Pilkington, and C. W. Corti, *Platinum Met. Rev.*, **27**, 157 (1983).

2) S. Uemiya, T. Matsuda, and E. Kikuchi, *J. Membr. Sci.*, **56**, 315 (1991).

3) Y. S. Lin and A. J. Burggraaf, *AIChE J.*, **38**, 445 (1992).

4) S. W. Nam and G. R. Gavalas, *AIChE Symp. Ser.*, **85**, 68 (1989).

5) G. R. Gavalas, C. E. Megiris, and S. W. Nam, *Chem. Eng. Sci.*, **44**, 1829 (1989).

6) M. Tsapatsis, S. Kim, S. W. Nam, and G. Gavalas, *Ind. Eng. Chem. Res.*, **30**, 2152 (1991).

7) M. Asaeda, Y. Oki, and T. Manabe, "Priority-Area Research Supported by the Ministry of Education, Science and Culture," Japan, "Energy Conversion and Utilization with High Efficiency," Subarea C (1993), 1993 Research Report, p. 253.

8) A. B. Shelekhin, A. G. Dixon, and Y. H. Ma, *J. Membr. Sci.*, **75**, 233 (1992).

9) M. Bhandarkar, A. B. Shelekhin, A. G. Dixone, and Y. H. Ma, *J. Membr. Sci.*, **75**, 221 (1992).

10) P. Kolsch, D. Venzke, M. Noack, E. Lieske, P. Toussaint, and J. Caro, *Stud. Surf. Sci. Catal.*, **84**, 1075 (1994).

11) M. B. Rao and S. Sircar, *J. Membr. Sci.*, **85**, 253 (1993).

12) M. Niwa, S. Kato, T. Hattori, and Y. Murakami, *J. Chem. Soc., Faraday Trans.*, **80**, 3135 (1984).

13) S. T. Sie, *Stud. Surf. Sci. Catal.*, **84**, 587 (1994).

14) F. Kapteijn, W. J. W. Bakker, J. van de Graaf, G. Zheng, J. Poppe, and J. A. Moulijn, *Catal. Today*, **25**, 213 (1995).

15) H. Suzuki, U.S. Patent 4699892 (1987).

16) L. M. Lachman et al., U.S. Patent 4800187 (1989).

17) Tokkyo Koho, JP 59-213615.

18) Tokkyo Koho, JP 63-287504.

19) T. Sano, Y. Kiyozumi, M. Kawamura, F. Mizukami, H. Takaya, T. Mouri, W. Inaoka, Y. Toida, M. Watanabe, and K. Toyoda, *Zeolites*, **11**, 842 (1991).

20) T. Sano, Y. Kiyozumi, F. Mizukami, H. Takaya, T. Mouri, and M. Watanabe, *Zeolites*, **12**, 131 (1992).

21) T. Sano, F. Mizukami, H. Takaya, T. Mouri, and M. Watanabe, *Bull. Chem. Soc. Jpn.*, **65**, 146 (1992).

22) J. G. Tsikoyiannis and W. O. Haag, *Zeolites*, **12**, 126 (1992).

23) T. Sano, Y. Kiyozumi, K. Maeda, M. Toba, S. Niwa, and F. Mizukami, *J. Mater. Chem.*, **2**, 141 (1992).

24) Y. Kiyozumi, F. Mizukami, K. Maeda, T. Kozasa, M. Toda, and S. Niwa, *Stud. Surf. Sci. Catal.*, in press.

25) E. D. Geus, M. J. Exter, and H. Bekkum, *J. Chem. Soc., Faraday Trans.*, **88**, 3101 (1992).

26) E. D. Geus, H. Bekkum, W. J. W. Bakker, and J. A. Moulijin, *Microporous Mater.*, **1**, 131 (1993).

27) M.-D. Jia, K.-V. Peinemann, and R.-D. Behling, *J. Membr. Sci.*, **82**, 15 (1993).

28) T. Sano, M. Hasegawa, Y. Kawakami, Y. Kiyozumi, H. Yanagishita, D. Kitamoto, and F. Mizukami, *Stud. Surf. Sci. Catal.*, **84**, 1175 (1994).

29) T. Masuda, A. Sato, H. Hara, M. Kouno, and K. Hashimoto, *Appl. Catal., A: General*, **111**, 143 (1994).

30) M. D. Jia, B. Chen, R. D. Noble, and J. L. Falconer, *J. Membr. Sci.*, **90**, 1 (1994).

31) P. Meriaudeau, A. Thangaraj, and C. Naccache, *Microporous Mater.*, **4**, 213 (1995).

32) C. Bai, M.-D. Jia, J. L. Falconer,and R. D. Noble, *J. Membr. Sci.*, **105**, 79 (1995).

33) Y. Yan, M. Tsapatsis, G. R. Gavalas, and M. E. Davis, *J. Chem. Soc., Chem. Commun.*, **1995**, 227.

34) Y. Yan, M. E. Davis, and G. R. Gavalas, *Ind. Eng. Chem. Res.*, **34**, 1652 (1995).

35) Z. A. E. P. Vroon, K. Keizer, M. J. Gilde, H. Verweij, and A. J. Burggraaf, *J. Membr. Sci.*, **113**, 293 (1996).

36) Y. H. Chiou, T. G. Tsai, S. L. Sung, H. C. Shih, C. N. Wu, and K. J. Chao, *J. Chem. Soc., Faraday Trans.*, **92**, 1061 (1996).

37) K. Kusakabe, S. Yoneshige, A. Murata, and S. Morooka, *J. Membr. Sci.*, **116**, 39 (1996).

38) K. Suzuki, Y. Kiyozumi, T. Sekine, K. Obata, Y. Sindo, and S. Sin, *Chem. Express*, **5**, 793 (1990).

39) T. Masuda, H. Hara, M. Kouno, H. Kinoshita, and K. Hashimoto, *Microporous Mater.*, **3**, 565 (1995).

40) H. Mimura, T. Tezuka, and K. Akiba, *J. Nucl. Sci. Technol.*, **32**, 1250 (1995).

41) K. Kita, Horii, Y. Ohtoshi, K. Tanaka, and K. Okamoto, *J. Mater. Sci. Lett.*, **14**, 206 (1995).

42) S. Yamazaki and K. Tsutsumi, *Microporous Mater.*, **4**, 205 (1995).

43) S. Yamazaki and K. Tsutsumi, *Microporous Mater.*, **5**, 245 (1995).

44) G. J. Myatt, P. M. Budd, C. Price, and S. W. Carr, *J. Mater. Chem.*, **2**, 1103 (1992).

45) J. C. Jansen, D. Kashchiev, and A. Erdem-Senatalar, *Stud. Surf. Sci. Catal.*, **85**, 215 (1994).

46) V. Valtchev, S. Mintova, and L. Konstantinov, *Zeolites*, **15**, 679 (1995).

47) M. Tsapatsis, T. Okubo, M. Lovallo, and M. E. Davis, *Mater. Res. Soc. Symp. Proc.*, **371**, 21 (1995).

48) D. M. Bibby and M.P. Dale, *Nature*, **317**, 157 (1985).

49) Q. Huo, S. Feng, and R. Xu, *J. Chem. Soc., Chem. Commun.*, **1988**, 1486.

50) W. Xu, J. Li, W. Li, H. Zhang, and B. Liang, *Zeolites*, **9**, 468 (1989).

51) W. Xu, J. Dong, J. (Jinping) Li, J. (Jianquan) Li, and F. Wu, *J. Chem. Soc., Chem. Commun.*, **1990**, 755.

52) M. H. Kim, H. X. Li, and M. E. Davis, *Microporous Mater.*, **1**, 191 (1993).

53) M. Matsukata, N. Nishiyama, and K. Ueyama, *Microporous Mater.*, **1**, 219 (1993).

54) M. Matsukata, N. Nishiyama, and K. Ueyama, *Microporous Mater.*, **7**, 109 (1996).

55) M. Matsukata, N. Nishiyama, and K. Ueyama, *Stud. Surf. Sci. Catal.*, **84**, 1183 (1994).

56) N. Nishiyama, K. Ueyama, and M. Matsukata, *Microporous Mater.*, **7**, 299 (1996).

57) G. Alexander, "Chemistry in Action Series 1, Silica and Me," Doubleday & Company, Inc., (1967).

58) M. Matsukata, N. Nishiyama, and K. Ueyama, *J. Chem. Soc., Chem. Commun.*, **1994**, 339.

59) N. Nishiyama, K. Ueyama, and M. Matsukata, *J. Chem. Soc., Chem. Commun.*, **1995**, 1967.

60) N. Nishiyama, T. Matsufuji, K. Ueyama, and M. Matsukata, submitted to *Microporus Mater.*

61) N. Nishiyama, K. Ueyama, and M. Matsukata, *Stud. Surf. Sci. Catal.*, **105**, 2195 (1996).

62) E. Kikuchi, K. Yamashita, S. Hiromoto, K. Ueyama, and M. Matsukata, *Microporous Mater.*, in press.

63) W. J. W. Bakker, G. Zheng, F. Kapteijn, M. Makkee, J. A. Moulijn, E. R. Geus, and H. van Bekkum, "Precision Process

Technology," ed by M. P. C. Weijenen and A. A. H. Drinkenburg, Kluwer, Dordrecht (1993), p. 425.
64) W. J. W. Bakker, F. Kapteijn, J. Poppe, and J. A. Moulijn, *J. Membr. Sci.*, **117**, 57 (1996).
65) N. Nishiyama, K. Ueyama, and M. Matsukata, "Proc. 5th World Congr. Chem. Eng.," Vol. 4, p. 834 (1996); submitted to *AIChE J.*
66) R. D. Noble and J. L. Falconer, *Catal. Today*, **25**, 209 (1995).
67) T. Sano, H. Yanagisita, Y. Kiyozumi, F. Mizukami, and K. Haraya, *J. Membr. Sci.*, **95**, 221 (1994).
68) T. Sano, M. Hasegawa, Y. Kawakami, and H. Yanagishita, *J. Membr. Sci.*, **107**, 193 (1995).
69) C. D. Baertsch, H. H. Junke, J. L. Falconer, and R. D. Noble, *J. Phys. Chem.*, **100**, 7676 (1996).
70) D. B. Shah and H. Y. Liou, *Zeolites*, **14**, 541 (1994); D. B. Shah and H. Y. Liou, *Stud. Surf. Sci. Catal.*, **84**, 1347 (1994).

Masahiko Matsukata was born in Tokyo in 1960. He studied applied chemistry at Waseda University and obtained his Dr. Degree in 1989 from the same university under the supervision of Professors Yoshiro Morita and Eiichi Kikuchi. He was appointed research associate of industrial chemistry, Seikei University, in 1989 and then moved to Osaka University as research associate. He was promoted to Associate Professor of Chemical Engineering at Osaka University in 1996 and moved to Department of Applied Chemistry, Waseda University, as Associate Professor in 1997. His research interests range from materials chemistry and engineering, mostly focusing on microporous materials to environmental and energy issues with utilization of fossil fuels.

Eiichi Kikuchi was born in Urawa (Saitama) in 1942. He was graduated from the Department of Applied Chemistry, Waseda University in 1964, and received a Ph D from the same university in 1969 on the study of Nickel-catalyzed hydrogenolysis of hydrocarbons. After being a Research Associate (1969—1975) at Waseda University and a Postdoctoral Fellow (1972,73) at the University of Alberta (Canada), he was promoted to Associate Professor in 1975 and Professor in 1980 at Waseda University. Throughout his carrier he was engaged in heterogeneous catalysis, particularly in hydrocarbon conversions, CO hydrogenation, NO reduction, and membrane catalysis.

ELSEVIER

Microporous Materials 11 (1997) 107–116

MICROPOROUS
MATERIALS

Synthesis of a zeolitic thin layer by a vapor-phase transport method: appearance of a preferential orientation of MFI zeolite

Eiichi Kikuchi [a], Kazuhiko Yamashita [a], Sachioko Hiromoto [a], Korekazu Ueyama [b], Masahiko Matsukata [b]

[a] *Department of Applied Chemistry, Waseda University, Okubo, Shinjuku, Tokyo 169, Japan*
[b] *Department of Chemical Engineering, Osaka University, Machikaneyma, Toyonaka, Osaka 560, Japan*

Received 13 January 1997; accepted 24 February 1997

Abstract

Zeolitic membranes were synthesized on a porous alumina support by the vapor-phase transport method using one of two alumina sources: aluminum sulfate and sodium aluminate. By choosing the appropriate period and temperature for drying the aluminosilicate gel on the alumina support, MOR, FER and MFI could be synthesized. MOR was formed when the water content in the dry gel was high. As the water content decreased, FER and MFI were formed sequentially. Preferential formation of MFI was achieved by treating the dry gel at 373 K. The temperature at which the support was dipped in the parent gel also influenced the type of zeolite formed, although the effect of drying conditions was more pronounced. A similar trend was found for both aluminum sulfate and sodium aluminate.

When the alumina source was sodium aluminate and the aluminosilicate gel was treated at 373 K, a preferentially oriented MFI membrane could be synthesized, as the (*a*00) and (0*b*0) crystal faces were oriented in parallel to the surface of porous alumina support. The uniform and dense morphology of the dry gel seems to account for the appearance of the orientation. © 1997 Elsevier Science B.V.

Keywords: Preferentially oriented membrane; Synthesis; Vapor-phase transport; Zeolitic membrane

1. Introduction

Zeolites (i.e., crystalline aluminosilicates) have been widely used as adsorbents, catalysts and ion exchangers. They can be used as molecular sieves because of their micropore systems. They are more resistant to high temperatures and chemicals than organic materials. Recently, great attention has been paid to zeolitic membranes as separation membranes and chemical sensors.

Hydrothermal synthesis has generally been used to synthesize zeolites on a support. Self-supporting MFI membranes were prepared on a Teflon slab by Sano et al. [1], and by Tsikoyiannis and Haag [2]. The zeolitic membranes obtained were polycrystalline and formed through the successive accumulation of zeolite crystals [3]. Pinholes between crystals were avoided using this method. Yan et al. [4] recently synthesized defect-free MFI membranes on the bottom surface of an alumina support placed horizontally just below the surface of the liquid phase. They confirmed that 1,3,5-triisopropylbenzene (kinetic diameter 0.85 nm) did not permeate through the membrane. It was reported that the H_2O/SiO_2 ratio and the synthesis temperature played important roles in

PII S0927-6513(97)00019-9

the synthesis of a defect-free zeolitic membrane [1,5]. Silicalite membranes were synthesized on inner surface of an alumina tube [6,7] and on a porous stainless steel [8]. Noble et al. suggested that at least two or three syntheses were necessary to reduce the number of defects. From the results of gas permeation experiments using several molecules such as n-C_4H_{10}, i-C_4H_{10}, H_2 and N_2, they suggested that the mass transport through silicalite membranes was controlled by the molecular size and adsorption properties [6–8].

Matsukata et al. [9] also prepared pinhole-free FER and MOR membranes by a vapor-phase transport method. This synthetic method was first reported by Xu et al. [10], who successfuly synthesized MFI from a dry gel in 1990. Dong et al. [11] also prepared self-supporting ZSM-5 and ZSM-35 membranes using this method. Kim et al. [12] reported that water and a high pH value in the hydrogel were necessary for crystallization [12]. FER was synthesized under water-lean conditions by Matsukata et al. [13]. They reported that the Na_2O/Al_2O_3 ratio in the hydrogel affected the type of zeolite formed.

In order to favor permeability, zeolite crystals on supports should be formed in the orientation of the crystal faces. Highly oriented MFI films have formed on flat, uniform and non-porous plates such as mercury [14] and silicon (100) wafers [15]. High surface tension and uniformity of the support are considered to be the key for the orientation of the zeolite.

Matsukata et al. [13] have synthesized zeolites by a vapor-phase transport method, and reported that the Na_2O/SiO_2 ratio and the templating reagent affected the phase of the zeolite, and the support material affected the crystallinity. In this study, we investigate the effect of the alumina source, the water content of the dry gel and the dipping temperature of the alumina support in the hydrogel on the phase of zeolite formed. We synthesized a preferentially oriented MFI mem-

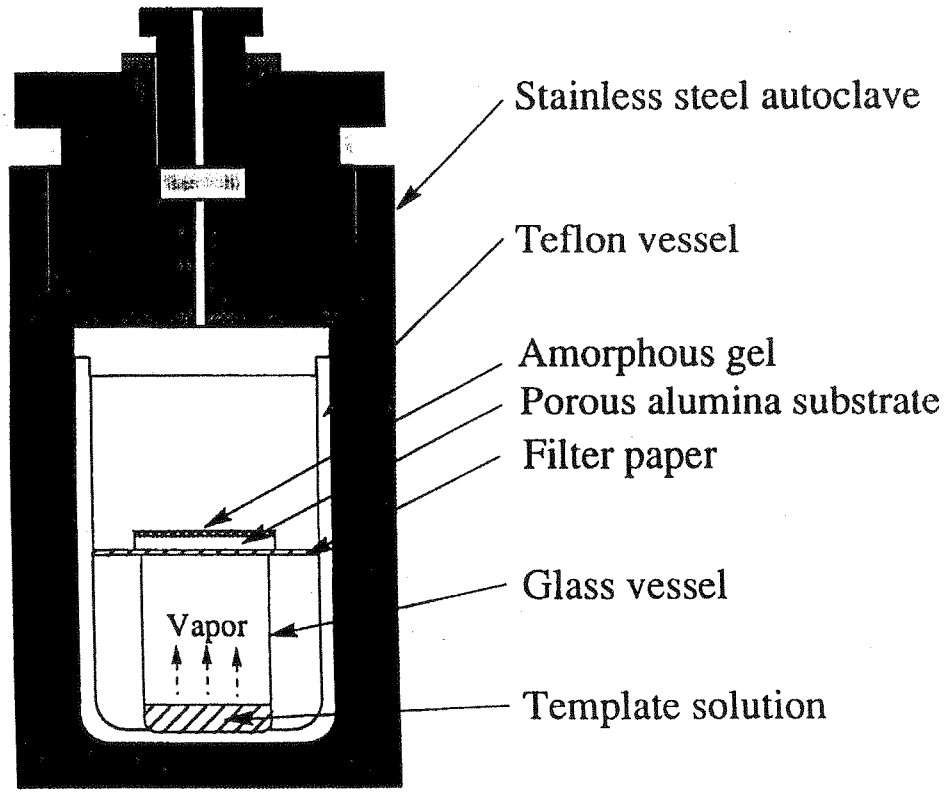

Fig. 1. Schematic illustration of the autoclave used for synthesizing zeolitic membranes by the vapor-phase transport method.

brane on a porous alumina support using sodium aluminate instead of aluminum sulfate as the alumina source.

2. Experimental

The zeolitic membranes were prepared using the vapor-phase transport method (VPT). A colloidal silica (ST-S; Nissan Chemical Co.) containing 30–31 wt.% SiO_2 and <0.6 wt.% Na_2O was used as the silica source. Two kinds of alumina source were used: anhydrous aluminum sulfate, $Al_2(SO_4)_3$ (Kanto Chemicals Co.), and sodium aluminate, $NaAlO_2$ (Kanto Chemicals Co.). The parent aluminosilicate gel was prepared as follows. Colloidal silica was stirred while adding 4 N sodium hydroxide and 0.24 M alumina source solutions. The composition of the gel was adjusted to $Na_2O:SiO_2:Al_2O_3 = 10.6–11.6:22.9:1$. The resultant gel was aged while stirring at 293 K for 6 h, and a porous alumina support (mean pore diameter 0.2 mm; Nippon Gaishi Co.) or a glass plate was dipped in the gel without stirring at various temperatures (276, 293 and 313 K) for 24 h. The aluminosilicate gel on the support was dried (a) at 293 K for 1 day, (b) at 293 K for 3 days, (c) at 293 K for 3 days followed by further drying at 333 K for 2 h, and (d) at 293 K for 3 days followed by further drying at 373 K for 2 h. Crystallization was carried out under a mixture of vapors of ethylenediamine (EDA), triethylamine (Et3N) and water in an autoclave which is shown schematically in Fig. 1. The composition of the mixture was 1EDA:1.9Et3N:3.7H_2O. The supported dry gel was placed in the middle of the autoclave. After crystallization at 453 K for 5 days, the product was washed with deionized water and dried at room temperature under evacuation.

The product was characterized using XRD and SEM. The dry gel removed from the support was characterized using TG-DTA to determine the water content and ^{27}Al-NMR to study the local structure of the gel.

3. Results and discussion

3.1. Effect of preparation conditions on product zeolite structure

The aluminosilicate gel was supported on the porous alumina plate by dip coating at 293 K, and the supported gel was dried at different temperatures. Table 1 lists the crystallization results obtained under various drying conditions. When aluminum sulfate was used and the dry gel was prepared at 293 K, drying for 1 day gave a mixture of mordenite (MOR) and ferrierite (FER). Interestingly, further drying led to different crystallization results. Prolonged drying at 293 K gave a pure phase of FER. When the parent gel was treated at a higher temperature after drying at 293 K for 3 days, MFI was observed in the product. In particular, pure MFI was formed when the parent gel was treated at 373 K for 2 h.

Different dipping temperatures of 276 and 313 K were applied for the preparation of the dry gel

Table 1
Effect of dipping temperature on the type of zeolite formed

Drying condition	Dipping temperature (K)					
	$Al_2(SO_4)_3$			$NaAlO_2$		
	276	293	313	276	293	313
293 K for one day	MOR	MOR + FER	MOR + FER	MOR	MOR + FER	MOR + FER
293 for three days	MOR + FER	FER	FER	FER + MFI	FER + MFI	FER
293 K for three days + 333 K for 2 h	FER	FER + MFI	FER	FER + MFI	FER + MFI	FER + MFI
293 K for three days + 373 K for 2 h	FER + MFI	MFI	FER + MFI	FER + MFI[a]	MFI[a]	FER + MFI[a]

Silica source: colloidal silica, $Na_2O:SiO_2:Al_2O_3 = 10.6–11.6:22.9:1$.
[a]Highly oriented products.

layer on the alumina support. The trend of the product shifting from MOR to MFI via FER, probably with increasing degree of drying, was maintained at these dipping temperatures. However, pure MFI was obtained only when the support was dipped at 293 K.

Similar results were obtained when sodium aluminate was used instead of aluminum sulfate. However, a preferentially oriented MFI thin layer was found to form on the support surface in the cases indicated in Table 1. This will be discussed later.

3.2. Formation of preferentially oriented MFI membranes

Fig. 2 shows the XRD patterns of the zeolites formed on the alumina support. When synthesized with aluminum sulfate, the relative intensities of the reflection peaks of MFI were coincident with those of a powder MFI sample, showing randomly oriented zeolite crystals. However, when sodium aluminate was used, a dramatically different XRD pattern was recorded for MFI. The relative intensities of the (*a*00) and (0*b*0) crystal faces of MFI were significantly large compared with those of the powder MFI. These results indicate that the (*a*00) and (0*b*0) faces of MFI are deposited in a parallel orientation along the surface of the alumina support, and that the *a*- and *b*-axes are perpendicular to its surface.

Fig. 3 shows an SEM image for MFI layers formed on the alumina support. In the case where aluminum sulfate was used, the MFI layer consists of an accumulation of randomly oriented polygonal crystals with a size of 10–20 μm (Fig. 3(a)). An intergrowth of crystals can be seen, although the cross-sectional view shows that there are large voids among the crystals (Fig. 3(b)). Figs. 3(c) and (d) show the top and cross-sectional views of a preferentially oriented MFI layer developed on the alumina support, obtained using sodium aluminate as the alumina source. The MFI layer is composed of large hexagonal crystals 50–100 μm in diameter, and the surface of the large crystals looks smooth. Voids between crystals were hardly observed in the cross-sectional view of this sample.

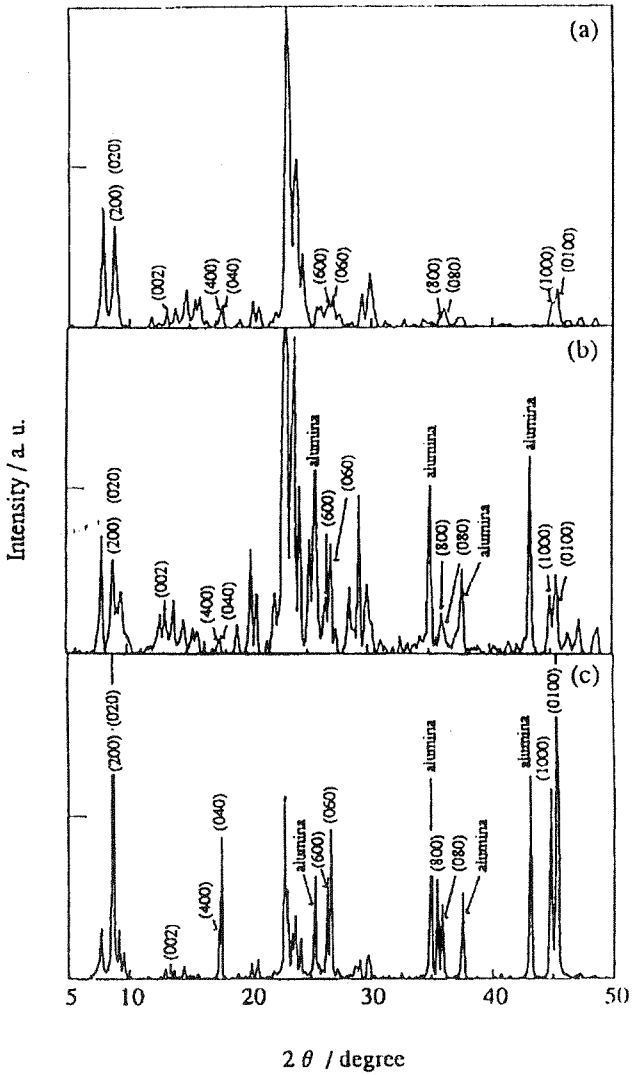

Fig. 2. XRD patterns of zeolites formed on alumina support and powder ZSM-5. (a) Powder ZSM-5 (SiO_2:Al_2O_3=23.8). (b) MFI on alumina support prepared using $Al_2(SO_4)_3$. (c) MFI on alumina support prepared using $NaAlO_2$. Dipping temperature: 293 K, drying condition: 293 K for 3 days followed by 373 K for 2 h.

3.3. Effect of preparation conditions of the aluminosilicate gel on the products

Judging from the results shown in Table 1, we supposed that the water content in the parent dry gel significantly influenced the phase of the synthesized zeolite. The water content in the dry gel was measured by means of TG-DTA for samples dried under various conditions. In these TG-DTA

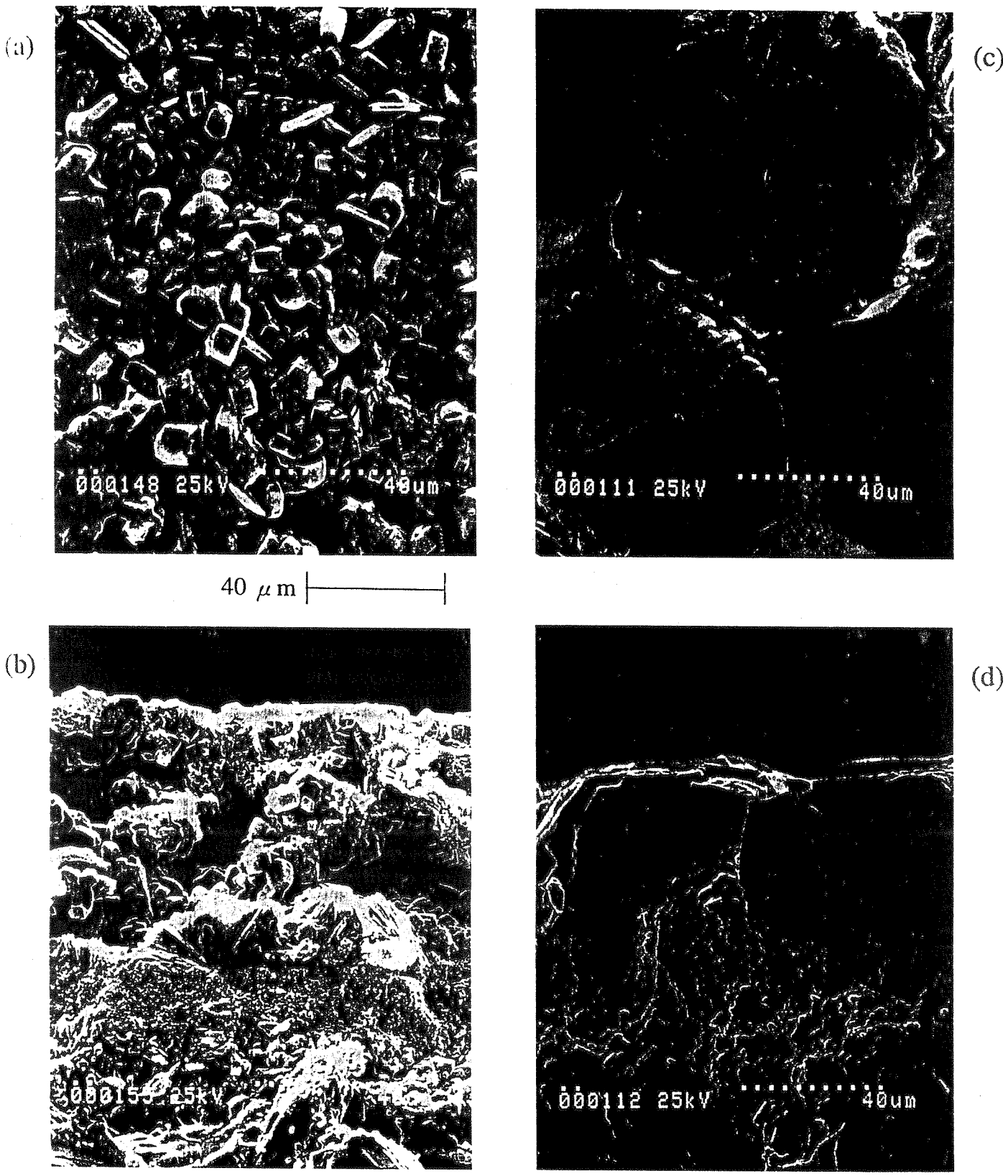

Fig. 3. SEM images (top and cross-sectional views) of the zeolite formed on the alumina support. SiO_2 source: colloidal silica, Al_2O_3 source: top view (a) $Al_2(SO_4)_3$, (c) $NaAlO_2$; cross-sectional view (b) $Al_2(SO4)_3$, (d) $NaAlO_2$. Dipping temperature: 293 K, drying condition: 293 K for 3 days followed by 373 K for 2 h.

experiments, the powdery dry gels removed from the alumina support were used after drying.

Table 2 lists the water content of the aluminosilicate gels. The water content gradually decreased with drying conditions from (a) to (c). In condition (d), when the parent gel was treated at 373 K, the water content was significantly low. Comparing with the results shown in Table 1, it is obvious that the zeolite phase formed changes in the order MOR, FER and MFI with decreasing water content. Kim et al. [9] proposed that there is a vapor–liquid equilibrium between water molecules condensed in the micropores of the gel and the amine in the vapor phase. It is similarly supposed that the water content in the dry gel controls the concentration of amines and decides the crystal structure of the zeolite synthesized.

Fig. 4 shows the results of DTA for aluminosilicate gels dried under conditions (a)–(d). As shown in Fig. 4(i), when aluminum sulfate was used, an endothermic peak appeared at about 373 K. The height of the peak decreased with increasing drying time and temperature. When the parent gel was dried at 293 K for 3 days followed by a further treatment at 373 K for 2 h, the endothermic peak was shifted to a higher temperature and was broadened. We propose that in the course of drying at 293 or 333 K, water evaporated gradually without changing the gel structure greatly, and as the temperature of gel treatment increased, polymerization of the aluminosilicate network proceeded and the structure consequently held water molecules more tightly. Thus, the type of zeolite synthesized depends on the degree of polymerization of the dry gel.

Table 2
Water content in dry gel

Drying conditions	Water content (wt.%)	
	$Al_2(SO_4)_3$	$NaAlO_2$
(a) 293 K for 1 day	72.0	71.7
(b) 293 K for 3 days	62.1	63.9
(c) 293 K for 3 days +333 K for 2 h	52.0	43.3
(d) 293 K for 3 days +373 K for 2 h	9.5	13.5

Silica source: colloidal silica, $Na_2O:SiO_2:Al_2O_3 = 10.6–11.6:22.9:1$; dipping temperature: 293 K.

The phase of synthesized zeolites did not depend significantly on the kind of alumina source used. As shown in Fig. 4(ii), a similar endothermic peak was observed for the gel sample prepared using sodium aluminate. The synthesized zeolites gave similar phases regardless of whether aluminum sulfate or sodium aluminate was used. The degree of polymerization in gel formation seems a more important factor in determining the phase of the zeolite.

It should be noted, however, that the DTA curve of the dry gel prepared using sodium aluminate gave another endothermic peak at about 400 or 550 K after prolonged drying at 333 or 373 K, respectively. The surface of the dry gel treated at 373 K had a lustered appearance. These results seem to show that exposure of the aluminosilicate gel to high temperatures accelerates polymerization and causes partial vitrification, and as a result, the network holds water molecules deep inside the gel pores. The second peak observed may be due to the evaporation of water which was held strongly and freed at higher temperatures. As stated above,a preferentially oriented MFI layer was obtained from the parent gel treated at 373 K. We believe that the structure of the dry gel should be related to the formation of the oriented MFI layer.

The results shown in Table 2 and Fig. 4 indicate that the water content and the degree of polymerization of the dry gel varied with the drying conditions for the gel. These factors seem to influence the structure of the synthesized zeolites strongly. In addition to the condition of gel drying, the temperature of dip coating is also important in determining the structure of the zeolites, as shown in Table 1. The effect of dipping temperature was reflected by the variation in the pH of the hydrogels to be mounted. Table 3 shows how pH varied with dipping temperature. It is shown that higher dipping temperatures gave lower pH values. We thus believe that Na^+ ions became incorporated in the network of hydrogels as polymerization progressed. The degree of polymerization of the hydrogels probably increased with increasing dipping temperature.

When the dipping temperature was 313 K, the

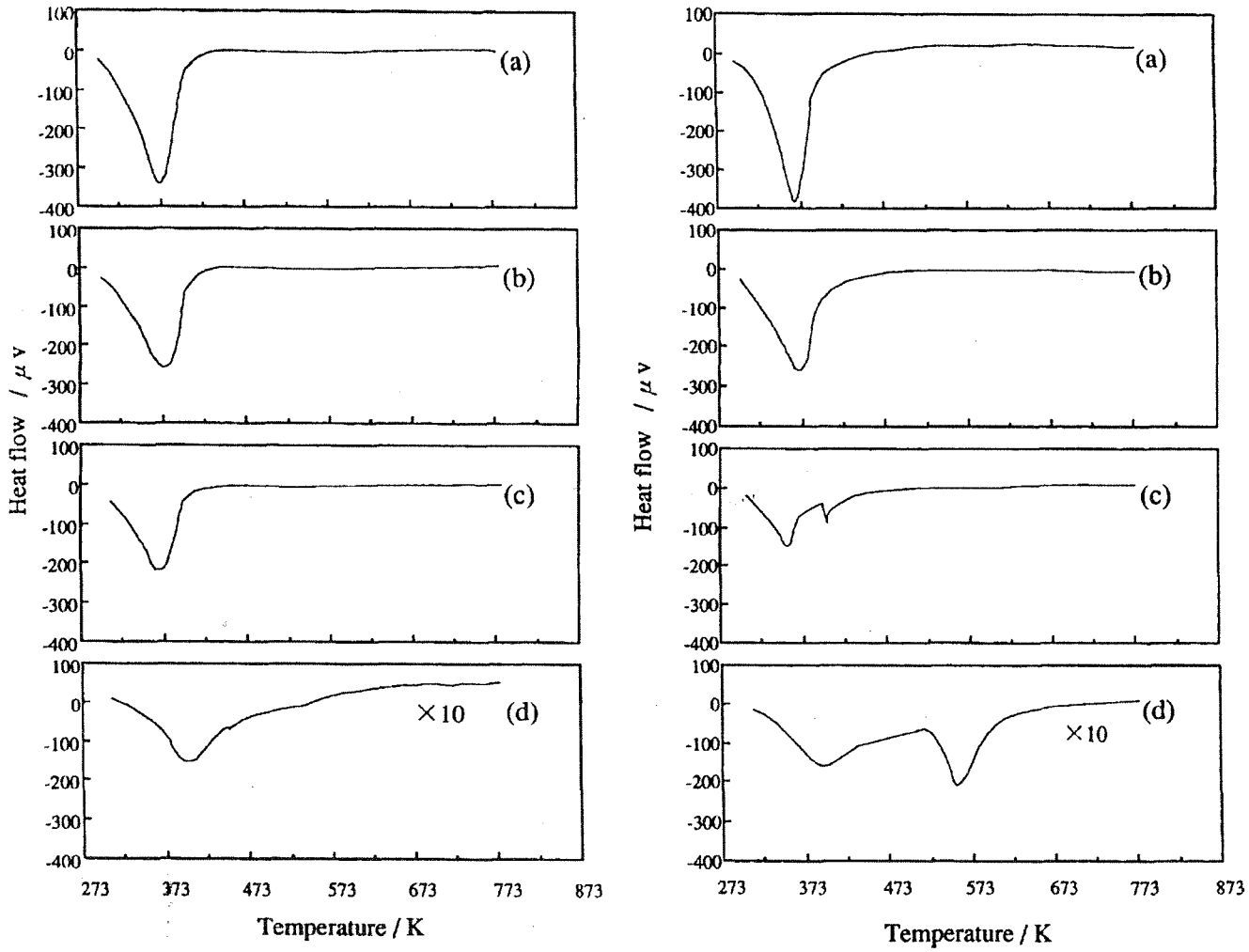

Fig. 4. (i) DTA curves for dry gels. SiO_2 source: colloidal silica, Al_2O_3 source: $Al_2(SO_4)_3$, drying conditions: (a) 293 K for 1 day, (b) 293 K for 3 days, (c) 293 K for 3 days followed by 333 K for 2 h, (d) 293 K for 3 days followed by 373 K for 2 h. (ii) DTA curves for dry gels. SiO_2 source: colloidal silica, Al_2O_3 source: $NaAlO_2$, drying conditions: (a) 293 K for 1 day, (b) 293 K for 3 days, (c) 293 K for 3 days followed by 333 K for 2 h, (d) 293 K for 3 days followed by 373 K for 2 h.

Table 3
pH of aluminosilicate gel after dipping the alumina support

Alumina source	Dipping temperature (K)		
	276	293	313
$Al_2(SO_4)_3$	Above 14	13.94	12.28
$NaAlO_2$	Above 14	13.92	12.88
	(Above 14)	(13.96)	(12.89)

Silica source: colloidal silica, $Na_2O:SiO_2:Al_2O_3 = 10.6–11.6:22.9:1$.

Figures in parentheses indicates the pH of the gel prepared without dipping the support.

pH of hydrogels prepared from aluminum sulfate was lower than that from sodium aluminate, as shown in Table 3. Table 1 shows that the zeolite phases obtained from aluminum sulfate, however, were similar to those from sodium aluminate, indicating that the structure of the dry gels prepared from these alumina sources were not significantly different. This probably suggests that the existence of SO_4^{2-} ions from aluminum sulfate may influence the decrease in pH, although it did not influence the degree of polymerization of the dry gel to vary the phase of zeolite synthesized.

FER was formed under all the drying conditions when the dipping temperature was 313 K, as shown

in Table 1. After dipping at higher temperatures, the degree of polymerization of the hydrogels and the Na^+ ion content in the gel may be increased. It was reported by Matsukata et al. [13] that for VPT synthesis, MFI was synthesized from dry gels with low Na_2O/Al_2O_3 ratios, and FER was synthesised from gels with higher Na_2O/Al_2O_3 ratios. Similarly, FER was synthesized in the present study, probably because the content of Na^+ ions in the parent gel was sufficiently high to form FER rather than MFI.

Tables 1 and 2 show that when the water content of the dry gel was high, MOR was formed in the products. MOR is a type of zeolite in which the SiO_2/Al_2O_3 ratio is generally lower than that in MFI and FER. It is thus supposed that the formation of MOR is caused by dissolution of the alumina support followed by occlusion of the Al^{3+} ions into the dry gel layer.

Table 4 shows the products prepared from the gel dried at 293 K for 1 day on a glass plate with aluminum sulfate. In this case, MOR was not formed on the glass plate; this could be due to the dissolution of glass, because the surface of the glass plate became dim after dipping it in the aluminosilicate gel. Similarly, it is supposed that when the water content of the dry gel is high, alumina is probably easily dissolved into the gel layer from the support. A higher water content in the dry gel makes dissolution of the alumina support easier. In such a case, the interaction between the gel layer and the support would play an important role in the crystallization process.

3.4. *Preferentially oriented MFI membrane*

The MFI layers prepared using sodium aluminate or aluminum sulfate have a completely different morphology, as shown in Fig. 3. It is probable that the chemical and/or the mechanical structure of zeolites largely depend on those of their parent dry gel in the VPT method. SEM images of dry gels prepared using these alumina sources are shown in Fig. 5. The dry gel layer from aluminum sulfate was created by the accumulation of gel particles having diameters of ca. 1–5 μm (Fig. 5(a)). The cross-sectional view (Fig. 5(b)) shows that there are many voids as in the resultant zeolite layer (Fig. 3(b)). On the other hand, the dry gel prepared using sodium aluminate is so dense that primary gel particles cannot be distinguished, as shown in Figs. 5(c) and (d). Such a dense and uniform morphology of the dry gel could allow the growth of large crystals. Prolonged growth along specific crystal axes was probably allowed in this uniform and dense parent dry gel, and thus the anisotropy of the crystal faces was emphasized, leading to the formation of a preferentially oriented MFI layer.

The coordination number of Al cations in these dry gels was determined by means of ^{27}Al MAS NMR. As shown in Fig. 6, two peaks appeared at 50–55 ppm (tetrahedral) and 0 ppm (octahedral) from the dry gel prepared from aluminum sulfate. This shows that all the octahedrally coordinated Al^{3+} ions in aluminum sulfate could not be changed to tetrahedral coordination in the course of gelation. The non-uniformity in the coordination number of the Al^{3+} ions may obstruct polymerization and lead to the formation of smaller gel particles with voids among them. The dry gel obtained from sodium aluminate contained only tetrahedrally coordinated Al^{3+} atoms, as shown in Fig. 6(b). The observed NMR peak width was narrow as compared with the case of aluminum sulfate, suggesting a uniform local coordination environment around Al^{3+} ions. As sodium aluminate gives AlO_2^- ions, which are stable as a tetrahedrally coordinated form, we believe that the Al^{3+} ions can easily form –Al–O–Si– networks while keeping the tetrahedrally coordinated formation. As a result, most of the Al^{3+} ions may be occluded in the gel structure. The uniform coordinated formation of Al^{3+} ions may cause extended gelation to form the uniform gel structure.

Table 4
Effect of support materials on the type of zeolite formed

Support	Dipping temperature (K)		
	276	293	313
Glass plate	FER	FER	
Porous alumina	MOR	MOR + FER	MOR + FER

Silica source: colloidal silica; Al_2O_3 source: $Al_2(SO_4)_3$, $Na_2O:SiO_2:Al_2O_3 = 10.6:22.9:1$; drying condition: 293 K for one day.

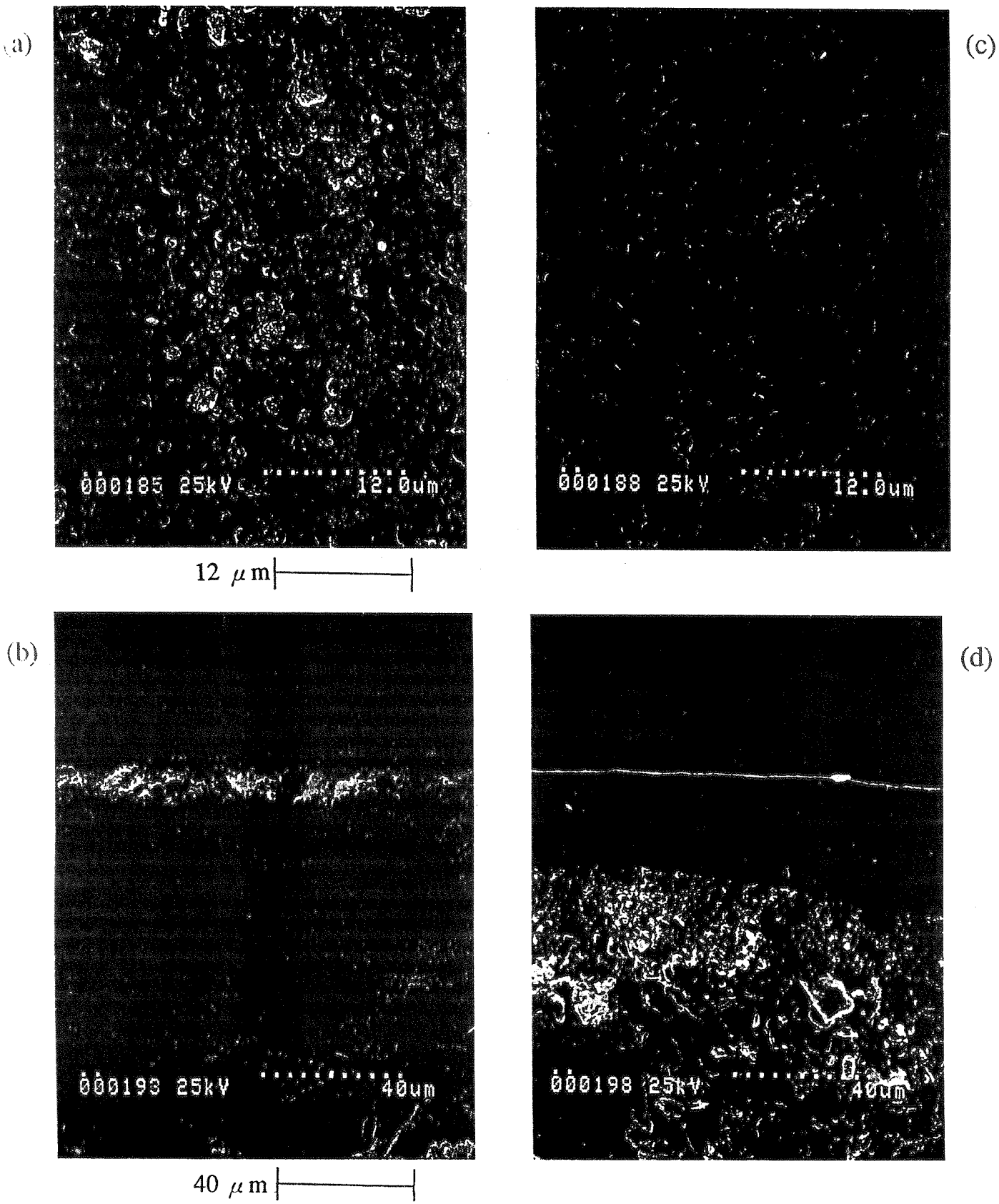

Fig. 5. SEM images for the dry gels. Al_2O_3 source: top view (a) $Al_2(SO_4)_3$, (c) $NaAlO_2$; cross-sectional view (b) $Al_2(SO_4)_3$, (d) $NaAlO_2$.

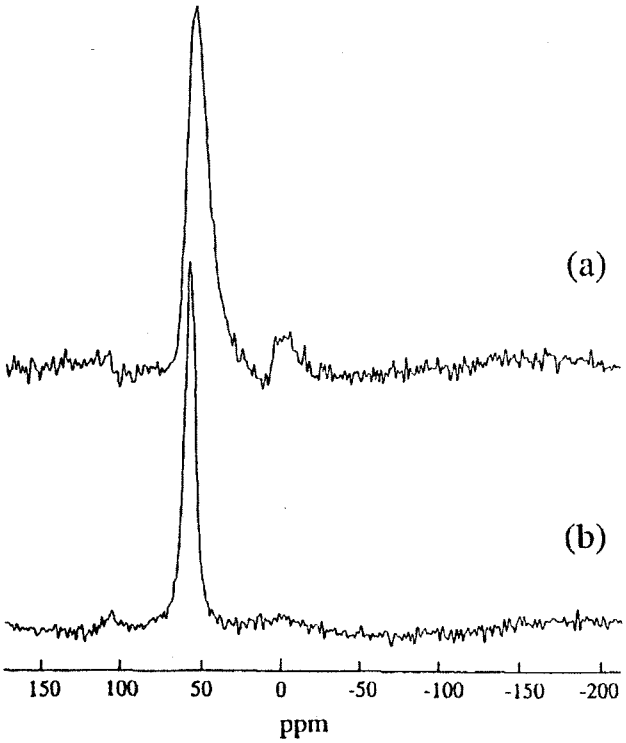

Fig. 6. ^{27}Al MAS NMR spectra for dry gels. The chemical shift was calibrated by using aqueous 1 N $Al_2(SO_4)_3$. Al_2O_3 source: (a) $Al_2(SO_4)_3$, (b) $NaAlO_2$.

4. Conclusions

(1) When the dipping temperature of the porous alumina support and/or the drying temperature and the time of the aluminosilicate gel on the support were varied, MOR, FER and MFI were synthesized from the same composition material.

(2) When sodium aluminate was used as the alumina source, a preferentially oriented MFI layer was formed on a porous alumina plate.

References

[1] T. Sano, Y. Kiyozumi, M. Kawamura, F. Mizukami, H. Takaya, T. Mouri, W. Inaoka, Y. Toida, M. Watanabe, K. Toyoda, Zeolites 11 (1991) 842.
[2] J.G. Tsikoyiannis, W.O. Haag, Zeolites 12 (1992) 126.
[3] T. Sano, F. Mizukami, H. Takaya, T. Mouri, M. Watanabe, Bull. Chem. Soc. Jpn. 65 (1992) 146.
[4] Y. Yan, M. Tsapatsis, G.R. Gavalas, M.E. Davis, J. Chem. Soc., Chem. Commun. (1995) 227.
[5] Y. Yan, M.E. Davis, G.R. Gavalas, Ind. Eng. Chem. Res. 34 (1995) 1652.
[6] M.-D. Jia, B. Chen, R.D. Noble, J.L. Falconer, J. Membrane Sci. 90 (1994) 1.
[7] C. Bai, M.-D. Jia, J.L. Falconer, R.D. Noble, J. Membrane Sci. 105 (1995) 79.
[8] E.R. Geus, H. van Bekkum, W.J.W. Bakker, J.A. Moulijn, Microporous Mater. 1 (1993) 131.
[9] M. Matsukata, N. Nishiyama, K. Ueyama, Stud. Surf. Sci. Catal. 84 (1994) 1183.
[10] W. Xu, J. Dong, J. Li, J. Li, F. Wu, J. Chem. Soc., Chem. Commun. (1990) 755.
[11] J. Dong, T. Dou, X. Zhao, L. Gao, J. Chem. Soc., Chem. Commun. (1992) 1056.
[12] M.H. Kim, H.X. Li, M.E. Davis, Microporous Mater. 1 (1993) 191.
[13] M. Matsukata, N. Nishiyama, K. Ueyama, Microporous Mater. 7 (1996) 109.
[14] Y. Kiyozumi, K. Maeda, F. Mizukami, Stud. Surf. Sci. Catal. 98 (1994) 278.
[15] J. C. Jansen, W. Nugroho, H. van Bekkum, in: Proceedings of the Ninth International Zeolite Conference, Montreal, 1992, R. van Ballmoos, J.B. Higgins and M.M.J. Treacy, eds., Butterworth-Heinemann, Oxford, p. 247.

Gas Permeation through Zeolite-Alumina Composite Membranes

Norikazu Nishiyama, Korekazu Ueyama, and Masahiko Matsukata
Dept. of Chemical Engineering, Osaka University, Osaka 560, Japan

Mordenite (MOR) and ferrierite (FER) membranes without any pinhole and crack were synthesized by a vapor-phase transport method. The permeance of H_2, He, CH_4, N_2, O_2 and CO_2 was determined at 290–400 K, which showed minimum with increasing temperatures for most cases. In the parallel diffusion model was proposed, molecules adsorbed in a micropore are assumed to diffuse in parallel through the central region of the pore and along the wall region of the pore. This parallel diffusion model accounts for the effect of pore size of MOR and FER on the permeation and expresses the experimental data well. The interaction between gas molecules and pore walls are evaluated for each gas.

Introduction

Much attention has been paid to inorganic membranes having molecular sieving properties for gas separation and membrane reactors due to their high thermal resistance, chemical inertness, and high mechanical strength. Zeolites are very promising materials for such molecular sieving membranes because of their unique pore sizes.

In most researches on zeolitic membranes, ZSM-5 (MFI) membranes have been synthesized by conventional hydrothermal synthesis. Tsikoyiannis and Hagg (1992) synthesized a self-supporting MFI membrane on a Teflon slab. However, for the lack of its mechanical strength, porous materials have been used to support a thin layer of zeolite (Geus et al., 1992, 1993; Yan et al., 1995; Sano et al., 1994).

Permeation measurements of single-component gas including inorganic gases and light hydrocarbons such as *n*-butane and *i*-butane through MFI membranes have previously been studied. Jia et al. (1993) reported that the permeance ratio as high as 6.2 for *n*-butane over *i*-butane through an MFI membrane was obtained. The results from several other groups also show higher permeances of *n*-butane than that of *i*-butane. Yan et al. (1995) synthesized defect-free MFI membranes on a porous α-alumina support and observed good permeation selectivities for butane isomers: the permeability ratio of *n*-butane to *i*-butane was 18 to 303 K. Transient gas permeation measurements were performed by Geus et al. (1993) for CH_4, *n*-butane, neon, *i*-butane at room temperature. Those values were in the following order: CH_4 > *n*-butane > neon > *i*-butane. In particular, they found that the permeance ratio of *n*-butane to *i*-butane was as high as 64 at 298 K.

The permeation tests for a mixed gas through zeolitic membranes have been performed using a Wicke-Kallenbach cell. Tsikoyiannis and Hagg (1992) studied the permeances for three binary mixtures (O_2/N_2, H_2/CO_2, and *n*-hexane/2,2-dimethylbutane) through self-supporting MFI membranes at 296 and 322 K. The observed selectivity for an *n*-hexane/2,2-dimethylbutane mixture was 17.2, much higher than that in the Knudsen region, 1. Bai et al. (1995) reported that the separation selectivities for H_2/SF_6 and H_2/*i*-butane were 12.8 and 11.9, respectively, at 583 K, and were significantly greater than those predicted from the Knudsen diffusion mechanism. Geus et al. (1993) studied the permeation behavior of the 50/50 methane/*n*-butane mixture with elevating temperature. *n*-Butane, which was preferentially adsorbed at lower temperatures, was desorbed with increasing temperature, and methane started to permeate at a higher temperature. Similar trends have been found for H_2/*n*-butane mixture (Kapteijn et al., 1995). The H_2 permeation flux at a steady state was reduced by a factor of more than 100 compared with that for a single-component measurement, while the *n*-butane flux remained unaltered, indicating that the permeation behavior of *n*-butane was hardly affected by the permeation of H_2.

Shah et al. (1993) and Sun et al. (1996) fabricated MFI (Al-free) membranes by embedding a large ($300 \times 100 \times 100$

Correspondence concerning this article should be addressed to M. Matsukata, who is currently at the Dept. of Applied Chemistry, Waseda University, Tokyo 169, Japan.

μm) single MFI crystal in an epoxy resin to measure the transport rates of C_1–C_4 and aromatic hydrocarbons in an MFI crystal. The diffusivities of both *n*-butane and *i*-butane in MFI crystals were determined as about 10^{-12} $m^2 \cdot s^{-1}$. Lewis et al. (1997) synthesized large single crystals of pure-silica ferrierite (FER) ($600 \times 500 \times 20$ μm). They mounted the FER crystal so that only the ten-membered or eight-membered ring channels are accessible for gas permeation. Methane, *n*-butane, and *i*-butane were used for the gas permeation tests. They showed that the ten-membered ring channel was permeable to these three kinds of the gases, but the eight-membered ring channel was permeable to only methane.

Recently, a novel synthetic method, vapor-phase transport (VPT), has developed for crystallization of zeolite powders and zeolitic membranes. In the VPT method, zeolites are crystallized from dry aluminosilicate gels under vapors of organic templates and/or water. Xu et al. (1990) have first synthesized MFI powders by the VPT method. Kim et al. (1993) and Matsukata et al. (1993) showed that various kinds of zeolites can by synthesized by the VPT method.

We have applied the VPT method to synthesize zeolitic membranes composed of FER (Matsukata et al., 1994a), mordenite (MOR) (Nishiyama et al., 1995, 1996), and a mixture of FER and MFI (Matsukata et al., 1994b) on a porous alumina support. Yan et al. (1995) postulated that a defect-free zeolitic membrane is possible to be synthesized hydrothermally by the intergrowth of crystals formed on the surface of support. On the other hand, we have proposed that a defect-free zeolitic membrane can be obtained when a compact composite layer consisting of zeolite crystals and a porous support is formed (Nishiyama et al., 1996).

In this study, we synthesized defect-free MOR and FER membranes on a porous alumina support by the VPT method. The dimension of the main channel of MOR (0.65×0.70 nm) is larger than that of FER (0.42×0.54 nm). Permeation tests of gases were carried out using these zeolitic membranes. We shall propose a parallel diffusion model and analyze the temperature dependence of permeances for gases. The effect of the pore size on permeation properties was discussed using the diffusion model.

Experimental Studies

Preparation of MOR and FER membranes

Preparation of Dry Gel on Porous Alumina Support. MOR and FER membranes with an effective membrane area of 2 cm^2 were synthesized from different types of parent gels. Both types of parent gel were prepared at room temperature. For the synthesis of the MOR membrane, colloidal silica containing 30.3 wt. % of SiO_2 and 0.42 wt. % of Na_2O (ST-S; Nissan Chem. Ind.) was used as silica source. Aluminum sulfate anhydride, $Al_2(SO_4)_3$, (Wako Pure Chem. Ind. Co.) was used as the alumina source. A NaOH solution was added to colloidal silica to adjust the pH of gel. The resultant gel was mixed with an $Al_2(SO_4)_3$ aqueous solution. The composition of the parent gel was $10Na_2O$: Al_2O_3: 25 SiO_2: 700 H_2O. A porous alumina plate with an average pore diameter of 0.1 μm (Nihon Gaishi Co.) was used as support. The support was dipped in the parent gel for 1 day and dried for 2 h at 363 K.

For the synthesis of the FER membrane, the parent gel was prepared in the same procedure as that described above, except for using different source materials. Sodium silicate solution containing 35–38 wt. % of SiO_2 and 17–19 wt. % of Na_2O (Kanto Chem. Co.) and concentrated H_2SO_4 were used as the silica source and pH adjustment agent, respectively. The composition of the gel was $12Na_2O$: Al_2O_3: 25 SiO_2: 700 H_2O. The surface of the support was treated with colloidal silica at the pH of about 10 to depress the dissolution of alumina from the support (Nishiyama et al., 1996). The treated support was dipped in the parent gel. By evacuating the support from one side, the gel was forced to penetrate into the pores of the alumina support.

Crystallization. A mixture of triethylamine(Et_3N), ethylenediamine(EDA) and water was poured into the bottom of an autoclave as the vapor source. The composition was 1.5 Et_3N: EDA: 3.0 H_2O. The porous alumina support coated with aluminosilicate dry gel was set in the autoclave. The gel was crystallized in the mixed vapors of Et_3N, EDA and water under autogeneous pressure at 453 K for 4 days. The membranes were rinsed with deionized water and dried at 363 K overnight. An as-synthesized membrane was calcined at 773 K for 4 h. We adopted 0.1 $K \cdot min^{-1}$ of the heating rate at the temperature range 473–773 K. Products were characterized by X-ray diffraction (XRD) and scanning electron microscope (SEM).

Evaluation of the compactness of zeolitic membranes

The compactness of the products was checked by the permeation of 1,3,5-triisopropylbenzene (TIPB) at room temperature. The zeolitic membrane, attached on an end of a stainless-tube with a cross-sectional area of 2.2 cm^2, was placed in liquid TIPB. The permeation side was kept under vacuum. The permeant was collected for 10 h in a cold trap using liquid nitrogen. After that, we put 3–5 cm^3 of methanol and 6.1×10^{-6} mol of *n*-octane into the trap. Methanol was used as a solvent and *n*-octane as a standard material. We injected 4 μL of the mixture into a gas chromatograph. We assumed that peak areas less than five counts cannot be detected on an integrator. Then, the minimum detectable flux was determined as 1×10^{-9} $mol \cdot m^{-2} \cdot s^{-1}$ under our experimental conditions.

Gas permeation test

The permeances of H_2, He, CH_4, N_2, O_2 and CO_2 through the zeolitic membranes were determined. The pressure difference between the feed and permeate sides was kept at 0.2 MPa. The permeation side was set at an atmospheric pressure. The permeation rates of gases through the zeolitic membranes were measured at 290–400 K. The experimental apparatus for the gas permeation tests was shown by Matsukata et al. (1994a).

Results and Discussion

Figure 1 shows the XRD patterns from MOR and FER membranes. These patterns were similar to those from common powder MOR and FER, respectively, indicating that randomly-oriented polycrystalline MOR and FER were formed on the alumina support.

The pervaporation of TIPB, which has a kinetic diameter

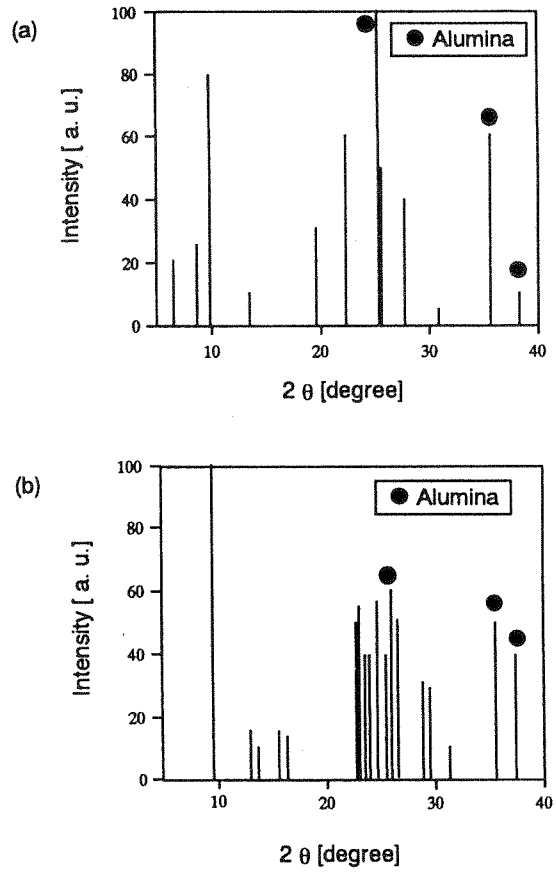

Figure 1. XRD patterns for (a) MOR and (b) FER membranes.

(0.85 nm) greater than the pore dimensions of MOR and FER, was carried out. No permeation of TIPB was detected through both zeolitic membranes. The minimum detectable flux was 1×10^{-9} mol·m^{-2}·s^{-1} under our experimental conditions as described above. These zeolitic membranes were practically defect-free.

We performed the permeation tests of benzene before and after the permeation test of TIPB. The flux of benzene after the permeation test of TIPB was 7×10^{-5} mol·s^{-1}·m^{-2} and almost the same as that before the permeation test of TIPB. No TIPB was detected in the later permeation test of benzene. Thus, we concluded that no TIPB existed in the micropore of FER. In addition, the TIPB adsorbed around the entrance of micropore could easily be substituted by benzene. Therefore, there clearly existed no pinhole and no crack, which would allow the entrance of TIPB into the FER membrane.

Figure 2 shows the SEM images of the cross-sectional views for the MOR and FER membranes. A composite layer consisting of porous alumina and zeolite was clearly formed. Voids among the MOR or FER crystals on the porous alumina support were observed in the SEM images for both membrane surfaces. We thus believe that the zeolite-alumina composite layer is compact. The thickness of the composite layer was about 20 μm for the MOR membrane and 40 μm for the FER membrane. A detailed discussion on the structure of these zeolite-alumina composite layer will be reported in the near future.

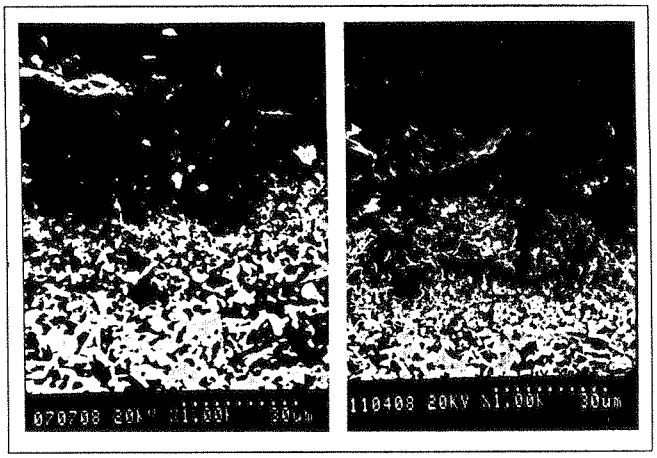

Figure 2. SEM images of the cross-sectional views of (a) MOR and (b) FER membranes.

Figure 3 shows the permeances of H_2, He, CH_4, N_2, O_2 and CO_2 through the MOR and FER membranes in the temperature range from 290 to 400 K. Judging from the results of the permeation tests of TIPB, we concluded that these gases permeated through the micropores of zeolite. The permeance of each gas through the MOR membrane was about 100 times greater than those through that of FER. This is due presumably to the pore diameter of MOR larger than that of FER, since the thickness of the compact layer in the MOR membrane was almost comparable to that of FER as described above.

The permeances of H_2, He and CH_4 through the MOR membrane monotonously increased with increasing temperature, indicating that the controlling mechanism of permeation did not change in this temperature range. This temperature dependence of the permeances is evidently caused by the activated diffusion. The permeances of gases through the MOR and FER membranes, except for H_2, He, and CH_4 through the MOR membrane, showed minimums with increasing temperature, suggesting that a different controlling mechanism should be taken into consideration.

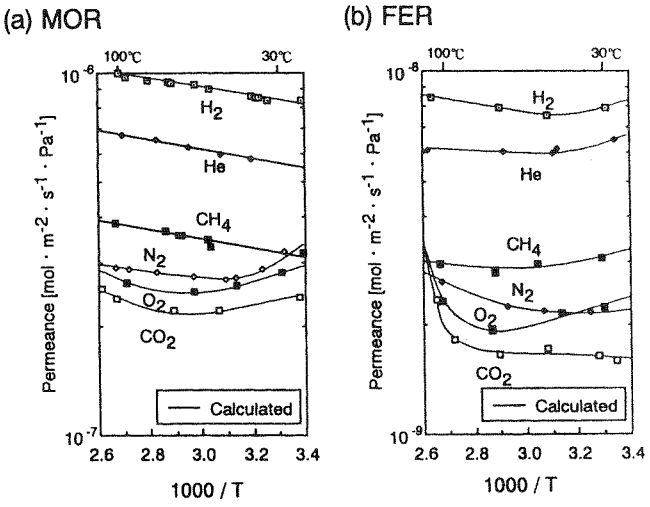

Figure 3. Permeances of single gases through (a) MOR and (b) FER membranes.

At higher temperatures, the temperature dependency of the permeances of all gases through both membranes indicated that the activated diffusion mechanism governed permeation: the interaction between molecules and pore wall played dominant role of permeation. It can be said that at lower temperatures the molecule-pore wall interaction significantly contributed to permeation mechanism. Therefore, we excluded the contribution of Knudsen diffusion mechanism.

Analysis of the permeance through the membranes

Barrer (1990, 1991) first discussed the permeation through a zeolitic membrane. His theory was based on the assumption that the entry of molecules into the membrane and their escape from there proceed via an externally adsorbed layer, which is called the interface process. He concluded that the contribution of the interface processes to the steady flow through zeolitic membrane would become less significant with increasing temperature and membrane thickness. On the basis of his theory, the role of the interface processes would be negligibly small at room temperature if the membrane thickness is greater than 1 μm, indicating that the rate-limiting process of the permeation through zeolitic membranes is the intracrystalline diffusion in the micropores of zeolite under our experimental conditions.

Shelekhin et al. (1995) modeled the single gas permeation through the molecular-sieve glass membranes. In their model, the total concentration of gas molecules inside the membrane is the sum of the gas-phase and adsorbed-phase concentrations. They concluded that the effect of the adsorbed diffusant on the total flow is significant for highly adsorbable gas.

Shelekhin's approach and the simple Fick formulation considering the concentration dependence of diffusivity cannot account for the appearance of the minimum permeances through the MOR and FER membranes. To explain the temperature dependence, the micropores of zeolite should be considered as the energetically heterogeneous surface. Seidel and Carl (1989) and Kapoor and Yang (1989) assumed that the surface consists of parallel paths such that each path has uniform, but different, energy, and surface diffusion occurs along these parallel paths. Their parallel-paths assumption contains a continuous energy distribution. Their parallel paths conception is, however, rather complicated. Actually, molecules in the micropore collide with each other and with the wall of the micropore as depicted in Figure 4a. We consider two parallel paths in the micropores in our simplified parallel diffusion model as depicted in Figure 4b. The molecules adsorbed in the micropore diffuse in parallel through the central region of a pore and along the wall region of a pore. In other words, there are two types of molecules with different adsorption energies and activation energies of diffusion in the micropores.

We assumed that the adsorption equilibrium between the center and wall region of the pores is always accomplished and that the movement of molecules between the center and wall regions of the pores is very rapid and that in the direction parallel to zeolite pores is relatively slow. The ratio of the numbers of molecules diffusing through each path expresses the probability of the existence of molecules in each path.

Furukawa and Nitta (1997) have recently studied gas permeation through nanoporous carbon membranes by nonequilibrium molecular dynamics. They showed the snapshots in simulation cell for ethane in the pore of four different pore widths. According to their snapshots, most of molecules in the broad pore diffused near the wall. However, in narrower pore of carbon, the number of the molecules diffusing around the center of pore became increased, suggesting that a parallel diffusion possibly occurs in the micropores of zeolites for small molecules. Their results strongly support that the parallel diffusion model is a reasonable concept.

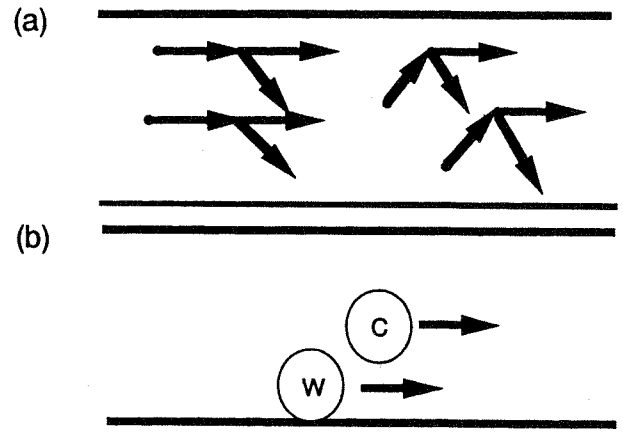

Figure 4. Parallel diffusion model.

Based on Barrer (1990)'s discussion, we assumed that the rate-limiting process of permeation through a zeolitic membrane is intracrystalline diffusion. The diffusive flux is generally written as

$$J = -D_F\frac{dC}{dx} = -D\frac{d\ln p}{d\ln C}\frac{dC}{dx} = -D\frac{d\ln p}{d\ln C}\frac{dC}{dp}\frac{dp}{dx}. \quad (1)$$

In this case, the adsorption equilibrium at the interface between the gas phase and membrane is accomplished. If gas adsorption on a zeolitic membrane at temperatures higher than room temperature is assumed to follow Henry's law, the derivatives are

$$\frac{d\ln p}{d\ln C} = 1, \quad \frac{dC}{dp} = \frac{K_H}{RT} = \frac{K_{H0}}{RT}\exp\left(\frac{q_{st}}{RT}\right) \quad (2)$$

where K_H and q_{st} represent Henry's constant and isosteric heat of adsorption, respectively. This model does not consider molecule-molecule interaction but wall-molecule interaction, because the low concentration (Henry law) region is assumed here. Diffusivity in activated process can be written as

$$D = D_0\exp\left(\frac{-E}{RT}\right) \quad (3)$$

where D and E represent diffusivity and activation energy of diffusion, respectively. By introducing Eqs. 2 and 3 into Eq. 1, we obtain

$$J = -\frac{D_0K_{H0}}{RT}\exp\left(\frac{q_{st}-E}{RT}\right)\frac{dp}{dx}. \quad (4)$$

At the steady state,

$$\frac{dJ}{dx}=0, \quad \text{then} \quad \frac{dp}{dx}=\frac{\Delta p}{d} \tag{5}$$

where Δp represents the pressure difference. The permeance through a zeolitic membrane is, then, expressed as

$$P=-\frac{\theta}{\tau d}\frac{D_0K_{H0}}{RT}\exp\left(\frac{q_{st}-E}{RT}\right). \tag{6}$$

Here, a parallel diffusion mechanism is applied to Eq. 6. The molecules adsorbed in the micropore diffuse in parallel through the central region of a pore and along the wall region of a pore. The permeance is expressed as the sum of both contributions:

$$P=-\frac{\theta}{\tau d}\sum_{i=c,w}\frac{D_{0,i}K_{H0,i}}{RT}\exp\left(\frac{q_{st,i}-E_i}{RT}\right). \tag{7}$$

Suffixes, c and w, correspond to the diffusion through the central region of a pore and along the wall region of the pore, respectively.

We considered that both types of diffusion contributed to the permeation of gases under these experimental conditions, except for the permeation of H_2, He and CH_4 through the MOR membrane. The parameter fitting was carried out using Eq. 7 on the assumption that molecules dominantly diffuse through the central region at higher temperatures and along the wall region at lower temperatures. The parameter fitting contains a set of two adjustable parameters, $\epsilon D_0K_{H0}/\tau d$ and $q-E$, for each path. Solid lines in Figure 3 represent the values calculated from Eq. 7. The proposed parallel diffusion model expresses the experimental data well.

Based on the calculated results, we separated the permeance, P, into two types of mass transportation through the central region of a pore, P_C, and along the wall region of a pore, P_W, where $P=P_C+P_W$. Figure 5 shows the temperature dependence of P_C, P_W and P calculated for He and CO_2 through the FER membrane, suggesting that the diffusion along the wall region of the FER pore cannot be ignored even for the permeation of He. The adsorbable gas, CO_2, diffuses dominantly along the pore wall at room temperature for the FER membrane.

Figure 6 shows the ratios of P_W to P for each gas. The diffusants along the wall region were more dominant through the FER membrane compared with those through the MOR membrane. This seems reasonable because the interaction between molecules and a pore wall should become more significant in a narrower pore. In the MOR membrane, H_2, He and CH_4 exclusively diffused through the central region of the pore. In other words, the interaction between molecules and the pore wall of MOR was not strong enough to make the diffusion along the pore wall remarkable. For both membranes, the values of P_W/P for CO_2 were greater than any other gas and those for He were the smallest. These results imply that the parallel diffusion model can account for the effect of the interaction between molecules and a pore wall.

One can note that the permeation behavior depends clearly on not only the pore size of zeolites but also the SiO_2/Al_2O_3 ratio of zeolites. Sun et al. (1996) used a membrane made of a large single crystal of pure-silica MFI with a size of $100\times100\times300$ μm for the single-gas permeation tests of methane, ethane, propane and butane. The permeances of these gases through a single-crystal of MFI increased with increasing temperature in the temperature range 303–343 K. Lewis et

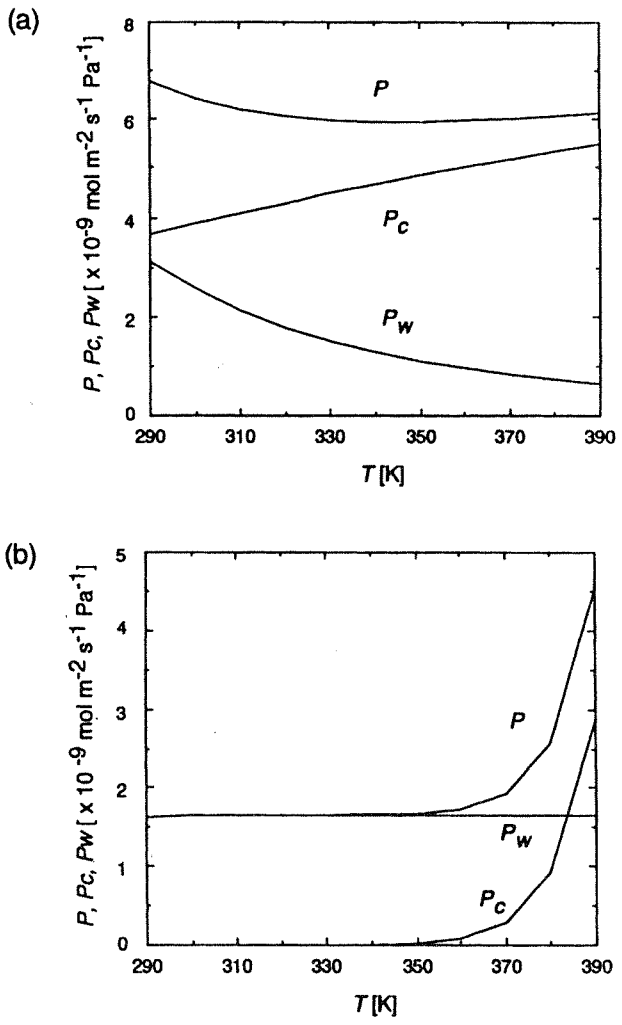

Figure 5. P, P_c, and P_w for (a) He and (b) CO_2 through FER membrane.

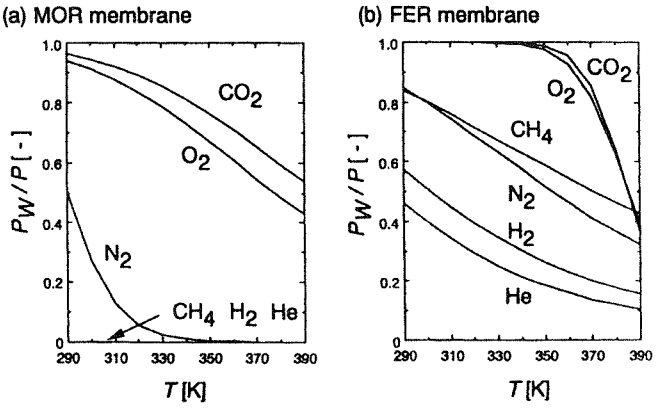

Figure 6. Temperature dependence of P_w/P.

Table 1. $(q_{st} - E)$ and $(\epsilon D_0 K_{HO}/\tau d)$ for MOR and FER Membranes

		$q_{st,c} - E_c$ [kJ·mol^{-1}]	$\epsilon D_{0,c} K_{H0,c}/\tau d$ [m·s^{-1}]	$q_{st,w} - E_w$ [kJ·mol^{-1}]	$\epsilon D_{0,w} K_{H0,w}/\tau d$ [m·s^{-1}]
MOR	H_2	−5.1	1.9×10^{-3}		
	He	−5.5	1.5×10^{-3}		
	CH_4	−5.0	7.1×10^{-4}		
	N_2	−6.6	5.7×10^{-4}	34	5.3×10^{-17}
	O_2	−23	8.8×10^{-2}	4.9	1.1×10^{-5}
	CO_2	−27	1.9×10^{-1}	2.1	2.9×10^{-5}
FER	H_2	−9.8	5.9×10^{-5}	8.9	3.4×10^{-8}
	He	−6.6	1.6×10^{-5}	12	6.3×10^{-9}
	CH_4	−14	5.0×10^{-5}	4.2	1.4×10^{-7}
	N_2	−19	2.6×10^{-4}	3.9	1.1×10^{-7}
	O_2	−110	3.8×10^{9}	0.7	5.2×10^{-7}
	CO_2	−140	1.6×10^{13}	−2.8	1.5×10^{-6}

al. (1997) also carried out single-gas permeation tests of methane using a membrane made of a single crystal of pure-silica FER ($600\times500\times20$ μm). The permeances of methane through the pure-silica FER membrane increased with increasing temperature in the temperature range 323–398 K.

Through pure-silica zeolite membranes, the diffusants in central region of the pore should be dominant compared with those through Al-containing zeolite membranes. Thus, minimum permeances should appear at lower temperatures for pure-silica zeolite membranes.

Table 1 summarizes the fitting parameters, $(q_{st,i} - E_i)$ and $\epsilon D_0/\tau d K_{H0}$. All the values of $(q_{st,w} - E_w)$ were much greater than those of $(q_{st,c} - E_c)$: the values of $(q_{st,w} - q_{st,c})$ were much greater than those of $(E_W - E_C)$. This result suggests that the activation energies of diffusion along the pore wall, E_W, are not much greater than those through the central region of pore, E_C, although there are large differences in the heats of adsorption between molecules on the pore wall, q_{stw}, and in the central region, q_{stc}. The value of $(q_{st,c} - E_C)$ for CO_2 was much less than that of any other gas for both MOR and FER membranes, possibly suggesting that the activation energy, E_C, of CO_2 was much greater than those for other gases.

Conclusions

The permeances of H_2, He, CH_4, N_2, O_2 and CO_2 through defect-free MOR and FER membranes were determined at 290–400 K. The temperature dependencies of the permeances were analyzed using a parallel diffusion model in which the permeance was separated into two contributions, molecules diffusing through the central region of the pore and along the wall region of the pore. The contribution of the diffusion at the wall region to the total permeation decreased with increasing temperature. The effect of diffusion along the pore wall on the total permeation was significant for adsorbable gas-like CO_2. In contrast, the diffusion through the central region of the pore was dominant for He. The molecules, which diffuse along the pore wall, were more dominant through the FER membrane compared with those through the MOR membrane, indicating that the effect of difference in the pore size between MOR and FER appeared. The proposed parallel diffusion model is useful for analyzing the interaction between gas molecules and a pore wall.

Acknowledgments

This study was supported partly by the grants-in-aid for Encouragement of Young Scientists (No. 07750850) and Scientific Research on Priority Areas (No. 07242250), the Ministry of Education, Science, Sports and Culture and by Mikiya Foundation.

Notation

C = concentration of molecule in membrane, mol·m^{-3}
D_F = Fickian diffusivity, m^2·s^{-1}
D = intrinsic diffusivity, m^2·s^{-1}
d = membrane thickness, m
E = activation energy, J·mol^{-1}
J = flux, mol·m^{-2}·s^{-1}
K_H = Henry's constant
p = pressure, Pa
Δp = pressure difference, Pa
P = permeance, mol·m^{-2}·s^{-1}·Pa^{-1}
q_{st} = isosteric heat of adsorption, J·mol^{-1}
R = gas constant, 8.314 J·mol^{-1}·K^{-1}
T = temperature, K
x = direction coordinate, m
θ = porosity of membrane
τ = tortuosity of membrane

Subscripts

c = center of pore
i = c or w
w = wall of pore
0 = constant

Literature Cited

Bai, C., M.-D. Jia, J. L. Falconer, and R. D. Noble, "Preparation and Separation Properties of Silicalite Composite Membranes," *J. Memb. Sci.*, **105**, 79 (1995).

Barrer, R. M., "Porous Crystal Membrane," *J. Chem. Soc. Farad. Trans.*, **86**, 1123 (1990).

Barrer, R. M., "Zeolite as Membrane: The Role of the Gas-Crystal Interface," *Stud. Surf. Sci. Catal.*, **65**, 257 (1991).

Furukawa, S., and T. Nitta, "Computer Simulation Studies on Gas Permeation through Nanoporous Carbon Membranes by Non-equilibrium Molecular Dynamics," *J. Chem. Eng. Japan*, **30**, 116 (1997).

Geus, E. D., M. J. Exter, and H. van Bekkum, "Synthesis and Characterization of Zeolite (MFI) Membranes on Porous Ceramic Supports," *J. Chem. Soc. Farad. Trans.*, **88**, 3101 (1992).

Geus, E. D., H. van Bekkum, W. J. W. Bakker, and J. A. Moulijin, "High-Temperature Stainless Steel Supported Zeolite (MFI) Membranes: Preparation, Module Construction, and Permeation Experiments," *Microporous Mater.*, **1**, 131 (1993).

Jia, M.-D., K.-V. Peinemann, and R.-D. Behling, "Ceramic Zeolite Composite Membranes: Preparation, Characterization and Gas Permeation," *J. Memb. Sci.*, **82**, 15 (1993).

Jia, M. D., B. Chen, R. D. Noble, and J. L. Falconer, "Ceramic-Zeolite Composite Membranes and Their Application for Separation of Vapor/Gas Mixtures," *J. Memb. Sci.*, **90**, 1 (1994).

Kapoor, A., and R. T. Yang, "Surface Diffusion on Energetically Heterogeneous Surfaces," *AIChE J.*, **35**, 1735 (1989).

Kapteijn, F., W. J. W. Bakker, J. van de Graaf, G. Zheng, J. Poppe, and J. A. Moulijn, "Permeation and Separation Behavior of a Silicalite: 1. Membrane," *Catal. Today*, **25**, 213 (1995).

Kim, M. H., H. X. Li, and M. E. Davis, "Synthesis of Zeolites by Water-Organic Vapor-Phase Transport," *Microporous Mater.*, **1**, 191 (1993).
Lewis, J. E., Jr., G. R. Gavalas, and M. E. Davis, "Permeation Studies on Oriented Single-Crystal Ferrierite Membranes," *AIChE J.*, **43**, 83 (1997).
Matsukata, M., N. Nishiyama, and K. Ueyama, "Synthesis of Zeolite under Vapor Atmosphere: Effect of synthetic conditions on zeolite structure," *Microporous Mater.*, **1**, 219 (1993).
Matsukata, M., N. Nishiyama, and K. Ueyama, "Preparation of a Thin Zeolite Membrane," *Stud. Surf. Sci. Catal.*, **84**, 1184 (1994).
Matsukata, M., N Nishiyama, and K. Ueyama, "Zeolitic Membrane Synthesized on a Porous Alumina Support," *J. Chem. Soc. Chem. Commun.*, 339 (1994).
Nishiyama, N., K. Ueyama, and M. Matsukata, "A Defect-free Mordenite Membrane Synthesized by Vapor-Phase Transport Method," *J. Chem. Soc. Chem. Commun.*, 1967 (1995).
Nishiyama, N., K. Ueyama, and M. Matsukata, "Synthesis of Defect-free Zeolite-Alumina Composite Membranes by a Vapor-Phase Transport Method," *Microporous Mater.*, in press (1997).
Sano, T., H. Yanagisita, Y. Kiyozumi, F. Mizukami, and K. Haraya, "Separation of Ethanol/Water Mixture by Silicalite Membrane on Pervaporation," *J. Memb. Sci.*, **95**, 221 (1994).
Seidel, A., and P. S. Carl, "The Concentration Dependence of Surface Diffusion for Adsorption on Energetically Heterogeneous Adsorbents," *Chem. Eng. Sci.*, **44**, 189 (1989).
Shah, D. B., S. Chokchal-acha, and D. T. Hayhurst, "Measurement of Transport Rates of C_4 Hydrocarbons across a Single-Crystal Silicalite Membrane," *J. Chem. Soc., Farad. Trans.*, **89**, 3161 (1993).
Shelekhin, A. B., A. G. Dixon, and Y. H. Ma, "Theory of Gas Diffusion and Permeation in Inorganic Molecular-Sieve Membranes," *AIChE J.*, **41**, 58 (1995).
Sun, M. S., O. Taru, and D. B. Shah, "Diffusion Measurements through Embedded Zeolite Crystals," *AIChE J.*, **42**, 3001 (1996).
Tsikoyiannis, J. G., and W. O. Hagg, "Synthesis and Characterization of a Pure Zeolitic Membrane," *Zeolites*, **12**, 126 (1992).
Xu, W., J. Dong, J. Li, J. Li, and F. Wu, "A Novel Method for the Preparation of Zeolite ZSM-5," *J. Chem. Soc. Chem. Commun.*, 755 (1990).
Yan, Y., M. E. Davis, and G. R. Gavalas, "Preparation of Zeolite ZSM-5 Membranes by *in-situ* Crystallization on Porous α-Al_2O_3," *Ind. Eng. Chem. Res.*, **34**, 1652 (1995).

Manuscript received Oct. 28, 1996, and revision received Sept. 8, 1997.

ELSEVIER

Microporous Materials 12 (1997) 293–303

MICROPOROUS
MATERIALS

FER membrane synthesized by a vapor-phase transport method: its structure and separation characteristics

Norikazu Nishiyama [a], Takaaki Matsufuji [a], Korekazu Ueyama [a], Masahiko Matsukata [b,*]

[a] *Department of Chemical Engineering, Osaka University, 1–3 Machikaneyama-cho, Toyonaka-shi, Osaka 560, Japan*
[b] *Department of Applied Chemistry, Waseda University, 3-4-1 Okubo, Shinjuku-ku, Tokyo 169, Japan*

Received 31 May 1997; accepted 31 July 1997

Abstract

The mechanism of formation of ferrierite (FER) membrane on an alumina support by a vapor-phase transport (VPT) method was studied using XRD, SEM, FE-SEM and EDX. The XRD measurement for a FER membrane after the removal of FER particles formed on the support showed that FER was formed in the pores of the alumina support, namely, a FER-alumina composite layer was formed. The FE-SEM image for the cross-sectional view of the FER-alumina composite layer showed that FER nanocrystals of about 50 nm diameter grew in the pores of the alumina support. Pervaporation tests for benzene/*p*-xylene mixtures were performed at 303 K. Even when the concentration of benzene in the feed solution was extremely small (0.5 mol%), the flux of benzene through the FER membrane was still greater than that of *p*-xylene. Therefore, a separation factor as high as 600 was obtained in the low feed concentration of benzene. Such a high selectivity for the benzene/*p*-xylene mixture suggested that the selectivity for the benzene/*p*-xylene mixture appears at the pore mouths of FER on the feed side of the FER-alumina composite layer. © 1997 Elsevier Science B.V.

Keywords: Ferrierite; Zeolitic membrane; Vapor-phase transport synthesis; Pervaporation

1. Introduction

Zeolites are recognized as attractive materials to prepare inorganic membranes because of their molecular sieving properties, high thermal resistance, chemical inertness and high mechanical strength. Taking into account that zeolites have inherent pore diameter and their physicochemical properties can be modified by ion exchange, fine control of permeability could be expected.

In most researches on zeolitic membranes, ZSM-5 (MFI) membranes have been synthesized by conventional hydrothermal synthesis. Tsikoyiannis and Hagg [1] synthesized a self-supporting MFI membrane on a Teflon slab. Due to the lack of its mechanical strength, however, porous supports have been used for supporting a thin layer of zeolite [2–9].

Another preparation method of zeolites, vapor-phase transport (VPT) method, was developed by Xu *et al.* [10], who synthesized MFI from dry aluminosilicate gels under mixed vapors of ethylenediamine (EDA), triethylamine (Et_3N) and water. Following this work, Kim *et al.* [11] and our previous research [12] confirmed that various types

* Corresponding author. Tel/Fax: +81 3 52863850; e-mail: mmatsu@mn.waseda.ac.jp

PII S0927-6513(97)00076-X

of zeolite such as ferrierite (FER), mordenite (MOR) and analcime (ANA) can be synthesized by the VPT method.

We have recently applied the VPT method to prepare zeolitic membranes on a porous alumina support [13–17]. In these previous studies, zeolitic membranes have been synthesized in two steps: (1) preparation of a dry aluminosilicate gel layer on a porous alumina support by a dip-coating method, and (2) crystallization under vapors of amines and water. One of the advantages of the VPT method is that it seems easy to prepare membranes even on supports which have complicated shapes like honeycombs. In addition, aluminosilicate dry gels can be fully crystallized to zeolite by the VPT method [18]. Namely, zeolites with the same SiO_2/Al_2O_3 ratio as that of the parent gel can be synthesized, although it is difficult to crystallize all Si and Al atoms in the solution by hydrothermal synthesis [19].

We previously synthesized FER and MOR membranes using the VPT method [16]. Both FER and MOR membranes were confirmed to be defect-free because no permeation of 1,3,5-triisopropylbenzene (TIPB) was detected. Although the top layer of these zeolitic membranes synthesized on an alumina support had numerous voids between crystals, continuous layers showing a dark contrast were observed in the SEM images for the cross-sectional views of a zeolitic membranes. These dark contrast continuous layers were believed to be compact tentatively. However, SEM observations do not give conclusive evidence that zeolite crystals formed in the pores of alumina support. In addition, the formation mechanism of a zeolite–alumina composite layer is still open question. The objective of this study is, first, to elucidate the formation mechanism of zeolitic membranes.

Recent studies on separation tests by pervaporation have indicated that zeolitic membranes have high separation potential for a variety of organic/water mixtures including water/ethanol [20–22], water/acetone [23] and water/methylethylketone [24]. It was suggested that separation performance for these mixtures was governed by hydrophilic/hydrophobic nature of zeolites. On the contrary, the separation of aromatic hydrocarbons can be achieved by the shape selectivity of zeolites as well as the interaction between molecules and pore walls of zeolite. However, only a few attempts have been made to date for the separation of aromatic hydrocarbons [25,26]. In the present study, benzene/*p*-xylene mixtures were examined for the pervaporation tests using a FER membrane prepared by the VPT method.

2. Experimental

2.1. Preparation of parent gel

A parent aluminosilicate gel was prepared using sodium silicate solution containing 35–38 wt.% of SiO_2 and 17–19 wt.% of Na_2O (Kanto Chem. Co., Inc.) as a silica source. Aluminum sulfate anhydride, $Al_2(SO_4)_3$, (Wako Pure Chem. Ind. Co., Ltd.) was used as an alumina source. An appropriate amount of conc. H_2SO_4 was added to the sodium silicate solution to adjust the pH of resultant gel. After the silicate gel was mixed with an $Al_2(SO_4)_3$ aqueous solution, the pH of resultant gel was 11.7. The composition of mixture was 25 SiO_2: Al_2O_3: 12 Na_2O.

A porous α-alumina plate (Nihon Gaishi Co., Ltd.) was used as a support. The surface of alumina support was treated with colloidal silica to depress dissolution of alumina in the cource of crystallization [16], unless otherwise mentioned. Two types of dipping method were examined for the preparation of FER membranes. First, the porous alumina support was dipped in a gel for 1 day. Secondly, after the support was dipped in the gel for 1 day, the gel was forced to penetrate into the pores of the alumina support by evacuating the support from one side. Hereafter, the first and second methods are called dipping methods (1) and (2), respectively.

2.2. Crystallization by vapor-phase transport method

The alumina support coated with the aluminosilicate dry gel was set horizontally in an autoclave. The gel was crystallized in the mixed vapors of Et_3N, EDA and water under autogeneous pressure

at 453 K for 4 days. The mixture having a molar ratio of 1 EDA: 2 Et_3N: 2.5 H_2O was used to produce vapor.

An as-synthesized FER membrane was calcined in air at 773 K for 4 h. Heating rate should be as small as possible because a high heating rate probably causes formation of cracks in the FER membrane owing to the difference in the thermal expansivity between FER and α-alumina support. The heating rate of 0.1 K min^{-1} was adopted in the temperature range of 473–773 K.

The structure and crystallinity of the products were determined by X-ray diffraction (XRD) with Cu Kα radiation (Simadzu VD-1 and Philips X's Pert-MRD).

The morphology of product was examined by scanning electron microscopy (SEM) (Hitachi S-800 and S-2250). Field emission SEM (FE-SEM) (Hitachi S-5000L) was also used for characterization.

Concentration profiles for Si and Al in the membrane were taken by an energy-dispersive X-ray (EDX) analyser (Philips, EDAX DX-4) attached to the scanning electron microscope (Hitachi, S-2250N).

2.3. Pervaporation of benzene/p-xylene mixtures

Pervaporation measurements for benzene/*p*-xylene mixtures were performed at 303 K using the FER membrane. The experimental apparatus was previously described [16]. The FER membrane, attached on a stainless tube with a cross-sectional area of 2.2 cm^2, was placed in 200 cm^3 of solution. The permeation side was kept under vacuum. The permeate was collected in the cold trap using liquid nitrogen every 30 min. Steady state fluxes were always obtained after 2 h. The amount of permeate was determined by a gas chromatograph.

Flux and separation factor $\alpha_{(a/b)}$ were calculated from the following equations

$$\text{Flux} = \frac{n}{t \cdot A} \tag{1}$$

$$\alpha(a/b) = \frac{(x_a/x_b)_{\text{permeate}}}{(x_a/x_b)_{\text{feed}}} \tag{2}$$

where n, t, A and x represent permeated amount (mol), time (s), membrane area (m^2) and mole fraction (-), respectively.

3. Results and discussion

3.1. Structure of the FER membrane

The formation mechanism of the FER membrane was studied using FER membranes prepared by the dipping method (1). In order to investigate the growth of FER in the pores of alumina support after crystallization, FER particles formed on the surface of alumina support were removed by polishing with sand paper. Fig. 1(a) and (b) show the XRD patterns for the FER membranes before and after the removal of FER particles on the surface of support, respectively. Fig. 2(a) and (b) show the top views of FER membrane before and

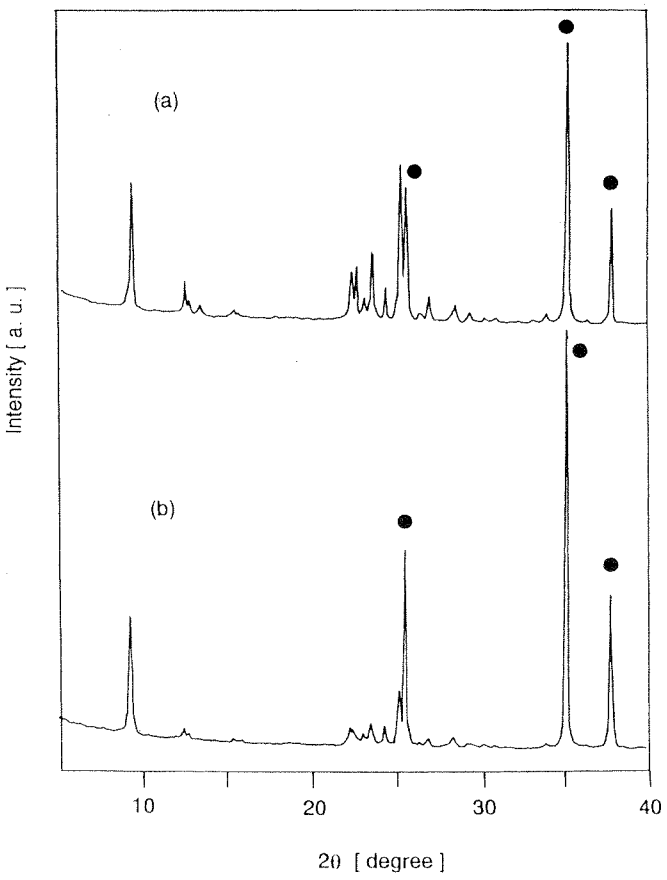

Fig. 1. XRD patterns for FER membranes (a) before and (b) after removal of FER particles on alumina support. Solid symbol, alumina.

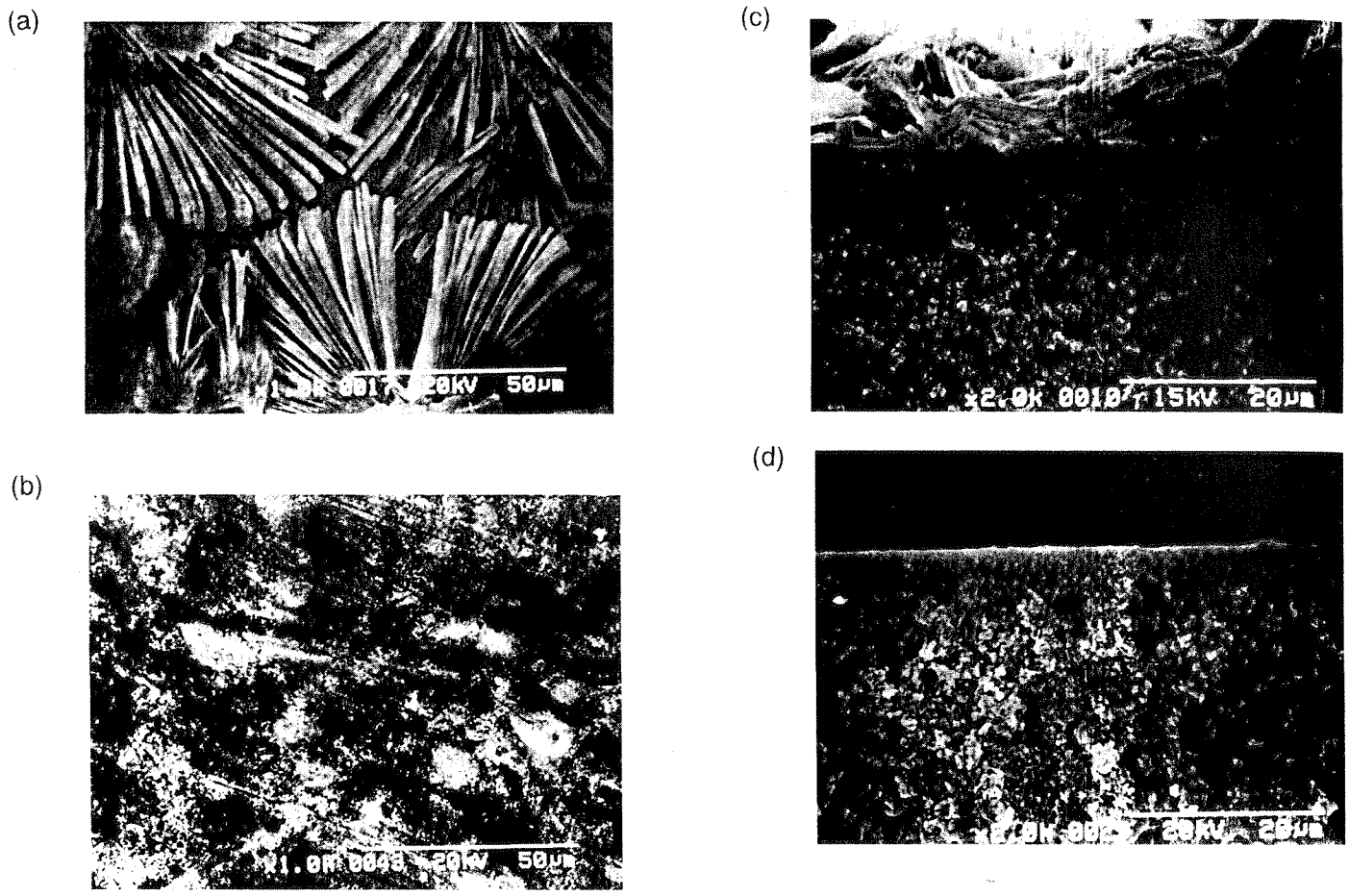

Fig. 2. SEM images for the top views of FER membranes (a) before and (b) after removal of FER particles on alumina support, and the cross-sectional views of FER membranes (c) before and (d) after removal of FER particles on alumina support

after the removal of FER particles on the alumina support, respectively. Fig. 2(c) and (d) show their corresponding cross-sectional views. No FER particle was observed over the whole surface of alumina support after polishing the membrane surface. The strong reflection peaks for FER were still observed in Fig. 1(b) although no FER crystal existed on the surface of alumina support. These XRD results indicated that FER was formed even in the pores of alumina support, namely, an FER-alumina composite layer was formed. From Fig. 2(c), the thickness of the FER layer on the alumina support and that of the FER-alumina composite layer were about 10 μm and 15 μm, respectively.

Fig. 3(a) and (b) show the FE-SEM images for the cross-section of porous alumina support and the center of FER-alumina composite layer, respectively. From Fig. 3(a), the average pore diameter of alumina support is found to be about 0.1 μm. In Fig. 3(b), nanoparticles with diameters of about 50 nm are observed in the pores of alumina support. Fig. 4 shows the FE-SEM images for FER powder produced by the VPT method. We first determined that a large plate-like FER particle is composed of assembled needle-like FER nanocrystals with a diameter of about 30 nm. By comparing Fig. 3(b) with Fig. 4, we believe that the nanoparticles observed in the alumina pores correspond to FER nanocrystals. In conclusion, FER nanocrystals grew in the pores of alumina support and filled up there to form a composite layer of FER and alumina.

3.2. *Formation mechanism of FER-alumina composite layer*

EDX analysis was carried out to clarify whether an aluminosilicate gel was penetrated into the

(a)

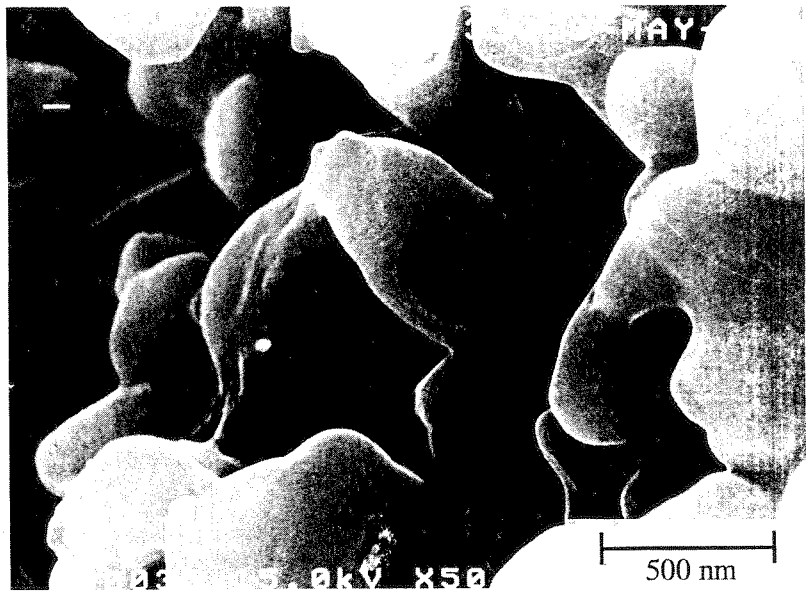

(b)

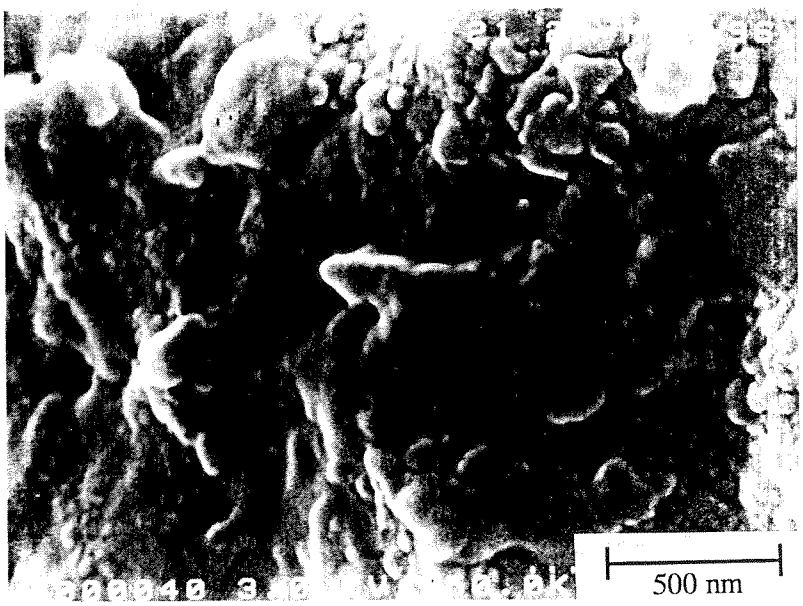

Fig. 3. FE-SEM images for the cross-section of (a) porous alumina support and (b) FER membrane.

(a)

(b)

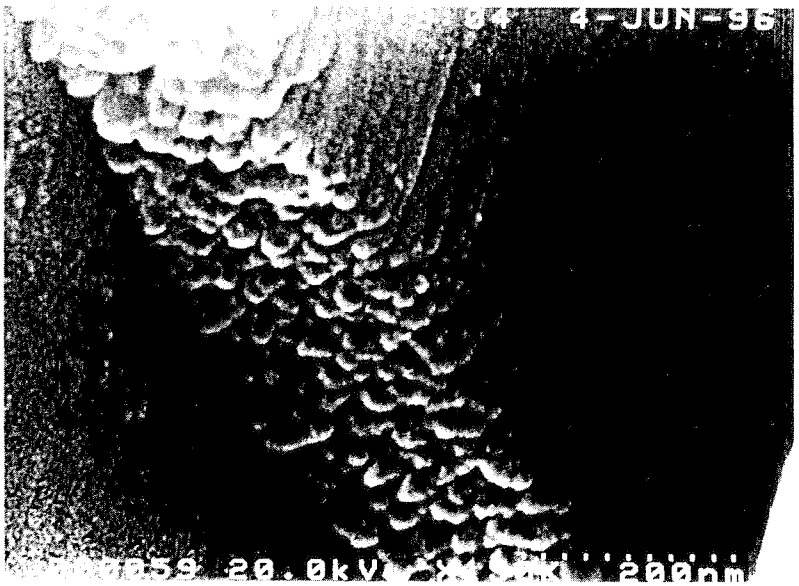

Fig. 4. FE-SEM images for FER powder produced by VPT method.

pores of alumina support during the dipping process. In this experiment, a support without surface treatment with colloidal silica was used. Fig. 5(a) and (b) show the SEM and EDX elemental images for the cross-section of alumina support coated with an aluminosilicate gel, respectively. White dots in Fig. 5(b) represent the presence of silicon. In Fig. 5(b), silicon was observed in the interior of alumina support, indicating that the aluminosilicate gel partly penetrated into the pores of alumina before crystallization.

The amount of aluminosilicate gel in the alumina support after the dipping process (2) should be larger than that prepared by method (1), because the support was evacuated from one side during a dipping process (2). We reported that the FER membrane prepared by method (2) could be practically defect-free, although the FER membrane prepared by method (1) was permeable to TIPB [17]. We consider that a larger initial amount of aluminosilicate gel in the pores of alumina makes it easier to fill up the voids in the composite layer. Therefore, it seems that the FER membrane prepared by the dipping method (2) became compact [17].

We previously proposed the formation of zeolite alumina composite layer only by SEM observation for the cross-sectional views of zeolitic membrane [16]. The XRD and EDX measurements in this study gave evidence that zeolite crystals formed in the pores of the alumina support. A schematic diagram of a plausible formation mechanism of zeolitic membrane is shown in Fig. 6(a). An aluminosilicate gel partly penetrates into the pores of alumina support before crystallization. Crystallization starts on the surface of alumina support. Then, crystallization proceeds both on the alumina support and in the pores of alumina. Zeolite crystals formed are composed of nano particles. The gel may successively be supplied into the pores of alumina support from the gel layer on the support to fill up the pores of alumina. Finally a zeolite–alumina composite layer formed can be compact, while voids remain among the crystals on the surface of alumina support.

The formation mechanism of a defect-free zeolitic membrane hydrothermally obtained has been proposed as shown in Fig. 6(b). Sano *et al.* [27] synthesized an MFI membrane on a Teflon slab hydrothermally and suggested that the MFI membrane is formed mainly through a successive accumulation of zeolite crystals which are formed via homogeneous nucleation in the liquid phase. On the contrary, Geus *et al.* [3,4] suggested that crystallization starts by heterogeneous nucleation on a support surface. They claimed that the layer made of intergrown polycrystals on the surface of the support was compact under their hydrothermal conditions. Another formation mechanism was proposed by Jansen *et al.* [28] and Kita [29] who have proposed that a gel layer is formed on a support at first and then the gel layer is crystallized to zeolitic membrane.

Irrespective of these formation mechanisms of membrane, once a zeolite layer or gel layer is formed on the surface of a support, an aluminosilicate solution may find it difficult to penetrate into the support to fill up the pores. The intergrowth of crystals in contact with a solution preferentially occurs under their hydrothermal conditions.

3.3. *Separation of benzene/p-xylene mixtures through FER membrane*

The pervaporation tests for benzene/*p*-xylene mixtures with various feed concentrations were performed at 303 K using an FER membrane prepared by the dipping method (2). The FER membrane used here was confirmed to be practically defect-free, because no permeation of TIPB was detected in the pervaporation of TIPB [17]. Fig. 7 shows the change in fluxes of benzene and *p*-xylene and the separation factor as a function of the feed concentration of benzene. Fluxes of benzene and *p*-xylene for single component permeation measurements are also plotted in Fig. 7. When the molar fraction of benzene in the feed solution was 57 mol%, the separation factor a (benzene/*p*-xylene) for the benzene/*p*-xylene mixture exceeded 100 which was much greater than 10.3 predicted from the vapor–liquid equilibrium. The separation factor for benzene/*p*-xylene mixtures largely increased with decreasing benzene concentration in the feed. This results suggests that even when the concentration of benzene in feed solution was extremely small, 0.5 mol%, the

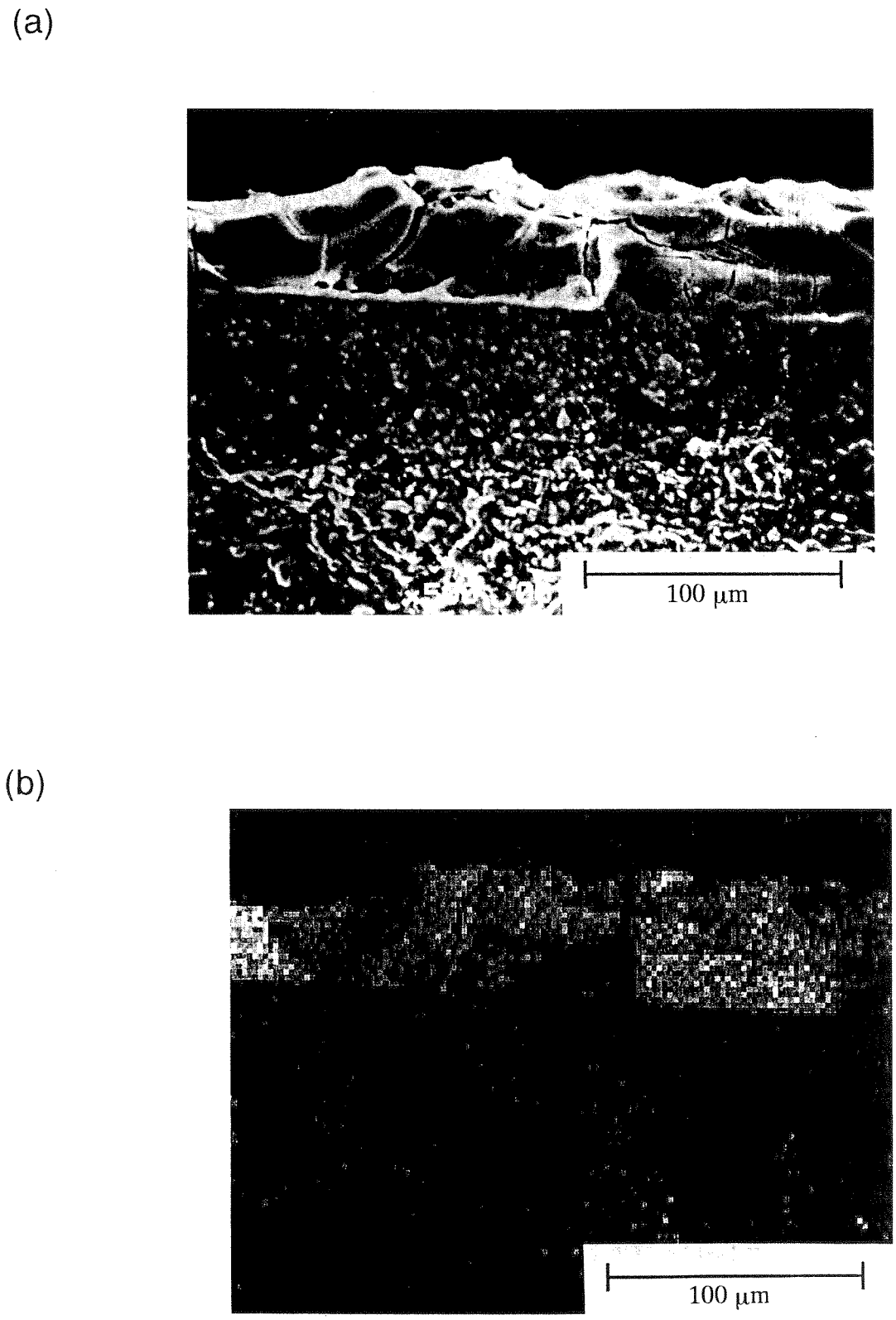

Fig. 5. (a) SEM and (b) EDX elemental images for the cross-section of alumina support coated with aluminosilicate gel. White dots: Si.

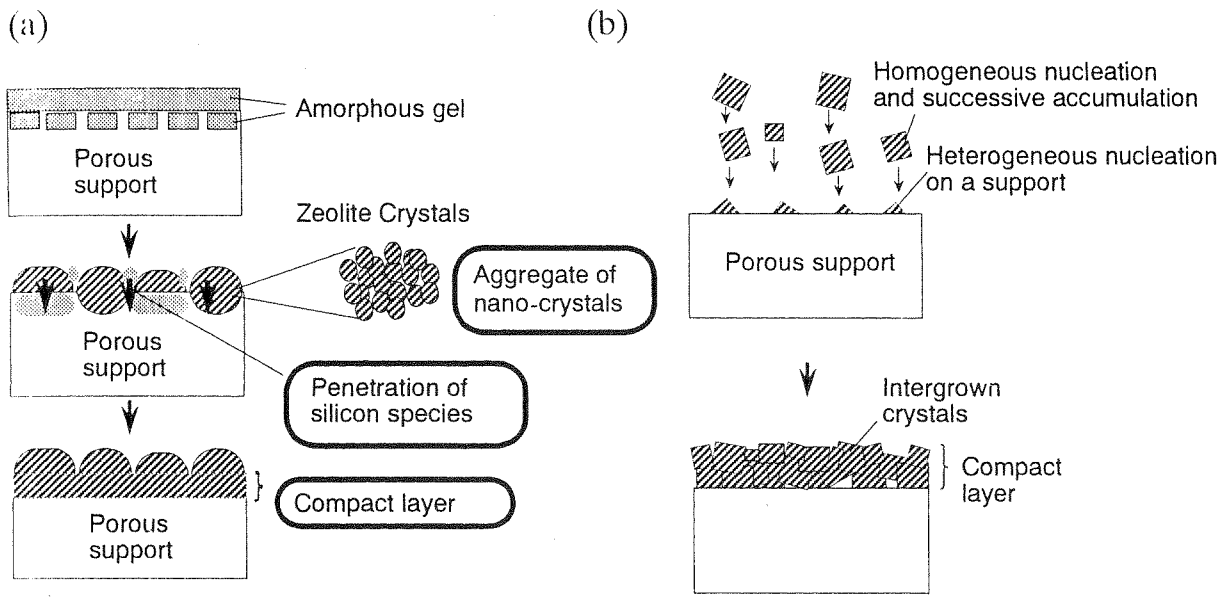

Fig. 6. Plausible formation mechanism of zeolitic membranes (a) by vapor-phase transport method and (b) by hydrothermal synthesis.

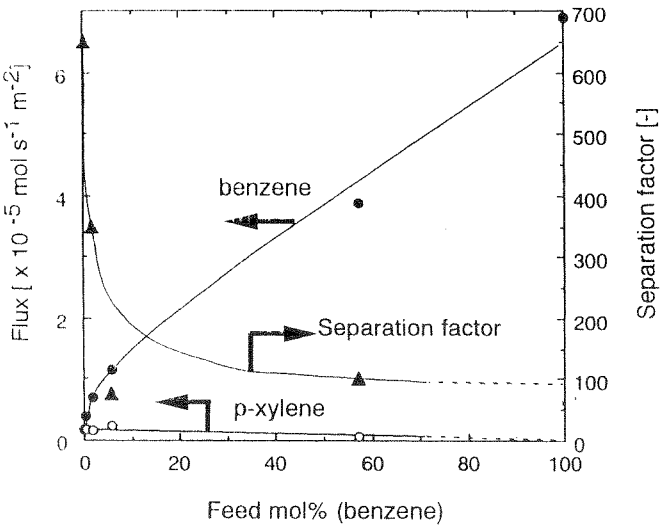

Fig. 7. Effect of benzene feed concentration on flux of benzene and *p*-xylene and separation factor in pervaporation of benzene/*p*-xylene mixtures. (T=303 K) ●, flux of benzene, ○, flux of *p*-xylene, ▲, separation factor.

sorption rate of benzene into the FER pores was still higher than that of *p*-xylene. The separation factor was as high as 600 when the feed concentration of benzene was 0.5 mol%. While the flux of *p*-xylene varied in proportion to the *p*-xylene concentration in the feed, the flux of benzene did not behave linearly with feed concentration: a large increase in the flux of benzene was observed with increasing concentration from 0 to 5 mol%. Therefore, a high separation factor was obtained at a low feed concentration of benzene.

We reported the pervaporation results of benzene/*p*-xylene (0.86: 1) mixture through MOR membranes [16]. The fluxes of benzene and *p*-xylene were 1.7×10^{-4} and 8.0×10^{-7} mol $s^{-1}\,m^{-2}$ at 295 K, respectively. Both fluxes of benzene and *p*-xylene through the FER membrane were about a quarter of those through the MOR membrane. The difference in fluxes between these two types of zeolitic membrane can be attributed to the difference in pore dimensions of MOR (0.70×0.65 nm) and FER (0.54×0.42 nm).

We previously carried out pervaporation using a FER membrane for a *p*-xylene/*o*-xylene mixture at 303 K [17]. The separation factor for a *p*-xylene/*o*-xylene mixture was about 3. It is considered that the shape selectivity of FER pores for xylene isomers appeared because it was reported that the MFI membrane which possessed pinholes with a diameter of about 1 nm showed no selectivity for a *p*-xylene/*m*-xylene mixture [22].

Vapor permeation of *p*-xylene, *m*-xylene, ethylbenzene and toluene through an MFI membrane was carried out by Baertsch *et al.* [25] who reported that no separation was achieved for binary mixtures of *p*-xylene/*o*-xylene, *p*-xylene/ethylbenzene, *p*-xylene/toluene and *m*-

xylene/ethylbenzene at 380–480 K. They claimed that the molecule with the slowest permeation rate limits diffusion and slows the other species down to its own rate in single-file transport. Funke *et al.* [26] used the same MFI membrane as that used by Baertsch *et al.* for the separation of octane isomers and found that n-octane preferentially permeated through the MFI membrane. They concluded that n-octane molecules prevented i-octane molecules from entering the zeolite pores.

When the single-file transport occurs in the membrane, the overall selectivity should always be governed by the selectivity on the feed side of membrane. Thus, taking into account that the FER-alumina composite layer is compact, high selectivities for the benzene/*p*-xylene mixtures suggest that the selectivity for the benzene/*p*-xylene mixture appears at the pore mouths of FER on the feed side of the FER-alumina composite layer. The intracrystalline diffusivity of benzene in MFI crystals was reported to be comparable to that of *p*-xylene [30,31]. Therefore, it seems that the difference in the sorption rates of benzene and *p*-xylene molecules into the zeolite pores on the feed side governed selectivity in pervaporation. We presume that the difference of sorption rates between benzene and *p*-xylene were caused by not only the difference in the shape of molecules but also by the difference in the affinity of molecules with pore mouth.

4. Conclusions

A gel in the pores of alumina support crystallized to zeolite and then zeolite–alumina composite layer formed by the VPT method. Zeolite crystals were composed of zeolite nanocrystals.

In the pervaporation tests performed at 303 K for benzene/*p*-xylene mixtures, we found that even when the concentration of benzene in the feed solution was extremely small, the flux of benzene through the FER membrane exceeds that of *p*-xylene. The separation factor of a benzene/*p*-xylene mixture was as high as 600 when the feed concentration of benzene was 0.5 mol%. High selectivities for the benzene/*p*-xylene mixtures suggest that the selectivity for the benzene/*p*-xylene mixture appeared at the pore mouths of FER on the feed side of the FER-alumina composite layer, because benzene and *p*-xylene molecules are difficult to pass through each other in the micropore of FER (single-file transport). The zeolitic membranes showed a promising potential to separate organic compounds such as aromatic hydrocarbons.

Acknowledgement

The authors express their appreciation to GHAS at Department of Chemical Engineering of Osaka University for XRD, SEM, FE-SEM measurements. This study was partly supported by the Grants-in-aid for Scientific Research on Priority Areas (No. 08232256).

References

[1] J.G. Tsikoyiannis, W.O. Haag, Zeolites 12 (1992) 126.
[2] C. Bai, M.-D. Jia, J.L. Falconer, R.D. Noble, J. Membrane Sci. 105 (1995) 79.
[3] E.D. Geus, M.J. Exter, H. van Bekkum, Chem. Soc. Faraday Trans. 88 (1992) 3101–3109.
[4] E.D. Geus, H. van Bekkum, W.J.W. Bakker, J.A. Moulijin, Microporous Mater. 1 (1993) 131.
[5] M.-D. Jia, K.-V. Peinemann, R.-D. Behling, J. Membrane Sci. 82 (1993) 15.
[6] M.-D. Jia, B. Chen, R.D. Noble, J.L. Falconer, J. Membrane Sci. 90 (1994) 1.
[7] T. Sano, Y. Kiyozumi, M. Kawamura, F. Mizukami, H. Takaya, T. Mouri, W. Inaoka, Y. Toida, M. Watanabe, K. Toyoda, Zeolites 11 (1991) 842.
[8] Y. Yan, M. Tsapatsis, G.R. Gavalas, M.E. Davis, J. Chem. Soc., Chem. Commun. (1995) 227.
[9] Y. Yan, M.E. Davis, G.R. Gavalas, Ind. Eng. Chem. Res. 34 (1995) 1652.
[10] W. Xu, J. Dong, J.(Jinping) Li, J.(Jianquan) Li, F. Wu, J. Chem. Soc., Chem. Commun., (1990) 755.
[11] M.H. Kim, H.X. Li, M.E. Davis, Microporous Mater. 1 (1993) 191.
[12] M. Matsukata, N. Nishiyama, K. Ueyama, Microporous Mater. 1 (1993) 219.
[13] M. Matsukata, N. Nishiyama, K. Ueyama, Stud. Surf. Sci. Catal. 84 (1994) 1183.
[14] M. Matsukata, N. Nishiyama, K. Ueyama, J. Chem. Soc. Chem. Commun., (1994) 339.
[15] N. Nishiyama, K. Ueyama, M. Matsukata, J. Chem. Soc. Chem. Commun., (1995) 1967.
[16] N. Nishiyama, K. Ueyama, M. Matsukata, Microporous Mater. 7 (1996) 299.

[17] N. Nishiyama, K. Ueyama, M. Matsukata, Stud. Surf. Sci. Catal. 105 (1996) 2195.
[18] M. Matsukata, N. Nishiyama, K. Ueyama, Microporous Mater. 7 (1996) 109.
[19] H. Lechert, P. Staelin, C. Kuntz, Zeolites 16 (1996) 149.
[20] H. Kita, K. Horii, Y. Ohtoshi, K. Tanaka, K. Okamoto, J. Mater. Sci. Lett. 14 (1995) 206.
[21] T. Sano, M. Hasegawa, Y. Kawakami, Y. Kiyozumi, H. Yanagishita, D. Kitamoto, F. Mizukami, Stud. Surf. Sci. Catal. 84 (1994) 1175.
[22] T. Sano, H. Yanagisita, Y. Kiyozumi, F. Mizukami, K. Haraya, J. Membrane Sci. 95 (1994) 221.
[23] Q. Liu, R.D. Noble, J.L. Falconer, H.H. Funke, J. Membrane Sci. 117 (1996) 163.
[24] J.F. Smetana, J.L. Falconer, R.D. Noble, J. Membrane Sci. 114 (1996) 127.
[25] C.D. Baertsch, H.H. Junke, J.L. Falconer, R.D. Noble, J. Phys. Chem. 100 (1996) 7676.
[26] H. Funke, A.M. Argo, C.D. Baertsch, J.L. Falconer, R.D. Noble, J. Chem. Soc., Faraday Trans. 92 (1996) 2499.
[27] T. Sano, F. Mizukami, H. Takaya, T. Mouri, M. Watanabe, Bull. Chem. Soc. Jpn 65 (1992) 146.
[28] J.C. Jansen, D. Kashchiev, A. Erdem-Senatalar, Stud. Surf. Sci. Catal. 85 (1994) 215.
[29] H. Kita, Maku (Membrane) 20 (1995) 169.
[30] D.B. Shah, H.Y. Liou, Zeolites 14 (1994) 541.
[31] D.B. Shah, H.Y. Liou, Stud. Surf. Sci. Catal. 84 (1994) 1347.

EFFECT OF PINHOLES ON PERMSELECTIVITIES OF MFI MEMBRANES

M. MATSUKATA*, J.D. WANG**, N. NISHIYAMA**, M. NOMURA*
and K. UEYAMA**

*Department of Applied Chemistry, Waseda University, Tokyo, Japan;
mmatsu@mn.waseda.ac.jp
**Department of Chemical Engineering, Osaka University, Osaka, Japan

ABSTRACT

MFI membranes were prepared by a vapor-phase transport (VPT) method in which a dry aluminosilicate thin layer prepared on a porous α-alumina support was crystallized in vapors of water, ethylenediamine (EDA) and triethylamine (Et_3N) at 453 K and autogeneous pressure. Gel preparation temperature, H_2O/SiO_2 ratio, Na_2O/SiO_2 ratio, aging temperature and time, dipping temperature and time governed the crystallinity of MFI and compactness of membrane. Particularly, Na_2O/SiO_2 ratio was important to prepare a compact MFI membrane. An MFI membrane that had a compact composite layer comprised of randomly oriented MFI crystals and porous alumina was successfully synthesized. It was confirmed that pervaporation of triisopropylbenzene (TIPB) is a suitable method for evaluating the amount of pinholes possibly forming at the boundaries of MFI crystals, and that the flux of TIPB well correlates with the permselectivities for inorganic gases (He, N_2, CH_4, and CO_2) and hydrocarbons (benzene/hexane) separation. The permeation results strongly suggested that MFI membrane should be pinhole-free for the appearance of permselectivity.

INTRODUCTION

Zeolites have been an attractive candidate as a component of inorganic membranes for separation mostly because of their unique, uniform micropore systems and catalytic properties. Zeolitic membranes have been synthesized using conventional hydrothermal synthetic method [1-7]. On the other hand, we have applied a new synthetic method, the VPT method [8-10], to prepare zeolitic membranes on a porous α-alumina support [11-16]. In the synthesis of zeolitic membranes by the VPT method, after an amorphous aluminosilicate gel is applied on

12th International Zeolite Conference © 1999 Materials Research Society

a porous ceramic support and dried, the resultant thin layer is crystallized to zeolite to give a supported zeolitic membrane. One of the advantages of the VPT method could be that this method is easily applicable to the synthesis of a thin zeolitic layer even on a surface having a complicated structure like honeycombs and monoliths irrespective of scale. Conventional, established synthetic methods of ceramic thin layers on a support can be employed to prepare a parent aluminosilicate thin layer.

Understanding the effect of pinholes often forming at the boundaries among zeolite crystals on the permeation and separation properties is one of the current key issues in zeolitic membranes research. The discrepancies in separation properties in the literature may be due to the lack of knowledge about this issue.

In the present study, appropriate conditions for synthesizing a high silica MFI zeolitic membrane by the VPT method were explored. By using MFI membranes giving different fluxes of TIPB, the effect of pinholes on permeation and separation properties for inorganic gases and hydrocarbon mixtures was investigated.

EXPERIMENTAL

MFI-type zeolitic membranes were prepared in the following procedure. A parent aluminosilicate gel suspension was prepared by mixing colloidal silica (Nissan Chemical Co., Ltd.) and a NaOH aqueous solution. The composition was SiO_2: 0.1-0.33 Na_2O: 7.77 H_2O in molar ratio. Since the colloidal silica contained aluminum itself, Si/Al ratio of the parent gel was 515. A porous, plate-like α-alumina substrate (NGK Insulators, Ltd.) was dipped in the gel suspension at 273 - 303 K for 24 - 48 h, and dried to obtain the substrate coated with the gel. The substrate had an asymmetric porous structure, and the mean pore size of the top layer was 0.1 mm. The coated substrate was placed in the middle of a special autoclave and EDA, Et_3N and water was poured to the bottom of the autoclave as vapor source. Crystallization of the resultant dry thin layer to zeolite was carried out in a mixed vapor of EDA, Et_3N and water at autogeneous pressure and 455 K for 4 days. It should be noted that the membrane never contacted with the liquid phase throughout its crystallization. An as-synthesized membrane was calcined in air at 773 K for 4 h. XRD measurements were carried out for the characterization of the membranes.

Pervaporation of TIPB was carried out to evaluate the amount of pinholes forming in MFI membranes. One side of a membrane was contacted with liquid TIPB at 303 K and evacuated from another side for 10 h. The permeant was trapped at 77 K and determined by gas

chromatography with an FID detector. The detection limit of TIPB flux was $1x10^{-9}$ mol m^{-2} s^{-1}. Gas permeation properties through MFI membranes were evaluated using the measurements of single gas flux for He, N_2, CO_2 and CH_4 at 300 – 373 K. The pressure of the permeation side was kept at atmospheric pressure and that of feed side was controlled to give pressure difference of 0 - 0.2 MPa. Pervaporation of binary hydrocarbon mixtures, benzene/n-hexane, was also carried out at 303 K.

RESULTS AND DISCUSSION

First, water content, aging temperature and time and dipping temperature and time were explored and tentatively optimized. A highly crystallized MFI was obtained with H_2O/SiO_2 ratio = 7.77, at 303 K of aging temperature for 2 h, and at 303 K of dipping temperature.

Run	Parent Gel Composition		Crystallization	Dipping	Product	TIPB Flux
	Si/Al	Na_2O/SiO_2	Time/h	Time/h		/mol m^{-2} s^{-1}
1	515	0.100	72	24	amorphous	-
2	515	0.130	72	24	MFI	High
3	515	0.145	72	24	MFI	High
4	515	0.190	72	24	MFI	$3.34X10^{-7}$
5	515	0.233	72	24	MFI	$4.33X10^{-5}$
6	515	0.333	72	24	amorphous	-
7	515	0.190	72	48	MFI	$<1.0X10^{-9}$
8	515	0.190	96	48	MFI + U*	-
9	515	0.190	120	48	MFI + U*	-

Table 1: Crystallization results of MFI membranes by vapor-phase transport method. H_2O/SiO_2 ratio = 7.77; Dipping temperature, 303 K; *unidentified phase

Table 1 compares the crystallization results mainly with different Na_2O/SiO_2 ratios and the fluxes of TIPB. Though the product was amorphous when Na_2O/SiO_2 ratio = 0.100 (Run 1), MFI was formed with Na_2O/SiO_2 ratio = 0.130 (Run 2). The intensities of reflection peaks for MFI in the XRD patterns were increased with increasing Na_2O/SiO_2 ratio and reached a maximum at Na_2O/SiO_2 ratio = 0.145 (Run 3). The product became amorphous again when Na_2O/SiO_2 ratio = 0.333 (Run 6). It was observed with the products of Runs 3 and 4 that liquid TIPB permeated soon to the permeation side because of the low vapor pressure of TIPB, indicating that the MFI layers in these products were not compact. Nicely crystallized and fairly

compact membranes were obtained in Runs 4 and 5. These results suggest that though the most intense reflection peaks for MFI in XRD patterns do not always indicate a compact membrane, the sodium concentration in parent gel is an important factor governing crystallinity and compactness of membrane. Sodium concentration may significantly influence both the formation of intermediate species by hydrolysis of Si-O-Si linkage in amorphous dry gel and that of zeolite framework by condensation of silanol groups. Sodium concentration may also have great effects on the mobility and migration of the parent gel into the substrate pores. We suppose that sodium concentration was insufficient to produce intermediate in Run 1, and too high to allow sufficient condensation of silanol groups in Run 6.

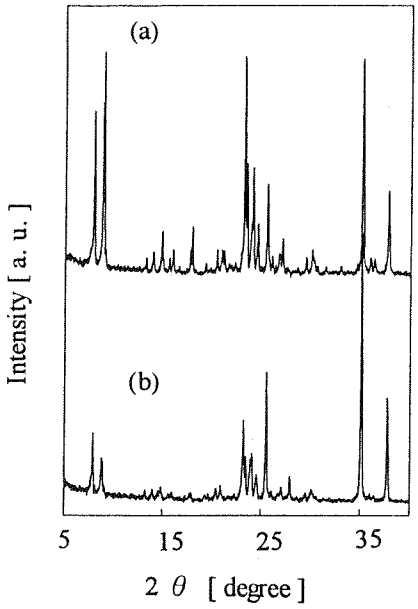

Figure 1 XRD patterns (a) for the as-synthesized membrane (Run 7) and (b) the membrane (Run 7) after removing the top layer.

Further optimization of synthetic conditions were attempted. Prolonged crystallization, however, resulted in the formation of an unidentified phase (Runs 8 and 9). The most compact membrane was obtained with prolonged dipping time from 24 h (Run 4) to 48 h (Run 7). No permeation of TIPB was detected with the membrane obtained in Run 7.

Figure 1a shows the XRD pattern for the product in Run 7. A randomly oriented MFI polycrystalline layer was formed as a top layer on the porous α-alumina support. This top layer is not compact because a lot of voids among MFI particles are observed as shown in Fig. 2a. This top layer was removed by mechanically polishing the membrane surface (Fig. 2b). It is worth noting that the XRD reflection peaks for MFI still remained as shown in Fig. 1b, suggesting that a composite layer of porous alumina and randomly oriented MFI crystals was formed inside the support. Even after the removal of the top layer, no permeation of TIPB was

detected with the membrane obtained in Run 7. We, thus, concluded that this composite layer was compact, being in good agreement with our previous report on FER membrane [15].

Let us discuss the effect of pinholes forming among zeolite crystals on the permeation and separation properties. Permeation properties of MFI membranes were studied using membranes (Runs 4, 5 and 7) giving different TIPB fluxes.

Figure 3 shows the permeabilities of inorganic gases through these MFI membranes. When a less compact MFI membrane (Run 5) was used, the permeance of He was about $2X10^{-8}$ mol m^{-2} s^{-1} Pa^{-1} and those of N_2, CH_4 and CO_2 were similar with each other (about $1X10^{-8}$ mol m^{-2} s^{-1} Pa^{-1}). These permeances were almost independent of temperature. The permeance of He through the membrane (Run 7) showing no TIPB permeation was smaller than that through the membrane obtained in Run 5, and showed apparent positive temperature dependency. The order of permeances was He > CO_2 > CH_4 > N_2 except for the order of CH_4 and N_2 at 303 K. Clearly, the permeation of these inorganic gases was largely governed by activated diffusion mechanism. In the case of the membrane obtained in Run 5, the contribution of permeation through pinholes (Knudsen diffusion) to the observed permeance was probably significant, resulting in less temperature dependency. The membrane obtained in Run 4 showed inter-mediate behavior, as shown in Fig. 3b. Argon adsorption isotherms were taken with these two membranes at 77 K and the distribution of pore size was analyzed using the H-K method (not shown). The membrane synthesized in Run 7 possessed only zeolitic micropores

(a)

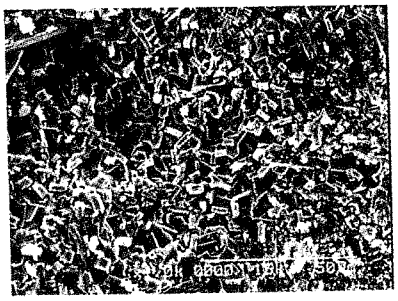

(b)

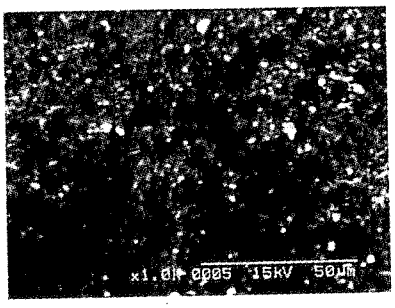

(c)

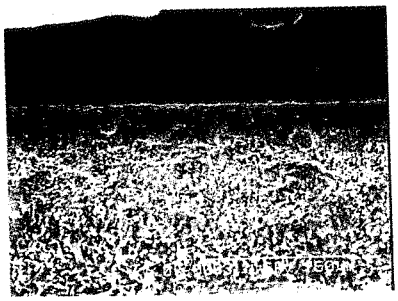

Figure 2 SEM images for the membrane (Run 7)
(a) Top view for the as-synthesized product
(b) Top view of the product after removing the top layer
(c) cross section of the product after removing the top layer.

whereas a trace amount of pore appeared at around 1 nm in the membrane obtained in Run 5. These results described above imply that a very small amount of pinholes are harmful for the separation of inorganic gases.

Pervaporation of benzene/n-hexane mixtures was carried out for exploring possibility of hydrocarbon separation. Figure 4 shows the permeation results with different compositions. The fluxes of benzene and hexane through the membrane obtained in Run 5 were in the order of 10^{-4} mol m^{-2} s^{-1}. The separation factor was almost unity. On the other hand, the membrane obtained in Run 7 separated the benzene/hexane mixture, though the fluxes were decreased to the order of 10^{-6} mol m^{-2} s^{-1}. With increasing molar fraction of benzene from 0.2 to 0.5, the flux of benzene increased while that of hexane was almost constant, resulting in the increase of the separation factor from unity to about 4. The difference in the fluxes between these two membranes indicates that most of molecules passed through pinholes in the case of the membrane obtained in Run 5 and thereby no separation was achieved.

For the appearance of permselectivity, a membrane should be pinhole-free. Pervaporation of TIPB was confirmed to be a good technique for evaluating the amount of pinholes. The determination of the apparent size of pinholes would be possible by pervaporation tests of molecules having different

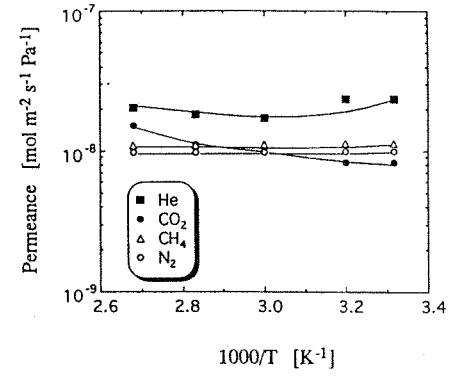

(a) TIPB flux 4.33×10^{-5} [mol m^{-2} s^{-1}]

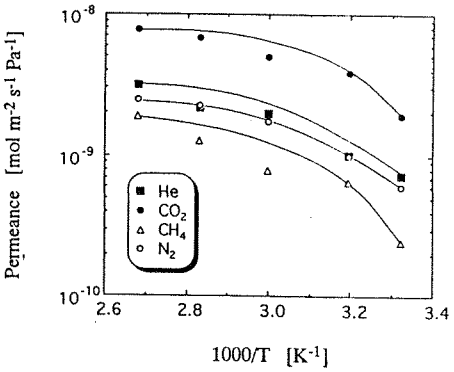

(b) TIPB flux 3.34×10^{-7} [mol m^{-2} s^{-1}]

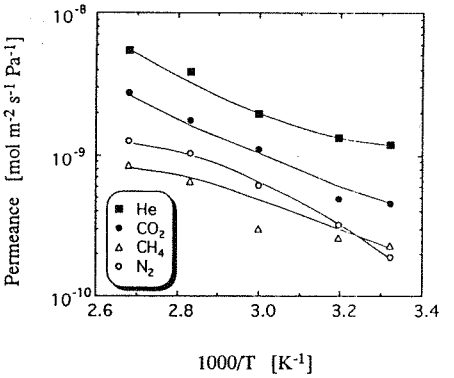

(c) TIPB flux $<1.0 \times 10^{-9}$ [mol m^{-2} s^{-1}]

Figure 3 Temperature dependency of the permeances of inorganic gases through MFI membranes formed in (a) Run 5, (b) Run 4 and (c) Run 7.

molecular sizes.

CONCLUSIONS

Synthesis of high silica MFI membrane supported on porous α-alumina was performed using the vapor-phase transport method. Among a variety of synthetic conditions, Na_2O/SiO_2 ratio in a parent aluminosilicate gel was essential to prepare a compact MFI membrane. Pinholes among MFI crystals seriously hinder the appearance of permselectivity in separation of inorganic gases and of hydrocarbon mixtures.

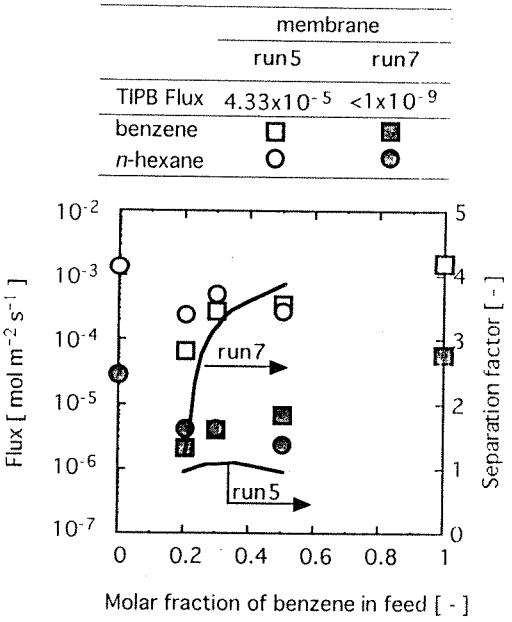

Figure 4 Separation results of benzene/hexane mixtures by pervaporation at 303 K.

ACKNOWLEDGMENTS

This study was supported partly by the grant-in-aid for Encouragement of Young Scientists (No.09750839) and Scientific Research (B) (No.09555247), the Ministry of Education, Science, Sports and Culture and by the Asahi Grass Foundation.

REFERENCES

1. T. Sano, Y. Kiyozumi, M. Kawamura, F. Mizukami, H. Takaya, T. Mouri, W. Inaoka, Y. Toida, M. Watanabe and K. Toyoda, *Zeolites*, **11**, 842 (1991).
2. Y. Yan, M. E. Davis and G. R. Gavalas, *Ind. Eng. Chem. Res.*, **34**, 1652 (1995).
3. H. Kita, K. Horii, Y. Ohtoshi, K. Tanaka and K. Okamoto, *J. Mater. Sci. Lett.*, **14**, 206 (1995).
4. K. Kusakabe, S. Yoneshige, A. Murata and S. Morooka, *J. Memb. Sci.*, **39**, 116 (1996).
5. Z.A.E.P. Vroon, K. Keizer, M. J. Gilde, H. Verweij and A. J. Burggraaf, *J. Memb. Sci.*, **113**, 293 (1996).

6. W. J. W. Bakker, F. Kapteijn, J. Poppe and J. A. Moulijn, *J. Memb. Sci.*, **117**, 57 (1996).
7. C. D. Baertsch, H. H. Funke, J. L. Falconer and R. D. Noble, *J. Phys. Chem.*, **100**, 7676 (1996).
8. W. Xu, J. Dong., J. Li, J. Li and F. Wu, *J. Chem. Soc., Chem. Commun.*, 755 (1990).
9. M.H. Kim, H.X. Li and M. E. Davis, *Microporous Mater.*, **1**, 191 (1993).
10. M. Matsukata, N. Nishiyama and K. Ueyama, *Microporous Mater.*, **1**, 219 (1996).
11. M. Matsukata, N. Nishiyama and K. Ueyama, *Stud. Surf. Sci. Catal.*, **84**, 1183 (1996).
12. M. Matsukata, N. Nishiyama and K. Ueyama, *Microporous Mater.*, **7**, 299 (1996).
13. M. Matsukata, N. Nishiyama and K. Ueyama, *Stud. Surf. Sci. Catal.*, **105**, 2195 (1996).
14. M. Matsukata and E. Kikuchi, *Bull. Chem. Soc. Jpn.*, **70**, 2341 (1997).
15. N. Nishiyama, K. Ueyama and M. Matsukata, *Microporous Mater.*, **11**, 107 (1997).
16. N. Nishiyama, K. Ueyama and M. Matsukata, *AIChE J.*, **43**, 2724 (1997).

ELSEVIER

Microporous and Mesoporous Materials 32 (1999) 159–168

MICROPOROUS AND MESOPOROUS MATERIALS

www.elsevier.nl/locate/micmat

Crystallization of ferrierite (FER) on a porous alumina support by a vapor-phase transport method

Takaaki Matsufuji [a], Norikazu Nishiyama [a], Korekazu Ueyama [a], Masahiko Matsukata [b,*]

[a] *Department of Chemical Engineering, Faculty of Engineering Science, Osaka University, 1-3 Machikaneyama-cho, Toyonaka-shi, Osaka 560-8531, Japan*

[b] *Department of Applied Chemistry, Waseda University, 3-4-1 Okubo, Shinnjyuku-ku, Tokyo 169-8555, Japan*

Received 14 January 1999; accepted for publication 10 May 1999

Abstract

The formation of a ferrierite (FER) membrane by a vapor-phase transport method is discussed. The formation process was studied using X-ray diffraction, scanning electron microscopy (SEM), field emission-SEM and energy dispersive X-ray analysis. The same location on the top surface was repeatedly observed at different crystallization times using SEM. It was found that an aluminosilicate species formed from a dry gel layer was mobile over the surface of support during crystallization. This intermediate aluminosilicate species penetrated into the pores of the alumina support to fill them, generating a compact FER–alumina composite layer. © 1999 Elsevier Science B.V. All rights reserved.

Keywords: Formation process; Synthesis; Vapor-phase transport; Zeolitic membrane

1. Introduction

There is much discussion in the literature of zeolitic membranes for gas separation and pervaporation [1–16]. Zeolitic membranes are useful for separating gas and liquid mixtures. However, the synthesis of defect-free zeolitic membranes suffers from lack of reproducibility. The main reason seems to be the uncontrolled formation of defects (pinholes) among zeolite crystals. To overcome this problem, it is necessary to understand the formation process of zeolitic membranes.

Most studies of the synthesis of zeolitic membranes have used a hydrothermal synthetic method, which is standard in the preparation of powder zeolites. Many formation mechanisms for defect-free zeolitic membranes prepared by the hydrothermal synthetic method have proposed. Myatt et al. [17] have proposed four such mechanisms: (1) production of nuclei and growth of crystals in the bulk solution followed by their attraction to a substrate, or collision and association with it; (2) production of nuclei in the bulk solution, followed by diffusion to and accumulation at a substrate before significant growth occurs; (3) diffusion of colloidal and amorphous aluminosilicate material to a substrate followed by concentration there, providing more favorable conditions for nucleation and growth in the vicinity of the surface; (4) production of nuclei on a substrate

* Corresponding author. Tel.: +81-3-5286-3850; fax: +81-3-5286-3850.

E-mail address: mmatsu@mn.waseda.ac.jp (M. Matsukata)

1387-1811/99/$ – see front matter
PII: S1387-1811(99)00101-8

surface, followed by surface growth. Sano et al. [18] hydrothermally crystallized an MFI membrane on a Teflon slab, and suggested that the MFI membrane was formed mainly by successive accumulation of zeolite crystals formed by homogeneous nucleation in the liquid phase. However, Geus et al. [2] and others (Tsikoyiannis and Haag [19]; Jansen et al. [20]; Yan and coworkers [5,6]) have suggested that crystallization begins by heterogeneous nucleation on the surface of a support. Whatever the formation mechanism of zeolitic membranes, once a zeolite layer is formed on the surface of the support it seems to be difficult for aluminosilicate solution to penetrate into the support to fill up the pores. The intergrowth of crystals formed on the surface of a support is probably essential to obtain a defect-free zeolitic membrane in crystallization under hydrothermal conditions.

A novel vapor-phase transport (VPT) method for zeolites has been developed by Xu et al. [21], who first reported that aluminosilicate dry gel was transformed to MFI in contact with mixed vapors of water, ethylenediamine (EDA), triethylamine (Et_3N) at 453 K. They claimed that this method reduced the consumption of expensive organic materials. Following this work, Kim et al. [22] and our group [23,24] studied this novel VPT synthetic method, and confirmed that it is useful for synthesizing ferrierite (FER) and mordenite (MOR). The VPT formation process seems to be different from that under hydrothermal conditions. The top layer of zeolitic membrane synthesized by the VPT method was clearly non-compact, indicating that any compact layer of FER and porous alumina (FER–alumina composite layer) seems to be formed in the porous alumina support [25].

We have previously proposed a formation process for FER membrane synthesized by the VPT method [25]. In this formation process we suppose that aluminosilicate species are mobile during crystallization. The morphological change as crystallization progresses is evidence for the mobility of aluminosilicate species. In this study we therefore repeatedly observed the same location on the top surface as crystallization progressed, using scanning electron microscopy (SEM), to study the morphological change of the resulting membrane.

2. Experimental

2.1. Preparation of parent gel

Parent aluminosilicate sol with an SiO_2/Al_2O_3 ratio of 18 was prepared, using colloidal silica containing 30 wt% of SiO_2 and 0.4 wt% of Na_2O (Nissan Chemical) as a silica source and aluminum sulfate anhydride, $Al_2(SO_4)_3$ (Wako), as an alumina source. Colloidal silica was initially mixed with $Al_2(SO_4)_3$, deionized water and NaOH (4 N) at 273 K. The composition of the parent sol was $18SiO_2{:}Al_2O_3{:}4.3Na_2O{:}450H_2O$. A porous α-alumina support (Nihon Gaishi) with an average pore diameter of 0.1 μm was then dipped into the parent sol at 303 K for 1 day. When it was necessary to depress dissolution of alumina from the support during crystallization, the alumina support was treated with colloidal silica of $pH \approx 10$.

2.2. Crystallization of dry gel by vapor-phase transport method

The support, coated with the parent sol, was dried for 24 h at 298 K. A mixture of EDA, Et_3N and water ($EDA{:}2.0Et_3N{:}H_2O$, volume ratio) was poured into the bottom of an autoclave to produce vapor. Crystallization was then performed at 453 K for up to 7 days at autogenous pressure. A synthesized FER membrane was calcined in air at 773 K for 4 h. A heating rate of 0.1 K min^{-1} was adopted in the range 473–773 K. The crystallinity and structure of the products were analyzed by X-ray diffraction (XRD) using Cu Kα radiation (Philips X's Pert-MRD). The resulting morphology was examined by SEM (Hitachi S-2250) and field emission-SEM (FE-SEM, Hitachi S-5000L). Energy-dispersive X-ray analysis (EDX, Philips, EDAX DX-4) in conjunction with SEM was also used for measuring the concentration profiles for silicon and aluminum.

3. Results and discussion

3.1. Formation process of FER–alumina composite layer

We have previously reported that a compact layer of FER and porous alumina is formed [25].

To understand the formation process of this FER–alumina composite layer, FE-SEM and EDX measurements were made on the product cross-sections. Fig. 1 shows FE-SEM images of the product cross-sections crystallized for different periods. FE-SEM observation was carried out at a depth of 20–30 μm below the surface of the alumina support. After 18 h crystallization, many voids are observed in the pores of the alumina support. The number of voids decreased after 2 days, and they were hardly observed after 4 days.

To confirm the formation of FER in the pores of the alumina support, the FER particles formed on the surface were removed with sandpaper. Fig. 2 shows XRD patterns before and after removal of the top layer. After removal of the top layer, reflection peaks for FER were still observed. We confirmed using SEM that no FER particles were observed on the surface of the alumina support. The intensities of the reflection peaks for FER increased with prolonged crystallization, both before and after the removal of FER particles, indicating that the crystallinity of FER formed in the pores of the support was improved. These XRD measurements strongly support the notion that FER is formed in the pores of the alumina support, to create an FER–alumina composite [25].

The EDX images of the cross-section of the FER membranes crystallized at 1, 2, 5 and 7 days are shown in Fig. 3. Black dots in Fig. 3(a) and (b) correspond to silicon and aluminum respectively. The interface between a surface gel layer and the porous alumina support was clearly observed. The black dots, indicating spreading of Si into the alumina support with prolonged crystal-

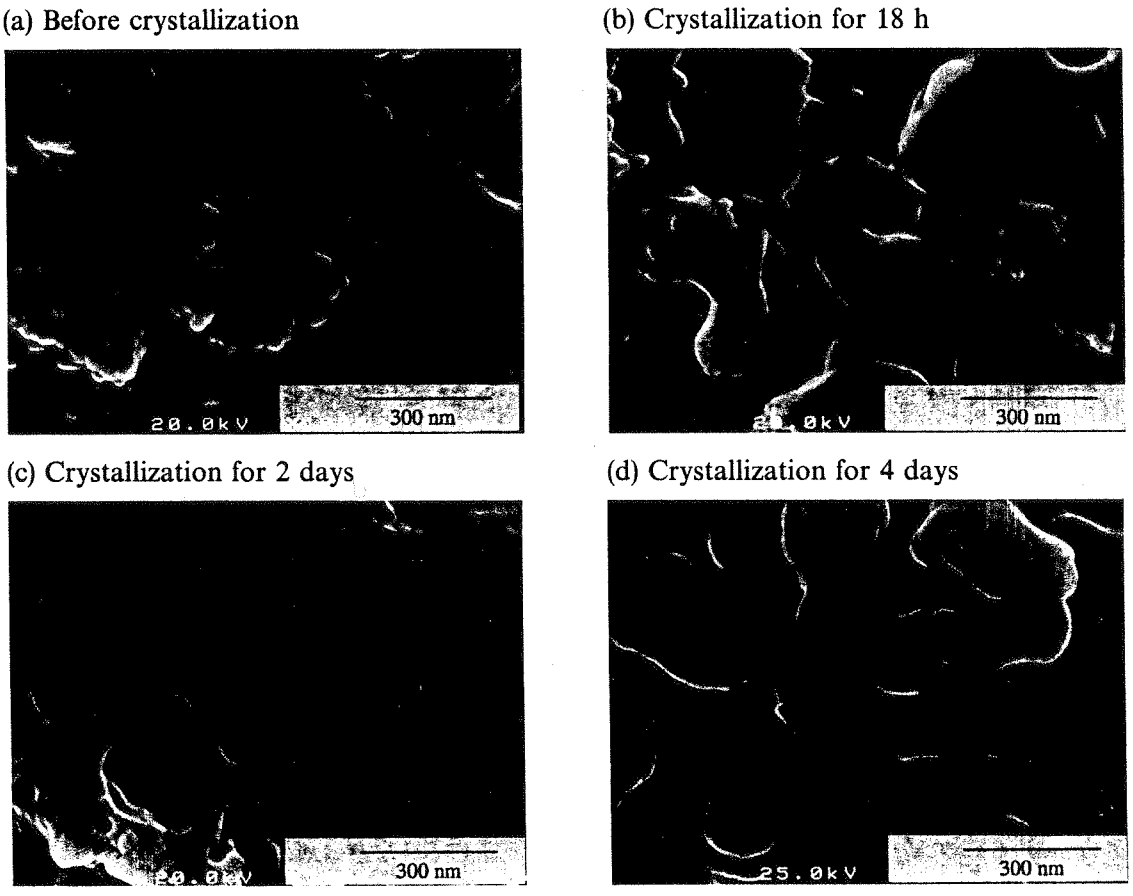

Fig. 1. FE-SEM cross-sectional images of (a) porous α-alumina support coated by the parent gel, (b) after crystallization for 18 h (c) after crystallization for 2 days and (d) after crystallization for 4 days.

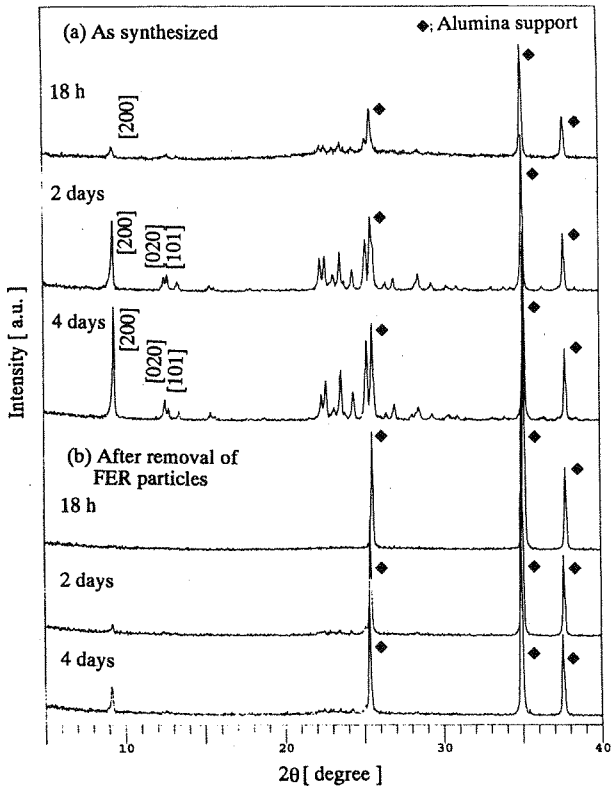

Fig. 2. XRD patterns for FER membranes (a) as synthesized and (b) after removal of FER particles on the alumina support.

lization, suggest that the dry gel formed as a surface layer on the support and then penetrated into the pores of the alumina support during crystallization. As a result, a continuous FER–alumina composite layer was formed.

3.2. *Mobility of aluminosilicate gel during crystallization*

We performed crystallization of a gel layer for 0, 1, 2, 5 and 7 days, using the same sample. The intensity of the reflection peaks for FER became greater with longer crystallization, implying that the crystallinity of FER improved over the period from 1 to 7 days. This trend is similar to the result shown in Fig. 2(a).

To investigate whether aluminosilicate gel on the surface of support was mobile during crystallization, the SEM observations were carried out for the top surfaces of the products with different crystallization.

Fig. 4 shows the morphological change of the top surface with the progress of crystallization, according to the VPT method. The same location was repeatedly observed at different crystallization times. The SiO_2/Al_2O_3 ratio of the parent gel was ~ 18. An amorphous gel is certainly consumed and takes part in the growth of FER crystals. This phenomenon is clearly indicated in Fig. 4(b) and (c) by the growth of particles denoted by arrows in these SEM images for the products after 1 to 2 days of crystallization. These results strongly support the hypothesis that aluminosilicate intermediate species, possibly formed from the gel, can migrate on the order of micrometers along the surfaces of the gel layer.

Intermediate alminosilicate species can be formed by hydrolysis of amorphous gel or by the dissolution of FER crystals crystallized on the support. When amorphous dry gel powder with $SiO_2/Al_2O_3 = 18$ was placed by itself on the support and crystallized under the same conditions as for membrane preparation, the SEM image of the top surface and the EDX elemental images for the cross-section gave information on the mobility of aluminosilicate species and the direction of their migration. To eliminate any contribution of silicon from colloidal silica to an EDX Si map, the treatment of the support with colloidal silica was not performed in these experiments.

After 4 days of crystallization the product was a mixture of FER and MOR, as indicated in the XRD pattern of Fig. 5. Dissolution of the alumina support gave the FER and MOR mixture, with no surface treatment by colloidal silica. Fig. 6(a) shows the SEM image, and Fig. 6(b) and (c) shows the EDX elemental maps for the cross-section of the product formed from the gel powder on the alumina surface. An interface between the surface zeolite crystals and the alumina support was observed. The gel powder was crystallized on the alumina support and gave crystals that seem to exist in the pores of the alumina, as shown in Fig. 6(a). Black dots shown in Fig. 6(b) and (c) correspond to silicon and aluminum respectively. The EDX measurements also clearly show that black dots corresponding to Si, denoted by an arrow in Fig. 6(b), spread into the alumina sup-

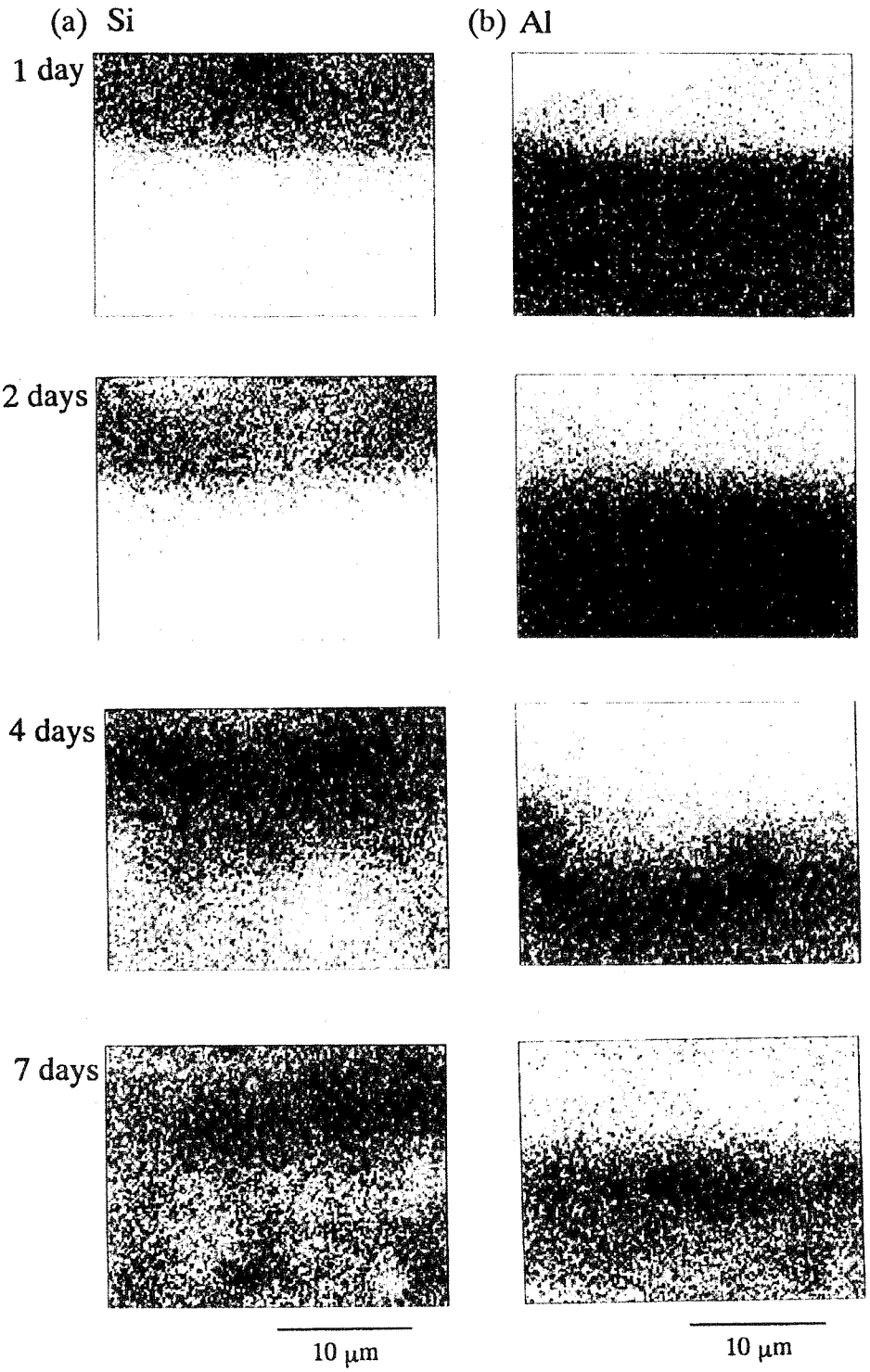

Fig. 3. EDX elemental cross-sectional images of FER membranes crystallized for 1, 2, 5 and 7 days. Black dots: (a) Si and (b) Al.

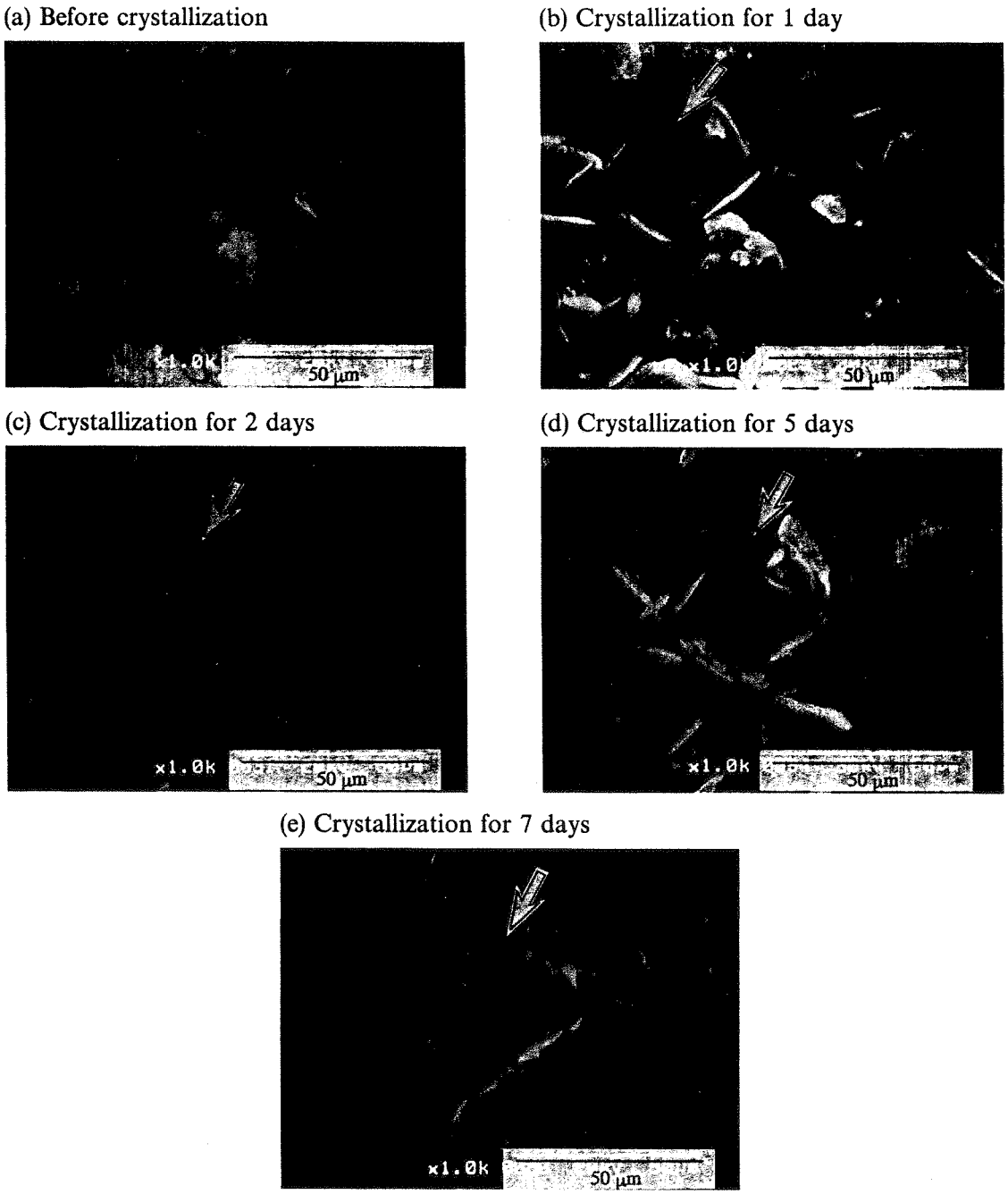

Fig. 4. SEM images for the top views of (a) alumina support with parent gel, and FER membranes crystallized for (b) 1 day, (c) 2 days, (d) 5 days and (e) 7 days.

port through the interface between the zeolite crystals on the support surface and the alumina support. It was confirmed that Si (and Al) species from the amorphous gel apparently migrate to the interior of the alumina support.

The migration of aluminosilicate intermediate species formed by the hydrolysis of FER powder on the support was also studied. The FER powder

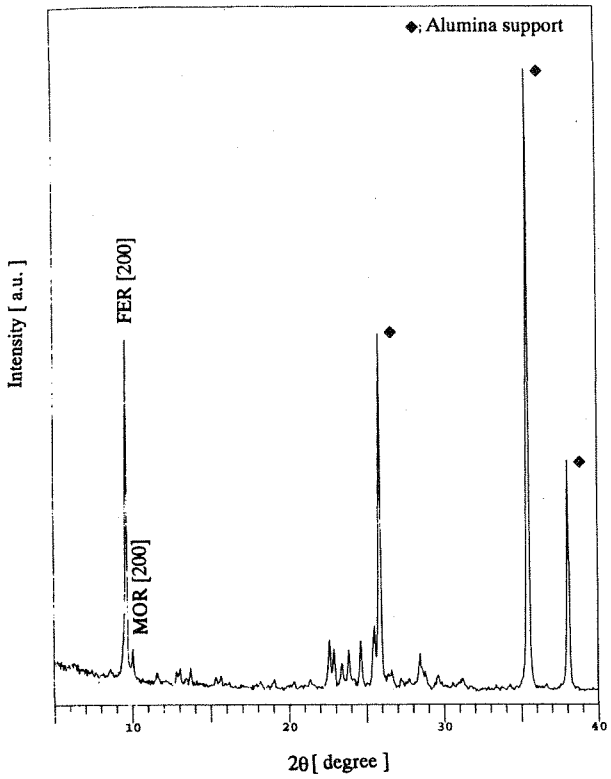

Fig. 5. XRD patterns for the product formed from gel powder on the support by the VPT method.

was made of this amorphous dry gel powder under the same conditions as for membrane preparation. Then FER powder was placed on the alumina surface and treated for 4 days under the same conditions as for membrane preparation. Fig. 7(a) shows the XRD patterns for the FER powder produced by the VPT method and Fig. 7(b) after removal of the product formed from FER powder placed on the support using the VPT method. After 4 days the XRD pattern corresponding to FER was still observed, as shown in Fig. 7(b). Fig. 8(a) shows an SEM image, and Fig. 8(b) and (c) EDX elemental maps for the cross-section of the product. Fig. 8(a) implies that FER particles were strongly attached to the alumina support. From the EDX measurement, black dots corresponding to Si, denoted by an arrow, also spread into the alumina support, as shown in Fig. 8(b) and (c). It seems that the outer surface of the crystals decomposes by hydrolysis, and oligomeric Si and Al species and amines apparently migrate

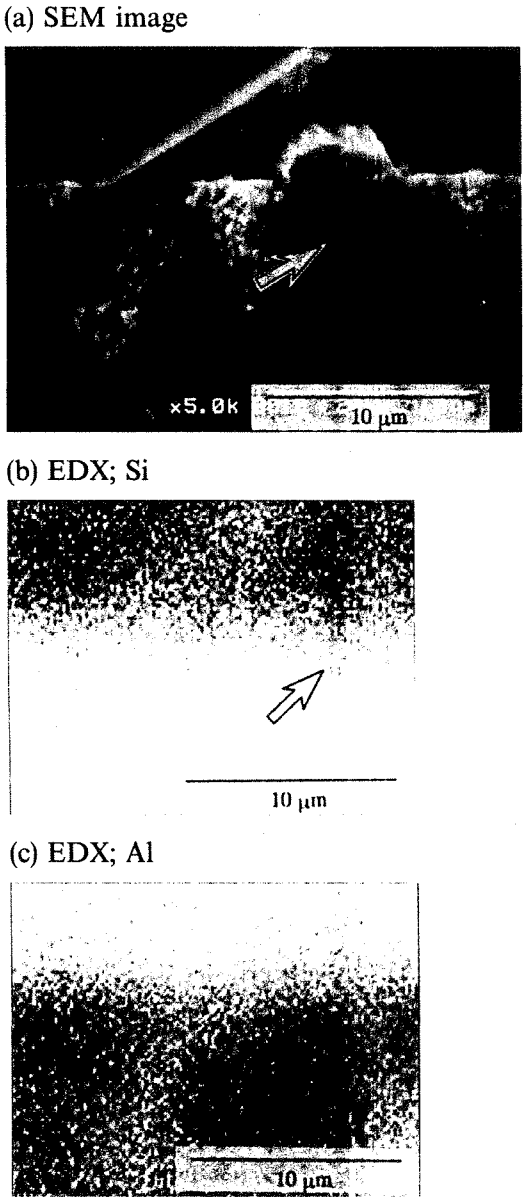

Fig. 6. (a) SEM, (b) and (c) EDX elemental cross-sectional images of the product formed from gel powder placed on the support. Black dots: (b) Si and (c) Al.

along the surface and into the pores of the alumina support, crystallizing into further crystals. The driving force of this migration could be the concentration gradient.

In conclusion, aluminosilicate species from both the amorphous gel and FER powder are successively supplied to the surface and into pores of the alumina support during the crystallization process.

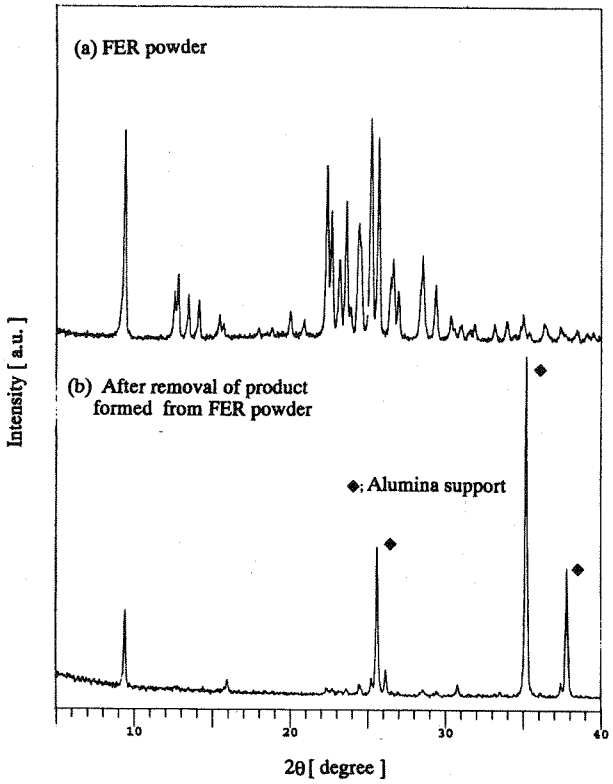

Fig. 7. XRD patterns for (a) FER powder and (b) after removal of the product formed from FER powder placed on the support using the VPT method.

3.3. Formation of zeolitic membrane by the VPT method

For the formation of defect-free zeolitic membranes by the hydrothermal synthesis method, the intergrowth of crystals formed on the surface of the support is probably necessary. On the other hand, on the surface of pinhole-free FER and MOR membranes obtained by a vapor-phase transport (VPT) method, numerous voids were observed among zeolite particles [25]. The zeolitic layers that formed on the surface of the alumina support were clearly non-compact. The compact layer was an FER–alumina composite layer within the support.

We accordingly consider that the present formation process is different from that under hydrothermal conditions. A plausible formation process for the zeolitic membrane by the VPT method is shown in Fig. 9. Aluminosilicate gel penetrates

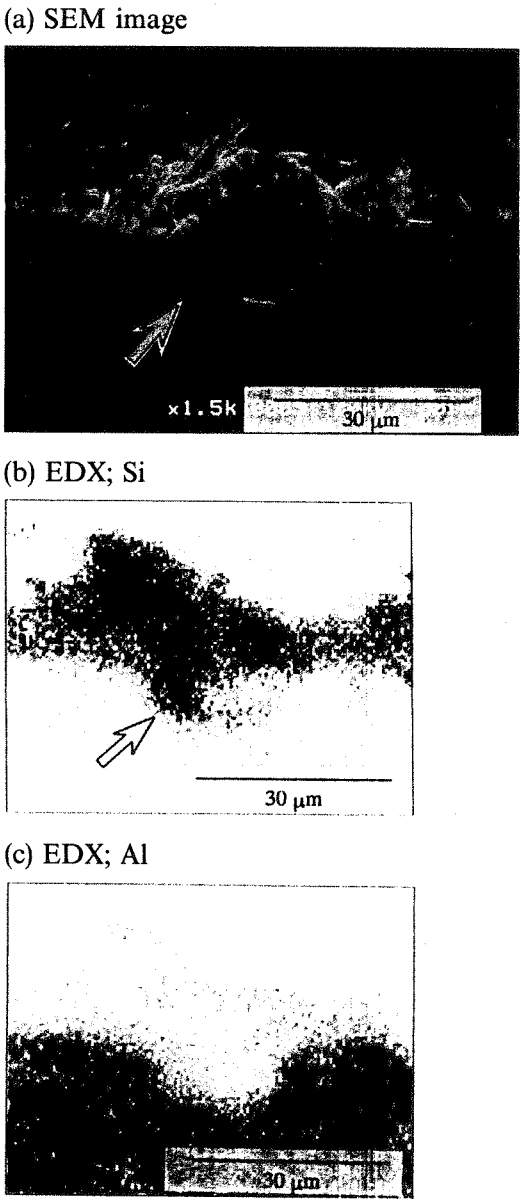

Fig. 8. (a) SEM, (b) and (c) EDX elemental cross-sectional images of the product formed from FER powder placed on the support. Black dots: (b) Si and (c) Al.

into the pores of the alumina support during the course of dip coating [25]. Crystallization begins on the surface of the alumina support. Crystallization then proceeds both on the alumina support and in the pores. On the alumina support, the crystallinity of the zeolite particles improves considerably with increasing duration of crystallization time. Voids remain in the alumina support

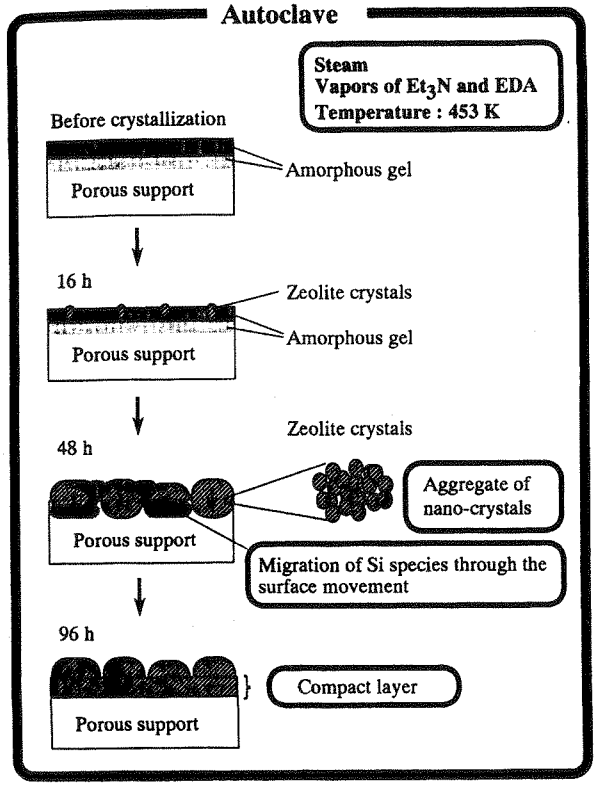

Fig. 9. Plausible formation process of FER membranes by the vapor-phase transport method.

in the early stage of crystallization. The aluminosilicate species are successively supplied, probably by the concentration gradient, into the pores of the alumina support from the gel layer on the support. Since the intermediate species formed from the gel is mobile on the alumina surface and is crystallized in the pores of the support, such voids can be filled up with zeolite crystals, leading to a compact FER–alumina composite layer.

4. Conclusions

The morphological change of the dry gel layer on and within a porous alumina support during crystallization has been examined to study the formation of zeolitic membranes by the VPT method. The same location on the top surface was observed repeatedly at different crystallization times. Samples prepared using the same hydrogel were also crystallized for different periods to observe the cross-section of the product. SEM observations and EDX elemental mappings strongly suggest that aluminosilicate intermediate species migrate over the top surface and into the pores of the alumina support, and successively crystallize to zeolite to give a compact membrane.

Acknowledgements

The authors are grateful to Nihon Gaishi Co. Ltd. for supplying α-alumina supports. We thank Mr Masao Kawashima (GHAS, Department of Chemical Engineering, Osaka University) for the FE-SEM measurements. We also express our gratitude to Grant-in-Aids for Scientific Research on Priority Areas (Grant No. 09218237).

References

[1] E.R. Geus, M.J. den Exter, H. Bekkum, J. Chem. Soc. Faraday Trans. 88 (1992) 3101–3109.
[2] E.R. Geus, H. Bekkum, W.J.W. Bakker, J.A. Moulijin, Micropor. Mater. 1 (1993) 131–147.
[3] F. Kapteijn, W.J.W. Bakker, J. van de Graaf, G. Zheng, J. Poppe, J.A. Moulijn, Catal. Today 25 (1995) 213–218.
[4] T. Sano, M. Hasegawa, Y. Kawakami, Y. Kiyozumi, H. Yanagishita, D. Kitamoto, F. Mizukami, Stud. Surf. Sci. Catal. 84 (1994) 1175–1182.
[5] Y. Yan, M. Tsapatsis, G.R. Gavalas, M.E. Davis, J. Chem. Soc. Chem. Commun. (1995) 227–228.
[6] Y. Yan, M.E. Davis, G.R. Gavalas, Ind. Eng. Chem. Res. 34 (1995) 1652–1661.
[7] R.D. Noble, J.L. Falconer, Catal. Today 25 (1995) 209–212.
[8] C. Bai, M.D. Jia, J.L. Falconer, R.D. Noble, J. Membr. Sci. 105 (1995) 79–87.
[9] M.J. den Exter, J.C. Jansen, J. van de Graaf, F. Kapteijn, H. van Bekkum, Stud. Surf. Sci. Catal. 102 (1996) 413–454.
[10] H. Kita, Maku (Membrane) 20 (1995) 169–182.
[11] Q. Liu, R.D. Noble, J.L. Falconer, H.H. Funke, J. Membr. Sci. 117 (1996) 163–174.
[12] C.D. Baertsch, H.H. Junke, J.L. Falconer, R.D. Noble, J. Phys. Chem. 100 (1996) 7676–7679.
[13] H. Funke, A.M. Argo, C.D. Baertsch, J.L. Falconer, R.D. Noble, J. Chem. Soc. Faraday Trans. 92 (1996) 2499–2502.
[14] J.F. Smetana, J.L. Falconer, R.D. Noble, J. Membr. Sci. 114 (1996) 127–130.
[15] Z.A.E.P. Vroon, K. Keizer, M.J. Gilde, H. Verweij, A.J. Burggraaf, J. Membr. Sci. 113 (1996) 293–300.

[16] J.E. Lewis Jr., G.R. Gavalas, M.E. Davis, AIChE J. 43 (1997) 83–90.
[17] G.J. Myatt, P.M. Budd, C. Price, S.W. Carr, J. Mater. Chem. 2 (1992) 1103–1104.
[18] T. Sano, F. Mizukami, H. Takaya, T. Mouri, M. Watanabe, Bull. Chem. Soc. Jpn. 65 (1992) 146–154.
[19] J.G. Tsikoyiannis, W.O. Haag, Zeolites 12 (1992) 126–130.
[20] J.C. Jansen, D. Kashchiev, A. Erdem-Senatalar, Stud. Surf. Sci. Catal. 85 (1994) 215–250.
[21] W. Xu, J. Dong, J. Li, J. Li, F. Wu, J. Chem. Soc. Chem. Commun. (1990) 755–756.
[22] M.H. Kim, H.X. Li, M.E. Davis, Micropor. Mater. 1 (1993) 191–200.
[23] M. Matsukata, N. Nishiyama, K. Ueyama, Micropor. Mater. 1 (1993) 219–222.
[24] N. Nishiyama, K. Ueyama, M. Matsukata, Micropor. Mater. 7 (1996) 299–308.
[25] N. Nishiyama, T. Matsufuji, K. Ueyama, M. Matsukata, Micropor. Mater. 12 (1997) 293–303.

ELSEVIER

Catalysis Today 56 (2000) 265–273

CATALYSIS TODAY

www.elsevier.com/locate/cattod

Permeation characteristics of butane isomers through MFI-type zeolitic membranes

Takaaki Matsufuji [a], Norikazu Nishiyama [a], Korekazu Ueyama [a], Masahiko Matsukata [b,*]

[a] *Division of Chemical Engineering, Graduate School of Engineering Science, Osaka University, 1-3 Machikaneyama-cho, Toyonaka-shi, Osaka 560-8531, Japan*

[b] *Department of Applied Chemistry, Waseda University, 3-4-1 Okubo, Shinnjyuku-ku, Tokyo 169-8555, Japan*

Abstract

MFI-type◆ zeolitic membranes were prepared by a vapor-phase transport method on porous α-alumina flat disks. Pure or mixed gas permeation measurements of butane isomers were performed at 375 K using two methods: pressure gradient (PG) and concentration gradient (CG) methods. Pure gas permeation measurements of H_2, He, CH_4, N_2, O_2, CO_2 and SF_6 were also carried out using PG method. Counter-diffusion of helium as a sweep gas was evaluated by determining the gas composition at the outlet of the feed side. It was confirmed that the counter-diffusion of helium occurs only when the total pressure of the feed side was <80 kPa.

In the mixed gas permeation measurements, the value of separation factor depended on the method of gas permeation. The separation factors of *n*-butane to *i*-butane were ca. 10 in the PG method and 30–60 in the CG method.

Keywords: Butane isomers; Zeolitic membranes; Pressure gradient; Concentration gradient

1. Introduction

In this decade, much attention has been paid to zeolitic membranes for gas separation, pervaporation and membrane catalysis [1–22]. Zeolitic membranes can be useful for separating mixtures of isomer with similar boiling points but different molecular sizes. Most of the zeolitic membranes reported in the literature are MFI-type zeolitic membranes synthesized by a hydrothermal technique, which is conventional for the preparation of granular zeolites.

Zeolite has been known to be a catalyst for catalytic cracking. Zeolitic membrane also possesses catalytic activity, either acid activity, or metal activity, or both. The catalytic activity can be modified according to the needs of the reaction involved [1]. For example, the acid activity of siliceous zeolites can be adjusted by the amount of trivalent elements (especially aluminum). Substitution by a trivalent element such as aluminum introduces a negative charge. The charge is to be balanced by cation exchange with proton and alkaline earth metal cations.

Suzuki [2] presented a large number of examples of membrane catalysis with ultrathin zeolitic membranes. He added reactants to one side of the zeolitic membrane and removed products from the other side. A good example of the zeolitic membrane reactor is for a feed of hydrogen/propene/*i*-butane mixture over a Pt–Ca A-type zeolitic membrane. Only hydrogen and propane appeared on the permeate side, indicating that hydrogenation and separation simultaneously

* Corresponding author. Tel./fax: +81-3-5286-3850.
E-mail address: mmatsu@mn.waseda.ac.jp (M. Matsukata).

0920-5861/00/$ – see front matter
PII: S0920-5861(99)00284-9

Table 1
Results of the separation of butane isomers with MFI-type zeolitic membrane

Support	Permeation method method	Temperature (K)	Ideal selectivity (–) *n*-/*i*-butane	Separation factor (–) *n*-/*i*-butane	Reference
Stainless steel/disk	CG	298	ca. 50	–	[3]
γ-Alumina/tube	PG, CG	298	22	–	[4]
		443	0.6	–	
α-Alumina/disk	PG	303	18.4	–	[5,6]
		458	33.1	–	
α-Alumina/disk	CG	298	90	52	[7]
		473	11	11	
Stainless steel/disk	CG	295	58	27	[8]
		403	–	23	
α-Almunia/disk	CG	373	1.5–12	18–26	[9]
γ-Alumina/tube	PG	300	14 (γ-Alumina)	33 (365 K)	[11]
α-Alumina/tube	PG	461	4.8 (α-Alumina)	18 (383 K)	

occurred. They did not report the information on numerical values of fluxes or stabilities of the membranes. These results would significantly expand the potential application of membrane catalysis using zeolite.

The quality of the membrane is important for the application of zeolitic membranes in industrial processes. Many research groups reported the pure and mixed gas permeation measurements of butane isomers, as listed in Table 1. *n*-Butane/*i*-butane permselectivity shows good indication of the quality of MFI-type zeolitic membrane. For single or mixed gas permeation measurements of butane isomers, two types of measurements have generally been performed: pressure gradient (PG) and concentration gradient (CG) methods.

In the PG method, the flux is determined at a given PG. On the other hand, the total pressure on both sides of membrane is generally kept at atmospheric pressure in the CG method. Helium or argon was generally used as a sweep gas in the gas permeation measurements. These sweep gases seemed to diffuse to the feed side during permeation measurements. To evaluate the permeation measurements, van de Graaf et al. [13] compared the data obtained from both PG and Wicke–Kallenbach methods. They claimed that the sweep gas significantly influenced permeation and such effect depended on the nature of sweep gas and on the magnitude of its counter permeation. It is difficult to conclude that previous permeation data were free from the effect of the counter-diffusion of sweep gas.

In this study, MFI-type zeolitic membranes were prepared by vapor-phase transport (VPT) method [23–30]. Both single gas permeation measurements and mixed gas separations were carried out to evaluate the influence of the method used for permeation measurement of butane isomers (pressure or concentration gradient) on the selectivity and on the counter-diffusion of the sweep gas with compact and less compact MFI-type zeolitic membrane.

2. Experimental

2.1. Preparation of parent gel

A parent aluminosilicate sol with SiO_2/Al_2O_3 ratio of 1000 was prepared using colloidal silica containing 30 wt.% of SiO_2, 0.5 wt.% of Al_2O_3 and 0.4 wt.% of Na_2O (Nissan Chemical Co., Ltd.). First, colloidal silica was mixed with NaOH(4N) at 303 K. A flat porous α-alumina support (Nihon Gaishi Co., Ltd.) with a cross-sectional area of 1.0×10^{-4} m^2 and an average pore diameter of 0.1 μm was dipped into the parent sol at 303 K for 1 day. Then the sol was forced to penetrate into the pores of alumina support by evacuating the support from one side for 1 h, as shown in Fig. 1. As a pretreatment of an alumina support, the support was treated with colloidal silica at the pH of about 10 to depress the dissolution of alumina during membrane synthesis.

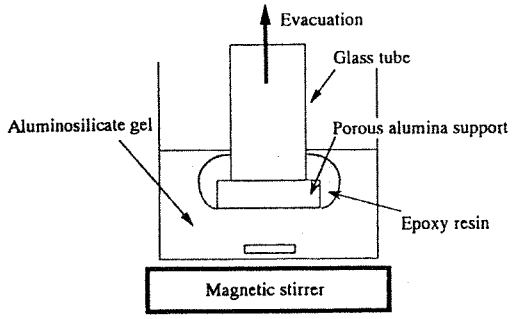

Fig. 1. Schematic diagram of experimental apparatus for coating α-alumina support with aluminosilicate sol.

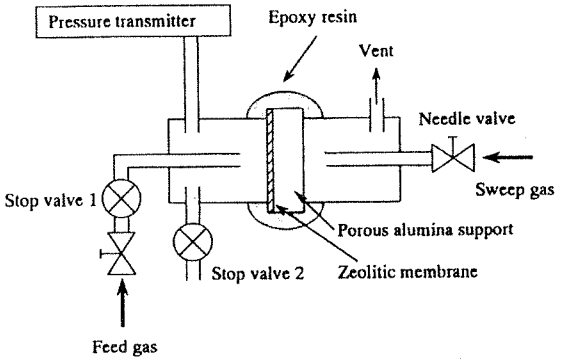

Fig. 2. Schematic diagram of experimental apparatus for permeation measurements.

2.2. Crystallization of dry gel by vapor-phase transport method

Crystallization was carried out in an autoclave. A mixture of ethylenediamine (EDA), triethylamine (Et_3N) and water (EDA: 2.0 Et_3N: H_2O, volume ratio) was poured in the bottom to produce vapor. The support coated with the parent gel was horizontally set on the partition in the middle of the autoclave. Crystallization was performed in gaseous environment at 453 K for 72 h at autogenous pressure. As-synthesized MFI membranes were calcined in air at 773 K for 10 h. The heating rate of 0.05–0.1 K min^{-1} was adopted in the temperature range from 473 to 773 K. The weight gain of alumina support during gel coating, crystallization and calcination was ca. 100 mg. The crystallinity and structure of the products were analyzed by X-ray diffraction (XRD) with Cu Kα radiation (Philips X's Pert-MRD). The morphology of products was examined by scanning electron microscopy (SEM) (Hitachi S-2250).

2.3. Evaluation of the compactness of zeolitic membranes

For evaluating compactness of MFI membranes, the pervaporation of 1,3,5-triisopropylbenzene (TIPB), which has a kinetic diameter (0.85 nm) larger than the pore dimensions of MFI (0.53 × 0.56, 0.51 × 0.55 nm), was carried out for 10 h at 295 K. A zeolitic membrane with a cross-sectional area of 0.50×10^{-4} m^2 was attached on an end of a glass tube, and placed in liquid TIPB. The permeation side was kept under vacuum. The permeant was collected for 10 h in a cold trap using liquid nitrogen and analyzed by a gas chromatograph with a flame ionization detector.

2.4. Gas permeation measurements

2.4.1. Pure gas permeation measurement

The pure gas permeation tests for H_2, He, CH_4, N_2, O_2, CO_2, *n*-butane, *i*-butane and SF_6 were performed using the PG method at 375 K. Fig. 2 shows the schematic diagram of experimental apparatus for determining the permeance. Epoxy resin was used as a seal material between a glass tube with a membrane and an apparatus. As a pretreatment for a gas permeation test, water adsorbed in the zeolitic membrane was removed by evacuating at 420 K for 2 h. The heating rate of 0.5–1.0 K min^{-1} was adopted. The total pressure of feed side was measured using the pressure transmitter. Helium was used as a sweep gas in the permeate side at atmospheric pressure. The permeance of H_2, He, CH_4, N_2, O_2, CO_2, *n*-butane, *i*-butane and SF_6 through an MFI membrane at 160 kPa was determined by using the rate of pressure reduction of the feed side from 165 to 155 kPa. They were calculated by using Eqs. (1) and (2):

$$\frac{\partial n}{\partial t} = \frac{\partial p}{\partial t} \times \frac{V}{RT} \quad (1)$$

$$\text{Permeance (mol m}^{-2}\,\text{s}^{-1}\,\text{Pa}^{-1}) = \frac{\partial n}{\partial t} \times \frac{1}{A\Delta p} \quad (2)$$

where n represents the amount of permeant (mol), t, time (s), p, pressure on the feed side (Pa), V, dead

volume on the feed side ($7.0\,cm^3$), R, gas constant ($8.314\,J\,mol^{-1}\,K^{-1}$), T, temperature (K), A, effective membrane area ($0.50 \times 10^{-4}\,m^2$) and Δp, partial pressure difference between the feed and permeant sides (Pa).

2.4.2. Evaluation of counter-diffusion of helium

The total pressure of feed side was kept at 180 kPa by feeding pure *n*-butane, after the pretreatment. After 24 h, feeding of *n*-butane was stopped by closing stop valve 2 shown in Fig. 2. The measurement was started after the total pressure of feed side was decreased to 160 kPa. Helium was used as a sweep gas and the pressure of permeate side was kept at atmospheric pressure throughout the permeation measurements. The feed gas was analyzed for the mole fraction of gas in the feed side by a gas chromatograph (Ohkura, Model 802) with a TC detector and a packed column (Porapak Type Q, 2 m × 1/8 in. (3.2 mm)). Similar procedure was used for measuring *i*-butane permeation, whereas only the total pressure of feed side was measured.

2.4.3. Mixed gas permeation measurement

In the PG method, the total pressure difference between the feed and permeation sides was kept at 60 kPa, while both sides of the membrane were kept at atmospheric pressure in the CG method, as shown in Fig. 3. Helium was used as a sweep gas. In the CG method, the total feed rates of butane isomers were 50–60 $cm^3\,min^{-1}$. The permeate and retentate gas were analyzed by gas chromatograph. Ideal selectivity was calculated from the flux ratio of *n*-butane to *i*-butane. Separation factor was calculated from the following equation,

$$\text{Separation factor} = \frac{(X_n/X_i)\ \text{permeate}}{(X_n/X_i)\ \text{feed}} \quad (3)$$

where X_n and X_i represent mole fractions of *n*-butane (%) and *i*-butane (%), respectively.

3. Results and discussion

3.1. Compactness of MFI-type zeolitic membrane

Almost half synthesized membranes were gas-tight (flux of helium $< 1.0 \times 10^{-8}\,mol\,m^{-2}\,s^{-1}$) after synthesis. When crystallization was not complete, a small amount of helium permeation was observed. The quality of the membranes after calcination was tested by the pervaporation of TIPB. After calcination, we obtained three polycrystalline MFI-type zeolitic membranes (membranes A, B and C) which were gas-tight before calcination.

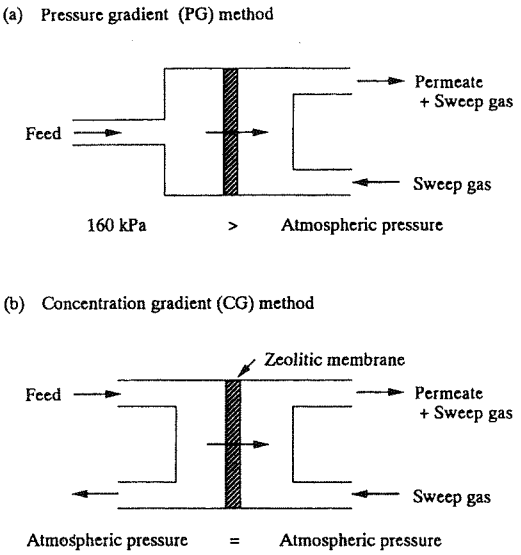

Fig. 3. Schematic diagram of gas permeation measurements.

Table 2 shows the flux of TIPB through the MFI membranes. After the pervaporation test, no permeation of TIPB through membrane A was detected, indicating that the flux of TIPB was less than $1.0 \times 10^{-9}\,mol\,m^{-2}\,s^{-1}$, the detection limit in this experiment. Therefore, it was concluded that membrane A was practically pinhole-free. On the other hand, the permeation fluxes of TIPB were 3.0×10^{-7} and $1.2 \times 10^{-6}\,mol\,m^{-2}\,s^{-1}$ for membrane B and C, respectively. Membranes B and C have pinholes larger than TIPB molecule.

Fig. 4 shows the SEM images of top and cross-sectional views of membrane A. On membrane

Table 2
Flux of TIPB through the MFI membranes

	Flux of TIPB ($mol\,m^{-2}\,s^{-1}$)
Membrane A	$<1.0 \times 10^{-9}$
Membrane B	3.0×10^{-7}
Membrane C	1.2×10^{-6}

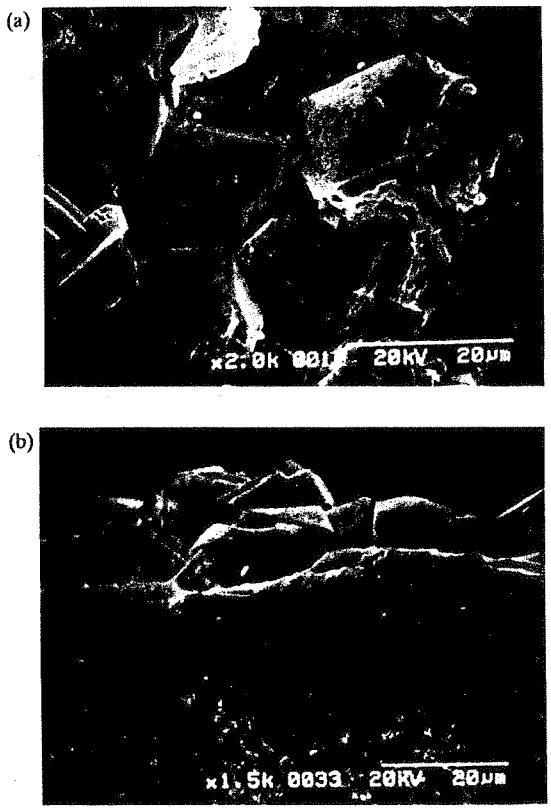

Fig. 4. SEM images for the (a) top view and (b) cross-sectional view of membrane A.

A, a top layer formed on the alumina support was ca. 20 μm thick and MFI zeolite was also formed in the interior of support was also ca. 20 μm thick.

3.2. Pure gas permeation measurement

Fig. 5 shows the permeances of H_2, He, CH_4, N_2, O_2, CO_2, *n*-butane, *i*-butane and SF_6 through membrane A as a function of kinetic diameter of molecule at 375 K. Molecules such as CO_2 and *n*-butane smaller than the channels of an MFI (0.53 × 0.56, 0.51 × 0.55 nm) showed greater permeances. On the other hand, the permeance of *i*-butane (0.50 nm) and SF_6 (0.55 nm), whose sizes are comparable to the size of the channels of MFI, were very low. The permeance ratios of *n*-butane/*i*-butane and *n*-butane/SF_6 were 60 and 385, respectively.

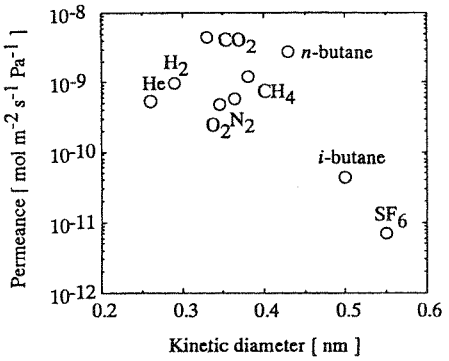

Fig. 5. Permeances as a function of kinetic diameter. Temperature: 375 K; partial pressure difference: 160 kPa.

3.3. Evaluation of counter-diffusion of helium

Counter-diffusion of the inert sweep gas can usually affect the permeation of feed components. The evaluation of counter-diffusion of the sweep gas is essential to understand the inherent permeances of feed components.

Fig. 6 shows the time course of the total pressure of feed side and the mole fraction of *n*-butane on the feed side for membrane A. It is worth noting that the total pressure of feed side had a minimum with time course and its value of 44.0 kPa was less than atmospheric pressure for the *n*-butane permeation test with membrane A. As shown in Fig. 6, the counter-diffusion of helium occurs only when the total pressure of the feed side was <80 kPa. Namely, *n*-butane dominantly permeated through membrane A from the feed side to the permeate one, and helium was difficult to enter the micropores of MFI crystals, even under the conditions that the total pressure of feed side was less than that of permeate side. When the total pressure of feed side was above 80 kPa, thus, the permeation data seemed to be free from the effect of the counter-diffusion of sweep gas. In the permeation measurement of *i*-butane with membrane A (not shown), the total pressure of feed side also had a minimum at 80.0 kPa.

On the other hand, in the permeation test with membrane B, the mole fraction of *n*-butane on the feed side started to decrease even when the total pressure of the feed side was higher than atmospheric pressure, as shown in Fig. 7. For membrane C, only the

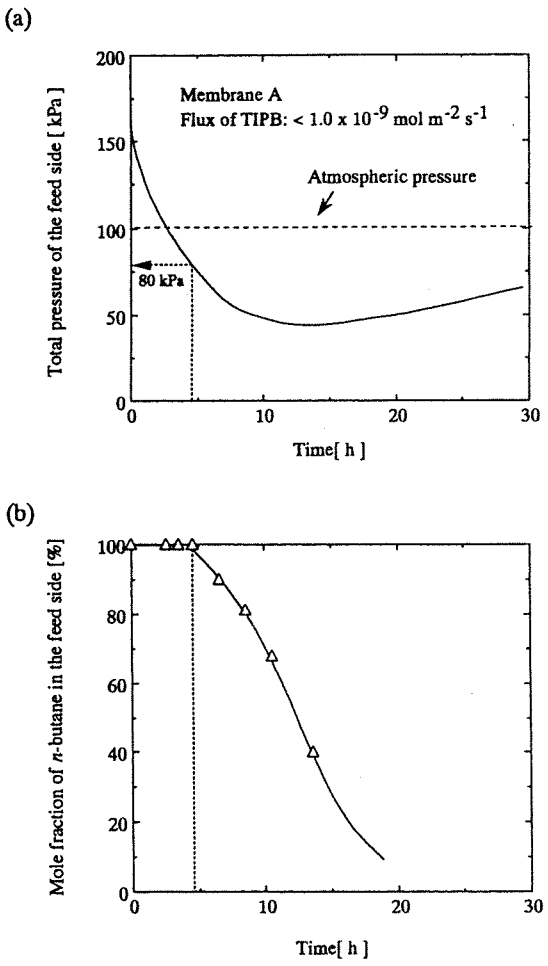

Fig. 6. Time course of (a) the total pressure of feed side and (b) the mole fraction of *n*-butane in the feed side with membrane A. Temperature: 375 K.

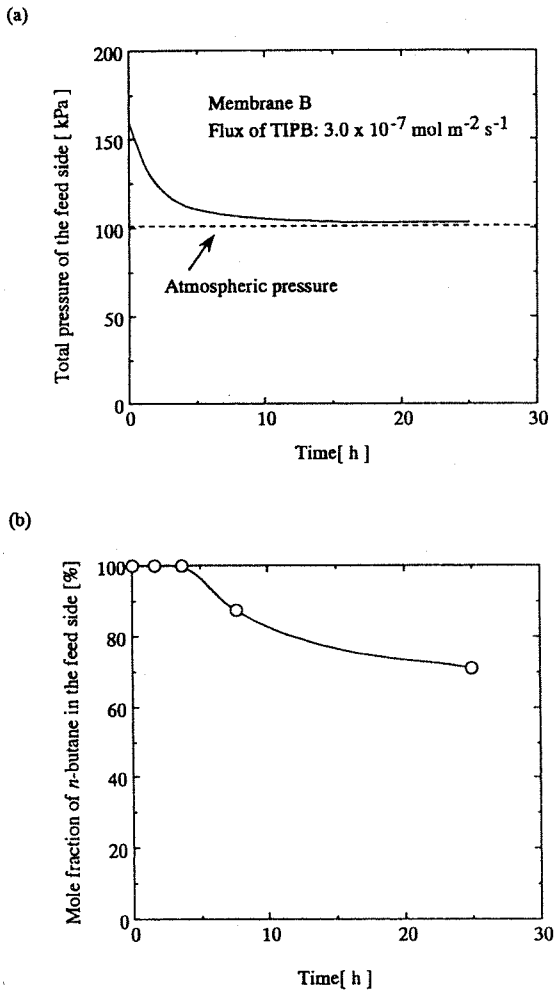

Fig. 7. Time course of (a) the total pressure of feed side and (b) the mole fraction of *n*-butane in the feed side with membrane B. Temperature: 375 K.

pressure change of the feed side was measured, and it quickly and monotonously approached to atmospheric pressure.

The compactness of MFI membrane would be essential to explain these permeation behavior. *n*-Butane molecules adsorbed might have filled the micropores of MFI crystals. Such pore filling would particularly be apparent with a compact membrane at lower temperatures. Even if the total pressure of feed side was lower than atmospheric pressure, the effect of pore filling possibly would still dominate the permeation behavior. *n*-Butane molecules filling the micropores of MFI crystals may inhibit the entrance of helium into the micropores of MFI.

On the other hand, *n*-butane seemed to permeate through pinholes in membrane B rather than the micropores of MFI crystals. *n*-Butane and helium can pass through each other in the pinholes of membrane B.

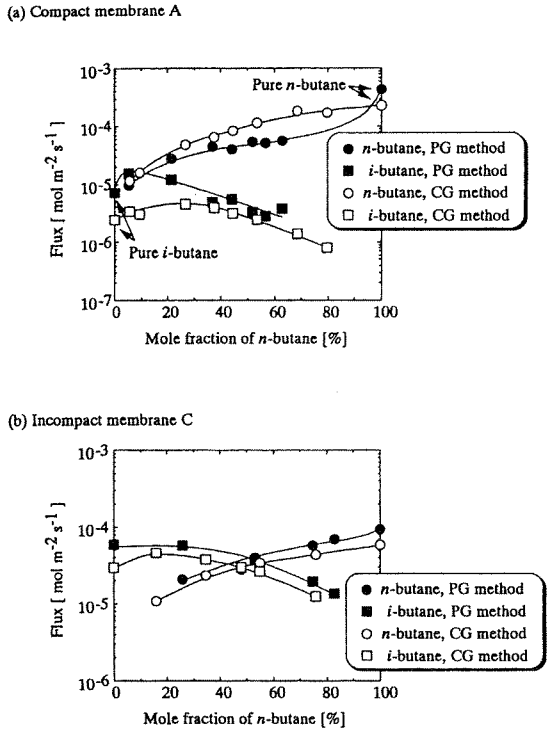

Fig. 8. Fluxes of butane isomers through MFI membranes as a function of mole fraction of *n*-butane in the feed. Temperature: 375 K; closed key: PG method; open key: CG method.

3.4. *n*-Butane/*i*-butane mixed gas separations

The permeation behaviors of *n*-butane and *i*-butane were studied with two types of gas permeation measurements at 375 K; PG and CG methods. It is not necessary to consider the effects of the counter-diffusion of helium with membrane A, because the total pressure of feed side was always above 80 kPa in these experimental procedure. Fig. 8 shows the fluxes of butane isomers through compact membrane A and incompact membrane C as a function of the mole fraction of *n*-butane in the feed.

In both permeation measurements using the PG and CG methods with membrane A, the flux of *n*-butane increased with increasing mole fraction of *n*-butane in the feed. It should be noted that the flux of *i*-butane had a maximum at around 25% of the mole fraction of *n*-butane in the CG method and 10% in the PG method, respectively. These results reveal that the permeation of *i*-butane was enhanced in the binary mixture. The results shown in Fig. 8 for the binary mixture show unique trend. *i*-Butane molecules might squeeze into the pore, accompanied by *n*-butane molecules. In the CG method, the flux of *n*-butane is higher than the flux of *i*-butane at low *n*-butane concentration for the membrane A. We suppose that a preferential distribution of *n*-butane and *i*-butane in the zeolite channels strongly depends on the concentration of the butane isomers on the feed side.

On the other hand, this is not true for the membrane C. Butane isomers seemed to permeate through pinholes in membrane C rather than the micropores of MFI crystals.

The PG method, where 60 kPa of total pressure difference was employed, gave a higher flux of *i*-butane and a lower flux of *n*-butane using membrane A, compared with those for the CG method. *i*-Butane molecules, adsorbed in the micropores of MFI, seem to reduce the diffusion and permeability of *n*-butane. On the other hand, the fluxes of both *n*-butane and *i*-butane in the PG method with membrane C were greater than those in the CG method.

Takaba et al. [31] presented the MD simulation of the mixed gas separation of butane isomers at 373 K. They reported that the permeation *n*-butane was observed, whereas *i*-butane did not permeate. However the diffusion of both isomers into the zeolite pores was observed. They concluded that the few diffused *i*-butane molecules reduced the diffusion and permeability of *n*-butane. The kinetic diameter of *i*-butane (0.50 nm) is larger than that of *n*-butane (0.43 nm). The micropores of MFI crystals are so narrow that *n*-butane and *i*-butane cannot pass through each other, possibly except at an intersection. The diffusion in such a narrow pore seems to be controlled by a molecule with a smaller permeation rate, i.e., *i*-butane molecule.

Fig. 9 shows the separation factor of butane isomer mixture through compact membrane A and incompact membrane C as a function of the mole fraction of *n*-butane in the feed. In the unary gas system, the ideal selectivity of *n*-butane to *i*-butane for membrane A was 60 in the PG method and 95 in the CG method. For binary mixtures, the separation factor also depended on the method of gas permeation: that of *n*-butane to *i*-butane was ca. 10 in the PG method and 30–60 in the CG method.

(a) Compact membrane A

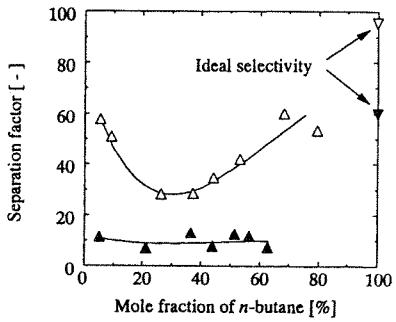

(b) Incompact membrane C

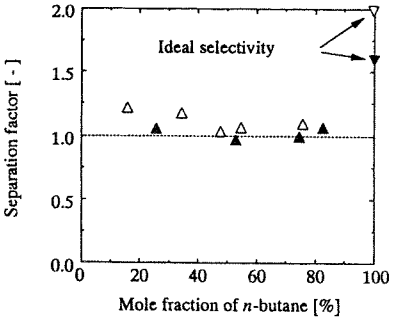

Fig. 9. Separation factor of butane isomers as a function of mole fraction of *n*-butane in the feed. Temperature: 375 K; closed key: PG method; open key: CG method.

On the other hand, the ideal selectivity of *n*-butane to *i*-butane using membrane C was only 1.6 in the PG method and 2.0 in the CG method. For the binary mixtures, the separation factors of *n*-butane to *i*-butane were ca. 1.0 in the PG method and 1.1 in the CG method, which are 1/30–1/60 of those for membrane A. These lead to a conclusion that the compactness of MFI membrane is essential to separate butane isomer mixtures at 375 K.

4. Conclusions

Polycrystalline MFI-type zeolitic membranes have been prepared by using vapor-phase transport method. In the permeation measurements, the compactness of MFI membrane is essential to obtain data, which are intrinsic to discuss the permeation through zeolitic layer. Using compact membrane, the permeation data free from the effects of counter-diffusion of helium were obtained by both PG method and CG method were free from the effects of counter-diffusion of helium. On the other hand, inert sweep gas permeated through pinholes of incompact membranes.

In the unary system using a compact membrane, small molecules such as CO_2 and *n*-butane showed greater permeances than those for large molecules, such as *i*-butane and SF_6. The permeance ratios of *n*-butane/*i*-butane and *n*-butane/SF_6 were 60 and 385, respectively.

In the binary system, the flux of *i*-butane had a maximum at around 25% of mole fraction of *n*-butane in the CG method and 10% in the PG method, respectively. This result reveals that permeation of *i*-butane was encouraged in the binary system.

The PG method gave a higher flux of *i*-butane and a lower flux of *n*-butane, compared with those for the CG method. *i*-Butane molecules may fill the micropore of MFI crystals and block their pore mouth. For binary mixtures, the separation factor depends on the method of gas permeation. The separation factors of *n*-butane to *i*-butane were ca. 10 in the PG method and 30–60 in the CG method at 375 K.

Acknowledgements

The authors are grateful to NGK Insulators, Ltd. for supplying α-alumina supports, and the authors thank GHAS laboratory at Osaka University form the SEM measurements.

References

[1] J.L. Falconer, R.D. Noble, D.P. Sperry, in: R.D. Noble, S.A., Stern (Eds.), Membrane Separations Technology. Principles and Applications, Elsevier, Amsterdam, 1995 (Chapter 14).
[2] H. Suzuki, US patent 4699892, 1987.
[3] E.R. Geus, H. Bekkum, W.J.W. Bakker, J.A. Moulijin, Microporous Mater. 1 (1993) 131–147.
[4] C. Bai, M.-D. Jia, J.L. Falconer, R.D. Noble, J. Membr. Sci. 105 (1995) 79–87.
[5] Y. Yan, M. Tsapatsis, G.R. Gavalas, M.E. Davis, J. Chem. Soc., Chem. Commun. (1995) 227–228.

[6] Y. Yan, M.E. Davis, G.R. Gavalas, Ind. Eng. Chem. Res. 34 (1995) 1652–1661.
[7] Z.A.E.P. Vroon, K. Keizer, M.J. Gilde, H. Verweij, A.J. Burggraaf, J. Membr. Sci. 113 (1996) 293–300.
[8] W.J.W. Bakker, F. Kapteijn, J. Poppe, J.A. Moulijn, J. Membr. Sci. 117 (1996) 57–78.
[9] K. Kusakabe, S. Yoneshige, A. Murata, S. Morooka, J. Membr. Sci. 116 (1996) 39–46.
[10] K. Kusakabe, A. Murata, T. Kuroda, S. Morooka, J. Chem. Eng. Jpn. 30 (1997) 72–78.
[11] J. Coronas, J.L. Falconer, R.D. Noble, AIChE J. 43 (1997) 1797–1812.
[12] R.D. Noble, J.L. Falconer, Catal. Today 25 (1995) 209–212.
[13] J.M. van de Graaf, F. Kapteijn, J.A. Moulijn, J. Membr. Sci. 144 (1998) 87–104.
[14] F. Kapteijn, W.J.W. Bakker, J. van de Graaf, G. Zheng, J. Poppe, J.A. Moulijn, Catal. Today 25 (1995) 213–218.
[15] T. Sano, M. Hasegawa, Y. Kawakami, Y. Kiyozumi, H. Yanagishita, D. Kitamoto, F. Mizukami, Stud. Surf. Sci. Catal. 84 (1994) 1175–1182.
[16] M.J. den Exter, J.C. Jansen, J.M. van de Graaf, F. Kapteijn, H. van Bekkum, Stud. Surf. Sci. Catal. 102 (1996) 413–454.
[17] H. Kita, Maku (Membrane) 20 (1995) 169–182.
[18] Q. Liu, R.D. Noble, J.L. Falconer, H.H. Funke, J. Membr. Sci. 117 (1996) 163–174.
[19] C.D. Baertsch, H.H. Junke, J.L. Falconer, R.D. Noble, J. Phys. Chem. 100 (1996) 7676–7679.
[20] H. Funke, A.M. Argo, C.D. Baertsch, J.L. Falconer, R.D. Noble, J. Chem. Soc., Faraday Trans. 92 (1996) 2499–2502.
[21] J.F. Smetana, J.L. Falconer, R.D. Noble, J. Membr. Sci. 114 (1996) 127–130.
[22] E. Lewis John Jr., G.R. Gavalas, M.E. Davis, AIChE J. 43 (1997) 83–90.
[23] W. Xu, J. Dong, Jinping Li, Jianquan Li, F. Wu, J. Chem. Soc., Chem. Commun. (1990) 755–756.
[24] M.H. Kim, H.X. Li, M.E. Davis, Microporous Mater. 1 (1993) 191–200.
[25] M. Matsukata, N. Nishiyama, K. Ueyama, Microporous Mater. 1 (1993) 219–222.
[26] M. Matsukata, N. Nishiyama, K. Ueyama, Microporous Mater. 7 (1996) 109–117.
[27] N. Nishiyama, K. Ueyama, M. Matsukata, Microporous Mater. 7 (1996) 299–308.
[28] N. Nishiyama, T. Matsufuji, K. Ueyama, M. Matsukata, Microporous Mater. 12 (1997) 293–303.
[29] E. Kikuchi, K. Yamashita, S. Hiromoto, K. Ueyama, M. Matsukata, Microporous Mater. 11 (1997) 107–116.
[30] N. Nishiyama, Synthesis of zeolitic membranes by vapor-phase transport method and their separation properties, Ph.D. Thesis, 1997.
[31] H. Takaba, R. Koshita, K. Mizukami, Y. Oumi, N. Ito, M. Kubo, A. Miyamoto, J. Membr. Sci. 134 (1997) 127–139.

ELSEVIER

Microporous and Mesoporous Materials 38 (2000) 43–50

MICROPOROUS AND MESOPOROUS MATERIALS

www.elsevier.nl/locate/micromeso

Synthesis and permeation studies of ferrierite/alumina composite membranes

Takaaki Matsufuji [a], Syuichi Nakagawa [a], Norikazu Nishiyama [a], Masahiko Matsukata [b,1], Korekazu Ueyama [a,*]

[a] *Division of Chemical Engineering, Graduate school of Engineering Science, Osaka University, 1-3 Machikaneyama-cho, Toyonaka-shi, Osaka 560-8531, Japan*

[b] *Department of Applied Chemistry, Waseda University, 3-4-1 Okubo, Shinnjyuku-ku, Tokyo 169-8555, Japan*

Received 2 August 1999; received in revised form 15 November 1999; accepted 17 November 1999

Abstract

Polycrystalline ferrierite/alumina composite membranes were prepared by a vapor-phase transport method. Pervaporation of *m*-xylene and 1,3,5-triisopropylbenzene was then used to evaluate the compactness of the membranes.

Permeation measurements were carried out for hydrogen, helium, methane, *n*-butane, *i*-butane and sulfur hexafluoride at 300–375 K. Ideal selectivities and the mixed gas separation factors were compared. The separation factor of butane isomers depended on the compactness of the membrane. The separation factor of *n*-butane/*i*-butane was as high as 40–70 at 375 K, and no detectable permeation flux of *m*-xylene was observed at 303 K.

Separation of a 25/75 *p*-xylene/*m*-xylene mixture was also performed at 303 K using pervaporation. The permeation of *p*-xylene was detectable, whereas that of *m*-xylene was below the detection limit of the experiment. The separation factor of *p*-xylene to *m*-xylene was greater than 16, which is much higher than the value of 1.0 expected from the vapor–liquid equilibrium.

Keywords: Ferrierite; Zeolitic membrane; Vapor-phase transport synthesis; Gas permeation; Pervaporation

1. Introduction

In the 1990s, zeolitic membranes have been synthesized by hydrothermal methods [1–21] and vapor-phase transport (VPT) methods [22–31]. The synthetic hydrothermal method is common for preparing powder zeolites. The VPT method is a novel synthetic method for zeolites which were first reported by Xu et al. [29], who synthesized ZSM-5 (MFI) from a aluminosilicate dry gel in contact with mixed vapors of water, ethylenediamine (EDA) and triethylamine (Et_3N) at 453 K. Following this work, Kim et al. [30] and our group [22–28,31] reported that the VPT method is useful to prepare zeolites [27,30] and zeolitic membranes [22–26,28,31]. As the size of zeolite pores is similar to the molecular dimension, both selective adsorption and molecular sieving play an important role in the separation of hydrocarbon mixtures.

* Corresponding author. Tel.: +81-6-6850-6255; fax: +81-6-6850-6255.

E-mail addresses: mmatsu@mn.waseda.ac.jp (M. Matsukata), ueyama@cheng.es.osaka-u.ac.jp (K. Ueyama).

[1] Tel.: +81-3-5286-3850; fax: +81-3-5286-3850.

1387-1811/00/$ - see front matter
PII: S1387-1811(99)00298-X

Interesting features of the separation of hydrocarbons using zeolitic membranes have been reported [1–28,31].

The compactness of the membrane is important for industrial applications of polycrystalline zeolitic membranes. The presence of intercrystalline defects is unavoidable in such membranes. When the sizes of the defects are larger than the pores of the zeolite, the membrane exhibits a very poor performance in separating hydrocarbon mixtures. By permeating through the membrane, a probe molecule with a size larger than the pores of the zeolite, but smaller than the size of the defects, the degree of defect can be evaluated from the permeation flux. We have used 1,3,5-triisopropylbenzene (TIPB) as a probe molecule, with a kinetic diameter of 0.85 nm which is a little larger than the pores of ferrierite (FER) (0.54×0.42 and 0.46×0.37 nm^2) and MFI (0.53×0.56 and 0.51×0.55 nm) [22–25,31].

Many research groups have reported the results of pure and mixed gas permeation for butane isomers through medium-pore zeolitic membranes including MFI and FER membranes [4,6–13, 16–19]. MFI has a framework structure composed of two types of intersecting channels which were both defined by 10-membered rings (MR). On the contrary, FER has 10-MR and 8-MR channels. The reported separation factors for the *n*-butane/*i*-butane were in the range of 20–60 using the polycrystalline MFI membranes at room temperature [6–12]. On the contrary, permeation results using a pure-silica oriented single-crystal FER membrane were reported by Lewis et al. [13]. They found an upper limit of *n*-butane/*i*-butane separation factor as high as 116 at 383 K.

In addition to the separation of mixtures of butane isomers, the separation of xylene isomers has been studied using MFI or FER membranes as well [13,20,21,24,25]. Table 1 lists the literature data obtained with the MFI and the FER membranes. Sano et al. [20] showed that it is difficult to separate *p*-xylene/*m*-xylene mixtures if the membrane has pinholes as large as 1 nm. Keizer et al. [12] obtained separation factors, $\alpha_{(p\text{-xylene}/o\text{-xylene})}$, of values <1.0 at 298 K and >200 at 375–415 K, showing that the separation factors of a binary mixture of *p*-xylene/*o*-xylene significantly depended on the operation temperature.

We previously reported the separation of *p*-xylene/*o*-xylene binary mixtures through the FER membrane synthesized by the VPT method. The separation factor, $\alpha_{(p\text{-xylene}/o\text{-xylene})}$, was 3.1 at 303 K [24,25]. We can expect higher separation factors of xylene isomers through FER membranes, as the pore sizes of FER were slightly smaller than those of MFI.

In this study, we used polycrystalline FER-type zeolitic membranes synthesized by the VPT method. Compactness of the membranes was evaluated by pervaporation tests, using *m*-xylene and TIPB as probe molecules. Permeation measurements of pure gas and mixed gas separations of butane isomers were carried out to study the importance of the compactness of polycrystalline FER membrane. The separation of a *p*-xylene/*m*-xylene mixture is also discussed using the most compact membrane.

Table 1
Separation of xylene isomer mixtures using MFI and FER membranes at room temperature

Component	Permeation method	Flux of *p*-xylene (mol m^{-2} s^{-1})	Separation factor α (*p*-/*m*- or *o*-xylene)	References
MFI membrane				
p-/*m*-xylene	Pervaporation	8.4×10^{-4}	1	[20]
p-/*o*-xylene	Vapor permeation	$\approx 5 \times 10^{-4}$	1	[21]
p-/*o*-xylene	Vapor permeation	$\approx 1 \times 10^{-7}$	0.5–0.9	[12]
p-/*m*-xylene	Pervaporation	9.4×10^{-8}	0.43	[31]
FER membrane				
p-/*o*-xylene	Pervaporation	6.6×10^{-7}	3.1	[24,25]

2. Experimental

2.1. Preparation of the parent gel

A flat porous α-alumina disk (NGK Insulators, Ltd.), with a cross-sectional area of 1.0×10^{-4} m^2 and an average pore diameter of 0.1 μm, was used as a support. This alumina support was treated with colloidal silica of pH about 10 in order to reduce the dissolution of alumina during synthesis. A parent aluminosilicate sol was prepared using a sodium silicate solution containing 35–38 wt.% of SiO_2 and 17–19 wt.% of Na_2O (Kanto Chemical Co., Inc.) as a silica source, and aluminum sulfate anhydride, $Al_2(SO_4)_3$, (Wako Pure Chem. Ind. Co., Ltd.), as an alumina source. The sodium silicate solution was mixed with $Al_2(SO_4)_3$, deionized water and H_2SO_4 at 273 K. The composition of the parent sol was $24SiO_2$:Al_2O_3:$12Na_2O$:$470H_2O$:$0.77H_2SO_4$. The colloidal silica-treated support was dipped into the parent sol for one day at 303 K. The sol was then forced into the pores of the alumina support by evacuating the support from one side for 1 h.

2.2. Crystallization of dry gel by the vapor-phase transport method

The support coated with the parent sol was dried for 24 h at 298 K and placed in the center of an autoclave. A mixture of EDA, Et_3N and water (EDA:$2.0Et_3N$:H_2O, volume ratio) was poured into the bottom of the autoclave to produce vapor. Crystallization was then performed at 453 K and under autogenous pressure for up to five days. A synthesized FER membrane was calcined in air at 773 K for 4 h. A heating rate of 0.1 K min^{-1} was adopted in the range of 473–773 K. The crystallinity and structure of the products were analyzed by X-ray diffraction (XRD) using CuKα radiation (Philips X's Pert-MRD).

2.3. Evaluation of the compactness of zeolitic membranes

To evaluate the compactness of the FER membranes, pervaporation of *m*-xylene and TIPB having the kinetic diameters of 0.68 and 0.85 nm, respectively, (which are larger than the pore dimensions of FER: 0.54×0.42, 0.46×0.37 nm^2), was carried out for 25 h at 303 K. The effective cross-sectional area of the membrane was 0.50×10^{-4} m^2. Vacuum was applied on the permeation side. The permeant was continuously collected for 25 h in a cold trap using liquid nitrogen, and was analyzed by a gas chromatograph equipped with a flame ionization detector.

2.4. Permeation measurements

Epoxy resin was used as a sealant between the membrane and the apparatus. As a pre-treatment for a permeation test, water adsorbed on the zeolitic membrane was removed by evacuation at 420 K for 2 h. Between each set of permeation experiments, the membrane was calcined for 6 h at 773 K to remove the adsorbed components and the epoxy resin. This treatment gave reproducible separation results.

2.4.1. Pure gas permeation measurements

The pure gas permeation tests for hydrogen, helium, methane, *n*-butane, *i*-butane and SF_6 were performed in a batchwise manner at 300–375 K. Vacuum was applied on the permeation side. The total pressure on the feed side was measured using a pressure transmitter. The permeances of hydrogen, helium, methane, *n*-butane, *i*-butane and SF_6 through an FER membrane at 100 kPa were determined from the rate of pressure reduction, from 102 to 98 kPa, on the feed side. The permeance was calculated using Eqs. (1) and (2):

$$\frac{dn}{dt} = \frac{dp}{dt} \times \frac{V}{RT}, \tag{1}$$

$$\text{Permeance (mol m}^{-2}\text{ s}^{-1}\text{ Pa}^{-1}) = \frac{dn}{dt}\frac{1}{A\,\Delta p}, \tag{2}$$

where n represents the amount of permeant (mol), t is the time (s), p, the pressure on the feed side (Pa), V, the dead volume on the feed side (5.3 cm^3), R, the gas constant (8.314 J mol^{-1} K^{-1}), T, the temperature (K), A, the effective membrane area (0.50×10^{-4} m^2) and Δp, the partial pressure difference between the feed and the permeation sides

(Pa). An ideal selectivity was calculated from the permeance ratio of the molecules.

2.4.2. Mixed gas permeation measurements

The same experimental apparatus was used for the mixed gas permeation measurements. The total permeances of both *n*-butane and *i*-butane were calculated from Eqs. (1) and (2), as mentioned above. The separation factor was calculated from the total amount of permeant and the change of composition on the feed side. The initial feed gas and final feed gas were analyzed with a gas chromatograph (Ohkura, Model 802) with a TC detector and a packed column (Porapak Type Q, 2 m × 1/8 in. (3.2 mm)). The initial molar ratio of butane isomers on the feed side was 51/49 *n*-butane/*i*-butane. The composition of the gas on the feed side was successively changed from 51/49 *n*-butane/*i*-butane to ≈49/51 *n*-butane/*i*-butane during the mixed gas permeation measurements. The permeance of each butane isomer was determined by GC-analysis.

2.4.3. Permeation measurements of xylene isomers

Permeation measurements of *p*-xylene and *m*-xylene were performed using the pervaporation technique referred above at 303 K. Experiments were carried out for single component and binary systems. For the binary mixtures, the composition of the feed was 25 mol% *p*-xylene and 75 mol% *m*-xylene.

2.5. Amount of butane isomers adsorbed on ferrierite powders

Adsorption measurements of butane isomers were carried out in a conventional volumetric apparatus at ≈100 kPa in the temperature range of 303–375 K. 0.5 g of FER powder in the sample cell was degassed at 395 K for 2 h. The pressure of the sample cell was measured by a Baratron absolute pressure transducer (model CMLB-31S06).

Competitive adsorption of butane isomers at ≈100 kPa was also carried out at 375 K in the same manner as the pure gas adsorption measurements. The initial composition of feed gas was analyzed by GC before adsorption. The initial molar ratio of butane isomers on the feed side was ≈52/48 *n*-butane/*i*-butane. The composition of the feed gas was progressively changed during the adsorption measurement. The amount of each butane isomer adsorbed was determined by GC analysis in the gas phase.

3. Results and discussion

3.1. Compactness of the FER-type zeolitic membrane

Although we prepared three polycrystalline FER-type zeolitic membranes (membranes A, B and C) under the same conditions, different permeation characteristics were found.

Table 2 shows the permeation flux of TIPB and *m*-xylene through the FER membranes. After the pervaporation test, the permeation of TIPB through membranes A and B was not detectable, indicating that the flux of TIPB was less than the detection limit of 1.0×10^{-9} mol m^{-2} s^{-1}. In addition, the permeation flux of *m*-xylene through membrane A was less than 4.0×10^{-10} mol m^{-2} s^{-1}, corresponding to the detection limit of *m*-xylene.

The permeation flux of *m*-xylene through membrane B was 2.9×10^{-9} mol m^{-2} s^{-1}, as shown in Table 2. Membrane B has pinholes larger than the *m*-xylene molecule. The permeation flux of TIPB was 7.6×10^{-6} mol m^{-2} s^{-1} for membrane C, suggesting that membrane C has pinholes larger than the TIPB molecule. Therefore, it is concluded that the compactness of membranes is decreasing in the order A > B > C.

3.2. Pure gas permeation measurement

Fig. 1 shows the permeances of hydrogen, helium, methane, *n*-butane, *i*-butane and sulfur

Table 2
Pervaporation tests for the compactness of FER membranes

Membrane	Flux of TIPB (mol m^{-2} s^{-1})	Flux of *m*-xylene (mol m^{-2} s^{-1})
A	$< 1.0 \times 10^{-9}$	$< 4.0 \times 10^{-10}$
B	$< 1.0 \times 10^{-9}$	2.9×10^{-9}
C	7.6×10^{-6}	n/a[a]

[a] not analyzed.

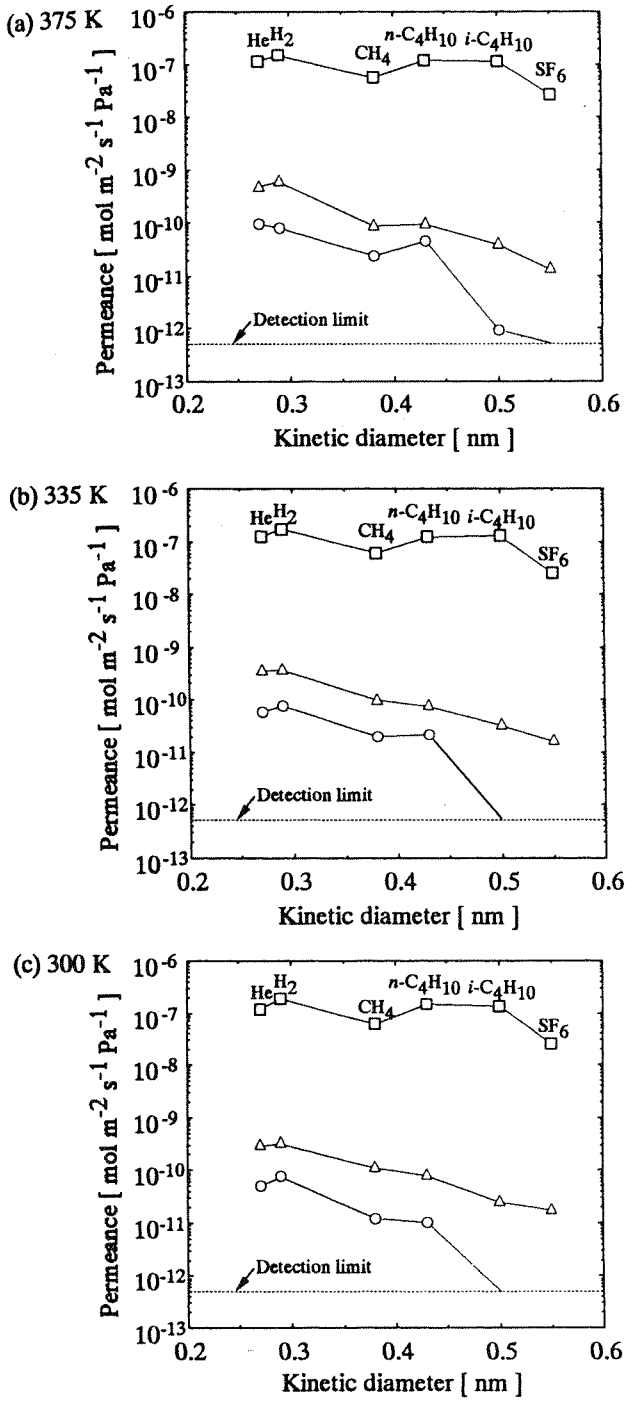

Fig. 1. Pure gas permeances through FER membranes as a function of the kinetic diameter of the molecules: ○: membrane A, △: membrane B, □: membrane C.

hexafluoride through membranes A, B, and C as a function of the kinetic diameter of the molecules. For membranes A and B, molecules such as hydrogen, helium, methane, *n*-butane, (smaller than the 10-MR channel of an FER (0.54×0.42 nm^2)) showed permeances higher than those of *i*-butane and sulfur hexafluoride. The permeance of *i*-butane (0.50 nm) and SF_6 (0.55 nm), the sizes of which are comparable to the size of the FER channels, were very low. For membrane A, the permeance of *i*-butane at 300–335 K and sulfur hexafluoride at 300–375 K was below the detection limit (5.0×10^{-13} mol m^{-2} s^{-1} Pa^{-1}) of this experiment. The ideal selectivities of hydrogen to *i*-butane at 375 K were 702 for membrane A, 14.7 for membrane B, and 1.3 for membrane C. The ideal selectivities of *n*-butane to *i*-butane at 375 K were 40 for membrane A, 2.5 for membrane B, and 1.0 for membrane C, as listed in Table 3. Therefore, the ideal selectivities of small/large molecules such as hydrogen/*i*-butane and *n*-butane/*i*-butane depend on the compactness of the membrane.

3.3. *n*-butane/*i*-butane mixed gas separations

The results of the mixed gas permeation experiments are summarized in Table 3. The initial molar ratio of butane isomers on the feed side was ≈51/49 *n*-butane/*i*-butane. The mixed gas permeances of butane isomers follow the order: membrane A < membrane B < membrane C. Ideal selectivities at 375 K follow the order: membrane A > membrane B > membrane C. The separation factors in mixed gas permeation measurements at 375 K follow the same order. The separation factors are always higher than the ideal selectivities in these experiments. The separation factor of *n*-butane/*i*-butane using membrane C was 1.3–1.4 in the range 300–375 K, indicating that the compactness of membrane C was very poor. Higher separation factors are obtained at the cost of smaller permeances of butane isomers. It was found that the pervaporation results of TIPB were a good indication of the capability of a membrane for separation of butane isomer mixtures, as listed in Table 2.

Adsorption data of butane isomers are listed in Table 4. The amounts of butane isomers adsorbed

Table 3
Mixed gas permeation results for the FER membranes

	Temperature (K)	Permeance (mol m^{-2} s^{-1} Pa^{-1})		αi^a	α^b
		n-butane	*i*-butane		
Membrane A	375	2.5×10^{-11}	$3.7–7.1 \times 10^{-13}$	40	40–70
Membrane B	375	1.2×10^{-10}	5.4×10^{-12}	2.5	23
	335	1.3×10^{-10}	1.3×10^{-11}	2.3	10
	300	9.4×10^{-11}	1.1×10^{-11}	3.3	8.5
Membrane C	375	1.3×10^{-7}	9.0×10^{-8}	1.0	1.4
	335	1.2×10^{-7}	9.5×10^{-8}	0.97	1.3
	300	1.4×10^{-7}	9.9×10^{-8}	1.1	1.4

[a] ideal selectivity.
[b] separation factor.

Table 4
Amount of butane isomers adsorbed on FER powder

	Temperature (K)	Amount adsorbed (mg/g-FER)		αi^a or α^b
		n-butane	*i*-butane	
Pure gas	375	41	11	3.7
	335	52	17	3.1
	300	59	21	2.8
Mixed gas	375	40	0.7–1.2	30–60

[a] ideal selectivity.
[b] separation factor.

on FER particles synthesized by the VPT method was measured at 100 kPa. At 300–375 K, the amount of *n*-butane adsorbed was higher than that of *i*-butane. The amount of butane isomer adsorbed increased with decreasing temperature. The ideal selectivities (the ratios of amount adsorbed) were 3.7 at 300 K, 3.1 at 335 K, and 2.8 at 375 K, respectively. The separation factor of *n*-butane/*i*-butane, calculated from the competitive adsorption data at 375 K, was 30–60, which is similar to the separation factor ($\alpha_{(n\text{-butane}/i\text{-butane})} = 40–70$) in the binary gas permeation test. The separation factor ($\alpha_{(n\text{-butane}/i\text{-butane})}$) is much higher than the ideal selectivities calculated from the sorption data. *n*-butane seems to effectively block the adsorption and/or the entering of *i*-butane. This blocking effect in a mixed gas system is an important factor in interpreting the permeation results through the FER membrane.

Lewis et al. reported a separation factor of 45/55 *n*-butane/*i*-butane mixture at 383 K, using a pure-silica oriented single-crystal FER membrane (10-MR channels) [13]. This can be regarded as the upper limit of separation factors for *n*-butane/*i*-butane. A direct comparison of the results reported there using single-crystal ferrierite with our polycrystalline FER membrane seems to be possible, as all the parameters used like the mixed gas composition, pressure difference between the feed side and permeate side and the temperature are similar. While the separation factor for the 45/55 *n*-butane/*i*-butane mixed gas permeation measurement was reported to be 116 at 383 K for the pure-silica oriented single-crystal FER membrane [13], that for membrane A at 375 K was 40–70, which is lesser than the upper limit of 116. The compactness of membrane A was the highest of our three membranes; however, there is still room for improvement in realizing higher separation factors.

3.4. Permeation measurements of xylene isomers

The pervaporation tests of *p*-xylene and *m*-xylene in the single component system were performed at 303 K using membrane A, which is the most compact one. The flux of *p*-xylene in the single component system was 3.3×10^{-9} mol m^{-2} s^{-1}; however, the flux of *m*-xylene was below the detection limit ($< 4.0 \times 10^{-10}$ mol m^{-2} s^{-1}), as shown in Table 5.

Separation of a 25/75 *p*-xylene/*m*-xylene mixture was also performed at 303 K. Only the permeation of *p*-xylene was detectable. The separation factor of *p*-xylene to *m*-xylene was greater than 16, which exceeds the value of 1.0 expected

Table 5
Permeation measurements of *p*-xylene/*m*-xylene isomers using membrane A at 303 K

		Flux ($mol\,m^{-2}\,s^{-1}$)	αi^a or α^b
Pure	*p*-xylene	3.3×10^{-9}	> 8.3
	m-xylene	$< 4.0 \times 10^{-10}$	
Mixture	*p*-xylene (25 mol%)	2.1×10^{-9}	> 16
	m-xylene (75 mol%)	$< 4.0 \times 10^{-10}$	

[a] ideal selectivity (flux ratio of *p*-/*m*-xylene).
[b] separation factor.

from the vapor–liquid equilibrium. Although the kinetic diameter of *p*-xylene (0.59 nm) is comparable to the size of the channels of FER, the kinetic diameter of *m*-xylene (0.68 nm) is apparently greater than the channel size. The permeation results, therefore, suggest that shape-selective separation for *p*-xylene/*m*-xylene takes place at the pore mouth of the FER membrane.

We reported previously the separation of 49/51 *p*-xylene/*o*-xylene mixture through the FER membrane at 303 K [24]. The separation factor of *p*-/*o*-xylene was 3.1. Although a direct comparison of the data is not possible as the xylene isomers used and the feed composition are both different, the fluxes of *p*-xylene can be compared. The flux of *p*-xylene through the FER membrane reported previously was 6.6×10^{-7} $mol\,m^{-2}\,s^{-1}$, which is about 200 times higher than for membrane A. The higher separation factor was accompanied by smaller fluxes of xylene isomers, as shown in the butane permeation results.

The flux of *p*-xylene in this work was lesser than the existing data obtained with MFI membranes at room temperature [12,20,21,31]. On the contrary, the separation factors of a binary mixture of *p*-xylene/*o*-xylene or of *p*-xylene/*m*-xylene were higher than those for MFI membranes, as shown in Table 1. These tendencies agree with the smaller pore size of FER than MFI. For a higher flux of *p*-xylene, it is necessary to establish a technique for decreasing the membrane thickness.

4. Conclusions

Polycrystalline FER-type zeolitic membranes have been prepared using the VPT method. The ideal selectivity and the separation factor of butane isomer mixture both depend on the compactness of the membrane. The most compact membrane in this experiment gave the highest separation factor, 40–70. This membrane can separate *p*-xylene and *m*-xylene mixtures. The separation factor of *p*-xylene to *m*-xylene was higher than 16, which is greater than the value of 1.0 expected from the vapor–liquid equilibrium. The FER-type zeolitic membranes have a great potential in separating hydrocarbon mixtures.

References

[1] T. Sano, H. Yanagisita, Y. Kiyozumi, F. Mizukami, K. Haraya, J. Membr. Sci. 95 (1994) 221.
[2] H. Kita, K. Horii, Y. Ohtoshi, K. Tanaka, K. Okamoto, J. Mater. Sci. Lett. 14 (1995) 206.
[3] H. Kita, Maku (Membrane) 20 (1995) 169.
[4] E.D. Geus, H. Bekkum, W.J.W. Bakker, J.A. Moulijin, Microporous Mater. 1 (1993) 131.
[5] F. Kapteijn, W.J.W. Bakker, J. van de Graaf, G. Zheng, J. Poppe, J.A. Moulijn, Catal. Today 25 (1995) 213.
[6] Z.A.E.P. Vroon, K. Keizer, M.J. Gilde, H. Verweij, A.J. Burggraaf, J. Membr. Sci. 113 (1996) 293.
[7] W.J.W. Bakker, F. Kapteijn, J. Poppe, J.A. Moulijn, J. Membr. Sci. 117 (1996) 57.
[8] K. Kusakabe, A. Murata, T. Kuroda, S. Morooka, J. Chem. Engng. Jpn. 30 (1997) 72.
[9] J. Coronas, J.L. Falconer, R.D. Noble, AIChE J. 43 (1997) 1797.
[10] J. Coronas, R.D. Noble, J.L. Falconer, Ind. Engng. Chem. Res. 37 (1998) 166.
[11] J.M. Van de Graaf, F. Kapteijn, J.A. Moulijn, Ind. Engng. Chem. Res. 37 (1998) 4071.
[12] K. Keizer, A.J. Burggraaf, Z.A.E.P. Vroon, H. Verweij, J. Membr. Sci. 147 (1998) 159.
[13] J.E. Lewis Jr., G.R. Gavalas, M.E. Davis, AIChE J. 43 (1997) 83.
[14] P. Meriaudeau, A. Thangaraj, C. Naccache, Microporous Mater. 4 (1995) 213.
[15] Y. Kiyozumi, F. Mizukami, Proceeding of the International Workshop on Zeolitic Membranes and Films, 1998, p. 13.
[16] C. Bai, M.D. Jia, J.L. Falconer, R.D. Noble, J. Membr. Sci. 105 (1995) 79.
[17] K. Kusakabe, S. Yoneshige, A. Murata, S. Morooka, J. Membr. Sci. 116 (1996) 39.
[18] Y. Yan, M.E. Davis, G.R. Gavalas, Ind. Engng. Chem. Res. 34 (1995) 1652.
[19] Y. Yan, M.E. Davis, G.R. Gavalas, J. Membr. Sci. 123 (1997) 95.

[20] T. Sano, M. Hasegawa, Y. Kawakami, Y. Kiyozumi, H. Yanagishita, D. Kitamoto, F. Mizukami, in: J. Weitkamp, H.G. Karge, H. Pfeifer, W. Hölderich (Eds.), Zeolites and Related Microporous Materials: State of the Art 1994, Stud. Surf. Sci. Catal. 84 (1994) 1175.
[21] C.D. Baertsch, H.H. Funke, J.L. Falconer, R.D. Noble, J. Phys. Chem. 100 (1996) 7676.
[22] N. Nishiyama, K. Ueyama, M. Matsukata, Microporous Mater. 7 (1996) 299.
[23] N. Nishiyama, T. Matsufuji, K. Ueyama, M. Matsukata, Microporous Mater. 12 (1997) 293.
[24] N. Nishiyama, K. Ueyama, M. Matsukata, in: H. Chou, S.-K. Ihm, Y.S. Uh (Eds.), Progress in Zeolite and Microporous Materials, Stud. Surf. Sci. Catal. 105 (1996) 2195.
[25] N. Nishiyama, Ph.D. Thesis, Osaka University, Japan, 1997.
[26] N. Nishiyama, K. Ueyama, M. Matsukata, J. Chem. Soc. Chem. Commun. (1995) 1967.
[27] M. Matsukata, N. Nishiyama, K. Ueyama, Microporous Mater. 7 (1996) 109.
[28] N. Nishiyama, K. Ueyama, M. Matsukata, AIChE J. 43 (11A) (1997) 2724.
[29] W. Xu, J. Dong, J. Li, J. Li, F. Wu, J. Chem. Soc. Chem. Commun. (1990) 755.
[30] M.H. Kim, H.X. Li, M.E. Davis, Microporous Mater. 1 (1993) 191.
[31] T. Matsufuji, N. Nishiyama, M. Matsukata, K. Ueyama, submitted to J. Membr. Sci.

ELSEVIER

Journal of Membrane Science 178 (2000) 25–34

journal of MEMBRANE SCIENCE

www.elsevier.nl/locate/memsci

Separation of butane and xylene isomers with MFI-type zeolitic membrane synthesized by a vapor-phase transport method

Takaaki Matsufuji[a], Norikazu Nishiyama[a], Masahiko Matsukata[b,1], Korekazu Ueyama[a,*]

[a] *Division of Chemical Engineering, Graduate School of Engineering Science, Osaka University, 1-3 Machikaneyama-cho, Toyonaka-shi, Osaka 560-8531, Japan*

[b] *Department of Applied Chemistry, Waseda University, 3-4-1 Okubo, Shinnjyuku-ku, Tokyo 169-8555, Japan*

Received 25 October 1999; received in revised form 2 March 2000; accepted 1 May 2000

Abstract

MFI-type zeolitic membranes were prepared by a vapor-phase transport (VPT) method on porous α-alumina flat disks. Single- and mixed-gas permeation measurements of butane isomers were performed in the temperature range of 300–375 K. The separation factor was always greater than the ideal selectivity. This result is explained by the preferential adsorption of *n*-butane on MFI in the binary system.

The pervaporation tests for xylene isomers were performed at 303 K. *p*-Xylene was the most permeable component in the unary system. In the permeation measurements of a binary mixture of *p*-xylene/*m*-xylene and a ternary mixture of *p*-xylene/*m*-xylene/*o*-xylene, *p*-xylene predominantly permeated in the early stage, and then, the flux of *p*-xylene decreased gradually and finally became lower than that of the other xylene isomers. The adsorption of *m*-xylene in the pores of MFI seemed to block the permeation of *p*-xylene.

Keywords: Zeolite membrane; MFI; Gas separation; Adsorption; Pervaporation

1. Introduction

In recent years, zeolitic membranes have been synthesized by a hydrothermal method [1–21] and a vapor-phase transport (VPT) method [22–28]. Since the size of zeolite pores is similar to the molecular dimension, both selective adsorption and molecular sieving play an important role in the separation of hydrocarbon mixtures. Interesting features on the separation of hydrocarbons using zeolitic membranes have been reported [1–28].

Separation using MFI-type zeolitic membranes were reported most often with respect to the separation of linear and branched hydrocarbon mixtures such as *n*-butane/*i*-butane [4,5,7,8,10–12] and *n*-hexane/2,2-dimethylbutane [4,10,12]. MFI has a framework structure composed of two types of intersecting channels which are both defined by 10-membered rings (MRs). Reported separation factors for the *n*-butane/*i*-butane and *n*-hexane/2,2-dimethylbutane mixtures were in the range of 20–60 and over 600, respectively, at room temperature.

In addition to the separation of linear and branched hydrocarbon mixtures, the separation of aromatic

* Corresponding author. Tel.: +81-6-6850-6255; fax: +81-6-6850-6255.
E-mail addresses: mmatsu@mn.waseda.ac.jp (M. Matsukata), ueyama@cheng.es.osaka-u.ac.jp (K. Ueyama).
[1] Tel.: +81-3-5286-3850; fax: +81-3-5286-3850.

0376-7388/00/$ – see front matter
PII: S0376-7388(00)00462-2

hydrocarbons has been studied using MFI or ferrierite (FER) membranes [12,14,21,24,25]. Sano et al. [14] prepared pure silica MFI membranes by hydrothermal synthesis on a porous sintered stainless steel and α-alumina supports. They showed that it is difficult to separate *p*-xylene/*m*-xylene mixtures if the membrane has pinholes as large as 1 nm. Baertsch et al. [21] reported the vapor permeation results of aromatic hydrocarbons through a pure silica MFI membrane. The permeances in the binary and ternary systems were identical to the permeance of the slowest component in the unary system measurements. They explained the separation results by a single-file transport. The pores of MFI were so narrow that aromatic hydrocarbon molecules could not pass each other. Consequently, the molecule with the slowest permeation rate inhibited the permeation of the other species. The selective adsorption at the entrance of pore seems to play an important role in the separation of an aromatic hydrocarbon mixture. However, no separation was obtained for binary mixtures of *p*-xylene/*o*-xylene, *p*-xylene/ethylbenzene, *m*-xylene/ethylbenzene and *p*-xylene/toluene in the temperature range of 380–480 K. Their results showed that the selective adsorption of the most permeable component in the unary system hardly occurred at the entrance of the pore in the binary and ternary systems.

On the other hand, Keizer et al. [12] obtained separation factors, $\alpha_{(p\text{-xylene}/o\text{-xylene})}$, of <1.0 at 298 K and >200 at 375–415 K, showing that the separation factors of a binary mixture of *p*-xylene/*o*-xylene significantly depended on operation temperature. Their membrane shows a possibility of the separation of a mixture of xylene isomers with the MFI membranes in vapor permeation.

We previously reported the separation of *p*-xylene/*o*-xylene binary mixtures through the FER membrane at 303 K [24,25]. The separation factor, $\alpha_{(p\text{-xylene}/o\text{-xylene})}$, was 3.1 at room temperature.

Further investigation is necessary to assure the possibility of the separation of a mixture of xylene isomers using a membrane composed of zeolite with a 10-MR channel. FER has 10-MR channels, for instance. We can expect larger fluxes of xylene isomers through MFI membranes, because the pore sizes of MFI (0.53 nm×0.56 nm and 0.51 nm×0.55 nm) were slightly larger than the pore sizes of FER (0.54 nm×0.42 nm and 0.46 nm×0.37 nm).

In this study, MFI membranes were prepared by the VPT method. Both single-gas permeation measurements and mixed-gas separations of butane isomers were carried out. Permeation behavior of xylene isomers through the MFI membrane was studied using a pervaporation technique.

2. Experimental

2.1. Preparation of parent gel

A flat porous α-alumina disk (NGK Insulators Ltd.) with a membrane area of 1.0×10^{-4} m^2 and an average pore diameter of 0.1 μm was used as a support. The alumina support was treated with colloidal silica with a pH of 10 to depress the dissolution of alumina from the support during synthesis. Parent aluminosilicate sol was prepared using colloidal silica containing 30 wt.% of SiO_2, 0.04 wt.% of Al_2O_3 and 0.4 wt.% of Na_2O (Nissan Chemical Co. Ltd.), and NaOH solution (4 N) (Wako Pure Chem. Ind. Co. Ltd.) at 303 K. The colloidal silica was mixed with NaOH solution at 303 K. The composition of the parent sol was 1000 SiO_2:1.0 Al_2O_3:210 Na_2O:25 000 H_2O. The support treated with the colloidal silica was dipped into the parent sol at 303 K for 1 day. Then, the sol was forced to penetrate into the pores of alumina support by evacuating the support from one side for 1 h.

2.2. Crystallization of dry gel by the vapor-phase transport method

The support coated with the parent sol was dried for 24 h at 298 K and placed in the middle of an autoclave. The inner volume of the autoclave was 100 cm^3. A mixture of ethylenediamine (0.5 cm^3), triethylamine (1.0 cm^3) and water (0.5 cm^3) was poured into the bottom of the autoclave to produce vapor. Crystallization was then performed at 453 K and autogenous pressure for 4 days. An as-synthesized MFI membrane was calcined in air at 773 K for 10 h. A heating rate of 0.1 K min^{-1} was adopted in the temperature range of 473–773 K. The crystallinity and structure of the product were analyzed by X-ray diffraction (XRD) using Cu Kα radiation (Philips X's Pert-MRD). The resulting morphology was examined by scanning electron microscopy (SEM, Hitachi S-2250).

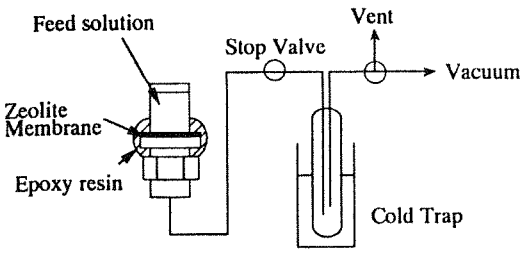

Fig. 1. Schematic diagram of the experimental apparatus for pervaporation.

2.3. Permeation measurements

Epoxy resin was used as a sealant between membrane and apparatus. As pretreatment for permeation tests, water adsorbed in the zeolitic membrane was removed by evacuation at 420 K for 2 h. Before each permeation experiment, the membrane was calcined for 4–10 h at 773 K to remove adsorbed components and epoxy resin.

2.3.1. Pervaporation

In order to evaluate the compactness of the MFI membranes, the pervaporation of 1,3,5-triisopropylbenzene (TIPB) with a kinetic diameter (0.85 nm) larger than the pore dimensions of MFI (0.53 nm×0.56 nm, 0.51 nm×0.55 nm) was carried out for 25 h at 303 K. The zeolitic membrane was attached at one end of a glass tube with a cross-sectional area of 0.50×10^{-4} m^2. Liquid TIPB were poured in the glass tube, as shown in Fig. 1. The permeation side was kept under vacuum. The permeant was continuously collected for 25 h in a cold trap using liquid nitrogen and analyzed by a gas chromatograph equipped with a flame ionization detector.

Pervaporation of xylene isomers were also performed at 303 K. Single, binary (*p*-xylene/*m*-xylene) and ternary (*p*-xylene/*m*-xylene/*o*-xylene) components of xylene isomers were tested. The compositions of the feed mixture were determined by the gas chromatograph.

2.3.2. Gas permeation measurements

Gas permeation measurements were performed using a pressure gradient (PG) method. The permeation measurements were operated in a batch-wise manner, as shown in Fig. 2.

In the PG method, the total pressure of the feed side was monitored using the pressure transmitter during the permeation measurement. The permeation side was evacuated to less than 50 Pa. This condition is referred to as vacuum. Single-gas permeation tests for He, N_2, *n*-butane, *i*-butane and SF_6 were performed in the temperature range of 300–375 K. The permeances of these gases at atmospheric pressure were determined by using the rate of pressure decrease of the feed side from 105 to 95 kPa. Ideal selectivity was calculated from the ratio of permeances.

Mixed-gas permeation measurements of butane isomers mixture were performed in the temperature range of 300–375 K. The initial feed gas and final feed gas were analyzed with a gas chromatograph (Ohkura, Model 802) with a TC detector and a packed

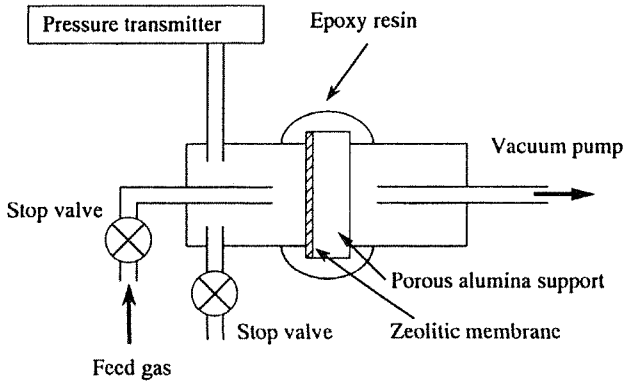

Fig. 2. Schematic diagram of gas permeation measurements.

column (Porapak Type Q, 2 m × 1/8 in. (3.2 mm)). The initial composition of the feed gas was 52/48 *n*-butane/*i*-butane (molar ratio). The permeances of each butane isomer and separation factor (*n*-butane/*i*-butane) were calculated from the total amount of permeant and the change in composition on the feed side.

Separation factors in the mixed-gas permeation measurements were defined as the following equation:

$$\text{Separation factor} = \frac{(X_n/X_i)_{\text{permeate}}}{(X_n/X_i)_{\text{feed}}}$$

where X_n and X_i represent mole fractions of *n*-butane (%) and *i*-butane (%), respectively.

2.4. Adsorption of butane isomers on MFI powder

Adsorption measurements using MFI powder synthesized by the VPT method were carried out by a conventional volumetric method at 100±5 kPa in the temperature range of 303–375 K. Prior to the experiments, 0.5 g of MFI (with SiO_2/Al_2O_3 ratio=1000) powder in the sample cell was degassed at 400 K for 2 h. The pressure of the sample cell was monitored with a Baratron absolute pressure transducer (model CMLB-31S06) until the change in pressure was not observed anymore.

The binary component adsorption measurements of butane isomers were carried out in the temperature range of 303–375 K, in the same manner as that in the unary system. A mixture of butane isomers with a 52/48 *n*-butane/*i*-butane molar ratio was introduced into a closed cell containing MFI powder. The decrease in pressure was monitored during the adsorption measurement. After the pressure reached an equilibrium value, the composition of the gas phase was measured by a gas chromatograph analysis.

3. Results and discussion

3.1. Compactness of MFI-type zeolitic membrane

We previously reported that the formation of FER/alumina composite layer in the interior of the support was compact [23,25]. Fig. 3 shows XRD patterns for (a) MFI powder synthesized by the VPT method, (b) as-synthesized membrane and (c) MFI membrane after removal of the top layer. Reflection peaks for MFI were still observed after removal of the top layer. Fig. 4 shows SEM images for (a) the top surface before removal of the top layer and (b) cross-section of the product before removal of the top layer and (c) after removal of the top layer. Numerous voids were observed among zeolite crystals on the top surface of MFI membrane, as shown in Fig. 4(a). After removal of the top layer, a ca. 20 μm thick of MFI/alumina composite layer was observed in the interior of the support, as shown in Fig. 4(c).

The permeation measurement of molecules larger than the zeolite pore seems to be a useful technique to evaluate the compactness of zeolitic membranes. We employed TIPB as a probe molecule for the pervaporation of the MFI membrane. No permeation of TIPB through the MFI membrane was detected, indicating that the permeation flux of TIPB was less than 1.0×10^{-9} mol m^{-2} s^{-1}, the detection limit in this experiment. Therefore, it was concluded that the MFI membrane was practically pinhole-free.

In the literature [8,10,11], the ideal selectivities of a specific pair of components such as N_2/SF_6 and *n*-butane/*i*-butane are taken as a good index of membrane compactness. The ideal selectivities for the N_2/SF_6 and *n*-butane/*i*-butane systems were in the range of 1.6–138 and 10–90, respectively, at ca. 300 K [4,5,7,8,10–12]. Widely varying selectivities reported so far are due to the different permeation methods used and conditions in permeation measurements.

Fig. 5 shows the permeances of N_2 and SF_6 through the MFI membrane as a function of temperature. The permeances of both N_2 and SF_6 increased with increasing temperature. The ideal selectivities for the N_2/SF_6 system were in the range of 8–13 in the temperature range of 303–375 K. Fig. 6 shows the permeation results of butane isomers. The permeances of butane isomers in the unary system increased with increasing temperature. The ideal selectivities of *n*-butane/*i*-butane in the PG method were 22 at 300 K, 16 at 335 K and 14 at 375 K, as shown in Fig. 6(b). The values of ideal selectivities for the N_2/SF_6 and *n*-butane/*i*-butane systems obtained in this study were in the range reported in the literature [4,5,7,8,10–12].

3.2. n-Butane/i-butane separations

In the binary system, the permeances of butane isomers also increased with increasing temperature. The

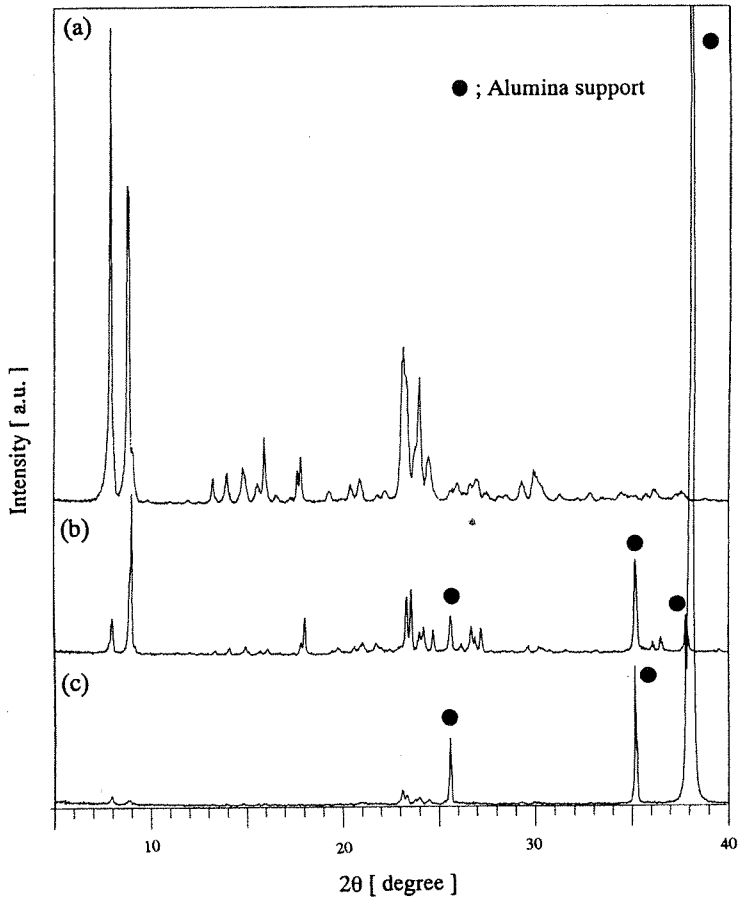

Fig. 3. XRD patterns for (a) MFI powder, (b) as-synthesized membrane and (c) MFI membrane after removal of the top layer.

separation factors of *n*-butane to *i*-butane were 28 at 300 K, 40 at 335 K and 69 at 375 K, as shown in Fig. 6(b). The separation factor is always greater than the ideal selectivity.

Adsorption of butane isomers in single and binary systems on MFI powder synthesized by the VPT method was measured. Table 1 shows the amounts of butane isomers adsorbed on MFI powder in the unary system. The ratio of the adsorbed amount of *n*-butane to that of *i*-butane (α_i) increased from 1.2 to 1.9 with increasing temperature (from 300 to 375 K).

Table 2 shows the amounts of butane isomers adsorbed on MFI powder in the binary-component adsorption measurements. The separation factor (α_{mix}) was always greater than the ideal selectivity. These results show that the preferential adsorption of *n*-butane on MFI plays an important role in the selective separation of a mixture of butane isomers using an MFI membrane. The difference in diffusivity between *n*-butane and *i*-butane in the zeolite pores might contribute to the selectivity in membrane separation in addition to the preferential adsorption of *n*-butane, because the selectivities in membrane separation were much larger than those in adsorption.

3.3. Separations of xylene isomers

Table 3 lists the fluxes of xylene isomers in the unary system. The flux of *p*-xylene is the largest among three kinds of isomers. The order of these selectivities can

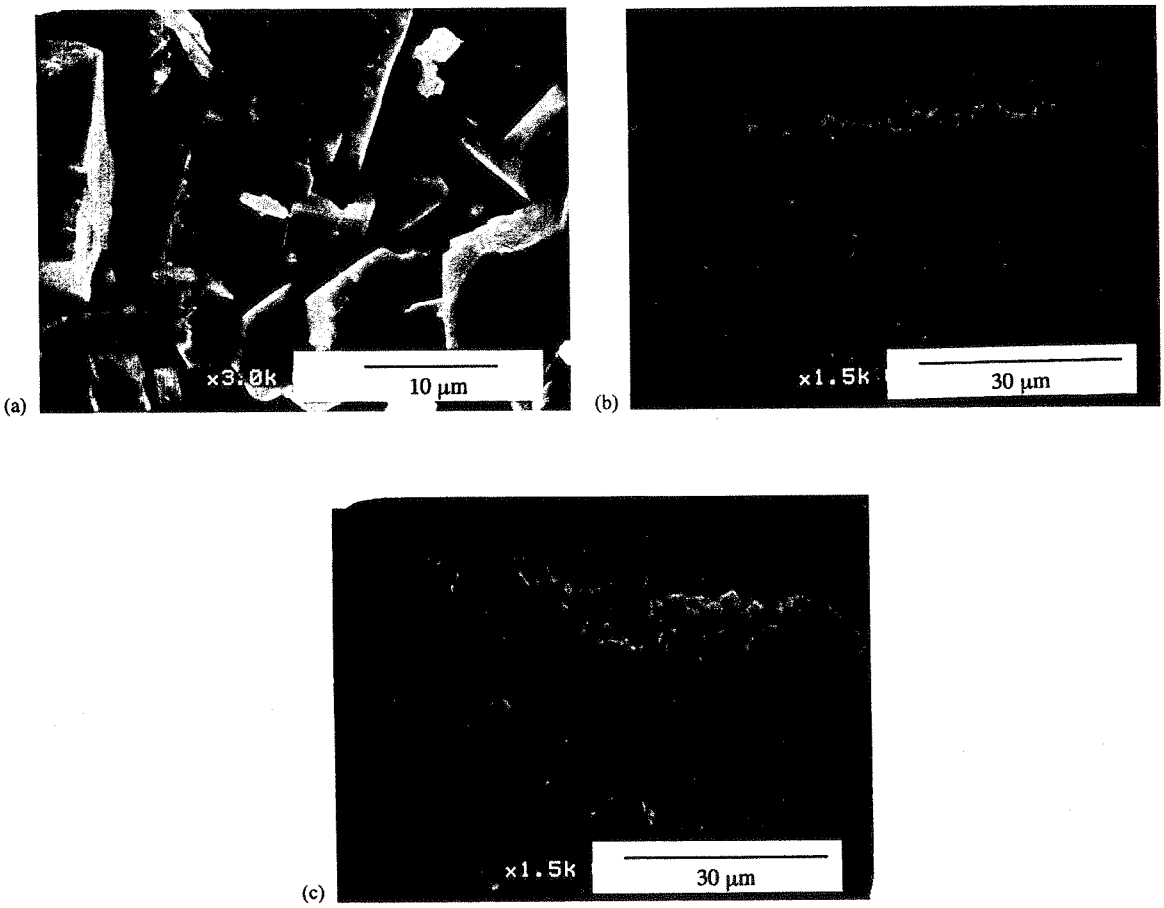

Fig. 4. SEM images for (a) the top surface before removal of the top layer, (b) cross-section of the product before removal of the top layer and (c) after removal of the top layer.

be explained by the size effect. The kinetic diameter of *p*-xylene is 0.59 nm and that of *m*-xylene and *o*-xylene is 0.68 nm.

Fig. 7(a) shows the transient profiles of the fluxes of *p*-xylene and *m*-xylene in the pervaporation of a 50/50 *p*-xylene/*m*-xylene mixture. *p*-Xylene preferentially permeated in the early stage and has a maximum value of flux, while the flux of *m*-xylene gradually increases and the flux of *m*-xylene at steady state becomes larger than that of *p*-xylene. The separation factor of the *p*-xylene/*m*-xylene system at steady state was 0.43, showing *meta*-selectivity.

In Fig. 7(b), *p*-xylene also predominantly permeates in the early stage and finally becomes the slowest component in the permeation measurement of a ternary mixture. In the permeation measurements of mixtures, the MFI membrane showed *para*-selectivity only in the early stage, suggesting that the kinetic diameter is not a limiting factor for the separation of a xylene isomer mixture. The separation factors of $\alpha_{(p\text{-xylene}/m\text{-xylene})}$, $\alpha_{(p\text{-xylene}/o\text{-xylene})}$ and $\alpha_{(m\text{-xylene}/o\text{-xylene})}$ at steady state were 0.16, 0.18 and 1.1, respectively.

Karsli et al. [29] reported that pre-loading with *p*-xylene at room temperature caused symmetry changes and lattice distortions to increase the sorption rates of *m*-xylene and *o*-xylene in the pores. It is considered that *p*-xylene adsorbed in the pores of

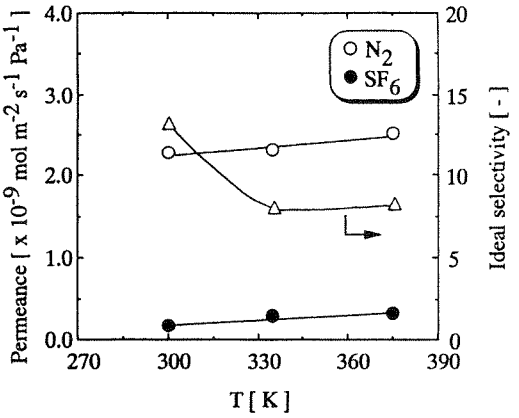

Fig. 5. Permeances of N_2 and SF_6 through an MFI membrane and ideal selectivities of N_2/SF_6 as a function of temperature.

MFI in the early stage of pervaporation opened the pores of MFI. Consequently, *m*-xylene and *o*-xylene were easily permeated through the MFI membrane.

Fig. 8 shows the pervaporation results of a ternary mixture of xylene isomers after the permeation measurement of *m*-xylene in the unary system. The flux of *m*-xylene dropped gradually after the exchange of the feed. The flux of *m*-xylene was reduced because of the lower concentration of *m*-xylene in the feed. The steady-state flux of *o*-xylene became large and then reached almost the same value as that shown in

Table 1
Amounts of butane isomer adsorbed on MFI powder in a unary system

Temperature (K)	Adsorbed amount (molecule u.c.$^{-1}$[a])		α_i[b]
	n-Butane	*i*-Butane	
375	5.0	2.6	1.9
335	6.0	3.5	1.7
300	7.2	6.0	1.2

[a] u.c.: unit cell.
[b] α_I: ratio of the adsorbed amount of *n*-butane/*i*-butane.

Table 2
Amounts of butane isomer adsorbed on MFI powder in a binary system

Temperature (K)	Adsorbed amount (molecule u.c.$^{-1}$[a])		α_i[b]
	n-Butane	*i*-Butane	
375	3.4	0.5	6.7
335	4.8	0.8	6.0
300	6.3	1.1	5.6

[a] u.c.: unit cell.
[b] α_{mix}: separation factor of *n*-butane/*i*-butane in the adsorption measurement.

Fig. 7(b). However, the flux of *p*-xylene was less than 1.0×10^{-9} mol m^{-2} s^{-1}, the detection limit in this experiment, indicating that the loading of *m*-xylene in the pores of MFI inhibited the permeation of *p*-xylene. *meta*(*ortho*)-selective separation at steady

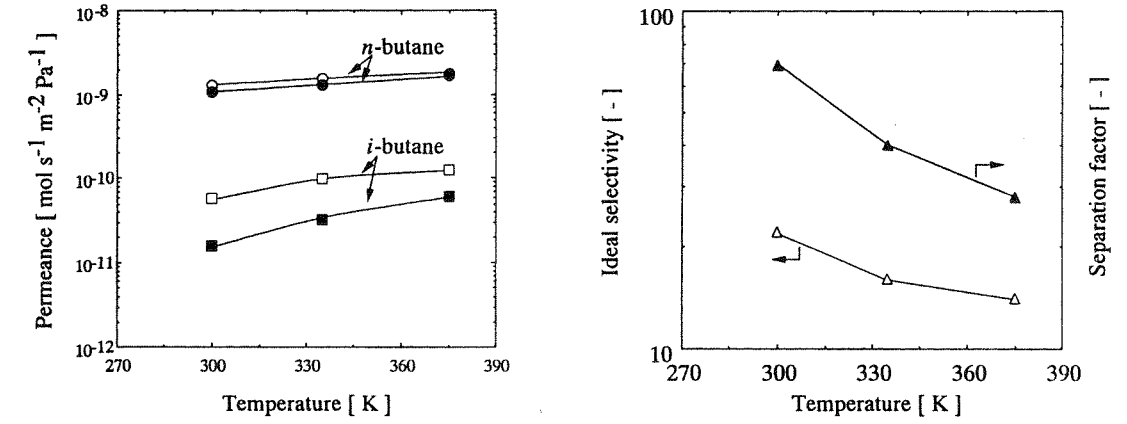

Fig. 6. Permeation results of butane isomers through MFI membrane. Open key: unary system. Closed key: 52/48 *n*-butane/*i*-butane mixed-gas system.

Table 3
Pervaporation results for a single liquid component of xylene isomers at 303 K

	Flux ($\times 10^{-7}$ mol m^{-2} s^{-1})
p-Xylene	5.5
m-Xylene	3.9
o-Xylene	3.4

state suggests that *m*-xylene or *o*-xylene is adsorbed more strongly than *p*-xylene in the pores of the MFI membrane.

3.4. Comparison of the separation of xylene isomers with the separation of butane isomers

The kinetic diameters of *n*-butane and *i*-butane are 0.43 and 0.50 nm, respectively, which is smaller than those of xylene isomers. In the unary system, smaller *n*-butane permeated faster than *i*-butane, which is a behavior similar to that of *p*-xylene in the xylene permeation measurements. Smaller *n*-butane also preferentially permeated in the separation of butane isomers, because *n*-butane is a more adsorptive component. On the other hand, the reverse in selectivity occurred while separating mixtures of xylene isomers, although *p*-xylene was the most permeable component in the early stage of permeation measurement. It is considered that *p*-xylene is a faster but less adsorptive component compared to *m*-xylene and *o*-xylene in the pores of MFI. Therefore, the permeation of

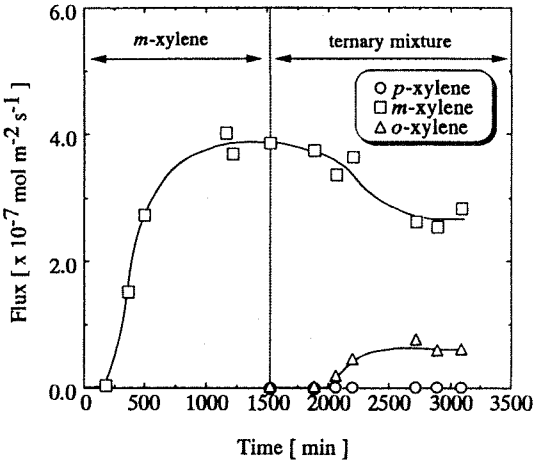

Fig. 8. Pervaporation results of a ternary mixture of xylene isomers after the permeation measurement of *m*-xylene. Composition of ternary mixture: *p*-xylene, 24 mol%; *m*-xylene, 51 mol%; *o*-xylene, 25 mol%.

p-xylene might have been blocked by strongly adsorbed *m*-xylene and *o*-xylene which were slower components. However, since the kinetic diameters of xylene isomers are close to the pore size of MFI, the reverse in selectivity occurred very slowly.

3.5. Reproducibility of permeation data after calcination

We performed 35 calcination procedures to remove adsorbed components over the whole of the permea-

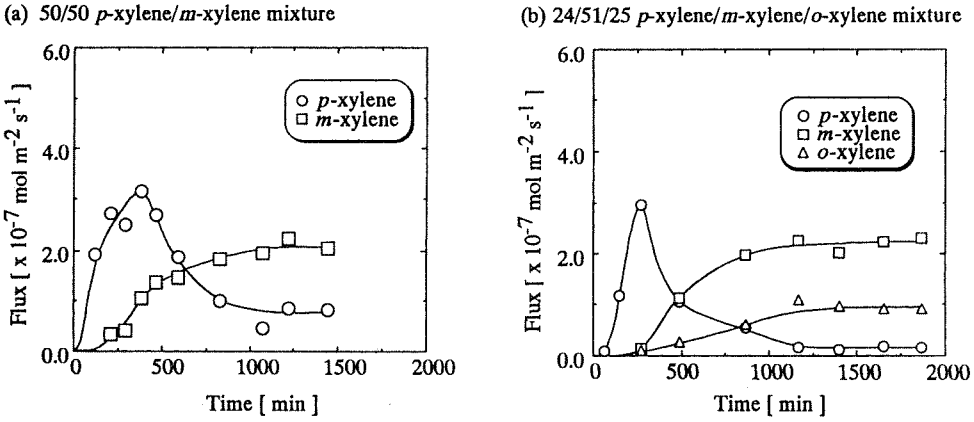

Fig. 7. Pervaporation results for xylene isomers at 303 K through MFI-type zeolitic membrane.

tion experiments. The influence of calcination on permeation properties was studied. The reproducibility of permeation data was tested using He as a probe molecule. The permeance of He after the first permeation measurement was 1.9×10^{-9} mol m^{-2} s^{-1} Pa^{-1} at 375 K. After the last permeation measurement, the permeance of He was 1.8×10^{-9} mol m^{-2} s^{-1} Pa^{-1}, indicating that the permeances of He were reproducible. Moreover, the permeation properties of membrane were reproducible on repeated runs of butane and xylene separation measurements. It seems that the MFI membrane has an excellent stability over the permeation and calcination conditions.

4. Conclusions

The competitive adsorption of butane isomers is one of the important factors in the separation of butane isomer mixture using the MFI membrane.

In the pervaporation of xylene isomers, *p*-xylene was the most permeable component in the unary system. However, *m*-xylene and *o*-xylene permeated faster than *p*-xylene in the binary and ternary systems. The adsorption of *m*-xylene in the pores of MFI seemed to inhibit the permeation of *p*-xylene.

Acknowledgements

The authors are grateful to NGK Insulators Ltd. for supplying α-alumina supports, and the authors appreciate Dr. Yasuyuki Egashira (Department of Chemical Engineering, Osaka University) for the helpful discussions. The authors express their appreciation to GHAS at the Department of Chemical Engineering of Osaka University for XRD and SEM measurements.

References

[1] E.R. Geus, H. Bekkum, W.J.W. Bakker, J.A. Moulijin, High-temperature stainless steel supported zeolite (MFI) membranes: preparation, module concentration, and permeation experiments, Microporous Mater. 1 (1993) 131–147.

[2] Y. Yan, M.E. Davis, G.R. Gavalas, Preparation of zeolite ZSM-5 membranes by in-situ crystallization on porous α-Al_2O_3, Ind. Eng. Chem. Res. 34 (1995) 1652–1661.

[3] C. Bai, M.D. Jia, J.L. Falconer, R.D. Noble, Preparation and separation properties of silicalite composite membranes, J. Membr. Sci. 105 (1995) 79–87.

[4] Z.A.E.P. Vroon, K. Keizer, M.J. Gilde, H. Verweij, A.J. Burggraaf, Transport properties of alkanes through ceramic thin zeolite MFI membranes, J. Membr. Sci. 113 (1996) 293–300.

[5] W.J.W. Bakker, F. Kapteijn, J. Poppe, J.A. Moulijn, Permeation characteristics of a metal-supported silicalite-1 zeolite membrane, J. Membr. Sci. 117 (1996) 57–78.

[6] K. Kusakabe, S. Yoneshige, A. Murata, S. Morooka, Morphology and gas permeance of ZSM-5-type zeolite membrane formed on porous α-alumina support tube, J. Membr. Sci. 116 (1996) 39–46.

[7] K. Kusakabe, A. Murata, T. Kuroda, S. Morooka, Preparation of MFI zeolite membranes and their use in separating *n*-butane and *i*-butane, J. Chem. Eng. Jpn. 30 (1997) 72–78.

[8] J. Coronas, J.L. Falconer, R.D. Noble, Characterization and permeation properties of ZSM-5 tubular membranes, AIChE J. 43 (1997) 1797–1812.

[9] Y. Yan, M.E. Davis, G.R. Gavalas, Preparation of highly selective zeolite ZSM-5 membranes by a post-synthetic coking treatment, J. Membr. Sci. 123 (1997) 95–103.

[10] J. Coronas, R.D. Noble, J.L. Falconer, Separation of C_4 and C_6 isomers in ZSM-5 tubular membranes, Ind. Eng. Chem. Res. 37 (1998) 166–176.

[11] J.M. van de Graaf, F. Kapteijn, J.A. Moulijn, Effect of operating conditions and membrane quality on the separation performance of composite silicalite-1 membrane, Ind. Eng. Chem. Res. 10 (1998) 4071–4078.

[12] K. Keizer, A.J. Burggraaf, Z.A.E.P. Vroon, H. Verweij, Two component permeation through thin zeolite MFI membranes, J. Membr. Sci. 147 (1998) 159–172.

[13] J.M. van de Graaf, F. Kaptaijn, J.A. Moulijn, Methodological and operational aspects of permeation measurements on silicalite-1 membranes, J. Membr. Sci. 144 (1998) 87–104.

[14] T. Sano, M. Hasegawa, Y. Kawakami, Y. Kiyozumi, H. Yanagishita, D. Kitamoto, F. Mizukami, Potentials of silicalite membranes for the separation of alcohol/water mixtures, Stud. Surf. Sci. Catal. 84 (1994) 1175–1182.

[15] T. Sano, H. Yanagisita, Y. Kiyozumi, F. Mizukami, K. Haraya, Separation of ethanol/water mixture by silicalite membrane on pervaporation, J. Membr. Sci. 95 (1994) 221.

[16] H. Kita, Pervaporation through zeolite membranes, Maku (Membrane) 20 (1995) 169–182.

[17] H. Kita, K. Horii, Y. Ohtoshi, K. Tanaka, K. Okamoto, Synthesis of a zeolite NaA membrane for pervaporation of water/organic liquid mixtures, J. Mater. Sci. Lett. 14 (1995) 206–208.

[18] M. Nomura, T. Yamaguchi, S. Nakao, Ethanol/water transport through silicalite membranes, J. Membr. Sci. 144 (1998) 161–171.

[19] Q. Liu, R.D. Noble, J.L. Falconer, H.H. Funke, Organics/water separation by pervaporation with a zeolite membrane, J. Membr. Sci. 117 (1996) 163–174.

[20] J.F. Smetana, J.L. Falconer, R.D. Noble, Separation of methyl ethyl ketone from water by pervaporation using a silicalite membrane, J. Membr. Sci. 114 (1996) 127–130.

[21] C.D. Baertsch, H.H. Funke, J.L. Falconer, R.D. Noble, Permeation of aromatic hydrocarbon vapors through silicalite-zeolite membranes, J. Phys. Chem. 100 (1996) 7676–7679.

[22] N. Nishiyama, K. Ueyama, M. Matsukata, Synthesis of defect-free zeolite-alumina composite membranes by a vapor-phase transport method, Microporous Mater. 7 (1996) 299–308.
[23] N. Nishiyama, T. Matsufuji, K. Ueyama, M. Matsukata, FER membrane synthesized by vapor-phase transport method: its structure and separation characteristics, Microporous Mater. 12 (1997) 293–303.
[24] N. Nishiyama, K. Ueyama, M. Matsukata, Synthesis of FER membrane on an alumina support its separation properties, Stud. Surf. Sci. Catal. 105 (1996) 2195–2202.
[25] N. Nishiyama, Synthesis of zeolitic membranes by vapor-phase transport method and their separation properties, Ph.D. Thesis, Osaka University, 1997.
[26] N. Nishiyama, K. Ueyama, M. Matsukata, A defect-free mordenite membrane synthesized by vapor phase transport method, J. Chem. Soc., Chem. Commun. (1995) 1967–1968.
[27] M. Matsukata, N. Nishiyama, K. Ueyama, Crystallization of FER and MFI zeolites by a vapor-phase transport method, Microporous Mater. 7 (1996) 109–117.
[28] N. Nishiyama, K. Ueyama, M. Matsukata, Gas permeation through zeolite-alumina composite membranes, AIChE J. 43 (11A) (1997) 2724–2730.
[29] H. Karsli, A. Culfaz, H. Yucel, Sorption properties of silicalite-1: influence of sorption history on sorption kinetics of critically sized molecules, Zeolites 12 (1992) 728–732.

Permeation of Hexane Isomers through an MFI Membrane

Takaaki Matsufuji,[†] Kensuke Watanabe,[†] Norikazu Nishiyama,[†] Yasuyuki Egashira,[†] Masahiko Matsukata,[‡] and Korekazu Ueyama*[,†]

Division of Chemical Engineering, Graduate School of Engineering Science, Osaka University, 1−3 Machikaneyama-cho, Toyonaka-shi, Osaka 560-8531, Japan, and Department of Applied Chemistry, Waseda University, 3−4−1 Okubo, Shinnjyuku-ku, Tokyo 169-8555, Japan

The pervaporation tests for *n*-hexane, 2-methylpentane (2-MP), and 2,3-dimethylbutane (2,3-DMB) were performed using an MFI-type zeolitic membrane at 303 K. In the unary systems, those fluxes followed the order *n*-hexane ≫ monobranched hexane (2-MP), > dibranched hexane (2,3-DMB). The ideal selectivities of *n*-hexane/2-MP and *n*-hexane/2,3-DMB were 37 and 50, respectively. *n*-Hexane preferentially permeated in the measurements of a binary mixture of *n*-hexane/2-MP and *n*-hexane/2,3-DMB. The feed composition dependence in separating *n*-hexane/2,3-DMB binary mixtures was studied. The separation factor for the 50/50 *n*-hexane/2,3-DMB mixture exceeded 120, which was much greater than 54 in the 50/50 *n*-hexane/2-MP system. When the feed concentration of *n*-hexane was 10 mol %, the separation factor α(*n*-hexane/2,3-DMB) at the steady state was as high as 270. *n*-Hexane effectively inhibited the permeation of 2,3-DMB, even when the concentration of *n*-hexane was very small.

1. Introduction

In recent years, interesting features on the separation of hydrocarbons using zeolitic membranes have been reported.[1−24] Since the size of the zeolite pore is similar to the molecular dimensions, both shape-selective adsorption and molecular sieving play an important role in the separation of hydrocarbon mixtures.

For practical applications, it is important to know the membrane performance as a function of operating conditions such as temperature, total pressure, and feed composition. Temperature and total pressure are usually constant in the separation unit. Feed composition changes during the operation until the desired purity is achieved. For the proper design of separation units, the composition dependence of the separation features of the membrane is an important factor. Knowledge about the feed composition dependence of the membrane performance is required to choose the optimal conditions. However, attention has primarily been paid to the temperature dependence of the separation factor.

Some research groups have reported the composition dependence of separation performance for hydrocarbon mixtures using an MFI membrane.[1−5] In separating butane isomers, the separation factor increased with increasing fraction of *n*-butane in the feed, when the fraction of *n*-butane was >25%.[2−4] These results show that the permeation of isobutane is significantly inhibited by the presence of *n*-butane in the micropores.

In addition, the separation of *n*-hexane/2,2-dimethylbutane (2,2-DMB) has been studied using MFI membranes.[3,5−9] The kinetic diameter of 2,2-DMB is 0.6 nm, which is larger than the pore size of MFI (ca. 0.55 nm). However, molecules that are larger than the zeolite pores are able to adsorb into deformed pores, because the framework of the zeolites is not a rigid structure. For example, *m*-xylene (0.68 nm × 0.38 nm)[10] and naphthalene (0.74 nm × 0.38 nm)[11] are able to adsorb in MFI. Separation factors, α(*n*-hexane/2,2-DMB), of 17−2580 were reported in the vapor permeation measurement.[3,5−9] Compared with the separation of butane isomers, less is known about the feed composition dependence in separating mixtures of hexane isomers.

Funke et al.[1] and Baertsch et al.[12] found that the same MFI membranes showed high selectivity for the *n*-octane/isooctane mixture[1] and no selectivity for the *p*-xylene/*o*-xylene mixture.[12] They reported that subtle differences in molecule size and shape could result in opposite trends in permeation behavior.

In this study, an MFI membrane was prepared by the vapor-phase transport (VPT) method.[4,13−17] To compare with our previous studies on the separation of xylene isomers,[17] the same MFI membrane as that used in the previous study[17] was employed for the pervaporation of hexane isomers. The separations of *n*-hexane/2-methylpentane (2-MP) and *n*-hexane/2,3-dimethylbutane (DMB) binary mixtures were performed at 303 K. The feed composition dependence in separating *n*-hexane/2,3-DMB binary mixtures was studied.

2. Experimental Section

2.1. Preparation of Parent Gel. A flat porous α-alumina disk (NGK Insulators, Ltd.) with a membrane area of 1.0×10^{-4} m^2 and an average pore diameter of 0.1 μm was used as a support. The alumina support was treated with colloidal silica with pH of 10 to depress the dissolution of alumina from the support during synthesis.

The parent aluminosilicate sol was prepared using colloidal silica containing 30 wt % SiO_2, 0.04 wt % Al_2O_3, 0.4 wt % Na_2O (Nissan Chemical Co., Ltd.), and NaOH solution (4 N) (Wako Pure Chem. Ind. Co., Ltd.). The colloidal silica was mixed with an NaOH solution at 303 K. The composition of the parent sol was 1000 SiO_2/1.0 Al_2O_3/210 Na_2O/25000 H_2O. The support treated with the colloidal silica was dipped into the parent sol at 303 K for 1 day.

* Corresponding author. TEL/FAX: +81-6-6850-6255. E-mail: ueyama@cheng.es.osaka-u.ac.jp.
[†] Osaka University.
[‡] Waseda University. TEL/FAX: +81-3-5286-3850. E-mail: mmatsu@mn.waseda.ac.jp.

10.1021/ie000026z CCC: $19.00
Published on Web 06/03/2000

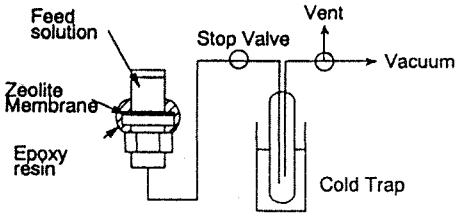

Figure 1. Schematic diagram of experimental apparatus for pervaporation.

2.2. Crystallization of Dry Gel by the Vapor-Phase Transport Method. The support coated with the parent sol was dried for 24 h at room temperature. A mixture of ethylenediamine (EDA; 0.5 cm^3), triethylamine (Et_3N; 1.0 cm^3), and water (0.5 cm^3) was poured into the bottom of an autoclave with an inner volume of 100 cm^3 to produce vapor. Crystallization was then performed at 453 K and autogenous pressure for 96 h. An as-synthesized zeolitic membrane was calcined in air at 773 K for 4−10 h. The heating rate 0.1 K min^{-1} was adopted in the range 473−773 K.

2.3. Pervaporation. Figure 1 shows the schematic diagram of the experimental apparatus for pervaporation. Epoxy resin was used as a sealant between the membrane and the apparatus. Between each set of permeation experiments, the membrane was calcined for 6 h at 773 K to remove adsorbed components and epoxy resin. This treatment gave reproducible separation results.

To evaluate the compactness of the MFI membrane, pervaporation experiments of *n*-hexane, 1,3,5-triisopropylbenzene (TIPB), and the 95/5 *n*-hexane/TIPB binary mixture were carried out at 303 K. The kinetic diameter of TIPB is 0.85 nm, which is larger than the pore dimensions of MFI (0.53 nm × 0.56 nm, 0.51 nm × 0.55 nm). The zeolitic membrane was attached on an end of a glass tube with the cross-sectional area 0.50 × 10^{-4} m^2. Feed solutions were poured on the feed side. The permeation side was kept under vacuum. The permeant was continuously collected in a cold trap using liquid nitrogen and analyzed for composition with a gas chromatograph equipped with a flame ionization detector. *n*-Octane (1.5 × 10^{-3} mol, 200 μL) was put into the trap, and 10−20 μL of the mixture was injected into a gas chromatograph. The amount of permeant can be determined by comparing the peak area for the permeant with that for *n*-octane.

The flux and the separation factor $\alpha_{(a/b)}$ were calculated from the following equations

$$\text{flux} = \frac{n}{tA} \tag{1}$$

$$\alpha_{(a/b)} = \frac{(x_a/x_b)_{\text{permeate}}}{(x_a/x_b)_{\text{feed}}} \tag{2}$$

where n, t, A, x_a, and x_b are the permeation amount (mol), the permeation time (s), the membrane area (m^2), the mole fraction of *n*-hexane (dimensionless), and the mole fraction of other hexane isomers (dimensionless), respectively.

Pervaporation of 2-MP and 2,3-DMB was performed at 303 K. The kinetic diameters 2-MP and 2,3-DMB are 0.50 and 0.62 nm, respectively, which are larger than the kinetic diameter of *n*-hexane (0.43 nm). Unary and binary (*n*-hexane/2-MP and *n*-hexane/2,3-DMB) systems were adopted. The compositions of the feed mixture were determined with the gas chromatograph. Ideal selectivities were calculated from the fluxes in the unary system.

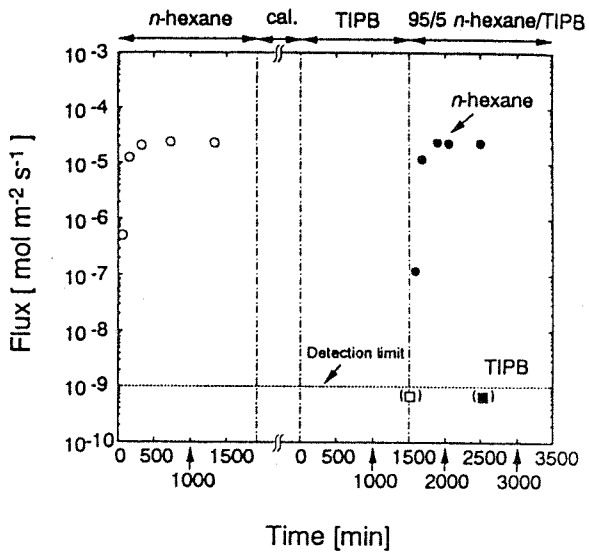

Figure 2. Pervaporation tests for the compactness of MFI membranes: cal, calcination.

Table 1. Pervaporation Results in the Unary System

	flux (mol m^{-2} s^{-1})	α_i[a] (dimensionless)
n-hexane	2.2 × 10^{-5}	
2-methylpentane	6.0 × 10^{-7}	37
2,3-dimethylbutane	4.4 × 10^{-7}	50

[a] α_i, ideal selectivity.

3. Results and Discussion

3.1. Compactness of MFI Membrane. Figure 2 shows the pervaporation results of *n*-hexane, TIPB, and the 95/5 *n*-hexane/TIPB mixture through the MFI membrane. First, the pervaporation test of *n*-hexane in the unary system was carried out. After the pervaporation test, the membrane was calcined for 10 h at 773 K. Second, the pervaporation test of TIPB in the unary system was carried out. After storing TIPB for 1500 min, no permeation of TIPB through the MFI membrane was detected, indicating that the flux of TIPB was <1.0 × 10^{-9} mol m^{-2} s^{-1}, the detection limit in this experiment. Finally, the pervaporation test of the 95/5 *n*-hexane/TIPB binary mixture was performed. In the pervaporation test of the 95/5 *n*-hexane/TIPB binary mixture, only *n*-hexane permeated through the MFI membrane. The flux of *n*-hexane was 2.3 × 10^{-5} mol m^{-2} s^{-1}, which was the same as that (2.2 × 10^{-5} mol m^{-2} s^{-1}) in the unary system, indicating that TIPB did not enter the membrane and hardly affected the permeation of *n*-hexane in the binary system. These results strongly suggest that the MFI membrane has no pinhole larger than the molecular dimension of TIPB.

3.2. Separation of Linear and Branched Hexane Isomers. The fluxes of *n*-hexane, 2-methylpentane (2-MP), and 2,3-dimethylbutane (2,3-DMB) in the unary systems are listed in Table 1. The fluxes followed the order *n*-hexane ≫ monobranched hexane (2-MP) > dibranched hexane (2,3-DMB). The ideal selectivities of *n*-hexane/2-MP and *n*-hexane/2,3-DMB were 37 and 50, respectively.

The pervaporation test for the 50/50 *n*-hexane/2-MP mixture was performed at 303 K. Figure 3 shows the

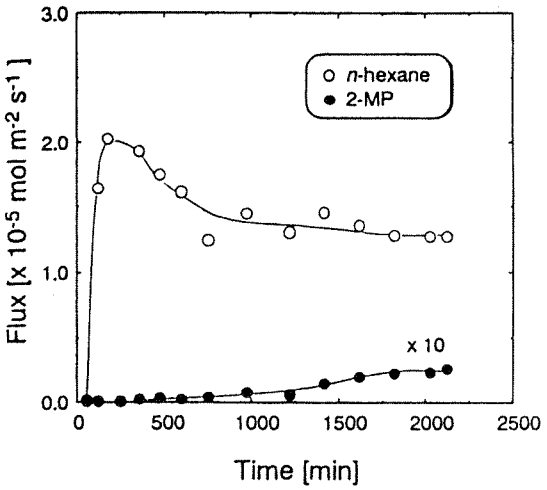

Figure 3. Transient profile of fluxes of *n*-hexane and 2-methylpentane (2-MP) in separating the 50/50 *n*-hexane/2-MP binary mixture at 303 K.

transient profile of *n*-hexane and 2-MP permeation. The value of the 2-MP flux was multiplied by 10 and plotted in Figure 3. *n*-Hexane predominantly permeated in the early stage and had a maximum in the range 180−400 min. The maximum value of the flux of *n*-hexane was smaller than the flux obtained in the unary system, shown in Table 1. The flux of 2-MP increased monotonically and reached the steady state after 1800 min. In the steady state, the separation factor α(*n*-hexane/2-MP) was 54, which was greater than the value of 0.91 theoretically calculated by the vapor−liquid equilibrium with the Antoine equation. The separation factor α(*n*-hexane/2-MP) was also greater than the ideal selectivity (α_i(*n*-henxane/2-MP) = 37) in the unary system.

Vlugt et al.[18] reported the adsorption isotherms for *n*-hexane and 2-MP on pure-silica MFI. They used the configurational-bias Monte Carlo (CBMC) technique for computing the adsorption isotherms for hexane isomers. Their CBMC simulations of isotherms of the 50/50 *n*-hexane/2-MP binary mixture showed that *n*-hexane was preferentially adsorbed and 2-MP was almost completely replaced by *n*-hexane. The preferential adsorption of *n*-hexane in the binary system seems to provide a larger separation factor than the ideal selectivity in separating the *n*-hexane/2-MP binary mixture using the MFI membrane.

The pervaporation tests for the *n*-hexane/2,3-DMB mixture with various feed concentrations were performed at 303 K. Figure 4 shows the transient profile of the fluxes of *n*-hexane and 2,3-DMB. The flux of 2,3-DMB was multiplied by 100 and plotted in Figure 4 a. The flux of 2,3-DMB was multiplied by 10 and plotted in Figure 4b or c. *n*-Hexane also permeated predominantly in the early stage and had a maximum in the range 180−400 min. The flux of *n*-hexane was monotonically decreased with the passing of time and reached the stationary state. The maximum value of the flux of *n*-hexane in the binary mixtures was slightly smaller than the flux obtained in the unary system.

Figure 5 shows the change in the fluxes of *n*-hexane and 2,3-DMB and the separation factor α(*n*-hexane/2,3-DMB) at the steady states as a function of the feed concentration of *n*-hexane. The value of the 2,3-DMB flux was multiplied by 10 in Figure 5. In the separation of the equimolar mixture, the separation factor exceeded 100, which was much greater than 0.83 calculated from

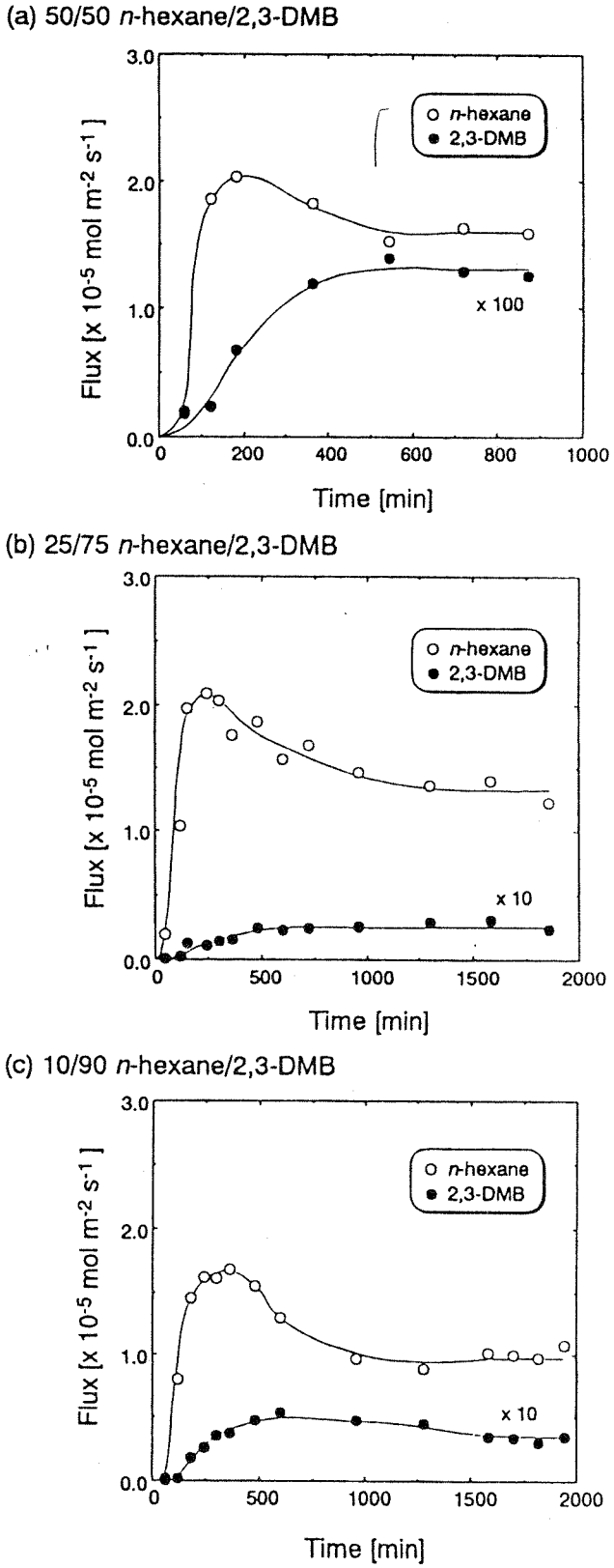

Figure 4. Transient profile of fluxes of *n*-hexane and 2,3-dimethylbutane (2,3-DMB) in the pervaporation at 303 K.

the vapor−liquid equilibrium. The separation factor α(*n*-hexane/2,3-DMB) was also greater than the ideal selectivity (α_i(*n*-henxane/2,3-DMB) = 50) in the unary system. The separation factor increased with decreasing *n*-hexane concentration in the feed. The separation factor α(*n*-hexane/2,3-DMB) at steady state was as high as 270 when the feed concentration of *n*-hexane was 10

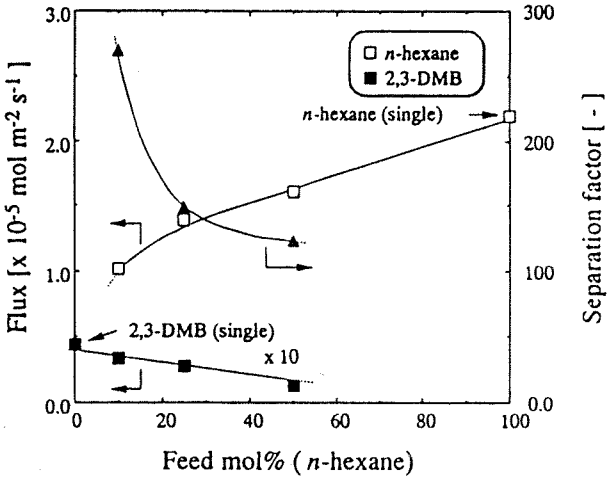

Figure 5. Effect of *n*-hexane feed concentration on the fluxes of *n*-hexane and 2,3-DMB and the separation factor of *n*-hexane/2,3-DMB mixtures using an MFI membrane.

mol %. While the flux of 2,3-DMB varied almost in proportion to the 2,3-DMB concentration in the feed, the flux of *n*-hexane did not behave linearly with the feed concentration. It seemed that *n*-hexane preferentially adsorbed in the pores of the MFI, even when the concentration of *n*-hexane was as small as 10 mol %.

3.3. Comparison of Fluxes in This Study to Reported Data. Direct comparison of the data obtained by others seems to be very difficult because both the permeation method (vapor permeation) used and the operation temperature are different. However, the fluxes of hexane isomers obtained by pervaporation may be comparable to the fluxes of those obtained by vapor permeation when the adsorption of hexane isomers at the feed side is saturated. The fluxes of *n*-hexane in the unary system (2.2×10^{-5} mol m^{-2} s^{-1} at 303 K) appeared to be about 2 orders of magnitude lower than those reported by Gump et al.[5] (ca. 2×10^{-3} mol m^{-2} s^{-1} at 373 K). Though the operation temperature was different, the flux obtained in this study was low. This low flux value took a long time to approach the steady-state value in both unary system and binary systems.

We previously reported that the compact layer of the membrane was the zeolite–alumina support composite layer interior of the alumina support (Nishiyama et al.[15,16]). The porosity of the alumina support is approximately 0.4, indicating that the effective membrane area is smaller than that of the membrane synthesized on the support surface. Moreover, the MFI membrane has no pinholes larger than the molecular dimension of TIPB. The hexane isomers seem to permeate the pores of MFI rather than the pinholes in this study.

4. Conclusions

n-Hexane preferentially permeated though the MFI membrane in the pervaporation tests for binary mixtures of *n*-hexane/2-MP and *n*-hexane/2,3-DMB. The separation factors (α(*n*-hexane/2-MP) and α(*n*-hexane/2,3-DMB)) were always greater than their ideal selectivities. Moreover, α(*n*-hexane/2,3-DMB) was larger than α(*n*-hexane/2-MP), indicating that *n*-hexane effectively blocked the larger 2,3-DMB.

The flux of *n*-hexane was still larger than that of 2,3-DMB in the pervaporation tests for binary mixtures of *n*-hexane/2,3-DMB, even when the concentration of *n*-hexane was small. The separation factor α(*n*-hexane/2,3-DMB) was as high as 270 when the feed concentration of *n*-hexane was 10 mol %. The MFI membrane showed promising potential to separate *n*-hexane and branched hexane isomer mixtures.

Acknowledgment

The authors are grateful to NGK Insulators, Ltd. for supplying α-alumina supports.

Literature Cited

(1) Funke, H. H.; Kovalchick; Falconer, J. L.; Noble, R. D. Separation of hydrocarbon isomer vapors with silicalite zeolite membranes. *Ind. Eng. Chem. Res.* **1996**, *35*, 1575.

(2) Kusakabe, K.; Murata, A.; Kuroda, T.; Morooka, S. Preparation of MFI zeolite membranes and their use in separating *n*-butane and *i*-butane. *J. Chem. Eng. Jpn.* **1997**, *30*, 72.

(3) van de Graaf, J. M.; Kapteijn, F.; Moulijn, J. A. Effect of operating conditions and membrane quality on the separation performance of composite silicalite-1 membrane. *Ind. Eng. Chem. Res.* **1998**, *37*, 4071.

(4) Matsufuji, T.; Mano, Y.; Nishiyama, N.; Ueyama, K.; Matsukata, M. Permeation studies of butane isomers through MFI-type zeolitic membranes; Proceedings of the Fifth International Conference on Inorganic Membranes, June 22–26, Nagoya, Japan, 1998; p 568.

(5) Gump, C. J.; Noble, R. D.; Falconer, J. L. Separation of hexane isomers through nonzeolite pores in ZSM-5 zeolite membranes. *Ind. Eng. Chem. Res.* **1999**, *38*, 2775.

(6) Tsikoyiannis, J. G.; Haag, W. O. Synthesis and characterization of a pure zeolitic membrane. *Zeolites* **1992**, *12*, 126.

(7) Vroon, Z. A. E. P.; Keizer, K.; Gilde, M. J.; Verweij, H.; Burggraaf, A. J. Transport properties of alkanes through ceramic thin zeolite MFI membranes. *J. Membr. Sci.* **1996**, *113*, 293.

(8) Funke, H. H.; Argo, A. M.; Falconer J. L.; Noble, R. D. Separation of cyclic, branched and linear hydrocarbon mixtures through silicalite membranes. *Ind. Eng. Chem. Res.* **1997**, *36*, 137.

(9) Coronas, J.; Noble, R. D.; Falconer, J. L. Separation of C_4 and C_6 isomers in ZSM-5 tubular membranes. *Ind. Eng. Chem. Res.* **1998**, *37*, 166.

(10) Funke, H.; Argo, A. M.; Baertsch, C. D.; Falconer, J. L.; Noble, R. D. Separation of close-boiling hydrocarbons with silicalite zeolite membranes. *J. Chem. Soc., Faraday Trans.* **1996**, *92*, 2499.

(11) van Koningsveld, H.; Jansen, J. C. Single-crystal structure analysis of zeolite H–ZSM-5 loaded with naphthalene. *Microporous Mater.* **1996**, *6*, 159.

(12) Baertsch, C. D.; Funke, H. H.; Falconer, J. L.; Noble, R. D. Permeation of aromatic hydrocarbon vapors through silicalite-zeolite membranes. *J. Phys. Chem.* **1996**, *100*, 7676.

(13) Nishiyama, N.; Ueyama, K.; Matsukata, M. Synthesis of defect-free zeolite-alumina composite membranes by a vapor-phase transport method. *Microporous Mater.* **1996**, *7*, 299.

(14) Nishiyama, N.; Ueyama, K.; Matsukata, M. Synthesis of FER membrane on an alumina support and its separation properties. *Stud. Surf. Sci. Catal.* **1996**, *105*, 2195.

(15) Nishiyama, N.; Matsufuji, T.; Ueyama, K.; Matsukata, M. FER membrane synthesized by vapor-phase transport method: Its structure and separation characteristics. *Microporous Mater.* **1997**, *12*, 293.

(16) Nishiyama, N. Synthesis of zeolitic membranes by vapor-phase transport method and their separation properties. Ph.D. Thesis, Osaka University, 1997.

(17) Matsufuji, T.; Nishiyama, N.; Matsukata, M.; Ueyama, K. Separation of butane and xylene isomers with MFI-type zeolitic membrane synthesized by a vapor-phase transport method. *J. Membr. Sci.*, in press.

(18) Vlugt, T. J. H.; Krishna R.; Smit, B. Molecular simulation of adsorption isotherms for linear and branched alkanes and their mixtures in silicalite. *J. Phys. Chem. B* **1999**, *103*, 1102.

(19) Geus, E. R.; Bekkum, H.; Bakker, W. J. W.; Moulijin, J. A. High-temperature stainless steel supported zeolite (MFI) membranes: preparation, module concentration, and permeation experiments. *Microporous Mater.* **1993**, *1*, 131.

(20) Yan, Y.; Davis, M. E.; Gavalas, G. R. Preparation of zeolite ZSM-5 membranes by in-situ crystallization on porous α-Al_2O_3. *Ind. Eng. Chem. Res.* **1995**, *34*, 1652.

(21) Bakker, W. J. W.; Kapteijn, F.; Poppe, J.; Moulijn, J. A. Permeation characteristics of a metal–supported silicalite-1 zeolite membrane. *J. Membr. Sci.* **1996**, *117*, 57.

(22) Coronas, J.; Falconer, J. L.; Noble, R. D. Characterization and permeation properties of ZSM-5 tubular membranes. *AIChE J.* **1997**, *43*, 1797.

(23) Keizer, K.; Burggraaf, A. J.; Vroon, Z. A. E. P.; Verweij, H. Two component permeation through thin zeolite MFI membranes. *J. Membr. Sci.* **1998**, *147*, 159.

(24) Kita, H. Pervaporation using zeolite membranes; Proceedings of the International Workshop on zeolitic membranes and films, Post conference of ICIM 98, June 28–30, Gifu, Japan, 1998; p 43.

Received for review January 3, 2000
Revised manuscript received April 11, 2000
Accepted April 19, 2000

IE000026Z

Preparation of mordenite membranes on α-alumina tubular supports for pervaporation of water–isopropyl alcohol mixtures

X. Lin, E. Kikuchi and M. Matsukata*

Department of Applied Chemistry, Waseda University, 3-4-1 Okubo, Shinjuku, Tokyo 169-8555, Japan. E-mail: mmatsu@mn.waseda.ac.jp

Received (in Cambridge, UK) 15th December 1999, Accepted 20th April 2000

Mordenite membranes prepared on α-alumina tubular supports by *in situ* hydrothermal synthesis using organic template-free media showed high water permselectivity for pervaporation of water–isopropyl alcohol mixtures.

Zeolite membranes have been widely studied in recent years because of their great potential applications in separations, membrane reactors and sensors. A continuous zeolite layer can be grown on various supports, including α-alumina and stainless steel generally by *in situ* hydrothermal synthesis. Different types of zeolites such as MFI, zeolite A, zeolite Y, mordenite and ferrierite have been synthesized on flat and tubular supports. Research has so far mainly focused on MFI (silicalite and ZSM-5) membranes for gas separation because their pore sizes, which are close to the sizes of gas molecules, allow separation of molecules based on their size. In addition, MFI crystals are easily grown on a support with structure-directing agents (SDAs). Some MFI membranes showing good separation of hydrocarbon isomers such as *n*-butane–isobutane have been reported by several groups.[1–3]

With respect to pervaporation separation, not only the pore sizes of zeolites, but also their surface properties (hydrophobicity and hydrophilicity) play an important role. Hydrophobic MFI membranes exhibit preferential alcohol permeation for pervaporation of a water–alcohol mixture although the molecular size of water is smaller than that of the alcohol.[4] In contrast, water permeated much faster than alcohols through hydrophilic zeolite A and Y membranes.[5,6] Since mordenite zeolite with large channels of 0.67 × 0.7 nm and small channels of 0.26 × 0.56 nm is hydrophilic, mordenite membranes would be selective for permeating water against alcohols.

In 1990, Suzuki *et al.*[7] first claimed the synthesis of a zeolite membrane (mordenite) onto a porous silica–alumina plate using an *in situ* hydrothermal synthesis method. Their membrane, synthesized at 160 °C for 2 days, exhibited Knudsen-diffusion behavior. Matsukata and coworkers[8] applied the vapor-phase transport method to obtain a mordenite membrane on a porous α-alumina disk. Their membranes showed a good separation factor of 160 for pervaporation of a benzene–*p*-xylene mixture. Very recently, Santamaría and coworkers[9,10] synthesized mordenite membranes onto a tubular support by *in situ* hydrothermal synthesis using TEAOH and reported the formation of composite mordenite/ZSM-5/chabazite membranes. They studied the separation of a water–n-propanol mixture through their composite membranes by a sweep gas method. Permeance ratios as high as 70 to 140 for water and *n*-propanol were achieved through their membranes. To our knowledge, the synthesis of mordenite membranes under SDA-free conditions on tubular supports has not been reported. Here we report the synthesis of a mordenite membrane onto a tubular support for pervaporation of a water–isopropyl alcohol mixture.

Mordenite membranes were synthesized on porous 6 cm long α-alumina tubes (NGK, Ltd.) with 0.1 μm diameter pores by *in situ* hydrothermal synthesis. The parent aluminosilicate gel was prepared as follows. An appropriate amount of alumina sulfate (Wako Pure Chem. Ind. Co. Ltd.) was added to a NaOH solution and stirred at room temperature until it dissolved. Colloidal silica containing 30–31 wt% of SiO_2 and 0.6 wt% of Na_2O ST-S, Nissan Chem. Ind. Ltd.) was then added to this solution and stirred vigorously for 1 h to give a gel of molar composition $0.38Na_2O:SiO_2:0.025Al_2O_3:40H_2O$.[7] The tubular support was washed, coated with a water slurry of seed crystals of zeolite mordenite (HSZ600, 70A, Tosoh Co.), SiO_2/Al_2O_3 ratio = 10.2), and then dried at 100 °C for 15 min. The support was then vertically immersed in the gel. Crystallization was carried out at 180 °C for a given period. After the crystallization, the sample was removed, washed carefully with distilled water, and then dried at 100 °C.

The membranes obtained were characterized by X-ray diffraction (XRD) with Cu-Kα radiation (Rigaku RINT2000). Fig. 1 shows the XRD patterns for the products crystallized at 180 °C for 8 and 24 h together with that for the seed powder. These XRD patterns were consistent with the mordenite structure. The XRD patterns of the membranes crystallized for different periods of crystallization showed that the (150) reflection intensity at 22.24°, became dominant with increasing crystallization time. Thus, mordenite crystals appear to grow randomly in the early stages of crystallization, and further crystal growth occurred mainly with the (150) face parallel to the support surface. Mordenite crystals were also grown on an unseeded support and gave almost the same XRD pattern as those on the seeded supports.

The morphology of the mordenite membranes was studied by scanning electron microscopy (SEM) (Hitachi S2150) and Fig. 2 shows SEM images for the surface and cross section of the mordenite membrane crystallized at 180 °C for 24 h. A continuous, intergrown layer fully covers the surface of support. The crystal sizes are *ca.* 6–7 μm, and the thickness of crystal

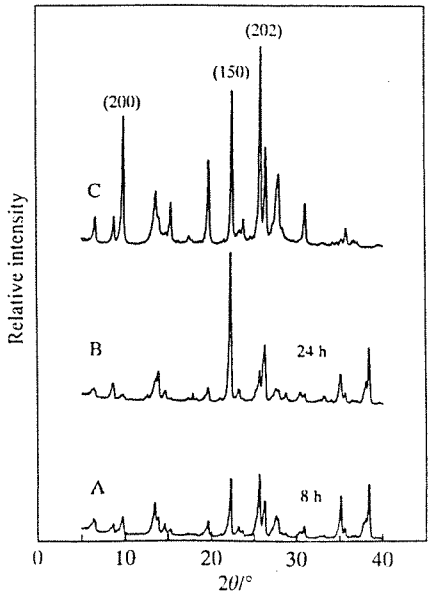

Fig. 1 XRD patterns for mordenite membranes crystallized at 180 °C for (A) 8 and (B) 24 h, and (C) mordenite seed powder.

DOI: 10.1039/a909867d

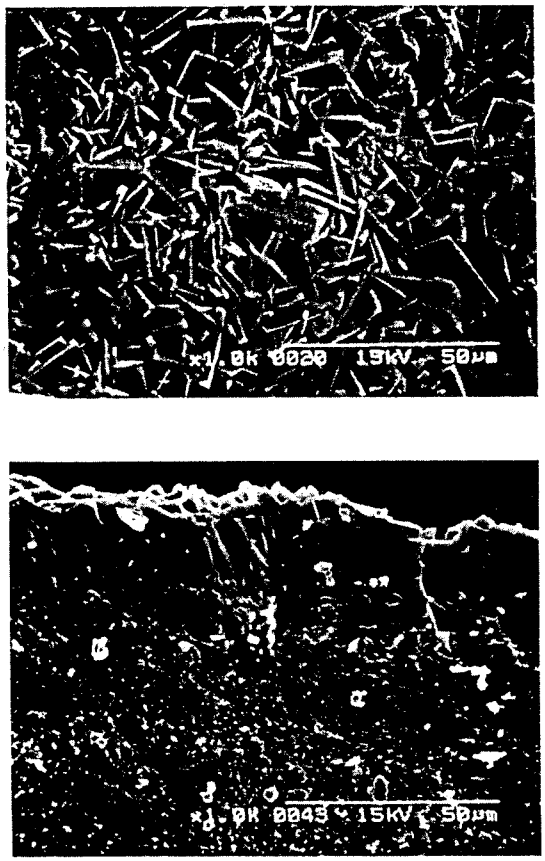

Fig. 2 SEM images for the surface and cross section of the mordenite membrane synthesized at 180 °C for 24 h.

layer is *ca.* 35 μm. The SiO_2/Al_2O_3 ratio of the mordenite zeolites determined by EDAX was *ca.* 12. In addition, the mordenite crystals have a rectangular form.

The pervaporation (PV) tests for water–isopropyl alcohol, and water–n-propanol mixtures were carried out at 75 °C using the pervaporation experimental apparatus described elsewhere.[8] The effective membrane area was *ca.* 15 cm^2 and the permeation side was kept under vacuum. The flux was calculated by weighing the condensed permeate. The separation factor was determined as $\alpha_{A/B} = (Y_A/Y_B)/X_A/X_B)$, where X_A, X_B, Y_A and Y_B denote the mass fractions of components A and B in the feed and permeate sides. The pervaporation results through the mordenite membranes crystallized at 180 °C for 24 h are listed in Table 1 and clearly show that water preferentially permeated through the mordenite membranes. The membrane synthesized on the seeded support exhibited a very high separation factor of 3360 for the water–isopropyl alcohol mixture compared with that of the unseeded support (192). We propose that the seed crystals increased the density of mordenite crystals on the support, resulting in a pinhole-free structure in contrast to the membrane formed on the unseeded support.

Table 1 Pervaporation results through mordenite membranes

Membrane[a]	Feed solution (A/B) (wt% of A)	Separation factor (A/B)[b]	Flux/ kg m^{-2}
M1	Water–n-propanol (10)	1782	0.2
M2	Water–isopropyl alcohol (10)	3360	0.1
M3[c]	Water–isopropyl alcohol (10)	192	0.2

[a] Membranes were crystallized at 180 °C for 24 h; [b] PV carried out at 75 °C. [c] Prepared without seeds.

Mordenite is formed for Si/Al ratios of *ca.* 5–6, higher than those for LTA (Si/Al = 1) and Y (Si/Al ratio = *ca.* 2.5). Thus, in comparison with LTA and Y, mordenite has potential application in acidic solutions under which esterification can occur. In addition, it is known that the effective pore size of mordenite can be precisely controlled in the range of *ca.* 0.3–0.6 nm by ion exchange, possibly leading to a wide variety of applications such as hydrocarbon separation and use as membrane reactors.

Notes and references

1 W. J. Bakker, F. Kapteijn, J. Poppe and J. A. Moulijn, *J. Membr. Sci.*, 1996, **117**, 57.
2 Z. A. P. Vroon, K. Keizer, M. J. Gilde, H. Verweij and A. J. Burggraaf, *J. Membr. Sci.*, 1996, **113**, 293.
3 X. Lin, J. L. Falconer and R. D. Noble, *Chem. Mater.*, 1998, **10**, 3716.
4 T. Sano, H. Yanagishita, Y. Kiyozumi, F. Mizukami and K. Haraya, *J. Membr. Sci.*, 1994, **95**, 221.
5 H. Kita, K. Horii, Y. Ohtoshi and K. Okamoto, *J. Mater. Sci. Lett.*, 1995, **14**, 206.
6 H. Kita, T. Inoue, H. Asamura, K. Tanaka and K. Okamoto, *Chem. Commun.*, 1997, 45.
7 K. Suzuki, Y. Kiyozumi, T. Sekine, K. Obata, Y. Shindo and S. Shin, *Chem. Express*, 1990, **5**, 793.
8 N. Nishiyama, K. Ueyama and M. Matsukata, *Microporous Mater.*, 1996, **7**, 299.
9 M. A. Salomón, J. Coronas, M. Menéndez and J. Santamaría, *Chem. Commun.*, 1998, 125.
10 E. Piera, M. A. Salomón, J. Coronas, M. Menéndez and J. Santamaría, *J. Membr. Sci.*, 1998, **149**, 99.

ゼオライトの合成及び膜作製技術の最近の進歩

Recent Progress of Zeolite Synthesis and Zeolitic Membrane Preparation

Key-words: Zeolites, Synthesis, Membrane, Separation

松方　正彦　Masahiko MATSUKATA
(Department of Applied Chemistry, Waseda University)

1. はじめに

ここ10年ほどの間に，TEM等の構造研究のための機器や，コンピューターケミストリーの進歩に伴って，次々と新しい構造をもつゼオライトが報告されており，ゼオライト合成化学は長足の進歩を遂げている．

ゼオライトの応用分野も，1980年代以降環境分野を中心に広がりを見せ，新規なゼオライト利用プロセスの開発が進められている．1990年代に入ってからは旧来にないゼオライトの応用も提案されるようになり，分離膜，センサー，電極修飾材料，光学材料などへの展開が幅広く志向されるようになってきた．

利用分野の発展に伴って，ゼオライト結晶の質，物性に対する要求も厳しくなり，水熱合成法の抜本的な改良も必要になりつつある．

本稿では，ゼオライトの利用プロセス，合成とその応用に関して，膜分離技術への展開を含むいくつかのトピックスについて述べ，ゼオライト合成技術を展望したい．

2. 環境分野におけるゼオライト利用技術の展開

1980年代以降，環境分野においてゼオライトが幅広く用いられるようになってきた．環境触媒としての応用例は別稿で述べられると思うので，ここでは触媒以外の分野におけるトピックスを紹介したい．利用されているゼオライトはローシリカとハイシリカの2種類に大別される．

2.1 ローシリカゼオライト

ローシリカゼオライトでは，Si-O-Alのネットワーク構造（Al上で電子過剰）上のカチオンに起因する静電場によって分子が分極する性質に基づいて，吸着分離プロセスが開発されている．

燃焼排ガス，化学プラントプロセスガスからのCO_2回収については，A型あるいはX型を用いた圧力スイング吸収（PSA）法が実用化されている[1]．図1には，15 vol%程度のCO_2を含む燃焼排ガスからのCO_2回収プロセスのフローシートを示す．回収CO_2濃度は99 %に達する．PSA法は環境分野で幅広く用いられ，Na-X，Ca-Xを用いて放射性オフガスからキセノンを選択的に吸着し，放射性クリプトンを除去するプロセスなども検討されている．

2.2 ハイシリカゼオライト

Si-O-Si上の酸素は強い親油性を示すため，シリカライトを代表とするハイシリカゼオライトは疎水性を発揮する．このため，ハイシリカゼオライトは有機物等の回収に優れた性能を示す．

スウェーデンのムーンタース・ゼオール社は，プラスチックスモークの処理にハイシリカゼオライトを用いたシステムを実用化している[2]．プラスチックスモークには高沸点成分が含まれており，吸着剤の再生が500°C以上で可能なことがポイントである．

ガソリンの積み下ろしの際に発生する蒸気をハイシリカゼオライトを用いて吸着・回収するプロセスが実用化されている（ウルトラ・ブライス）．こうしたVOCs（Volatile Organic Com-

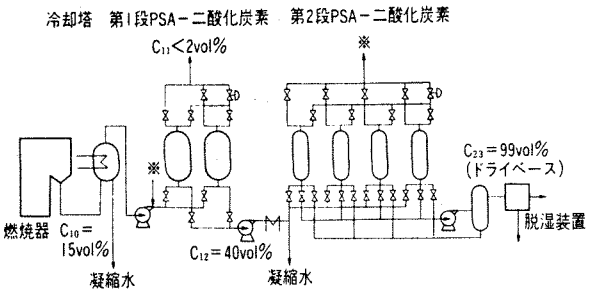

図1　PSA-二酸化炭素フローシート

pounds）に対する環境規制は，今後強化される傾向にあり，ハイシリカゼオライトの重要な利用分野となると思われる．

ゼオライトを用いた脱臭剤も開発されており，場合によっては従来の活性炭以上の性能を示す．吸着するのは，硫黄化合物，含酸素有機化合物などで，メルカプタン，硫化水素，アンモニア等の除去についてはアモルファスのアルミノケイ酸塩などを混合して用いる．その他，SO_2回収，塩化メチレン回収など，ハイシリカゼオライトの吸着剤としての利用は急速に広がりつつある．

3.　ゼオライト合成におけるトピックス

3.1　マルチディメンショナルなゼオライト

ゼオライトの細孔入口の大きさは，細孔を形成している酸素の数で決まる．2種類の大きさの細孔径をあわせもつゼオライトは数多く知られており，例えばモルデナイトは酸素12員環と8員環の細孔よりなっている．しかし，モルデナイトの酸素8員環は小さすぎ，多くの反応には有効ではなく実用的には12員環の1次元細孔をもつゼオライトと見なされている．

最近，酸素10員環と12員環のインターセクションをもつ，新規なゼオライトが合成された．小さな分子は10員環を，多環芳香族などやや大きな分子は12員環を拡散させ，インターセクションにおいて両者を反応させる（Molecular Traffic Control）ことによって，高選択的な反応が可能と期待されている．

モービルが発明したMCM-22[3]は，こうしたゼオライトの一種であり，既に一部で工業的に利用されているらしい．MCM-22は界面活性剤をテンプレート（鋳型剤）として用いて合成

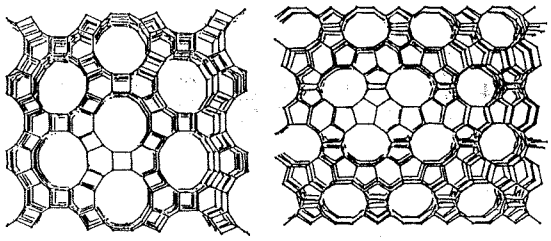

図2　SSZ-26，33の構造

される．Chevronの開発したSSZ-26，-33，Davisらの開発したCIT-1も，酸素10員環と12員環のインターセクションをもつ新規な構造のゼオライト（図2）[4]として期待される．

3.2　キラルなゼオライト

ゼオライトベータ[5]は，12員環の細孔が三次元的に連結している．ベータには，Polymorph A，B，Cと呼ばれる構造異性体が存在し（図3），これまで合成されてきたベータはすべてPolymorph AとBがc軸方向に積層欠陥を介して連なった混晶である．Polymorph Aはキラルであり，これを選択的に合成できれば，無機の光学活性物質となり，興味深い．光学異性体転換反応用触媒としても期待される．今のところPolymorph Aが選択的に合成された例はない．

3.3　大口径ゼオライト

$AlPO_4$-nやガロフォスフェートでは，酸素14員環以上の細孔入口径をもつ大口径ゼオライトが合成されている（VPI-5（18員環）[6]，Cloverite（20員環）[7]）．大口径ゼオライトには，既往のゼオライトでは吸着できない大きな分子の吸着分離，触媒反応が期待されている．しかし，これらは水熱安定性に欠け，実用性には問題があった．

1996年ついに14員環の細孔をもつアルミノシリケートUTD-1[8]が，合成された（図4）．UTD-1合成のためのテンプレートは，コバルトのキレートCp_2CoOHである．今後の展開が期待される．

3.4　水熱合成法の改良

大久保も指摘している[9]ように，従来の水熱合成では核発生と結晶成長が同時に起きている（Spontaneous Nucleation）．このため既往の水熱合成では，固相の析出に伴い溶液の各成分濃

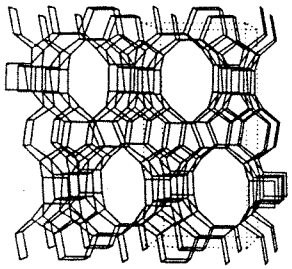

図3　ベータ（Polymorph A）の構造

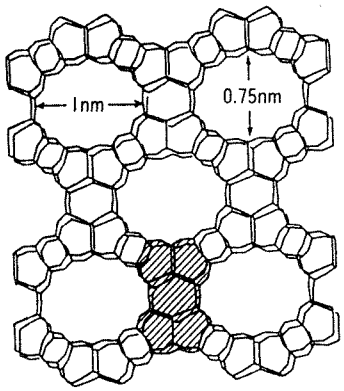

図4　UTD-1の構造

度が連続的に変化し，真に均一な粒子径，組成をもつゼオライトの合成は難しいと思われる．

東ソーのKasaharaらは，Nuclei Solutionの合成と，Nucleiの成長を分離した2段階の合成法を開発することにより，撹拌条件下でのフォージャサイトの合成に初めて成功した[10]．それまでは，フォージャサイトの合成は無撹拌下で行われており，撹拌すると十分な結晶化が起こらない．無撹拌下での合成は，装置内における対流等流れの制御が難しく，スケールアップが困難である．彼らの成果は，ゼオライトの合成分野において，核発生と結晶成長を分離するという概念を導入した点で先駆的である．

近年，Tsapatisらは，ゼオライトL[11]及びZSM-5[12]の合成に対して，この概念を用い，ゼオライトナノコロイドの合成，ゼオライト膜合成を報告している．ゼオライトの核を捉え，積極的に合成し，薄膜合成に利用する試みは各国で始まっており[13]，今後の展開が期待される．

水熱合成において，溶液中の濃度変化を抑制し均一なゼオライトを合成するためには，回分式から流通系への展開も視野に入れた研究開発がなされるべきだろう．

4.　水熱合成法以外の新規な合成法

4.1　非水溶媒を用いるゼオライト合成

Bibbyら[14]が，1985年にエチレングリコールを溶媒としてソーダライトの合成に成功して以来，水を溶媒としない合成法に関心が向けられている．ZSM-5，フェリエライトなど有用なゼオライトの合成も報告されている[15]．

4.2　ドライゲルコンバージョン

4.2.1　気相輸送法

1990年にXuらによって，水，エチレンジアミン，トリエチルアミンの混合蒸気中で，乾燥ゲルがZSM-5へと結晶化することが報告された[16]．その後，この合成法が各種のゼオライト合成に有効であることが報告されている[17),18]．

気相輸送法では，テンプレートを含まないアルミノシリケートゲルを調製し，乾燥する．乾燥ゲルをオートクレーブ中段に仕込み，底部にテンプレート水溶液を入れる．テンプレート蒸気と水蒸気は加熱に伴ってゲル中に浸透し，結晶化が起きる．

4.2.2　水蒸気処理法

気相輸送法では，テンプレートが気化することが必要であるため，合成に一般に用いられる4級アンモニウム塩は用いることができない．筆者らは気化できないテンプレートを乾燥ゲル中に混合し，水蒸気中で結晶化させる方法を開発した．

テトラエチルアンモニウムをテンプレートに用いると，水熱合成では得られない幅広いシリカアルミナ比のベータが合成可能である[19]．また，数十nmのほぼ均一な粒子径をもつベータが得られ，かつ結晶化が速いことが特徴である．ベータ以外にも，クラウンエーテルの一種である18-Crown-6を用いるとハイシリカなY型ゼオライトやEMT（フォージャサイトの一種でY型ゼオライトとは構造異性体）が得られる[20]など幅広い応用が可能である．

4.2.3　ドライゲルコンバージョン法のメリット

ドライゲルコンバージョン法によるゼオライト合成では，水熱合成と異なり原料のゲルの結

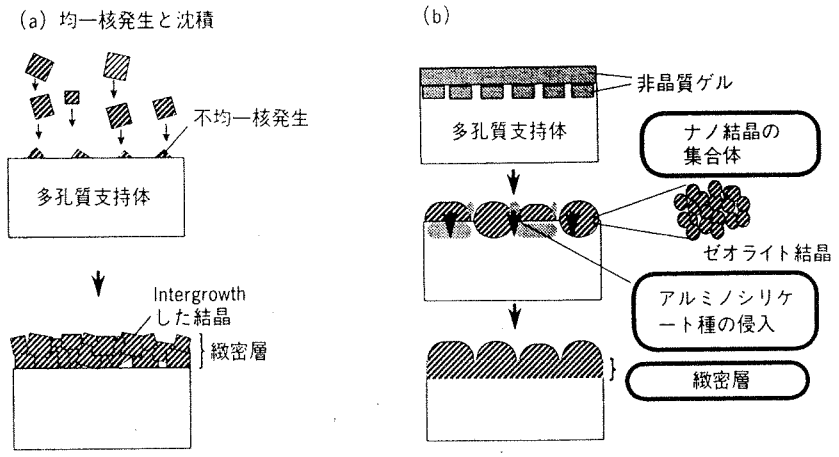

図5　ゼオライト膜の生成機構

(a) 水熱合成法，(b) ドライゲルコンバージョン法

晶化はほぼ100％に達する．また，原料ゲルを乾燥して用いるので反応器容積を小さくできる．高価なテンプレートの使用量も少なくてすむ．気相輸送法では，テンプレートの再使用が可能となるし，水蒸気処理法では結晶化をするときには液相に水しか用いないので，廃液の処理は不要である．連続合成も可能と期待できる．

5．ゼオライトの薄膜化技術

ゼオライト膜は急速に研究が展開しつつある．分子レベルでの高選択性が期待され，実際に水/アルコール系の浸透気化分離（A型[21]，シリカライト[22]），ブタン/イソブタン系（ZSM-5，シリカライト[23]）及び水素/炭化水素（シリカライト[24]）系のガス分離，芳香族炭化水素混合物の浸透気化分離（フェリエライト[25]，モルデナイト[26]）などで高い透過選択性を発揮する例が次々と報告されている．膜には，自立した膜と，多孔質支持体上に合成された支持膜の2種類があるが，自立膜は機械的強度に乏しく，今後は支持膜が主流になると思われる．ここでは紙数の制約もあり，これまでに明らかになった膜形成過程の概要を述べる．分離性能の詳細，及び合成技術の詳細については文献及び最近の総説[27]を参照して頂ければ幸いである．

ゼオライト膜の合成法には，様々な手法が提案されているが，最も研究例が多いのは水熱合成法である．図5 (a) には，水熱合成法によるゼオライト膜の生成過程を示した．大別して，均一核発生によるゼオライト粒子生成と支持体上への沈着による膜形成，あるいは基板表面における不均一核発生，の2説あるが，いずれの場合も緻密なゼオライト膜生成には，膜を構成するゼオライト粒子間のIntergrowthが重要となる．

一方，ドライゲルコンバージョン法を用いると，乾燥ゲルを多孔質支持体にあらかじめ塗布した後，気相中で結晶化することによりゼオライト膜を合成することができる[25)~27)]．この方法では，ゲルが結晶化過程で支持体細孔内に浸透し，多孔質支持体とゼオライトのコンポジット層が生成する（図5 (b)）．

他にも既に述べたようにゼオライトナノ結晶を支持体に植え付け，これを成長させる方法[11]など，様々な手法が提案されている．ゼオライト膜の合成に当たっての，絶対的な方法は今のところない．透過・分離性能の評価と合わせて今後の一層の発展が期待される．

6．おわりに

ゼオライトの利用分野は拡大の一途をたどっており，また新規なゼオライトが次々と見いだされているが，必ずしもこれらニーズとシーズが結びついていないのが現状である．

ゼオライトの物性（耐熱性，耐薬品性など）に対する要求も厳しくなりつつある．また，薄膜化技術は結晶をいかに緻密に生成させるかと

いう新しい問題を投げ掛けている．ゼオライト利用分野の拡大には，ゼオライトの合成化学の発展が不可欠である．新規なゼオライト群の発見と，薄膜化等精密合成手法の発展が，ゼオライトを利用した環境技術をはじめ，新規なプロセスの開発へと結実することを願ってやまない．

文　献

1) 泉　順，ケミカルエンジニアリング，[7] 53 (1996).
2) 原田雅志，ケミカルエンジニアリング，[4] 46 (1996).
3) USP, 4788169.
4) R.F. Lobo and M.E. Davis, *J.A.C.S.*, 117, 3766 (1995), R.F. Lobo, M. Pan, I. Chan, R.C. Medrud, S.I. Zones, P.A. Crozier and M.E. Davis, *Science*, 262, 1543 (1993).
5) J.M. Newsam, M.M. Treacy, W.T. Koetsier and C.B. DeGruyter, *Proc. R. Soc. Lond.* A420, 375 (1988).
6) M.E. Davis, C. Saldarriaga, C. Montes, J. Garces and C. Crowder, *Nature*, 331, 698 (1988).
7) M. Estermann, L.B. MuCusker, Ch. Baerlocher, A. Merrouche and H. Kessler, *Nature*, 352, 320 (1991).
8) C.C. Freyhartdt, M. Tsapatsis, R.F. Lobo, K.J. Balkus Jr. and M.E. Davis, *Nature*, 381, 295 (1996); USP 548424.
9) 大久保達也，ゼオライト，13, 49 (1996).
10) S. Katahira K. Itabashi and K. Igawa, Proc. 7th. Intern. Zeolite Conf., Ed. Y. Murakami, A. Iijima and J.W. Ward, Kodansha (1986) p.185.
11) M. Tsapatis, M.C. Lovallo, T. Okubo, M.E. Davis and M. Sadakata, *Chem. Mater.*, 7, 1734 (1995); M. Tsapatis, M.C. Lovallo and M.E. Davis, *Microporous Mater.*, 5, 381 (1996).
12) M.C. Lovallo and M. Tsapatsis, *AIChE J.*, 42, 3020 (1996).
13) 例えば，B.J. Schoeman, *Stud. Surf. Sci. Catal.*, 105, 617 (1996).
14) D.M. Bibby and M.P. Dale, *Nature*, 317, 157 (1985).
15) Q. Huo, S. Feng and R. Xu, *J. Chem. Soc., Chem. Commun.*, 1486 (1998); W. Xu, J. Li, W. Li, H. Zhang and B. Liang, *Zeolites*, 9, 468 (1989).
16) W. Xu, J. Dong, J. Li, J. Li and F. Wu, *J. Chem. Soc., Chem. Commun.*, 755 (1990).
17) M.H. Kim, H.X. Li and M.E. Davis, *Microporous Mater.*, 1, 191 (1993).
18) M. Matsukata, N. Nishiyama and K. Ueyama, *Microporous Mater.*, 1, 219 (1993), *Microporous Mater.*, 7, 109 (1996).
19) P.R.H. Prasad Rao and M. Matsukata, *Chem. Commun.*, 1441 (1996).
20) 菊地英一，木津功一，小松原祥子，松方正彦，上山惟一，第12回ゼオライト研究発表会予稿集 (1996) p.45.
21) 喜多英敏，井上　勉，堀井康司，田中一宏，岡本健一，化学工学会第28回秋季大会研究発表予稿集 (1995) M 207.
22) T. Sano, H. Yanagishita, Y. Kiyozumi, F. Mizukami and K. Haraya, *J. Membr. Sci.*, 95, 221 (1994).
23) Y. Yan, M.E. Davis and G.R. Gavalas, *Ind. Eng. Chem. Res.*, 34, 1652 (1995).
24) F. Kapteijn, W.J.W. Bakker, J. van de Graaf, G. Zheng, J. Poppe and J.A. Moulijn, *Catal. Today*, 25, 213 (1995).
25) N. Nishiyama, K. Ueyama, M. Matsukata, *Stud. Surf. Sci. Catal.*, 105, 2195 (1996).
26) N. Nishiyama, K. Ueyama, M. Matsukata, *Microporous Mater.*, 7, 299 (1996).
27) 松方正彦，表面，34, 385 (1996)；触媒，38, 585 (1996).

[筆　者　紹　介]

松方　正彦（まつかた　まさひこ）
平成元年早稲田大学理工学研究科博士後期課程修了．工学博士．同年成蹊大学工学部助手．同4年大阪大学基礎工学部助手．同8年同助教授，同9年早稲田大学理工学部助教授，現在に至る．専門：反応工学．
[連絡先]　〒169　東京都新宿区大久保3-4-1　早稲田大学理工学部

10. 無機ガス分離膜の開発動向

松 方 正 彦*

1．はじめに

ガス分離に対して無機膜が応用されたのは有機高分子膜より古く，第2次世界大戦当時の1940年代米国のマンハッタン計画において，多孔質アルミナを用いて^{238}Uと^{235}Uの同位体分離が行われたのが始まりである．ウランをガスとして扱うために，UF_6が用いられ，選択性は$^{235}UF_6$ $^{238}UF_6$の膜細胞孔内における拡散係数の差によるものであった．その後，有機高分子膜の台頭と共に，無機膜の開発は希ガスの同位体分離など特殊な分野を除いて，勢いを失っていった．

1980年代に入って，有機高分子膜の開発が高度に進み，さらに分離膜の要求性能が高くなるとともに，再び無機膜がガス分離を始めとした分離技術開発の対象として見直されるようになってきた．1991年には，H_2/N_2系の理想分離係数が1000を越えるアモルファスシリカ膜が報告され(Tsapatsis *et al.*, 1991)，この報告がきっかけとなって，以降無機膜研究全般が活発になり現在に至っている．

本稿では，ガス分離用無機膜の用途・分離対象を述べた後，無機膜のガス分離性能の現状について紹介し，最後に展望を述べてみたい．

2．無機ガス分離膜の要求性能

有機高分子膜を用いた分離プロセスは，動力が小さくてすむこと，簡便な操作性，安価な装置コストから，既往の分離プロセスである蒸留，深冷分離，圧力スイング吸着法，液吸収法などより有利となる場合があるため，ガス分離の分野では1980年代初期より工業的に用いられてきた．

膜として必要な性能の3要件は，透過選択性(目的物の回収率に影響)，透過流束(必要な膜面積を決定)，寿命(交換，メンテナンスのコストに影響)である．無機膜の場合には，通常有機高分子膜より著しく高価で，かつ重いため，無機高分子膜がガス分離の分野で実用化されるには，これら3要件について有機高分子膜と比べて著しく劣ってはならないことは勿論のこと，コスト面で競争力をつける必要がある．コスト高となる原因のひとつは，Transport Layerを支える支持体層にあり，支持体自身のコストダウンとモジュール化によって大面積化を図ることが重要な課題である．まず，既往の有機高分子膜が対応できない過酷な条件にある分離対象は，無機膜分離にとって有望である．多くの高分子膜の最高使用温度は数十℃であり，ポリイミド樹脂でも200℃程度である．無機物を膜材料として用いれば，数百℃で使用可能な分離膜が実現できると期待されている．ただし，高温では膜のミクロ構造の安定性，膜材料と雰囲気ガスとの反応に注意する必要がある．

一般論としては，既往の分離プロセスと比較して，無機膜による分離が有利となるためには，0.01 $cm^3(STP)s^{-1}cm^{-2}cmHg$程度の透過能が目標となる(Hsieh, 1996)．また，分離係数は5～10程度必要

* 早稲田大学 理工学部 応用化学科

で，製品の要求純度が95%以下の場合が望ましい．

膜分離プロセスにおいては，供給側と透過側の圧力差が推進力となるため，モジュール内のシール部分におけるリークの防止が必要であるが，高温におけるシールについては現在のところ確立された技術はない．

3．無機ガス分離膜の開発対象

無機膜が対象とする工業的に重要なガス分離の対象を表1に示す．これらはいずれも開発の端緒に付いたばかりのものが多いが，検討に値する有望な利用分野として紹介したい．

水素の回収・製造技術は，発電，石油精製などエネルギー産業，各種化学産業において重要な技術である．水素分離はガス分離膜の分野としても重要な開発目標であり，多くの研究例が報告されている．高純度水素の製造については，これまで非多孔性の緻密な金属膜の開発が進められてきた．水素は，多くの金属中において酸素・窒素の拡散係数と比べて$10^{15\sim20}$大きい拡散係数をもつため，緻密な金属膜を用いると水素の選択的透過による高純度水素の生産が期待できる．これまで検討されてきた金属膜は，水素の透過流束の観点からパラジウムが多い．半導体工業向けや，燃料電池向けの水素製造に用いることができる．

複合サイクル発電あるいは化学品製造プロセスの一部として，天然ガス，重質油，石炭などの化石資源を原料として，酸素による部分ガス化，水蒸気改質プロセスにより水素あるいは合成ガスが製造される．これらのプロセスでは，水素と一酸化炭素の分離，水素と二酸化炭素の分離が望まれる．ガス製造プロセスの後段にメタノール合成やオキソ合成などの化学品合成プロセスを配する場合には，原料となるH_2/CO比が重要で，H_2/CO比を調節するために通常シフトコンバーターを設けて，水性ガスシフト反応を行う．このとき，膜分離を組み合わせて水素分離を行う方式が考えられている．ガス製造反応器からの出口ガスには硫化水素，二酸化炭素が含まれているため，1段目の膜分離器でこれらを分離し，2段目で水素を分離する方式が提案されている．ガス製造プロセスおよび後段の化学反応プロセスは加圧下で運転されるが，膜分離プロセスのフィード側の残留物である合成ガスが，後段プロセスの原料となるため，エネルギー的に有利となる．石炭ガス化プロセスにおける水素分離の目標となる分離条件は，約540℃，5～35気圧，硫黄酸化物あるいは硫化水素の濃度は1%以下である．ガス化剤となる酸素は，一般に圧力スイング法によって製造されるが，規模によっては空気分離も膜分離の対象となる．

アンモニア合成は，500℃，300気圧といった過酷な条件で操業され，未反応ガスをリサイクルする必要がある．このとき，ガス中には不活性なアルゴン，メタンが濃縮してくるため，原料の水素・

表1　無機ガス分離膜の用途

分離対象	用途
高純度水素の回収	半導体工業，燃料電池用水素製造
水素／一酸化炭素／二酸化炭素	水蒸気改質による水素・合成ガス製造，石炭ガス化複合サイクル発電における水素製造
水素／炭化水素	石油精製オフガスからの水素回収
水素／窒素／アルゴン・メタン	アンモニア合成
二酸化炭素／窒素	燃焼排ガスからの二酸化炭素回収
窒素／酸素	空気分離
メタン／二酸化炭素・硫化水素・窒素・炭化水素	天然ガス分離
オレフィン／パラフィン系炭化水素	石油化学原料
直鎖炭化水素／分枝状炭化水素	石油化学原料
キシレン異性体	石油化学原料
空気／炭化水素	VOC(ガソリン蒸気等)回収

窒素をこれら不活性ガスと分離する必要がある．このとき，高温のまま未反応水素/窒素を膜分離できれば意義深い．ただし，選択透過した水素は再昇圧する必要がある．

近年の地球温暖化に対する問題意識の高まりと共に，特に火力発電設備を対象として二酸化炭素の膜分離回収プロセスの開発が進められている．ここでは，二酸化炭素は窒素，水蒸気，酸素といった他の排ガス成分との分離が試みられている．目標温度は約400℃である．

石油精製プロセスのオフガスは，水素とC_2～C_4の低級炭化水素を含み，かつ石油精製プロセスにおける水素の需要は原油の重質化とともに増加の一途を辿っている．したがって，オフガスからの水素の分離回収は，石油精製において有望な応用対象である．また，炭化水素の脱水素プロセスから生成する炭化水素と水素の分離も有用である．

天然ガスを供給するためのパイプラインでは，窒素・二酸化炭素・硫化水素はカロリー低下およびパイプラインの腐食の原因となる．そこで，これらを膜分離によって天然ガスから除去する分離精製プロセスが検討されている(Meyer and Gamez, 1995)．このとき，供給側にメタンが残留すれば，再昇圧の必要がなく実用化に有利となる．

ガス状炭化水素混合物の分離も，無機ガス分離膜の対象として魅力的である．C_2～C_4のオレフィンとパラフィンの分離は，パラフィンは燃料として，オレフィンは基幹化学原料としての価値が高いため，分離膜の開発が望まれている．また，直鎖炭化水素と分枝状炭化水素の分離も，石油化学工業において幅広い用途がある．Sie(1994)は，異性化触媒とゼオライト膜を組み合わせた膜反応器による，分枝状炭化水素(あるいは直鎖炭化水素)の選択的合成プロセスを提案した．また，キシレン混合物ガスなど芳香族炭化水素混合ガスの高温分離プロセスも，炭化水素製造プロセスの簡略化，高効率化によって魅力的な対象である．空気とガソリン蒸気などの有機蒸気分離も，環境中へのVOC(Volatile Organic Compounds)の放出抑制技術として重要となりつつある．

4．無機ガス分離膜の開発動向

無機ガス分離膜は，非多孔性膜と多孔性膜に大きく分類される．非多孔性膜には，水素の選択的透過を目的とした金属膜と，酸素の選択的透過を目的とした酸化物膜がある．従来，主として前者の膜の開発はパラジウムを中心として進められてきたが，メタンの酸化カップリングやアルカンの部分酸化反応など，化学原料としての未利用炭化水素の選択的部分酸化反応の実現を目指して，酸素透過性酸化物膜も開発が進められるようになってきた．

多孔性膜には，非晶質シリカ膜などの非晶質酸化物膜，ゼオライトなどの結晶性ミクロ多孔性膜，多孔質炭素膜があり，それぞれ積極的に開発が行われている．

4．1 緻密膜

4．1．1 金属膜

パラジウム金属膜は，当初金属管そのままが用いられていたが，現在では透過流束の向上とパラジウムのコスト削減を目指して，無電解めっき，化学気相析出(CVD)，スパッタリングなどを用いて，多孔質体に薄膜状に製膜する方法が検討されている．パラジウムはα，βの2つの相をもち熱サイクルによってスピノーダル分相を起こすため，高温における水素製造に用いると膜性能の低下が避けられない．このため，Agと合金化し膜構造の安定化が図られる．400℃，68気圧，25μmの膜厚をもつPd-Ag合金膜で，4.1×10^4Barrer(1 Barrer$=10^{-10}$cm^3(STP)/cm s^{-1}cm^{-2}cmHg)の性能が報告されており，水素の純度99.9999%以上を得ることは難しくない．無機膜の中では例外的に高い選択性が達成されている例である．

Kikuchi(1997)は，無電解めっきによってα-アルミナ多孔質支持体上に膜厚5μm程度までのパ

ラジウム薄膜を製膜することに成功し，高温の各種水素製造反応への応用を試みている．メタンの水蒸気改質では，水素の分離によって平衡を著しく生成物側へシフトさせることにより，反応温度の低温化が可能であることを示した．一般に，水素の透過は水素の解離を伴う金属パラジウム中への水素の溶解拡散機構に従う．現在の開発課題は，水素透過能の向上であり，さらなる薄膜化が必要である．

最近，上宮ら(1997)は，無電解めっき法によって白金薄膜の製膜に成功した．透過機構は明らかではないが，白金薄膜の場合にも水素の選択的透過が起きることが見出された．パラジウム膜と比較して，白金薄膜には耐硫黄性，析出炭素に対する耐性が期待できる．今後，パラジウム以外の金属薄膜にも注目が集まると思われる．

4．1．2　酸化物膜

酸素選択透過膜として，安定化ジルコニア(YSZ)が古くから知られている．酸化物結晶中の格子酸素が移動するため，酸素の選択的透過が起こる．アルケン，アルカンの部分酸化反応用の膜反応器の材料として検討されている(竹平，1997)．YSZ中の格子酸素が十分な易動性を示すのは，動作温度が450℃以上とやや高いため，CeO_2など他の酸化物系の検討も始まっている．

近年ペロブスカイト型の酸化物による酸素透過膜が注目され，メタンと酸素からの合成ガス製造や，酸化カップリングによるC_2以上の炭化水素の合成など，さまざまな酸化反応膜反応器を構築する試みが行われている．しかし，多くのペロブスカイト型の酸化物は，反応によって格子酸素が過剰に消費されると膜の破壊が起きてしまい，膜の安定性に欠ける．Balachandranら(1997)は最近，Sr-Fe-Co系ペロブスカイト($SrFe_{0.2}Co_{0.8}O_x$)と極めて近い組成をもつ，非ペロブスカイト酸化物$SrFeCoO_x$を提案している．この膜をメタンと酸素からの合成ガス製造に用いると，850℃において40日以上にわたって膜の破壊は起きないこと，その間CO選択性98%以上を維持したことが報告された高性能を発揮するとされており，今後の展開が期待される．

4．2　多孔性膜

多孔性膜は，その細孔径と透過分子のサイズによる分子ふるい作用，あるいは細孔壁と分子の相互作用による表面拡散によって，高い分離性能が発現することが期待されている．

4．2．1　非晶質膜

非晶質の多孔酸化物膜としては，シリカ膜がもっとも活発に研究されている．多くはゾルゲル法によって合成され，1 nm以下のミクロ孔をもつ膜の合成の報告も増えつつある．Tsapatsisら(1991)は，シリカ膜によつて水素/窒素の分離を行い，水素の透過係数こそ約7×10^{-7} cm³(STP)$s^{-1}cm^{-2}$cmHgと小さいものの，1000～5000と例外的に大きい分離係数の発現を報告した．現在，この結果はシリカの網目構造中の微細な細孔によって分子ふるい的な透過選択性が発現したと理解されている．Wuら(1994)は，CVD法により合成したシリカ膜を用いて，水素/窒素の分離において透過係数約1×10^{-5} cm³(STP)$s^{-1}cm^{-2}$cmHgにおいて分離係数72を達成している．

ゾルゲル法によってシリカ微粒子を合成し，これを支持体上にコーティングすることでナノあるいはサブナノスケールの細孔径をもつ膜の合成が可能である．Asaedaら(1994)は，ゾルゲル法により平均細孔径1 nm以下のシリカ膜を合成し，35℃においてプロピレン/プロパンの分離係数30を報告している．両者の分子径はほとんど変わらず，分子ふるい効果は期待できないので，高い分離能の発現は細孔内へのプロピレンの選択的吸着によると考えられている．こうした細孔内への吸着による透過選択性の発現は，後述するようにミクロ細孔をもつ分離膜においては分子ふるい作用以上に重要となることが多いことが明らかにされつつある．

膜の透過選択性の改良を目的として，膜の表面修飾がしばしば報告されるようになってきた．テト

ラエトキシオルトシリケート(TEOS)の加水分解により生成したシリカ粒子で薄層コーティングすることにより，γ-アルミナ多孔膜の表面を修飾することができる(Cho *et al.*, 1995, Lange *et al.*, 1995). Lang 等(1995)は，この方法により 200℃において水素/メタン系で 40，水素/イソブタン系で 200 と高い選択性が発現することを報告した．他にも，γ-アルミナ多孔膜の表面をフェニルトリエトキシシランなどのシランカップリング剤を用いて修飾を試みた例(Hym *et al.*, 1996)，シリカ膜の表面層をγ-アルミナ薄層にてコーティングした例(Naira *et al.*, 1996)等が報告されている．これらは，いずれも膜表面の吸着特性の制御を目的としており，今後ともこの方向の研究は活発になると思われる．

Takaba ら(1996)は，分子動力学計算により二酸化炭素，窒素の膜透過・分離について検討し，高温においても分子と細孔壁の相互作用は重要で，分離には二酸化炭素を強く吸着する材料が好ましいことを報告しており，計算機科学の面からも膜透過・分離における吸着現象の重要性が指摘されている．

ただし，シリカ膜のような非晶質膜は，水蒸気によるシンタリングを受けやすく，選択性の低下を招きやすい．高温のガス分離に応用する際には注意が必要である．

4. 2. 2 ゼオライト膜

ゼオライトは 0.3～0.7nm 程度の均一で剛直な細孔をもつアルミノシリケートの総称である．膜材料としては，ゼオライトの細孔が結晶構造に基ずくことから，高温における安定性，および細孔径の均一さに基づく高い分離性能(分子ふるい作用)が期待されており，急速に発展してきた分野である(Matsukata and Kikuchi, 1997)．分子ふるい作用以外にも，細孔内の静電場による選択的吸着能，親疎水性などによる分離機能の発現が期待される．

ゼオライト膜合成には，粉末状ゼオライトの合成手法である水熱合成がよく用いられる．自立膜は機械的強度に乏しく，多孔支持体上に製膜することが望ましい．支持体の材質としては，焼結金属(Geus *et al.*, 1992, 1993)，α-アルミナ(Yan *et al.*, 1995, 1997)，γ-アルミナ(Bai *et al.*,1994)等が用いられる．ZSM-5 ゼオライト(有効細孔径 0.55nm 程度)が，多くの場合研究対象とされている．図 1 には，Kapteijn ら(1995)が報告した，水素と *n*-ブタンの単独系(図 1 (a))，混合系(図 2 (b))の初期における非定常な透過挙動を示す．膜には焼結金属上に製膜したシリカライト(アルミニウムを含まない ZSM-5)が用いられた．*n*-ブタンの分圧が 5 kPa，水素の 95kPa である．単独系では分子径が小さく，吸着が弱く，分圧の高い水素の透過が圧倒的に大きい．一方，混合系では初期において水素の優先的な透過がみられるが，ブタンが透過するようになると水素の透過は著しく阻害され，ブ

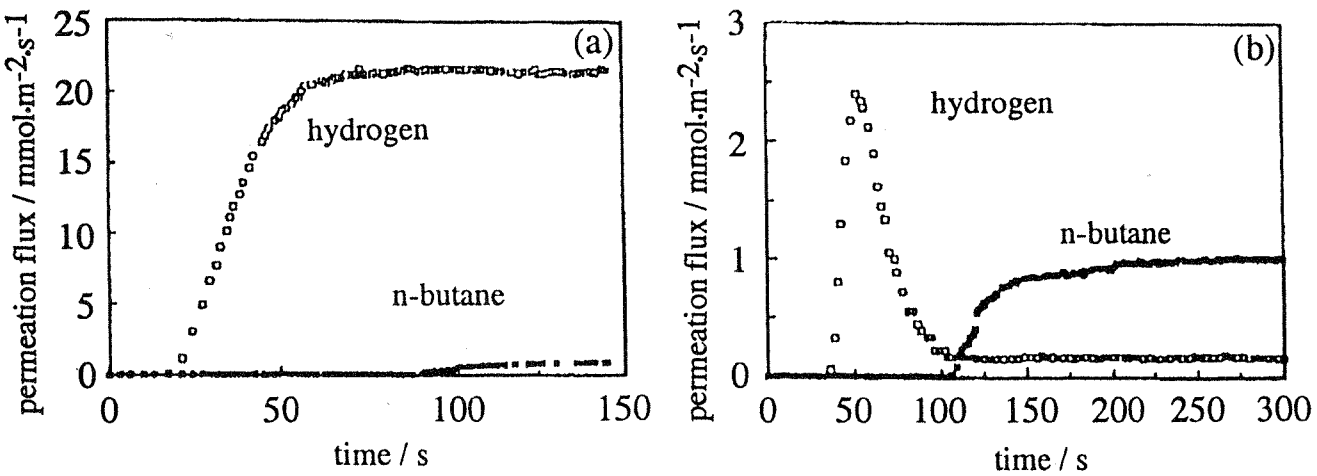

図 1　水素(95kPa)，*n*-ブタン(5 kPa)の 27℃における透過流速の経時変化．(a)単成分系，(b)混合系，シリカライト

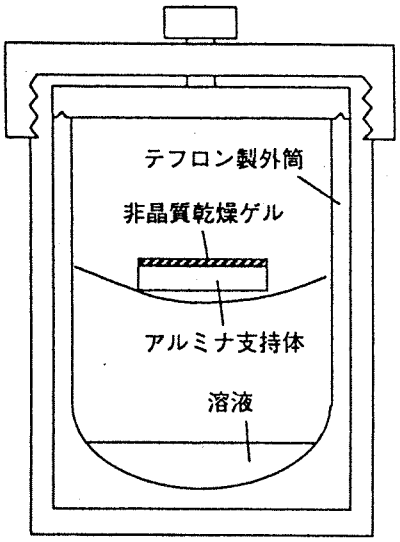

図2　気層輸送法によるゼオライト膜合成用オートクレーブ

タンが選択的に透過するようになる．これはバルキーで吸着力の大きいブタンによって細孔内が占有された結果と考えられる．図1の結果は水素/炭化水素の混合系においてゼオライト膜を用いた炭化水素の選択的透過が可能であることを実験的に証明したものである．パラジウム膜が水素の選択的透過能を示すことはよく知られているが，それとは反対の機能の発現であり，極めて興味深い．また，吸着性ガスにおいては，非晶質膜の場合と同様，分子サイズよりも吸着性が透過選択性に支配的であることを示している．最近，Kusakabe ら(1997)は，Y型ゼオライト膜の製膜を行い，30℃において二酸化炭素/窒素の分離係数20～100と，非常に高い分離係数を実現した．二酸化炭素の透過率も 10^{-7}mol m^{-2} s^{-2} Pa^{-1} と比較的大きい．この場合にも，吸着性の大きい二酸化炭素がゼオライトの細孔を充填することにより，選択的に透過したとされている．

ゼオライト膜は，通常ランダムに配向した多結晶の集積体として得られるため，その結晶粒界に生じるピンホール，クラックの透過・分離性能に対する影響を考えなくてはならない．なお，図1で用いられた膜はほぼピンホールフリーと考えられている．ゼオライト膜の性能を評価する際に，しばしば *n*-ブタンと *iso*-ブタンの透過流束の比が比較される．一般的にはピンホールが埋まるほど *n*-ブタンが選択的に透過する．ピンホールがある場合には *iso*-ブタン選択性となることもあるようである．これはピンホール内に沸点の高い *iso*-ブタンが毛管凝縮するためと推察される．Yan ら(1997)は，トリイソプロピルベンゼン(分子径0.85nm)を膜に吸着させると，ZSM-5型ゼオライトの細孔内部に入らないためピンホールのみに浸透し，これを熱分解することにより(Post-coking Treatment)ピンホールがある程度ブロックされることを報告した．この方法によって，*n*-ブタン/*iso*-ブタン系の理想分離係数が，185℃において45と，処理前と比べて4倍向上する．ただし，ゼオライト膜のピンホールあるいは粒界の評価手法は確立されておらず，緊急の研究課題と思われる．

水熱合成法以外のゼオライト膜合成手法として，気相輸送法によるゼオライト膜合成が提案されている(Matsukata *et al.*, 1993, 1994a)．Xu ら(1990)により報告された気相輸送法は，その後一般的なゼオライト合成法として確立されてきた(Kim *et al.*, 1994, Matsukata *et al.*, 1994)．気相輸送法では水熱合成と異なり結晶化剤を含まないシリカアルミナゾルを調製し，一旦乾燥させる．この固相状態の乾燥ゲルを結晶化剤を含む蒸気中で処理することにより結晶化剤をゲル中に浸透させ，ゼオライトへと結晶化せしめる．Matsukata ら(1994a, b)が合成に用いたオートクレーブを図1に示す．オートクレーブ中段に乾燥ゲルを置き，底部には結晶化剤および水を充填する．

この手法を用いて合成したモルデナイト膜(Nishiyama *et al.*, 1996；細孔径0.65×0.75nm)およびフェリエライト膜(Matsukata *et al.*, 1994b；細孔径0.35×0.48nm)を用いて，30～100℃の範囲で無機ガスの透過実験を行った結果を図3に示す．細孔径の大きいモルデナイト膜では，2桁ほど大きい透過流束を示している．モルデナイト膜における H_2，He，CH_4 は右肩下がりの傾向を示した．クヌッセン拡散の場合には右肩上がりの直線となるはずで，この結果は水素，ヘリウム，メタンの透過もゼオライト細孔内における活性化過程が支配的であることを示している．また，その他の場合はいずれも極小値を示し，このことは2種類以上の透過機構が存在することを示唆する．この透過現象を説明するために，透過分子にはゼオライト細孔中央付近を透過するものと，細孔壁とより強い相互作用(細孔壁への吸着)をもちながら透過するものの2種類が存在するとする，Parallel diffusion model を提案した(Nishiyama *et al.*, in press)．高温側では前者が支配的であり，温度が高いほど

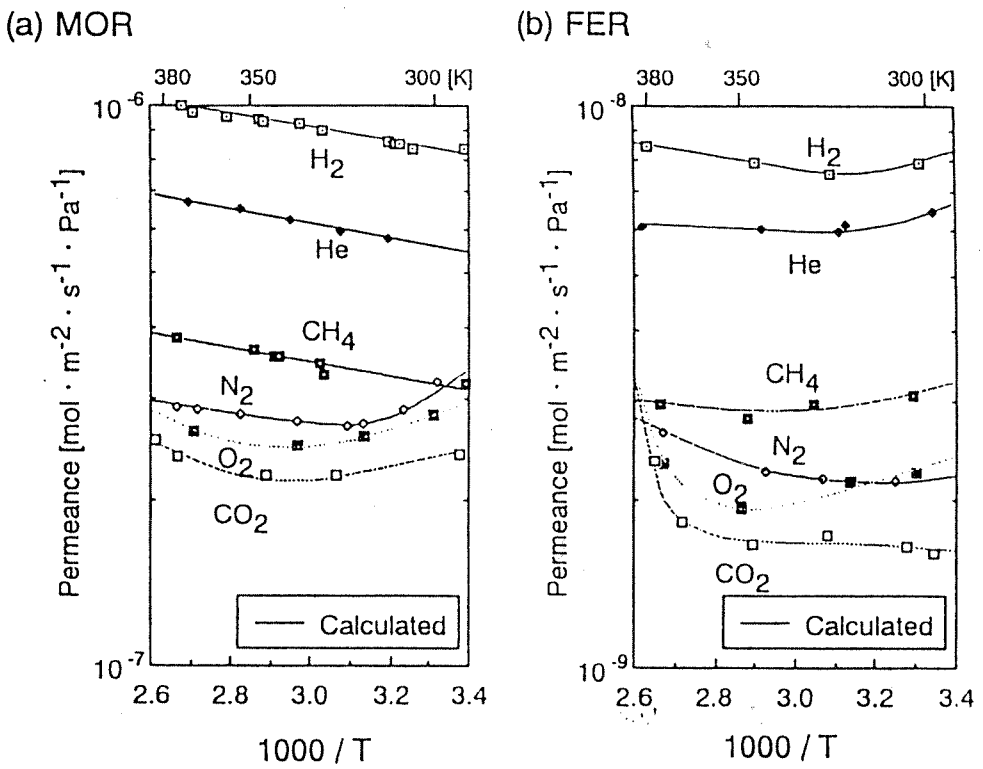

図3　モルデナイト膜(MOR)，フェリエライト膜(FER)の無機ガス透過性能

透過分子数が増えるが，低温になると今度は低温ほど細孔壁への吸着量が大きくなり，後者の機構により再び透過量が増加する．モルデナイトは細孔径が大きく，その細孔内における水素，ヘリウム，メタンのような吸着の弱い分子は前者の機構が常に支配的であるため，右肩下がりの直線となったと考えられる．これら吸着の弱い分子でもFER膜ではその透過率は温度に対して極小値をもつようになる．

実験的に透過側にスイープガスを用いるか，あるいは真空排気するかは研究者によって異なる．ミクロポーラス膜の場合，スイープガスに用いた分子が対向拡散し，目的分子の透過挙動に影響することが予想されるため，異なる研究者の結果を比較する際には注意が必要である．特に，分子径の大きいアルゴンなどをスイープガスとして用いた場合には注意が必要である．

4．2．3　炭素膜

ミクロポーラス炭素は，1nm以下の細孔制御が可能なため，膜材料として有望とみられている．ただし，炭素膜は酸化雰囲気では安定性がないので，分離対象の選択が重要である．

Air Products社は積極的に炭素膜(SSF™膜)の開発を進めている(Rao and Sircar, 1993, 1996)．彼らは，平均細孔径0.7μmのマクロポーラスグラファイト上にPoly(vinylidene chrolide)-acrylate terpolymer latexを薄膜コーティングし，これを1000℃にて炭化することで，平均細孔径0.55nm程度のミクロポーラス炭素膜を合成した．この膜は石油精製オフガスからの水素回収に高性能を発揮する．**図4**に，SSF™膜分離と圧力スイング法を用いた水素回収システムを示す(Rao and sircar, 1993)．Kapteijnらの結果と同様，SSF™膜においても吸着性の炭化水素が選択的に透過し，水素が供給側で濃縮される．特にC_3以上の炭化水素はほぼ透過・除去される．したがって，水素の圧力低下を最小限に抑えることができ，水素をリサイクルする際に有利となる．膜のモジュール化も進んでおり，両端をO-リングでシールした管状膜のモジュールが発表されている(Rao and Sircar, 1996)．

SudaとHaraya(1997)は，Kaptonポリイミドフィルムを1000℃で炭化し，これを若干水蒸気処

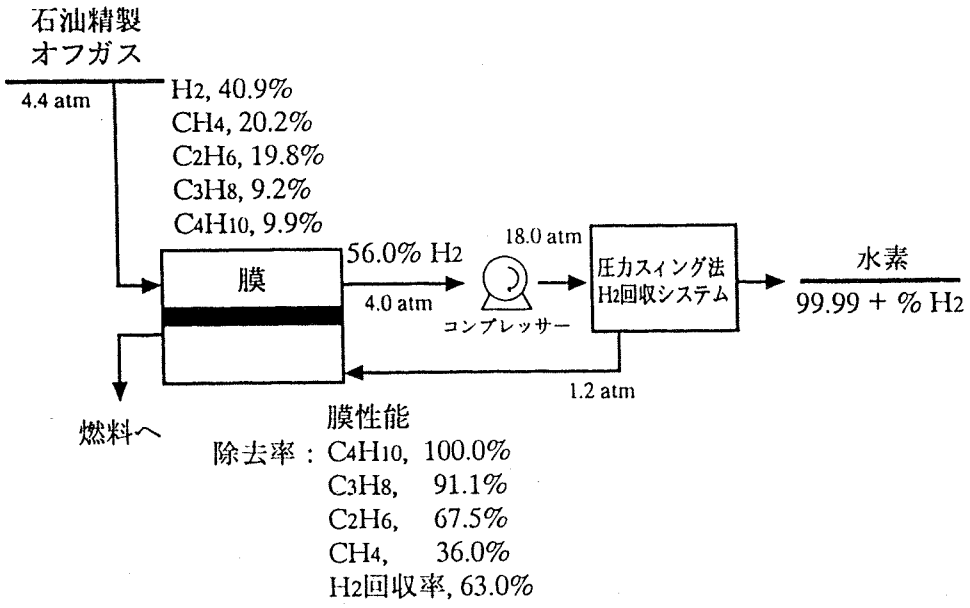

図4　SSF™膜を用いた石油精製オフガスからの水素回収プロセス

理することにより，細孔径0.40～0.43nmの炭素膜を合成した．この膜は35℃において，水素/窒素，二酸化炭素/窒素系で，それぞれ1000，100と高い理想分離係数を示した．また，オレフィンとパラフィンの分離が可能で，プロピレン/プロパン系において100を越える分離係数が報告されている．

5．おわりに

無機化合物を用いたガス分離膜の現状を述べてきた．数年前と比較して開発対象・目標がより明確になってきたこと，続々と新規な膜合成のアイデアがされることが相まって，近年の無機膜開発研究は大変な活況である．分離性能のみで判断する限り，分野によっては実用化可能な領域にまで達しているものもある．しかし，無機ガス分離膜の特徴が真に発揮できる高温において優れた性能(透過流束，分離係数，寿命)を発揮する膜の報告例は決して多くない．実験室レベルから実用レベルに至るまで，支持体と分離装置の高温シールの方法は共通の工学的問題であり，実際に高温における透過実験を難しくしている．

ミクロ細孔内の物質移動現象は，溶解拡散機構による説明ができない場合が多く，新しい研究テーマである．また，膜性能を簡便に評価可能な膜のキャラクタリゼーション手法も確立されておらず，透過性能発現の理由を論議することが難しい．

現実に使用可能な膜モジュールの開発と共に，膜の合成・評価手法が確立され，両者が両輪となって効率的な無機ガス分離膜の開発が進められ，大規模で高効率な無機膜分離プロセスが一日も早く実現されることを願ってやまない．

引用文献

上宮成之，畠山紀子，梶原昌高，小島紀徳，水元和成，土井　正，1997，表面技術，**48**(4)，470
竹平勝臣，1997，触媒，**39**(5)，330
Asaeda, M., A. Yamamichi, M. Satoh and M. Kamakura, 1994, Proc. 3rd Intern. Conf. on Inorg. Membr.
Bai, C., M.D. Jia, J.L. Falconer and R.D. Noble, 1995, *J. Membr. Sci.*, **105**, 79
Balachandran, U., J.T. Dustek, P.S. Maiya, B. Ma, R.L. Mieville, M.S. Kleefisch and C.A. Udovicli, 1997, *Catal. Today*, **36**, 265
Chen, Y.D. and R.T. Yang., 1994, *Ind. Eng. Chem. Res.*, 3146

Cho, Y.K., K. Han and K.H. Lee, 1995, *Microporous Mater.*, 219
Geus, E.R., M.J. den Exter and H. van Bekkum, 1992, *J. Chem. Soc.*, Faraday Trans., **88**, 3101.
Geus, E.R., H. van Bekkum, W.J.W. Bakker and J.A. Moulijn, 1993, *Microporous Mater*, **1**, 131
Hsieh, H.P., 1996 "Inorganic Membranes for Separation and Reaction", Elsevier, pp.256
Hyun, S.H., S.Y. Jo and B.S. Kang, 1996, *J. Membr. Sci.*, **120**, 197
Kapteijn, F., W.J.W. Bakker, J. van de Graaf, G. Zheng, J. Poppe and J.A. Moulijn, *Catal. Today*, **25**, 213 (1995)
Kikuchi, E., 1997, CATTECH, 67
Kim, M.H., H.X. Li and M.E. Davis, 1993, *Microporous Mater.*, **1**, 191
de Lange, R.S.A., J.H.A. Hekkink, K. Keizer and A.J. Burggraaf, 1995, *Microporous Mater.*, **4**, 169
Kusakabe, K., T. Kuroda, A. Murata and S. Morooka, 1997, *Ind. Eng. Chem. Res.*, **36**, 649
Matsukata, M., N. Nishiyama and K. Ueyama, 1993, *Microporous Mater.*, **1**, 219
Matsukata, M., N. Nishiyama and K. Ueyama, 1994a, *J. Chem. Soc. Chem. Commun.*, 339
Matsukata, M., N. Nishiyama and K. Ueyarna, 1994b, *Stud. Surf. Sci. Catal.*, **84**, 1183
Matsukata, M. and E. Kikuchi, 1997, *Bull. Chem. Soc. Jpn.*, **70**, 2341
Meyer, H.S. and J.P. Gomez, 1995, Proc. 45th Anuual Laurence Reid Gas Conditioning Conf., 284
Nair, B.N., K. Keizer, W.J. Elferink, M.J. Gilde, H. Verweij and A.J. Burggraaf, 1996, 116, 161
Nishiyama, N., Ueyama, K. and Matsukata, M., 1995, *J. Chem. Soc. Chem. Commun.*, 1967
Nishiyama, N., Ueyama, K. and Matsukata, M., 1996, *Microporous Mater.*, **7**, 299
Nishiyama, N., K. Ueyarna and M. Matsukata, *AIChE J.*, in press
Rao, M.B. and S. Sircar, 1993, *J. Membr. Sci.*, **85**, 253
Rao, M.B. and S. Sircar, 1996, *J. Membr. Sci.*, **110**, 109
Sie, S.T., 1994, *Stud. Surf. Sci. Catal.*, **85**, 587
Suda, H. and K. Haraya, 1997, *Chem. Commun.*, 93
Tsapatsis, M., T. Okubo, M. Lovallo and M.E. Davis, 1995, *Mat. Res. Soc., Symp. Proc.*, Vol.371, 21
Tsapatsis, M., S. Kim, S.W. Nam and G. Gavalas, 1991, *Ind. Engi Chem. Res.*, **30**, 2152
Takaba, H., K. Mizukami, M. Kubo, A. Stirling and A. Miyamoto, 1996, *J. Membr. Sci.*, 251.
Wu, J.C.S., H. Sabol, G.W. Smith, D.L. Flowers and P.K.T. Liu, 1994, *J. Membr. Sci.*, **96**, 275.
Xu, W., J. Dong, J. Li, J. Li and F. Wu, 1990, *J. Chem. Soc. Chem. Commun.*, 755
Yan, Y.S., M.E. Davis and G. Gavalas, 1995, *Ind. Eng. Chem. Res.*, 1652
Yan, Y.S., M.E. Davis and G. Gavalas, 1997, *J. Membr. Sci.*, **126**, 53

総　説（Review Article）：膜（MEMBRANE），23 (2)，55-61 (1998)

●特集　無機分子ふるい膜を展望する

無機膜による炭化水素分離

松　方　正　彦

早稲田大学　理工学部応用化学科　〒 169-8555　東京都新宿区大久保 3-4-1

State-of-the Art of Hydrocarbon Separation through Inorganic Membranes

Masahiko Matsukata

Department of Applied Chemistry, Waseda University
3-4-1 Okubo, Shinjyuku-ku, Tokyo 169-8555, Japan

State-of-the art of hydrocarbon separation technology by inorganic membranes is reviewed. Targets for hydrocarbon separation are classified into five groups : H_2/Lower hydrocarbons, alkane/alkene, straight chain hydrocarbons/branched hydrocarbons, aliphatic hydrocarbons/aromatic hydrocarbons, and aromatic hydrocarbon mixtures. Various types of microporous inorganic membranes, amorphous silica, zeolites and carbon membranes, have been under development. Some of them show very high permselectivities, indicating the promising prospects of inorganic membrane technology. While molecular sieving property has long been anticipated to appear on the basis of size recognition by micropores smaller than 1 nm, there have been a few reports with conclusive evidence on the separation by molecular sieving. On the other hand, the difference in adsorption properties into a membrane can lead to the appearance of permselectivity particularly at lower temperatures.

Keywords : inorganic membranes／carbon／zeolites／silica／hydrocarbon separation

1.　はじめに

分子レベルの分離が可能な無機膜開発にあたっての大きなターゲットは，電力・石油といったエネルギー産業である．なかでも世界の１次エネルギー源として石油は依然として重要な位置を占めており，無機膜による石油系炭化水素混合物の分離精製は，大規模な応用が期待できる分野である．石油は幅広い分子量分布をもつ炭化水素の混合物であり，膜分離技術の開発対象として恰好のターゲットである．多くの高分子膜の耐熱性の上限は数十°C で，かつ有機溶媒に対する膨潤・溶解が問題となるため，石油系炭化水素の分離には無機膜が望ましいと言われている．同じく１次エネルギー源の主役である天然ガスは C1-C4 の炭化水素，N_2，CO_2 の混合物であり，エネルギー大量消費型の深冷分離法に替わって，膜分離技術が検討されているが，天然ガス分離の場合には扱う原

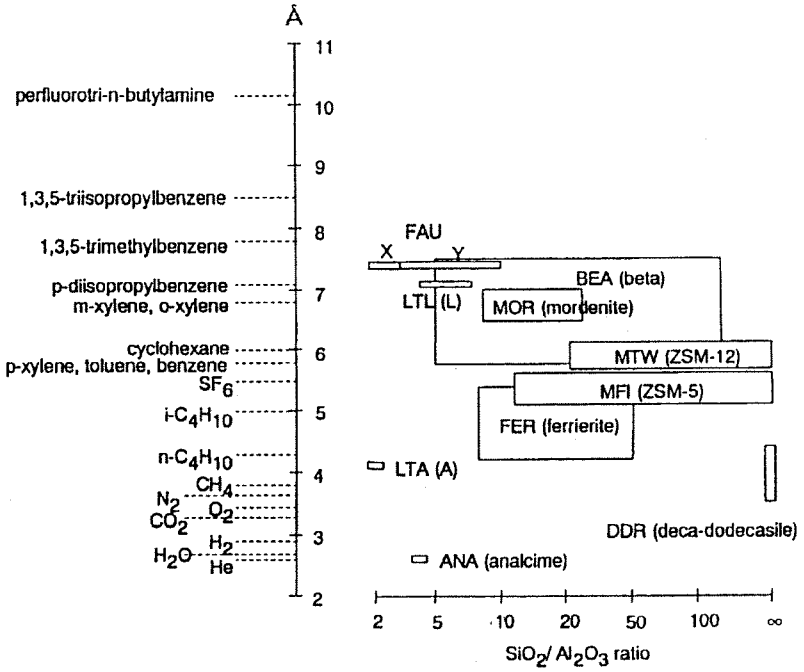

Fig. 1　Relation between micropore size of zeolite and molecular diameter.

料がすべて気体であるため，有機高分子膜との競合となる．本稿では，こうした炭化水素分離分野における無機分離膜の研究開発の現状を整理し，研究開発課題を概観したい．

2.　分離対象

石油系炭化水素分離における膜利用技術は，既往の石油精製プロセスに追加的に使用できプロセスの高効率化・省エネルギー化に貢献し得る技術と，既往のプロセスを置き換えるための技術に分類できる．前者としては，石油精製プロセスオフガスからの H_2 回収などが，後者としては直鎖炭化水素と分枝状炭化水素の分離，脂肪族炭化水素と芳香族炭化水素の分離，芳香族炭化水素混合物の分離，さらにはこれらの分離機能をインテグレートした蒸留塔（トッパー）の代替としての原油の直接分離などが考えられている．

個々の分離対象については後に詳しく述べるが，直鎖／分枝状炭化水素の分離には，n-/*iso* ブタン，C7-C8 炭化水素分離によるガソリンのオクタン価向上，セタン価向上用ディーゼル油精製などが考えられる．脂肪族／芳香族炭化水素の分離はガソリンからの脱ベンゼンなどに有用である．芳香族炭化水素分離としては，何と言っても C8 炭化水素混合物からのキシレンの異性体分離精製が大きなターゲットである．現在でも p- キシレンの製造プロセスは複雑であることから，C8 混合物から p- キシレンが一段で分離できればプロセス革新に直結すると期待されている．既往の研究では，単純な分離に関する研究が多いが，今後は無機膜と触媒反応とを組み合わせて，目的生成物を一段で合成する膜反応器の研究が盛んになるであろう．

3.　炭化水素分離用無機膜材料

炭化水素分離用無機膜材料としては，これまでシリカ系アモルファス多孔体，ゼオライト，炭素が検討されている．

シリカ膜は一般にゾルーゲル法によって合成され，シリカ粒子の１次粒子径およびその凝集過程の制御によって，細孔径が制御される．したがって，シリカ膜中に生成する細孔はこれら１次粒子間に生成する空隙となる．ゾルーゲルの科学の発展に伴って，細孔径の精密制御も可能となりつつ

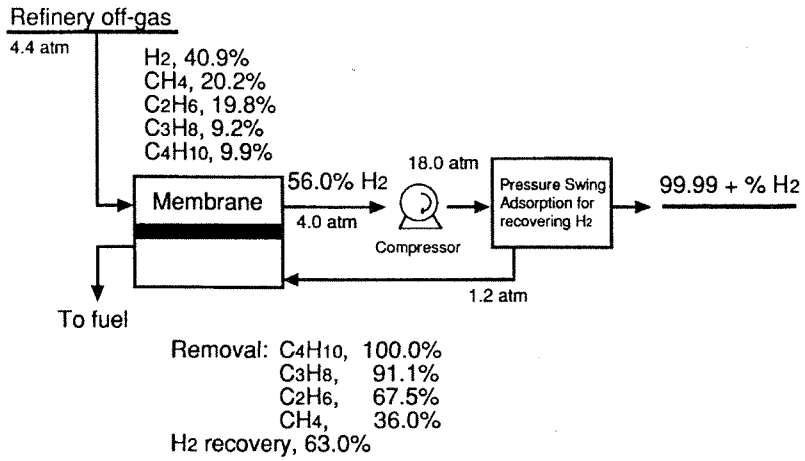

Fig. 2 Mass Balance of H_2 recovery process from refinery waste with SSF membrane.

ある.

ゼオライトは，均一で剛直な分子レベルの細孔をもつ結晶性アルミノシリケートであり，100 種類以上の異なる構造のゼオライトが人工的に合成されている．Fig. 1 には，代表的なゼオライトの細孔径と分子径の関係を示す．多くのゼオライトの細孔入り口は，酸素の 8, 10 あるいは 12 員環よりなっており，それらは石油系炭化水素の分子系とほぼ等しいことから，分子の大きさによって選択的な吸着（分子ふるい作用あるいは形状選択性）を示すことが知られている．また，ゼオライトは様々な SiO_2/Al_2O_3 比を得ることができるが，構造中の Al は陽イオン交換サイトとなり様々な金属イオンを固定することができる．このことから，交換カチオンの種類および交換率の制御によって，ゼオライト細孔と吸着分子間の相互作用の精密な制御が可能となると期待される．細孔径が結晶学的に均一であることのほか，比較的耐熱性が高いこと（MFI で 900°C程度），空気焼成による再生が期待されることが魅力である．その一方で，ゼオライト膜は通常多結晶体であり，ゼオライト結晶粒界に生じやすいピンホールの評価，制御が難しい．

炭素膜の多くは高分子樹脂薄膜を，高温で分解・炭化して得る．適当な原料の選択・炭化条件（ガス雰囲気，温度プロファイルなど）の精密な制御が均質なミクロ細孔を得るために重要である．炭素は酸化を受けやすいので，高温で使用する場合には注意が必要となろう．

4. 炭化水素分離に関する既往の研究

4.1 水素・メタン／低級炭化水素系

Air Products 社の Rao and Sircar およびその共同研究者ら[1~3]は，石油精製オフガス分離に対して有用な炭素膜 (Surface Selective Flow (SSF) Membrane, 細孔径 0.5–0.6 nm) を開発している．Fig. 2[1] にはプロセス内の物質収支を示す．分子径が H_2 より大きい炭化水素が選択的に透過し，H_2 が供給側に残留することが特長である．これにより水素圧の著しい低下が避けられ，H_2 を効率的に石油精製プロセスへとフィードバックすることができ，透過した炭化水素は燃料となる．回収したい物質が供給側に残留することは重要である．膜の透過側では圧力の著しい低下が避けられないため，透過側から原料へのフィードバックに際しては再度昇圧が必要で，その動力コストは全体のコストに対して無視できないことが多いようである．彼らはチューブ状に製膜した（内径 6 mm, 外形 9 mm, 長さ 106 cm）SSF 膜を O-リングでシールし，これをバンドルすることでモジュールを作成した．すでに，6 ヶ月に渡るフィールドテストも行われ，実験室規模の分離性能が長期間維持されることも確認されている[3]．

分離のメカニズムは，炭化水素と炭素膜細孔壁との強い相互作用により，炭化水素の膜内への優先的な吸着が起きるので，H_2 が排除されるためとされている．こうした優先的な吸着による透過選択性の発現は，炭素膜に限られているわけではない．Delft 工科大学（オランダ）の研究グループでは，アルミニウムを含まない MFI 型ゼオライト（シリカライト-I）膜を，水熱合成により多孔性焼結金属板上に製膜した．やはり，H_2/n-ブタン系[4]，CH_4/n-ブタン系[5] について，同様に n-ブタンが選択的に透過し，吸着力の弱い小分子が排除される結果が報告されている．CH_4/低級炭化水素系の分離のターゲットは，天然ガスの精製である．

4.2　アルケン／アルカン系

C2 あるいは C3 のアルカンとアルケンの分離は，石油化学工業に有用なアルケンの製造に有用である．Asaeda ら[6] は，ゾルゲル法により調製したシリカ膜を用いて，単成分系の透過実験より求めたプロピレン／プロパンの透過係数比が約 20（プロピレンの透過係数＝約 $10^{-3}m^3m^{-2}s^{-1}$, 35°C）となることを報告している．また，混合系では組成によるが，プロピレンの透過係数は余り変化しないが，プロパンの透過が阻害され分離係数は 2〜3 倍に向上する．これらの結果は，プロピレン／プロパンの有効分子径には大きな差がないことから，プロピレンのシリカ細孔内への優先的な吸着が起きることが理由とされている．Nair ら[7] は，プロピレン／プロパン系について選択性を示さないシリカ膜表面に，アルミナゾルを用いてアルミナ薄層によるコーティングを施すと，室温から 150°C 程度の範囲で分離係数 1.3〜2 となることを見出した．ある物質を優先的に吸着するための吸着層を表面修飾により導入することで，分離性能が発現したと考えられている．Suda and Haraya は，Kapton ポリイミド薄膜を 1,000°C, 真空中にて炭化すると，平均細孔径約 0.37 nm の炭素膜が得られることを報告した[8]．このままでは，細孔は炭化水素分離には小さすぎるが，この膜を 400°C にて 20 mmHg の水蒸気で穏和に酸化するとわずかに 0.03 nm 程度細孔径が広がる．このとき，プロピレン／プロパン系において，プロピレンの透過係数は 10 barrer 程度と比較的大きく，かつその透過係数比は 1,000 を超えた（プロピレンが選択的に透過）．分離機能の発現機構については，分子ふるい作用と吸着特性の差の両方が寄与したと推察されている．極めて精密な細孔径の制御が実現された例として大変興味深い．

一方，Kapteijn ら[9] は上記と同じ MFI 膜を用いると，シリカ膜とは逆にアルカンがアルケンより優先的に透過することを報告している．分離係数はたかだか 2 程度と高くないが興味深い．彼等は，膜に対する吸着力の違いではなく，拡散係数の濃度依存性を考慮した Maxwell-Stefan 則を用いて選択性の発現の原因を説明している．理論的取り扱いの詳細については当該文献を参照していただきたい[4, 10]．

4.3　直鎖／分枝状炭化水素系

直鎖／分枝状炭化水素の分離に関しては，ゼオライト膜による n-/*iso* ブタン系の分離に関する報告が多い．これは，Fig. 1 からわかるように，酸素 10 員環の細孔入り口をもつ MFI や FER 型のゼオライトは，ちょうど直鎖／分枝状炭化水素と同程度の細孔径をもつため，分子ふるい作用による分離が期待されている．

ゼオライト膜による n-/*iso* ブタン系の分離に関しては，一般には分子径の小さい n-ブタンが選択的に透過すると報告されている[5, 11-13] が，*iso* ブタンの方が選択的に透過したという報告[14] もある．Yan らの報告[12] では，単成分系の透過実験より求めた透過係数比が，室温では 18.4 (n- ブタン透過率＝7.5×10^{-9} mol・m^{-2}・s^{-1}・Pa^{-1}), 185°C では 31.1 (n-ブタン透過率＝5.85×10^{-8}mol・m^{-2}・s^{-1}・Pa^{-1}) と高い値が得られている．C5以上のアルカンについての検討例は多くないが，Meriaudeau ら[15] は多孔質ガラス上に製膜した MFI 型ゼオライト膜を用いて，n-ヘキサンと 2,2-ジメチルブタンの蒸気分離について検討し，60 °C において透過係数比 3.5 と，n-

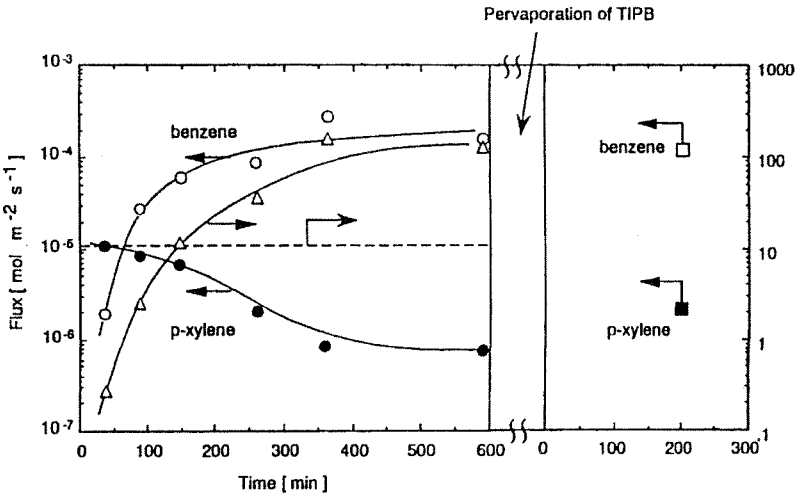

Fig. 3 Pervaporation results for a benzene/p-xylene mixture through a MORmembrane at 295 K.
○ : Flux of benzene, ●, ■ : flux of p-xylene and △ : separation factor.
Dashed line : theoretical separation factor (11.3) determined at the vapor-liquid equilibrium.

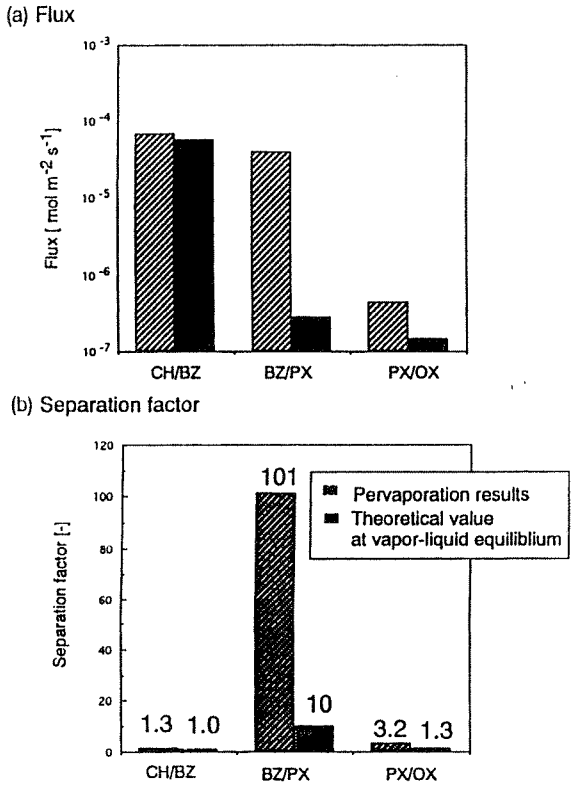

Fig. 4 Pervaporation results for mixtures using an FER membrane at 303 K.
Feed molar ratio : CH/BZ, 0.95 ; BZ/PX, 1.34 ; PX/OX, 0.96.

ヘキサンの方が大きな透過流束を与えることを報告している.

ゼオライト膜を用いたときの理想的な分離能に関しての研究には，単結晶を樹脂などに埋め込んだ単結晶膜が有効である[16, 17]. Lewisら[17]は，FER ゼオライトの単結晶をエポキシ樹脂に埋め込み，n-/*iso* ブタンの透過実験を行った．このときの透過係数比は，50°Cで 30 (n-ブタン透過率 $=2.5\times10^{-11}$ mol・m^{-2}・s^{-1}・Pa^{-1})，125°C で 152 (n-ブタン透過率 $=1.6\times10^{-10}$ mol・m^{-2}・s^{-1}・Pa^{-1}) と，酸素 10 員環よりなる細孔では，n-ブタンの透過が *iso* ブタンより速いことが明らかとなった．また，等モル混合系でも，110°C においてn-ブタンの透過流束が低下することなく，116という高い分離係数を示した. 以上の実験結果は，ゼオライト膜によって直鎖／分枝状炭化水素の分離が可能であることを証明した点で意義深い.

結晶学的に同じ構造をもつ多結晶ゼオライト膜（例えば MFI 型ゼオライト膜）で，小さな分離係数が種々報告されている[5, 11~13]ことは，ゼオライト結晶粒界に生成したピンホールを透過する流束の，全透過流束に対する寄与が大きいことを示していると思われる．ピンホールのキャラクタリゼーション法，および制御法の研究は稀で，今後の重要な研究課題である.

Table 1 Vapor permeation results through an MFI-type zeolitic membrane. Carrier gas : He

Temperature/°C	25	150	150	500	500
Water/vol %	0	0	7	0	7
	Permeation				
O_2(20 %)	yes	yes	yes	yes	yes
CH_4(1,000 ppm)	yes	yes	yes	yes	yes
C_3H_8(1,000 ppm)	yes	yes	yes	yes	yes
C_3H_6(1,000 ppm)	yes	yes	yes	yes	yes
Toluene (1,000 ppm)	yes	yes	yes	yes	no
p-xylene (500 ppm)	yes	-	-	-	-
m-xylene (500 ppm)	no	no	no	no	no

4. 4　芳香族炭化水素の分離

Matsukata らは，気相輸送法を用いてゼオライト膜の合成を試みている[18, 19]．水熱合成法では，多孔質支持体をアルミノシリケート溶液中に浸漬しゼオライト膜を成長させるが，気相輸送法ではあらかじめ乾燥アルミノシリケートゲルを製膜し，これを気相中で結晶化させる方法である．

FER[20]，MOR[21]（モルデナイト，酸素 12 員環よりなる大口径ゼオライト），MFI[22] ゼオライト膜が気相輸送法により合成されている．

Fig. 3には，MOR 膜を用いて行ったベンゼン／パラキシレン混合物の浸透気化分離試験の結果を示す[21]．この実験の前には，パラキシレン単成分の透過試験を行ったため，初期ではパラキシレンが選択的に透過したが，定常状態ではベンゼン／パラキシレンの分離係数は 160 を越えた．この MOR 膜は 1, 3, 5-トリイソプロピルベンゼン (TIPB, 有効分子径 0.85 nm) を通さない膜，すなわちの結晶粒界のピンホールがゼオライト結晶内のミクロ細孔と同程度に小さい膜であり，分離の発現はゼオライトのミクロ細孔に由来すると考えられる．TIPB の透過実験をいったん行った後で，再度分離試験を行っても透過分離性能には再現性がある．これは，TIPB が膜のピンホールに吸着して他の分子の透過を阻害することがないことを意味し，膜に TIPB を吸着できる大きさのピンホールが存在しないことと一致する．

Fig. 4には FER を用いて，シクロヘキサン (CH) ／ベンゼン (BZ)，ベンゼン／パラキシレン (PX)，パラキシレン／オルトキシレン (OX) の混合物の浸透気化分離の結果を示す[20]．BZ/PX 系では同様に 100 を越える高い分離係数が得られた．また，PX/OX 系においても分離係数 3.2 とパラキシレンが選択的に透過する．

Figs. 3, 4 の場合の分離機構については，ベンゼンとパラキシレンの有効分子径に差がないことと，ベンゼン濃度が極めて低い場合でもベンゼンの優先的な吸着が起きる（ベンゼン濃度 0.5% で分離係数約 700）ことから，分子ふるい作用よりは，吸着特性の違いが支配的と考えられている．一方，PX/OX 系では，オルトキシレンの分子径がパラキシレンより大きいことから，分子ふるい作用が寄与している可能性もある．

Table 1 には MFI 膜を用いて 500°C までの範囲で単成分系の蒸気透過実験を行った結果を示す．ただし，同伴ガスには He を用いている．500°C までの範囲で，メタキシレンが透過しないことがわかる．メタキシレンが MFI 型ゼオライトの細孔内にほとんど吸着できないためで，分子ふるい作用が発現した結果と考えられる．一方，トルエンは室温付近では膜を透過するにも関わらず，500°C では透過がみられなかった．透過選択性に関する温度の影響についてはさらに検討が必要である．

5.　おわりに

無機膜の開発は，ゼオライトに代表されるように，ミクロ細孔をもつ多孔体を膜化することにより，分子ふるい作用が発現することを期待して研究が始まったと思われる．しかし，炭化水素混合物の分離においては，膜に対する吸着力の差によって分離性能が発現する場合が多いようである．吸着力の違いによって分離性能が発現する場合には，単成分系の吸着・透過測定から混合系の分離性能を予測することは難しく，混合系における膜透過，吸着の実験的・理論的研究の充実が望まれる．無機膜の細孔，特に膜厚，粒界などの制御技術は開発途上であり，解決すべき課題は多い．

炭化水素分離の研究は欧米においても石油精製会社を始めとして開発研究が企業においても活発化しているようである．無機分離膜技術が実用化されるにあたっては，再現性ある膜合成技術の開発はもちろんのこと，高温シール法の開発，モジュール化による大面積化の実現，安価な支持体の開発など課題は多い．幸いにして我が国の多孔質セラミック支持体の合成技術は欧米に先んじており，高性能の無機膜開発にあたっての基盤は充分にあると思われる．我が国から世界に先駆けて，無機膜による炭化水素分離プロセスが実現されることを期待したい．

文　献

1) M. B. Rao and S. Sircar, *J. Membr. Sci.*, **85**, 253-264, 1993.
2) M. B. Rao and S. Sircar, *J. Membr. Sci.*, **110**, 109-118, 1996.
3) T. Naheiri, K. A. Ludwig, M. Anand, M. B. Rao and S. Sircar, *Sep. Sci. and Technol.*, **32**, 1589-1602, 1997.
4) F. Kapteijn, W.J.W. Bakker, J. van de Graaf, G. Zheng, *J. Poppe and J. A. Moulijn, Catal. Today*, **25**, 213-218, 1995.
5) E. D. Geus, H. van Bekkum, W. J. W. Bakker and J. A. Moulijn, *Microporous mater.*, **1**, 131-147, 1993
6) M. Asaeda, A. Yamamichi, M. Stoh and M. Kamakura, Proc. of Third Intern. Conf. on Inorg. Membr., 1994
7) B. N. Nair., K. Keizer, H. Verweij and A. J. Burgraaf, *Sep. Sci. Technol.*, **31**, 1907-1914, 1996
8) H. Suda and K. Haraya, Chem. Commun., 93-94 1997
9) F. Kapteijn, W. J.W. Bakker, G. Zheng, J. Poppe and J. A. Moulijn, *Chem.Eng. J.*, **57**, 145-153, 1995
10) J. M. van de Graaf, F. Kapteijn and J. A. Moulijn, "Structured Catalysts and Reactors," Ed. by A. Cybulski and J. A. Moulijn, Marcel Dekker, pp. 543-573, 1998
11) W. J. W. Bakker, G. Zheng, F. Kapteijn, M. Makkee and J. A. Moulijn, "Precision Process Technology," Ed. by M. P. C. Weijenen and A. A. H. Drinkenburg, Kluwer, Dordrecht, pp.425-436, 1993
12) Kusakabe, A. Murata, T. Kuroda and S. Morooka, *J. Membr. Sci.*, **116**, 39-46, 1996.
13) Y. Yan, M. E. Davis and G. R. Gavalas, *Ind. Eng. Chem. Res.*, **34**, 1652-1661 (1995)
14) M.D. Jia, B. Chen, R.D. Noble, J. L. Falconer, *J. Membr. Sci.*, **90**, 1-10, 1994
15) P. Meriaudeau, A. Thangaraj and C. Naccache, *Microporous mater.*, **4**, 213-219, 1995
16) M. S. Sun, O. Talu and D. B. Shah, *AIChE J.*, **42**, 3001-3007, 1996
17) J. E. Lewis. Jr., G. R. Gavalas and M. E. Davis, *AIChE J.*, **43**, 83-89 1997
18) W. Xu, J. Dong, J. Li, J. Li and F. Wu, J. Chem. Soc., Chem. Commun., 755-756 1990, M. H. Kim, H. X. Li. and M.E. Davis, *Microporous Mater.*, **1**, 219-225, 1993, M. Matsukata, N. Nishiyama and K. Ueyama, *Microporous Mater.*, **7**, 109-117, 1996
19) M. Matsukata and E. Kikuchi, *Bull. Chem. Soc. Jpn.*, **70**, 2341-2356, 1997
20) N. Nishiyama, K. Ueyama and M. Matsukata, *Microporous Mater.*, **7**, 299-308, 1996
21) N. Nishiyama, K. Ueyama and M. Matsukata, *Stud. Surf. Sci. Catal.*, **105**, 2195-2202, 1997, *Microporous Mater.*, in press
22) 松方正彦，西山憲和，上山惟一，高橋　章，高橋知典，化学工学会第63年会要旨集，1998

（受付　1998年1月28日　掲載決定2月14日）

R/D フィロソフィーシリーズ (2)

新しいゼオライト合成法とその展開*

松　方　正　彦

筆者が早稲田大学において学位を取得後，平成元年から助手としてお世話になったのは成蹊大学工学部の小島紀徳助教授（現教授）の研究室であった。小島先生は，今ではすっかり環境問題，とりわけ地球温暖化問題の専門家であるが，当時は当該分野に乗り出そうと準備を進められている時期であった。さて，当時小島研究室の柱の一つは液体膜であり，筆者も学生時代に研究室（早稲田大学理工学部応用化学科燃料化学研究室）の同僚が無電解メッキによるPd薄膜合成に関する研究を行っていたことから，まんざら膜になじみがないわけでもなかった。平成元年当時は，ちょうど反応分離の概念が浸透し，世界的にも研究が広がりを見せ始めた頃であり，関心も高かった。

さて，液体膜の研究は当時既にずいぶんと進んでいたし，小島先生のご専門でもあったことから，筆者はなんとか自分なりの特色が出せる研究を始められないかと，もんもんとテーマを探していた。そのとき出会った論文が，W. Xu, J. Dong, J. Li, J. Li, and F. Wu : *J. Chem. Soc., Chem. Commun.*, 755 (1990) である。そこには，アルミノシリケート水性ゲルを乾燥してドライゲルとし，これを180℃の圧力容器（オートクレーブ）中，水，エチレンジアミン（EDA），トリエチルアミン（Et_3N）の混合蒸気で処理すると代表的ゼオライトであるZSM-5が生成したことが報告されていた。

ゼオライトは，狭義にはミクロ細孔をもつ結晶性アルミノシリケートの総称であり，そのミクロ細孔は結晶の骨格構造に由来して，均一で剛直である。最近では，アルミニウムを含まない純シリカ系から，珪素，アルミニウム以外の金属イオンを骨格に含む酸化物にいたるまで，ミクロ細孔をもつ酸化物結晶の総称として用いられることが多い。ゼオライトのミクロ細孔は0.3～0.7 nm程度と，炭化水素分子と同程度のサイズをもつため，いわゆる「分子ふるい」機能を発揮し，触媒・吸着剤として多くの研究者・技術者の興味を引いてきた。

ゼオライトは天然にも多く産出し，工業的にも利用されてきたが，ゼオライト研究の分野により一層の発展をもたらしたのは，Barrer and Dennyによる水熱合成による人工ゼオライト合成の成功[2]であった。以来約40年に渡って，ゼオライト合成研究はほとんど水熱合成を用いて行われてきた。ゼオライトの水熱合成における水の果たす役割について疑問をもち，水はゼオライト合成における必須のメディアではないことを初めて示したのは，Bibby and Daleである。1985年に発表されたこの論文には，エチレングリコール溶媒中でシリカソーダライト（酸素6員環による細孔入り口をもつ）が生成することが報告された。その後，有機溶媒をメディアとするゼオライト合成は数多く報告されるようになり，工業的に有用なフェリエライトやZSM-5（いずれも酸素10員環の細孔入り口をもつ）の合成も報告されるようになった[4]。

こうした研究の動向の中で，Xuら[1]は溶媒を用いることなく，ガス中で結晶化が起きないかと考えたものと思われる。この論文に出会ったときの感覚を今でもはっきりと覚えている。研究室の自分の机で，この論文のアブストラクトを読んだ瞬間に，この方法を使えばゼオライトを薄膜化できるし，ゼオライト膜はおそらく分子を選択的に分ける無機膜になると直感し，興奮した。その後，すぐにゼオライト膜に関する文献・特許の調査をしたところ，我が国では1980年代初頭より，いくつか特許が提出されていたものの，学術的な研究はほとんどなされていないことがわかったので，ゼオライト膜を研究テーマとしたいという気持ちが強くなっていった。

その後すぐに，大阪大学基礎工学部化学工学科の上山惟一先生の研究室にお世話になることになり，本格的にゼオライト膜の研究を進める機会を得た。

まず，はじめに着手したのは，Xuらの合成法の再現性を確認することであったが，幸いなことに彼らの方法は再現が容易な優れた方法であった。合成条件などを若干検討し，Microporous Materials誌にすぐに報告した[5]。驚いたのは，

Development and Application of New Synthetic Method of Zeolites
Masahiko Matsukata（正会員）
1989年3月　早稲田大学理工学研究科博士後期課程修了　工学博士
同　年4月　成蹊大学工学部助手
1992年1月　大阪大学基礎工学部助手
助教授を経て
1997年4月　早稲田大学理工学部助教授
現在に至る
連絡先；〒169-8555　新宿区大久保3-4-1
早稲田大学理工学部応用化学科

* 1999年5月17日受理

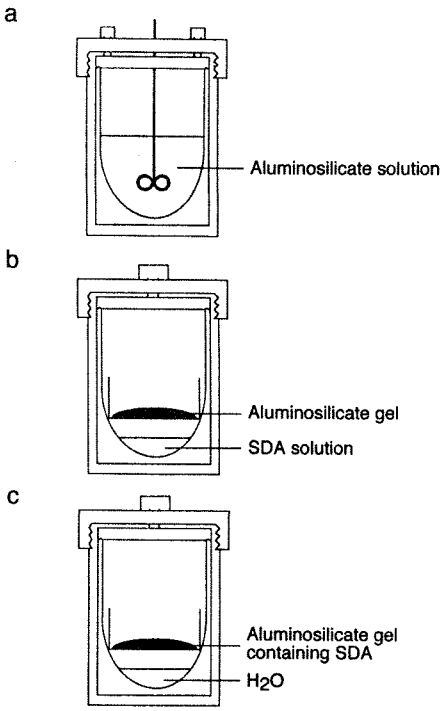

図 1 各種のゼオライト合成法
(a) 水熱合成法，(b) 気相輸送法，(c) ドライゲルコンバージョン法

米国のCaltechのグループが，全く同じ号にほとんど同様の報告をしていた[6]ことであり，研究はやはり一刻を争うのだということを，まさに実感させられた。この合成方法はVapor-phase Transport (VPT) 法と命名され[6]，我々はこれを気相輸送法と和訳して用いている。**図1**には，既往の方法である水熱合成法と，気相輸送法を比較してある。

さて，粉末合成法としての気相輸送法が有効であることがわかったので，多孔質アルミナディスク上に乾燥ゲルを製膜し，これを気相輸送法にて結晶化させる方法の研究をさっそく始めた。幸いにして，うまく製膜する手法を見いだすことができ，それ以来ゼオライト膜の研究を行っている[7]。最近では，ゼオライト膜をきっかけとして無機膜全般の研究を行うようになった。

さて，ゼオライトの結晶化に当たっては，EDAやEt_3Nのような，気化できる結晶化剤ばかりでなく，4級アンモニウム塩のように気化が難しい物質を結晶化剤とすることが多い。代表的な合成ゼオライトであるZSM-5も，テトラプロピルアンモニウムカチオンを用いる研究例が多い。そこで，我々は，ゲルを調製する際にあらかじめ4級アンモニウム塩を混合しておき，これを乾燥後，水蒸気中で処理するとゼオライトが得られるのではないかと考えた（図1c)。実際，この合成手法によって各種のゼオライトを合成することができ，たとえばテトラエチルアンモニウム(TEA) カチオンを用いると，ベータ型ゼオライトが得られた（**図2a**)。そこで我々はこの合成方法をドライゲルコンバージョン（DGC）法と名付けた。詳細については総説を参照していただきたいが，本合成法の工学的特徴としては，

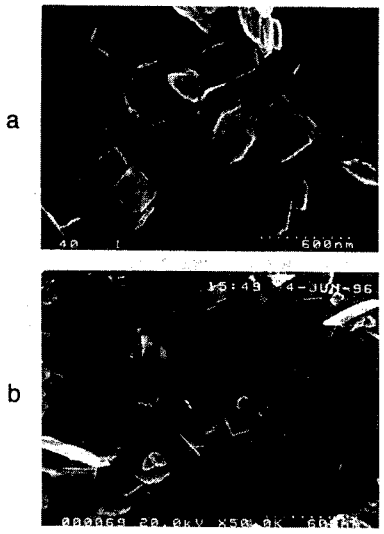

図 2 ドライゲルコンバージョン法によって合成されたゼオライト
(a) ベータ，酸素12員環よりなる3次元細孔をもつゼオライト．
(b) OU-1，ベータの相変態によって得られた新規なゼオライト．酸素12員環よりなる1次元細孔をもつ[8]

(1) 高価な有機結晶化剤の使用量の削減，(2) 水熱合成と比較して結晶化速度の向上，(3) 結晶化装置の小型化，(4) 廃水処理費用の低減，(5) 結晶化装置の連続化，などの可能性が考えられる。また，水熱合成法では合成が難しい組成，あるいは新規なゼオライトの合成も可能（図2b）であり，DGC法は水熱合成法の代替ではなく，新規な合成法として大きな可能性をもっていると考えている。DGC法によるゼオライトベータの合成の成功をきっかけとして，その後我々は種々の新規な組成・構造をもつゼオライトの合成，ゼオライトの生成機構，ゼオライトの触媒作用・吸着特性に関する研究へと展開してきた[8]。

こうして振り返ってみると，筆者の研究は，一つ見つけるとより新しい分野へとアメーバ状に広がってきたように思われる。それらを支えているのは好奇心と知識欲のはずであり，ゼオライト研究は筆者にとってそれらの大切さを改めて教えてくれた。また，研究というのは論文の発表に至るまで，スピードが要求されることも痛切に感じてきた。今後とも，新しい方法によって合成した，新しいマテリアルの工学的利用を夢見て，研究開発に邁進したい。

最後になりましたが，本稿の執筆を通じて，自らの研究の進め方の経緯を反芻と反省をする貴重な機会を与えて頂いたことに，感謝を申し上げます。

引用文献

1) W. Xu, J. Dong, J. Li, J. Li and F. Wu : *J. Chem. Soc., Chem. Commun.*, 755 (1990)
2) R. M. Barrer and P. J. Denny : *J. Chem. Soc.*, 983 (1961)
3) D. M. Bibby and M. P. Dale : *Nature*, **317**, 157 (1985)
4) Q. Huo, S. Feng and R. Xu : *J. Chem. Soc., Chem,. Commun.*, 1486 (1989) ; W. Xu, J. Li, W. Li, H. Zhang and B. Liang : *Zeolites*, **9**, 468 (1989)
5) M. Matsukata, N. Nishiyama and K. Ueyama : *Microporous Mater.*, **1**, 219 (1993)
6) M. H. Kim, H.X. Li and M. E. Davis : *Microporous Mater.*, **1**, 191 (1993)
7) M. Matsukata and E. Kikuchi : *Bull. Chem. Soc. Jpn.*, **70**, 2341 (1997)
8) M. Matsukata, M. Ogura, T. Osaki, P. R. H. Prasad Rao, M. Nomura and E. Kikuchi : *Topics in Catalysis*, in press

●解説

無機膜の最近の開発動向

早稲田大学　松方　正彦*，野村　幹弘**

これまで工業化されてきた膜材料は有機高分子膜がほとんどであったが，1980年代に入ってからは濾過，ガス分離などを対象として，無機膜を研究開発の対象として見直す機運が徐々に高まってきた．1980年代では，金属Pdが水素を溶解する機能があることを利用して，Pd膜を用いた水素分離に関する研究[1]が無機膜研究の主体であったが，1991年にはH_2/N_2の理想分離係数が1000を超えるアモルファスシリカ膜[2]が報告されるに至り，無機膜研究全体が大きな盛り上がりを見せるようになった．以後，無機材料の耐熱性・耐圧性・耐有機溶剤性あるいは材料自身の環境負荷の小さいことを利用した，有機膜では実現できなかった分野への応用が志向されている．

ここでは，最近の無機膜の研究開発を概観し，今後の展望を考えてみることとしたい．ただし，紙数の制限もあり細孔径2nm以上の限外濾過，あるいは精密濾過といった，いわゆる濾過膜は取り上げていないので，ご了承いただきたい．

*まつかた　まさひこ：理工学部応用化学科　助教授
**のむら　みきひろ：同学科　助手
〒169-8555　東京都新宿区大久保3-4-1
☎03-5286-3850

無機膜素材と用途

表1には，既報の無機膜による分離対象と，適用が検討されている膜素材について，主なものをまとめた．表2には，これまで検討されてきた無機膜の製法を示す．

両表中の膜素材は，無孔質材料（緻密膜）と多孔質材料に分類できる．無孔質材料としては，パラジウムを代表とする金属およびペロブスカイトを代表とする酸素欠損型複合酸化物があげられる．一方，多孔質材料としては，シリカなどのアモルファス酸化物，ゼオライトなどのミクロポーラス結晶，炭素などが検討されている．

分離対象は幅広いが，波及効果の大きさを考えると，エネルギー・環境分野，石油精製・石油化学分野における利用が実用化されることが望まれる．また，表中では環境分野における用途が欠け

表1　無機膜の応用分野の代表例

分離対象	膜素材	用途
高純度水素の回収	パラジウム，シリカ	半導体，燃料電池
水素／一酸化炭素／二酸化炭素	パラジウム，シリカ	水蒸気改質反応による合成ガス製造
水素／炭化水素	パラジウム，シリカ，ゼオライト	石油精製オフガスからの水素製造
水素／窒素／アルゴン・メタン	パラジウム，シリカ	アンモニア合成
二酸化炭素／窒素	ゼオライト，カーボン	燃焼排ガス
窒素／酸素	酸素欠損型複合酸化物（ペロブスカイトなど）	空気分離
メタン／二酸化炭素・硫化水素・窒素・炭化水素	ゼオライト，カーボン	天然ガス分離
オレフィン／パラフィン系炭化水素	ゼオライト，カーボン	石油化学原料
直鎖炭化水素／分枝炭化水素	ゼオライト，カーボン	石油化学原料
キシレン異性体	ゼオライト，カーボン	石油化学原料
空気／炭化水素	ゼオライト，カーボン	VOC（ガソリン蒸気など）回収

表2　代表的な無機膜の製膜方法

構造	製膜方法	材質	細孔径
無孔質	無電解めっき	パラジウム	—
	CVD	パラジウム	—
	焼結	複合酸化物（ペロブスカイトなど）	—
多孔質	焼結	金属	0.1～100 μm
		酸化物	0.1～100 μm
	相分離	ガラス	4nm～5 μm
	陽極酸化	アルミナ	10～250nm
	ゾル-ゲル	アルミナ	4～100nm
		シリカ	4～100nm
		ジルコニア	4～100nm
	CVD	シリカ	＞0.3nm
		白金	—
	熱分解	カーボン	＜1nm
	水熱合成	ゼオライト	＜1nm
	ドライゲルコンバージョン	ゼオライト	＜1nm

ているが，有害有機化合物除去など環境保全分野における利用も魅力的な適用対象となろう．

無機膜材料の研究の動向

図1には，1990年代に入ってからの無機膜研究に関する報告数の検索結果をまとめた．報告には，論文，特許，会議報告などが含まれている．調査対象としては，シリカ，ゼオライト，金属パラジウム，炭素，酸素透過性複合酸化物といった，無機膜を代表する分野を取り上げた．

全体として1990年代に入って報告数が増加しており，近年の無機膜研究の活況を裏付けている．特にアモルファスシリカとゼオライトは1990年代後半の報告数の伸びが大きく，分野の広がりが伺える結果となった．

報告の数としては，シリカ膜が圧倒的に多いが，これは多孔質シリカガラス（例えばコーニング社のバイコールガラス）に関する研究とアモルファスシリカ膜の両者が含まれているためである．シリケートの化学に関する知見がこれまでに十分蓄積されていたことにより，多くの研究者が取り付きやすい分野であることが，報告が圧倒的に多く，かつ近年も伸びている一因であろう．細孔径は，0.3nm程度から数nmにわたって制御が可能であり，製法もゾル-ゲル法[3]，気相化学析出（CVD）法[4]などが活発に研究されている．

一方，アモルファス物質である必然として，シリカ膜の細孔径は分布をもつため，より均一なミクロ細孔をもつ膜材料としてゼオライトが登場した[5),6)]．ゼオライトは，均一で剛直なミクロ細孔をもつアルミノシリケート系の結晶の総称である．細孔径は0.3～0.9nmであり，表1の対象となる分子とほぼ同じサイズである．固体酸でもあるので，膜触媒としても期待できる．研究開発対象としては，ZSM-5（細孔径0.56×0.53nm），A型（細孔径0.4nm），Y型（細孔径0.74nm）といった，触媒，吸着剤として従来利用されてきたゼオライトが選ばれることが多い．

ゼオライトは，膜に限らず一般に水熱合成（熱水中での原料成分の溶解—再析出を用いる方法）によって合成されるが，筆者らはドライゲルコンバージョン法という新規な方法を提案している[6),7),8)]．この方法は，あらかじめ多孔質の支持体上に水性ゲルを製膜・乾燥した後，乾燥ゲル層を適当

図1　1990年代における無機膜研究の文献報告数の推移

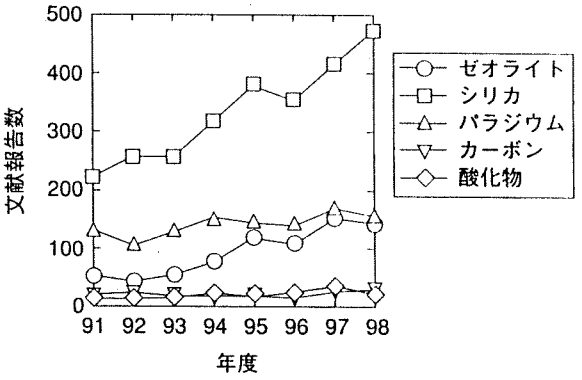

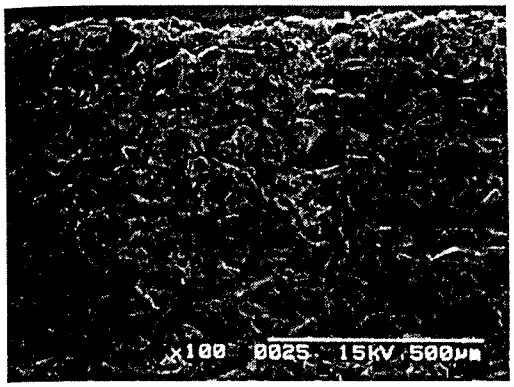

(a) 平均細孔径10μm

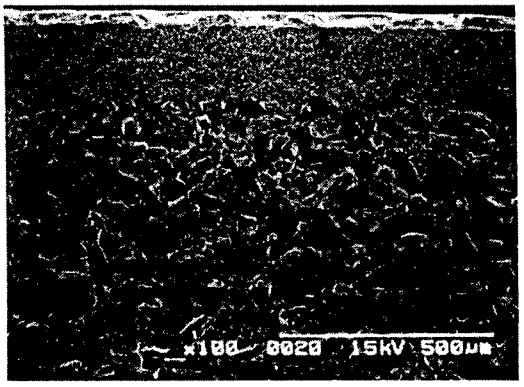

(b) 平均細孔径0.1μm

写真1　多孔質アルミナ支持体断面の電子顕微鏡像

な蒸気（通常，水蒸気を含む）中で結晶化する方法である．水熱合成が液相中から支持体上にゼオライトを析出させる手法であるのに対し，製膜の原理を異にする手法である．ゼオライトは，1990年代初頭から炭化水素の異性体分離用分子ふるい膜材料として期待されてきた一方，最近ではアルコール／水系の分離などを対象として，実用化例（A型ゼオライト膜）[9]も現れている．後者の場合には，ゼオライトの分子ふるい特性ではなく，A型ゼオライトのきわめて強い親水性を生かしている．

炭素膜は報告数こそ少ないが，有機高分子膜を炭化することにより得られるので，製膜性がよく，今後研究は増えると考えられる．石油精製オフガスからの水素回収用としてすでにベンチテストが行われている例もある．この膜は大変興味深く，石油精製オフガス中のC_1-C_4炭化水素を選択的に透過させ，最も分子径の小さい水素が供給（高圧）側に残る．このため，水素のコンプレッサー用動力が低減できるとされている．

金属膜の研究は，パラジウムによる水素透過膜に関する研究が中心である．金属パラジウムは選択的に水素を溶解する性質があることから，高純度水素製造に用いられている．また，天然ガスの水蒸気改質反応による水素製造や，エチルベンゼンの脱水素によるスチレン製造など，水素を反応系外に引き抜くことにより，熱力学的平衡値をシフトさせることができる反応系に対して反応分離膜として盛んに検討されてきた[1]．論文数はここ10年ほど横這いであるが，これは，他の無機膜と異なりパラジウム膜は古くから検討されてきたことが理由であり，今後とも水素の選択的透過を利用した反応分離用無機膜として主たる地位を占めるものと思われる．パラジウム膜の製造には，無電解めっき法[10]がしばしば用いられるが，CVDによる合成例も増えてきた．白金，ロジウムなど他の白金族の元素も，CVD法で製膜すると水素が選択的に透過する[11]ことが最近報告され，今後の展開が注目される．

ペロブスカイトを代表とする酸素欠損型複合酸化物を製膜すると，数百℃以上の高温において膜両側の酸素分圧差を駆動力として，酸素を選択的に透過させる．この性質を利用して，高温で空気から酸素を分離し，これを利用してメタンの酸素による部分酸化によって合成ガスを製造し，さらに合成ガスから灯・軽油，メタノール，ジメチルエーテルなどを製造する方法（Gas to Liquid：GTL）が欧米で注目を集めている．

報告数は他の膜材料と比較して多くないが，今後，わが国においても大きな発展が期待できる分野と思われる．

今後の課題

無機膜が幅広く実用化されるに当たっては，科学的にも技術的にもいくつかのブレークスルーが必要である．

まずは透過流束・分離性能の向上が必須である．これまで報告された無機膜には，透過流束・分離性能ともに満足すべき報告は残念ながら少ない．透過流束の向上には薄膜化以外になく，無孔質膜・多孔質膜ともに，多孔質の支持体上にごく薄

写真2　シリカライト膜の電子顕微鏡像
原料ゲル：0.1TPrABr-0.1 NaOH-SiO_2-80H_2O
合成条件：170℃，48時間

(a) 表面

(b) 断面

く（多くの場合，サブミクロン程度の厚みに），かつ再現性よく，緻密に（ピンホールがなく）製膜する手法が必要であろう．

写真1に，平均細孔径が10 μmと0.1 μmの多孔質アルミナ支持体断面の電子顕微鏡像を示す．細孔径10 μmの膜は対称膜であり，細孔径0.1 μmの膜は3層構造をもった非対称膜である．構成粒子の大きさや空隙の形状がまったく異なることがよく分かる．

写真2には，水熱合成法によって製膜したゼオライト（シリカライト）膜の表面および断面像[12]を示す．容易に想像できるように，ゼオライト結晶をいかに緻密に生成させるかが，膜としての機能を支配することになる．ゼオライト結晶生成を制御するには支持体の性状がきわめて重要であると想像される．

このことはゼオライト膜に限らず，すべての無機膜に対して共通であり，したがって製膜手法自身のブラッシュアップはもちろんのこと，支持体の形状・物性も膜性能の制御に重要と思われる．アルミナ支持体以外の一般的な支持体としては，多孔質焼結金属があげられるが，それらを含めて現在の無機膜研究は，支持体をメーカーから入手してそのまま使用することが多く，それぞれの製膜対象に応じて最適の支持体を設計することはほとんど行われていない．スケールアップを想定したモジュール化を含め，支持体開発と製膜技術がより一体となった研究開発体制の充実が望まれる．また，モジュールの強度計算，システム設計，高温シール技術の開発など，エンジニアリングサイドに立った検討がより真剣になされるべきと言えよう．

☆　　☆

無機膜は研究が活発に行われるようになってからわずか10年あまりの古くて新しい分野であり，新しい産業の創出にふさわしい分野の幅広さをもっている．今後の産官学一体となった研究開発の大きな発展に期待するとともに，筆者らも渾身の努力を傾注して，分野の発展に貢献したい．

参考文献

1）E. Kikuchi：Cattech, 1, 67 (1997)
2）M. Tsapatsis, S. Kim, S. W. Nam and G. Gavalas：Ind. Eng. Chem. Res., 30, 2152 (1991)
3）例えば，R. J. R. Uhlhorn, K. Keizer and A. J. Burggraaf：J. Membr. Sci., 66, 271 (1992)
4）例えば，G. R. Gavalas, C. E. Megiris and W. Nam：Chem. Eng. Sci., 44, 1829 (1989)
5）T. Sano, Y. Kiyozumi, M. Kawamura, F. Mizukami, H. Takaya, T. Mouri, W.Inaoka, Y. Toida, M. Watanabe and K. Toyoda：Zeolites., 11, 842 (1991)
6）M. Matsukata and E. Kikuchi：Bull. Chem. Soc. Jpn., 40, 2341 (1997)
7）M. Matsukata, N. Nishiyama and K. Ueyama：J. Chem Soc. Chem. Commun., 339 (1994)
8）N. Nishiyama, K. Ueyama, M. Matsukata：Microporous Mater., 7 (6), 299 (1996)
9）M. Kondo, Y. Matsuo, Y. Morigami and J. Abe：膜, 23 (2), 95 (1998)
10）S. Uemiya, N. Sato, H. Ando, Y. Kube, T. Matsuda and E. Kikuchi：J.Membr. Sci., 56, 303 (1991)
11）S. Uemiya, M. Kajiwara and T. Kojima：AIChE J., 43 (11A), 2715 (1997)
12）N. Nomura, T. Yamaguchi and S. Nakao：Ind. Eng. Chem. Res. 36 (1997) 4217

Microscopic Structure of a Ferrierite Membrane Synthesized by a Vapor-phase Transport Technique

Masahiko Matsukata, Norikazu Nishiyama, Takaaki Matsufuji,
and Korekazu Ueyama,
Department of Chemical Engineering, Osaka University,
Machikaneyama, Toyonaka, Osaka 560, Japan

Introduction: Zeolites are strong candidates for inorganic membrane materials which enable high temperature operation with separation at a molecular level. Most of the studies on the synthesis of zeolitic membranes have so far adopted conventional hydrothermal synthetic method. On the other hand, we have developed a new method for zeolitic membrane synthesis [1,2], the method of which adopted a vapor-phase transport method [3-5]. Pinhole-free ferrierite (FER) and mordenite (MOR) membranes have been successfully prepared on a porous alpha-alumina support[1,2]. In this study, we focused on the analysis of microscopic structure of a FER membrane.

Experimental: Aluminosilicate gel with SiO_2/Al_2O_3 ratio = 25 was prepared by mixing colloidal silica (Nissan Chemical Co., Ltd.), $Al_2(SO_4)_3$ and NaOH. A porous alpha-alumina plate (NGK Co., Ltd.) with an average pore diameter of 0.1 μm was dipped in the parent gel. After 1 day, the plate was taken out of the gel, and dried at room temperature. The plate was placed at the middle of the autoclave where a mixture of ethylenediamine, triethylamine and water was poured at the bottom. Crystallization was performed at 453 K for 1-4 days at autogeneous pressure. The structure of the autoclave and preparation procedure for a FER membrane were previously described [2]. Characterization of the product was mainly carried out with XRD and FE-SEM.

Results and Discussion: After 4 days of crystallization by the vapor-phase transport method, no amorphous phase remained. SEM observations showed that flake-like FER crystals were formed on the surface of the alumina support and that the parent gel penetrated into the pores of the support in the course of preparation. The top FER layer cannot be pinhole-free because there are numerous voids among FER crystals. We scraped the top layer with sand paper. After confirming by SEM that all FER crystals were removed, XRD measurements were carried out. The XRD results showed that randomly-oriented FER formed in the pores of alumina support with no amorphous phase.

Figure 1 showed the cross-sectional views of (a) the porous alumina support and

(b) the FER membrane. Taking the XRD results into consideration, we conclude that the pores of the alumina support were filled with FER crystals. It should be noted that the continuous layer observed for the FER membrane consisted of tiny particles with diameters of several tens nanometer. Figure 1(c) shows an FE-SEM image for the edge of a flake-like FER crystal synthesized by the vapor-phase transport, clearly indicating that this FER crystal are composed of needle-shaped nano-units with a diameter of 20 - 40 nm. We thus believe that nano-particles observed in the membrane are FER nanocrystals. In conclusion, a FER nanocrystals-porous alumina composite layer is formed and this layer can be pinhole-free.

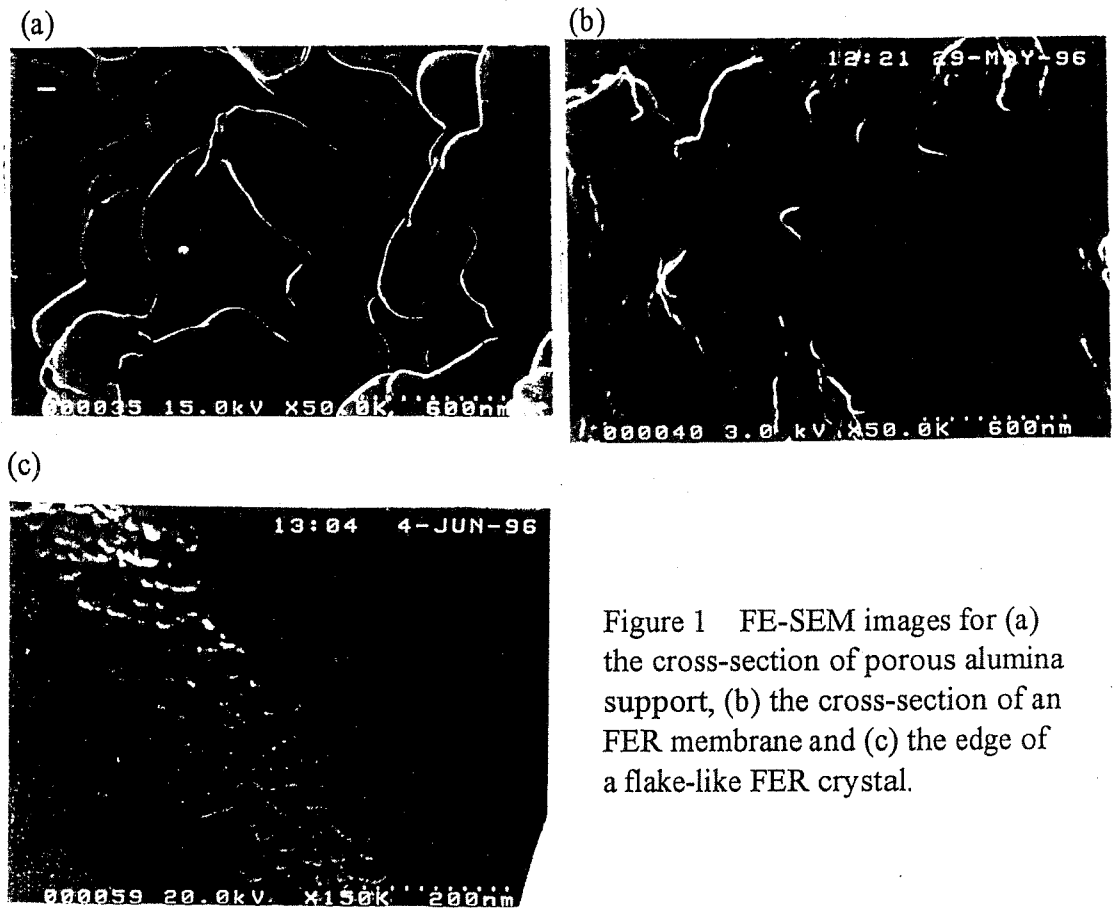

Figure 1 FE-SEM images for (a) the cross-section of porous alumina support, (b) the cross-section of an FER membrane and (c) the edge of a flake-like FER crystal.

References:

1. M. Matsukata, N. Nishiyama and K. Ueyama, Stud. Surf. Sci. Catal., 84 (1994) 1183, J. Chem. Soc., Chem. Commun., (1995) 1967, Microporous Mater., in press.
2. N. Nishiyama, K. Ueyama and M. Matsukata, Stud. Surf. Sci. Catal., in press.
3. W. Xu, J. Dong, J. Li and F. Wu, J. Chem. Soc. Chem. Commun., (1990) 755.
4. M.H. Kim, H.X. Li and M. E. Davis, Microporous Mater., 1 (1993) 191.
5. M. Matsukata, N. Nishiyama and K. Ueyama, *ibid.*, 1 (1993) 219, 7(1996) 109.

SELECTIVE PERMEATION OF HYDROCARBONS THROUGH A ZEOLITE MEMBRANE

Akira Takahashi, Tomonori Takahashi, Korekazu Ueyama*,
Norikazu Nishiyama*, and Masahiko Matsukata**

NGK Insulators, Ltd., Mizuho, Nagoya 467, Japan
*Department of Chemical Engineering, Osaka University, Toyonaka 560, Japan
**Department of Applied Chemistry, Waseda University, Tokyo 169, Japan

Introduction

Gas separation process using membrane is beneficial for various fields such as petrochemical and gas industries. Development of pinhole-free zeolite membrane is one of the most active research areas,[1,2] because it is suggested that molecules of different sizes can be separated with a zeolite membrane by molecular sieving effect. Recently unique preparation method called "vapor phase transport method" was developed to make zeolite membranes by Matsukata et al.[3] In this method, an amorphous dry gel coated on the substrate is converted to a zeolite membrane in the atmosphere containing water vapor at elevated temperature. Compared with the conventional hydrothermal method, this method would be suitable to prepare zeolite membranes on the inner surface of tubular substrate, when an amorphous gel is uniformly coated on the surface of the substrate.

In this paper, an MFI type and an MFI/FER type zeolite membranes were prepared by the vapor phase transport method on an α-Al_2O_3 porous substrate and their permeation properties of various hydrocarbons were investigated.

Experimental

Zeolite membranes were prepared as follows. A parent silicate gel suspension was prepared by mixing colloidal silica (Nissan Chemical Co., Ltd.) and a NaOH aqueous solution. In the case of aluminosilicate gel suspension, aluminum sulfate anhydride, $Al_2(SO_4)_3$ (Wako Pure Chem. Ind. Co., Ltd.) was added into the mixture. The SiO_2/Al_2O_3 ratio of the aluminosilicate gel mixture was 25/1 in molar ratio. Then the porous α-Al_2O_3 substrate (ϕ 13mm x 3mm circular plate, NGK Insulators, Ltd.) was dipped into the silicate or aluminosilicate gel suspension at 303 K for 1 day, and dried to obtain the substrate coated with the gel. The substrate had an asymmetric membrane structure, and the mean pore size of the top layer was 0.1 μ m. The coated substrate was treated in vapor of triethyleamine (Et_3N), ethylenediamine (EDA), and water at autogeneous pressure at 453 K for 4 days to crystallize zeolite at the surface of the substrate. The treated membranes were calcined in air at 773 K for 4 hrs. Crystal phases were characterized by XRD and morphology of membranes on the surface of the Al_2O_3 substrate was observed by a scanning electron microscope.

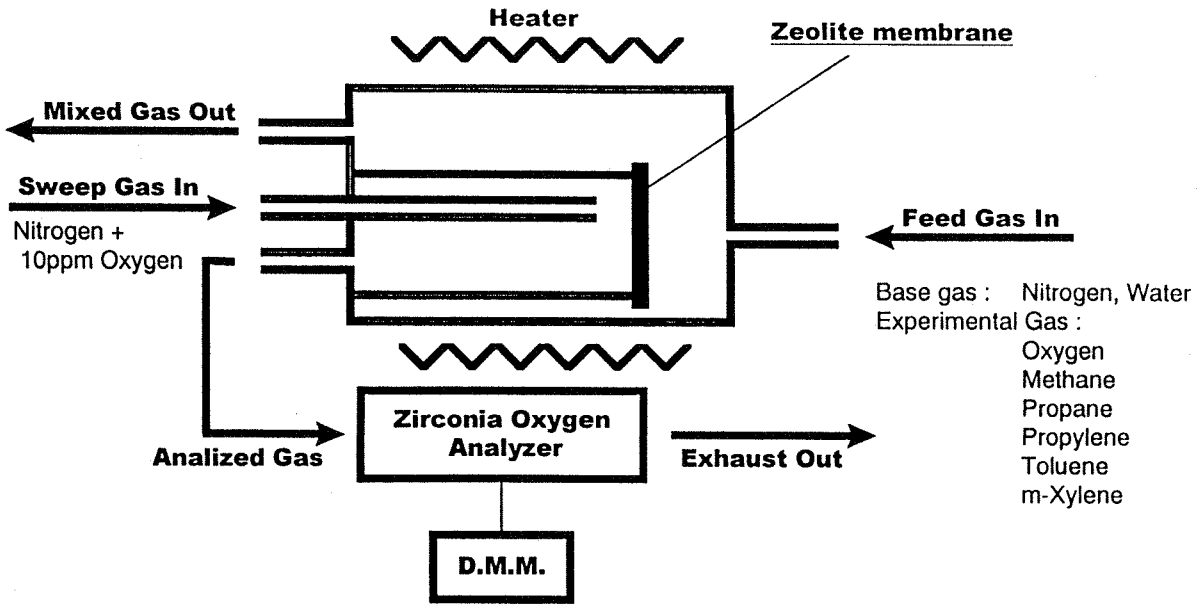

Figure 1. Schematic representation of experimental apparatus for gas permeation.

The permeation behavior was examined by the apparatus shown in Figure 1. Permeation of various hydrocarbon vapors such as methane, propane, propylene, toluene and m-xylene were tested at 298-773 K. Hydrocarbons were carried with N_2 and supplied to the feed side of the membrane, while nitrogen containing about 10 ppm of O_2 was supplied to the permeation side. At the outlet of the permeation side, the oxygen concentration was measured with a zirconia oxygen meter. Permeation of hydrocarbon was detected by measuring the electromotive force (EMF) of sensor cell. When a flammable component, namely hydrocarbon, permeated through the membrane, oxygen concentration measured should decrease with the consumption of oxygen on the surface of the zirconia sensing element. Influence of water on permeation behavior was also examined by adding the water vapor into the feed gas.

Results and Discussion

(1)CHARACTERIZATION OF MEMBRANES

The XRD patterns in Figure 2 revealed that the crystal phases of membranes formed on the Al_2O_3 substrate were MFI and MFI/FER which were prepared with silicate gel and aluminosilicate gel, respectively.

Surface and cross-sectional views of the membrane prepared with silicate gel are shown in Figure 3. Although needle-like crystals, which seems to be MFI crystals, grew on the surface of substrate, the surface of the Al_2O_3 substrate itself was also observed. Therefore, the MFI membrane did not seem to cover the whole surface of substrate. However, as a result of cross-sectional observation, zeolite seemed to grow inside the Al_2O_3 porous layer as well as the Al_2O_3 surface, because a dense layer was formed in the 0.1 μ m porous layer after preparation.

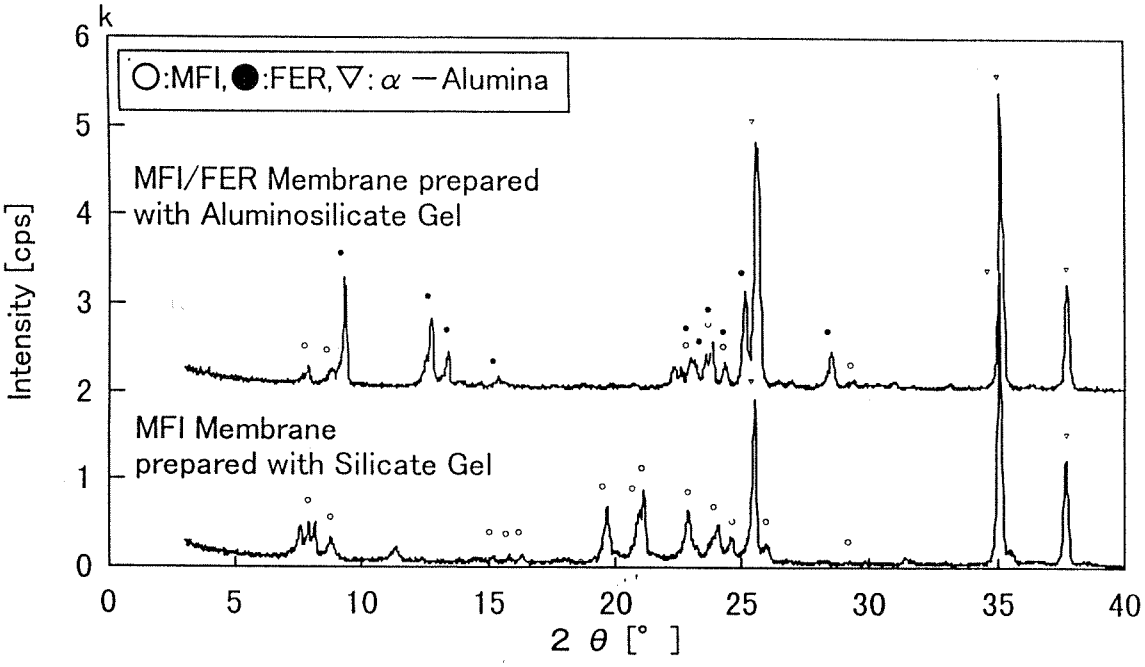

Figure 2. XRD Peak patterns of membranes formed on Al_2O_3 substrate.

(a)Surface of substrate (b)Cross-section of substrate

Figure 3. Surface and cross-sectional views of membrane prepared with silicate gel.

(2)HYDROCARBONS PERMEATION BEHAVIOR

When 1% O_2 or 100ppm CH_4 was supplied to the feed side of the membrane in order to check the response of zirconia meter, the EMF of sensor cell changed rapidly and leveled off within 10 minutes. Therefore this technique is thought to be suitable to investigate the permeation behavior of membrane.

Table 1 summarized the hydrocarbon permeation results. Both the MFI and MFI/FER membranes showed almost the same properties for hydrocarbons permeation except for toluene permeation.

When relatively small hydrocarbons such as propane and propylene were supplied at room temperature, a decrease of oxygen concentration was observed for both membranes. This behavior was maintained up to 773K even in the presence of 7 vol. % water. On the other hand, no permeation of m-xylene was

detected at each temperature.

Toluene permeation behavior was influenced by the temperature and water addition. Though toluene permeated through both membranes at room temperature and 423K, toluene did not permeate through both MFI and MFI/FER membranes at 773K in the absence of water. Water addition led to the toluene permeation through the FER/MFI membrane at 773K.

Based on these results, the membranes prepared in this study were practically pinhole-free and thereby a molecular sieving property appeared for the permeation of hydrocarbons of different molecular size. However, further investigation on permeation behavior is required for understanding the changes of toluene permeation by temperatures and water contents.

Table 1 Hydrocarbon permeation results.

Membrane		MFI					MFI/FER				
Test Condition	Temperature(K)	R.T.	423	423	773	773	R.T.	423	423	773	773
	Water (%)	0	0	7	0	7	0	0	7	0	7
Test Gas	Oxygen	YES	YES	YES	YES	YES	YES	YES	YES	YES	YES
	Methane	YES	YES	YES	YES	YES	YES	YES	YES	YES	YES
	Propane	YES	YES	YES	YES	YES	YES	YES	YES	YES	YES
	Propylene	YES	YES	YES	YES	YES	YES	YES	YES	YES	YES
	Toluene	YES	YES	YES	NO	NO	YES	YES	YES	NO	YES
	m-Xylene	NO	NO	NO	NO	NO	NO	NO	NO	NO	NO

Conclusions

MFI-type and MFI/FER type zeolite membranes were prepared by a vapor phase transport method on a α-Al_2O_3 substrate. Dense zeolite membrane was formed inside the 0.1 μ m α-Al_2O_3 porous layer as well as the surface of the substrate. A dense zeolite and Al_2O_3 composite layer was considered to be practically pin-hole free and thereby a molecular sieving property appeared for the permeation of hydrocarbons of different molecular size.

References

1)T. Sano, Y. Kiyozumi, K Maeda, M. Toa, S. Niwa and F. Mizukami, J. Mater. Chem., 2, 141 (1992).

2)J. G. Tsikoyiannis and W.O Haag, ZEOLITES, 12, 126 (1992).

3)Matsukata et al., Stud. Surf. Sci. Catal., 105, 2195 (1996), Microporous Mater., 11, 107 (1997), AIChE J., 43, 2724(1997).

PERMEATION STUDIES OF BUTANE ISOMERS THROUGH MFI-TYPE ZEOLITIC MEMBRANES

Takaaki Matsufuji[a)], Yurika Mano[a)], Norikazu Nishiyama[a)], Korekazu Ueyama[a)] and Masahiko Matsukata[b)]

a) Department of Chemical Engineering, Osaka University, 1-3 Machikaneyama-cho, Toyonaka-shi, Osaka 560-8531, Japan

b) Department of Applied Chemistry, Waseda University, 3-4-1 Okubo, Shinjuku-ku, Tokyo 169-8555, Japan

To separate butane isomers with similar boiling points, MFI-type zeolitic membranes were prepared by a vapor-phase transport method[1)] on porous α-alumina flat disks. A parent aluminosilicate gel with SiO_2 /Al_2O_3 ratio of 1000 was prepared using colloidal silica containing 30 wt% of SiO_2 and 0.4 wt% of Na_2O (Nissan Chemical Co., Ltd.). At first, colloidal silica was mixed with NaOH(4N) at 303 K. A porous alpha-alumina support (Nihon Gaishi Co., Ltd.) with an average pore diameter of 0.1 μm was dipped into the parent gel at 303 K for 1 day. Then, the gel was forced to penetrate into the pores of alumina support by evacuating the support from one side for an hour. Before the dip-coating process, the support was treated with colloidal silica with pH value of about 10 to depress dissolution of alumina during crystallization.

Crystallization was carried out in an autoclave. A mixture of ethylenediamine(EDA), triethylamine(Et_3N) and water (EDA: 2.0 Et_3N : H_2O, volume ratio) was poured in the bottom to produce vapor. The support coated with the parent gel was horizontally set on the partition. Crystallization was performed at 453 K for 72 h at autogeneous pressure. The weight gain of alumina support during synthesis was ca. 100 mg. As-synthesized MFI membranes were calcined in air at 773 K for 10 h. The heating rate of 0.05-0.1 K min^{-1} was adopted at 473-773 K. The crystallinity and structure of the products were analyzed by X-ray diffraction (XRD) with CuKα radiation (Philips X's Pert-MRD).

We prepared two membranes under the same conditions, however their permeation characteristics were different to each other. The membranes

are called membrane A and B hereafter.

For evaluating the compactness of MFI membranes, the pervaporation of 1, 3, 5-triisopropylbenzene (TIPB) , which has a kinetic diameter larger(0.85 nm) than the pore dimensions of MFI(0.53 x 0.56 nm), was carried out for 10 h at 295 K. No permeation of TIPB through membrane A was detected by a gas chromatograph with an FID, which indicates that the flux of TIPB was less than 1.0×10^{-9} mol m^{-2} s^{-1}. It was the detection limit in this experimental procedure. Therefore, it is concluded that membrane A was pinhole-free. On the other hand, the permeation of TIPB was detected for membrane B and its flux of TIPB was 1.2×10^{-6} mol m^{-2} s^{-1}. Thus, membrane B has some pinholes larger than TIPB molecule.

The permeation behavior of *n*-butane and *i*-butane was studied with two types of gas permeation measurements at 375 K: Pressure gradient (PG) and concentration gradient (CG) methods. **Figure 1** shows the schematic diagram of experimental apparatus for the permeation measurements. In the PG method, the total pressure difference between the feed and permeation sides was 60 kPa. The total pressure on the both sides of the membrane was kept at atmospheric pressure in the CG method. Helium was used as a sweep gas. The total feed rates were 50-60 cm^3/min. The permeate was analyzed by a gas chromatograph with a TC detector. Ideal selectivity was calculated from the flux ratio of *n*-butane to *i*-butane in the single gas permeation tests. Separation factor was calculated by the following equation,

$$\text{Separation factor} = \frac{(Xn/Xi)\text{permeate}}{(Xn/Xi)\text{feed}}$$

where Xn = mole fraction of *n*-butane [%] and Xi = mole fraction of *i*-butane [%].

Figure 2 shows the fluxes of butane isomers through compact membrane A and incompact membrane B as a function of mole fraction of *n*-butane in the feed. In the permeation test with membrane A, the flux of *n*-butane increased with increasing mole fraction of *n*-butane in the feed. However, the flux of *i*-butane had a maximum which was larger than those for the pure gas permeation measurements. This seems to reflect the

effect of the enhancement of permeation in the mixed-gas system. Kinetic diameter of *i*-butane(0.50 nm) was larger than that of *n*-butane(0.43 nm). For the diffusion of two kind of molecules in a micropore system, the molecules with a slower permeation rate generally control the diffusion phenomena. The pores of MFI are so narrow that *n*-butane and *i*-butane cannot pass through each other, possibly except at an intersection. The diffusion in such a narrow pore is generally controlled by a molecule with a smaller permeation rate, that is, *i*-butane molecule. The flux of *i*-butane for mixed-gas is expected to be lower than that in unary system. The results shown in **Figure 2** for the mixed-gas system shows unique trend. *n*-Butane molecules might squeeze into the pore with accompanying *i*-butane molecules.

Compared with the CG method, the PG method gave a higher flux of *i*-butane and a lower flux of n-butane in the mixed gas measurements using membrane A. *i*-Butane molecules adsorbed in the micropores of MFI might have blocked the pores. Such pore-blocking seems to play an important role in the permeation behavior of mixed-gas permeation measurements.

Figure 3 shows the separation factor of the mixture of butane isomers through the compact membrane A and the incompact membrane B as a function of the mole fraction of *n*-butane in the feed. The ideal selectivity of *n*-butane to *i*-butane for membrane A was 60 in the PG method and 95 in the CG method. The separation factor depends on the method of gas permeation. Those of n-butane to *i*-butane were ca. 10 in the PG method and 20-60 in the CG method.

On the other hand, the ideal selectivity of *n*-butane to *i*-butane using membrane B was only 1.6 in the PG method and 2.0 in the CG method. The separation factors of *n*-butane to *i*-butane were ca. 1.0 in the PG method and 1.1 in the CG method, leading to a conclusion that the compactness of MFI membrane is essential to separate butane isomer mixtures at 375 K.

1) Nishiyama, N., "Synthesis of zeolitic membranes by vapor-phase transport method and their separation properties", Ph.D. thesis, **1997**

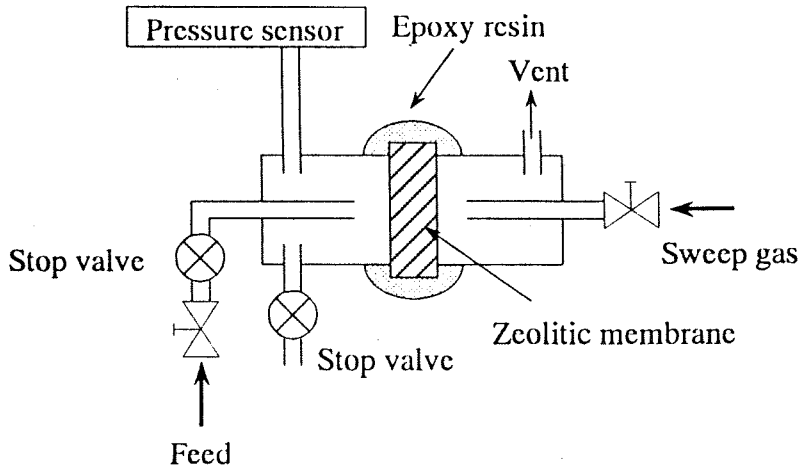

Fig. 1 Schematic diagram of experimental apparatus for permeation measurements.

(a) Compact membrane A

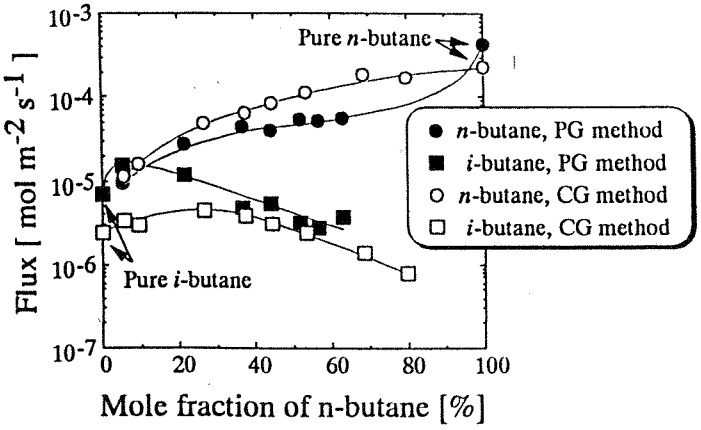

(b) Incompact membrane B

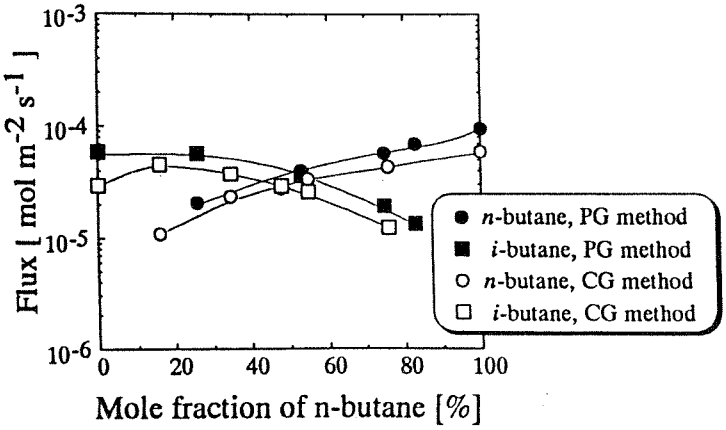

Fig. 2 Flux of butane isomers through MFI-type zeolitic membranes A and B as a function of mole fraction of n-butane in the feed.
Temperature: 375 K.
Closed key: PG method.
Open key: CG method.

(a) Compact membrane A

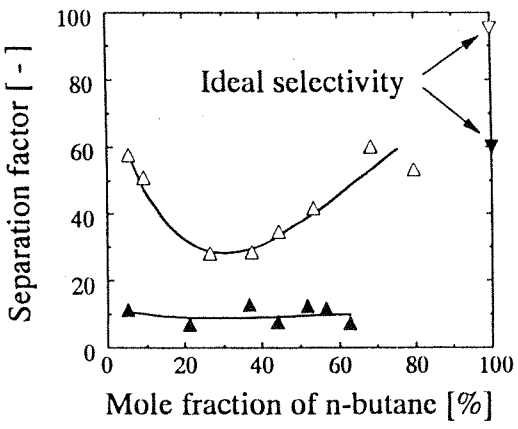

(b) Incompact membrane B

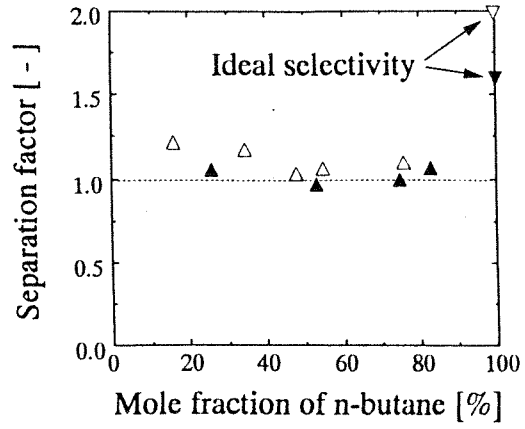

Fig. 3 Separation factor of butane isomers as a function of mole fraction of n-butane in the feed.
Temperature: 375 K.
Closed key: PG method.
Open key: CG method.

ELSEVIER

Applied Catalysis A: General 166 (1998) 97–103

APPLIED CATALYSIS A: GENERAL

Crystallization of high silica BEA by dry gel conversion

P.R. Hari Prasad Rao[a], K. Ueyama[a], M. Matsukata[b,*]

[a] *Department of Chemical Engineering, University of Osaka, Toyonaka, Osaka-560, Japan*
[b] *Department of Applied Chemistry, Waseda University, 3-4-1 Okubo, Shinjuku-ku, Tokyo 169, Japan*

Received 12 May 1997; received in revised form 11 July 1997; accepted 14 July 1997

Abstract

Zeolite with BEA structure was prepared using a new crystallization method called 'Dry Gel Conversion Technique'. This dry gel conversion technique is a convenient method to prepare zeolites and enables one to synthesize zeolite BEA with SiO_2/Al_2O_3 ratios from 30 to infinity using tetraethylammonium hydroxide (TEAOH) as a structure directing agent. Zeolite BEA with SiO_2/Al_2O_3 ratios from 30 to 730 were rapidly crystallized in 3 and 12 h, respectively. The ^{27}Al NMR spectrum for BEA with SiO_2/Al_2O_3 ratio of 30 confirmed the absence of octahedrally coordinated aluminum. The crystallization rates were higher for BEA with low SiO_2/Al_2O_3 ratios than for those with high SiO_2/Al_2O_3 ratios. BEA crystallized by this method had uniform particles of about 60 nm. Higher Na^+ ion concentrations in the gel promoted the formation of high silica BEA. Elimination of occluded TEA cations took place at lower temperatures (around 623 K) in high silica BEA than that in BEA with low SiO_2/Al_2O_3 ratios (around 900 K). This method also allowed to synthesize BEA in the form of self-bonded pellets.

Keywords: Zeolite BEA (beta); Dry gel conversion; High silica zeolite; Crystallization; Self-bonded zeolite pellet

1. Introduction

New crystallization methods for zeolite synthesis are interesting, as they may enable us to prepare zeolites with new structures, compositions and convenient forms such as membranes and films. One such vapor-phase transport method has been successfully employed for synthesis of powdery zeolites [1–3] and zeolitic membranes [4–6]. This method involves crystallization of dry aluminosilicate gel in the presence of volatile structure-directing agent(s) and steam. The amount of structure-directing agent required in this method is very small as compared to that used in the hydrothermal method. However, this method cannot be applied for the preparation of all types of zeolites, since many of them need non-volatile structure-directing agents for their crystallization. Recently, we have reported a new crystallization method Dry Gel Conversion Technique for crystallization of zeolite BEA [7].

Zeolite BEA, a three-dimensional wide-pore, a high silica zeolite, has potential technological applications in petrochemical processes and organic synthesis. Zeolite BEA synthesized by a hydrothermal method [8] always has a low product yield and could not be synthesized with SiO_2/Al_2O_3 ratios above 250 using

*Corresponding author. Tel.: +81-3-5286-3203; fax: +81-3-5286-3203; e-mail: mmatsu@mn.waseda.ac.jp.

0926-860X/98/$19.00
PII S0926-860X(97)00245-7

TEAOH (tetraethylammonium hydroxide), TEAOH-diethanolamine, TEABr-NH_3 or TEAOH-TEABr-triethanolamine [8,9]. van der Waal et al. [10] have reported an all silica BEA zeolite using dibenzyldimethyl ammonium cation, an expensive and not easily removable structure directing agent. Recently, Camblor et al. [11] have reported an all silica BEA using TEAOH and HF, however, its industrial production may not be possible since HF was used in the preparation.

In this study, we investigated the synthesis of zeolite BEA with various SiO_2/Al_2O_3 ratios using TEAOH as a structure-directing agent. We shall show that this method allows one to prepare zeolite BEA with higher SiO_2/Al_2O_3 ratios than those which have been obtained by the conventional hydrothermal synthesis method.

2. Experimental

2.1. Synthesis

Dry gels having compositions,

$SiO_2 : a\,Al_2O_3 : b\,Na_2O : c\,TEAOH$

where $a = 0 - 0.033$, $b = 0.014 - 0.092$ and $c = 0.16 - 0.50$ were prepared as follows.

Aluminum sulfate (Wako Pure Chem.) was dissolved in 10 g of distilled water at 353 K. A given amount of NaOH (4 M, Wako Pure Chem.) aqueous solution and TEAOH (20% in water, Wako Pure Chem.) were added to 10 g of colloidal silica (30.3% SiO_2, 0.42% Na_2O and 700 ppm of Al_2O_3, Nissan Chem.) at room temperature (298–303 K) while stirring. Fumed silica was used in the syntheses of all silica BEA. After 30 min, an appropriate amount of the aluminum sulfate solution and 5.5 g of water were added to the mixture and stirring was continued for 2 h. Then, the mixture was heated to 353 K and dried while stirring. When the gel became viscous, it was stirred using a teflon rod till it became a dry gel. The dry gel was crushed to powder and placed in a special autoclave (Fig. 1) where water as a source of steam was poured at the bottom. Crystallization of the dry gel was carried out in steam at 453 K and autogenous pressure for 3 to 12 h. All silica BEA was crystallized at 418 K for 120 h.

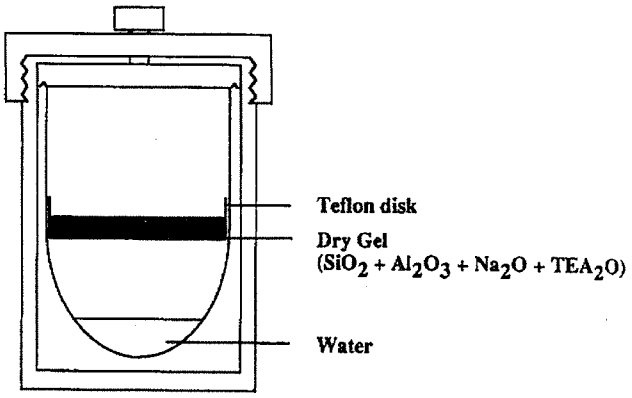

Fig. 1. Schematic diagram of the autoclave used in crystallization of BEA.

The product was washed thoroughly with deionized water and dried in air at 363 K for 12 h. The organic material was removed by calcination in air at 773 K. X-ray diffraction patterns were recorded on Philips X's Pert-MRD instrument using CuK_α radiation. Field Emission SEM (FE-SEM) images were taken by Hitachi S-5000L FE-SEM. Solid-state NMR measurements were carried out with GSX-400 (JEOL) spectrometer. ^{29}Si-NMR spectra were recorded at 79.30 MHz with a pulse length of 5.2 μs, a pulse interval of 10 s and a spinning rate of about 6 kHz. ^{27}Al-NMR spectra were recorded at 104.05 MHz with a pulse length of 5.1 μs, a pulse interval of 5 s and a spinning rate of about 6 kHz. TG–DTA experiments were performed with Shimadzu DTG-50/50H thermogravimetric analyzer.

3. Results and discussion

Fig. 2 shows the XRD patterns of the products obtained by crystallization of dry gels having different SiO_2/Al_2O_3 ratios and all silica BEA. Highly crystalline BEA samples with SiO_2/Al_2O_3 ratios from 30 to 730 were obtained directly in powdery form after crystallization was carried out for 3–12 h at 453 K. Zeolite BEA with SiO_2/Al_2O_3 ratios from 30 to 730 in which colloidal silica was used as a source of silica were fully crystalline without any impure phases (Fig. 2a–f). The crystallinity of all silica BEA (Fig. 2g) (fumed silica was used as the source of silica) was about 85% which has an additional reflec-

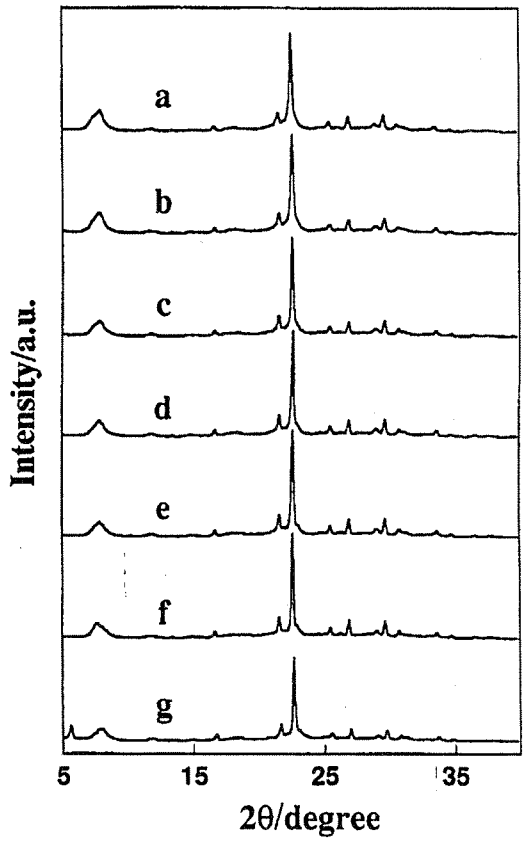

Fig. 2. X-ray diffraction patterns of as-synthesized BEA with different SiO_2/Al_2O_3 ratios. SiO_2/Al_2O_3 ratio: a, 30; b, 100; c, 200; d, 380; e, 480; f, 730; g, infinity.

tion at around $2\theta = 5.6°$. Further work on all silica BEA is in progress.

Fig. 3 shows the crystallization curves for samples with SiO_2/Al_2O_3 ratios from 30 to 730. Relative crystallinity was evaluated from the intensity of the most intense (302) reflection peak appearing at $2\theta = 22.4°$. For the sample with SiO_2/Al_2O_3 ratio of 30, crystallization was rapid and was completed within 3 h (Fig. 3a). The X-ray diffraction pattern of the sample is given in Fig. 2(a). The sample, which was amorphous even after 150 min of crystallization, converted to fully (100%) crystalline prod after 180 min of crystallization. Crystallizati rate decreased with increasing SiO_2/Al_2O_3 ratio a crystallization took as long as 12 h for the samp e with SiO_2/Al_2O_3 ratio of 730. The relative crystalli ity of product with SiO_2/Al_2O_3 ratio of 730 (Fig. 3 l) was lower as compared to that with SiO_2/Al_2O_3 rati of 30 (Fig. 3a). However, as shown in Fig. 3(c) (X-ray

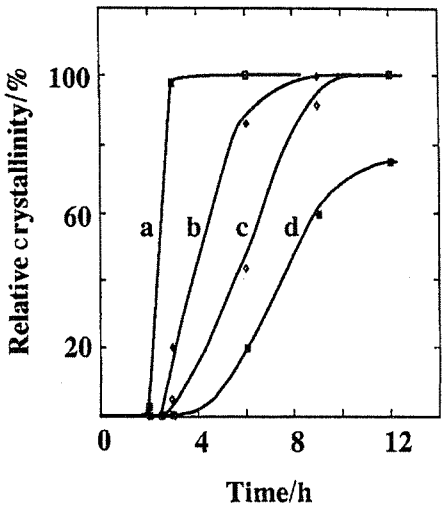

Fig. 3. Rate of crystallization of BEA with different chemical compositions. SiO_2/Al_2O_3, SiO_2/Na_2O and SiO_2/SO_4^{2-} ratios: a, 30, 23.8 and 20.9; b, 380, 23.8 and 528; c, 730, 10.9 and 10; d, 730, 23.8 and 0, respectively.

diffraction pattern is presented in Fig. 2f), its relative crystallinity could be improved to 100% by the addition of 0.005 mol of $NaHSO_4$ to the parent gel consisting of 0.05 mol of SiO_2. Recently, it was reported that anions such as sulfates can increase the rate of crystallization in hydrothermal synthesis [12]. In our experiments, owing to the use of aluminum sulfate as a source of aluminum, the sulfate ion concentration varied from 2.4×10^{-3} to 0 mol ($SO_4^{2+}/SiO_2 =$ 0.048–0) in the gels with SiO_2/Al_2O_3 ratios from 30 to 730. For SiO_2/Al_2O_3 ratio of 730, the addition of 0.71 g of $NaHSO_4$ (98%, 0.005 mol of sulfate ions) increased the relative crystallinity from 75 to 100%. However, in this experiment, Na^+ ion concentration also increased by the addition of $NaHSO_4$ and it is not clear which (Na^+ or SO_4^{2+}) ions are responsible for the increase in crystallinity.

Fig. 4 shows the XRD patterns of calcined samples. As shown in Table 1, the products were calcined between 723–823 K in air for 12 h to remove the occluded organic material present within the pores of BEA. They were stable after calcination. In order to remove organic material from BEA with SiO_2/Al_2O_3 ratios of 30, a temperature as high as 823 K was required, whereas for the sample with SiO_2/Al_2O_3 ratios of 730 a calcination temperature of 723 K was sufficient. As shown in Table 1, BEA samples after calcination had BET surface areas in the range of 500–

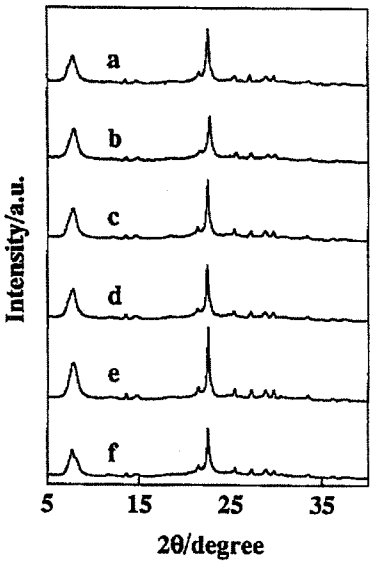

Fig. 4. X-ray diffraction patterns of calcined BEA with different SiO_2/Al_2O_3 ratios. SiO_2/Al_2O_3 ratios: a, 30; b, 100; c, 200; d, 380; e, 480; f, 730.

Table 1
SiO_2/Al_2O_3 ratios of parent gel and product and BET surface area of product

SiO_2/Al_2O_3 ratio		Calcination temperature (K)	BET surface area [a] (m^2g^{-1})	Langmuir surface area (m^2g^{-1})
Gel	Product			
30	30	823	599	787
60	60	823	—	—
100	100	773	507	—
380	380	723	529	—
480	480	723	595	720
730	730	723	580	653

[a] Surface areas are at liquid nitrogen temperature by single point BET method.

600 m^2g^{-1}. This indicates that zeolite pores were not blocked by any non-removable occluded material. Chemical analysis of BEA samples were compared with those of their gels in Table 1. SiO_2/Al_2O_3 ratios of BEA samples are the same as those of their initial gels suggesting that the gel was completely transformed into zeolite.

Fig. 5 shows the ^{27}Al and ^{29}Si NMR spectra for the sample with SiO_2/Al_2O_3 ratio of 30. The absence of a peak at 0 ppm in the ^{27}Al NMR spectrum indicates that no extra-framework aluminum was present in the sample. The SiO_2/Al_2O_3 ratio calculated from ^{29}Si

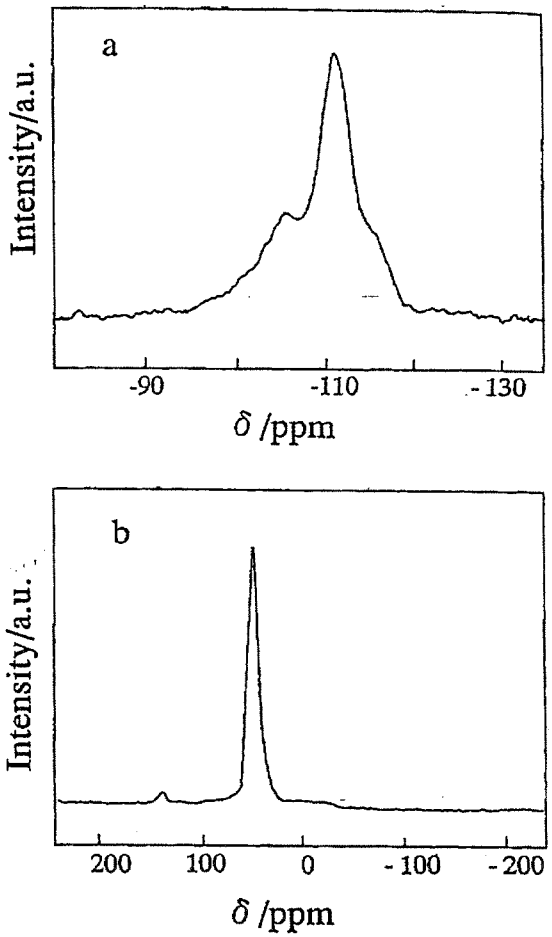

Fig. 5. ^{29}Si-NMR (a) and ^{27}Al-NMR (b) spectra of BEA with $SiO_2/Al_2O_3 = 30$.

NMR as well as chemical analysis matches with that of the initial gel, such results confirm the complete transformation of gel into the zeolite phase.

Fig. 6 shows the FE-SEM images for BEA with SiO_2/Al_2O_3 ratio of 30 (crystallized from the gel with SiO_2/Al_2O_3, SiO_2/Na_2O and SiO_2/SO_4^{2-} ratios of 30, 23.8 and 20.9, respectively). Uniform particles of about 60 nm in length were obtained. No amorphous phase seems to exist in the sample. Formation of uniform nano-crystals from dry gel powder is of particular interest to understand the mechanism of zeolite formation.

Table 2 compare the effect of Na^+ ions on the product. BEA can be synthesized using wide ratios of SiO_2/Na_2O from 10 to 71. As shown in Table 2, when SiO_2/Na_2O ratio was 71 (which was originally present in the colloidal silica), the products from the

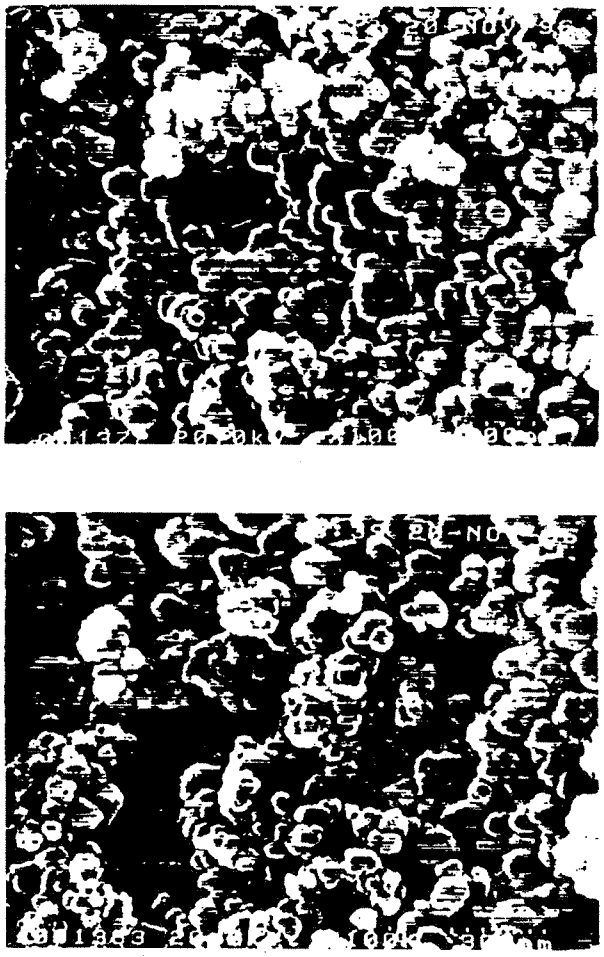

Fig. 6. FE-SEM images for BEA crystallized from the gel with SiO_2/Al_2O_3, SiO_2/Na_2O and SiO_2/SO_4^{2-} ratios =30, 23.8 and 20.9, respectively. Crystallization time: a – 3 h; b – 120 h.

Table 2
Effect of sodium content on synthesis of BEA [a]

SiO_2/Al_2O_3	SiO_2/Na_2O				
	13.5	20	23.8	29.4	71
30	—	BEA	BEA	BEA	Amorphous
60	BEA	BEA	BEA	BEA	—
100	—	BEA	BEA	—	BEA
200	—	BEA	BEA	BEA	BEA
380	—	BEA	BEA	BEA	MTW
480	—	BEA	BEA	BEA	MTW
730	BEA	—	BEA [b]	BEA [b]	Amorphous

[a] SiO_2/TEA_2O = 5.4. Relative crystallinity of BEA is 100%.
[b] Relative crystallinity around 75%.

gels with SiO_2/Al_2O_3 ratios from 100 to 300 were BEA. On the other hand, the gel with SiO_2/Al_2O_3 ratio of 380 and 480 produced MTW and the gel with SiO_2/Al_2O_3 ratio of 30 gave amorphous material. In the gel with SiO_2/Al_2O_3 ratio of 380 and 480, when SiO_2/Na_2O ratio changed from 71 to 29.4 highly crystalline BEA with no MTW impurity was obtained. This shows that for the gels with SiO_2/Al_2O_3 ratios of 380 and 480, higher sodium concentrations promoted the formation of BEA rather than MTW. In our experimental conditions, an insufficient amount of Na^+ could not initiate crystallization when SiO_2/Al_2O_3 ratios of the gel were either low ($SiO_2/Al_2O_3 = 30$) or very high ($SiO_2/Al_2O_3 = 730$). Even with the small concentrations of Na^+ ions ($SiO_2/Na_2O = 71$), gels with SiO_2/Al_2O_3 ratios between 100 to 480 were crystallized and the type of product depended on SiO_2/Al_2O_3 ratio. When SiO_2/Al_2O_3 ratios of 380 and 480, the product was MTW. When the concentration of Na^+ ion in the gel was increased ($SiO_2/Na_2O = 29.4$), the product was BEA instead of MTW. This clearly shows that higher Na^+ ion concentrations promoted the formation of BEA rather than MTW for gels with SiO_2/Al_2O_3 ratios of 380 and 480.

Table 3 lists the products formed by using different SiO_2/TEA_2O ratios. While several patents claim the formation of BEA with SiO_2/TEA_2O ratio from 4 to 20 [13], in most of the published papers BEA was synthesized using SiO_2/TEA_2O ratios around 4. Recently, Clearfield et al. [14] reported synthesis of BEA with SiO_2/Al_2O_3 ratios from 14 to 32 using SiO_2/TEA_2O ratio of 12. Using our method, it is possible to synthesize BEA with SiO_2/Al_2O_3 ratios 30–480 using SiO_2/TEA_2O ratio of 8.

When water was not added in the autoclave, the product was always amorphous. A small amount of steam can still be formed by the dehydration of gel at

Table 3
Effect of SiO_2/TEA_2O ratio on the synthesis of BEA

SiO_2/TEA_2O	Product
4.0	BEA
5.4	BEA
8.0	BEA
12.5	BEA+MTW

SiO_2/Al_2O_3 = 60.

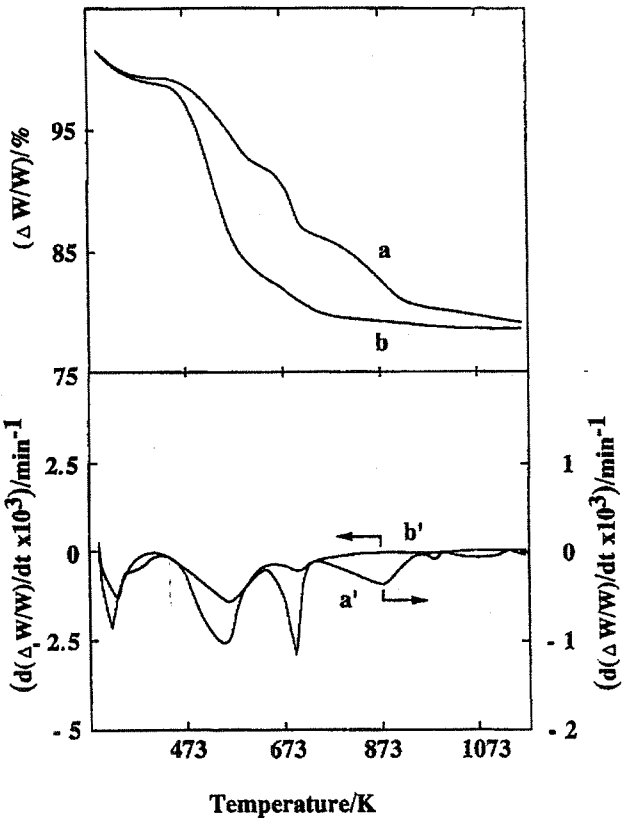

Fig. 7. TG–DTG patterns of BEA samples treated in the stream of air. a and b: TG patterns for BEA with SiO_2/Al_2O_3 ratios 30 and 730, respectively; and a'and b': DTG patterns for BEA with SiO_2/Al_2O_3 ratios 30 and 730, respectively.

the crystallization temperature of 453 K. Such a small amount of steam is, however, insufficient to transform the amorphous gel into a crystalline phase. A small amount of additional water to produce a sufficient amount of steam is essential for the crystallization of the dry gel.

Hydrothermal crystallization of BEA from the gel with a composition of SiO_2: 0.033 Al_2O_3: 0.05 Na_2O: 0.37 TEAOH: 20 H_2O (similar to the one used in the dry gel conversion method) at 453 K failed and the product was amorphous.

Fig. 7 shows the TG–DTG patterns of BEA samples with SiO_2/Al_2O_3 ratios 30 and 730 in the stream of air. The elimination of TEA ions from as-synthesized BEA with SiO_2/Al_2O_3 ratios of 30 and 730 was completed at around 723 and 950 K, respectively. The TG–DTG pattern for BEA with SiO_2/Al_2O_3 ratio of 730 has three steps. The first step appearing between 300–423 K was due to elimination of water. Most of the organic material was removed in the second step between 423–623 K and the third step between 623–723 K was due to either partial or complete oxidation of a small amount of remaining organic material. The TG–DTG pattern for BEA with SiO_2/Al_2O_3 ratio of 30 has four steps that include elimination of water between 300–423 K, partial elimination of TEA ions between 423–623 K, oxidative decomposition of TEA ions between 623–773 K and complete elimination of remaining organic material between 773–923 K. The second step appearing between 423–623 K is minor as compared to that for BEA with SiO_2/Al_2O_3 ratio of 730, indicating that only a small amount of organic material is eliminated in this temperature range. TEA ions in BEA with SiO_2/Al_2O_3 ratio of 730 possibly have interactions

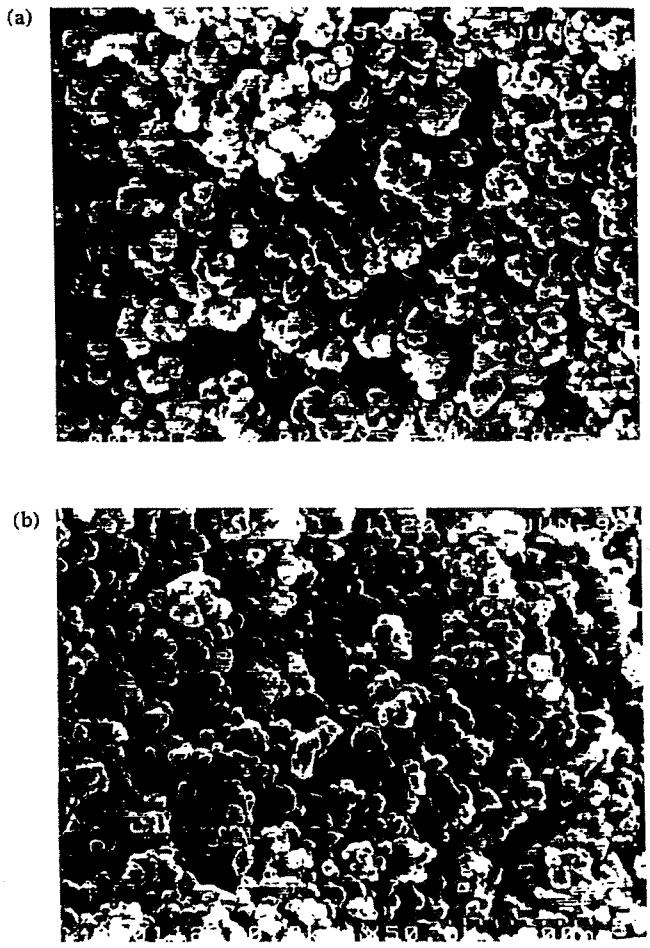

Fig. 8. SEM images of surface (a) and inner (b) portions of a self-bonded BEA with SiO_2/Al_2O_3 = 150.

mostly with oxygens of Si–O–Si linkages as fewer Si–O–Al groups are present compared to BEA with SiO_2/Al_2O_3 ratio of 30. Since the interaction between TEA ions and oxygen of Si–O–Si linkages is believed to be weaker than that between TEA ion and oxygen of Si–O–Al linkage, TEA ions were eliminated at lower temperatures in BEA with SiO_2/Al_2O_3 ratio of 730. The TG–DTG pattern for BEA with SiO_2/Al_2O_3 ratio of 30 is in consistent with previous results on BEA synthesized by the hydrothermal method [15]. This shows that neither decomposition nor degradation of TEA ions occurred while preparing the dry gels.

Fig. 8 shows the SEM images of surface and inner portions of a self-bonded BEA pellet with SiO_2/Al_2O_3 ratio of 150. This method enables one to synthesize zeolite in convenient forms such as self-bonded pellets. Self-bonded pellets with 4 cm diameter (equivalent to the inner diameter of the gel container) were formed when the SiO_2/Al_2O_3 ratios > 100. Depending on the form of support used, we can synthesize convenient forms of self-bonded BEA. Crystallinity and particle sizes are uniform both at surface and inner portions with crystallinity as high as that for powder forms of BEA.

These experiments confirm that zeolites with a high crystallinity and a uniform particle size can be synthesized from amorphous dry gel powder in the presence of steam.

4. Conclusion

A new method was developed for the crystallization of zeolites, where BEA can be rapidly crystallized. BEA with SiO_2/Al_2O_3 ratios 30–730 were synthesized using TEAOH as a structure-directing agent. Complete conversion of gel to zeolite was obtained. Particle size of the products synthesized using this method was uniform even for high silica BEA zeolite. This method enables reduction in template concentration and synthesis of zeolite in convenient forms such as self-bonded pellets. This method may be useful for the synthesis of zeolitic membranes. Also this method might enable continuous production of zeolite, reduction in reactor volume and elimination of waste water treatment.

Acknowledgements

P.R.H. thanks Japan Society for Promotion of Science, Japan, for a research fellowship. We thank GHAS laboratory for providing XRD facility.

References

[1] W. Xu, J. Dong, J. Li, F. Wu, J. Chem. Soc. Chem. Commun., (1990) 755.
[2] M.H. Kim, H.X. Li, M.E. Davis, Microporus Materials 1 (1993) 191.
[3] M. Matsukata, N. Nishiyama, K. Ueyama, Microporus Materials 1 (1993) 219.
[4] M. Matsukata, N. Nishiyama, K. Ueyama, J. Chem. Soc. Chem. Commun., (1994) 339.
[5] N. Nishiyama, K. Ueyama, M. Matsukata, Stud. Surf. Sci. Catal. 84 (1994) 1183.
[6] N. Nishiyama, K. Ueyama, M. Matsukata, Chem. J. Soc. Chem. Commun., (1995) 1967; N. Nishiyama K. Ueyama, M. Matsukata, Microporus Materials 7 (1996) 299.
[7] P.R. Hari Prasad Rao, M. Matsukata, Chem. Commun., (1996) 1441.
[8] J. Perez-Pariente, J.A. Martens, P.A. Jacobs, Zeolites 8 (1988) 46.
[9] U. Lohse, B. Altrichter, R. Donath, R. Fricke, K. Jancke, B. Parlitz, E. Schreier, J. Chem. Soc. Faraday Trans., (1996) 159.
[10] J.C. van der Waal, M.S. Rigutto, H. van Bekkum, J. Chem. Soc. Chem. Commun., (1994) 1241.
[11] M.A. Camblor, A. Corma, S. Valencia, Chem. Commun., (1996) 2365.
[12] R. Kumar, A. Bahumik, R.K. Ahedi, S. Ganapathy, Nature 381 (1996) 298.
[13] R. Szostak, Hand book of Molecular Sieves, Van Nostrand Reinhold, New York, 1992, p. 95.
[14] A.B. Borade, A. Clearfield, Catal. Lett. 26 (1994) 285.
[15] E.B. Lami, F.D. Renzo, F. Fajula, P.H. Mutin, T.D. Courieres, J. Phy. Chem. 96 (1992) 3807.

Phase Transformation of High Silica BEA to OU-1 and MTW

P.R. Hari Prasad Rao, Korekazu Ueyama, Eiichi Kikuchi,† and Masahiko Matsukata*†
Department of Chemical Engineering, Osaka University, Toyonaka, Osaka 560
†*Department of Applied Chemistry, Waseda University, Tokyo 169*

(Received December 2, 1997; CL-970911)

Phase transformation of high silica BEA to OU-1 and MTW was demonstrated for the first time. Zeolite OU-1, an analogous material to SSZ-31 and NCL-1, was synthesized using tetraethylammonium hydroxide (TEAOH) as a structure directing agent. The influence of Na and Al ions on stabilization of BEA phase during crystallization is presented.

Zeolites are materials widely used in catalysis, adsorption and ion exchange. Zeolite pore structure and chemical compositions are very important since they determine shape selectivity and catalytic activity. A major part of recent research on zeolites is focused on synthesis of zeolites with new structures, synthesis using low cost organic materials as structure directing agents and new crystallization methods to perform crystallization in a dense media,[1] from or in a gas phase.[2-7]

Barrer described the transformation of zeolite structures during crystallization.[8] Transformation of LTA to hydroxy-sodalite and zeolite P was reported.[9] Norby pointed out such transformation as one of the possible routes for the synthesis of zeolites.[10] We recently reported the synthesis of highly crystalline BEA by dry gel conversion method. This method allowed to prepare BEA with SiO_2/Al_2O_3 = 30 to infinity using TEAOH as a structure directing agent in an alkaline medium.[4-6] In this study, we report the transformation of high silica BEA to zeolite OU-1 (an analogous material to SSZ-31[11] and NCL-1[12]) and MTW and the effect of gel compositions on the phase transformation.

Dry gels having compositions, SiO_2 : 0.0013 - 0.33 Al_2O_3 : 0.042-0.94 Na_2O : 0.37 - 0.38 TEAOH, were prepared as described elsewhere.[5,6] Crystallization of the dry gel was carried out in the presence of steam at 453 K and autogeneous pressure for 3 to 120 h. The products were characterized by XRD, SEM and N_2 adsorption.

Highly crystalline BEA was obtained by crystallization of dry gels with SiO_2/Al_2O_3 ratios = 30 - 730 for 3 - 12 h under autogenous pressure at 453 K. Crystallization was completed for the gels with SiO_2/Al_2O_3 = 30 within 3 h and produced highly crystalline BEA as previously reported.[5,6] No change in the crystallinity as well as particle sizes was observed in the products obtained from these gels (SiO_2/Al_2O_3 ratios = 30) even after 120 h of crystallization (Figure 1A). However, gels with SiO_2/Al_2O_3 ratios = 380 and 730, which produced pure BEA after crystallization for 12 h, transformed to other phases after prolonged crystallization. The products formed depended on the gel compositions as well as crystallization time. As shown in Figure 1B, a gel with SiO_2/Al_2O_3 = 380 produced BEA after crystallization time of 12 h. When the crystallization was carried out for 24 h, the product showed additional reflections in its XRD pattern typically at 2θ = 6.2, 7.4, 8.2, 21.2 and 24.9°, other than those for BEA. These reflections can be attributed to a new phase OU-1. Enrichment of these reflections and diminish of the reflections for BEA continued till 60 h of crystalllization, suggesting that BEA is transforming to another phase. Further prolonged crystallization led to the formation of cristoballite. The product crystallized for 60 h, after calcination at 723 K did not contain BEA, and a different phase OU-1 (an analogous material to SSZ-31 and NCL-1) was produced. XRD patterns of Figure 1B do not show any broad peak characteristic of amorphous material. Similarly, SEM images also show the absence of any amorphous phase. These results suggest the direct phase transformation from BEA to OU-1. SSZ-31 and NCL-1 were synthesized using N,N,N-trimethyltricyclo[5.2.1.$0^{2,6}$]

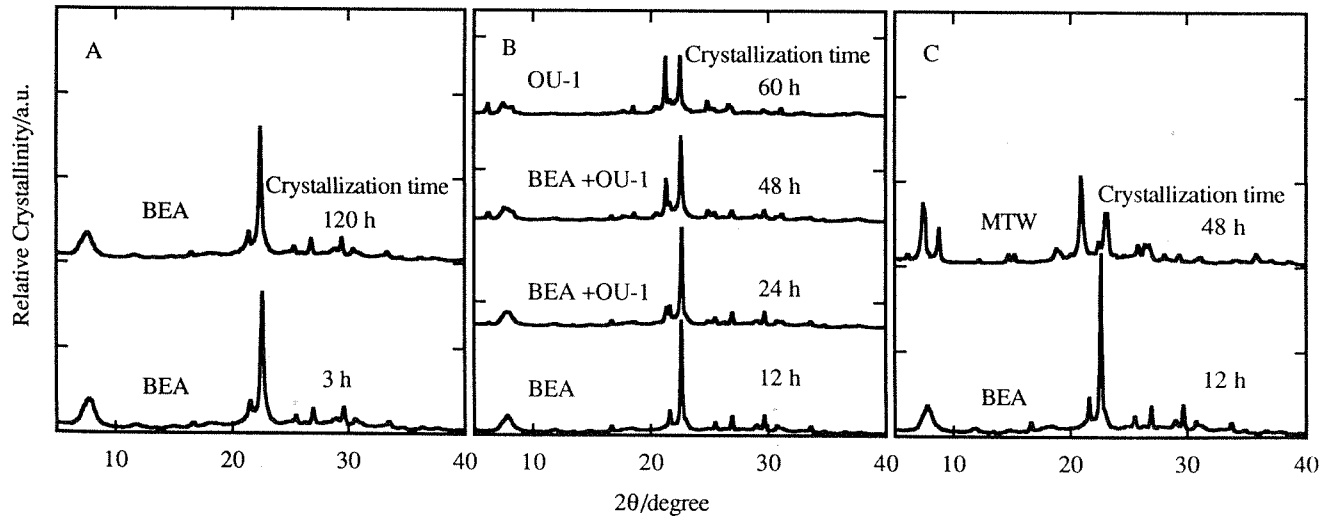

Figure 1. Effect of gel composition and crystallization time on zeolite product.
SiO_2/Al_2O_3 and Na_2O/SiO_2 ratios : A, 30 and 0.042; B, 380 and 0.042; C, 730 and 0.094, respectively.

decaneammonium and hexamethylene bis(triethylammonium bromide), respectively, as structure directing agents.[11,12] These structure directing agents are commercially not available. Lobo *et al.*[11] have shown that BEA, MTW and SSZ-31 have a similar (related) framework structure (projection). These zeolites have 12 membered pore opening with the difference in the connectivity of T-atoms and rearrangement of these T-atoms may lead to the formation of different structures. Our method enables to synthesize these three structurally related zeolites using TEAOH as a structure directing agent.

When the Na^+ ion concentration in the gel having SiO_2/Al_2O_3 ratio = 380 was Na_2O/SiO_2 ratio = 0.014, the product was transformed to MTW instead of OU-1. When the Na^+ ion concentration of the gel was raised to Na_2O/SiO_2 ratio = 0.094, stability of BEA phase was improved and product did not transform to other phases even after 60 h of crystallization. This suggests Na^+ ions play an important role in directing the structure of product. A lower Na^+ ion concentration (Na_2O/SiO_2 = 0.014) favors the formation of MTW and an increased Na^+ ion concentration (Na_2O/SiO_2 = 0.042) is required for the formation of OU-1. A further higher Na^+ ion concentration (Na_2O/SiO_2 = 0.094) improves the stability of BEA with SiO_2/Al_2O_3 ratio = 380 during crystallization. The gel having SiO_2/Al_2O_3 ratio = 730 and Na_2O/SiO_2 ratio = 0.014 did not crystallize and the product remained amorphous. When the Na_2O/SiO_2 ratio was raised to 0.042, the products after 12 and 48 h of crystallization were BEA (relative crystallinity = 75 %) and MTW, respectively. Gel with SiO_2/Al_2O_3 ratio = 730 and Na_2O/SiO_2 ratio = 0.094 formed highly crystalline BEA after 12 h of crystallization. However, when the crystallization was prolonged to 48 h, the product transformed from BEA to MTW (Figure 1C). This suggests that during crystallization, the stability of BEA phase decreases with increasing SiO_2/Al_2O_3 ratios, though their stability could be improved by increasing Na_2O/SiO_2 ratios to a certain extent. After crystallization, pure BEA samples with SiO_2/Al_2O_3 ratios = 380-730 were found to have high thermal stability and after transforming to H-form: They were stable even after calcination at 1373 K[6]. This suggests that a less stable phase during crystallization needs not be thermally a less stable phase.

Figure 2 shows FE-SEM images of BEA and OU-1. OU-1 crystals are rectangular in shape with 2 μm length and 1 μm width: Namely, the crystal shape of this phase is totally different from that of BEA. The BET surface areas of BEA, OU-1 and MTW were 529, 290 and 310 $m^2 g^{-1}$, respectively. Sorption capacities for cyclohexane and m-xylene were measured at 303 K by TG. These two kinds of hydrocarbons saturated at 298 K in a stream of helium were supplied. The sorption capacities were about 4 and 2 wt% for cyclohexane and m-xylene, respectively.

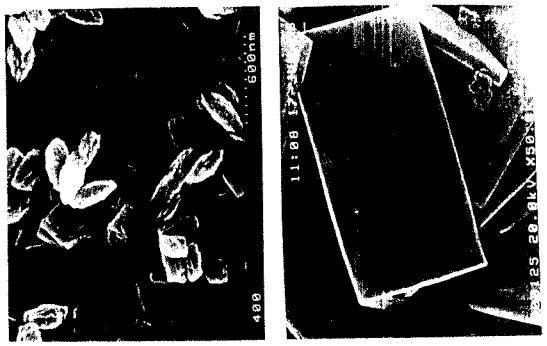

A B

600 nm

Figure 2. FE-SEM images of BEA (A) and OU-1 (B). SiO_2/Al_2O_3, Na_2O/Al_2O_3 and crystallization time: A, 400, 18.4 and 12 h; B, 380, 15.96, 60 h.

These adsorption properties strongly indicate that OU-1 is a high silica zeolite with 12-membered ring opening. Our preliminary studies on structural analysis by HRTEM and XRD confirmed that OU-1 is a large pore molecular sieve and has pore opening similar to that of SSZ-31.[13]

One of the authors (PRH) thanks Japan Society for the Promotion of Science for a research fellowship.

References

1 A.B. Borade and A. Clearfield, *Catal. Lett.*, **26**, 285 (1994).
2 W. Xu, J. Dong, J. Li, and F. Wu, *J. Chem. Soc., Chem. Commun.*, **1990**, 755.
3 M. Matsukata, N. Nishiyama, and K. Ueyama, *Microporus Mater.*, **1**, 219, (1993).
4 P.R. Hari Prasad Rao and M. Matsukata, *Chem. Commun.*, **1996**, 1441.
5 P.R. Hari Prasad Rao, K. Ueyama, and M. Matsukata, *Appl. Catal. A*, **166**, 97, (1998).
6 P.R. Hari Prasad Rao, C. A. Leon y Leon, K. Ueyama and M. Matsukata, *Microporous Mater.*, in press.
7 U.Deforth, K.K. Unger, and F. Schuth, *Microporous Mater.*, **9**, 287 (1997).
8 R.M. Barrer, "Hydrothermal Chemistry of Zeolites", Academic Press, London (1982).
9 B. Subotic, N. Masic, and I. Smit, *Zeolites*, **5**, 207, (1985).
10 P. Norby, *J. Amer. Chem. Soc.*, **119**, 5215, (1997).
11 R.F. Lobo, M. Tsapatsis, C.C. Freyhardt, I. Chan, C.C. Chen, S. I. Zones, and M. E. Davis, *J. Amer. Chem. Soc.*, **119**, 3732, (1997).
12 R. Kumar, K. R. Reddy, and P. Ratnasamy, U.S. patent 5219813 (1993).
13 M. Matsukata, K. Ueyama, E. Kikuchi, Y.Sasaki, T. Suzuki, M. Kato, and P.R. Hari Prasad Rao, in preparation.

ELSEVIER

Microporous and Mesoporous Materials 21 (1998) 305–313

MICROPOROUS AND MESOPOROUS MATERIALS

Synthesis of BEA by dry gel conversion and its characterization

P.R. Hari Prasad Rao [a], C.A. Leon y Leon [b], K. Ueyama [a], M. Matsukata [c,*]

[a] *Department of Chemical Engineering, Osaka University, Toyonaka, Osaka 560, Japan*
[b] *Quantachrome Corp., 1900 Corporate Drive, Boynton Beach, FL 33426, USA*
[c] *Department of Applied Chemistry, Waseda University, 3-4-1 Okubo, Shinjuku-ku, Tokyo 169, Japan*

Received 25 August 1997; received in revised form 12 December 1997; accepted 12 December 1997

Abstract

Zeolite BEA with SiO_2/Al_2O_3 ratios ranging from 30 to 740 were crystallized at 413 and 453 K by the dry gel conversion technique. The particle size of the products increased with increasing SiO_2/Al_2O_3 ratio as well as with increasing crystallization temperature. In as-synthesized BEA, the TEA^+ ions interacting with $Si-O^-$ decomposed between 473 and 673 K and those interacting with $Al-O^-$ were cleaved between 673 and 798 K. During their elimination, the TEA^+ ions interacting with $Al-O^-$ underwent higher degradation than those interacting with $Si-O^-$. Chemical compositions showed the least influence on the fractions of decomposition product during the elimination between 473 and 673 K. The framework of H-BEA and NH_4-BEA zeolites with SiO_2/Al_2O_3 ratios ranging from 400 to 740 were stable even at 1373 K, whereas H-BEA with $SiO_2/Al_2O_3 = 30$ was stable only up to 1173 K and became amorphous when calcined at 1373 K. After calcination at 1373 K, Na-BEA with $SiO_2/Al_2O_3 = 400$ and 730 were transformed to tridymite (dense phase) whereas that with $SiO_2/Al_2O_3 = 30$ became amorphous. The elimination of Na^+ ions is necessary to have a BEA remain stable above 1173 K.

Keywords: Zeolite BEA (beta); Dry gel conversion; High silica zeolite; Crystallization; Interaction of TEA^+ ions with zeolite; Thermal stability

1. Introduction

Zeolites are mostly synthesized by hydrothermal crystallization methods at autogenous pressure. Numerous types of aluminosilicate, metallosilicate and aluminophosphate molecular sieves have been prepared by this method [1]. Each zeolite has a definite structure and a unique pore size and most of them have limitations on their chemical compositions. Some zeolites can be synthesized by using a specific structure-directing agent and some by using two or more kinds of structure-directing agents. Recently, new crystallization methods [2–7] have been developed in order to reduce the consumption of structure-directing agents employed and to prepare zeolites in convenient forms such as membranes. We have recently shown that a new crystallization method, the dry gel conversion technique, is useful for the synthesis of BEA with SiO_2/Al_2O_3 ratios ranging from 30 to infinity. In this method, BEA was crystallized from dry gels containing tetraethylammonium hydroxide (TEAOH) as a structure-directing agent [6,8–10]. This method has the following advantages

* Corresponding author. Tel./fax: (+81) 3 5286 3203; e-mail: mmatsu@mn.waseda.ac.jp

1387-1811/98/$19.00
PII: S1387-1811(98)00033-X

over the hydrothermal crystallization method: preparation of zeolites in convenient forms such as membranes [8]; possible development of new structures [10]; reduction of limitations on chemical compositions [8–10]; improvement in catalytic activity [11]; reduction in template concentration [8,9].

In this study, BEA was synthesized from gels having different compositions at 413 K and at 453 K by the dry gel conversion method. The crystallization behavior of BEA, including the interaction of TEA^+ ions with the framework and their sorption properties, and thermal stabilities were investigated.

2. Experimental

Table 1 describes the compositions of gels for the samples BEA-30-1, BEA-400-1, BEA-730-1, BEA-400-2, BEA-730-2, BEA-400-3 and BEA-730-3, where figures in the middle represent SiO_2/Al_2O_3 ratios of the parent gel and those on the right represent run number. Dry gels, having the compositions given in Table 1, were prepared by mixing 0.8 ml of NaOH (4 M aqueous solution, Wako Pure Chem.; 2.05 ml in the case of BEA-730-2) and 13.7 g of TEAOH (20% aqueous solution, Wako Pure Chem.) with 10 g of colloidal silica (30.3% SiO_2, 0.42% Na_2O and 700 ppm of Al_2O_3, Nissan Chem.) while stirring at room temperature. After 30 min, a desired amount of aluminum sulfate dissolved in deionized water was added to the mixture and the resultant gel was aged for about 2 h. For the gels of BEA-730-1, BEA-400-2 and BEA-730-3, 0.005 mol of $NaHSO_4$ was added after aging the gel for 1 h. Finally, the gel was heated to 353 K and dried for all cases. The resultant dry gel was crushed to powder and placed in a special autoclave of 100 ml volume containing 1 ml of water at its bottom as a source of steam. The dry gels for BEA-400-3 and BEA-730-3 were crystallized in steam at 413 K for 60 h and those for other samples were crystallized at 453 K for 3 to 12 h at autogenous pressures. The products were calcined in air between 723 and 823 K for 12 h to remove organic material. They were treated with a 1 M NH_4NO_3 solution at 333 K for 3 h, filtered and washed with deionized water. This procedure was repeated twice for each sample. The samples were dried at 388 K for 12 h and subsequently calcined at 723 K for 12 h to get the H-form of BEA.

X-ray diffraction patterns were recorded on Rigaku RAD-1C instrument with Cu Kα radiation. The chemical analysis of the products was carried out by ICP (ICAP 575 II). Field emission scanning electron microscope (FE-SEM) images

Table 1
Chemical compositions

Sample	Chemical composition/molar ratio							
	Gel				As-synthesized form		H-form	
	SiO_2/Al_2O_3	Na_2O/Al_2O_3 [a]	TEA_2O/SiO_2	OH/SiO_2 [b]	SiO_2/Al_2O_3	Na_2O/Al_2O_3	SiO_2/Al_2O_3	Na_2O/Al_2O_3
BEA-30-1[c]	30	1.39	0.185	0.434	30	0.034	34	0.012
BEA-400-1[c]	400	18.4	0.185	0.434	400	1.72	387	0.050
BEA-730-1[c]	730	70.0	0.190	0.444	730	1.31	782	0.127
BEA-400-2[c]	400	37.2	0.185	0.434	404	1.21	377	0.040
BEA-730-2[c]	730	68.6	0.190	0.540	682	1.38	653	0.080
BEA-400-3[d]	400	18.4	0.185	0.434	398	1.32	—	—
BEA-730-3[d]	730	70.0	0.190	0.444	740	2.56	—	—

[a] $Na_2O/Al_2O_3 = ([Na_2O \text{ from colloidal silica}] + 0.5 \times [NaOH] + 0.5 \times [NaHSO_4])/([Al_2O_3 \text{ from colloidal silica}] + [Al_2(SO_4)_3])$; [] = concentration in moles.
[b] $OH/SiO_2 = ([NaOH] + [TEAOH])/[SiO_2]$; [] = concentration in moles.
[c] Crystallization at 453 K.
[d] Crystallization at 413 K.

were taken using Hitachi (S-4500S) FE-SEM apparatus.

Temperature-programmed desorption mass spectrometry (TPD-MS) experiments were performed by heating about 50 mg of an as-synthesized zeolite sample in a specially designed cell for the TPD-MS instrument (Bell Company Inc.) in a stream of He (50 ml min^{-1}). The sample was heated to 423 K at a rate of 10 K min^{-1} in a stream of He and kept for 1 h at 423 K under the flowing carrier gas. Then the sample were evacuated for 10 min and heated to 1023 or 1173 K at a rate of 10 K min^{-1}. The relative concentrations of the following molecules were measured by mass spectrometer (TPD-MS) during heating: H_2, NH_3, C_2H_4, $EtNH_2$, C_3^+, Et_2NH and Et_3N.

Thermogravimetric differential thermal analysis (TG-DTA) experiments were performed with a Shimadzu DTG-50/50H thermogravimetric analyzer in a stream of N_2. The heating rate was the same as that used for TPD-MS experiments.

As-synthesized samples were treated between 473 and 673 K in vacuum and their sorption properties were compared with those of the calcined samples. Surface areas (BET method) and micropore volumes (t-method) of BEA were determined using an AUTOSORB-3B gas sorption analyzer (Quantachrome Corp.). Care was taken to ensure that samples were outgassed prior to their analyses at conditions that did not alter their original structure.

Thermal stabilities were tested by calcining about 100 mg of H-BEA at 973, 1173 and 1373 K with a heating rate of 3 K min^{-1} and the sample was kept at the final temperature for 2 h.

3. Results and discussion

3.1. Crystallization

Fig. 1 shows the X-ray diffraction patterns of the products with SiO_2/Al_2O_3 ratios of 30, 400 and 730 (BEA-30-1, BEA-400-1 and BEA-730-1 respectively) crystallized at 453 K and the product with $SiO_2/Al_2O_3 = 740$ (BEA-730-3) crystallized at 413 K. The crystallization of the gel (BEA-30-1) with composition $SiO_2 : 0.033\ Al_2O_3 : 0.042\ Na_2O$:0.37 TEAOH occurred very rapidly at 453 K and completed within 3 h to give a highly crystalline BEA with $SiO_2/Al_2O_3 = 30$, as previously reported [8]. When the Al concentration was decreased to 0.0013 mol of Al_2O_3 per mole of SiO_2 ($SiO_2/Al_2O_3 = 730$) its crystallization took longer than 12 h to complete. The relative crystallinity of this product remained at about 75% after 12 h of crystallization (not shown in the figure) and prolonged crystallization resulted in the appearance of other phases. Relative crystallinity was evaluated from the intensity of the most intense (302) reflection peak, which appears at $2\theta = 22.4°$. However, the addition of 0.005 mol of $NaHSO_4$ or NaOH to the parent gel consisting of 0.05 mol of SiO_2 to make a gel (BEA-730-1) having a composition $SiO_2 : 0.0013\ Al_2O_3 : 0.093\ Na_2O : 0.37$ TEAOH increased the relative crystallinity of the product to 100% after 12 h of crystallization. In our previous study [8], we found that a higher Na concentration in high silica gels promoted the formation of BEA rather than MTW. Our previous experiments on all-silica BEA also showed that higher Na concentrations are

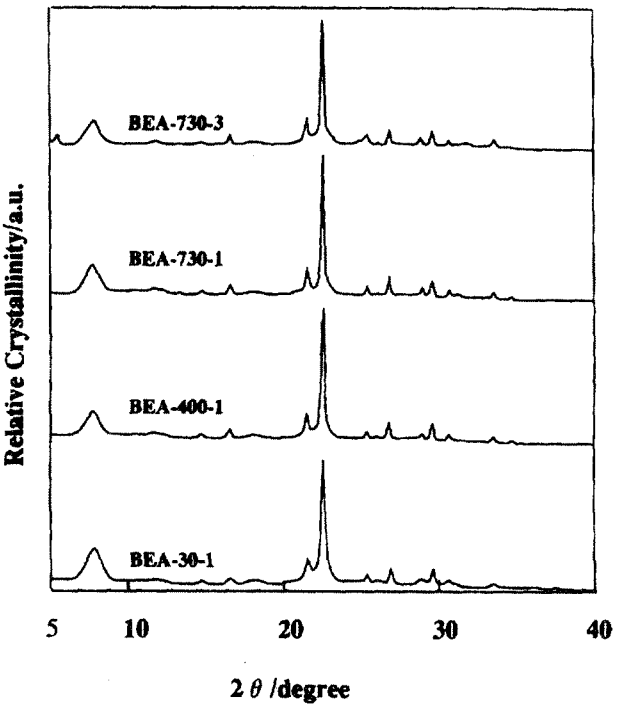

Fig. 1. X-ray diffraction patterns of as-synthesized BEA.

required to crystallize silicious gels [10]. Gopper et al. [12] have reported similar observations on the synthesis of all-silica MTW.

Table 1 lists the chemical compositions of the products. The gel for BEA-730-2, which had a higher OH^- ion concentration ($OH^-/SiO_2=0.54$) compared with that for BEA-730-1 ($OH^-/SiO_2=0.44$), gave a product with $SiO_2/Al_2O_3=682$. This SiO_2/Al_2O_3 ratio is lower than that of BEA-730-1 (SiO_2/Al_2O_3 of the product was 730). It is interesting to note that, in spite of having an excess amount Na ($Na_2O/Al_2O_3=1.39$) in the gel for BEA-30-1, the product retained only a negligible amount of Na ($Na_2O/Al_2O_3=0.034$), indicating that in the product most of the $Al-O^-$ groups were compensated by TEA^+ ions. However, the products of BEA-400-1 and BEA-730-1 retained excess amounts of Na compared with the amounts of Al ions ($Na_2O/Al_2O_3=1.72$ and 1.31 respectively).

We found that high silica BEA could be crystallized at a lower temperature of 413 K, though a longer crystallization time was required. Crystallization of the gels for BEA-400-3 and BEA-730-3 at 413 K for 60 h produced BEA with $SiO_2/Al_2O_3=398$ and 740 respectively. SiO_2/Al_2O_3 ratios of these products were comparable with those of BEA-400-1 and BEA-730-1 crystallized at 453 K ($SiO_2/Al_2O_3=400$ and 730 respectively). BEA-400-3 and BEA-730-3 crystallized at 413 K also retained excess amounts of Na compared with the amounts of Al ions found in the cases of BEA-400-1 and BEA-730-1 crystallized at 453 K. As shown in Fig. 1, the as-synthesized BEA-730-3 showed an additional reflection peak at around $2\theta=5.6°$. This, however, disappeared after calcination at 723 K. We have also observed the appearance of this peak in all-silica BEA [8,10] and BEA-400-3.

Fig. 2 shows the FE-SEM images for the products of BEA-30-1, BEA-400-1, BEA-730-1, BEA-730-2 and BEA-730-3. The particle sizes of the products BEA-30-1, BEA-400-1 and BEA-730-1 are about 60 nm, 250 nm and 400 nm respectively. This shows that the particle size increased with increasing SiO_2/Al_2O_3 ratio. The product of BEA-730-2 ($SiO_2/Al_2O_3=682$) has a particle size (550 nm) larger than that of

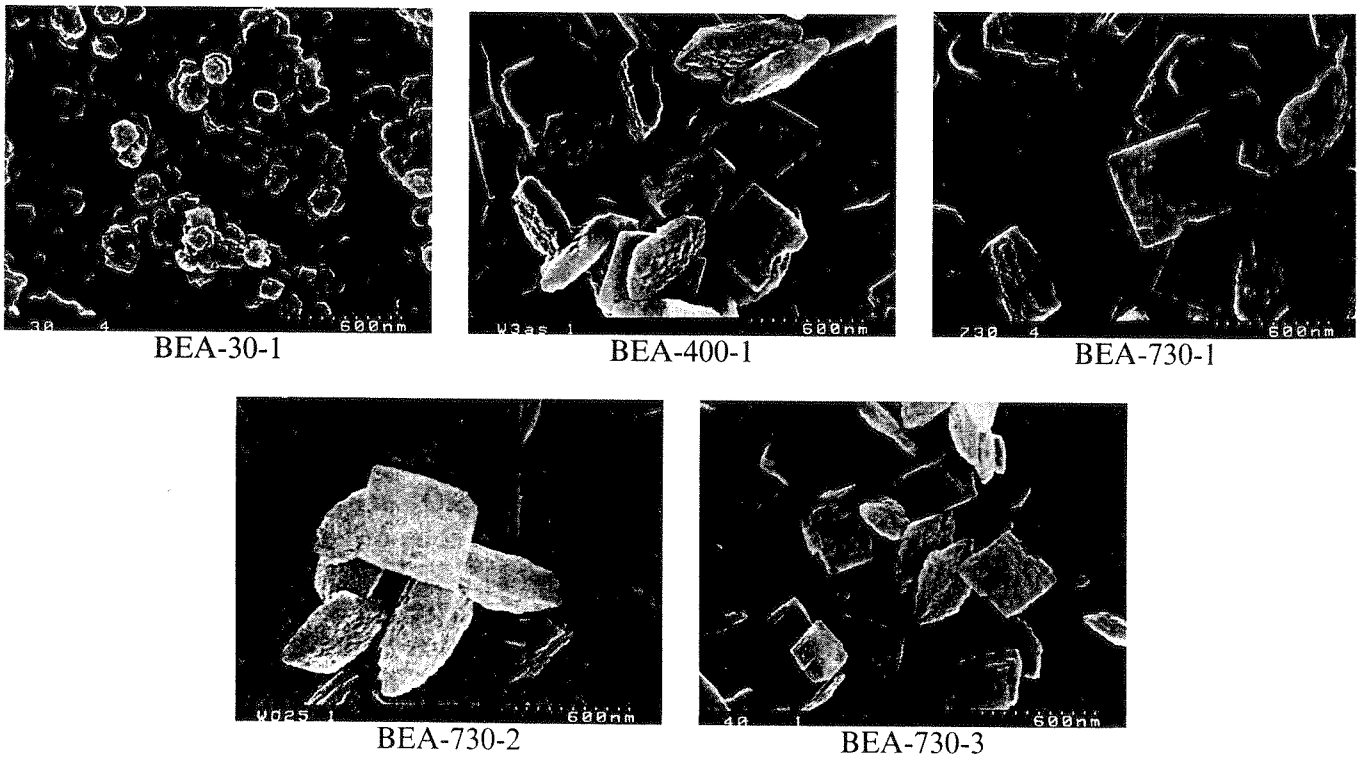

Fig. 2. FE-SEM images for BEA crystallized from gels having different compositions and at different temperatures.

BEA-730-1 ($SiO_2/Al_2O_3=730$, 400 nm). This may be due to the OH^- ion concentration of the gel for BEA-730-2 ($OH^-/SiO_2=0.53$) being higher than that for BEA-730-2 ($OH^-/SiO_2=0.44$). With increasing SiO_2/Al_2O_3 ratio, as well as OH^-/SiO_2 ratio, the number of nuclei formed may be reduced, resulting in an increase in particle size. The particle size of the product of BEA-730-3 crystallized at 413 K is about 300 nm and is about 100 nm smaller than that of BEA-730-1 crystallized at 453 K. This shows that crystallization at lower temperatures produces smaller particles.

Fig. 3 shows the thermal decomposition spectra of TEA^+ ions occluded in as-synthesized BEA-730-1 and BEA-30-1 in a stream of He. In BEA-730-1, which has $SiO_2/Al_2O_3=730$, most of the occluded TEA^+ ions decomposed and were eliminated between 473 and 673 K. Major decomposition products at this temperature included $EtNH_2$ and C_2H_4. H_2, NH_3 and C_3^+ hydrocarbons were also evolved as minor products. Lami et al. [13] have reported a mechanism for the decomposition of TEA^+ ions in BEA with SiO_2/Al_2O_3 ratios of 27.6–55 when BEA was treated in Ar and air. They proposed degradation of TEA^+ ions via Hofmann elimination:

$$(C_2H_5)_4N^+X^- \rightarrow C_2H_4+(C_2H_5)_3N+XH$$

where X^- can be $S-O^-$ or $Al-O^-$; the formation of amines occurs by successive β elimination:

$$(C_2H_5)_3N \rightarrow C_2H_4+(C_2H_5)2NH$$

$$(C_2H_5)_2NH \rightarrow C_2H_4+(C_2H_5)NH_2$$

$$(C_2H_5)NH_2 \rightarrow C_2H_4+NH_3$$

Most of the products observed in the decomposition spectra are explained by these successive eliminations of C_2H_4. Ethylene was the only product eliminated between 673 and 823 K. The absence of evolution of other products along with ethylene between 673 and 823 K suggests that C_2H_4 formed during the decomposition of TEA^+ ions at around 573 K might have been readsorbed. The TEA^+ ion decomposition pattern for as-synthesized BEA-730-3 ($SiO_2/Al_2O_3=740$) crystallized at 413 K is similar to that of BEA-730-1.

We have observed a different decomposition spectra for the product with a lower SiO_2/Al_2O_3 ratio (see Fig. 3). The TEA^+ decomposition pattern of as-synthesized BEA-30-1 ($SiO_2/Al_2O_3=30$) showed the evolution of various TEA^+ decomposition fragments between 473 and 673 K and between 673 and 798 K. The decomposition products between 473 and 673 K were similar to those for BEA-730-1, although the intensities of these evolved products were smaller. Between 673 and 798 K the decomposition products of TEA^+ ions include mainly C_2H_4, NH_3 and H_2. It can be seen from Fig. 3 (BEA-30-1)

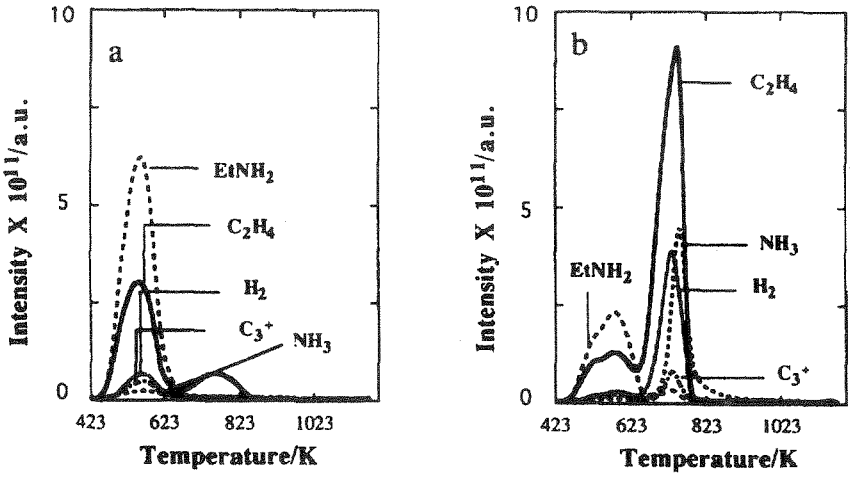

Fig. 3. Thermal decomposition spectra (TPD-MS) of TEA^+ ions occluded in as-synthesized BEA-730-1 (a) and BEA-30-1 (b) in a stream of He.

that NH_3 was desorbed at a slightly higher temperature than were C_2H_4 and H_2, suggesting that it was adsorbed on acid sites and then desorbed. Hydrogen was another major product; its formation was accompanied by C_2H_4. We observed that hydrogen was also formed from the decomposition of TEA^+ ions in amorphous gel (not shown in the figure), suggesting that H_2 might form during the decomposition of TEA^+ ions. BEA-30-1 remained black, even after treating at 1173 K in He, indicating the presence of carbonaceous materials. However, BEA-400-1 and BEA-730-1 ($SiO_2/Al_2O_3=400$ and 730 respectively) became white after treating them in a flow of He at 1023 K.

The elimination pattern of TEA^+ ions from BEA with $SiO_2/Al_2O_3=400$ was similar to that from BEA with $SiO_2/Al_2O_3=730$ (not shown in the figure). The desorption of readsorbed C_2H_4 occurred at a temperature slightly lower than that from BEA with $SiO_2/Al_2O_3=730$, but still higher than that from BEA with $SiO_2/Al_2O_3=30$.

Judging from the results described above, we concluded that the decomposition products between 473 and 673 K probably evolved through the decomposition of TEA^+ ions interacting with $Si-O^-$ and those between 673 and 798 K evolved through the decomposition of TEA^+ ions interacting with $Al-O^-$. As the interaction between TEA^+ ions and $Al-O^-$ seems to be stronger than that between TEA^+ ions and $Si-O^-$, a higher temperature is presumably required to decompose TEA^+ ions associated with $Al-O^-$. BEA-730-1 had fewer $Al-O^-$ groups because of the high SiO_2/Al_2O_3 ratio ($SiO_2/Al_2O_3=730$) and an Na_2O/Al_2O_3 ratio of 1.31, suggesting the absence of free $Al-O^-$ groups to interact with TEA^- ions. Hence, we concluded that in BEA-730-1 most of the TEA^+ ions interacted with $Si-O^-$ groups and decomposed between 473 and 673 K. In contrast, the as-synthesized form of BEA-30-1 had an Na_2O/Al_2O_3 ratio of 0.034, indicating the presence of free $Al-O^-$ groups. Therefore, in BEA-30-1 the TEA^+ ions interacted with these free $Al-O^-$ groups and gave decomposition peaks between 673 and 798 K. The appearance of decomposition peaks at 473–673 K for BEA-30-1 inferred that some TEA^+ ions still interacted with $Si-O^-$.

Fig. 4 shows the differential thermogravimetry

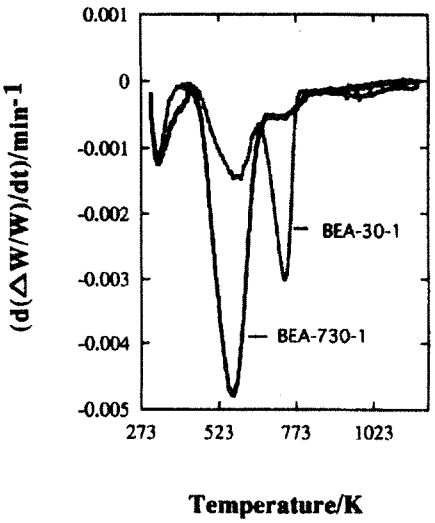

Fig. 4. DTG patterns of TEA^+ ions occluded in as-synthesized BEA-30-1 and BEA-730-1 in a stream of N_2.

(DTG) patterns of BEA-30-1 and BEA-730-1 in a stream of N_2. The DTG pattern for BEA-730-1 showed two major peaks for weight loss. The first peak between 300 and 423 K may be due to the loss of water, and the most intense peak between 423 and 673 K indicates the elimination of most of the TEA^+ ions. A minor peak appearing between 673 and 798 K may be due to the elimination of the readsorbed materials, such as C_2H_4, NH_3 and other molecules undetected by TPD-MS. The DTG pattern for BEA-30-1 showed three major peaks for weight loss. As with the case of BEA-730-1, the first peak between 423 and 673 K may be due to the loss of water, whereas the second and third peaks at 423–673 K and 673–798 K could be due to the elimination of TEA ions associated with $Si-O^-$ and $Al-O^-$. The DTG pattern for BEA-730-3 ($SiO_2/Al_2O_3=740$, crystallized at 413 K) was similar to that for BEA-730-1 crystallized at 453 K.

The TEA^+ ion decomposition patterns and the DTG patterns clearly confirm that TEA^+ ions in BEA with $SiO_2/Al_2O_3=730$ can be eliminated at a lower temperature than those in BEA with $SiO_2/Al_2O_3=30$.

3.2. Sorption properties and thermal stability

Table 2 compares the results of nitrogen sorption measurements at 77 K for the samples treated

Table 2
Surface area and micropore volume of BEA

SiO_2/Al_2O_3	BET surface area/$m^2\,g^{-1}$									
	Vacuum treatment temperature/K			Air calcination temperature/K						
	473	573	673	473	573	723	823	973	1173	1373
BEA-30-1	—	538 (0.15)	765 (0.023)	198 (0.014)	483 (0.11)	—	770 (0.27)			
H-BEA-30-1	—					726		716	618	—
BEA-400-1	529 (0.16)	724 (0.27)	—	175 (0.021)	597 (0.17)	730 (0.34)	—			
BEA-730-1	467 (0.17)	734 (0.31)	—	146 (0.023)	613 (0.17)	633 (0.29)	—			
H-BEA-730-1						631		674	656	587

Values in parentheses indicate micropore volume/$cm^3\,g^{-1}$.

in air at 473–823 K (as-synthesized form), 723–1373 K (H-form) and in vacuum at 473–673 K (as-synthesized form). The sample with $SiO_2/Al_2O_3=30$ after pretreatment in vacuum at 673 K showed a BET surface area of 765 $m^2\,g^{-1}$, which is similar to that of the sample calcined in air at 823 K (770 $m^2\,g^{-1}$). It should be noted that this sample appeared black even after the treatment in vacuum at 673 K, indicating the presence of carbonaceous materials which might have formed by the interaction between decomposition products of TEA^+ ions and acid sites. However, such carbonaceous materials did not block the micropores of BEA. For this sample, a pretreatment temperature of 573 K in vacuum was insufficient to decompose TEA^+ ions present in the zeolite pores, as indicated by its lower BET surface area: 538 $m^2\,g^{-1}$. For BEA with $SiO_2/Al_2O_3=400$ and 730, the heat treatment in vacuum at 573 K gave almost the same results as the calcination in air at 723 K, clearly indicating that the TEA^+ ions occluded in the micropores of these as-synthesized high silica BEA can be decomposed and removed without oxidants. When these samples (BEA with $SiO_2/Al_2O_3=400$ and 730) were calcined in air at 723 K, the occluded materials were completely removed and they had high BET surface areas (730 $m^2\,g^{-1}$ and 633 $m^2\,g^{-1}$ respectively). For the sample with $SiO_2/Al_2O_3=730$ the calcination in air at 723 K led to a decrease in its surface area, which may indicate the loss of crystallinity. However, this sample remained stable even after calcination at 823 K and, after transforming to the H-form, remained stable even at 1373 K. These experiments clearly indicate that an oxidant is necessary to eliminate TEA^+ ions from BEA with $SiO_2/Al_2O_3=30$, whereas such an oxidant is not necessary for the samples with $SiO_2/Al_2O_3=400$ and 730.

Fig. 5 shows the X-ray diffraction patterns for H-BEA with $SiO_2/Al_2O_3=782$ (H-BEA-730-1) calcined at temperatures between 723 and 1373 K. It can be seen that H-BEA-730-1 is stable even after calcination at 1373 K. With increasing calcination temperature from 723 to 973 K, the intensity of the peak appearing at a lower angle, i.e. $2\theta=7.5°$, increased, whereas the peaks appearing at $2\theta\approx22°$ remain unchanged. As shown in Table 2, this was accompanied by a small increase in BET surface area from 631 to 674 $m^2\,g^{-1}$. The X-ray diffraction patterns for the samples calcined at 973 and 1173 K have the same intensities for all reflection peaks, indicating that no change in the structure has occurred at these temperatures. When the calcination temperature was further raised to 1373 K, a small decrease in the intensity of the peaks at $2\theta\approx22°$ was observed, with no change in the intensity of peak at $2\theta\approx7.5°$. This was accompanied by a decrease in the surface area from 656 to 587 $m^2\,g^{-1}$, indicating a small reduction in the degree of crystallinity. The H-form samples of BEA-400-1, BEA-400-2 and BEA-730-2

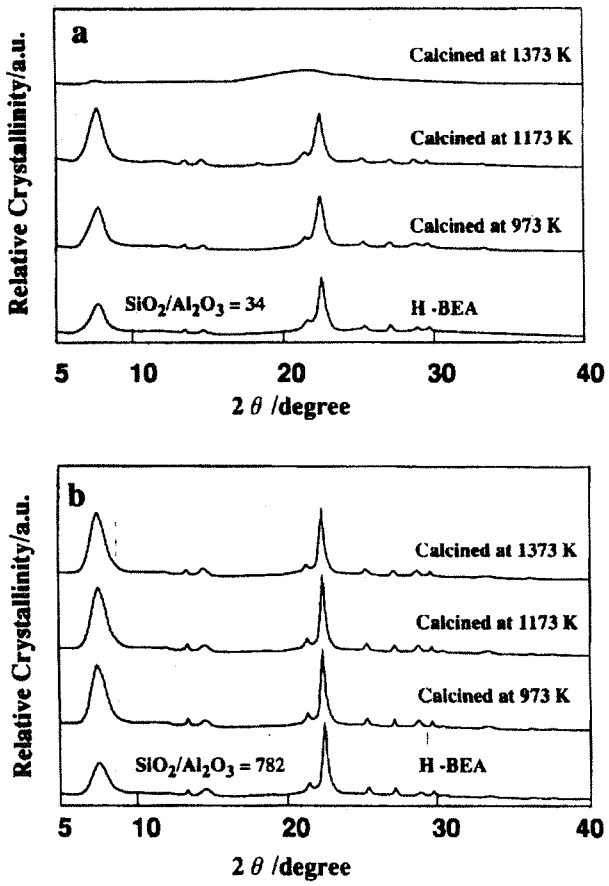

Fig. 5. X-ray diffraction pattern of H-forms of BEA-30-1 (a) and BEA-730-1 (b) calcined at different temperatures (indicated in the figure).

crystallized from the gels having different Na^+, OH^- and SO_4^{2+} ion concentrations and BEA-730-3 crystallized at 413 K were also stable at 1373 K. This shows that Na^+, OH^- and SO_4^{2+} ion concentrations in the gel and crystallization temperature do effect the thermal stability of the product.

In contrast, H-BEA with $SiO_2/Al_2O_3 = 34$ (H-BEA-30-1) lost its crystallinity and became amorphous when calcined at 1373 K in air, though it was stable at 1173 K. Compared with H-BEA-730-1, the Al content of H-BEA-30-1 is 23 times greater and that of H-BEA-400-1 is twice as great. Thus, Al possibly reduces the thermal stability of zeolite BEA. Na-BEA-30-1, when calcined in air at 1373 K, gave amorphous material, whereas Na-BEA-400-1 and Na-BEA-730-1 formed a dense phase, namely tridymite. This is not surprising, since it is known that Na cleaves Si–O–Si bonds and promotes the formation of dense phases.

4. Conclusions

Zeolite BEA with $SiO_2/Al_2O_3 = 30$ to 740 were crystallized by dry gel conversion. Temperatures in the range 413–453 K can be employed for the crystallization of BEA in this method. The particle size of BEA increased with increasing SiO_2/Al_2O_3 ratio as well as with increasing crystallization temperature. In a stream of He, the TEA^+ ions presumably interacting with $Si–O^-$ were decomposed at around 573 K and those interacting with $Al–O^-$ decomposed at around 743 K. Sorption studies confirmed that the TEA^+ ions occluded in BEA with $SiO_2/Al_2O_3 = 400$ and 730 can be eliminated by evacuation at 573 K. Zeolite H-BEA with $SiO_2/Al_2O_3 = 387$ and 782 are stable even at 1373 K and have higher thermal stabilities than those with $SiO_2/Al_2O_3 = 34$. The elimination of Na from the BEA structure improves the thermal stability of BEA. BEA crystallized at 413 K and at 453 K has similar thermal stabilities.

Acknowledgement

This study was partially supported by Grant-in-Aid for Scientific Reasearch (No. 09750839, 09555247), from the Ministry of Education, Science, Sports and Culture. PR thanks the Japan Society for the Promotion of Science for a post-doctoral fellowship. PR, KU and MM express their appreciation to Yuasa Ionics Co. for their assistance with the gas sorption study.

References

[1] R. Szostak, Handbook of Molecular Sieves, Van Nostrand Reinhold, New York, 1992.
[2] W. Xu, J. Dong, J. Li, F. Wu, J. Chem. Soc. Chem. Commun. (1990) 755.
[3] M.H. Kim, H.X. Li, M.E. Davis, Micropor. Mater. 1 (1993) 191.

[4] M. Matsukata, N. Nishiyama, K. Ueyama, Micropor. Mater. 1 (1993) 219.
[5] N. Nishiyama, M. Matsukata, K. Ueyama, J. Chem. Soc. Chem. Commun. (1995) 1967.
[6] P.R. Hari Prasad Rao, M. Matsukata, Chem. Commun. (1996) 1441.
[7] U. Deforth, K. Unger, F. Schuth, Micropor. Mater. 9 (1997) 287.
[8] P.R. Hari Prasad Rao, K. Ueyama, M. Matsukata, Appl. Catal. A: 166 (1998) 97.
[9] P.R. Hari Prasad Rao, M. Matsukata, Proc. 7th Asian Chem. Cong., Hiroshima, Japan, May 16–20, 1997, p. 567.
[10] P.R. Hari Prasad Rao, K. Ueyama E. Kikuchi, M. Matsukata, submitted to Chem. Lett.
[11] T. Tatsumi, Q. Xia, N. Jappar, Chem. Lett. (1997), 677.
[12] M. Gopper, H.X. Li, M.E. Davis, J. Chem. Soc. Chem. Commun. (1992) 1665.
[13] E.B. Lami, F.D. Renzo, F. Fajula, P.H. Mutin, T.D. Courieres, J. Phys. Chem. 96 (1992) 3807.

SYNTHESIS OF PURE SILICA BETA AND Al-FREE Ti-BETA USING TEAOH AND THEIR CHARACTERIZATION

P. R. HARI PRASAD RAO[1], K. UEYAMA[1], E. KIKUCHI[2] and M. MATSUKATA[2]

[1]Department of Chemical Engineering, Osaka University, Toyonaka, Osaka, Japan.
[2]Department of Applied Chemistry, Waseda University, Tokyo, Japan;
mmatsu@mn.waseda.ac.jp

ABSTRACT :

Pure silica Beta and Al-free Ti-Beta were crystallized using tetraethylammonium hydroxide (TEAOH) as a structure-directing agent by dry gel conversion technique. A higher concentration of Na ion in the gel promoted the formation and stabilization of Beta phase during crystallization. Pure silica Beta crystallized at higher temperatures (at 433 K for 24 h and then at 453 K for 12 h) was thermally stable even at 1173 K and lost its crystallinity partially at 1373 K. Presence of impure phases reduces the thermal stability of Beta. Under similar crystallization conditions, Ti-Beta was successfully obtained even in the absence of Al. The incorporation of Ti into the framework of Beta was suggested by the appearance of an intense band at 960 cm^{-1} in the IR spectra and at 205-225 nm in the UV-VIS spectra for the sample that was treated with aqueous NH_4NO_3 solution after calcination and recalcined at 773 K.

INTRODUCTION

Pure silica and high silica large pore zeolites with high thermal stabilities are of interest, specially for high temperature applications such as gas clean up and separation processes, since they have less acidity so that less coke formation is anticipated. Incorporation of Ti into these structures imparts them oxidation activity for various organic intermediates. Hydrothermal synthesis of zeolite Beta with SiO_2/Al_2O_3 ratios = 10 - 250 were reported using TEAOH, TEAOH-diethanolamine, TEABr-NH_3 and TEAOH-TEABr-triethanolamine. van der Waal *et al.* (1) and Camblor *et al.* (2) have reported the formation of pure silica Beta using dibenzyldimethyl ammonium cation and TEAOH-HF, respectively. Several reports have appeared on the synthesis and catalytic activity of Ti-Beta (3,4). We have recently reported a new crystallization method, Dry Gel Conversion Technique, and shown the crystallization of zeolite Beta from dry gels containing TEAOH as a structure-directing agent (5-7). In the present study, the crystallization of pure silica Beta and Al-free Ti-Beta from dry gels containing TEAOH and their characterization were performed. We also compare thermal stability of Beta with different compositions.

EXPERIMENTAL

Pure silica Beta and Al-free Ti-Beta were prepared from dry gels having compositions given in Table 1. These gels were prepared, typically by mixing 1.5 g of fumed silica, 15 ml of

12th International Zeolite Conference

deionized water, a required amount of NaOH (4M aqueous solution, Wako Pure Chem.) and TEAOH (20 % in water, Wako Pure Chem.). A solution containing 1 ml of H_2O, 1 ml of H_2O_2 and 0.17 g of $Ti(OC_4H_9)_4$ was added after aging for 2 h while stirring for the case of sample C. The mixture was heated to 353 K after stirring for 2 h and dried while stirring. When the gel became viscous, it was stirred using a teflon rod till it became a dry gel. The dry gel was crushed to powder and placed in a special autoclave where water as a source of steam was poured at the bottom. Crystallization of samples A and D was carried out at 433 K for 24 h and then at 453 K for 12 h and that of samples B and C was carried out at 413 K for 168 h. Beta samples E and F with SiO_2/Al_2O_3 ratio = 400 were prepared as reported elsewhere (6,7).

X-ray diffraction patterns were recorded on Rigaku Miniflex instrument with Cu K α radiation. Field Emission SEM images were taken with a Hitachi (S-4500S) FE-SEM apparatus. Thermal stabilities were tested by calcining about 100 mg of H-Beta (calcined Beta after treating with NH_4NO_3 solution to remove Na^+ ions present at silanol sites) at 1173 -1523 K with a heating rate of 3 K min^{-1} and the sample was kept at the final temperature for 2 h.

Sample	Gel Composition				Cryst. Temp. /K and Time	Product	Rel. Crystal-linity/%
	Si/Ti	SiO_2/Al_2O_3	Na_2O/SiO_2	TEA_2O/SiO_2			
A	-	-	0.160	0.185	433 (24 h) & 453 (12 h)	Beta	70
B	-	-	0.096	0.220	413 (168 h)	Beta	80
C	50	-	0.096	0.220	413 (168 h)	Ti-Beta	80
D	-	-	0.160	0.220	433 (24 h) & 453 (12 h)	Beta (90%) + MFI (10%)	60
E	-	400	0.042	0.185	453 (12 h)	Beta	100
F	-	400	0.042	0.185	453 (36 h)	Beta (92%) + 8% OU-1	80

Table 1: Effect of gel compositions on the crystallization of Beta.

RESULTS AND DISCUSSION

Pure silica Beta

Figure 1 shows the X-ray diffraction patterns of as-synthesized pure silica products A and B. The X-ray diffraction patterns show relatively high crystallinity of the products. The relative crystallinity of sample A crystallized at 433 K for 24 h and then at 453 for 12 h is slightly lower than that of B crystallized at 413 K for 168 h. As shown in Fig. 1, the as-synthesized sample B showed a minor additional reflection peak at around $2\theta = 5.6°$. This peak

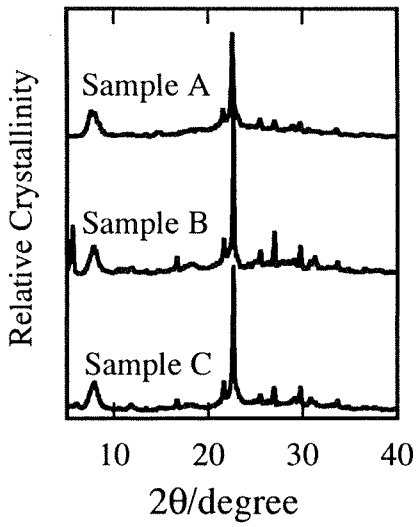

Figure 1. XRD patterns of as-synthesized pure silica Beta and Al-free Ti-Beta.

disappeared after treating the sample at temperatures above 453 K. A similar peak also appeared in Al-containing Beta crystallized at 413 K (6,7). Such an additional peak did not appear in sample A. When the samples A and B were crystallized only at 453 K, the product remained amorphous. However, when Al was introduced into these gels and crystallized at 453 K, highly crystalline Beta was produced.

Using the synthesis conditions used for sample A, pure silica Beta was successfully synthesized from the gels having molar ratios SiO_2: 0.15-2.0 Na_2O: 0.16-0.22 TEA_2O, though the composition SiO_2: 0.16 Na_2O: 0.185 TEA_2O is more suitable. A further increase in the concentration of either structure-directing agent or NaOH makes it difficult to obtain fine dry gel and that leads to the appearance of other phases such as MFI, along with Beta. Similarly when the crystallization was prolonged, the product contained impure phases such as MFI and MTW. When the crystallization of gel having same composition as that of sample B was carried out at 433 K for 24 h and then at 453 K for 12 h, the product was a mixture of MFI, Beta and MTW phases. In our previous study (8), we showed that high silica Beta transforms to other phases such as MTW and OU-1 depending on the gel composition during crystallization. The gel with SiO_2/Al_2O_3 ratio = 380 and Na_2O/SiO_2 ratio = 0.094 formed Beta after 9 h of crystallization and the product was stable even after 48 h of crystallization. The gel with SiO_2/Al_2O_3 ratio = 380 and Na_2O/SiO_2 ratio = 0.014 formed Beta initially and transformed to MTW after 12 h of crystallization, suggesting that such a higher Na ion concentration in the gel stabilized the Beta phase. Similarly, when the crystallization of gel having same composition as that of sample B was carried out at 433 K for 24 h and then at 453 K for 12 h, the product might transform to MFI even before full crystallization. Table 2 compares the chemical compositions and BET surface areas of samples A-C. As-synthesized samples retained a large amount of Na.

However, most of them were eliminated by treating the products with a NH_4NO_3 solution. The Na ions which were retained in the samples even after the treatment with NH_4NO_3 might be present at defect sites as Si-O-Na.

Figure 2 shows the FE-SEM images for the products. The particle sizes of products A and B are about 1.1 and 0.9 μm, respectively. In our previous report (7), we showed that the particle size of Beta increased from 60 to 400 nm, when SiO_2/Al_2O_3 ratio was raised from 30 to 730. A particle size of about 1 μm for pure silica Beta is in accordance with our previous results. The absence of hetero atoms might have reduced the number of nuclei formed leading to the products with larger particle sizes.

Sample	Chemical Composition				BET Surface Area
	As-synthesized		After treating with NH_4NO_3		($m^2.g^{-1}$)
	Si/Ti	Na/Si	Si/Ti	Na/Si	
A	-	0.017	-	0.0015	530
B		0.030	-	0.0022	506
C	41.73	0.052	41.05	0.0002	520

Table 2: Chemical compositions of products.

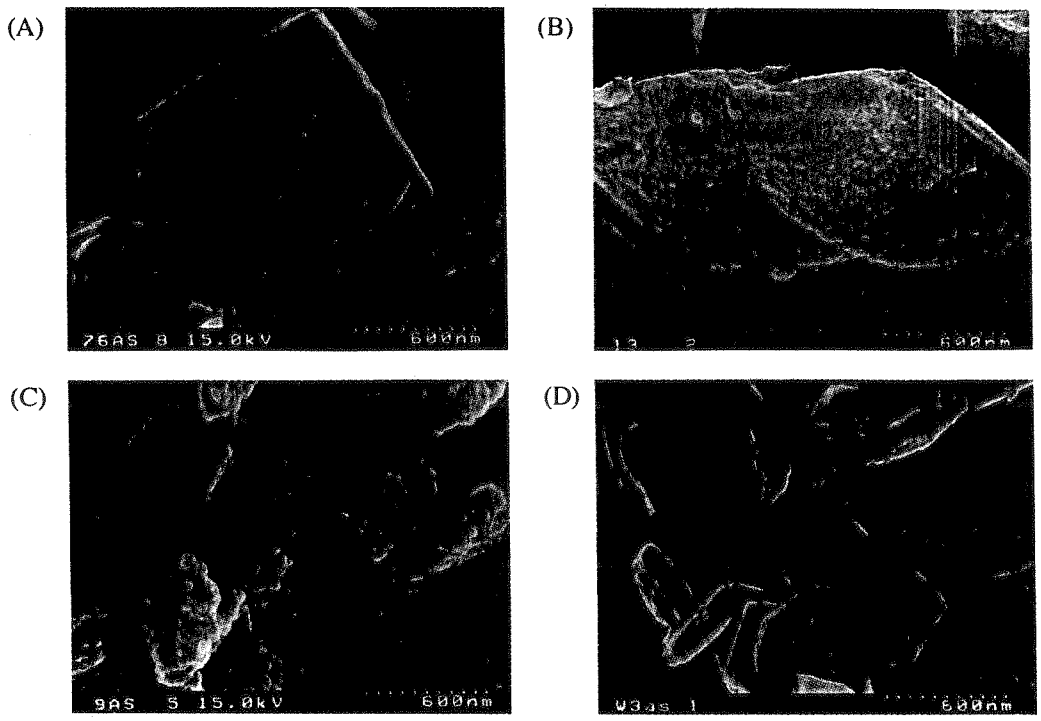

Figure 2. FE-SEM images of obtained Beta.
Pure silica Beta; samples A and B, and Al-free Ti-Beta; C.
Beta having SiO_2/Al_2O_3 molar ratio = 730 was also shown in D.

Figure 3 shows the X-ray diffraction patterns of samples A and B calcined at temperatures between 773 -1373 K. The as-synthesized samples were calcined at 773 K (Na-Beta) and treated with NH_4NO_3 and recalcined (H-Beta) before testing their thermal stability at higher temperatures. Sample A was stable even after calcination at 1173 K. It, however, lost crystallinity partially and a reflection peak at $2\theta = 26.4°$, probably due to crystoballite appearing after calcination at 1373 K. Sample B was thermally less stable and turned to amorphous material after calcination at 1173 K. The high thermal stability of sample A may be due to the presence of fewer defect sites. In our previous report (7) we have shown that Beta with SiO_2/Al_2O_3 ratio = 34 was stable at 1173 but turned to amorphous at 1373 K, and Beta with SiO_2/Al_2O_3 ratio = 782 was stable even at 1373 K. Sample A has higher thermal stability compared to Beta with SiO_2/Al_2O_3 ratio = 34 though being less stable compared to high silica Beta with SiO_2/Al_2O_3 ratio = 782.

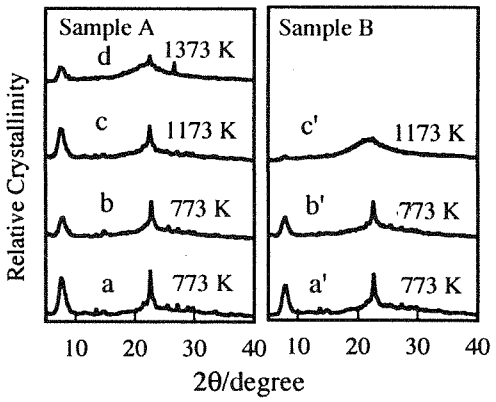

Figure 3. XRD patterns of sample A and B calcined at temperatures indicated in figure. A and a', Na-Beta; b-d and b' and c', H-Beta.

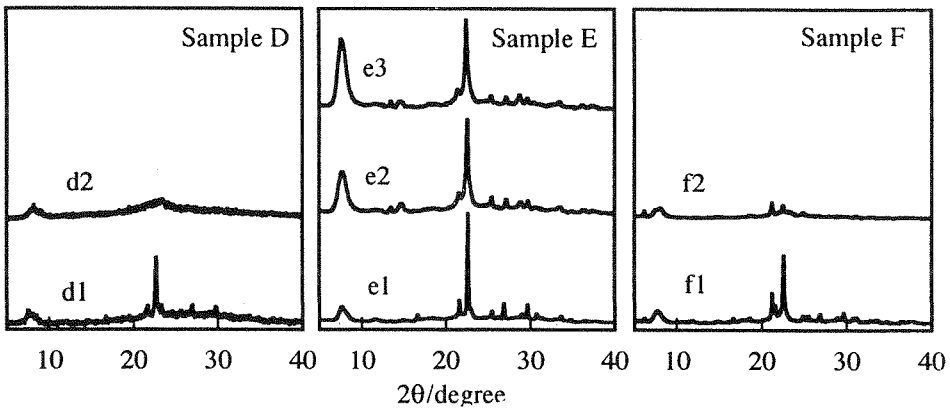

Figure 4. Comparison of thermal stability of samples D, E and F.
D1, e1 and f1, as-synthesized; d2, e2 and f2, calcined at 723 K; e3, calcined at 1373 K.

Figure 4 shows the effect of impure phases on the thermal stability of Beta. Sample D, a pure silica Beta which contained about 10 % of other phases such as MFI, was prepared under similar conditions used for preparation of sample A. This sample is thermally less stable and lost most of its crystallinity even when calcined only at 723 K. This suggests that the presence of impure phases may destabilize the structure of pure silica Beta. In order to confirm the effect of these impurities on the thermal stability Beta, high silica Beta samples E and F with $SiO_2/Al_2O_3 = 400$ were prepared. Samples E is a pure Beta which does not contain any impure phases. Sample F is a Beta containing about 8 % of zeolite OU-1. The sample E was stable after calcination at 773 K and after treating with NH_4NO_3 it was stable even after calcination at 1373 K. Whereas sample F which contains OU-1 impurity lost most of its crystallinity after calcination at 723 K. As a result, we presume that a pure high silica Beta has high thermal stability and the presence of any impure phases reduce its thermal stability.

Ti-Beta

The crystallization method used for preparation of sample B was used to crystallize Al-free Ti-Beta using TEAOH from the gels containing Na^+ ions. Khouw *et al.* (9) showed that the presence of small amounts of alkali (Si/Na = 100) promotes higher incorporation of Ti into zeolite framework and also improves the catalytic activity, and that in the presence of a larger amount of Na^+ ion (Si/Na= 10) Ti precipitates as TiO_2, resulting in difficult incorporation of Ti into the lattice. Recently Tatsumi *et al.* (4) have reported the crystallization of highly active Al-containing Ti-Beta in the presence of Na^+ ions using dry gel conversion method. In our experiments, the precipitation of Ti as TiO_2 was prevented by treating the Ti source with an aqueous H_2O_2 solution before adding to the gel containing Na^+ ions. By this method, the gels remained clear even after containing higher Na^+ ion concentrations (Si/Na= 5) and no precipitation was observed.

As shown in Figure 1c, highly crystalline Ti-Beta was obtained by the crystallization of sample C at 413 K for 168 h. No amorphous material was present after crystallization. The particle sizes of Ti-Beta were about 0.2 μm, suggesting that the presence of Ti in the gels reduced particle size of the products. This also supports that hetero atoms such as Al and Ti increase the number of nuclei formed, leading to smaller particle size of the products. We have not succeeded to prepare Ti-Beta using the gel and crystallization conditions used for the preparation sample A.

Figure 5 shows the IR spectra of Ti-Beta calcined at 773 K (Na-Ti-Beta) and after the treatment of calcined Na-Ti-Beta with NH_4NO_3 and successive recalcination (H-Ti-Beta). H-Ti-Beta showed an intense absorption peak appeared at 960 cm^{-1}, whereas the IR spectra of Na-Ti-Beta showed only a shoulder peak at around 985 cm^{-1}. Khouw *et al.* (9) showed that after treating TS-1 with NaOH the absorption band at 960 cm^{-1} transformed to a shoulder peak at 985 cm^{-1} and reappeared by acid washing. In our experiment due to the presence of Na^+ ions in the

gel, the crystallized product might have contained Na^+ ions at exchangeable positions and hence the shoulder peak possibly appeared in the Na-Ti-Beta. These Na ions were exchangeable with NH_4NO_3 and after the ion exchange the intense absorption peak appeared similar to Ti-MFI prepared in the absence of alkali (9). These results may suggest the presence of Ti at framework positions.

Figure 6 presents the UV-VIS spectra of H-Ti-Beta. The spectra has an intense band in the region between 205 -225 nm and a weak band around 270 nm. It was previously reported that the band at around 270 nm comes from partially polymerized hexacoordinated Ti species (10). A band at around 225 nm has been assigned to the ligand to metal charge transfer (CT) involving isolated Ti atoms in octahedral coordination. After dehydration, the peak at 225 nm shifts to 205 nm and the peak at 205 nm is characteristic of charge transfer spectra for tetrahedral Ti. This spectrum suggests the presence of Ti at framework positions. However, a weak band 270 nm and an absorption edge starting from 330 nm may also suggest the presence of a part of Ti either at distorted positions or as extra-framework Ti. These IR and UV-VIS results suggest the incorporation of Ti into the framework of Beta though a part of Ti may exist at extra-framework positions.

The catalytic activity of this Al-free Ti-Beta was tested in oxidation of cyclohexene. As shown in the Table 3, the calcined Ti-Beta which was not treated with NH_4NO_3 solution showed only negligible activity for the oxidation of cyclohexene in the presence dilute H_2O_2 and acetonitrile as a solvent. The oxidation products were cyclohexene epoxide and 1, 2 cyclohexene-di-ol. After treating the calcined Ti-Beta with NH_4NO_3 and recalcined the catalytic activity increased by about 11 times and the oxidation products were cyclohexene epoxide, 1, 2

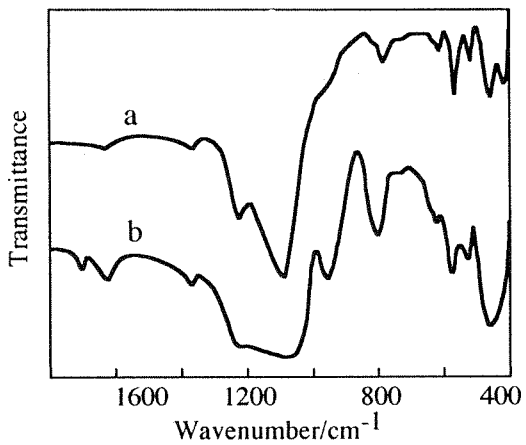

Figure 5. FTIR spectra of Ti-Beta.
a : Na-Ti-Beta; b : H-Ti-Beta.

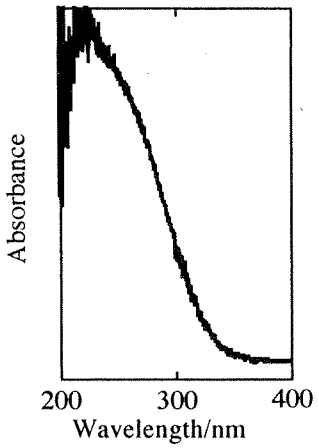

Figure 6. UV-VIS spectra of H-Ti-Beta.

cyclohexene-di-ol, cyclohexene-1-ol and cyclohexene-1-one. When the experiment was conducted using methanol as solvent instead of acetonitrile cyclohexene conversion was increased from 9.4 % (total products/(total products + cyclohexene) to 11.6 percentage and the products are mainly 1, 2 cyclohexene-di-ol, glycol ether, cyclohexene-1-ol and cyclohexene-1-one. However, products does not contain any epoxide. This suggests that initially formed epoxide was cleaved and secondary products were formed. van der Waal et al. (11) have suggested that Ti-Beta has strong acidic properties and the formation Brønsted acid centers on catalytically active Ti centers by the adsorption of either alcohol or peroxide. In our experiments also Brønsted acid sites might have formed by the adsorption of peroxide and these Brønsted acid sites might be responsible for cleaving the initially formed epoxide.

Sample	Solvent	Cyclohexene Conversion[a]	Product Selectivity				
			Epoxide	1-ol	1-one	Ether	di-ol
NaTiBeta	Acetonitrile	0.85	28.6	-	-	-	71.4
HTiBeta	Acetonitrile	9.40	16.2	6.9	12.1	-	64.7
HTiBeta	Methanol	11.6	-	2.0	14.8	27.2	56.0

Table 3: Oxidation of cyclohexene.
Reaction conditions: Catalyst, 100 mg; Cyclohexene, 17 mmol; Cyclohexene/H_2O_2, 3 (mole ratio); Solvent, 10 ml; Temperature, 333K, Duration, 3 h.
[a] : Total products/(Total products + Unreacted cyclohexene)

CONCLUSIONS

Pure silica Beta and Al-free Ti-Beta were crystallized using TEAOH as a structure-directing agent by dry gel conversion method. The pure silica Beta is stable even at 1173 K and lost crystallinity partially after calcination at 1373 K. Presence of impure phases in high silica and all silica Beta decreases the thermal stability of the products. IR and UV-VIS spectra confirm the incorporation of Ti into the framework of Beta. Catalytic experiments confirm the appearance acidic properties even on Al-free Ti-Beta.

ACKNOWLEDGEMENT

One of the authors (PR) thanks the Japan Society for the Promotion of Science for a post-doctoral fellowship.

REFERENCES

1 J.C. van der Waal, M.S. Rigutto and H. van Bekkum, *J. Chem. Soc. Chem. Commun.*, 1241 (1994).
2 M.A. Camblor, A. Corma and S. Valencia, *Chem. Commun.*, 2365 (1996).
3. M.A. Camblor, A. Corma, A. Martinez and J. Parez-pariente, *J. Chem. Soc. Chem. Commun.*, 589 (1992).
4. T. Tatsumi, Q. Xia and N. Jappar, *Chem. Lett.*, 677 (1997).
5. P.R. Hari Prasad Rao and M. Matsukata, *Chem. Commun.*, (1996) 1441.
6. P.R. Hari Prasad Rao, K. Ueyama and M. Matsukata, *Appl. Catal. A*, **166**, 97 (1998).
7. P.R. Hari Prasad Rao, K. Ueyama and M. Matsukata, *Microporous Mater.*, in press.
8. P.R. Hari Prasad Rao, K. Ueyama E. Kikuchi and M. Matsukata, *Chem. Lett.*, 311 (1998).
9. C.B. Khouw and M. E. Davis, *J. Catal.*, **151**, 77 (1995)
10. A. Corma, M.T. Navarro, J. Parez-pariente and F. Sanchez, *Stud. Surf. Sci. Catal.*, **84**, 69 (1994)
11. J. C. van der Waal and H. van Bekkum, J. Mol. Catal., **124**, 137 (1197).

SYNTHESIS OF OU-1, A LARGE-PORE, HIGH SILICA ZEOLITE, BY DRY GEL CONVERSION

M. MATSUKATA*, M. KATO**, T. SUZUKI***, Y. SASAKI****, E. KIKUCHI*, K. UEYAMA** and P.R. HARI PRASAD RAO**

*Department of Applied Chemistry, Waseda University, Tokyo, Japan; mmatsu@mn.waseda.ac.jp

**Osaka University, Osaka, Japan

***Toyohashi University of Technology, Nagoya, Japan

****Japan Fine Ceramics Center, Nagoya, Japan

ABSTRACT

A new high silica zeolite OU-1 was synthesized by a dry gel conversion technique using tetraethylammonium hydroxide as a structure-directing agent. OU-1 was formed via the phase transformation from Beta with prolonged crystallization. Structural analysis of OU-1 was performed by means of XRD, electron diffraction (ED), and high resolution TEM (HRTEM). It was concluded that OU-1 has one dimensional pore system with 12-membered ring opening, probably being analogous to SSZ-31 and NCL-1. The most striking characteristic of OU-1 is that similarly to Beta OU-1 is a highly faulted intergrowth of at least two distinct zeolite frameworks: The topological features of these two types of frameworks are the same as those of polymorphs A and B of Beta when the frameworks are projected from the direction of pore opening, while three dimensional T-O-T linkages of OU-1 are different from those of Beta. Phase transformation of Beta to another type of zeolites having a related-structure appears reasonable to occur. Such phase transformation could be a new route to develop a new structure.

INTRODUCTION

We have found that Beta zeolite is easily crystallized by the dry gel conversion[1-3]. In the dry gel conversion synthesis, an aluminosilicate aqueous solution or gel containing an organic structure-directing agent is dried to obtain a dry gel and then the resultant dry gel is crystallized not in continuous water phase but in steam at autogeneous pressure. This method allows us the synthesis of Beta with a broad range of SiO_2/Al_2O_3 ratio = 30 - ∞ using tetraethylammonium hydroxide (TEAOH), a common structure-directing agent, and extremely rapid crystallization of Beta; for instance, only 3 and 12 h for SiO_2/Al_2O_3 ratios = 30 and 700, respectively. We have recently found that high silica Beta zeolite transformed into another phase with prolonged crystallization[4]. Under appropriate conditions, a new phase, OU-1, was found to form via such phase transformation.

12th International Zeolite Conference

In the present study, the structure of OU-1 was discussed on the basis of the results of XRD, ED and HRTEM study. A interesting, highly faulted structure of OU-1 is presented.

EXPERIMENTAL

An aluminosilicate gel with a composition of SiO_2 : 0.0026 Al_2O_3 : 0.042 Na_2O : 0.37 TEAOH was prepared at room temperature. After being aged for 2 h while stirring, the gel was dried at 353 K. When the gel became viscous, it was stirred using a Teflon rod till it became a dry gel. The resultant dry gel was crushed and placed in the middle of a special autoclave where water as a source of steam was poured at the bottom. Crystallization was carried out at 453 K for 60 h.

The products were characterized with XRD, ED and HRTEM.

RESULTS AND DISCUSSION

Highly crystalline Beta with SiO_2/Al_2O_3 ratio = 380 was formed after 12 h of crystallization. As reported elsewhere[4], a new phase, OU-1, appeared with prolonged crystallization. As shown in Figure 1, the reflection peaks for Beta disappeared and the pure phase of OU-1 was formed after 60 h of crystallization. Further prolonged crystallization led to the formation of crystoballite (not shown). Typical positions of reflection peaks with Cu Ka radiation are 2q = 6.12 (70), 7.42 (21), 8.20 (36), 21.14 (100), 22.44 (62), and 22.68 (22). The figures in the parenthesis represents relative intensities. The XRD pattern of OU-1 is similar to NCL-1[5] and SSZ-31[6].

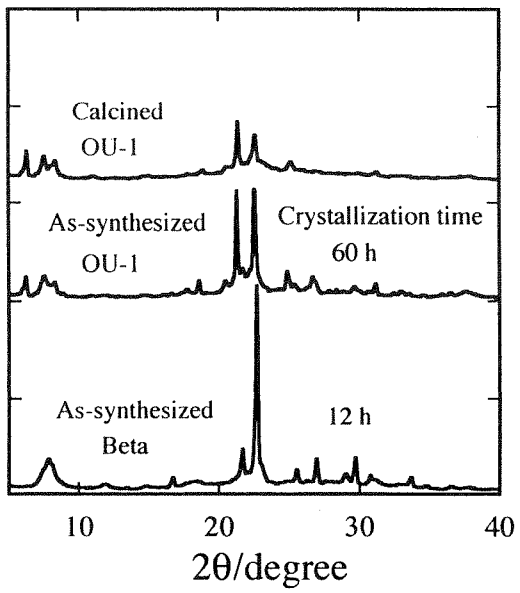

Fig. 1. XRD patterns of Beta and OU-1.

Figure 2 shows a typical morphology of OU-1. This zeolite is plate-like thin crystal. Judging from the results of XRD measurements and SEM observations, no amorphous phase was formed during the phase transformation from Beta to OU-1.

We have analyzed X-ray and electron diffraction patterns and concluded that OU-1 has one dimensional pore system with 12-membered ring opening as described in elsewhere[7]. Briefly, this zeolite is a highly faulted intergrowth of mainly two types of polymorphs. Figure 3 shows the schematic representation of these two types of framework structures: Type A is ABAB... stacking and type B is ABCABC... stacking. Figure 4 shows the HRTEM views of OU-1. The directions of observation are indicated in the figure. OU-1 has 12-membered oxygen ring opening along the longitudinal direction of crystal, though no pore opening is observed from the top of the plate, being in good agreement with the results of structural analysis.

As mentioned above, the XRD pattern of OU-1 is very similar to that of SSZ-31 of which the structure was recently solved by Lobo *et al.*[6] They concluded that SSZ-31 has a very complicated structure and a combination of several types of polymorphs. Though it is difficult to conclude clearly because of such complexity of structure, OU-1 would be analogous to SSZ-31.

Fig. 2 FE-SEM image of OU-1.

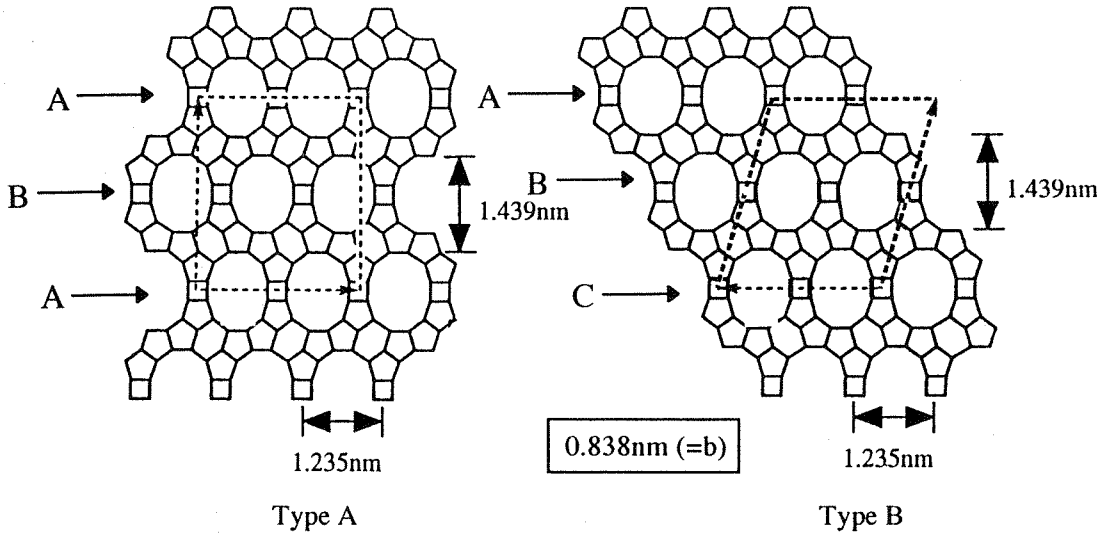

Fig. 3 Framework structures of OU-1.

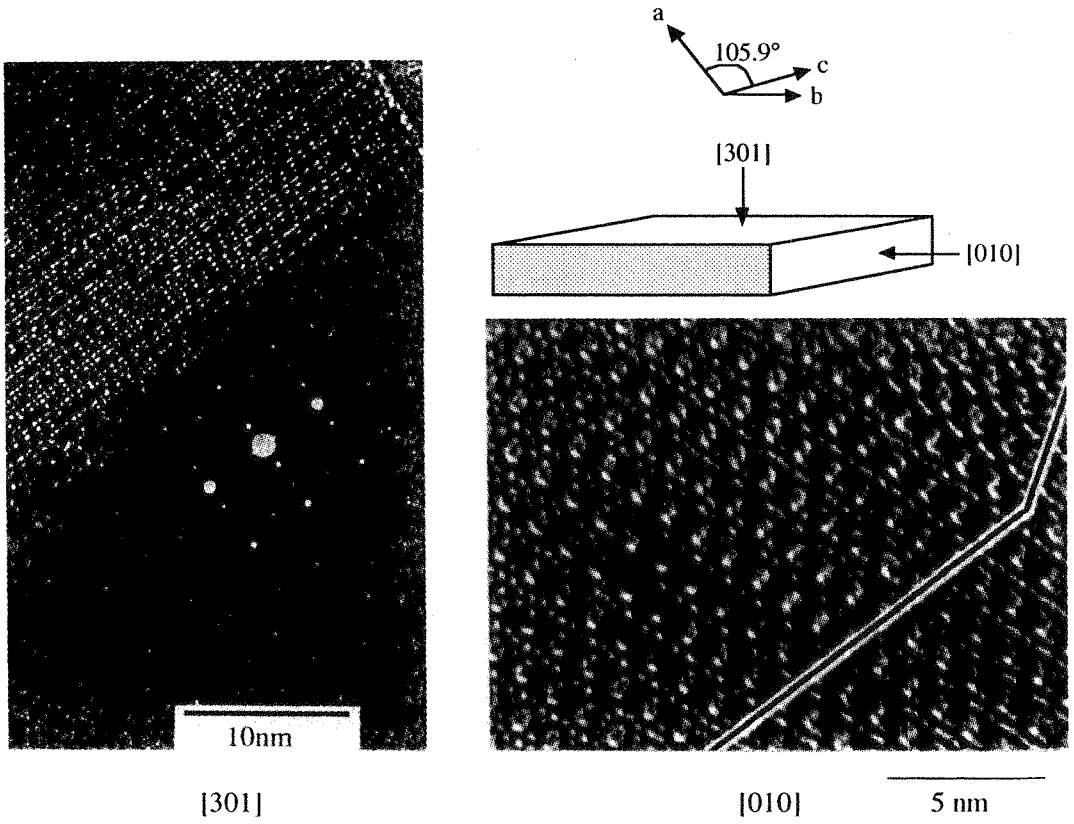

Fig. 4 HRTEM images for OU-1 observed along [301] and [010] directions which are indicated in figure.

It is noteworthy that the framework projections viewed along pore for OU-1 are the same as those for Beta zeolite: The projections for type A and B are the same topological features as those for the Beta framework structures of polymorph A viewed along [010] and polymorph B viewed along [110], respectively. Three dimensional linkage of T-O-T are different between the structures of Beta and OU-1, whereas their two dimensional projections of pore opening are the same.

As shown in Fig. 2, OU-1 has a morphology very different from Beta. Taking it into account that crystallization occurred in a gas medium and OU-1 was formed without formation of amorphous phase, we consider that intermediate species formed via hydrolysis of Beta migrates over the surface of Beta crystals and contributes to the nucleation of OU-1 there. The topological similarity of Beta and OU-1 probably rationalize the occurrence of phase transformation from Beta to OU-1. We suppose that intermediate species formed from Beta keeps sub-unit of Beta structure and OU-1 forms by rearrangement of such sub-units. Further, judging from the structures of OU-1 and Beta, the framework density of OU-1 would be greater than that of Beta. The transformation to a denser phase is possibly reasonable to occur.

CONCLUSIONS

It was found that high silica Beta containing TEA_2O as a structure-directing agent was transformed to a new zeolite OU-1 under the synthetic conditions of dry gel conversion. OU-1 is a very unique aluminosilicate zeolite from a view point of structure which is characterized by an one dimensional pore system with 12-membered ring opening and a highly faulted intergrowth of at least two distinct zeolite frameworks very similar to those of polymorphs A and B of Beta when the frameworks are projected from the direction of pore opening. Phase transformation between zeolites having similar structures would provide a possible new route to develop a new structure.

ACKNOWLEDGEMENTS

This study is supported partly by the Grant-in-aid for Scientific Research on Priority Area (No. 10136250), the Ministry of Education, Science, Sports and Culture and by the Asahi Grass Foundation.

REFERENCES

1. P. R. Hari Prasad Rao and M. Matsukata, Chem. Commun., 1441 (1996).
2. P. R. Hari Prasad Rao, K. Ueyama and M. Matsukata, Appl. Catal. A, **166**, 97 (1998).
3. P. R. Hari Prasad Rao, C. A. Leon y Leon, K. Ueyama and M. Matsukata, Microporous

and Mesoporous Mater., in press.

4. P. R. Hari Prasad Rao, K. Ueyama, E. Kikuchi, and M. Matsukata, Chem. Lett., 311 (1998).
5. R. F. Lobo, M. Tsapatsis, C. C. Freyhardt, I. Chan, C.C. Chen, S. I. Zones and M. E. Davis, J. Amer. Chem. Soc., **119**, 3732 (1997).
6. R. Kumar, K. R. Redy and P. Ratnasamy, U.S. Patent 5219813 (1993).
7. M. Matsukata, P.R. Hari Prasad Rao, K. Ueyama, E. Kikuchi, M. Kato, T. Suzuki and Y. Sasaki, in preparation.

Topics in Catalysis 9 (1999) 77–92

Conversion of dry gel to microporous crystals in gas phase

Masahiko Matsukata*, Masaru Ogura, Takayuki Osaki, Poladi Raja Hari Prasad Rao, Mikihiro Nomura and Eiichi Kikuchi

Department of Applied Chemistry, Waseda University, 3-4-1 Okubo, Shinjyuku-ku, Tokyo 169-8555, Japan
E-mail: mmatsu@mn.waseda.ac.jp

Recently the dry gel conversion (DGC) technique, where a hydrogel is dried and the resultant dry gel is converted into microporous crystals in steam or in a mixed vapor of steam and organic structure-directing agents (SDAs), has been developed. It has been shown that a wide variety of microporous crystals, pure silica microporous crystals, aluminosilicates, metallosilicates, and aluminophosphates, can be synthesized using the DGC method. Remarkable results have been reported in the synthesis of BEA types zeolites, namely aluminosilicate, titaniumsilicate, zincosilicate, and borosilicate with BEA topology, using tetraethylammonium hydroxide, a commercially available SDA. It has also been found that zeolite OU-1, probably analogous to SSZ-31 and NCL-1, is formed via phase transformation from BEA. Dense zeolite coatings like membranes are possible using this method. Characteristics of the DGC method are discussed in detail.

Keywords: dry gel conversion, zeolite synthesis, DGC method, beta zeolite, OU-1 zeolite

1. Introduction

Zeolites have so far been synthesized by hydrothermal methods that are solution-mediated methods using excess water. On the other hand, Bibby and Dale first reported the crystallization of silica sodalite in an ethylene glycol media in 1985 [1]. It has been reported that various types of zeolites including MFI and FER were synthesized in organic solvents without additional water [2,3]. These results suggest that water is not always essential as a media for zeolite synthesis.

In 1990, Xu et al. reported that a dry aluminosilicate gel could be transformed to MFI by contact with vapors of water and volatile amines [4]. Since then, such methods to transform dry gel to zeolite in vapor have extensively been developed and found a lot of applications for synthesizing microporous crystals with new compositions and structures. In this paper, the state of the art of the dry gel conversion (DGC) technique will be surveyed.

2. What is dry gel conversion technique?

Figure 1 presents the schematic presentation of synthetic methods for microporous crystals. Figure 1(a) shows a conventional hydrothermal synthetic method where a hydrogel containing all sources, for instance, aluminum, silicon and sodium, are converted to a crystalline microporous phase. Organic structure-directing agents (SDAs) are often included in the hydrogel. Crystallization is performed in a confined system, an autoclave, to maintain autogeneous pressure when crystallization needs a temperature above 373 K, as is well known.

Figures 1(b) and (c) are the schematic diagrams of reactors used for DGC methods. In using volatile SDAs such as ethylenediamine (EDA), a mixture of water and SDAs is poured into the bottom of the autoclave and then a dry gel, that does not contain SDAs, is placed in the middle [4–6]. Upon heating, steam and SDAs vaporize, reach the dry gel and bring about crystallization. This synthetic method is designated as "vapor-phase transport (VPT)" by Kim et al. [5].

Quaternary amines such as tetrapropylamine (TPA) hydroxide are often used as SDAs and are not volatile. When being used, such a non-volatile SDA can be involved in a dry gel, as shown in figure 1(c). Only steam is supplied from the gas phase. We call the last method "steam-assisted conversion (SAC)" here.

3. Crystallization using dry gel conversion methods

3.1. Vapor-phase transport synthesis

Table 1 lists the typical results of VPT syntheses found in the literature [4–6]. As mentioned above, Xu et al. [4] first reported the successful results of MFI synthesis using the VPT method: MFI zeolites are crystallized from dry gels with SiO_2/Al_2O_3 ratios = 44.8 and 86.4 in the presence of vapors of water, EDA and triethylamine (Et_3N) at 453–473 K. Kim et al. [5] and Matsukata et al. [6] followed their study and confirmed that the VPT method has wide applications in synthesizing various types of zeolites, MFI, FER, MOR and so on. While co-existence of EDA and Et_3N is essential to crystallize FER [6], without an organic SDA MFI can be obtained from a dry gel with an appropriate composition [5].

Figure 2 compares the compositions of the parent gels used in the VPT synthesis of MFI and FER with typical compositions of gels which have been reported in hydrothermal synthesis. It is noteworthy that the compositions

* To whom correspondence should be addressed.

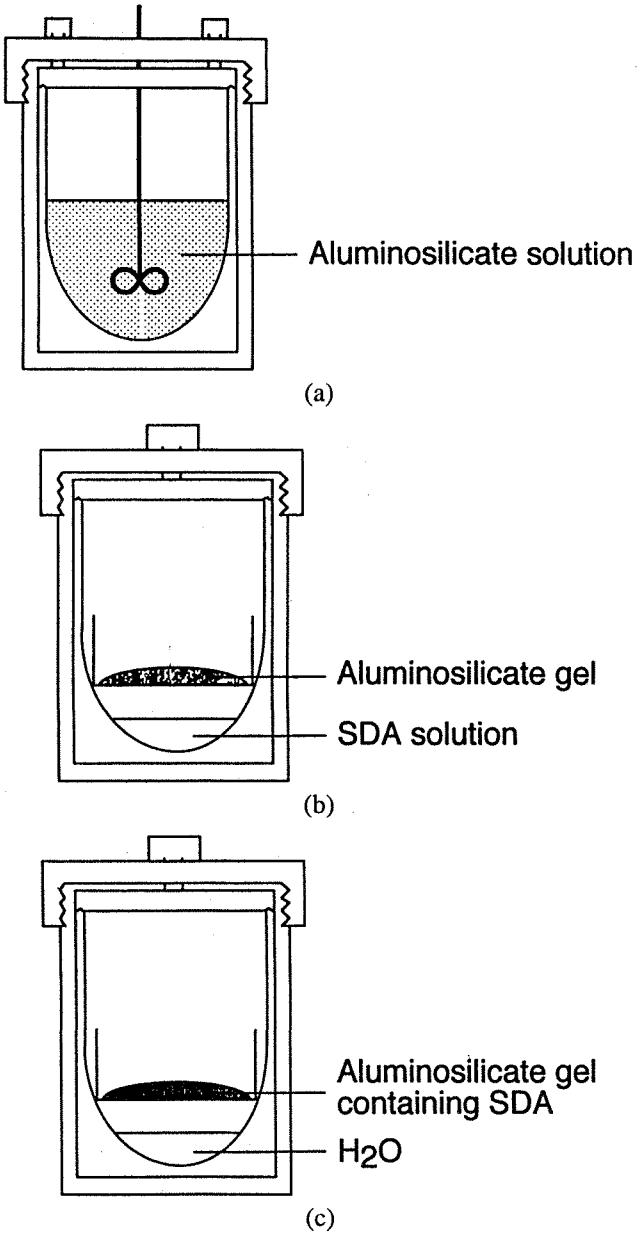

Figure 1. Schematic diagram of the methods for microporous crystal synthesis. (a) Hydrothermal method, (b) vapor-phase transport (VPT) method, and (c) steam-assisted crystallization (SAC) method. The latter two are the dry gel conversion (DGC) methods.

used in the VPT method can be plotted around the border of MFI and FER formation. For instance, MFI with a SiO_2/Al_2O_3 ratio = 25 is obtained in the VPT method even at a Na_2O/SiO_2 ratio of 0.48 which is higher than those used in the conventional hydrothermal synthesis. These results suggest that the VPT method has the possibility of expanding the compositions of zeolite formation.

3.2. Steam-assisted conversion of dry gel

3.2.1. Crystallization of aluminosilicate and pure silica BEA zeolite

Zeolite BEA, a three-dimensional large-pore, high silica zeolite, has potential technological applications in petrochemical process, organic synthesis and adsorption processes. Growing interest has been paid to the synthesis of zeolite BEA. In hydrothermal synthesis BEA using tetraethylammonium hydroxide (TEAOH), TEAOH-diethanolamine, TEABr-NH_3, or TEAOH-TEABr-triethanolamine as SDAs has always given a low product yield and its SiO_2/Al_2O_3 ratio produced has been limited up to about 250 [16–18]. Van der Waal et al. [19] and Burkett and Davis [20] have reported the formation of pure silica BEA hydrothermally using dibenzyldimethyl ammonium cation and 4,4′-trimethylenebis(N-butyl-N-methylpiperidinium) cations, respectively. These two kinds of SDAs were, however, not commercially available. Camblor et al. [21] successfully synthesized high silica BEA from a dense hydrogel with TEAOH-HF. Rao and Matsukata [22] first reported that the SAC method enables us to easily synthesize BEA having a wide range of SiO_2/Al_2O_3 ratios from 30 to infinity by using TEAOH, a commercially available SDA.

Synthetic method

Figure 3 shows a typical SAC synthetic method for the synthesis of BEA. Dry gels having compositions

$$SiO_2 : a\,Al_2O_3 : b\,Na_2O : c\,TEAOH$$

where a = 0–0.033, b = 0.014–0.092, and c = 0.16–0.50, are typically used for crystallization. A given amount of aluminum sulfate is dissolved in distilled water at 353 K except for the case of pure silica BEA synthesis. Given amounts of NaOH aq. and TEAOH aq. are added to a silica source (colloidal silica or fumed silica) at room temperature (298–303 K) while stirring. After 30 min, the aluminum sulfate solution is added and stirring is continued for 2 h. Then, the mixture is heated up to 353 K and dried while stirring. It is very important for good crystallinity that when the gel becomes viscous, it should be stirred till it becomes a dry gel, for instance, using a Teflon® rod. The dry gel is crushed to a powder and placed in the middle of the autoclave, as shown in figure 1(c). The amount of water required for crystallization is only 1.0 ml when one tries to crystallize 1.5 g of dry gel in 45 ml of autoclave.

Crystallization behavior

Figure 4 shows the crystallization curves of dry gels with SiO_2/Al_2O_3 ratios = 30–730 to BEA at 453 K [23]. The value of relative crystallinity shown in the ordinate was calculated using the intensity of the most intense (302) reflection peak appearing at $2\theta = 22.4°$ in the XRD patterns with Cu-Kα radiation. For the products with SiO_2/Al_2O_3 ratio = 30, crystallization was very rapid and was completed within 3 h, though no BEA phase was observed in the XRD pattern even after 2.5 h of crystallization. Although the crystallization rate decreased with increasing SiO_2/Al_2O_3 ratio, the dry gel with SiO_2/Al_2O_3 ratio = 730 was fully converted to BEA after 12 h.

Table 1
Typical results of zeolite synthesis using vapor-phase transport methods.

Reaction composition/molar ratio		Crystallization	Products	References
Amorphous gels	Liquid-phase[a]			
1.4 Na_2O : Al_2O_3 : 44.8 SiO_2 : 228 H_2O	EDA :4.3 Et_3N : 2.8 H_2O	200 °C, 5 days	MFI	[4]
1.5 Na_2O : Al_2O_3 : 86.4 SiO_2 : 325 H_2O	EDA :7.7 Et_3N : 10 H_2O	180 °C, 5 days	MFI	[4]
1.5 Na_2O : Al_2O_3 : 86.4 SiO_2	EDA :7.7 Et_3N : 10 H_2O	180 °C, 7 days	MFI	[4]
4.0 Na_2O : Al_2O_3 : 20 SiO_2	H_2O	175 °C, 7 days	MOR	[5]
8.0 Na_2O : Al_2O_3 : 40 SiO_2	H_2O	175 °C, 7 days	MFI	[5]
2.0 Na_2O : Al_2O_3 : 40 SiO_2	H_2O	175 °C, 7 days	MFI	[5]
2.0 Na_2O : Al_2O_3 : 10 SiO_2	Pr_3N : H_2O	175 °C, 7 days	MOR	[5]
4.0 Na_2O : Al_2O_3 : 20 SiO_2	Pr_3N : H_2O	175 °C, 7 days	MOR	[5]
4.0 Na_2O : Al_2O_3 : 40 SiO_2	Pr_3N : H_2O	175 °C, 7 days	MFI	[5]
2.0 Na_2O : Al_2O_3 : 10 SiO_2	Pr_2NH : H_2O	175 °C, 7 days	MOR	[5]
8.0 Na_2O : Al_2O_3 : 40 SiO_2	Pr_2NH : H_2O	175 °C, 7 days	MFI	[5]
Na_2O : Al_2O_3 : 10 SiO_2	Pr_2NH : H_2O	175 °C, 7 days	MOR	[5]
4.0 Na_2O : Al_2O_3 : 40 SiO_2	Pr_2NH : H_2O	175 °C, 7 days	MFI	[5]
Na_2O : Al_2O_3 : 20 SiO_2	Pr_2NH : H_2O	175 °C, 7 days	MFI	[5]
0.25 Na_2O : Al_2O_3 : 20 SiO_2	Pr_2NH : H_2O	175 °C, 7 days	MFI	[5]
2.0 Na_2O : Al_2O_3 : 10 SiO_2	$PrNH_2$: H_2O	175 °C, 7 days	MOR	[5]
16 Na_2O : Al_2O_3 : 80 SiO_2	$PrNH_2$: H_2O	175 °C, 7 days	MFI	[5]
0.50 Na_2O : Al_2O_3 : 5.0 SiO_2	$PrNH_2$: H_2O	175 °C, 7 days	FER	[5]
Na_2O : Al_2O_3 : 20 SiO_2	$PrNH_2$: H_2O	175 °C, 7 days	MFI	[5]
0.25 Na_2O : Al_2O_3 : 20 SiO_2	$PrNH_2$: H_2O	175 °C, 7 days	MFI	[5]
4.0 Na_2O : Al_2O_3 : 20 SiO_2	DAP : H_2O	175 °C, 7 days	MOR	[5]
Na_2O : Al_2O_3 : 10 SiO_2	DAP : H_2O	175 °C, 7 days	FER	[5]
4.0 Na_2O : Al_2O_3 : 40 SiO_2	DAP : H_2O	175 °C, 7 days	MFI	[5]
0.50 Na_2O : Al_2O_3 : 20 SiO_2	DAP : H_2O	175 °C, 7 days	MFI	[5]
0.25 Na_2O : Al_2O_3 : 20 SiO_2	DAP : H_2O	175 °C, 7 days	MFI	[5]
Na_2O : Al_2O_3 : 80 SiO_2	DAP : H_2O	175 °C, 7 days	MFI	[5]
0.10 TPABr : TEOS	60 H_2O : EDA	175 °C, 7 days	MFI	[5]
14 Na_2O : Al_2O_3 : 29 SiO_2	EDA : 5.3 Et_3N : 2.5 H_2O	180 °C, 3 days	FER	[6]
6.0 Na_2O : Al_2O_3 : 26 SiO_2	EDA : 5.3 Et_3N : 2.5 H_2O	180 °C, 3 days	MFI	[6]
15 Na_2O : Al_2O_3 : 31 SiO_2	1-PrOH : 2.0 Et_3N	160 °C, 6 days	MFI	[6]

[a] EDA: ethylene diamine; DAP: diaminopropane.

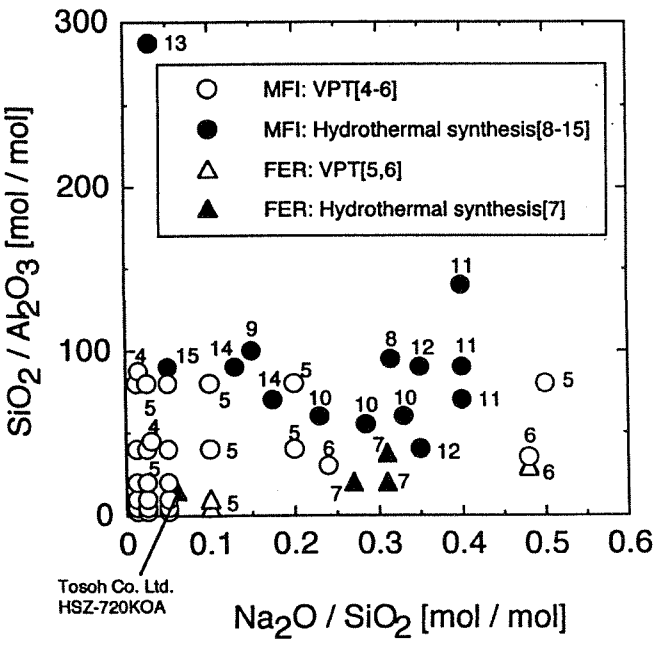

Figure 2. Compositions of parent gels for synthesis of MFI and FER. Figures given in the neighborhood of each plot correspond to the reference numbers.

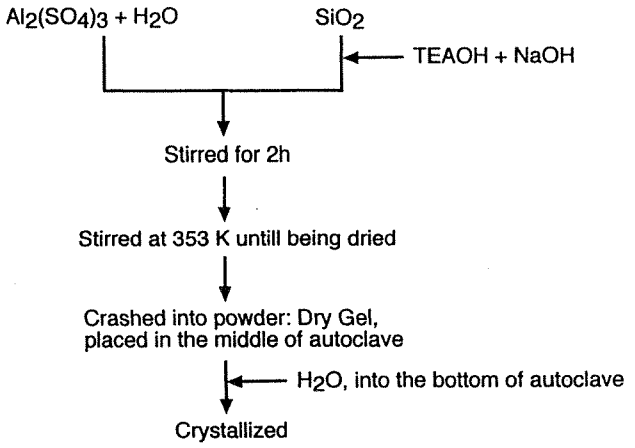

Figure 3. Typical synthetic method of zeolite BEA by the SAC method.

Important features of the SAC method can be drawn from these crystallization results. There exists an upper limit of SiO_2/Al_2O_3 ratio at about 250 in hydrothermally synthesizing BEA with TEAOH as a SDA [15], as described above. The SAC method using conventional TEAOH, easily gives even pure silica BEA. Very fast crystallization of BEA is also noteworthy. Generally, hydrothermal synthesis needs at least a few days for crystallization

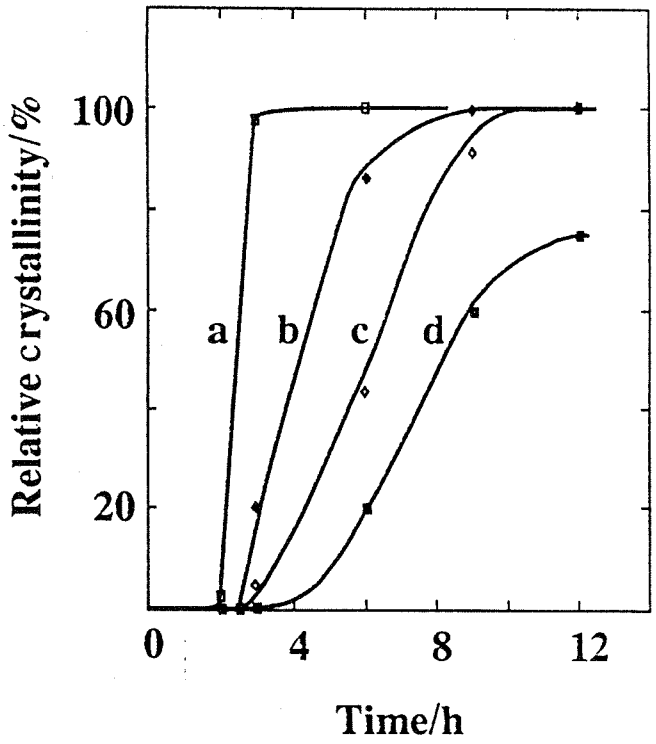

Figure 4. Crystallization curves of BEA with different chemical compositions at 453 K. SiO_2/Al_2O_3, SiO_2/Na_2O and SO_4^{2-}/SiO_2 ratios: (a) 30, 23.8 and 20.9; (b) 380, 23.8 and 528; (c) 730, 10.9 and 10; (d) 730, 23.8 and 0, respectively.

of BEA and it is difficult to crystallize a parent gel fully even after 1 week. Another feature to be noted in the SAC method is that BEA is crystallized at a higher temperature, as high as 453 K, in contrast to that hydrothermal synthesis of BEA which is performed up to 413 K. Crystals of uniform size are always formed, as shown in figure 5 where typical scanning electron micrograph (SEM) images for BEA via the SAC method are presented. BEA with SiO_2/Al_2O_3 ratio = 30 are the crystals of about 100–180 nm. Larger crystals of BEA are formed with increasing SiO_2/Al_2O_3 ratio and BEA with SiO_2/Al_2O_3 ratio = 730 gives about 400 nm size crystals. Such a trend has also been reported in hydrothermal synthesis of BEA [18].

Thermal stability

It has been found [23] that high silica BEA prepared by the SAC method has high thermal stability. Figure 6 presents the thermal stability of H-form BEA with SiO_2/Al_2O_3 ratio = 782. Up to 1173 K, no change in crystallinity was observed in the XRD pattern. In agreement with the XRD results, its BET specific surface area was almost unchanged: 631 and 656 $m^2 g^{-1}$ after calcination at 723 and 1173 K, respectively. It should be noted that even at 1373 K, the BEA structure remained though the BET specific surface area was slightly decreased to 587 $m^2 g^{-1}$ along with a small decrease in the reflection intensities as shown in figure 6. The high thermal stability shown here may be due to the high crystallinity. It has been known that BEA is a highly faulted zeolite consisting of polymorphs A and B which are stacked along the *c*-axis [25]. It is strongly suggested that such stacking defaults in the BEA structure do not cause the instability against temperature.

3.2.2. Phase transformation of BEA to MTW and OU-1

In the SAC synthesis, high silica BEA has been found to transform denser phases with prolonged crystallization. As shown in figure 7(a), BEA with SiO_2/Al_2O_3 ratio = 380 is gradually transformed to a new phase, OU-1, after 60 h [26]. Typical reflection peaks appear at 2θ = 6.2, 7.4, 8.2, 21.2 and 24.9°. With increasing SiO_2/Al_2O_3 ratio, BEA begins to transform to MTW, as shown in figure 7(b). Morphological features of OU-1 and its image of high resolution transmission electron micrograph (HR-TEM) are shown in figure 8. OU-1 possesses a one-dimensional,12-membered oxygen ring opening system (figure 8(b)), and forms very thin plate-like rectangular crystals (figure 8(a)). The large pore of OU-1 observed in figure 8(b) runs along the longitudinal [010] direction. The HRTEM images for OU-1 and its electron diffraction pattern suggest that OU-1 is a highly faulted zeolite containing at least two types of polymorphs.

Judging from the results of structural analysis [26,27], OU-1 is probably analogous to SSZ-31 [28] and NCL-1 [29]. SSZ-31 and NCL-1 were synthesized using N,N,N-trimethyltricyclo[5.2.1.$0^{2,6}$]decaneammonium and hexamethylenebis(triethylammonium bromide), respectively. It is interesting that OU-1, analogous to these zeolites, can be formed via the phase transformation from BEA containing conventional TEAOH as a SDA. Figure 9 shows plausible two-dimensional projections for the two types of polymorphs A (ABABAB... stacking) and B (ABCABCABC... stacking) of OU-1 [27]. These two-dimensional projections are the same as those for polymorphs A and B of BEA and MTW. This fact reveals that the difference in up-down sequence of T–O–T bonds (three-dimensional connectivity of T-atoms) can lead not only to various polymorphs but to different micropore systems. The phase transformation of BEA to OU-1 or MTW in the SAC method may be caused by the rearrangement of those T-atoms without complete destruction of BEA framework.

3.2.3. Synthesis of FAU and EMT with crown ethers

Delprato et al. reported that crown ethers whose sizes fit well in the supercage of faujasite, act as SDAs for its hydrothermal synthesis [30]. They found that among crown ethers, 1,4,7,10,13,16-hexaoxacyclooctadecane (18-crown-6) and 1,4,7,10,13-pentaoxacyclopentadecane (15-crown-5) selectively give hexagonal faujasite (EMT) and cubic faujasite (FAU), respectively. Their synthetic method using crown ethers as SDAs produce high silica FAU and EMT.

The DGC method can be applied to zeolite syntheses using SDAs other than amines. We have attempted to synthesize high silica EMT and FAU using the SAC method [31]. Table 2 lists the synthetic results using the SAC method together with the hydrothermal one. Col-

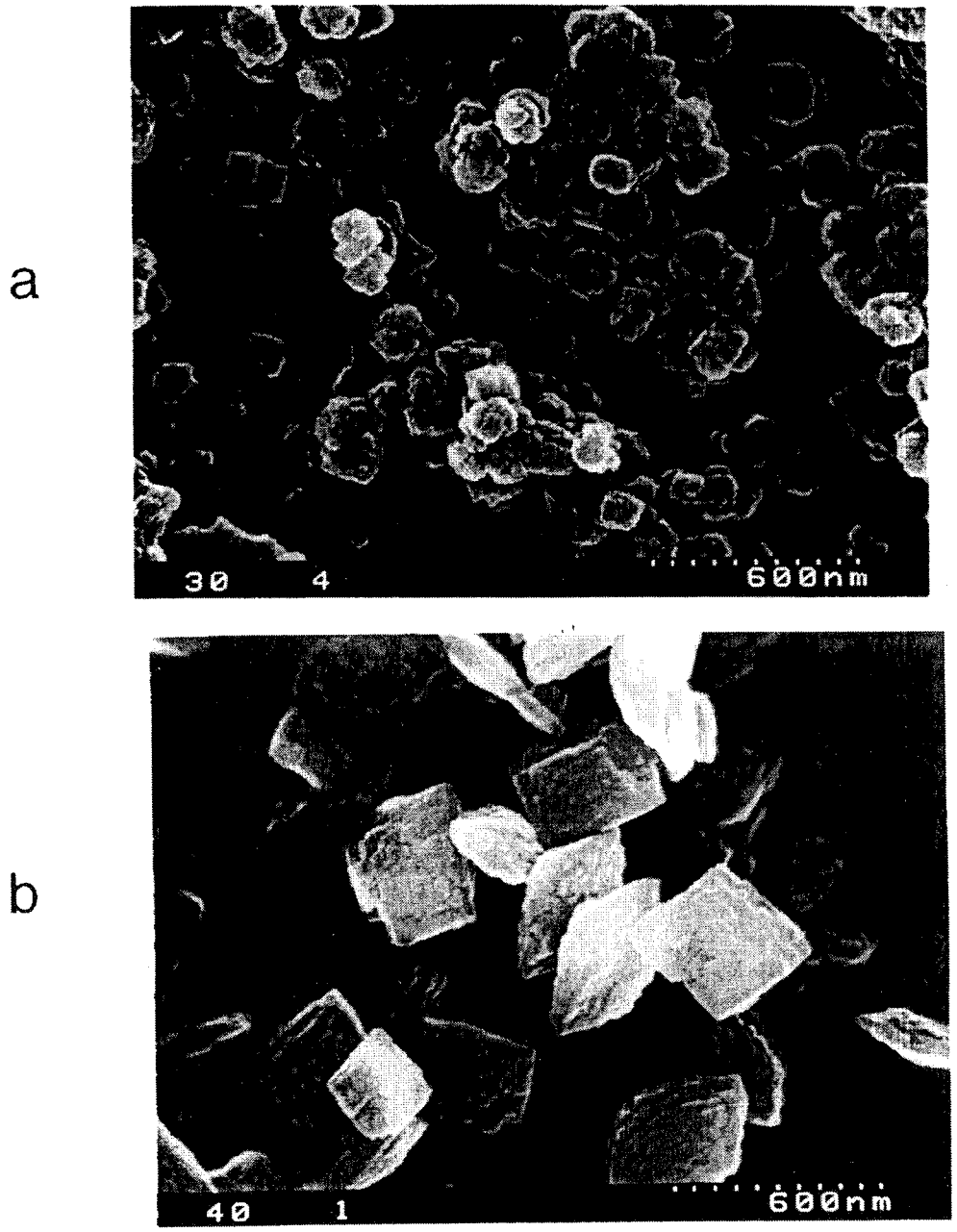

Figure 5. Typical SEM images for BEA synthesized via the SAC method. SiO_2/Al_2O_3 ratio: (a) 30; (b) 730.

loidal silica and aluminum hydroxide were used as silica and alumina sources, respectively. The chemical compositions used were 10 SiO_2 : Al_2O_3 : x Na_2O : 0.75 R : 140 H_2O (x = 2.1–3.3, R = 18-crown-6 or 15-crown-5). The hydrogel was aged at 308 K for 24 h. The resultant parent gel was hydrothermally crystallized in an autoclave at 388 K for 7 days. In the case of the SAC method, the parent gel, after aging, was dried and crushed into powder, and then crystallized in steam at 388 K and autogeneous pressure. The hydrothermal synthesis using 18-crown-6 gave EMT when $x < 2.7$. Pure FAU was formed with increasing values of x. It was found that EMT was formed using the SAC method whereas the range of the value of x to give EMT was narrow. Though FAU was also formed with increasing sodium content in the dry gel, GIS was easy to form as impurity. In agreement with the previous report by Delprato et al. [30], 15-crown-6 gave FAU by both hydrothermal and SAC methods.

Field emission SEM observations of EMT crystals give great insight into the zeolite growth mechanisms. Figure 10 compares the morphological features of EMT prepared by the hydrothermal and SAC methods. It is worth noting that EMT crystals synthesized hydrothermally consisted of thin hexagonal plates and have obvious facets randomly aligned at the edges of plates. The thickness of each sheet observed is ca. 10–20 nm. Such characteristic morphology observed is in good agreement with a layer-by-layer growth mechanism which has been proposed for the formation of

EMT by Burkett and Davis [32]. On the other hand, EMT crystals prepared by the SAC method have very different morphological features. As shown in figure 10(b), stripes indicating steps less than 10 nm thick, are observed on the surface of EMT crystals and have smoothe edges. In the SAC method, EMT crystals may grow by a spiral growth mechanism. Detailed investigation of crystal growth of EMT will be reported in the near future [31].

3.2.4. *Synthesis of metallosilicates*

Metallosicilates, a class of microporous silicates containing T-atoms other than silicon and aluminum, have found vast development and subsequent applications. The DGC method, especially the SAC method, has recently been shown useful for incorporation of heteroatoms into the zeolite framework.

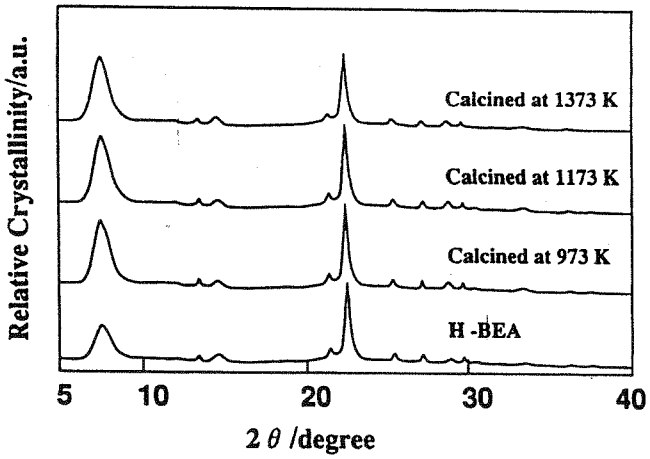

Figure 6. X-ray diffraction patterns of H-exchanged BEA with SiO_2/Al_2O_3 ratio = 782 [23]. Calcination was carried out in air for 2 h.

Titaniumsilicates

Titaniumsilicates having MFI topology (TS-1 and TS-2) have been shown to be highly active catalysts for the partial oxidation of a wide variety of organic substrates such as alkenes and aromatics, using H_2O_2 as the oxidant [33]. Because of its three-dimensional large-pore system, many efforts, including conventional hydrothermal syntheses [34–36], cogel method [37], seeding method [38], gas-solid [36, 39] and liquid-liquid [40] isomorphous substitution have been tried in an effort to obtain BEA containing Ti in its framework (Ti-BEA).

Tatsumi et al. [41,42] have reported that the SAC (they use the term "DGC") method is a useful technique for synthesizing Ti-BEA with high oxidation activity and in high synthesis yield. They pointed out that while Al in the framework of BEA has detrimental effects for oxidation activity and selectivity, the SAC method enables us to crystallize high silica Ti-BEA with high yield. Table 3 lists their typical crystallization results of Ti-BEA [41,42] together with our recent results on the syntheses of Al-free Ti-BEA [43]. Tetrabutyl orthotitanate was used as Ti-source by both groups. Zeolite yield is easy to manipulate to exceed 90%. All the Ti-BEA samples listed in table 3 gave a narrow UV band appearing at 205–225 nm [41,43], typical UV-Vis spectroscopic features for Ti-containing zeolites. It was reported that the treatment of as-made Ti-zeolites with 1 M H_2SO_4 effectively removes TiO_2 nanoparticles which can be occluded in the micropores of zeolites [32]. The SiO_2/TiO_2 ratio was not decreased seriously by the H_2SO_4 washing. These results strongly suggest that most of Ti in the parent dry gel can be incorporated in the framework positions without forming anatase and rutile phases.

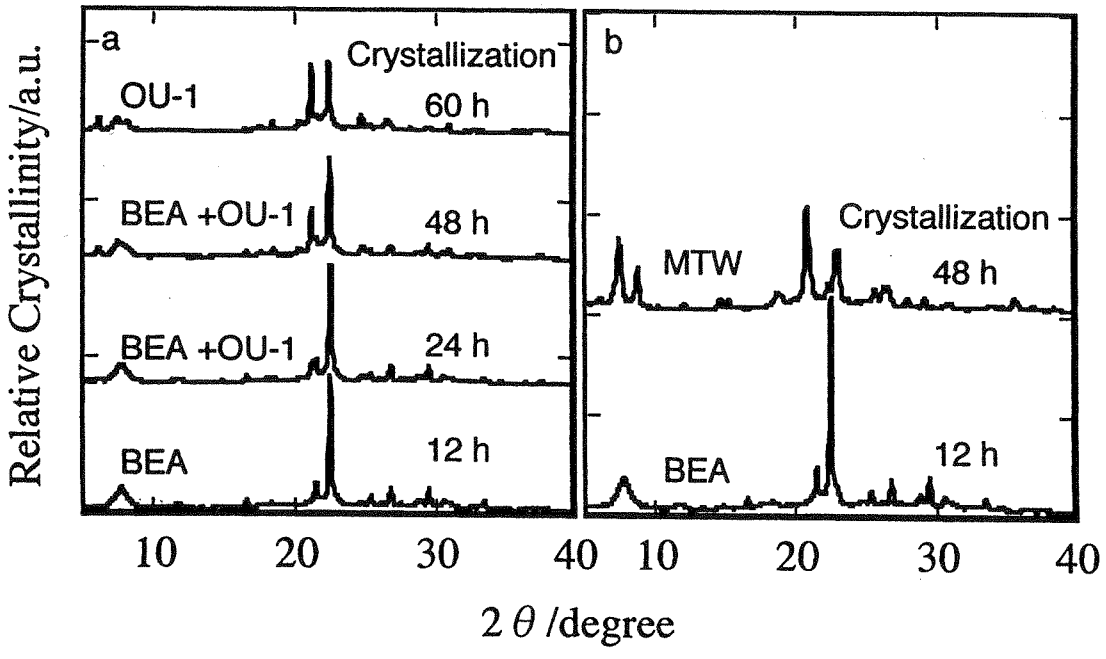

Figure 7. Phase transformation of BEA with prolonged crystallization at 453 K. SiO_2/Al_2O_3 and Na_2O/SiO_2 ratios: (A) 380 and 0.042; (B) 730 and 0.094.

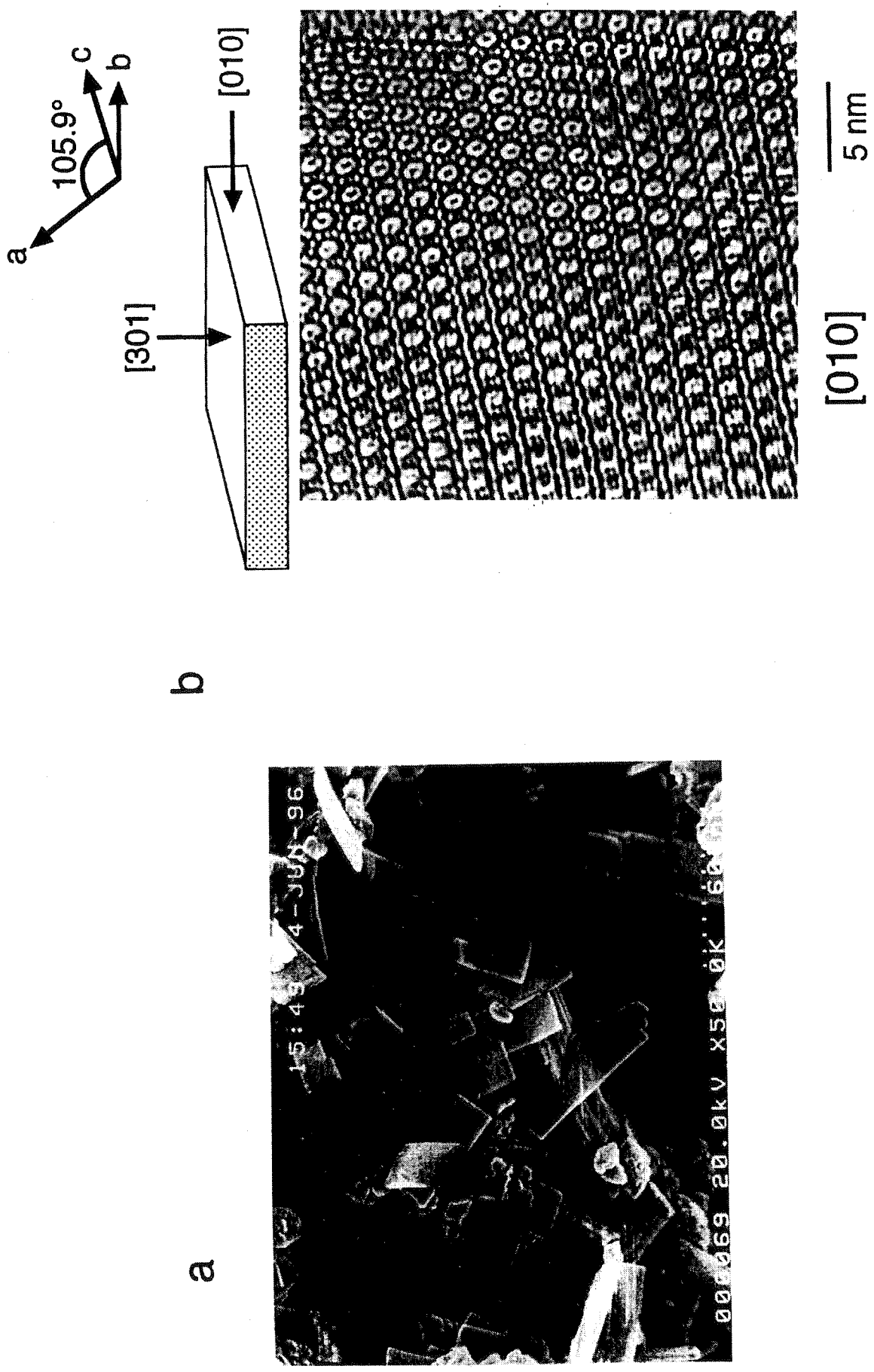

Figure 8. (a) SEM and (b) HRTEM images for OU-1.

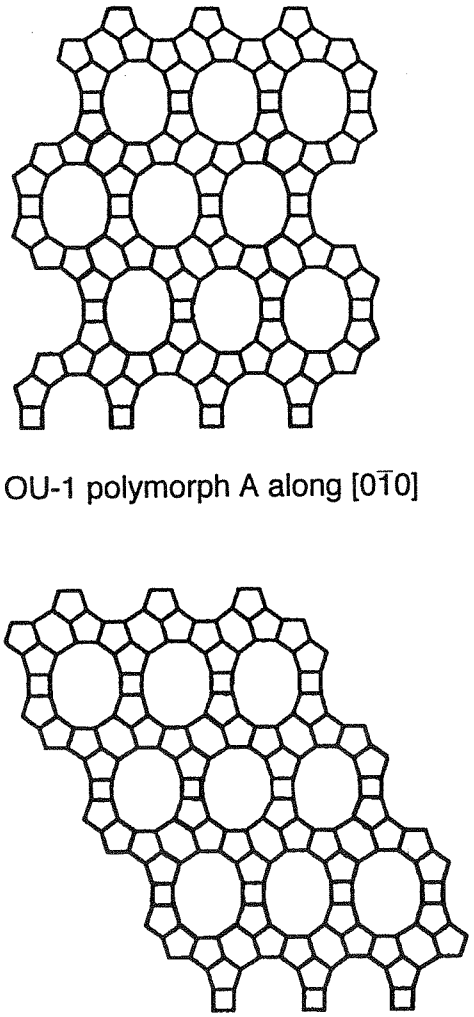

Figure 9. Framework topologies of polymorphs in OU-1.

There are some points to be noted in the SAC synthesis of Ti-BEA. First, the addition of Na is essential for the success of crystallization of Ti-BEA by the SAC method. Camblor et al. have reported [34] that the addition of alkali cations leads to a low crystallinity in the synthesis of Ti-BEA. This is not the case. Second, crystallization should start at a lower temperature of 403 K compared with the cases of BEA syntheses (453 K) described above. All attempts to crystallize Ti-BEA at 453 K directly have always failed, while an increase of temperature to 453 K after 96 h of crystallization at 403 K is effective to facilitate crystallization [41]. In addition, we have recently found that the gel aging temperature is critical. All the Al-free Ti-BEA samples listed in table 3 were the cases where their parent hydrogels were aged at 293 K for 2 h. When a hydrogel was aged at 273 K, the products were amorphous. With increasing aging temperature from 293 K, the crystallinity of the product decreased and became amorphous at 323 K of aging. In addition, Al-free TS-1 and TS-2 are also formed by the SAC method [43].

Tatsumi et al. reported that though cyclohexene is not oxidized with H_2O_2 over TS-1, because it is difficult to enter into the micropores of MFI, Ti-BEA gave high conversions of H_2O_2 and selectivities in the oxidation of cyclohexene [41,42]. They reported that the oxidation of C_6–C_8 cyclic alkenes and alcohols also effectively proceeds over Ti-BEA obtained by the SAC method, followed by calcination and H_2SO_4 washing.

Borosilicates

While being interesting in their catalytic properties, boron-substituted zeolites (borosilicates) are important materials since boron incorporated in the zeolitic framework can be extracted under mild conditions and replaced with other T-atoms [45]. Bandyopadhyay et al. performed the crystallization of dry gels with the compositions of SiO_2 : 0.002–0.033 B_2O_3 : 0.028–0.050 Na_2O : 0.36–1.2

Table 2
Typical results of EMT and FAU syntheses.[a]

SDA	x	Products	
		HTS	SAC
18-crown-6	2.10	EMT (8.18)	Amorphous
	2.20	EMT	EMT (8.00)
	2.40	EMT (7.14)	EMT (7.66)
	2.55	EMT	EMT + GIS
	2.70	EMT + FAU	FAU
	2.85	FAU	FAU + GIS
	3.00	FAU	FAU + GIS
	3.30	FAU	–
15-crown-5	2.10	Amorphous	–
	2.40	FAU (7.40)	FAU (7.21)
	2.55	FAU	–
	2.85	FAU	–

[a] Synthesis conditions: 388 K, 7 days. Gel composition: 10 SiO_2 : Al_2O_3 : x Na_2O : 0.75 R : 140 H_2O (R = 18-crown-6, 15-crown-5). Figures in parentheses are SiO_2/Al_2O_3 ratios determined by ^{29}Si-NMR.

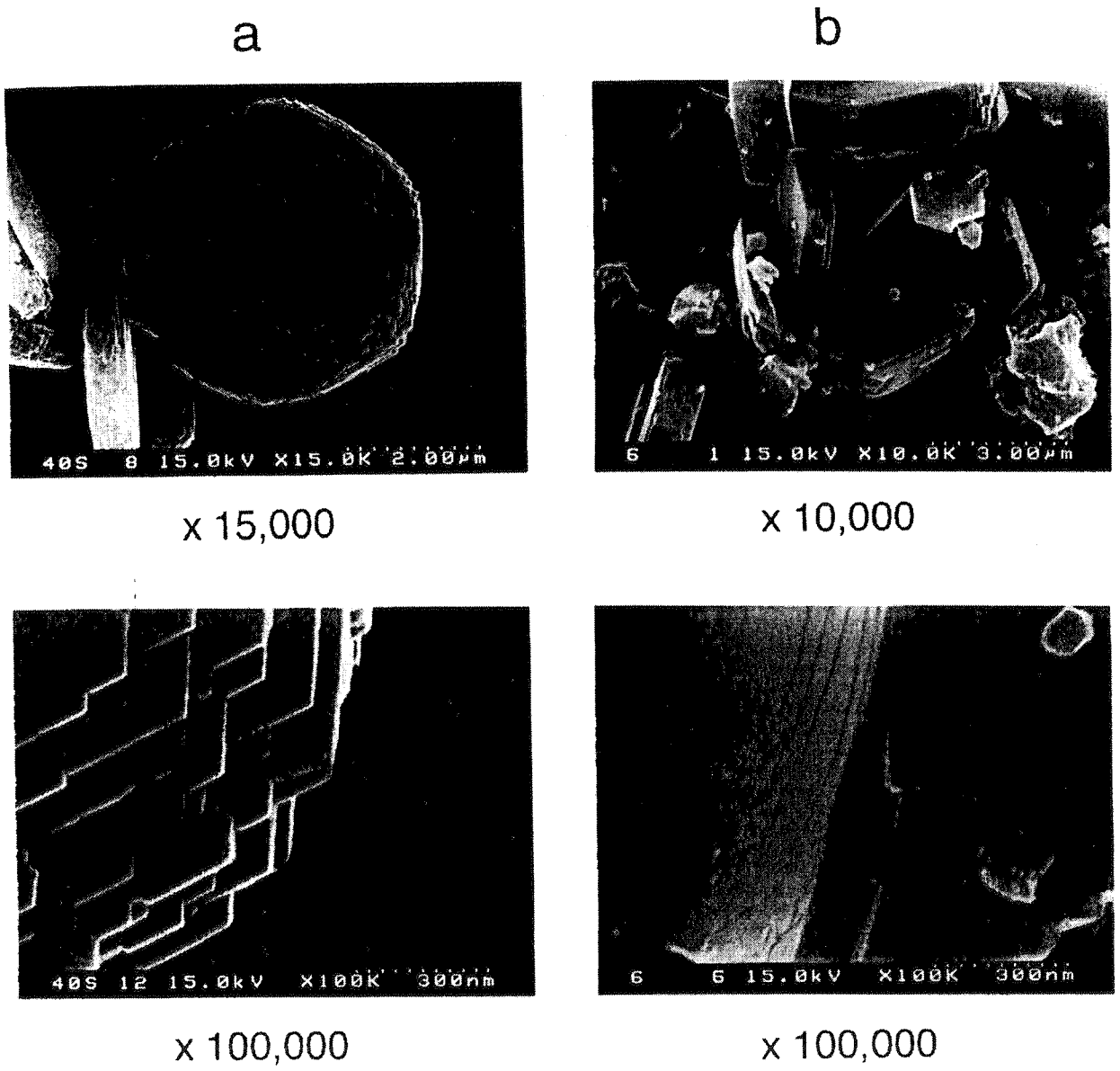

Figure 10. Field emission-SEM images for EMT synthesized by (a) the hydrothermal method and (b) the SAC method.

Table 3
Typical results of Ti-Beta synthesis.

Gel			Crystallization	Calcined			H_2SO_4-washed			References
SiO_2/TiO_2	SiO_2/Al_2O_3	Na_2O/SiO_2		SiO_2/TiO_2	SiO_2/Al_2O_3	Na_2O/SiO_2	SiO_2/TiO_2	SiO_2/Al_2O_3	Na_2O/SiO_2	
30.4	662	0.0051	403 K, 4 days + 448 K, 18 h	31.3	704	0.0053	36.6	1304	0.00094	[41]
30.2	664	0.0100	403 K, 4 days + 448 K, 18 h	28.4	648	0.0100	30.5	1416	0.00160	[41]
58.3	664	0.0051	403 K, 4 days + 448 K, 18 h	55.5	926	0.0054	N.d.	N.d.	N.d.	[41]
89.4	660	0.0051	403 K, 4 days + 448 K, 18 h	78.4	756	0.0053	92.4	1364	0.00079	[41]
58.3	660	0.0051	403 K, 5 days	56.4	682	0.0053	N.d.	N.d.	N.d.	[41]
50	–	0.0960	413 K, 7 days	65	–	0.0340	45	–	N.d.	[43]
100	–	0.0960	413 K, 7 days	76	–	0.0245	67	–	N.d.	[43]
300	–	0.0960	413 K, 7 days	207	–	0.0265	173	–	N.d.	[43]

Table 4
Zincosilicates synthesized by the SAC method.[a]

SiO_2/ZnO ratio	Structure
10	VET
20	VET + BEA
100	BEA
200	BEA
500	BEA + MTW
∞	BEA + MTW

[a] Gel composition: SiO_2 : 0.10 Li_2O : 0.020 Na_2O : 0.40 TEAOH : a ZnO, a = 0–0.10. Crystallization temperature: 423 K. Crystallization time: 48 h.

TEAOH by using the SAC method at 448 K for 72 h and found that phase selection of borosilicates strongly depended on the composition of dry gel. B-BEA was formed with TEAOH/SiO_2 ratios of 0.8–1.2 and SiO_2/B_2O_3 ratios = 30–50, while B-MTW was found to form with SiO_2/B_2O_3 ratios = 50–100 and TEAOH/SiO_2 ratios = 0.8–1.0. B-MFI was formed with increasing SiO_2/B_2O_3 ratio to 100–200. Apart from the postsynthesis of various metallosilicates using borosilicates as parent zeolites, mechanisms concerning such phase selections will be an interesting issue.

Zincosilicates

Zincosilicates are anticipated to realize a new class of molecular sieves having void spaces in excess of 50%, and

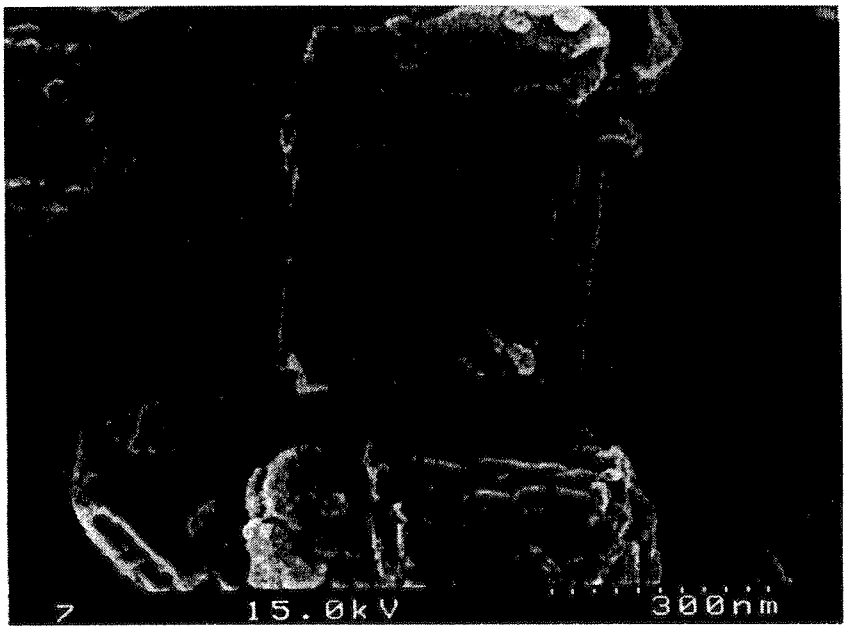

Figure 11. FE-SEM image for Zn-BEA.

Table 5
Examples of the DGC synthesis of $ALPO_4$.[a]

Synthetic method	Gel composition	Crystallization time	Products
SAC	$Al_2O_3 : P_2O_5$: 1.02 TMAOH	60 h	$ALPO_4$-41 + dense phase
	$Al_2O_3 : P_2O_5$: 1.02 TEAOH	30 h	$ALPO_4$-18
	$Al_2O_3 : P_2O_5$: 1.02 TEACl	40 h	$ALPO_4$-5 + dense phase
	$Al_2O_3 : P_2O_5$: 1.02 TEABr	40 h	Dense phase
	$Al_2O_3 : P_2O_5$: 1.02 TPAOH	60 h	$ALPO_4$-5 + dense phase
	$Al_2O_3 : P_2O_5$: 1.20 TPAOH	30 h	$ALPO_4$-5
	$Al_2O_3 : P_2O_5$: 1.02 TBAOH	30 h	Amorphous
	$Al_2O_3 : P_2O_5$: 1.02 TBAOH	40 h	Dense phase
	$Al_2O_3 : P_2O_5$: 1.02 N-methyldiethanolamine	30 h	Unknown
	$Al_2O_3 : P_2O_5$: 1.02 Piperidine	30 h	Unknown
	$Al_2O_3 : P_2O_5$: 1.02 Et_3N	30 h	Unknown
VPT	$Al_2O_3 : P_2O_5$: 1.02 Cyclohexylamine	30 h	Unknown[b]
	$Al_2O_3 : P_2O_5$: 1.02 Ethylenediamine	30 h	Unknown[c]

[a] Crystallization temperature, 453 K.
[b] In the XRD pattern, a distinct reflection peak appeared at $2\theta = 4.8°$.
[c] In the XRD pattern, a distinct reflection peak appeared at $2\theta = 8.8°$.

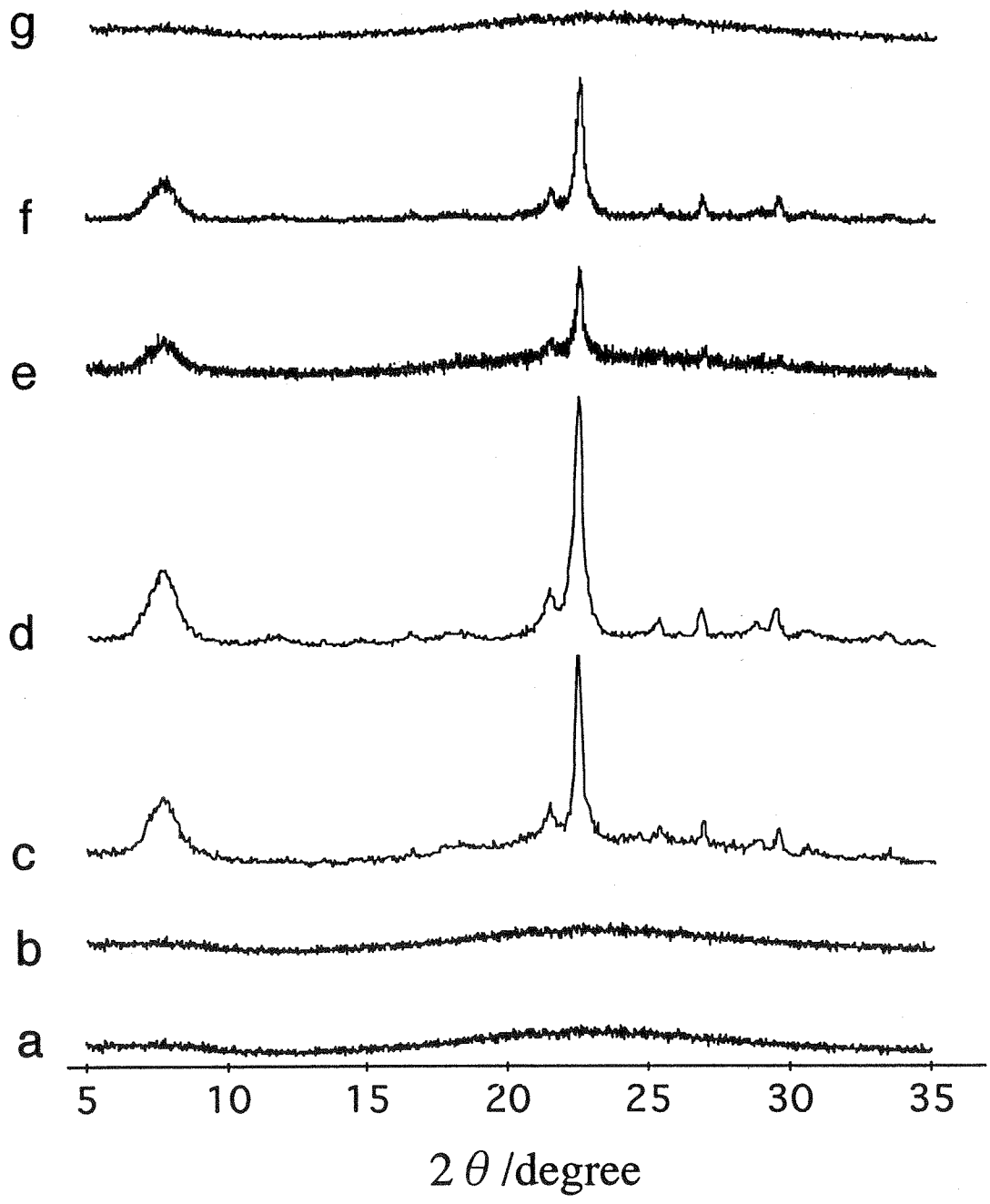

Figure 12. Effect of the amount of water at the bottom of autoclave in the synthesis of BEA by the SAC method. The synthetic procedure is the same as that shown in figure 3. The composition of dry gel, SiO_2 : 0.033 Al_2O_3 : 0.036 Na_2O : 0.37 TEAOH, the inner volume of autoclave, 45 ml; the amount of dry gel used for crystallization, 1.50 g; crystallization temperature, 453 K; crystallization time, 24 h. The amount of water used in ml: (a) 0; (b) 0.22; (c) 0.5; (d) 1.0; (d) 1.5; (e) 2.0; (f) 2.5.

large ion exchange capacities beyond the upper limit of zeolites with SiO_2/Al_2O_3 ratio = 2. Hydrothermal methods have been developed for synthesizing a variety of zincosilicates, including a series of VPI-7 to VPI-10 [46–49] and RUB-17 [50].

The SAC method is also useful for synthesizing zincosilicates [51]. Dry gels having the compositions of SiO_2 : 0.1 Li_2O : 0.4 TEAOH : a $Zn(CH_3COO)_2$ (a = 0–0.1) were crystallized at 423 K for 48 h. It was reported [48,49] that hydrogel having similar chemical compositions (a = 0.01–0.1, H_2O/SiO_2 ratio = 32) successfully gave VPI-8 (VET) in a hydrothermal synthesis at 423 K, though MTW was formed when a = 0. Typical results of the SAC synthesis are listed in table 4. Similar to the results of hydrothermal synthesis [49], the dry gel having SiO_2/ZnO ratio = 10 gave VET. It is worth noting that Zn-containing BEA is formed when the SiO_2/ZnO ratio = 100. An FE-SEM image of Zn-BEA with SiO_2/ZnO = 100 is shown in figure 11. With a further increase in SiO_2/ZnO, MTW was found mixed with BEA.

3.2.5. Microporous aluminum phosphates

Microporous aluminumphospates ($ALPO_4$) have been crystallized using hydrothermal synthesis in acidic conditions. The VPT and SAC methods are useful for synthesizing $ALPO_4$, as listed in table 5. $ALPO_4$-5, -18, and -41 are formed with conventional SDAs under appropriate conditions.

3.2.6. Membrane applications

Rapidly growing attention has been paid to zeolite membranes in this decade [52]. Compared with organic polymer membranes which have been commercialized for dialysis, gas separation and so on, zeolites are good candidates as novel membrane materials because of their molecular sieving properties, stability against higher temperatures and various solvents, easy control of hydrophobic and hydrophilic nature, and catalytic properties.

Zeolitic membranes are possible to synthesize using the DGC method. Matsukata et al. [53,54] have previously reported the synthetic results of supported-zeolitic membranes by using the VPT method using EDA and Et_3N as SDAs and the resulting membrane separation properties. A general preparation method is as follows. Porous alumina support was immersed in aluminosilicate hydrogel. After being taken out from the hydrogel, the resultant thin gel layer formed on the support surface is dried and crystallized under VPT conditions. Previously, MFI [53–55], FER [54,56,57], and MOR [54,57,58] membranes have been synthesized by the VPT method. Their synthetic results and separation properties for inorganic gas and hydrocarbon mixtures have mostly been reviewed in [59].

4. Role of water in crystallization by the DGC method

Perhaps the most profound question to be raised for the DGC method is the role of water during the synthesis. What is the difference between a conventional hydrothermal method and the DGC method? Though we have not had the final answer, we will discuss this problem here as far as possible.

As an attempt to check on the role of water in the DGC synthesis, especially the SAC synthesis, we carried out the crystallization of a TEA-containing dry gel with various amounts of water. Figure 12 shows the XRD patterns of the as-made products. One can notice that the amount of water should carefully be chosen since it significantly influences the crystallization results. Without the addition of water into the bottom of autoclave, no crystallization occurred, in agreement with the previous results of Ti-BEA [41] and B-BEA [45] synthesis. Taking into account that the saturated vapor pressure of steam is 10.224 atm at 453 K, the amount of water to produce the saturated vapor pressure of steam in the autoclave used in this study is 0.22 ml. As shown in figure 12, however, no crystallization occurred after 24 h of crystallization with 0.22 ml of water. While further increasing the amount of water added resulted in the formation of BEA, the crystallinity of product had a maximum when 1.0 ml of water was added to the autoclave. It should be noted that no crystalline phase was obtained with 2.5 ml of water. Since the water content in dry gel was typically 3.0–10.0% [54], water in the dry gel did not contribute to the total amount of water existing in the autoclave all that much, even if all water contained in the parent gel would come into the gas phase. As a result, keeping a certain saturated vapor pressure of steam is not enough to initiate crystallization of BEA, suggesting that adsorption and condensation of water on/in the dry gel are essentially required for crystallization. However, a large excess of water is detrimental to crystallization, the result of which seems to be worth discussing in understanding the difference in hydrothermal and SAC methods.

The requirement of an appropriate amount of water exceeding the exact amount to keep the saturated vapor pressure suggests that condensation of water would take place particularly in the pores of dry gel. One may consider that the SAC method is a hydrothermal synthetic method that is performed under extremely dense conditions. However, this idea cannot explain the result that BEA was not formed in the presence of a large excess amount of water.

Many of SDAs like quaternary ammonium cations, especially TEA^+, are unstable in an alkaline aqueous solution. TEA^+ cations in an as-received aqueous solution are easy to decompose even at 363 K giving a brown product. However, the dry gel system stays white at 423 K in an air oven, implying no degradation of TEA^+ cations contained in dry gel at this temperature. Stabilization of TEA^+ cations in the dry gel was confirmed by a temperature-programmed decomposition experiment (not shown) where TEA^+ cations decomposed above about 450 K. It has previously been reported [23] that in as-made BEA, TEA^+ cations are occluded and stabilized by interacting with the BEA framework by forming $Al–O^-$ TEA^+ bonds (decomposing above 600 K) and $Si–O^{\delta-}TEA^{\delta+}$ bonds (decomposing above 450 K). In conclusion, TEA^+ cations in a dry gel are forced to interact with (alumino)silicious species in the absence of a continuous phase of water. In principle, such stabilization of SDA molecules (or cations) is impossible in an alkaline hydrogel used in conventional hydrothermal synthesis.

Zeolite syntheses using SDAs can be regarded as competitive reactions between degradation of SDA molecules and a series of zeolite-forming reactions that includes hydrolysis of silicious species to give intermediates and dehydrocondensation to give T–O–T networks. Possible crystallization of BEA at a temperature as high as 453 K by the SAC method [22–24] is probably due to successful stabilization of TEA^+ cations in the dry gel, leading to rapid crystallization within 1 day. Crystallization of Ti-containing BEA by the SAC method still needs about 1 week. We suppose that in this slow crystallization the degradation of SDA is not negligible. In these cases, a lower crystallization temperature like 413 K [41–43] should be selected. Though zeolite-forming reactions require wa-

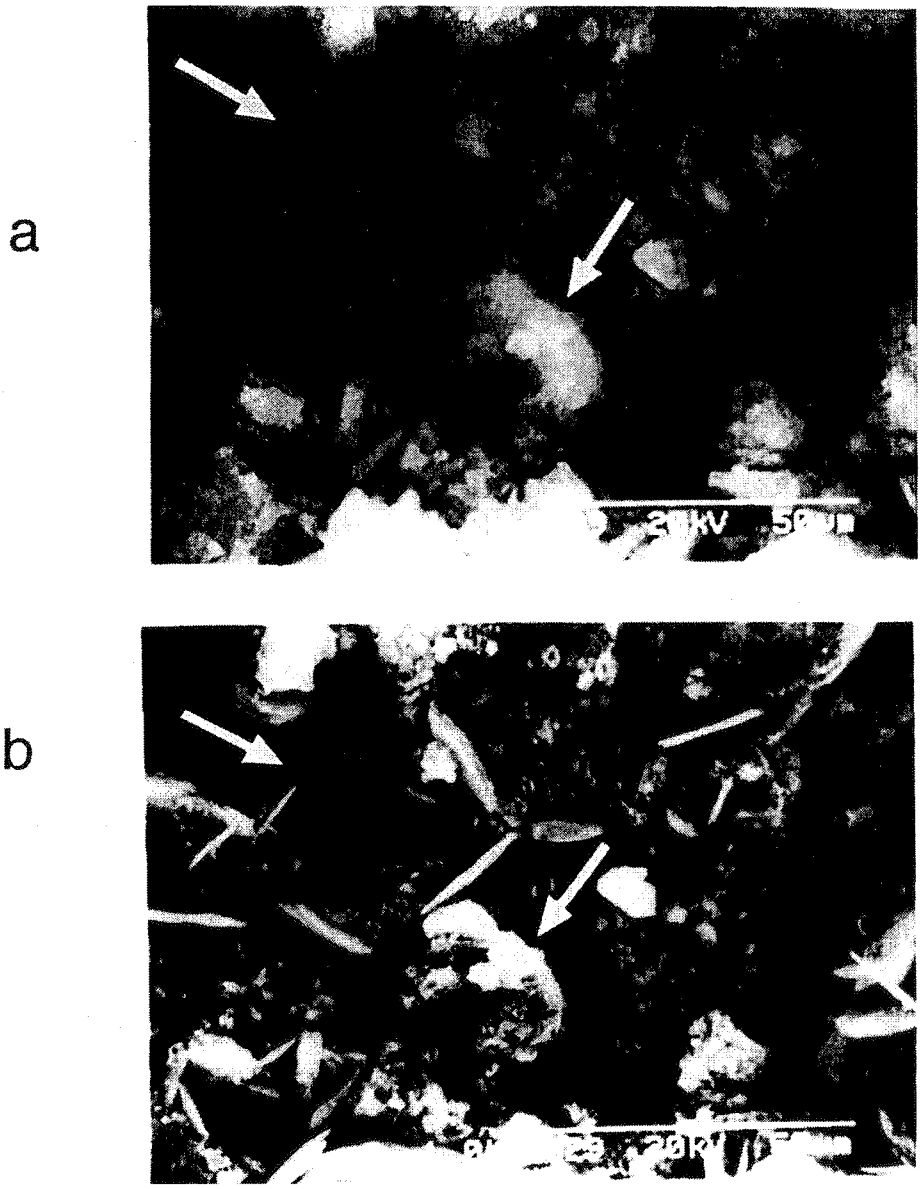

Figure 13. SEM images for the top views of (a) a gel layer formed on a porous alumina support, and products after crystallization times of (b) 1 day, (c) 2 days, (d) 5 days and (e) 7 days. A parent aluminosilicate gel with SiO_2/Al_2O_3 ratio = 18 was applied on the surface of a porous alumina disk. Crystallization was carried out at 453 K by the VPT method using a mixture of EDA : 2.0 Et_3N : H_2O. Since the same sample was repeatedly crystallized, the crystallization time represents total time for crystallization. From the XRD pattern of product, FER was found after 1 day of crystallization, and fully crystallized after 7 days.

ter as easily expected, the SDA would partially escape from the dry gel into the aqueous phase and then its degradation would take place when water condenses in the dry gel in large excess and forms a continuous phase. This is probably the case observed in figure 12(f).

Figure 13 gives the SEM images for the same position with repeated crystallization of a dry gel layer, which was formed on a porous alumina support [60]. The crystallization of the dry gel layer was performed by using the VPT method. As indicated by the arrows in figure 13, the growth of FER crystals is clearly observed with the consumption of dry gel. These SEM observations suggest that aluminosilicate intermediate species possibly formed by the hydrolysis of amorphous dry gel, migrate over the surface of the gel layer and participate in the crystal growth. However, since the positions and shapes of the parent dry gel are mostly retained, full dissolution of the dry gel did not occur.

Similar results were observed in the phase transformation from BEA to OU-1 [26,27]. No indication of the full dissolution of the parent dry gel and of the formation of amorphous phase was observed in the XRD patterns and SEM images during the phase transformation. OU-1 seemed to directly grow among the crystals without significant dissolution. While various possibilities have been suggested concerning phase transformation of zeolites [61,62], plausible mechanisms from BEA to OU-1 would be surface-mediated nucleation and growth: Partially hydrolyzed species are formed, and migrate over the

c

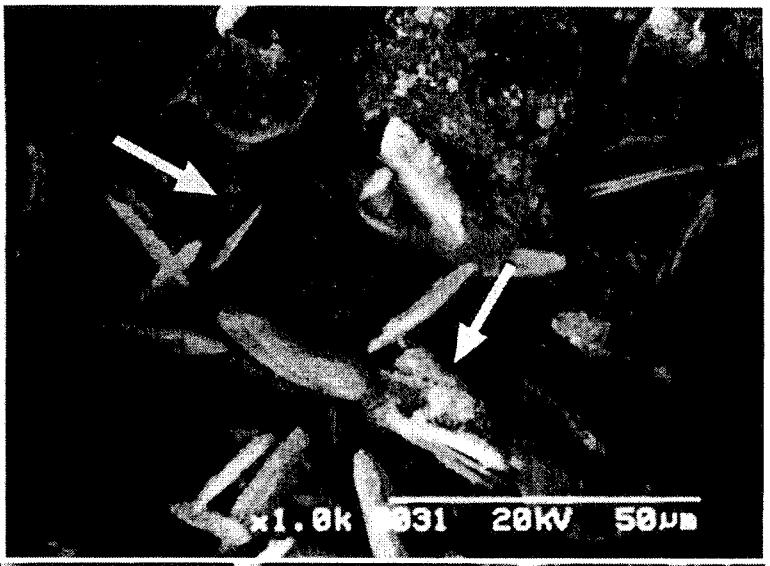

d

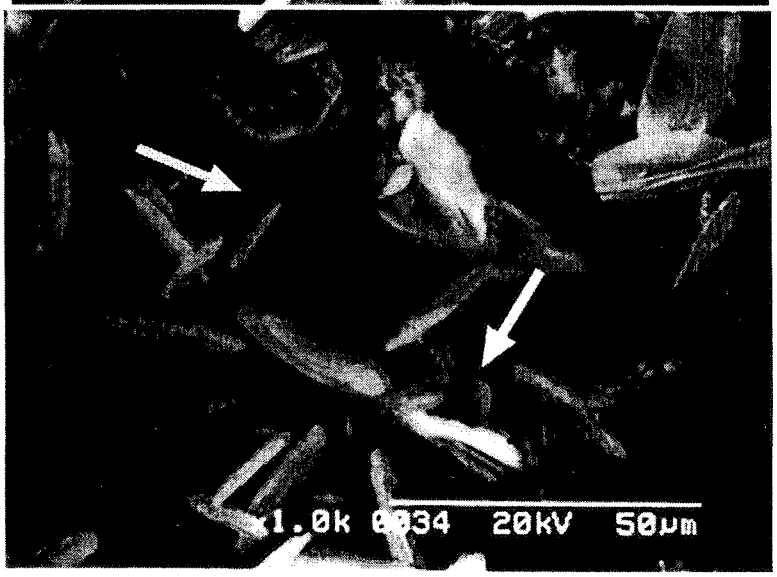

e

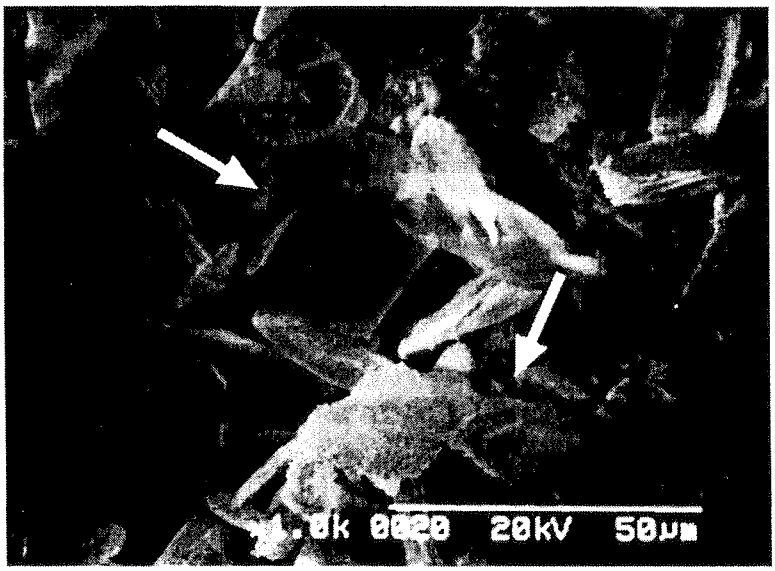

Figure 13. (Continued.)

surface of BEA crystals, and then OU-1 crystals nucleate and grow on the BEA surface.

In conclusion, we believe that the most striking characteristic of the DGC method is the stabilization of SDAs. In order to keep SDAs stable in the gel and product phases throughout crystallization, the amount of water should be as small as possible. Though keeping the saturated vapor pressure of water is essential for zeolite-forming reactions, a large excess amount of water condensing in the gel possesses a detrimental effect probably due to the degradation of SDA in the aqueous phase.

5. Concluding remarks

The DGC synthesis of microporous crystals is not a mere technique alternative to conventional hydrothermal synthesis. A wide variety of successful applications have been demonstrated in this paper. Syntheses of novel microporous crystals and crystallization mechanisms are worth investigating further. We consider that the DGC method has a great merit in studying crystallization mechanisms: All species expected to form the frameworks of microporous crystals stay in the solid phase, in contrast to the cases of hydrothermal syntheses where the information on crystallization is concerned with species dispersed into aqueous and gel (solid) phases. Elucidation of crystallization mechanisms involved in the DGC synthesis would also contribute to a better understanding of hydrothermal synthesis.

Apart from the scientific aspects described above, some advantages for industry can be drawn as follows: (1) Possible synthesis of zeolites possessing the same SiO_2/M_xO_y ratio to that of the parent gel, (2) possible continuous production of zeolites, (3) reduction of the consumption of expensive SDAs, (4) rapid crystallization, and (5) in the SAC method, no need for waste water treatment. Zeolite coatings using the DGC method are believed to be useful for creating novel structured catalysts and membranes.

We anticipate that these scientific and industrial merits will motivate the further study and development of the DGC method.

References

[1] D.M. Bibby and M.P. Dale, Nature 317 (1985) 157.
[2] Q. Huo, S. Feng and R. Xu, J. Chem. Soc., Chem. Commun. (1998) 1486.
[3] W. Xu, J. Li, W. Li, H. Zhang and B. Liang, Zeolites 9 (1989) 468.
[4] W. Xu, J. Dong, J. Li, W. Li and F. Wu, J. Chem. Soc., Chem. Commun. (1990) 755.
[5] M.H. Kim, H.X. Li and M. E. Davis, Microporous Mater. 1 (1993) 191.
[6] M. Matsukata, N. Nishiyama and N. Ueyama, Microporous Mater. 1 (1993) 219.
[7] T. Mole and J.A. Whiteside, J. Catal. 75 (1982) 284.
[8] E. Narita, K. Sato and T. Okabe, Chem. Lett. (1984) 1055.
[9] H. Hagiwara, Y. Kiyozumi, M. Kurita, T. Sato, H. Shimada, K. Suzuki, S. Shin, A. Nishijima and N. Todo, Chem. Lett. (1981) 1653.
[10] K. Chao, T.C. Tashi and M. Chen, J. Chem. Soc., Faraday Trans. 1 77(1981) 547.
[11] E. Costa, M.A. Ugina, A. De Lucas and J. Blanes, J. Catal. 107 (1987) 317.
[12] G. Boxhoorn, O. Sudmeijer and P.H.G. van Kasteren, J. Chem. Soc., Chem. Commun. (1983) 1416.
[13] T. Inui, Shokubai 25 (1984) 261.
[14] A. Nastro, C. Colela and R. Aiello, B. Drzaj, S. Hocevar and S. Penjovnic, eds., *Zeolites. Synthesis, Structure, Technology and Application* (Elsevier, Amsterdam, 1985) p. 39.
[15] J. Perez-Pariente, J.A. Martens and P.A. Jacobs, Zeolites 8 (1988) 46.
[16] U. Lohse, B. Altrichter, R. Donath, R. Fricke, K. Jancke, B. Parlitz and E. Schreiner, J. Chem. Soc., Faraday Trans. (1996) 159.
[17] M. Matsukata, N. Nishiyama and K. Ueyama, Microporous Mater. 7 (1996) 109.
[18] M.A. Camblor, A. Corma and S. Valencia, Microporous and Mesoporous Mater. 25 (1998) 59.
[19] J.C. van der Waal, M.S. Rigutto and H. van Bekkum, J. Chem. Soc., Chem. Commun. (1994) 1241.
[20] S.L. Burkett and M.E. Davis, Microporous Mater. 1 (1993) 265.
[21] M.A. Camblor, A. Corma and S. Valencia, Chem. Commun. (1996) 2365.
[22] P.R. Hari Prasad Rao and M. Matsukata, Chem. Commun. (1996) 1441.
[23] P.R. Hari Prasad Rao, C.A. Leon y Leon, K. Ueyama and M. Matsukata, Microporous and Mesoporous Mater. 21 (1998) 305.
[24] P.R. Hari Prasad Rao, K. Ueyama and M. Matsukata, Appl. Catal. A: General 166 (1998) 97.
[25] J.M. Newsam, M.M.J. Treacy, W.T. Koetsier and C.B. de Gruyter, Proc. Roy. Soc. London A 420 (1988) 375.
[26] P.R. Hari Prasad Rao, K. Ueyama, E. Kikuchi and M. Matsukata, Chem. Lett. (1998) 311.
[27] M. Matsukata, M. Kato T. Suzuki, Y. Sasaki, E. Kikuchi, K. Ueyama and P.R. Hari Prasad Rao, in: *Proc. 12th Intern. Zeolite Conf.*, Baltimore, 1998, eds. M.M.J. Treacy, B. Marcus, J.B. Higgins and M.E. Bisher, Mater. Res. Soc., in press.
[28] R.F. Lobo, M. Tsapatsis, C.C. Freyhardt, I. Chan, C.C. Chen, S.I. Zones and M.E. Davis, J. Am. Chem. Soc. 119 (1997) 3732.
[29] R. Kumar, K.R. Reddy and P. Ratnasamy, US Patent 5219813 (1993).
[30] F. Delprato, L. Delmotte, J.L. Guth and L. Huve, Zeolites 10 (1990) 546.
[31] M. Matsukata, K. Kizu and E. Kikuchi, in: *Proc. First Intern. Conf. on Inorganic Mater.*, Versailles, France, 1998, P20, in preparation.
[32] C.B. Khouw and M.E. Davis, J. Catal. 151 (1995) 77.
[33] B. Notari, Adv. Catal. 41 (1996) 253.
[34] M.A. Camblor, A. Corma, A. Martinez and J. Perez-Pariente, J. Chem. Soc., Chem. Commun. (1992) 589.
[35] A. Corma, M.A. Camblor, P. Esteve, A. Martinez and J. Perez-Pariente, J. Catal. 145 (1994) 151.
[36] R.J. Saxton, G.L. Crocco, J.G. Zajacek and K.S. Wijesekera, EP659685 A1 (1994).
[37] M.A. Camblor, M. Constantini, A. Corma, L. Gilbert, P. Esteve, A. Martinez and S. Valencia, Appl. Catal. 133 (1995) L185.
[38] M.A. Camblor, M. Constantini, A. Corma, L. Gilbert, P. Esteve, A. Martinez and S. Valencia, Chem. Commun. (1996) 1339.
[39] M.S. Rigutto, R. de Ruiter, J.P.M. Niederer and H. van Bekkum, Stud. Surf. Sci. Catal. 84 (1994) 2245.
[40] J.S. Reddy and A. Sayari, J. Chem. Soc., Chem. Commun. (1990) 755.
[41] T. Tatsumi, Q. Xia and N. Jappar, Chem. Lett. (1997) 677.
[42] N. Jappar, Q. Xia and T. Tatsumi, J. Catal. 180 (1998) 132.
[43] P.R. Hari Prasad Rao, K. Ueyama, E. Kikuchi and M. Matsukata, in: *Proc. 12th Intern. Zeolite Conf.*, Baltimore, 1998, eds. M.M.J. Treacy, B. Marcus, J.B. Higgins and M.E. Bisher, Mater. Res. Soc., in press.
[44] R. de Ruiter, A.P.M. Kentgens, J. Grootendorst, J.C. Jansen and H. van Bekkum, Zeolites 13 (1993) 128.

[45] R. Bandyopadhyay, Y. Kubota and Y. Sugi, Chem. Lett. (1998) 813.
[46] M.J. Annen, M.E. Davis, J.B. Higgins and J.L. Schlenker, J. Chem. Soc., Chem. Commun. (1991) 1175; L.B. McCuster, R.W. Grosse-Kunstleve, Ch. Baerlocher and M. Yoshikawa, Microporous Mater. 6 (1996) 295.
[47] M.J. Annen and M.E. Davis, Microporous Mater. 1 (1993) 57.
[48] C.C. Freyhardt, R.F. Lobo, S. Khodabandeh, J.E. Lewis Jr., M. Tsapatsis, M. Yoshikawa, M.A. Camblor, M. Pang, M.M. Helmkamp, S.I. Zones and M.E. Davis, J. Am. Chem. Soc. 118 (1996) 7299.
[49] M. Yoshikawa, S.I. Zones and M.E. Davis, Microporous Mater. 11 (1997) 127; 11 (1997) 137.
[50] C. Rohrig, H. Gies and B. Marler, Zeolites 14 (1994) 218.
[51] M. Nomura, E. Kikuchi and M. Matsukata, in preparation.
[52] For example:
(a) T. Sano, Y. Kiyozumi, M. Kawamura, H. Takaya, T. Mouri, W. Inaoka, M. Watanabe and K. Toyoda, Zeolites 11 (1991) 842;
(b) J.G. Tsikoyiannis and W.O. Haag, Zeolites 12 (1992) 126;
(c) E.D. Geus, M.J. Exter and H. van Bekkum, J. Chem. Soc., Faraday Trans. 88 (1992) 3101.
[53] M. Matsukata, N. Nishiyama and K. Ueyama, J. Chem. Soc., Chem. Commun. (1994) 339.
[54] N. Nishiyama, K. Ueyama and M. Matsukata, Microporous Mater. 7 (1996) 299.
[55] E. Kikuchi, K. Yamashita, S. Hiromoto, K. Ueyama and M. Matsukata, Microporous Mater. 11 (1997) 107.
[56] M. Matsukata, N. Nishiyama and K. Ueyama, Stud. Surf. Sci. Catal. 84 (1994) 1183;
N. Nishiyama, T. Matsufuji, K. Ueyama and M. Matsukata, Microporous Mater. 12 (1997) 293.
[57] N. Nishiyama, K. Ueyama and M. Matsukata, AIChE J. 43 (1997) 2724.
[58] N. Nishiyama, K. Ueyama and M. Matsukata, J. Chem. Soc., Chem. Commun. (1995) 1967.
[59] M. Matsukata and E. Kikuchi, Bull. Chem. Soc. Jpn. 70 (1997) 2341.
[60] T. Matsufuji, N. Nishiyama, K. Ueyama and M. Matsukata, Microporous and Mesoporous Mater., submitted.
[61] R.M. Barrer, *Hydrothermal Chemistry of Zeolites* (Academic Press, London, 1982).
[62] P. Norby, J. Am. Chem. Soc. 119 (1997) 3732.

Proceedings of the International Conference
on Solid-Solid Phase Transformations '99 (JIMIC-3)
Edited by M. Koiwa, K. Otsuka and T. Miyazaki
The Japan Institute of Metals, 1999.

Conversion of Dry Gels to Zeolites

Masahiko Matsukata, P.R.H. Prasad Rao, Takayuki Osaki, Masaru Ogura, and Eiichi Kikuchi
Department of Applied Chemistry, Waseda University
3-4-1 Okubo, Shinjuku, Tokyo 169-8555 Japan
e-mail: mmatsu@mn.waseda.ac.jp

Keywords: zeolite crystallization, Dry Gel Conversion, Beta, OU-1, structure-directing agent, phase transformation of zeolite

Abstract

Crystallization of zeolite using an organic compound as a structure-directing agent (SDA) and phase transformation of zeolite into another phase were investigated by means of a new crystallization method of dry gel conversion (DGC). Different types of zeolite were crystallized by DGC with SDAs having different sizes in alkyl chains of organics. Not the size of SDAs but the type of them determines the phase crystallized. Phase transformation of zeolite beta occurred into a new phase of zeolite OU-1, which has the same topology as zeolites SSZ-31 and NCL-1. From XRD and SEM observations, it can be concluded that the phase transformation occurs via surface-mediated nucleation and growth without significant dissolution nor destruction of zeolite structure.

Introduction

Zeolites, microporous aluminosilicate crystals, have so far been crystallized by using hydrothermal synthetic method [1]. We have recently developed an alternative new method to synthesize zeolites [2]. In this method, powdery aluminosilicate dry gel containing organic structure-directing agents is crystallized to zeolites in the presence of steam (Dry Gel Conversion method). Aluminosilicate hydrogels containing tetraethylammonium (TEA) cation were prepared, and dried at 353 K. The resultant dry gel was placed in a special autoclave and crystallized in steam at autogeneous pressure and 453 K. We have found that fully crystallized zeolite beta (BEA) having a three dimensional micropore system of 0.55x0.55 nm in [001] direction and 0.76x0.64 nm in <100> direction with a wide range of Si/2Al ratio from 30 to infinity could be obtained in this DGC method, whereas the range of Si/2Al ratio to give BEA is limited to ca. 20-250 in conventional hydrothermal synthesis. Moreover, high silica BEA was found to transform to other phases, zeolite MTW or OU-1 that is a novel phase found in our previous study [3], with prolonged crystallization, possibly via a surface-mediated phase transformation process. Phase selection of MTW and OU-1 was governed by sodium concentration in the parent dry gel.

In this presentation, we will report crystallization of zeolites by the dry gel conversion method using organic compounds with different lengths of alkyl chain in them, and further phase transformation of BEA to another phase of zeolite, OU-1, with prolonged crystallization.

Experimental

Zeolites were prepared from dry gel having compositions of SiO_2: $0.033Al_2O_3$: $0.44SDA$: $0.096Na_2O$. An aqueous solution including a hydroxide of SDA, tetramethylammonium (TMA), tetraethylammonium (TEA), or tetrapropylammonium (TPA) was used. An aqueous solution containing a required amount of $Al_2(SO_4)_3$ was added to the mixture. The mixture was heated to 353 K after stirring for 2 h and dried while stirring. The dried gel was crushed into powder and placed in a Teflon cup inside an autoclave, at the

bottom of which a small amount of water as a source of steam was poured. The amount of water poured was 0.5 ml. The volume of the autoclave was 45 cm^3, and the saturated water vapor pressure at 453 K was 10.2 atm. The amount of water in the autoclave was, thus, enough to achieve the saturated water vapor pressure during crystallization. Crystallization of the dry gel was carried out at 453 K for 12 h, followed by filtration and washing with distilled water.

Phase transformation of BEA into OU-1 was investigated using a dried gel of SiO_2: $0.0026Al_2O_3$: 0.042TEAOH: $0.096Na_2O$. Crystallization was prolonged to 60h at 453 K.

X-ray diffraction patterns were measured by RINT 2000 (Rigaku instrument Co.) with Cu K_α radiation. FE-SEM images were taken with Hitachi 2500S.

Results and Discussion

Figure 1 shows the X-ray diffraction patterns of products obtained by the DGC method with various organic amines in dry gels. When TMAOH, TEAOH, or TPAOH was used as a SDA, a zeolitic phase attributable to offretite (abbreviated to OFF), beta (BEA), or ZSM-5 (MFI) appeared after crystallization at 453 K, respectively. OFF has a three-dimensional structure with 0.36x0.52 nm pore-opening, while BEA and MFI has those with 0.64x0.76 and 0.55 nm, respectively. This result does not mean that either length or size of alkyl chain in amine molecules determines a crystal phase.

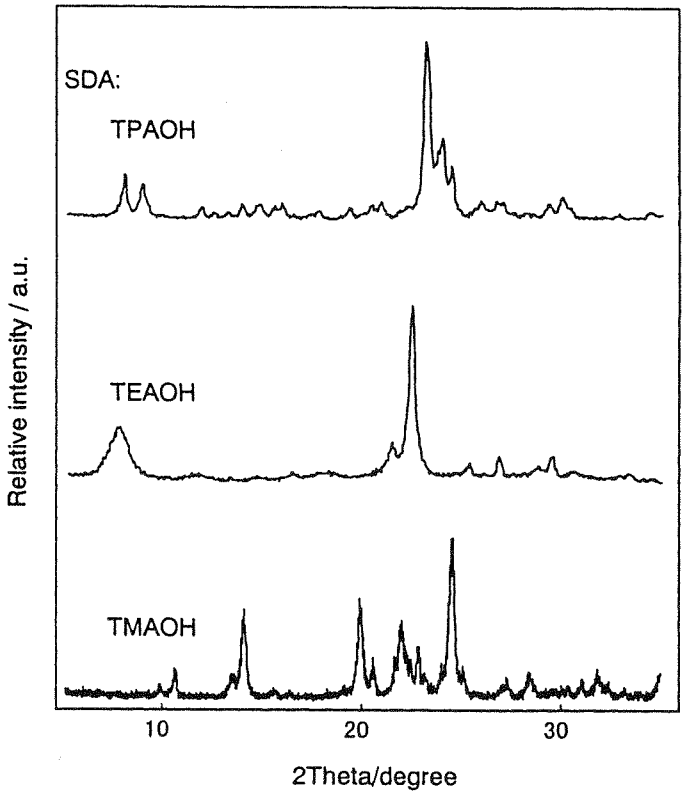

Figure 1. XRD patterns of products obtained by DGC method, using TMAOH, TEAOH, and TPAOH as structure-directing agents.

We have discussed about the crystallization of BEA by DGC [2]. In our previous study, TEA cation was found to interact with anionic silicon and aluminium oxides of Si-O and Al-O^- to form Si-O-TEA and Al-O-TEA bondings. Many of SDAs like quaternary ammonium cations, are unstable in an alkaline aqueous solution. A stabilization of SDA

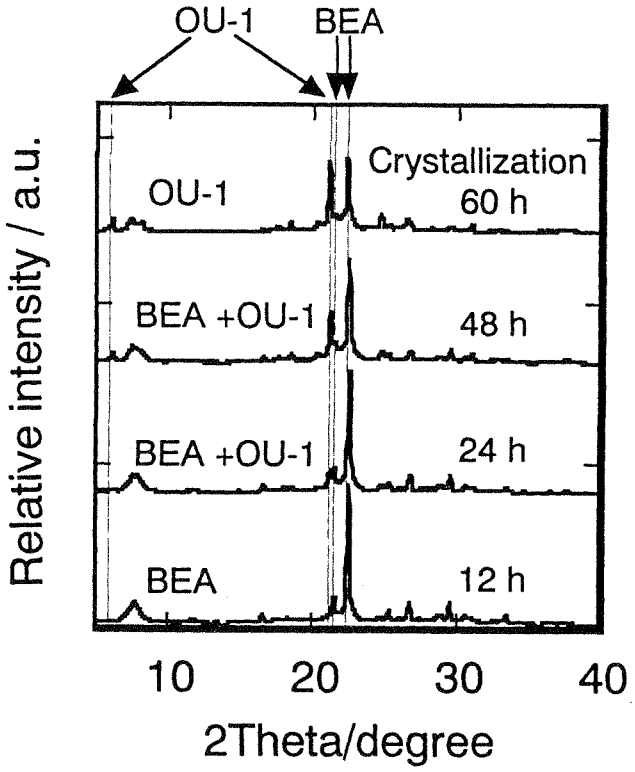

Figure 2. XRD patterns during phase transformation of BEA into OU-1.

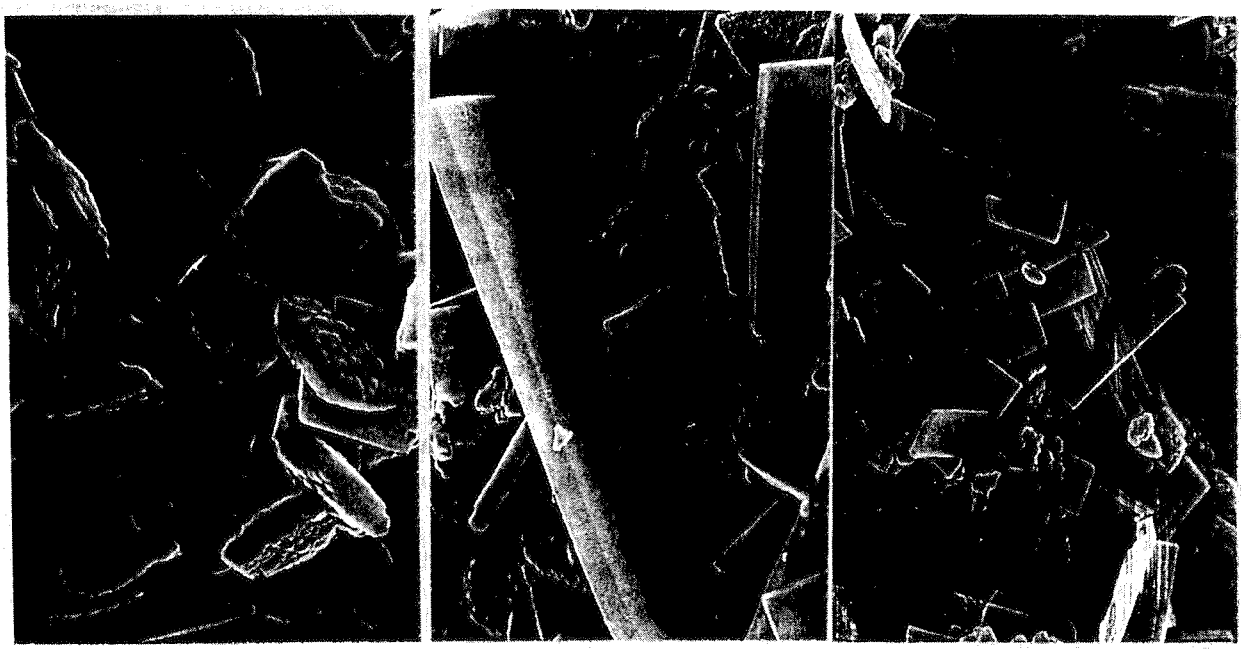

Figure 3. FE-SEM images of BEA and OU-1 in the course of phase transformation.

molecules or cations is impossible in an alkaline hydrogel used in conventional hydrothermal synthesis. TEA cation in an as-received aqueous solution is easy to decompose, while it is stabilized inside the BEA framework that is confirmed by thermal decomposition of TEA with as-made samples. The DGC allowing stabilization of SDA might lead us to obtain zeolites which cannot be obtained by hydrothermal synthesis.

We have already found that phase transformation of BEA occurs to form denser phases with prolonged crystallization [3]. As shown in Figure 2, a new phase in XRD pattern came after 60 h crystallization in the case of crystallization conditions of BEA with SiO_2/Al_2O_3=380 and Na_2O/SiO_2=0.042. Typical diffraction peaks appear at 6.2, 7.4, 8.2, 21.2 and 24.9 degree. The new phase has been named as OU-1, which has a topology analogous to the zeolite SSZ-31 [4] or NCL-1 [5]. From the results of structural analysis, OU-1 possesses one dimensional 12-membered oxygen ring pore-opening system, which runs along the longitudinal [001] direction. It is interesting that OU-1 can be obtained through the phase transformation using TEA as a SDA, more easily than the syntheses of SSZ-31 and NCL-1 requiring N,N,N-trimethyltricyclo[5.2.1.$0^{2,6}$]decaneammonium and hexamethylenebis(triethylammonium bromide), respectively. BEA and OU-1 have a similar type of polymorphs A (ABAB...stacking) and B (ABCABC...stacking). The phase transformation of BEA to OU-1 in DGC method might be caused by the rearrangement of T-atoms without complete destruction of BEA framework.

Figure 3 shows the SEM images of BEA and OU-1 formed during crystallization. It is clearly observed that tiny particles of BEA were transformed gradually into thin and plate-like rectangular particles, which are typical for OU-1. The results of SEM observation and XRD measurement indicated that dissolution of parent dry gel occurs, and that a formation of amorphous phase is not observed during the phase transformation. OU-1 seems to be crystallized among the BEA particles without significant dissolution. While various possibilities have been suggested, concerning phase transformation of zeolites [6], plausible mechanisms from BEA to OU-1 would be surface-mediated nucleation and growth: partially hydrolyzed species were formed, and migrated over the surface of BEA crystals, and then OU-1 crystals nucleated and grew on BEA surface.

Conclusions

The role of SDA during crystallization of zeolite is mainly on determination of crystal structure; nevertheless larger the molecular size of SDA is used, smaller the pore size of zeolite is crystallized. For example, TPA cation larger than TEA is used as a SDA, zeolite MFI having a smaller size of pore than that of BEA is formed. The most striking characteristic of the DGC method is the stabilization of SDAs during crystallization. Phase transformation of zeolite BEA occurs into much denser phase of OU-1, which has a same topology of SSZ-31 and NCL-1. Significant dissolution of zeolitic crystal structure is not observed in the course of the phase transformation. This phenomenon is attributed to the rearrangement of T-atoms according to a surface-mediated nucleation mechanism without destruction of zeolite structure.

References

[1] Davis, M. E., *Synthesis of Porous Materials: zeolites, clays, and nanostructures*, ed. by M.L. Occelli and H. Kessler, Marcel Dekker, Inc., p. 1 (1997).

[2] Rao, P.R.H.P., Matsukata, M., *Chem. Commun.*, (1996) 1441.

[3] Rao, P.R.H.P., Ueyama, K., Kikuchi, E., and Matsukata, M., *Chem. Lett.*, **1998**, 311.

[4] Lobo, R.F., Tsapatsis, M., Freyhardt, C.C., Chan, I., Chen, C.C., Zones, S.I., and Davis, M.E., *J. Am. Chem. Soc.*, **119**, 3732 (1997).

[5] Kumar, R., Reddy, K.R., and Ratnasamy, P., U.S. Patent 5219813 (1993).

[6] Norby, P., *J. Am. Chem. Soc.*, **119**, 5215 (1997).

酸化物：ドライゲルコンバージョン法を中心とするゼオライト合成とその特性

早稲田大学理工学部応用化学科　　松方正彦

1．はじめに

ゼオライトが人工的に合成されるようになって約30年が経つ。この間、ゼオライト合成と言えば、もっぱら水熱合成によって行われてきた。水熱合成によるゼオライト合成のメカニズムはいまだに明らかではなく、ゼオライト合成における核発生と結晶成長に関する議論はごく最近の研究のトピックスであるが、長年の疑問のひとつはゼオライト生成に果たす水の役割であった。

一方、ここ10年ほどの間、水を連続相としないゼオライト合成に関する研究が行われるようになってきた。本稿では、水を連続相としないゼオライト合成に関する既往の研究について紹介し、筆者らが最近進めているドライゲルコンバージョン法について、その特徴について述べたい。

2．非水系溶媒を用いた合成法

1985年にBibby and Dale[1]は、シリカソーダライトがフュームドシリカ・水酸化ナトリウム系からエチレングリコールを連続相として、150℃で生成することを報告した。この報告は、水を用いないゼオライト合成のはじめての例となり、連続相としての水がゼオライト合成にとって必ずしも必須ではないことを示したことで意義深い。彼らは、ゼオライトは、水熱合成と同様に水酸化ナトリウムによるSi-O-Si結合の切断と再縮合により生成し、エチレングリコールの役割は、反応途中で生成する中間体の溶媒和による安定化にあると推察している。

シリカソーダライトは、必ずしも工業的に有用なゼオライトではないが、Xuら[2]は、エチレンジアミン(EDA)とトリエチルアミン(Et_3N)の混合溶液を用いて、SiO_2/Al_2O_3比が18.8－70.0の範囲で、ZSM-5とフェリエライトが生成することを報告した。彼らはこの論文中で、結晶化途中の溶液中にアルミノシリケートの溶出が起きなかったので、Bibby and Daleの提案[1]とは異なり、非晶質アルミノシリケートの固相転移により直接ゼオライトが生成したと結論している。しかし、水熱合成においてゲル相の生成を経由する場合には、水相中のアルミニウム、珪素の濃度が極端に低下する(仕込みの数百～数千分の1以下)ことはしばしば起きるので、Xuらの提案[2]は測定法の正確さを含め、さらに吟味が必要と思われる。

Kupermanら[3]は、種々の非水溶媒系によるゼオライト合成を試み、0.4 - 5 mmといった巨大な結晶の合成に成功している。SiO_2･HF･ピリジン系からはDodecasil-3C、SiO_2･HF･ピリジン･プロピルアミン系およびSiO_2･Al_2O_3･HF･Et_3N･臭化テトラプロピルアンモニウム(TPA-Br)系からはフェリエライト、SiO_2･HF･Et_3N･TPA-Br系からはシリカライト、Al_2O_3･P_2O_5･Et_3N･ポリエチレングリコール系からはある種の$AlPO_4$-nが生成することが報告された。彼らが合成に成功したような大結晶は、ゼオライトのミクロ細孔をデバイス合成用の容器として使用する場合に必要である。この非水溶媒系の合成法は、こうした大きくかつ欠陥の少ないゼオラ

イト結晶の合成に有望となろう。

3．ドライゲルコンバージョン法

2項で述べたゼオライト合成の手法は、水を用いないまでも、連続相として液相を用いた方法であった。これに対して、あらかじめ原料ゲルを乾燥し、これを気相雰囲気下で結晶化する方法がドライゲルコンバージョン法である。筆者らが用いているドライゲルコンバージョン法には、気相輸送法および水蒸気処理による結晶化法の2種類がある。前者はエチレンジアミン(EDA)など気化が可能な有機物を結晶化剤(Structure-directing agent)として用いる場合であり、後者はクラウンエーテルのように結晶化温度における蒸気圧が低い結晶化剤、あるいは4級アンモニウム塩のように気化できない結晶化剤を用いる場合である。

3.1 気相輸送法

1990年にXuら[4]は、$0.15Na_2O:Al_2O_3:86.4SiO_2$の組成をもつゲルを823Kにて焼成した後、EDA、トリエチルアミン(Et_3N)および水の混合蒸気の自己圧下において453Kにて7日間処理すると、ZSM-5が得られることを初めて報告した。筆者ら[5][6]およびKimら[7]はこの報告に注目し、Xuらの合成方法によってZSM-5が生成することを追試して確認した。

図1には筆者らが用いているオートクレーブを示す。オートクレーブの中段に乾燥ゲルを、底部に結晶化剤を含む水溶液を入れる。このとき、水溶液の組成のみならず、仕込み量が生成物の結晶化速度、結晶径に著しく影響を及ぼすことが、経験的にわかっている。その原因については明らかではなく、今後検討が必要である。中段の乾燥ゲルを支えるには、筆者らは当初特注の多孔性テフロン板を用いていたが、濾紙で適当に工夫して支えを作ったり、あるいはテフロン製のカップを用いれば充分である。また、通常水性ゲルを乾燥後、適当に粉砕してから結晶化を行っているが、粉砕せずに塊状の乾燥ゲルを用いても充分に結晶化は可能である。

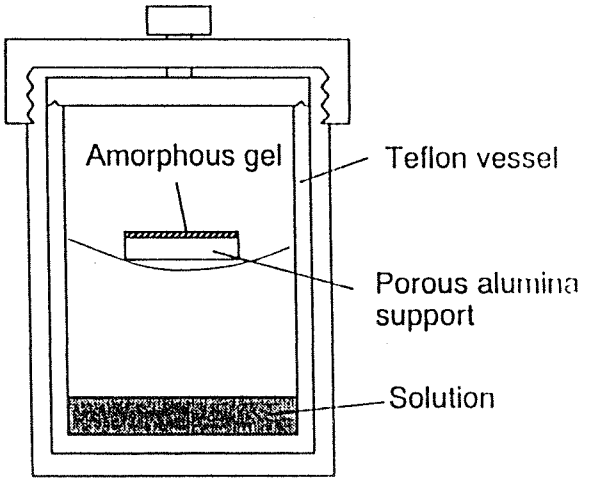

図1 ドライゲルコンバージョンに用いるオートクレーブ

表1には本合成法を用いて行った結晶化実験の結果を示す[5]。適当なゲル組成、結晶化剤水溶液組成(EDA、ET_3N混合水溶液)にて、ZSM-5、フェリエライト(FER)などの工業的にも有用なゼオライトが合成できることがわかる。ただし、EDAのみ、あるいはEt_3Nのみでは結晶化せず、両者の共存が必須である。興味深いのは、生成したFER結晶の元素分析を行ったところ、EDAのみが結晶化に存在し、Et_3Nは結晶内には取り込まれていなかったことである[6]。Et_3Nが結晶化に必須であるにもかかわらず、生成物中に存在しないのは理解が難しく、結晶化機構の解明が待たれる。なお、EDAの含有量からは、FERの酸素10員環よりなる細孔のインターセクションに丁度1分子づつEDAが存在していると計算され、これはEDAがフェリエライトの構造形成に主たる役割を果たしていることと矛盾しない。Kimら[7]はEDA, Et_3Nの替

わりにプロピレンジアミン、トリプロピルアミンの混合水溶液を蒸気源として結晶化を行い、ZSM-5、GIS、MORが得られることを報告している。本合成法では、アミン類など結晶剤がオートクレーブ底部の液層から蒸気として供給され、これがゲル中に浸透して結晶化が起きるため、Kimらは本合成法をVapor-phase transport methodと呼んだ。気相輸送法はその和訳である。

表1 気相輸送法による合成結果。結晶化：160℃、6日間。

Run	Initial amorphous gel Composition	pH	Liquid phase composition	Product
1	$14Na_2O:Al_2O_3:29SiO_2$	12.0	H_2O	ANA
2	$14Na_2O:Al_2O_3:29SiO_2$	12.0	$EDA:5.3Et_3N:2.5H_2O$	ANA
3	$14Na_2O:Al_2O_3:29SiO_2$	11.0	H_2O	Amorphous
4	$14Na_2O:Al_2O_3:29SiO_2$	11.0	$EDA:5.3Et_3N:2.5H_2O$	FER
5[a)]	$12Na_2O:Al_2O_3:26SiO_2$	9.3	$EDA:5.3Et_3N:2.5H_2O$	FER + MFI
6	$6Na_2O:Al_2O_3:26SiO_2$	10.9	$EDA:5.3Et_3N:2.5H_2O$	MFI
7[a,b)]	$15Na_2O:Al_2O_3:31SiO_2$	9.6	$1\text{-}PrOH:2.0Et_3N$	MFI
8	$14Na_2O:Al_2O_3:29SiO_2$	9.5	$EDA:5.3Et_3N:2.5H_2O$	FER
9	$14Na_2O:Al_2O_3:29SiO_2$	9.6	$EDA:17.3Et_3N:7.4H_2O$	TON
10[a)]	$14Na_2O:Al_2O_3:29SiO_2$	9.9	$2.5EDA:H_2O$	Amorphous
11[a)]	$14Na_2O:Al_2O_3:29SiO_2$	9.9	$2.1Et_3N:H_2O$	Amorphous
12[a)]	$14Na_2O:Al_2O_3:29SiO_2$	10.0	$1.1\ 1\text{-}PrOH:H_2O$	Amorphous
13	$12Na_2O:Al_2O_3:25SiO_2$	10.9	$EDA:5.3Et_3N$	FER

Initial gel compositions and pH are the values before rinse. Compositions are shown by using molar ratio. [a)] Gel was not dried before crystallization. [b)]

生成物の ^{29}Si-NMRおよび ^{28}Al-NMRスペクトルからは、原料乾燥ゲルの完全な結晶化が可能であることがわかった。通常の水熱合成では、原料に用いたAlは比較的有効に結晶化に使われるが、Si源が完全にゼオライト化する例は多くない。ただし、結晶化途中におけるSiO_2/Al_2O_3比の経時変化を検討すると、図2に示すように、常に生成物のSiO_2/Al_2O_3比が仕込みゲル組成と一致しているわけではなく、結晶化初期ではSiO_2/Al_2O_3比は仕込み組成よりかなり低く、Alの周囲から結晶化していることがわかる。やがて周囲のSi源が結晶化するため、結晶化が完了するに至って仕込みゲル組成と一致したSiO_2/Al_2O_3比のゼオライトが生成することになる。さらに、ほとんどのゼオライトでは、生成できるSiO_2/Al_2O_3比の範囲が限定されており、いかなるSiO_2/Al_2O_3比のゼオライトが合成できるというわけではない。

結晶化度が比較的容易に100%となり、原料乾燥ゲルと同じSiO_2/Al_2O_3比のゼオライトの合成が容易に行える（狙ったSiO_2/Al_2O_3比のゼオライトを容易に合成できる）ことは、気相輸送

法の重要な利点の一つである。また、ゼオライト合成において有機結晶化剤のコストは、工業的には常に頭の痛い問題であるが、本合成法では過剰の有機結晶化剤の大部分は、底部の溶液中に残るので再使用が可能と思われる。また、水熱合成と比べ、ゲルの体積は乾燥する分減少するため、合成容器単位体積あたりの生産性は向上するはずである。

以上は粉末状ゼオライト合成における気相輸送法の特長であるが、本合成法は薄膜状ゼオライトの合成にも有効である。薄膜状ゼオライトは、分子選択性無機分離膜、耐熱性センサー、光学材料、半導体デバイスなど様々な展開が期待されている新しい材料である。ゼオライト源は、自立膜としても合成可能であるが、機械強度が乏しいため、多孔性焼結金属あるいは多孔性セラミックス上に担持することになる。気相輸送法を用いて薄膜を合成する場合では、あらかじめ薄膜状にゲルを製膜しておき、これを結晶化するため、モノリスなど複雑な形状をもつ担体への均一な製膜が期待できる。一方、水熱法によるゼオライト合成では、よく知られているように、オートクレーブ壁から水性ゲルへの伝熱、粘土の高い水性ゲルの撹拌、混合の制御の困難が伴い、製膜条件および装置のスケールアップが難しいように想像される。筆者らは、これまでFER、MOR、ZSM-5膜の合成を多孔質α-アルミナ支持体を用いて行い、ガス透過、炭化水素混合物の浸透化気化分離において選択性が発現することを見いだしている[8]。

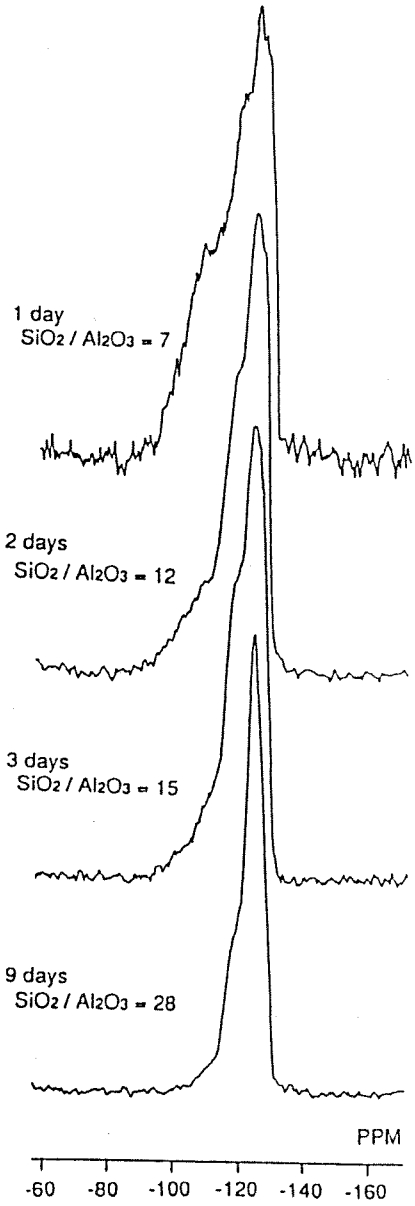

図2 気相輸送法によって合成したZSM-5の29Si-NMRスペクトル

3.2 水蒸気処理による結晶化法

ゼオライト合成に用いられる結晶化剤としては、EDAのような揮発性のアミンばかりではなく、4級アンモニウム塩が用いられる。4級アンモニウム塩は、気化が難しく、かつ水溶液中において数十℃以上では不安定で容易に分解することから、気相輸送法を適用することが出来ない。

そこで、筆者らは、アルミノシリケートゲルの調製段階であらかじめ結晶化剤を添加し、これを乾燥することにより結晶化剤を含む乾燥ゲルを得、これを水蒸気中で処理することによって結晶化を行う方法を提案してきた[9][10][11]。

3.2.1 BEAおよびOU-1

図3には、この方法によるBEAの合成レシピを示す。BEAは酸素12員環よりなる細孔が3次元的に繋がったLarge-poreゼオライトであり、最近触媒、吸着剤として注目されている。

水熱合成法によるBEAの合成には、テトラエチルアンモニウム(TEA)が結晶化剤として通常用いられるが、本合成法でもTEAを用いることが出来る。TEAは非常に不安定で、水溶液をそのまま加熱すると直ちに分解し溶液は茶褐色となるが、乾燥ゲル中に取り込まれたTEAは安定で、80-100℃程度で乾燥を行って、ゲルは白色のままである。このことは、TEA^+がSiO^-あるいはAlO^-とイオン結合することにより、ゲル中で安定化されることを示している。オートクレーブに仕込む水の量は極めて重要である。BEAの合成には例えば100mlのオートクレーブの場合、仕込水の量は0.5-1.0mlとごくわずかで充分であり、飽和水蒸気圧が得られる。ただし、合成条件下で水が飽和水蒸気圧以下になると、結晶化は充分に進行しない。また、水が過剰の場合には、乾燥ゲルに対して過剰の水の凝縮が起き、この場合にも結晶化は充分に進行しない。結晶化が成功している場合には、オートクレーブを開けると生成物は乾燥した粉末状で得られる。

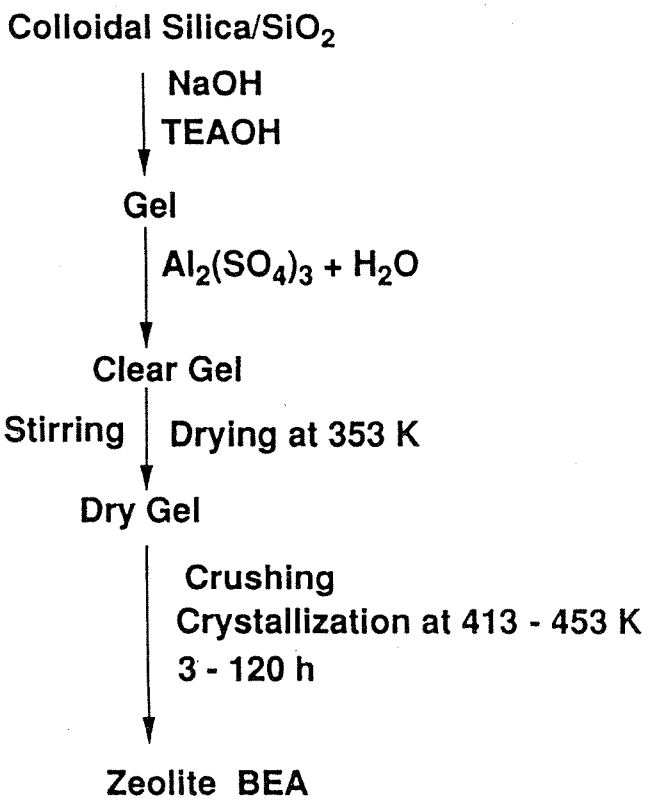

図3 ドライゲルコンバージョン法による
BEAの合成レシピ

図4には、種々のSiO_2/Al_2O_3比の乾燥ゲルを結晶化させたときの結晶化度の経時変化を示す。水熱合成では、数日以上必要であるが、図に示すように本合成法ではSiO_2/Al_2O_3比＝30の場合、わずか3hで結晶化が完了する。さらに、水熱合成では通常SiO_2/Al_2O_3比＞100のBEAは合成が難しいが、本合成法ではSiO_2/Al_2O_3＝730でも12hで結晶化が完了する。得られるBEAの粒径はSiO_2/Al_2O_3比＝30では数十nmと小さく、SiO_2/Al_2O_3比が高くなると大きくなり、SiO_2/Al_2O_3比＝730では約600nmである。いずれのSiO_2/Al_2O_3比においても粒径は均一である。現在までにSiO_2/Al_2O_3比＝30～∞の範囲で結晶化度の高いBEAの合成が可能であることを確認している。SiO_2/Al_2O_3比＝730のBEAを空気焼成して、窒素吸入によってBET表面積を求めると、450℃では631m^2g^{-1}、900℃では656m^2g^{-1}と安定である。1100℃でも587m^2g^{-1}と高比表面積を維持しており、本方法で合成されたBEAは熱的にも極めて安定である。ただし、耐熱性はSiO_2/Al_2O_3比に依存し、SiO_2/Al_2O_3比＝30の場合には1100℃焼成では構造は完全に崩壊し、非晶質となる。

本合成法は、気相輸送法と同様な特長があることは勿論のこと、それ以外にも、極めて結晶化が速いこと、結晶化は水蒸気中で行われるため排水処理が不要となること、といった利点がある。また、水熱合成では得られないハイシリカなゼオライトBEAが得られることから、水熱合成法の単なる代替ではないことも明らかとなってきた。メタロシリケートの合成

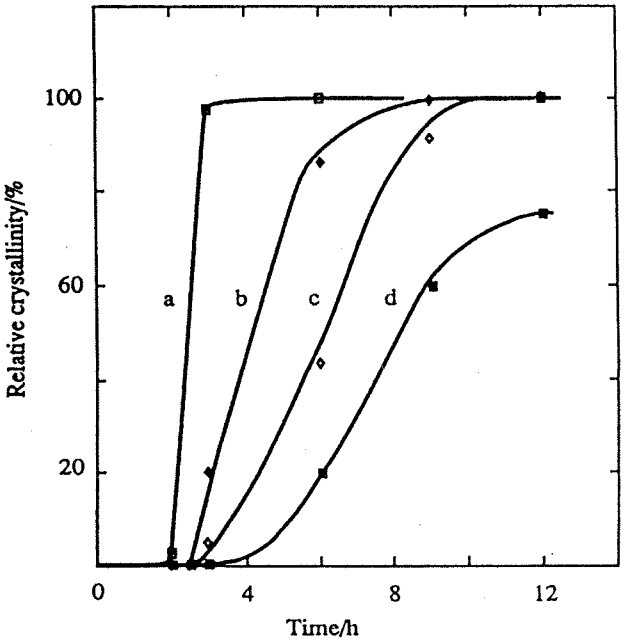

図4 BEAの結晶化曲線。原料組成（SiO_2/Al_2O_3比、SiO_2/Na_2O比、SiO_2/SO_4^{2-}比の順）：a, 30, 23.8, 20.9; b, 380, 23.8, 528; c, 730, 10.9, 10; d, 730, 23.8, 0。結晶化温度、180℃。SiO_2/SO_4^{2-}比は硫酸を添加することにより調整。

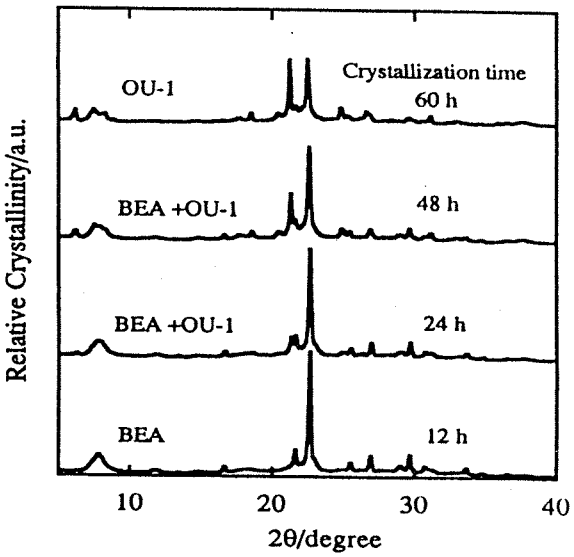

図5 SiO_2/Al_2O_3比＝380の乾燥ゲルからのBEAの生成およびOU-1への相転移。結晶化温度、180℃。SiO_2/Na_2O比＝23.8。

も可能であり、TatsumiらはTi-Al-BEAの合成に成功したことを報告している[12]。

さて、ハイシリカの場合には、BEAが得られる条件で、さらに結晶化時間を長くすると、相転移が起きる。図５には、SiO_2/Al_2O_3比＝380の場合の相転移現象を示す[13]。結晶化時間を長くすると、BEAのXRDパターンが消え、かわりに新しい相が生成してくることがわかる。筆者らは、このBEAから相転移により生成する新しい結晶相をOU-1と名付けた。OU-1は薄板状の直方体であり、BEAの結晶形態とは全く異なる。相転移途中では非晶質相の生成が全く認められないことから、BEAの構造の一部が加水分解して生成した中間体がBEA表面を移動し、BEA表面でOU-1の核発生および結晶成長が進行したと考えている。図６のHR-TEM像からもわかるようにOU-1は酸素12員環よりなる細孔をもつゼオライトである。この12員環細孔は１次元である。OU-1の構造は今のところ図７に示す２種類のPolymorphが主たる構造単位で、これらが積層欠陥を介して繋がっていると考えている。最も注目したいのは、これら２種類のPolymorphの構造を細孔方向から投影した図７が、BEAを構成するPolymorph A, Bとトポロジカルに全く一致する点である。すなわち、図のような細孔方向からの投影図からは、実はOU-1とBEAは区別できない。BEAは酸素12員環よりなる細孔が３次元のネットワークをもつ一方、OU-1は１次元細孔であることから、立体構造は全く異なるであろうことは直感的に理解できる。すなわち、Si-O-Siの立体的なLinkageがOU-1とBEAでは異なる。現在、OU-1結晶内で各Polymorphが形成するドメインの大きさ、および各ドメイン間の積層欠陥の構造について解析をさらにすすめているところである。

OU-1がBEAの相転移で得られたことと、OU-1とBEAが極めて近い構造をもっていることから考えて、BEAの加水分解により生成する中間体はBEAの構造の一部を維持しており、こ

の中間体からOU-1が核発生したと推察できる。ゼオライトの相転移現象は、人工ゼオライトの水熱合成の創始者であるBarrerによって指摘されていた古くから知られていた現象であるが、近い構造をもつゼオライト構造間の相転移現象を積極的に利用することで、さらに新しい構造をもつゼオライトの合成に繋がる可能性が秘められていると期待したい。

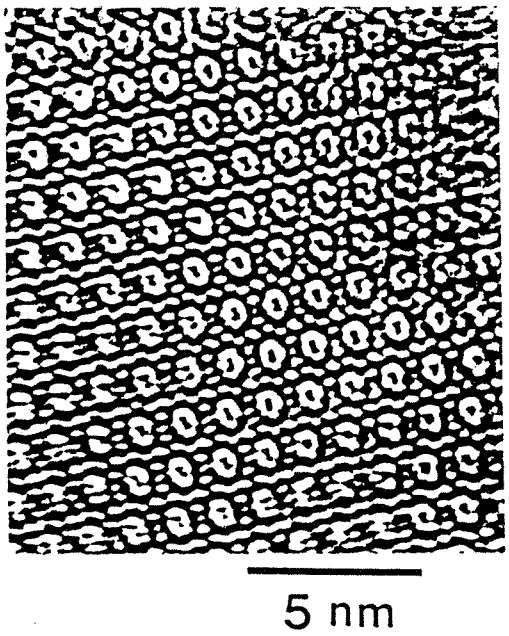

図6 OU-1のHR-TEM像。酸素12員環の細孔が観察できる。

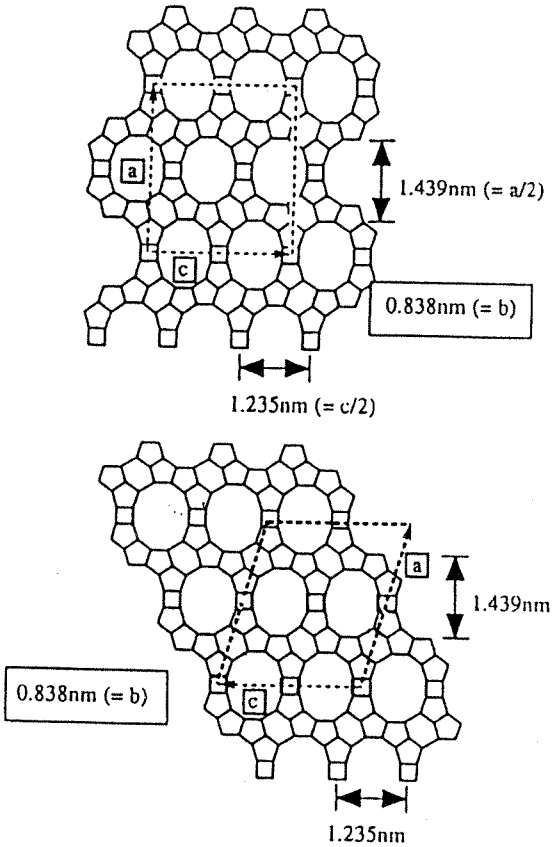

図7 電子線回析より推定されるOU-1の構造。主としてこの2種類のpolymorphより構成されていると考えられる。

3.2.2 FAUおよびEMT

本合成法は、フォージャサイト型ゼオライトであるFAU(Y型ゼラオイト、Cubic)、EMT(Hexagonal)などLarge poreゼラオイトの合成にも適用できる。ハイシリカのFAUおよびEMTの合成は、クラウンエーテルを用いて水熱合成できることは、Delpratoらによって示された[14]が、本合成法においても15-crown-5を用いるとFAUが、18-crown-5を用いるとEMTが、115℃、3日間で得られる[15]。水熱合成法の場合には、EMTは厚み20nm程度の極薄い層が積み重なって六角平板状の結晶へと成長する一方、本合成法の場合には、はじめに大きさ20nm程度のナノ粒子が六角平板状に凝集し、この凝集体が合一することによって平滑な表面をもつ六角平板結晶へと変化する。このナノ粒子の凝集体からは明瞭なEMTのXRDパターンは得られないものの、熱分析等の結果は18-crown-6がEMTのケージ中に取り込まれていることを支持しており、凝集物はすでにEMTの基本構造をもっていると思われる。水熱合成ではこうしたナノ粒子の凝集体は観察されない。このように、水熱合成法とドライゲルコンバージョン法では、同じ構造をもつゼオライトでもその結晶化過程が異なることがある。

3.2.3 AlPO4-n

燐酸アルミ系のゼラオイトである$AlPO_4$-nもドライゲルコンバージョン法を用いて合成することが出来る[16]。テフロンを支持体として用いると、TEAOHを含む乾燥ゲルからは$AlPO_4$-18(酸素8員環の2次元細孔)が、TPAOHを含む乾燥ゲル$AlPO_4$-5(酸素10員環の1次元細孔)が得られる。$AlPO_4$-n合成の場合には、乾燥後の粉末から非晶質部分から得られるハローな回析線のほかに、dense phaseと思われるXRDパターンが常に得られ、これがオートクレーブ中で$AlPO_4$-nへと相転移する。その意味では、$AlPO_4$-nへと結晶するための原料粉末をドライゲルと呼ぶことは厳密には正しくないかもしれない。dense phaseの構造の同定はできていない。

$AlPO_4$-nの合成の場合には、生成物相に原料粉末の支持体の材質が大きく影響する。たとえば、TEAOHを含む乾燥ゲルをアルミナ上で結晶化させると、$AlPO_4$-18ではなく$AlPO_4$-5が生成する。支持体の材質が生成物の構造に著しく影響することは、乾燥ゲル支持体の界面が$AlPO_4$-nの核発生に重要であることを示していると思われるが、支持体によって異なる生成物が得られる原因については今後検討が必要である。

4．気相合成法

これまで述べてきゼオライト合成法と異なり、完全に気相を経由する方法によってゼオライトを得る方法が、Schuthらによって提案されている[17)18)]。彼らの方法は、700℃で焼成したシリカアルミナなどを、塩化テトラメチルアンモニウムやTPABrなどの4級アンモニウム塩および弗化アンモニウムと混合し、210℃程度にて処理するというものである。この方法によって、ZSM-5、MTN型ゼオライト、MTW型ゼオライト(ZSM-12)などが合成されている。合成のメカニズムは、

$$SiO_2 + 4\,NH_4F \rightarrow SiF_4 + 2H_2O + 4\,NH_3$$

によって生成したSiF_4が気化し、これが再度水と反応後脱水することによりSi-O-Si結合が形成されるとされている。ただし、この場合も反応式からわかるように、完全に無水条件ではなく、Siと等モル量の水が生じることになるため、結晶化に対して水の果たす役割を明らかにする必要があると思われる。

5.おわりに

水熱合成に替わるゼオライト合成法として、ドライゲルコンバージョン法を中心として様々な新規合成法を紹介してきた。筆者らが行ってきた合成は、まだまだ限られた範囲で行われたものである。ドライゲルコンバージョン法は、もとより万能ではない。合成例もまだまだ足りないし、水蒸気の結晶化過程における役割に関しては研究は着手したばかりである。結晶化機構もわからない(もっとも水熱合成の機構も完全に理解できているわけではない)。本合成法によって得られたゼオライトの触媒特性など応用研究まではなかなか手が回っていないのが現状である。しかし、ドライゲルコンバージョン法は、水熱合成の代替ではなく、BEAの合成例で示したように水熱合成では合成できない組成をもつゼオライトの合成を達成することができる、あるいはEMTの例で示したように結晶化過程も水熱合成とは異なるなど、この合成法ならではの特徴があることが明らかになってきた。OU-1の合成は、新規な構造をもつゼオライトの合成が、この方法で可能であることを示してくれた。OU-1がBEAからの相転移によって得られたことも、ゼオライトの合成原理の新しい可能性を感じさせてく

れる。また、すでに述べたように分離膜、センサー、デバイスなど新規用途へ展開の可能性が期待されると共に、既知の構造をもつ粉末状ゼオライトの合成にしても多くの工業的利点が指摘できる。Schuthらが報告したようにSi源を気相を経由して供給しゼオライトを合成する方法を積極的に利用すれば、CVDを用いての基板上へのゼオライト合成することも可能かもしれない。半導体デバイスのCVDによる合成技術の発展の経緯に学べば、CVDによる合成は材料のマクロ構造制御のために目指すべき道のひとつであるようにも思われる。

Bibby and Daleが13年前に示した、"ゼオライト合成にとっては水は必須のメディアではない"という単純で明快な結論は、ゼオライト合成にとって広大な可能性を引き出してくれたし、確かな新しい道(科学技術)へと結実しつつあると期待したい。ますますゼオライト合成に関わる研究者・技術者が増え、多くの新しいゼオライト合成技術、ゼオライトの利用技術が我が国から発信されることを期待したい。

引用文献

1) D. M. Bibby and M. P. Dale, *Nature*, **317**, 157-158 (1985)
2) Xu, J. Li, W. Li, H. Zhang, and B. Liang, *ZEOLITES*, **9**, 468-473 (1989)
3) A. Kuperman, S.Nadimi, S. Oliver, G. A. Ozin, J. Garces, and M. M. Olken, *Nature*, **365**, 239-242 (1993)
4) W.Xu, J.Dong, J.Li, J.Li and F.Wu, *J. Chem. Soc., Chem, Commun.*,'755(1990)
5) M.Matsukata, N.Nishiyama and K.Ueyama, *Microporous Mater.*, **1**, 219(1993)
6) M.H.Kim, H.X. Li and M.E.Davis, *Microporous Mater.*, 1, 191(1993)
7) M.Matsukata, N.Nishiyama and K.Ueyama, *Microporous Mater*, 7, 109(1996)
8) 例えばM.Matsukata and E.Kikushi, *Bull. Chem. Soc. Jpn.*, 70, 2341(1997)
9) P.R.Hari Prasad Rao and M.Matsukata, *Chem. Commun.*, 1441(1996)
10)P.R.Hari Prasad Rao, K.Ueyama and M.Matsukata, *Appl. Catal., A.*, 166, 97(1998)
11)P.R.Hari Prasad Rao, C.A.Leon y Leon, K.Ueyama and M.Matsukata, *Microporous Mater.*, in press.
12)T.Tatsumi, Q.Xia and N.Japper, *Chem. Lett.*, 677(1997)
13)P.R.Hari Prasad Rao, K.Ueyama, E.Kikuchi and M.Matsukata, *Chem. Lett.*, in press
14)F.Delprato, L.Delmotte, J.L.Guth and L.Huve, *Zeolites*, 10, 546(1990)
15)松方正彦、木津功一、菊地英一、第13回ゼラオイト研究発表会講演予稿集、p.39(1997)
16)鈴木温雄、西山憲和、上山惟一、松方正彦、第13回ゼオライト研究発表会講演予稿集、p.41(1997)
17)R.Althoff, K.Unger and F.Schuth, Microporous Mater., 2, 557(1994)
18)U.Deforth, K.K.Unger and F.Schuth, Microporous Mater., 9, 287(1997)

《トピックス》

ゼオライトOU-1合成の経緯と構造

松 方 正 彦
早稲田大学理工学部応用化学科

1. はじめに

1994年，筆者が大阪大学基礎工学部化学工学科に助手として在職当時のことであった。インドの国立化学研究所(NCL)において，V-βゼオライトに関する研究で学位を取得し，その後1年間フランスのマリーキュリー大学(パリ第6大学)のBarthomeuf教授のもとで博士研究員をしていたP.R. Hari Prasad Rao博士が，井上科学振興財団のご援助で来日し，筆者の所属していた研究室(上山惟一教授)に加わることとなった。彼に担当してもらったテーマは多く，残念ながら成果に結びつかなかったものもあるが，筆者らのその後の研究活動にとって，エポックメイキングな成果となったのがドライゲルコンバージョン(DGC)法によるゼオライトβ(BEA，以下βと略す)の合成に関する研究であった。Rao博士は1998年4月まで筆者らとともにこの研究を行い，現在米国Woechester Polytechnic InstituteにおいてMa教授のもとでゼオライト膜に関する研究を行っている。

1995年の夏頃，彼がβの合成研究の途中でこれまでに見たことのないXRDパターンを持ってきた。よく知られているように，βは水熱合成，DGC法といった合成法，あるいはテトラエチルアンモニウムカチオン(TEA)など Structure-directing agent (SDA)の種類に関わらず，通常，polymorph AとBの混晶として成長する[1]。polymorphのAはキラルで，これは選択的に合成できれば無機酸化物による光学活性が期待されている。もっともpolymorph Aの光学活性となる構造単位は約2nmほどもあり，光学活性物質としての利用は限られるかもしれない。しかしなお，現在でもpolymorph AあるいはBの選択的合成が無機合成化学的に興味あるテーマであることには変わりがない。

さて，我々が見いだしたXRDパターンは一見polymorph Aによく似ていたので，当時大変興奮した。東京大学のT先生の研究室にも押し掛けて，「これはpolymorph Aではないだろうか？」と相談したことを覚えている。じつは，そのXRDパターンはpolymorph Aではなく，その後我々がOU-1と名付けたものであった。本稿では，OU-1の合成の経緯を織り交ぜながら，その合成方法，構造の特徴を紹介させていただきたい。

2. ドライゲルコンバージョン法によるゼオライト合成

まず，DGC法によるゼオライト合成法について簡単に説明したい。原料は(アルミノ)シリケート水性ゲルであり，その調製手順は通常の水熱合成法と変わりない。適当な組成をもつ水性ゲルを，所定の温度と時間熟成後，加熱してゲルを乾燥させる。通常我々が用いている乾燥温度は353Kである。ゲルを入れた容器から蒸気が立ち上らなくなるまで，十分に撹拌し続けることが，特にハイシリカβを合成する上でのノウハウの一つである。得られた乾燥ゲルを乳鉢で粉砕し，これを図1に示すようなオートクレーブに仕込む。乾燥ゲル粉末は，孔を開けたテフロン板などを支えとしてオートクレーブ中段に仕込んでもよいし，テフロン製のカップに入れてオートクレーブの底に置いてもよい。結晶化を開始するに当たっては，自己圧程度の水蒸気の存在が必須であり，このためオートクレーブに粉末とは接触しな

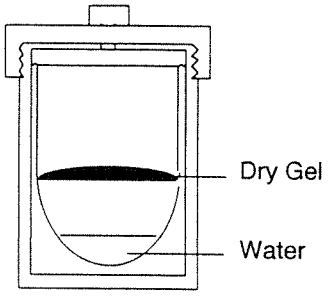

図1 ドライゲルコンバージョン法に用いるオートクレーブ

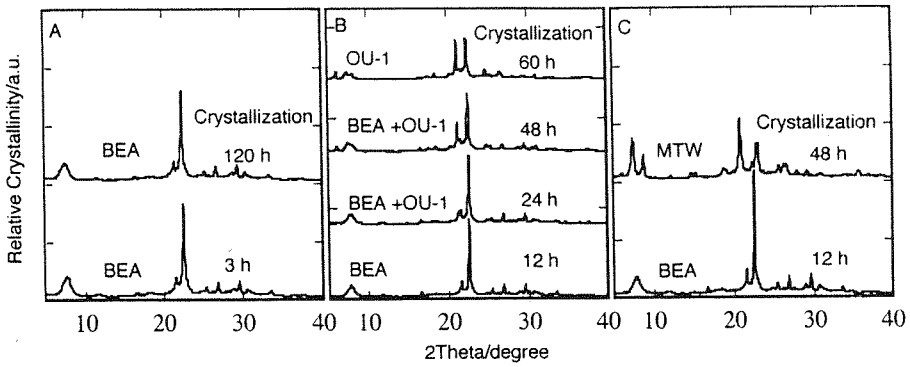

図2 BEAおよび相転移により生成したOU-1(B), MTW(C)のXRDパターン
SiO_2/Al_2O_3比：(A) 30；(B) 380；(C) 730.
Na_2O/SiO_2比：(A) 0.042；(B) 0.042；(C) 0.094.

いよう少量の水を入れる。図1中の水の量は充塡する場所を判りやすくするため誇張してあり，実際には例えば50 mlの内容積をもつオートクレーブであれば，0.5－2 ml程度の水で十分である。水の量が過剰であると結晶化しないことが多いが，理由は明らかではない。

3. OU-1の合成と構造

SiO_2：0.0013－0.33 Al_2O_3：0.042－0.094 Na_2O：0.38 TEAOHの組成をもつアルミノシリケート乾燥ゲルを453 Kにて結晶化したときの生成物のXRDパターンを，図2[2]に示す。SiO_2/Al_2O_3比は30，380，730の3通りである。SiO_2/Al_2O_3＝30の場合にはわずか3時間でβが生成し，120時間結晶化後もXRDパターンにほとんど変化はない。一方，SiO_2/Al_2O_3＝730の場合には，12時間の結晶化ではβが生成するが，48時間後にはβはほぼ消滅し，替わりにMTWが生成していることがわかる。このように，TEAをSDAとして用いてハイシリカゼオライトが得られること，結晶化時間が短いことはDGC法の特徴である。さて，OU-1はSiO_2/Al_2O_3＝100－400程度の狭い範囲で生成する。図2には，SiO_2/Al_2O_3＝380の場合のβからOU-1への相変化の様子を示してある。

OU-1のXRDパターンは，我々が当初βのpolymorph Aと見誤ったように，βとよく似ているが，60時間後にはβはほぼ消滅している。この相変化の様子をSEMにより観察した結果を図3に示す。図3aはβ，図3cはOU-1の純相であり，図3bは，相変化の途中に現れるβとOU-1の混晶である。結晶形態からも両者の違いは明らかである。

XRDに現れるOU-1の特徴的な回折線は，CuK_αをX線源に用いた場合，2θ＝6.2，7.4，8.2，21.2，24.9に現れる。

OU-1のXRDパターンは，インドのNCLから発表されたNCL-1[3]，シェブロン社から発表されたSSZ-31[4]と，大変よく似ており，OU-1を含めた3種のゼオライトは，構造的にanalogousと思われる。NCL-1はハイシリカなアルミノシリケートで，N, N, N-trimethyltricyclo〔5, 2, 1, $0^{2,6}$〕decaneammoniumをSDAとし，SSZ-31は通常ボロシリケートで，hexamethylene bis (triethylammonium bromide) をSDAとして合成される。いずれのSDAも市販品ではなく，かなりバルキーなSDAである。また，相変化によるものでなく，水性ゲルから水熱合成法により得られている。一方，OU-1はTEAという単純な構造をもつSDAから，βからの相変化によって得られることは興味深い。

さて，どうやら新しいゼオライトが生成したことは判ったのだが，困ったのは構造解析であった。もとより，我々は合成研究はしているものの構造解析手法の詳細には全く疎い。困ってあちこちらを尋ね歩いているうちに，東ソー(株)の板橋氏に仲介の労をとっていただき，豊橋技術科学大学の加藤正直先生にXRD構造解析をお願いできることになったが，1996年の終わり頃であった。また，高分解能TEM (HRTEM)および電子線回折を用いた構造解析については，日本ファインセラミックスセンターの佐々木優吉氏に縁あって，お願いできることになった。

解析はまだ完全には終わっていないが，これまでに得られている結論[5]を以下に示す。図4[5]は，2方向からのHRTEM像，図5はOU-1の細孔方向

(a)

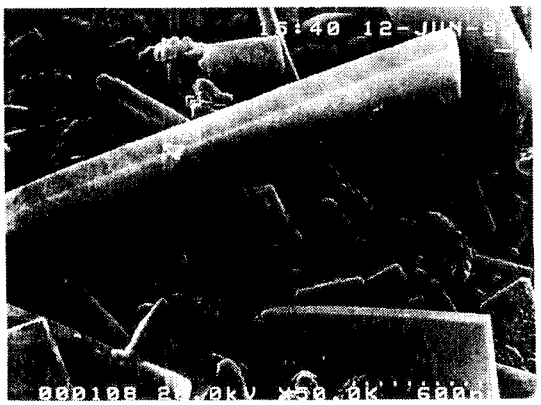

(b)

(c)

図3 BEAおよびOU-1のSEM像
(a) BEA; (b) BEA＋OU-1; (c) OU-1.

から見た骨格構造である。HRTEM像からわかるように，平板状結晶であるOU-1を平板の真上から観察した場合，すなわち〔301〕方向から見た場合にはミクロ細孔は見られず，平板を真横から長手方向に向かって観察した場合に限って，ミクロ細孔の観察ができる。ミクロ細孔はこの方向に1次元に開いているらしい。

OU-1は，少なくともType AとBの2種類よりなる混晶であり，Type AはABAB…の積層構造を，Type BはABCABC…の積層構造をもっている。Type A，Bとも酸素12員環よりなる1次元のストレートなミクロ細孔をもつ構造である。この12員環がHRTEM像の中に見られる。Type AとBという異なる構造が存在する理由は〔TO_4〕四面体ユニットの立体的なつながり方（up down sequence）が異なるためであるが，その詳細はともかく，図5のような2次元投影図中では，楕円形の12員環細孔の四隅に見られる6員環ユニットの向きが，1層目と2層目とで異なる方向を向いている場合はType A（ABAB…構造），すべての6員環ユニットが同じ方向を向いている場合にはType B（ABCABC…構造）となると考えるとわかりやすい。

先に述べたように，OU-1はハイシリカBEAからの相変化で生成するが，我々が興味深く思うのは，このType AとBの2次元投影図は，図5から明らかなようにβのpolymorphと全く同じことである。このことは，βの基本骨格の〔TO_4〕四面体ユニットの立体的なつながり方を変えると，OU-1の構造となることを意味している。こうしたゼオライトの相変化に関しては，水熱合成の場合には種々の機構が提案されている[6,7]が，DGC法によるOU-1生成の場合には連続的な液相が存在しない条件で合成しているので，β骨格の一部分が分解してアルミノシリケートの中間体が生成し，β結晶表面においてOU-1が核発生していることは確かと思われる。そうすると，3次元細孔構造をもつβから，βと似た構造をもち，より骨格密度の高い，1次元細孔をもつゼオライトが生成することは適当と思われるのである。

OU-1のように多くの積層欠陥を有するゼオライトの構造解析は容易でなく，まだ電子線回折像などを完全に説明するには至っていない。まず，OU-1の構造をきちんと明らかにすることが当面の課題であり，さらにβとの積層欠陥との比較などからOU-1の構造上の特徴に考察を加えたいと考えている。また，積層欠陥と相変化との関係なども興味ある課題である。

4. おわりに

βとOU-1の合成と構造に関する最近の研究の経緯について紹介させていただいた。本研究は，我々にとって新規構造の解析，相変化といったテーマについて，興味を抱くきっかけとなった。新しい合成

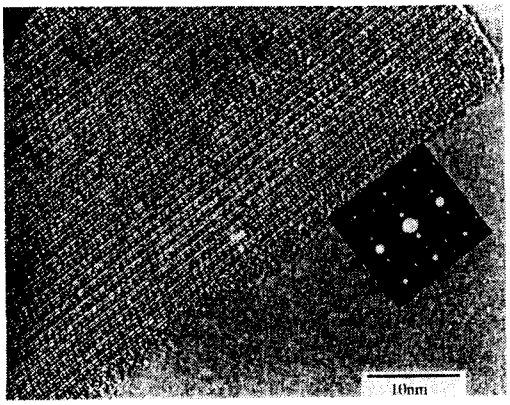

[301]

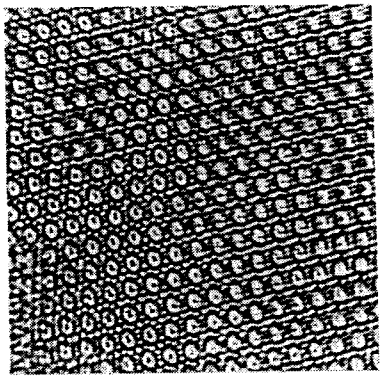

[010]

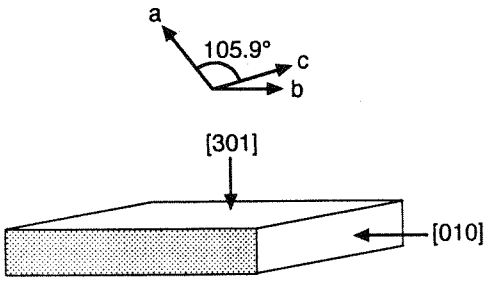

図4　HRTEMによるOU-1の〔301〕,〔010〕方向からの格子像

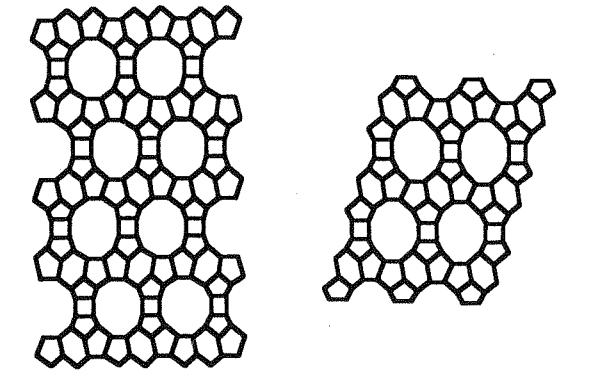

図5　BEAおよびOU-1の骨格構造

法は新しい構造を生み出す可能性があることを信じ，さらに新規ゼオライトの合成に挑戦を続けたい。

謝　辞

本文中でも述べたように，OU-1の構造解析は，豊橋技術科学大学の加藤正直先生，日本ファインセラミックスセンターの佐々木優吉氏の手によるものである。また，本研究の推進には，大阪大学大学院基礎工学研究科，上山惟一先生，西山憲和助手，P. R. Hari Prasad Rao博士(当時)，東ソー株式会社板橋慶治博士，早稲田大学の菊地英一先生，小倉賢学振研究員をはじめ多くの方々のお世話になった。ゼオライトの合成から構造解析，利用に至る研究においては，多くの方々との協力関係が欠かせないことを身をもって体験させていただいた。記して謝意を表する。

引用文献

1) J. M. Newsam, M. M. J. Treacy, W. T. Koetsier, and C. B. de Gruyter, *Proc. R. Soc. London,* **A240**, 375 (1988).
2) P. R. Hari Prasad Rao, K. Ueyama, E. Kikuchi, and M. Matsukata, *Chem. Lett.*, 311 (1998).
3) R. Kumar, K. R. Reddy, and P. Ratnasamy, USP 5219813 (1993).
4) R. F. Robo, M. Tsapatsis, C. C. Freyhardt, I. Chan, C. C. Chen, S. I. Zones, and M. E. Davis, *J. Amer. Chem. Soc.*, **119**, 3732 (1997).
5) M. Matsukata, M. Kato, T. Suzuki, Y. Sasaki, E. Kikuchi, K. Ueyama, and P. R. Hari Prasad Rao, Proc. 12th Intern. Zeolite Conf., Mater. Res. Soc., in press.
6) R. M. Barrer, "Hydrothermal Chemistry of Zeolites", Academic Press, London (1982).
7) P. Norby, *J. Amer. Chem. Soc.*, **119**, 3732 (1997).

Dry Gel Conversion Synthesis of beta and EMT Zeolites

Masahiko Matsukata, P. R. H. Prasad Rao, Department of Chemical Engineering, Osaka University,
Machikaneyama, Toyonaka, Osaka 560, Japan
Kouichi Kizu, Eiichi Kikuchi, School of Science and Engineering, Waseda University,
Okubo, Shinjyuku, Tokyo 180, Japan

Introduction: Recently, zeolites have been synthesized using amorphous aluminosilicate dry gel under the vapors of organic compounds and water. Since Xu et al.[1] have reported the synthesis of ZSM-5 using a vapor-phase transport method, several reports have appeared on the synthesis of zeolites such as ferrierite [2, 3] and zeolitic membranes[4]. Only a few kinds of zeolites can be synthesized using volatile organic compounds. We thus attempted to crystallize various zeolites by adding structure-directing agents to dry gel prior to crystallization and have previously reported that beta with a very wide range of SiO_2/Al_2O_3 ratio of 30 - 900 can be crystallized from dry gel containing TEAOH in steam at 453 K within 72 h [5]. In this paper, we report further results of beta synthesis by a dry gel conversion technique. In addition, we first report that EMT can be crystallized from dry gel with 18-crown-6 ether.

Experimental: Aluminosilicate gel having a given SiO_2/Al_2O_3 ratio was prepared by mixing colloidal silica (Nissan Chemical Co., Ltd.), an aluminum source($Al_2(SO_4)_3$ or $Al(OH)_3$) and sodium hydroxide. An amount of TEAOH or 18-crown-6 ether was added to the aluminosilicate gel as structure-directing agents. After drying up the aluminosilicate gel containing a structure directing agent, we transferred this parent gel in an special autoclave and then crystallized in steam at autogeneous pressure.

Results and Discussion:

Synthesis of beta In this study, we varied crystallization time to follow the progress of crystallization. The range of parent gel composition was SiO_2/Al_2O_3=30-900, SiO_2/Na_2O=10-30, SiO_2/TEA_2O=4.0-8.0. Beta was always obtained in this composition range at 453 K. The XRD patterns indicated that crystallization surprisingly completed within 3 and 12 h for SiO_2/Al_2O_3 ratios = 30 and 900, respectively. Judging from FE-SEM observations, the crystal size was about 60 nm and very uniform. Crystal size distribution interestingly became broader with prolonged crystallization. This result suggests that exchange of silicon and/or aluminum species occurred among crystals even after crystallization completed. Since

crystallization was carried out in gas phase, that is, there was no continuous water phase, these species might be mobile on the solid surface under the synthetic conditions.

Synthesis of EMT For the synthesis of EMT, a typical dry gel composition used in this study was $10SiO_2:Al_2O_3:2.4Na_2O:0.75$ 18-crown-6:xH_2O. Crystallization was carried out in steam at autogeneous pressure in the temperature range of 388 - 423 K. Table 1 lists typical crystallization results. We first found that EMT can be synthesized by the dry conversion technique. Pure EMT was obtained in the temperature range of 378 - 398 K after 4 days. Other phases like mordenite were observed when crystallization was carried out above 408 K. Taking into account that the boiling point of 18-crown-6 ether was ca. 403 K, the ether probably escaped from the dry gel at temperatures above 408 K, leading to the formation of other phases.

Table 1 Typical crystallization results for EMT synthesis

Crystallization time/day	**Temperature/K**					
	378	388	398	408	418	428
2	Am.	Am.	EMT, Am.	EMT	EMT, Am.	EMT, Am.
4	EMT	EMT	EMT	EMT, GIS	EMT, MOR, Am.	EMT, MOR, Am.
6	EMT	EMT	EMT	EMT, MOR	EMT, MOR, Am.	MOR, Am.

Am. Represents amorphous.

Conclusions: The dry conversion technique is useful to synthesize various kinds of zeolites. This synthetic method enables rapid crystallization, complete conversion of parent gel, elimination of waste-water treatment and continuous production. Further, it is possible that some of zeolites which are difficult to produce by conventional hydrothermal synthesis are produced by this dry gel conversion technique like the case of the synthesis of high silica beta.

References:

1. W. Xu, J. Dong, J. Li and F. Wu, J. Chem. Soc. Chem. Commun., (1990) 755.
2. M.H. Kim, H.X. Li and M. E. Davis, Microporous Mater., 1 (1993) 191.
3. M. Matsukata, N. Nishiyama and K. Ueyama, *ibid.*, 1 (1993) 219, 7(1996) 109.
4. For example, M. Matsukata, N. Nishiyama and K. Ueyama, Stud. Surf. Sci. Catal., 84 (1994) 1183, Microporous Mater., in press.
5. P.R.H. Prasad Rao and M. Matsukata, Chem. Commun., (1996) 1441.

ドライゲルコンバージョン法によるゼオライト合成

Synthesis of Zeolites by Dry Gel Conversion Method

松方正彦*1　小倉　賢*2

ゼオライトの用途は，従来の洗剤ビルダー，吸着剤，触媒といった分野から，分離膜，センサー，光学材料などへと広範に展開しつつある。機能性材料としてゼオライトはすでに多くの期待を担っており，さらなる高機能化のために結晶化機構に関する知見の集積が必要不可欠である。本稿では，われわれが開発したゼオライトの新規合成法に関して，結晶化機構の追究・高機能化を目標とした研究成果を中心に概説する。

1. はじめに

ゼオライトは結晶性アルミノシリケートの総称であり，均一で剛直な分子レベルの細孔を有する[1]。また，これらの多くは固体酸として機能し，その酸触媒作用により，重質油の接触分解や異性化などの実用化プロセスに用いられている。一方，ゼオライトの結晶化機構に関しては，近年優れた研究が多く報告されている[2]もののいまだに明らかでない点が多い。ゼオライトの結晶化剤には有機アミン類がしばしば用いられる[3]が，これら有機分子のゼオライトの結晶化過程における役割などは詳細が未解明である。ゼオライトの触媒あるいは吸着剤としての高度利用，機能向上，新規機能性材料の開発，さらには新規構造をもつゼオライトの合成には，結晶化機構の解明が避けては通れない重要な課題である。

われわれは，有機アミン類などの結晶化剤を含む乾燥ゲルを水蒸気自己圧下で処理することによりゼオライトが生成することを見出し，本合成法をドライゲルコンバージョン（DGC）法と名づけた[4]。たとえば本法によれば，ゼオライトベータが短時間で合成可能となること，従来の合成法である水熱法では得られないゼオライトが合成可能であることなどを明らかにしてきた。ゼオライトベータは酸素12員環の3次元細孔を有し，先に述べたような実用化プロセスでしばしば用いられているMFI型ゼオライト（酸素10員環）に比べるとその細孔径は大きく（ベータ：0.74nm，MFI：0.55nm，図1），よりバルキーな分子の反応への適用が期待されているゼオライトの一つである。ゼオライトベータは，水熱合成，DGC法といった合成法，あるいはテトラエチルアンモニウムカチオン（TEA）などStructure-directing agent（SDA）の種類にかかわらず，通常，polymorph AとBの混晶として成長する。polymorphのAはキラルで，これは選択的に合成できれば無機酸化物による光学活性が期待されている。現在でもpolymorph AあるいはBの選択的合成が無機合成化学的に興味あるテーマである。

*1　Masahiko Matsukata　早稲田大学　理工学部　応用化学科
*2　Masaru Ogura　早稲田大学　理工学部　応用化学科

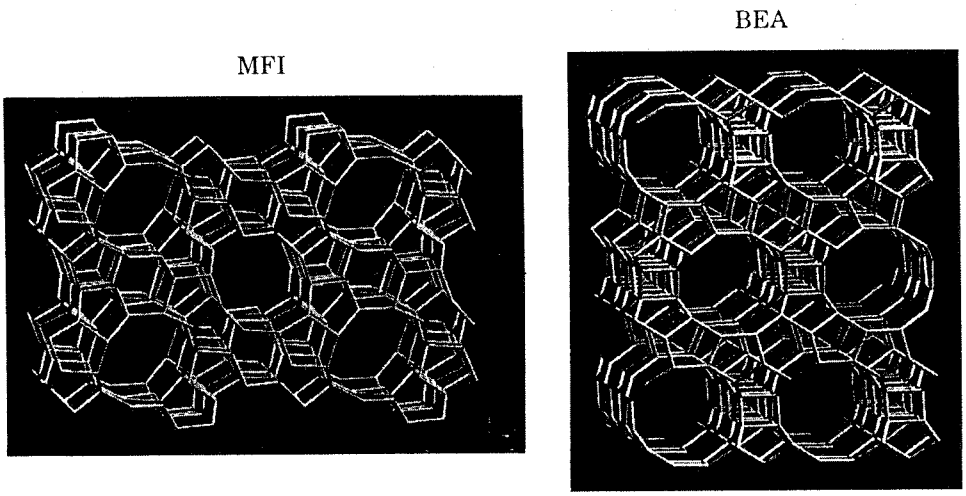

図1　MFIゼオライトおよびベータ（BEA）ゼオライトの骨格構造

本稿では，ゼオライトベータのDGC法による合成研究の経緯をたどり，その合成方法，得られたゼオライトの物理化学的特性を紹介させていただきたい。

2.　ドライゲルコンバージョン法とは

まず，DGC法によるゼオライト合成法について簡単に説明したい。原料は（アルミノ）シリケート水性ゲルであり，その調製手順は通常の水熱合成法と変わりない。適当な組成をもつ水性ゲルを，所定の温度と時間熟成後，加熱してゲルを乾燥させる。通常われわれが用いている乾燥温度は80℃である。ゲルを入れた容器から蒸気が立ち上がらなくなるまで，十分に攪拌・乾燥し続けることが，特にハイシリカゼオライトベータを合成するうえでのノウハウの一つである。得られた乾燥ゲルを乳鉢で粉砕し，これを**図2**に示すようなオートクレーブに仕込む。結晶化にあたっては，自己圧程度の水蒸気の存在が必須であり，このためオートクレーブに粉末とは接触しないよう少量の水を入れる。図2中の水の量は充填する場所をわかりやすくするため誇張してあり，実際にはたとえば50m*l*の内容積をもつオートクレーブであれば，0.5～2m*l*程度の水で十分である。水の量が過剰であると結晶化しないことが多い。

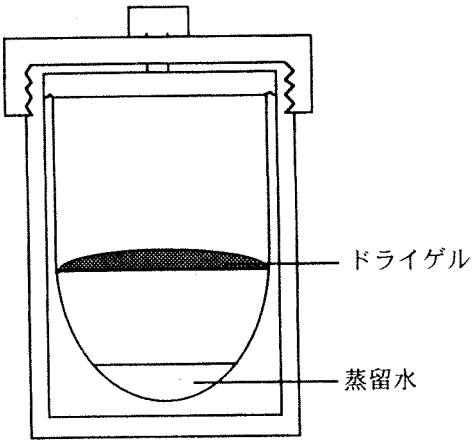

図2　DGC法で用いるオートクレーブ

3.　ドライゲルコンバージョン法によるゼオライトベータの合成

ゼオライトベータは，テトラエチルアンモニウム水酸化物（TEAOH）をStructure-directing agent（SDA）とする水熱合成法ではSiO_2/Al_2O_3が10～300程度の範囲で得られる。しかし，DGC法ではよりハイシリカなゼオライトベータが得られ，さらにはオールシリカベータが合成可能である[1]。本法により合成されたゼオライトベータは，粒子径が10～50nmであり非常に微細である（**図3**）。

ゼオライトの骨格内アルミニウムは酸性質を示すサイトであり，酸点が反応阻害性を示す液相酸化反応などではアルミニウムフリーのゼオライト

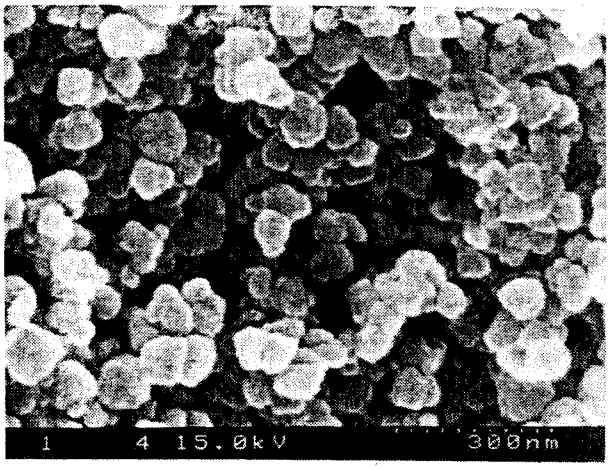

図3 DGC法で合成したゼオライトベータ（SiO_2/Al_2O_3＝100）のSEM像

が望まれる。後述するが，骨格内にTiを取り込んだTi-ベータゼオライトの液相エポキシ化反応では，アルミニウムフリーのベータにTiを導入したTi-Si-ベータがエポキシド選択性の高いゼオライトとなることが示された[6]。

一方，最近われわれのグループでは，SiO_2/Al_2O_3＝7.0とアルミニウム含有量が大きく，かつ非常に微細な粒子からなるゼオライトベータが合成されることを見出した[7]。酸触媒反応に適用しようとした場合に，酸点を多くもつことが重要であることはいうまでもなく，構造の安定性が必要不可欠であるが，本法にて合成されたゼオライトベータは1100℃で焼成しても構造が維持され，水熱条件下にさらされても脱アルミニウムを起こしにくいことがわかった[8]。これは，構造欠陥となるシラノール基（Si-OH）がほとんどないゼオライトベータが合成できる本法の特徴であると思われる。

4. ゼオライトベータの結晶化過程の追跡

水熱法の場合には結晶化過程の解明には固相（結晶相とゲル相）と液相の化学種の構造・反応を明らかにすることが必要であるが，DGC法の場合には水熱合成とは異なり連続相としての水が存在しないため，ゼオライト骨格を形成する化学種がつねにすべて固相中に存在している。このため，結晶化機構の研究にあたって情報が液相・固相両者に分散することなく，固相のみを解析することで結晶化に関する情報が得られる（図4）。その特長を生かし，ゼオライト合成におけるSDAの役割に関して着目し，ゼオライトの結晶化機構を検討した。

得られたゼオライトベータ中に含まれる有機結晶化剤のTEAカチオンを昇温分解させその生成物を質量分析計にて観察したところ，分解スペクトルはゼオライト骨格のシリカアルミナ比に大きく依存していることがわかった（図5）。アルミニウムをほとんど含まない（SiO_2/Al_2O_3＝730）ゼオライトベータの場合，200℃付近から分解生成物がみられ，アンモニア，エチルアミン，ジエチルアンモニウム，トリエチルアンモニウムなどが観測された。一方アルミニウムを多く含む（SiO_2/Al_2O_3＝30）ゼオライトベータの場合，主たる分解スペクトルは400℃以上で現れ，その生成物はアンモニアとエチレンであった。

一般に有機アミンは水溶液中でホフマン分解により炭素鎖が逐次的に分解するが，TEAカチオンの場合約90℃程度でも容易に分解する。このことを考慮すると，TEAカチオンはゼオライトベータ骨格内でアルミニウム（AlO_2^-）およびシリカ（SiO^0）と化学的な結合を形成していると考えられる。TEAカチオンのホフマン分解に対する反応性には，カウンターアニオンの塩基性度が重要であり，塩基性度の高いOH が存在する溶液ではTEAは容易に分解してしまうが，AlO_2^-やSiO^0はOH と比較して塩基性度が小さく，これらと相互作用したTEAカチオンは安定で，結晶化途中で分解することなくゼオライト結晶発生に有効に働くものと結論した。

生成物の形態・構造の経時変化をFE-SEMを用いて追跡した（図6）。XRDで観察されるような長周期的規則構造が形成される以前に，数十nmの前駆体微粒子の集合体が形成されていた。Si-NMRでは結晶化過程ではTEAカチオン周囲においてシロキサン結合の生成（脱水縮合）が連続的に進行することが明らかとなった。これらの

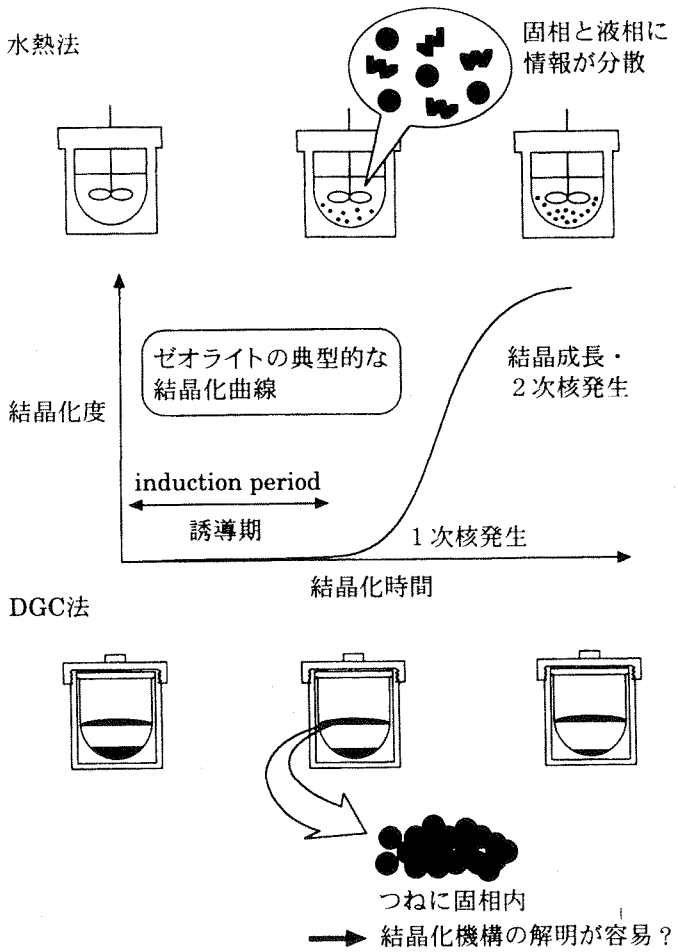

図4　DGC法の特徴

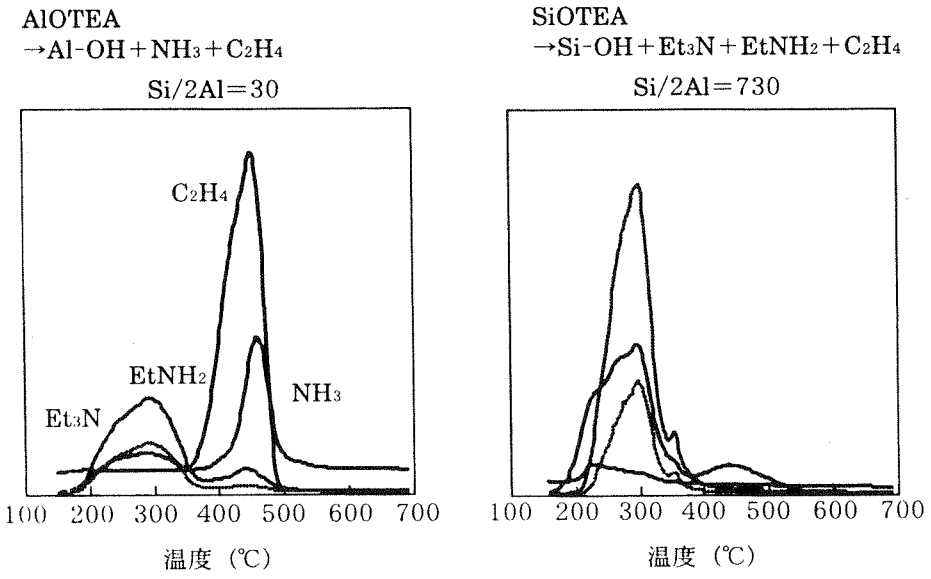

図5　ゼオライトベータ（SiO_2/Al_2O_3＝30，730）に取り込まれたTEAカチオンの昇温分解スペクトル

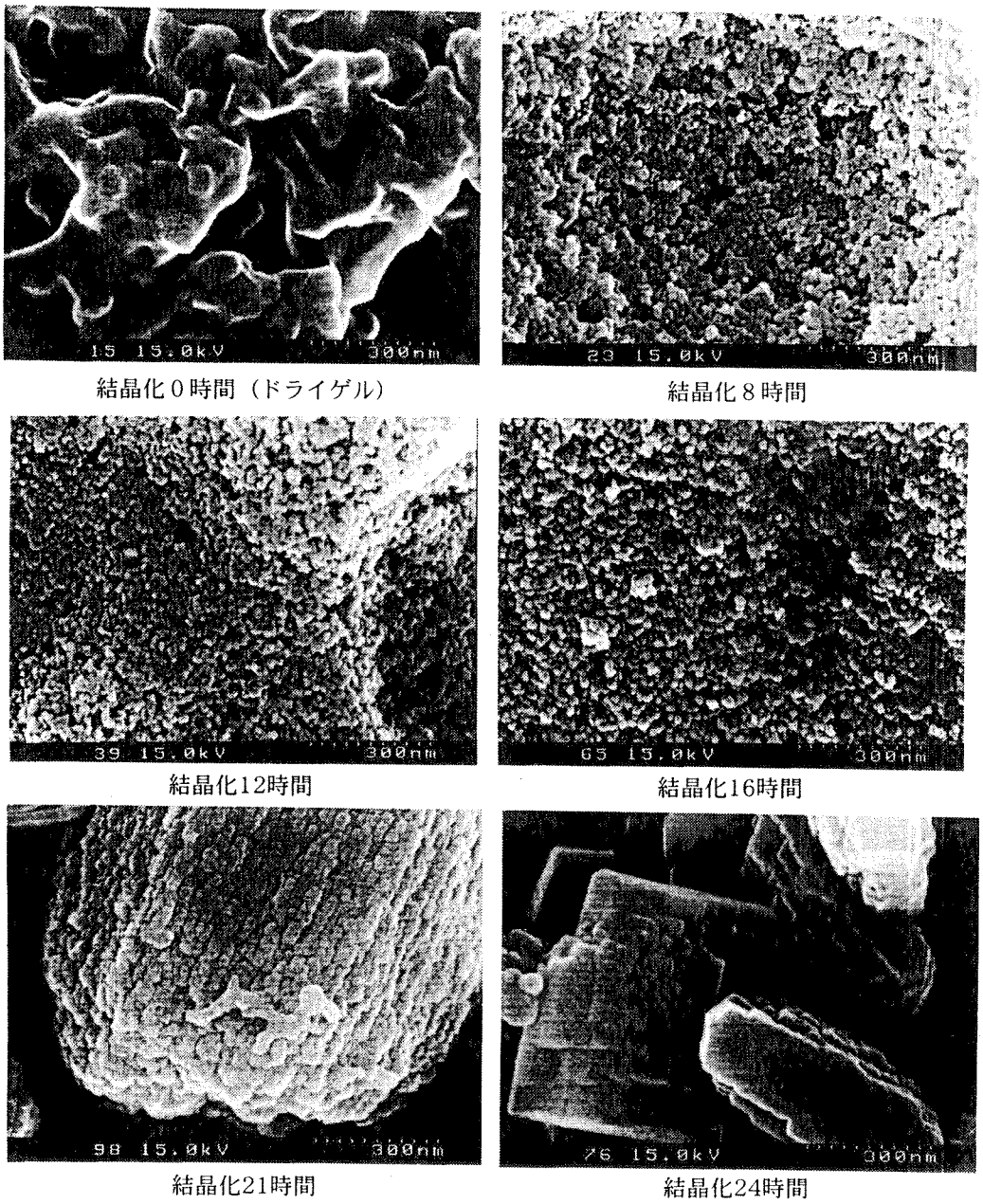

図６　ゼオライトベータ（SiO_2/Al_2O_3＝730）結晶化過程におけるモルフォロジー変化

ことから，結晶化に伴うTEAカチオン周囲環境変化およびシリケート骨格の形成過程を定性的に評価することができた。これは測定対象が固体(乾燥ゲルあるいはゼオライト)であったためであり，本法の特徴を生かして解明できたものである。

5.　新規構造を有するゼオライトOU-１の発見[9]

ゼオライトベータの結晶化過程を追跡している段階で，これまで報告されているゼオライトのX線回折パターンにはみられない構造が，ゼオライトベータからの相転移により形成されていることを見出した。SiO_2：0.0013～0.33，Al_2O_3：0.042～0.094，Na_2O：0.38 TEAOHの組成をもつアルミノシリケート乾燥ゲルを180℃にて結晶化したときの生成物のXRDパターンを図７に示す。SiO_2/Al_2O_3比は30，380，730の３通りである。SiO_2/Al_2O_3＝30の場合にはわずか３時間でベータが生成し，120時間結晶化後もXRDパターンにほとんど変化はない。一方，SiO_2/

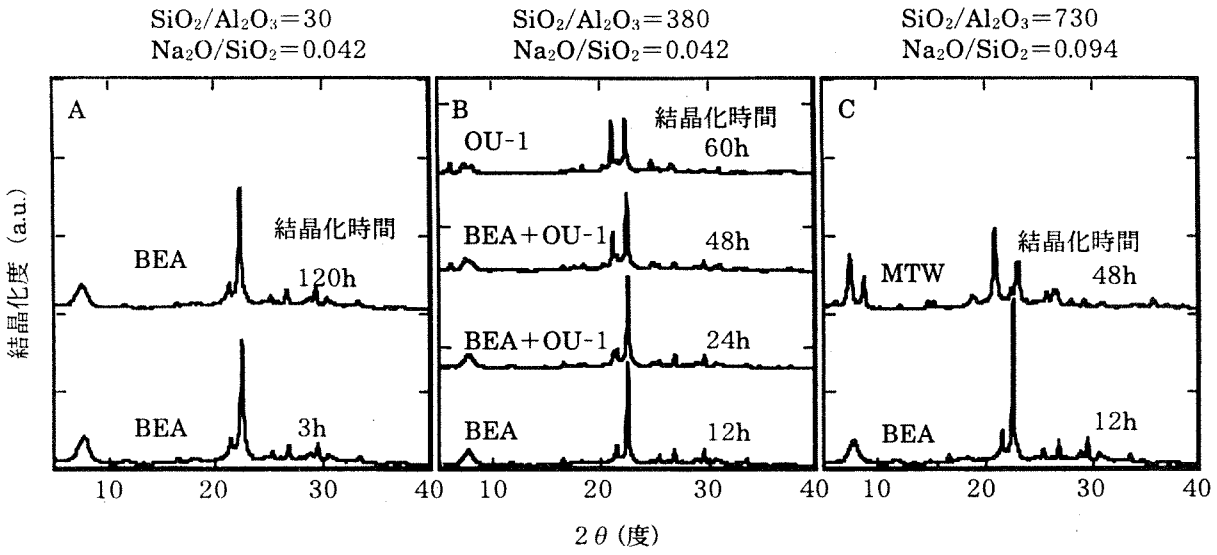

図7　ゼオライトベータの相転移によるOU-1ゼオライト，MTWゼオライトの生成
SiO_2/Al_2O_3=30 (A)，380 (B)，730 (C)

Al_2O_3=730の場合には，12時間の結晶化ではベータ相が生成するが，48時間後にはベータ相はほぼ消滅し，替わりにMTWゼオライトが生成した。また，SiO_2/Al_2O_3=100～400程度の狭い範囲で生成する新規ゼオライトをOU-1と名づけた。

OU-1のXRDパターンはベータとよく似ているが，60時間後にはベータ相はほぼ消滅した。この相変化をSEMにより観察したところ，結晶形態からも両者の違いは明らかであった。XRDに現れるOU-1の特徴的な回折線は，CuKαをX線源に用いた場合2θ=6.2, 7.4, 8.2, 21.2, 24.9に現れる。このXRDパターンは，インドのNational Chemical Laboratoryから発表されたNCL-1[10]，シェブロン社から発表されたSSZ-31[11]とたいへんよく似ており，OU-1を含めた3種のゼオライトは，構造的にanalogousと思われる。NCL-1はハイシリカなアルミノシリケートで，*N*, *N*, *N*-trimethyltricyclo［5,2,1,$0^{2,6}$］decaneammoniumをSDAとし，SSZ-31は通常ボロシリケートで，hexamethylene bis (triethylammonium bromide) をSDAとして合成される。いずれのSDAも市販品ではなく，かなりバルキーなSDAである。また，相変化によるものではなく，水性ゲルから水熱合成法により得られている。一方，OU-1はTEAという単純な構造をもつSDAから，ゼオライトベータからの相変化によって得られることは興味深い。こうしたゼオライトの相変化に関しては，水熱合成の場合には種々の機構が提案されている[12]が，DGC法によるOU-1生成の場合には連続的な液相が存在しない条件で合成しているので，ベータ骨格の一部分が分解してアルミノシリケートの中間体が生成し，ベータ結晶表面においてOU-1が核発生したと思われる。3次元細孔構造をもつベータから，ベータと似た構造をもち，より骨格密度の高い，1次元細孔をもつゼオライトが生成することは適当である（**図8**）。

OU-1のように多くの積層欠陥を有するゼオライトの構造解析は容易でなく，まだ電子線回折像などを完全に説明するには至っていない。まず，OU-1の構造をきちんと明らかにすることが当面の課題であり，さらにゼオライトベータとの積層欠陥との比較などから積層欠陥と相変化との関係なども興味ある課題である。

6. ゼオライトベータ内へのチタンの導入とポスト・シンセシスによる高性能化[6]

辰巳ら[13]によって，DGC法により合成されたTi-ベータゼオライトがシクロヘキサンなど比較的かさ高い分子である芳香族オレフィンのエポキ

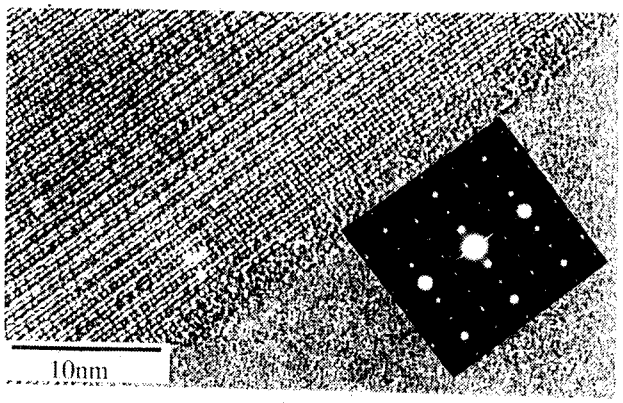

[301]

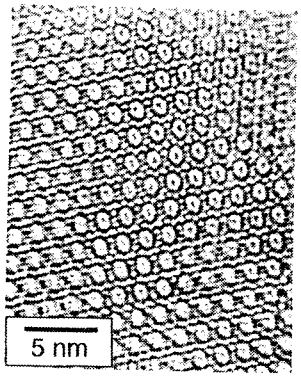

[010]

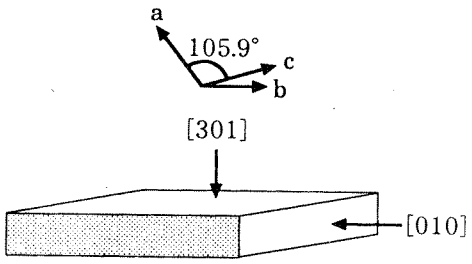

図8　OU-1ゼオライトの［301］および［010］方向からの高分解TEM像

シ化反応に有効であること，Alを少なくするだけでなく本法により合成されたTi-ベータゼオライトが疎水性であることが選択的なエポキシド生成に重要であることが報告された。われわれのもつ合成レシピを利用して，アルミニウムフリーのTi-Si-ベータゼオライトを合成することを試みた。アルミニウムを含むベータと比べてオールシリカベータはその適当な合成条件範囲が狭い。特に，水性ゲル段階に仕込むNa量が最終生成物の結晶化度に与える影響が大きいことがわかった。Si-ベータ合成の際にTiを導入したところ，Ti-Si-ベータがTi-Al-ベータと同等の高い結晶化度で得られた。

オールシリカのゼオライトベータ骨格内へ導入するTi量を変えて合成を行ったところ，水性ゲル（仕込み比）とほぼ同じモル比Si/Ti＝20～300でTi-ベータが合成可能であった。水熱合成法では結晶化度の高いTi-ゼオライトが1.05個/単位胞のTi導入まで可能であることが報告されている[10]が，本法によれば2.10個/単位胞までTiの導入が可能である。Ti導入量が大きくなるに従ってベータゼオライト結晶［302］面に相当する2theta＝22deg.付近の回折線の格子間隔（d値）がほぼ1次の相関で大きくなった（図9）。このことはTiが等価なサイトに逐次導入されていることを示しているものと思われる。またUVスペクトルによってTiの配位状態を検討したところ，いずれも220～250nm付近に吸収がみられた。これはシリケート骨格内に取り込まれた4配位チタン種に相当する。以上の結果から，Tiはゼオライト骨格内へ導入され，イオン半径の大きいTiによりゼオライト格子間隔が拡大されることがわかった。

Ti-Si-ベータにおけるの配位状態をUVスペクトル測定により検討した。合成後のサンプルは220～250nm付近のほかに270nmに吸収がみられる。前者は4配位Tiに起因するもので，後者は

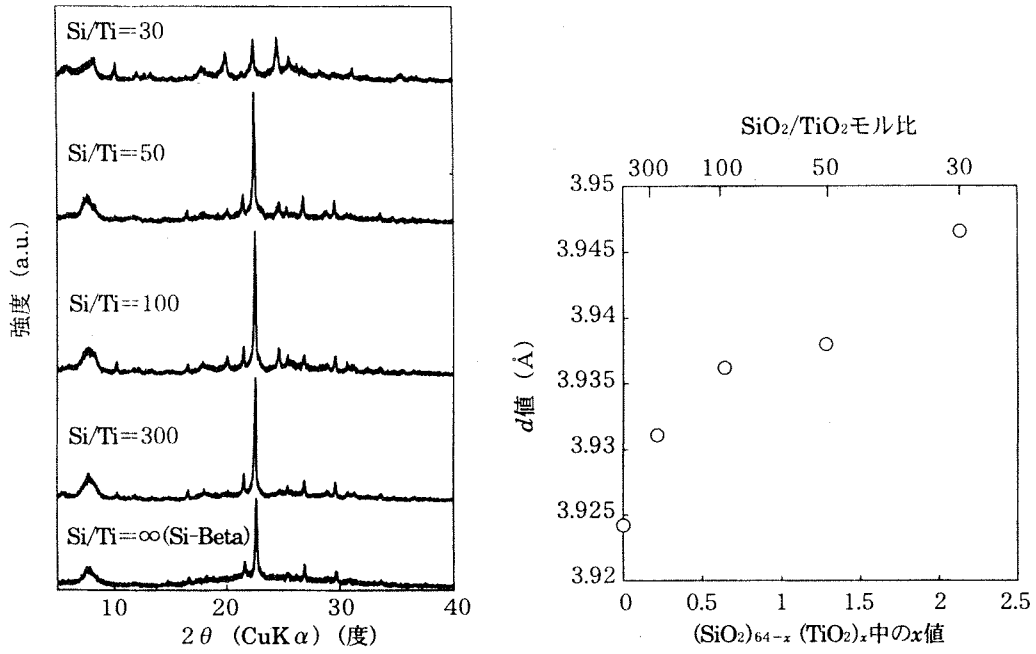

図9　DGC法によるTi-Si-ベータゼオライトの合成
生成物のXRDパターンと結晶内Ti量に対するBEA［302］結晶面のd値の変化

水などが配位したゼオライト骨格外Ti種に起因しているものと考えられている。この吸収は焼成後（Na/Ti-Si-ベータ）に強度が小さくなった。ゼオライト骨格外のTi種を取り除く方法として焼成前にH_2SO_4にて洗浄する方法が知られているため，焼成前にNH_4NO_3にて洗浄する方法とあわせてその効果を検討したところ，H_2SO_4/Ti-Si-ベータ，NH_4NO_3/Ti-Si-ベータともに骨格外のTi種量がほとんどみられなくなった。しかし，H_2SO_4洗浄では骨格のSi/Ti比が大きくなっており（すなわち脱Tiが起こり），NH_4NO_3洗浄ではその変化がなかった。このことからDGC法により調製されたTi-Si-ベータ中のTi種はほとんどすべて骨格内に存在しているものと思われる。また，NH_4NO_3によりH_2Oが吸着するようなTi種を改質することができる。

H_2O吸着等温線を測定し，疎水性の評価を行った（図10）。Na/Ti-Si-ベータには Ti-Al-ベータ（SiO_2/Al_2O_3＝380）とほぼ同量のH_2Oが吸着された。骨格内のAl量を減少させることによって（Ti-Al-ベータ（SiO_2/Al_2O_3＝730）），H_2O吸着量が減少していることがわかる。さらには，

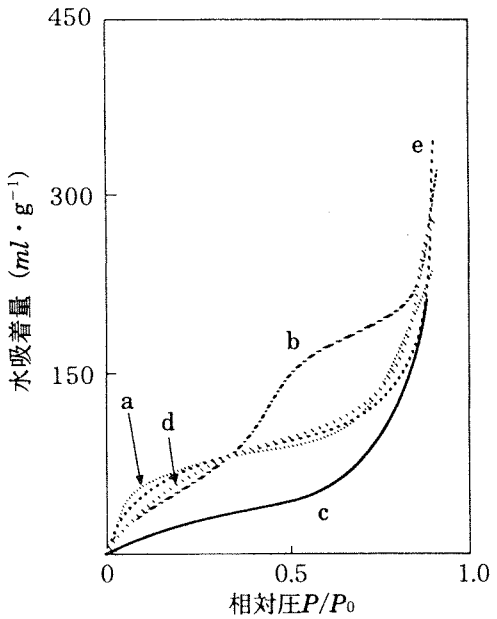

図10　Ti-ベータゼオライトへのH_2O吸着等温線とH_2O吸着量に対する前処理の効果
(a) Na/Ti-Si-ベータ，(b) H_2SO_4洗浄Ti-Si-ベータ，(c) NH_4NO_3イオン交換Ti-Si-ベータ，(d) Ti-Al-ベータ(SiO_2/Al_2O_3＝730)，(e) Ti-Al-ベータ(SiO_2/Al_2O_3＝380)

表1　合成したTi-ベータゼオライト上でのエポキシ化反応

サンプル	シクロヘキサン転化率（%）	エポキシド選択性（%）
Si-beta	0	0
Na/Ti-Si-beta	19	45
H_2SO_4/Ti-Si-beta	28	62
NH_4NO_3/Ti-Si-beta	35	89
Ti-Al-beta730	11	98
Ti-Al-beta380	11	98

反応条件：
シクロヘキセン：30mmol, 過酸化水素：10mmol,
溶媒：アセトニトリル，触媒：50mg,
反応温度：50℃，反応時間：2h

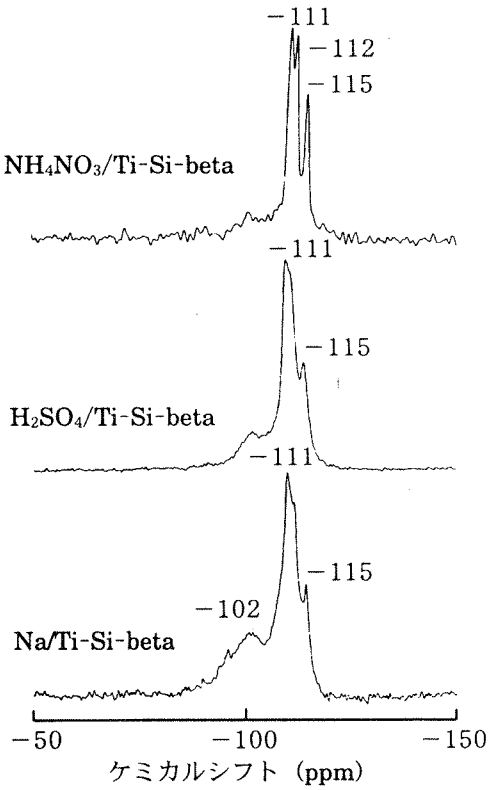

図11　Ti-Si-ベータゼオライトの^{29}Si-MASNMRスペクトル

H_2SO_4洗浄，NH_4NO_3イオン交換によってH_2O吸着量が大幅に減少した。NH_4NO_3/Ti-Si-ベータについては，すべてのサンプル中で最も疎水的になることが明らかとなった。また^{29}Si-NMRによる検討から，NH_4NO_3イオン交換では特にQ^3サイト（構造欠陥サイト）量減少に効果があることがわかった（図11）。

これらのサンプルを用いてシクロヘキサンのエポキシ化反応を行った（表1）。NH_4NO_3/Ti-Si-ベータが最も活性が高く，エポキシドへの選択性がNH_4NO_3イオン交換によって向上することが明らかとなった。

以上まとめると，DGC法によりオールシリカベータ内へTiを導入した高い結晶化度をもつTi-Si-ベータが合成可能であること，NH_4NO_3イオン交換により疎水的な反応サイトが構築可能であると結論した。本法により合成されたベータゼオライトにNH_4NO_3イオン交換を施すことにより，H_2O吸着量の少ないゼオライトに改質することが可能となる。これは骨格内の欠陥サイトが減少していることを示しており，耐水熱安定性を向上させる修飾法（ポスト・シンセシス）として期待できる。

7.　おわりに

新規ゼオライト合成法であるドライゲルコンバージョン法および本法により得られたゼオライトの特性について，ゼオライトベータを一例として概説した。本法はベータゼオライトだけでなくMTW，OU-1，MFI，SSZ-31[15]などのゼオライトも合成でき，一般にゼオライトの結晶化に有効な方法である。また，ポスト・シンセシスによっても高機能化を図ることができることを示すことができた。本法の特徴を生かすことにより結晶化過程の追跡が可能となり，新規ゼオライトや高機能ゼオライトの合成へと発展することが期待される。

謝辞：本研究は，工業技術院「独創的高機能材料創製技術の研究開発」プロジェクトの一部として，新エネルギー・産業技術総合開発機構（NEDO）からの開発依頼を受けて実施したものである。ここに記して感謝する。

文　献

1）富永博夫編，ゼオライトの科学と応用，講談社サイエンティフィク（1987）
2）R. Ravishankar *et al.*, *J. Phys. Chem.*, B103, 4960（1999）
3）M. E. Davis, S. I. Zones, Synthesis of Porous Materials：Zeolites, Clays and Nanostructures, p1, Marcel Dekker, New York（1996）
4）M. Matsukata *et al.*, *Topics in Catalysis*, 9, 77（1999）
5）P. R. H. P. Rao *et al.*, Proc. 12th International Zeolite Conference, Mater. Res. Soc., 1515（1999）
6）M. Ogura *et al.*, submitted for publication
7）A. Mitra *et al.*, submitted for publication
8）P. R. H. P. Rao *et al.*, *Microporous and Mesoporous Mater.*, 21, 305（1998）
9）P. R. H. P. Rao *et al.*, *Chem. Lett.*, 1998, 311
10）R. Kumar *et al.*, U.S. Patent 5219813（1993）
11）R. F. Lobo *et al.*, *J. Am. Chem. Soc.*, 119, 3732（1997）
12）P. Norby, *J. Am. Chem. Soc.*, 119, 5215（1997）
13）T. Tatsumi, Jappar, *J. Phys. Chem.*, B102, 7126（1998）
14）T. Blasco *et al.*, *J. Am. Chem. Soc.*, 115, 1806（1993）
15）R. Bandyopadhyay *et al.*, *Chem. Lett.*, 2000, 300